NanoSpain
Conf 2011

NANOIBERIAN CONFERENCE

NANOSPAIN POSTERS (170)

NANOSPAIN POSTERS (170)

NANOSPAIN POSTERS (170)

NANOSPAIN POSTERS (170)

NanoSpain Posters (170)

Autonomous catalytic motion of carbon nanotubes

A. Afshar Farniya[1], M.Esplandiu[1], P. Jimenez[2], A. Benito[2], W. Maser[2], P. Ortiz[3], A. Llobera[3] and A.Bachtold[1]

[1]Centre d'Investigació en Nanociència i Nanotecnologia CIN2 (ICN-CSIC), Campus UAB Bellaterra, Barcelona, Spain
[2]Instituto de Carboquimica de Zaragoza (CSIC), Departamento de Nanotecnología, Zaragoza, Spain
[3]Centro Nacional de Microelectrónica (CSIC), Campus UAB Bellaterra, Barcelona, Spain

Aafshar@icn.cat

Biomotors (or motor proteins) have attracted a lot of attention as nanomotors, since they can perform various tasks such as cell division and intracellular transport [1]. One problem of biomotors is that they degrade rapidly outside the physiology of the cell. Therefore, researchers have tried to look for alternatives. Applying man-made catalytic nanomotors is an appealing prospect. Catalytic motors can convert chemical fuel such as H_2O_2 molecules into autonomous motion and perform tasks, such as the transportation of cargo [2].

Catalytic motors typically consist of the assembly in series of two rods made of different materials (for instance, Au and Pt). The precise chemomechanical transduction mechanism is still the subject of current investigations. A possible mechanism is that the oxidation of H_2O_2 occurs preferentially on the Pt rod while the reduction of H_2O_2 and O_2 takes place on the Au rod [3]. These simultaneous reactions cause the electrons to be transferred from the Pt to the Au end. The electron flux is accompanied by the motion of the protons that are surrounding the rods in the solution. This proton flux pushes against the fluid, leading to the directional motion of the nanoscale motor. Interestingly, the direction of the motion can be controlled using solution with H_2O_2 gradient. The motor goes towards the concentration maximum [4].

We propose to develop catalytic motors based on single carbon nanotubes (Fig 1). Au will be patterned at one end of the carbon nanotube and Pt on the other one. One motivation is that the motion may be more efficient. Indeed, the friction from the surrounding liquid may be reduced due to size reduction. In addition, the speed may be enhanced, since (a) nanotubes can conduct electrons without any resistance over long distances and (b) conducting electrons are located at the tube surface, which allows for a larger interaction with protons.

These catalytic nanotube motors may be used for sorting applications. It may sort metal and semiconducting nanotubes, since semiconducting nanotubes are expected to remain more immobile (as they carry much lower electron currents).

References

[1] M. G. L. van den Heuvel and C. Dekker, Science, **317** (2007) 333
[2] S. Sundararajan, et al., Nano Lett. **8** (2008) 1271
[3] R. Laocharoensuk et al., ACS Nano **2** (2008) 1069
[4] T.R. Kline et al., Angew. Chem. **117** (2005) 754

Figures
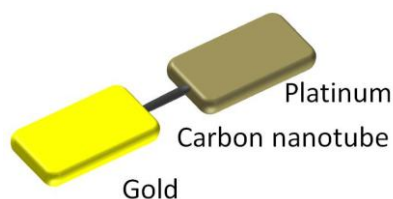
Figure 1 Carbon nanotube –based catalytic motor

Influence of substrates structure on magnetic and dielectric properties of $CoFe_2O_4$ and $BaTiO_3$ magneto-electric multilayer thin films

Frédéric Aguesse[1], Anna-Karin Axelsson[1], Matjaz Valant[2,1] and Neil McN Alford[1]

[1]Department of Materials, Imperial College London, Exhibition Rd, SW7 2AZ London, United Kingdom

and

[2]Materials Research Laboratory, University of Nova Gorica, 5000 Nova Gorica, Slovenia

e-mail: faguesse@imperial.ac.uk

The understanding of magnetoelectric (ME) materials, in which the magnetisation can be controlled in applying an electric field, or the electric order via magnetic field, are of great interest because of their potential novel applications in memory storage, field sensors and more generally for multifunctional devices. Combination of highly piezoelectric and magnetostrictive materials in the magneto-electric composite films [1] is expecting to give a high ME response via an elastic coupling at the interface. $BaTiO_3$ and $CoFe_2O_4$ are amongst the best oxide materials candidates for such elastic interaction.

Innovative multilayers superstructures of $BaTiO_3$ and $CoFe_2O_4$ were prepared by Pulsed Laser Deposition on different single crystal substrates such as MgO, $LaAlO_3$ and $SrTiO_3$. The in- and out-of-plane strain, induced in the structures, was studied by symmetric and asymmetric X-ray diffraction measurements. Furthermore, the interfaces between the layers were analysed by Transmission Electron Microscopy, which emphasizes the film growth mechanism and its relation to structural defects such as dislocations.

Despite various lattice mismatches (from -10% to +0.4%), the films were grown epitaxially and their in-plane crystallographic structure matches the substrates. The surface quality of the films was observed by AFM, SEM, and despite the good quality of the films, micro and nano defects and interfacial compatibility between the layers has a significant impact on the individual layers functionality. Magnetic and dielectric measurements will also be presented and discussed.

References

[1] M Fiebig, Journal of Physics D: Appl. Phys., **38** (2005) R123 Authors, Journal, **Issue** (Year) page.

Magnetization Configurations and Reversal of Magnetic Nanotubes with Uniaxial Anisotropy

Ai-Ping Chen[1], Julian M. Gonzalez[1], and Konstantin Y. Guslienko[1,2]

[1]Dpto. Física de Materiales, Universidad del Pais Vasco, M. Lardizabal, 3, San Sebastian 20018, Spain
[2]IKERBASQUE, the Basque Foundation for Science, Alameda Urquijo, 36-5, Plaza Bizkaia, Bilbao 48011, Spain
Contact@E-mail: sckguslk@ehu.es

Nanotubes and nanotube arrays, combining the attractive tubular structure with magnetic properties, are promising candidates for potential applications in a broad range of nano-technological areas, such as high-density data storage, nano-electromechanical devices, as well as biotechnology, like drug delivery, biosensors, chemical and biochemical separations etc. [1]. Therefore, study of the magnetic properties of nanotubes, such as their magnetization (**M**) distributions, magnetization reversal processes etc. became one of the important research directions in modern nanomagnetism.

We present calculations of the magnetization configurations and reversal behavior of magnetic nanotubes with uniaxial anisotropy by means of 2D micromagnetic simulations and analytical methods. The equilibrium state, the hysteresis loops and the switching field values are calculated as functions of the tube sizes and material parameters. There is an additional degree of freedom for magnetic nanotubes in comparison to nanowires, their thickness, ΔR. The tube radii R from 50 nm to 150 nm and the tube length (L) /radius aspect ratio $5 \leq L/R \leq 20$ were explored. For a finite length of magnetic nanotubes the magnetization configuration is characterized by the uniformly magnetized along the tube axis middle part and two non-uniform curling states of a length L_c in two ends of the tube with the same or opposite magnetization rotating senses, referring as C-state, or B-state, respectively. We found that the magnetization configuration of the C-state exists for thin nanotubes with the tube thickness, ΔR, in the range of $\Delta R/R \leq 0.2$ [2]. For thicker nanotubes the strong magnetostatic stray field forces the change of rotating senses of the end domains in opposite directions (B-state) [3]. The transition from the C-state to a vortex state with in-plane magnetization is described as function of the tube geometrical parameters. The nanotube hysteresis loops and switching fields were calculated. A simple analytical model was developed to describe the nanotube magnetization reversal reducing its description to the Stoner-Wohlfarth model with effective parameters. The equilibrium state of nanotube is described by Θ, the angle of the magnetization **M** deviation from the intrinsic tube easy axis (Fig. 1). Θ as the function of tube aspect ratio L/R, tube thickness ΔR, and uniaxial anisotropy constant K_u obtained by minimizing the total energy of **M** containing the anisotropy, the magnetostatic, and the exchange energy terms, well describes the dependences of the shape of hysteresis loop and switching field values on tube geometric and material parameters in the C- and B-state. For thick nanotubes with reducing tube length the uniformly magnetized middle part gradually diminishes and disappears. The different types of domain walls, such as the transverse domain wall, the asymmetric vortex wall, branch fashion wall, as well as horse-saddle wall, are nucleated in the tube, leading to the wide variety of magnetization reversal modes. We present simulations of the domain wall types and magnetization reversal modes for short nanotubes with R of 50 nm and 100 nm.

In the magnetic field applied along the tube axis **z** the simulated hysteresis loops of C- and B-state tubes (Figs. 1, 2) consist of the reversible rotation to the stable states and irreversible reversal of the magnetization. The coercive field H_c and the switching field H_s, increase with increasing of K_u for the given size nanotubes, and decreases with increasing R for the nanotubes. With reducing nanotubes length and increasing tube thickness the domain walls with the varied patterns, such as the transverse wall, vortex wall, branch wall, and horse-saddle wall, determine **M** distributions near the centre of the tube. The domain wall structure and magnetization reversal modes demonstrate sensitive dependences on the tube thickness, ΔR. For short nanotubes of $R=100$ nm, with ΔR increasing to 40 nm, 50 nm, and 60 nm the domain walls are induced. The magnetization processes of such domain walls are characterized by the periodic transitions of the wall structures from the respective initial patterns to the final unique structure of the branch fashion wall, which causes no closure of the magnetization loops for the z-component of the magnetization at zero fields with respect to the initial and the final states.

The simulations were performed using the typical soft magnetic material parameters: the exchange constant, $A=10^{-6}$ erg/cm, and the saturation magnetization, $M_s= 10^3$ G. In order to study dependence of the magnetization configuration and magnetization reversal on the values of the uniaxial anisotropy constant, K_u, two values of $K_u = 5 \times 10^4$ erg/cm^3, and $K_u = 10^5$ erg/cm^3, were chosen that satisfy the soft

magnetic materials condition of $M_s^2 \gg K_u$. The exchange length of the material is $l_{ex} = \sqrt{A}/M_s = 10$ nm. The dependences of H_c, H_s on the tube geometry ($L, R, \Delta R$) and material parameters (A, M_s, K_u) can be understood by the energy competition of the magnetostatic and Zeeman energy terms against the sum of the exchange and anisotropy energy terms.

References

[1] X. F. Han et al., *Adv. Mater.* **21** (2009) 4619.
[2] A. P. Chen, K. Y. Guslienko, and J. Gonzalez, *J. Appl. Phys.* **108** (2010) 083920.
[3] A. P. Chen, J. Gonzalez, and K. Y. Guslienko, submitted to *J. Appl. Phys*.

Figures
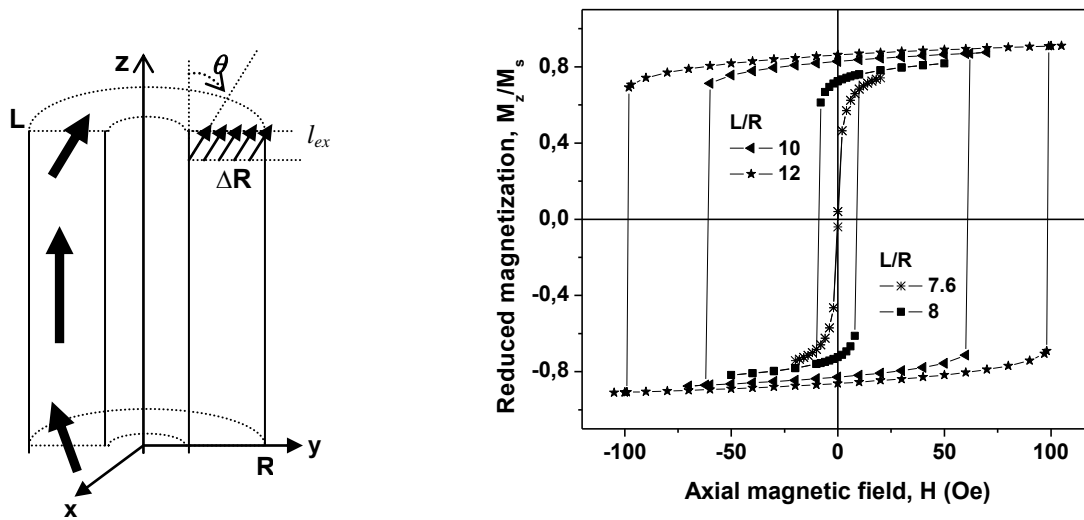
Fig. 1. Schematic representation of magnetization distribution in a nanotube (left). Hysteresis loops (right) of the C-state nanotubes of thickness ΔR=20 nm and radius R= 50 nm in the axial magnetic field for the different tube aspect ratios, L/R. $K_u = 10^5$ erg/cm^3.
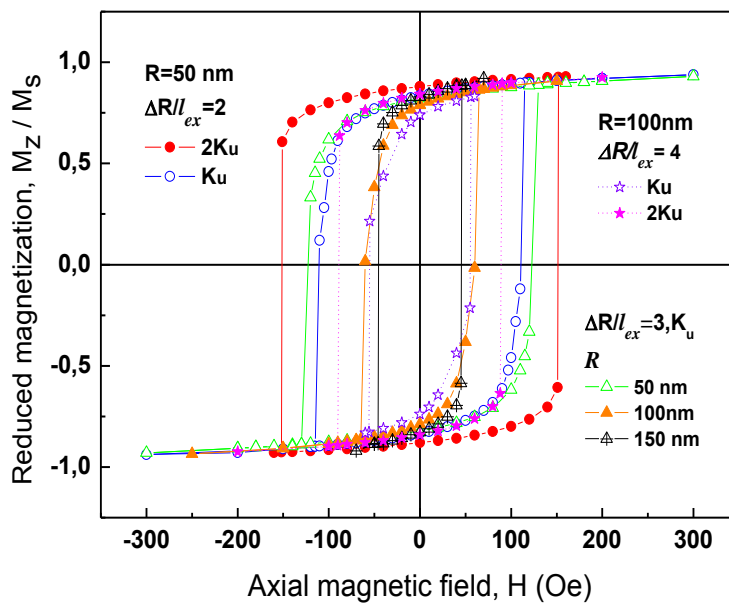
Fig.2. Hysteresis loops of the B-state nanotubes. The tube aspect ratio L/R=20. Geometrical parameters of the nanotubes: R=50 nm, ΔR/l$_{ex}$ =2; R=100 nm, ΔR/l$_{ex}$= 4; and ΔR/l$_{ex}$ = 3, R= 50 nm, 100 nm, 150 nm, respectively. The anisotropy constant is $K_u = 5 \times 10^4$ erg/cm^3.

Nanostructured Inorganic Thin Films prepared by Modified SILAR-method

Rune Wendelbo and Fatima Ait Medjane

Abalonyx AS, Sem Saelandsvei 26, 0371-Oslo, Norway
rw@abalonyx.no

Successive ionic layer adsorption and reaction (SILAR) represents a promising wet chemical approach for preparation of chalcogenide and oxide thin films. In its simplest form, a substrate is alternately introduced in solutions containing respectively the cations and the anions of the target material. One disadvantage with conventional SILAR is that heat treatment between successive layer depositions is not provided.

We present here an automated set-up for parallel processing of 24 samples, including heating, drop-removal and online measurement of conductivity and light transmission. An extensive range of sulfide-, oxide-, phosphate- and carbonate thin films have been prepared by our modified SILAR method. The films were deposited on substrates of glass by using an automated high-throughput set-up developed in-house for the purpose. A commercial robotic arm is used to dip 24 substrates in parallel in well plates containing different solutions followed by heating in inert or reactive gas (Fig1). Typically, one 24-well plate is prepared with six different salt solutions in rows of four wells, containing the target materials cations. Another 24-well plate is prepared with solutions of four different compounds containing the anions for the target materials. Additional well-plates are filled with distilled water for washing. The set-up includes in-house made instrumentation for on-line measurement of conductivity and transmittance. X-ray diffraction (XRD), SEM, AFM and XPS techniques have been employed to investigate the structure and surface morphology of as-deposited films, for example comparing films prepared with different heat treatments during the deposition sequence. The method is particularly suitable for the preparation of films with thickness ranging from a few nm to 1 micrometer, the thickness depending both on dipping cycles and solution concentrations. Specifically, we have been searching for new transparent conductive materials, and it was found that for sulfides, in a narrow compositional range around Zn/Cu = 10, semi-transparent films with sheet resistivity lower than 100 Ohms/sq were obtained for samples heated to around 200 ºC (Figs. 2a and 2b). This amounts to about 100 times higher conductivity than for materials of similar composition previously reported. When we prepared samples with the same chemical composition without heat treatment, the sheet resistance was above 200 MOhms/sq. SEM-analysis indicated that the films were not uniform in early stages of the deposition-process. Elongated "islands" could be observed, which grows with increasing number of dipping cycles. However, after 90 dipping-cycles, the SEM analysis shows continuous and homogeneous films.

In conclusion, we have shown that the modified SILAR-method can be used to prepare thin films with improved properties, by the introduction of on-line heating in the course of the process.

Figures
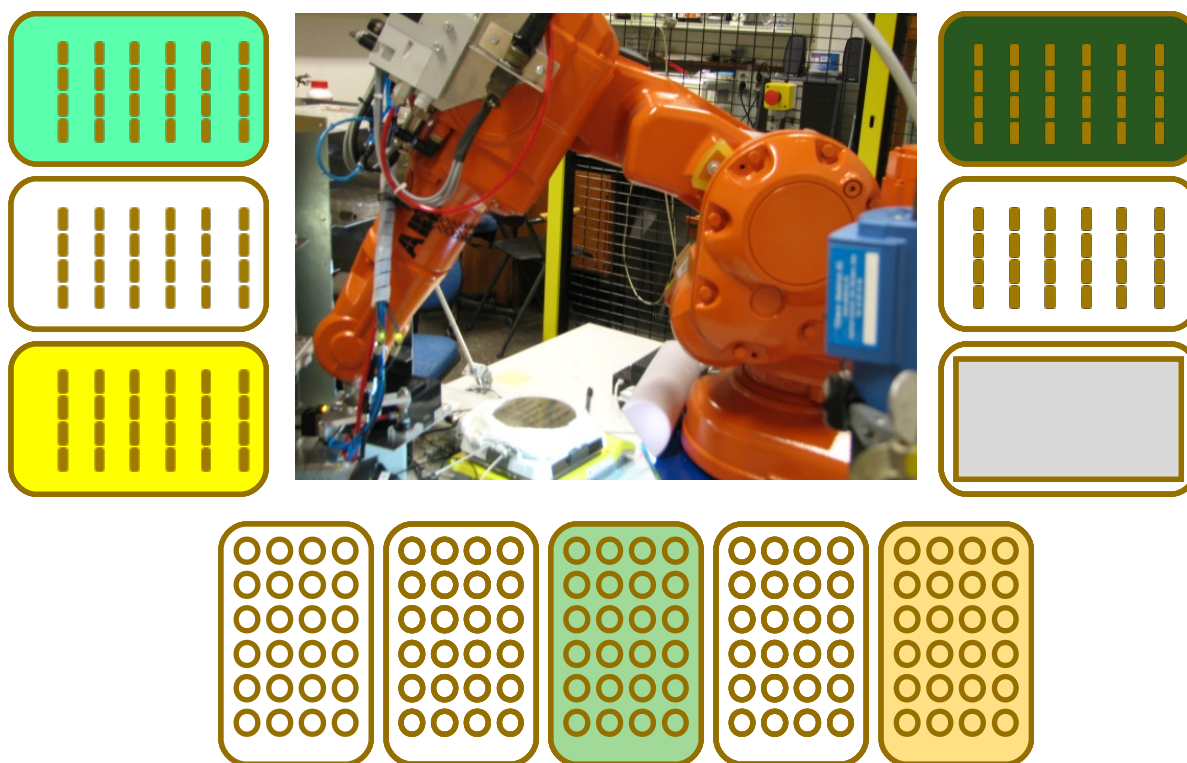
Figure 1. Robotic system used for SILAR. 24-well plates and 24-well format stations for treatment and characterizations shown schematically.
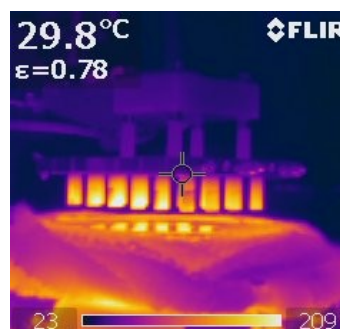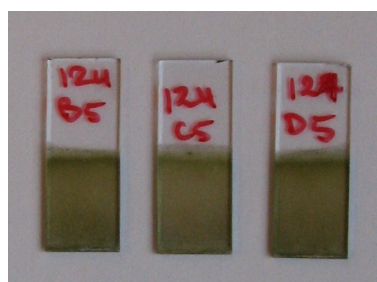
Figure 2. a) Highly conductive sulfide samples produced by modified SILAR. b) Sampleholder with 24 glasslides being withdrawn from heating station.

BITLLES: a quantum trajectory simulator for DC, AC, and noise with explicit Coulomb and exchange correlations among transport electrons

G. Albareda, A. Alarcón, F. L. Traversa, A. Benali, and X. Oriols

Dept. d'Enginyeria Electrònica, Universitat Autònoma de Barcelona, 08193 Bellaterra, Spain
guillem.albareda@uab.cat

With the aim of manufacturing smaller and faster devices, the electronic industry is today entering the nano and picosecond scales. In such particular scenarios, electron dynamics becomes affected by strongly correlated quantum dynamics, both in space and time. Thus, in order to provide an accurate enough description of the electron-electron correlations, quantum transport simulators must consider a reasonable approach to the many-particle problem. Anyway the big deal concerns the solution of the many-particle Schrödinger equation nowadays solvable only for very few degrees of freedom.

In this work we present a general purpose time-dependent 3D quantum electron transport simulator based on Bohmian trajectories that we call **BITLLES** [1-3]**.** It is based on a recently published algorithm [1] that, on the grounds of Bohmian Mechanics [2], solves the many-particle Schrödinger equation for hundreds of electrons in terms of multiple single-particle pseudo-Schrödinger equations without losing the explicit Coulomb and exchange correlations among electrons (at a level comparable to the Time Dependent Density Functional Theory) [1-3].

The adaptation of Bohmian mechanics to electron transport leads to a quantum Monte Carlo (MC) algorithm, where randomness appears because of the uncertainties in energies, initial positions of (Bohmian) trajectories, etc [2-4]. The ability of our simulator to deal with strongly correlated systems is shown here for a Resonant Tunneling Diode (RTD). Its characteristic I-V curve with Coulomb correlations introduced at different approximation levels is plotted in Fig. 1. As it can be observed, the effect of the correlations appear not only in the magnitude of the current but also in the position and shape of the resonant region [3,5]. Many-particle tunneling phenomena are reveled in the (super-Poissonian) behavior of the Fano factor shown in Figs. 2 and 3 [2]. In Fig. 4, we show the achievement of current continuity in the computation of the AC current for the same RTD [6]. The (time-dependent) current response to a voltage step is shown in Figs. 5 and 6.

References

[1] X. Oriols, Quantum trajectory approach to time dependent transport in mesoscopic systems with electron-electron interactions, *Phys. Rev. Let. 98, 066803* (2007).

[2] X. Oriols and J. Mompart, *Applied Bohmian Mechanics: From Nanoscale Systems to Cosmology*, Editorial Pan Stanford.

[3] G. Albareda, H. López, X. Cartoixà, J. Suné, and X. Oriols, Time-dependent boundary conditions with lead-sample Coulomb correlations:Application to classical and quantum nanoscale electron device simulators, *Phys. Rev. B, 82, 085301* (2010).

[4] G. Albareda, F. L. Traversa and X. Oriols, Full counting statistics within bohmian mechanics, *in preparation* (2011).

[5] G. Albareda, J. Suné, and X. Oriols, Many-particle hamiltonian for open systems with full coulomb interaction: Application to classical and quantum time-dependent simulations of nanoscale electron devices, *Phys. Rev. B. 79, 075315* (2009).

[6] A. Alarcón and X. Oriols, Computation of quantum electron transport with local current conservation using quantum trajectories, *J. Stat. Mec. Theor. Exp.. 2009, P01051* (2009).
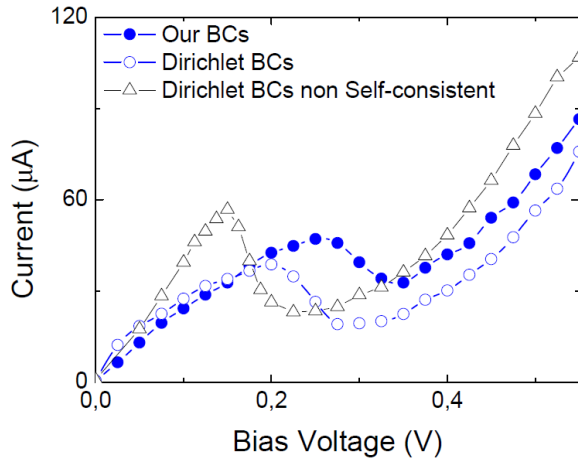
Fig. 1. DC Current for a RTD with Coulomb correlations introduced at different levels of accuracy.
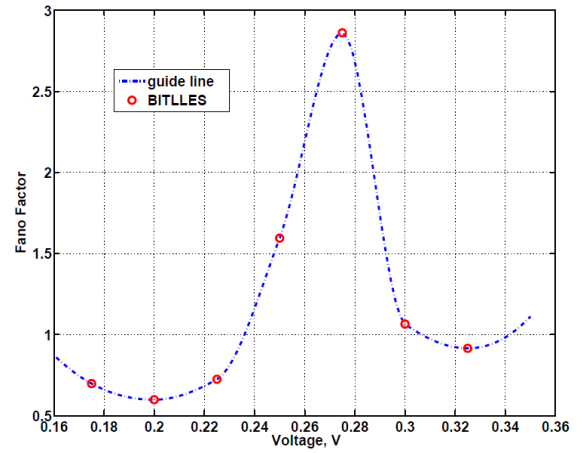
Fig. 2. Fano Factor computed for the RTD of Fig. 1 computed directly from the (time-dependent) current fluctuations.
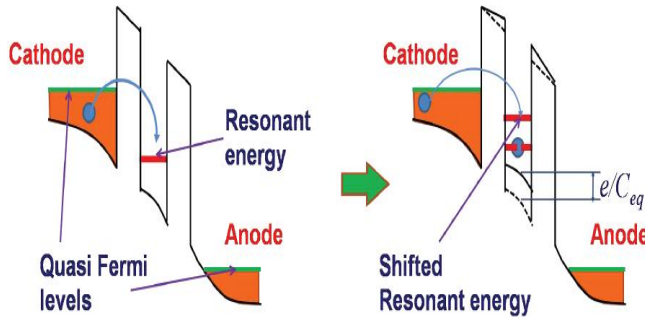
Fig. 3. RTD Band diagram. The potential deformation due to many-particle tunneling in the well is the basic mechanism of super-poissonian noise.
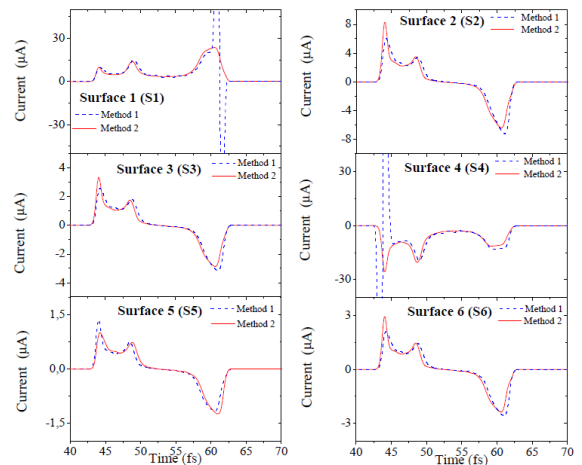
Fig. 4. Time-dependent total current computed on the six surfaces of an arbitrary parallelepiped. The sum of the current on the six surfaces is zero demonstrating the achievement of overall current continuity.
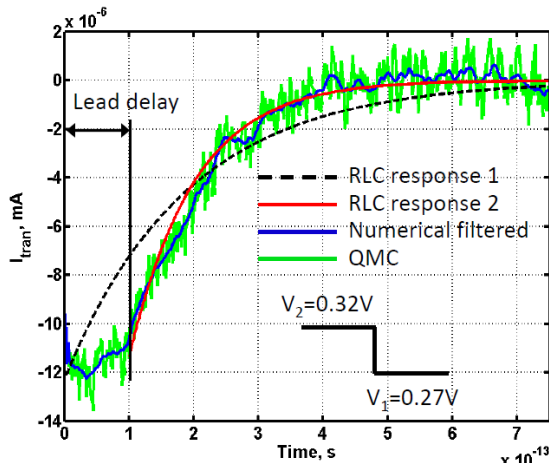
Fig. 5. Current response of the RTD to a step input voltage. Self-consistent boundary conditions including the leads are used.
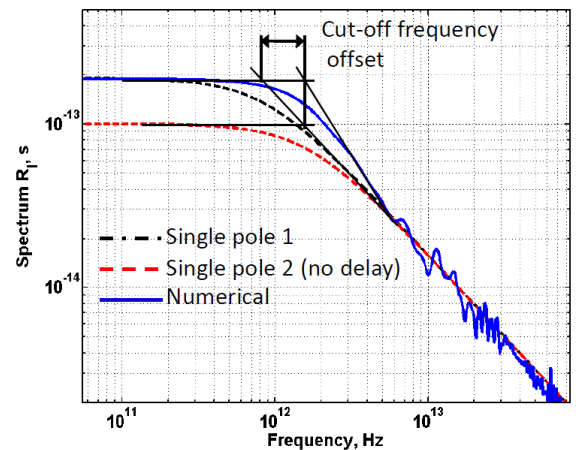
Fig. 6. Spectrum of the current response of Fig. 5. Cut off frequency and its offset due to the lead delay are pointed out.

10

Optical fiber biosensor based on Lossy Mode Resonances

Paula Aldaz, Beatriz Larrion, Joel Santos, Leyre Ruete, Miguel Hernaez, Carlos Ruiz-Zamarreño, Ignacio Del Villar, Ignacio R. Matias, Francisco J. Arregui

Department of Electrical and Electronic Engineering, Public University of Navarre, Campus Arrosadia S/N, 31006 Pamplona, Spain.
parregui@unavarra.es

The detection of the specific binding between antigen and antibody is perhaps the most used technique for diagnosis in medicine and biology. More specifically, the utilization of optical devices, which enable the detection of specific antigen-antibody binding by means of the monitorisation of their spectral response, is extensively exploited in immunoassays. In this field, Surface Plasmon Resonance (SPR) sensing has been established as a leading technique capable of detecting low analyte concentrations [1]. SPR optical fiber devices are based on semiconductor or metallic coatings, commonly gold and silver, which enable to monitor outer refractive index changes [2]. Hence, biological sensors can be fabricated by synthesizing a thin film on the sensor probe, the refractive index of which is sensitive to a target analyte. This variation of the refractive index leads to a modification of the sensor spectral response [1]. Among many other thin-film fabrication techniques, layer-by-layer (LbL) electrostatic self assembly, owing to its precise thickness control, has been proposed as a promising fabrication method suitable for the immobilization of immunoglobulin G (IgG) and anti-IgG [3].

Recently, optical fiber devices based on Lossy Mode Resonances (LMR) have been presented in the literature [4]. LMR are obtained by the coupling of light from an optical waveguide to a supporting layer of an optical absorbing material. LMR-based devices produce a response to external refractive index variations similar to that based on SPR. The main difference is that LMRs are produced by both TE and TM polarized light and more than one LMR can be generated without modifying the waveguide morphology [4]. Moreover, many different materials apart from metals and semiconductors can be used to produce LMR, such as Indium Tin Oxide [4], TiO2/PSS [5] films or even polymers [6]. Thanks to the characteristics and advantages mentioned above LMR can be exploited for the fabrication of biological sensing devices.

In this work, a LMR-based optical fiber biosensor that consists of a 200 µm optical fiber core coated with titanium oxide nanoparticles and poly (sodium 4-styrenesulfonate) (PSS) is studied [5]. The experimental setup and details of the sensor head are depicted in Figure 1. The cladding of a fragment of a multimode optical fiber (FT200EMT, Thorlabs Inc.) was chemically removed and then the core was sonicated and cleaned in both detergent and acetone and then rinsed in ultrapure water. After that, a 4 cm fragment was perpendicularly cleaved. In order to form a mirror on the end surface of the fiber, one of the end tips was coated with a reflective film (Ag) and protected with a plastic cap. Then, the LMR supporting overlay composed of $[TiO_2/PSS]$ bilayers was fabricated by using the LbL technique. In Figure 2 the spectral response as a function of the number of bilayers is represented, in this figures it can be easily observed the generated LMR. The $[TiO_2/PSS]_9$ structure was used as a precursor for the immunosensing layer and IgG molecules were adsorbed onto it by hydrophobic and electrostatic interactions [7]. In order to test the device, the sensor head was immersed in goat IgG solution (50µg/ml) for 90 min at room temperature and then in anti-goat IgG (50µg/ml). To reduce the non-specific binding, the sensor was rinsed with phosphate buffered saline (PBS) buffer solution. The results are plotted in Figure 3 showing the shift of the resonance between both cases. To our knowledge this is the first time that a biosensors based on LMR is presented in the literature.

References

[1] B. D. Gupta, R. K. Verma, Surface Plasmon Resonance-Based Fiber Optic Sensors: Principle, Journal of Sensors **979761** (2009) 12

[2] B. Larrión, M. Hernáez, F. J. Arregui, J. Goicoechea, J. Bravo, I. R. Matías, Photonic Crystal Fiber Temperature Sensor Based on Quantum Dot Nanocoatings, Journal of Sensors **932471** (2009) 6.

[3] F.Caruso, K. Niikura, D.N Furlong, Y.Okahata. Assembly of Alternating Polyelectrolyte and Protein Multilayer Films for Immunosensing. Langmuir, **13** *(*1997) 3427-3433

[4] I. Del Villar I, C. R. Zamarreño, M. Hernaez, I. R. Matias, F. J. Arregui, Generation of Lossy Mode Resonances With Absorbing Thin-Films, J. Lightwave Technol. **28** (2010) 3351-3357

[5] M. Hernaez, I. Del Villar, C. R. Zamarreño, F. J. Arregui, I.R. Matias. Optical fiber refractometers based on lossy mode resonances supported by TiO2 coatings. Applied Optics **49(20)** (2019) 3980-3985

[6] C.R. Zamarreño, M. Hernáez, I. Del Villar, I.R. Matías, F.J. Arregui, Optical fiber pH sensor based on lossy-mode resonances by means of thin polymeric coatings, Sens. Actuators B (2011) doi:10.1016/j.snb.2010.12.037

[7] Y. Zhang, H. Shibru, K. L. Cooper, A. Wang, Miniature fiber-optic multicavity Fabry-Perot interferometric biosensor, Opt. Lett. **30** (2005) 1021–1023.

Figures
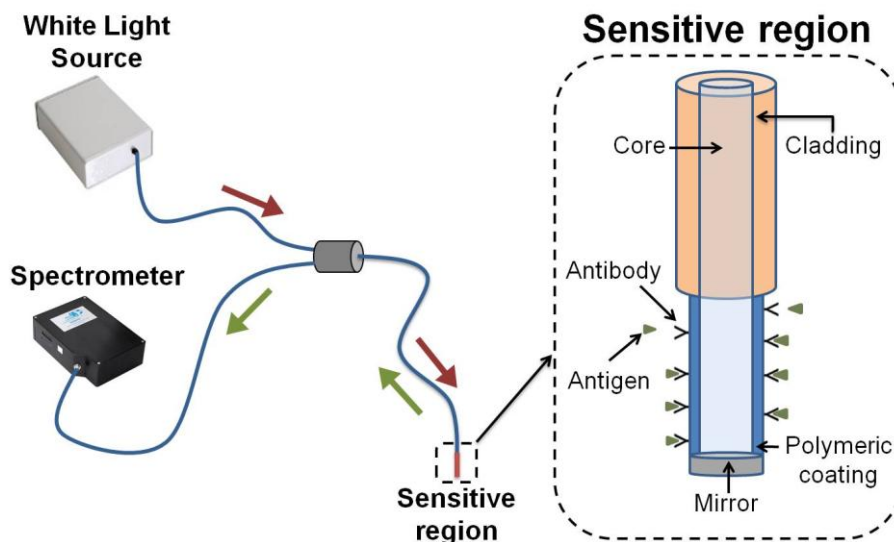
Figure 1. Experimental set-up
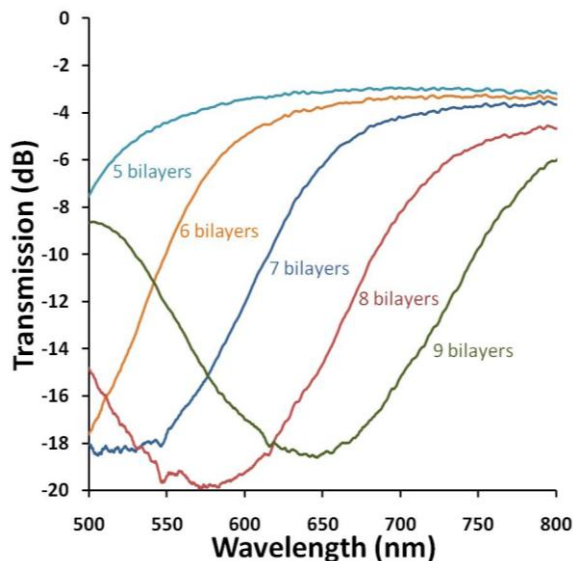
Figure 2. Spectral response of the LMR devices
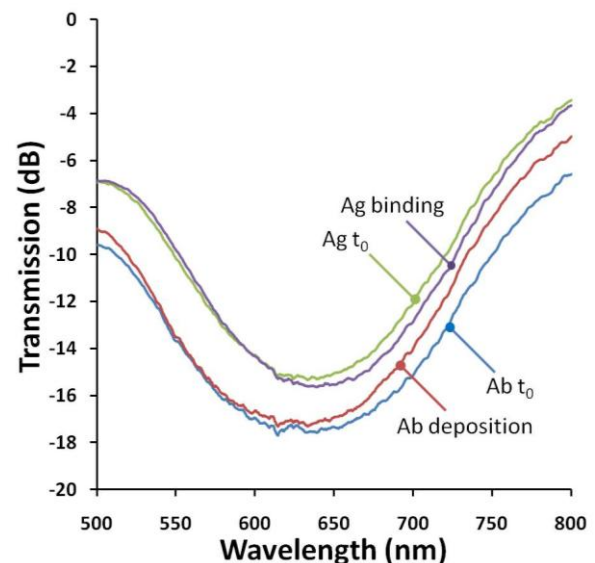
Figure 3. Spectral response before (Abt0) an after (Ab deposition) the deposition of antibodies and before (Agt0) and after (Ag binding) the attachment of antigens

Assembly and Properties of QDs Thin Films

T. Alejo, M. D. Merchán, and M. M. Velázquez

Departamento de Química Física, Universidad de Salamanca, Plaza de los Caidos
s/n,Salamanca 37008, Spain

teresaalejo@usal.es.

Quantum dots (QDs) are semiconductor that have recently attracted extensive interest due to their unique photoelectrochemical properties which can be placed between those of bulk semiconductor materials and those of isolated molecules or atoms. QDs are increasingly applied in bioanalytics and optoelectronics [1]. The photophysical and catalytic properties can be adjusted by changing the size of nanoparticles [2] or by changing the functional groups of molecules capping on the nanoparticles [3]. QDs at the air–water interface result in the formation of 2D Langmuir films. Advantages of this assembly technique include establishing limiting nanoparticle area, easy manipulation of the films, and interparticle distance control. To be utilized in solid devices, the QDs should be immobilized onto solid substrates. Langmuir-Blodgett (LB) films are prepared from Langmuir monolayers at the air-water interface therefore we need to know the properties of these monolayers.

In the present study, surface self assembled systems such us cationic gemini $C_{18}H_{37}$ $(CH_3)_2N^+$-$(CH_2)_2$-$N^+(CH_3)_2$ $C_{18}H_{37}$, (18-2-18) and the PMAO polymer. These systems are used as linking procedure to anchor the QDs onto substrates. The thermodynamic properties of these self assembled materials were investigated by surface pressure-area (Π-A) isotherms of the QDs monolayers. The morphology of films at the air-water interface was observed by Brewster Angle Microscopy (BAM). Langmuir-Blodgett (LB) films of QDs on solid substrates were characterized by Atomic Force Microscopy (AFM) and Transmission Electron Microscopy (TEM). The fluorescent properties of the LB film were also studied by Steady State Fluorescence Measurements.

The results obtained show that the morphology and properties of the films depend on the self assembled system employed to bind the QDs on the substrate. In addition the structures formed using different systems induce changes in the photophysical properties of the nanomateriales as is observed in the fluorescence emission of the LB nanomaterials.

References

[1] Somers, R.C.; Bawendi, M.G.; Nocera, D.G. Chem Soc Rev; **36,** (2007) 579.
[2] Hoffman, A. J.; Mills, G.; Yee, H.; Hoffman, M. R. J. Phys. Chem., **96,** (1992) 5546.
[3] Collier, C. P.; Saykally, R. J.; Shiang, J. J.; Henrichs, S. E, Science, **277,** (1997) 1978.
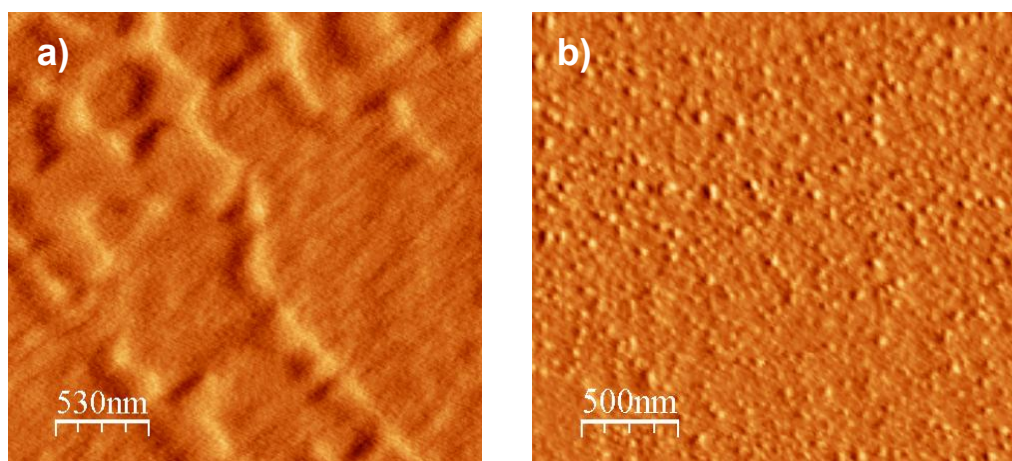
Figure 1 AFM images of mixtures QDs/18-2-18 (a), bilayer: QDs film onto 18-2-18 monolayer (b)

Influence of Cd-to-S and Cd-to-MAA molar ratios in the size and photoluminescence properties of CdS QDs synthesized in aqueous medium

María Jesús Almendral Parra, Ángel Alonso Mateos, Sara Sánchez Paradinas, Juan Francisco Boyero Benito, Julio J. Criado Talavera

University of Salamanca. Departamento of Química Analítica, Nutrición y Bromatología. Plaza de la Merced s/n, 37008-Salamanca, Spain

Among the many experimental variables affecting the stability, dispersion and photoluminescence properties of CdS nanoparticles synthesized in aqueous medium, the molar ratio of the species forming NPs is of great importance.

In order to choose the optimum molar ratios of the species involved, we carried out two types of experiments: on the one hand we studied the effect of the concentration of the dispersant agent (MAA, mercaptoacetic acid), keeping constant Cd-to-S ratio and, on the other hand we investigated the effect of the change of Cd-to-S ratio maintaining Cd-to-MAA ratio constant.

Experimental results obtained show that the environment in which the nanoparticles are formed is important in the processes of nucleation and growth and in the state and shape of the nanoparticle surface. The nucleation process does not merely involve the approach of Cd^{2+} y S^{2-} ions; Cd/MAA ions may also be involved and because of it the kinetics in the process of synthesis of nanoparticles may depend on the concentration of the dispersant agent. From a practical point of view the most fluorescent nanoparticles were obtained for a Cd-to-MAA ratio in the range 1:2. Moreover, our work demonstrates the need to have excess of cadmium in the synthesis of our NPs for the formation of a *nanoshell* of $Cd(OH)_2$, which directly affects the fluorescence intensity. The highest fluorescence intensity would be achieved for an optimum ratio between the thickness of the nanoshell and the mean diameter of the NPs. If the nanoshell is a very narrow deposit with regard to the mean diameter, only the transfer of electrons through it is improved, increasing slightly the quantum efficiency in the excitation-emission process. When the nanoshell is large regarding the nanoparticle diameter, the transfer of electrons through it in the excitation process increases but during the emission process the non-radiant energy fraction is increased. The intermediate situation, with an optimum ratio between nanoshell width and mean particle diameter affords the highest quantum efficiency.

Real time and real space observation of fluids on and in a bionanotube

José María Alonso[1], Thierry Ondarcuhu[2], Andrey Chuvilin[1], Alexander Michael Bittner[1,3]

[1]CIC-nanGUNE Consolider, Tolosa Hiribidea 76, 20018 Donostia-San Sebastián, Spain
[2]CEMES-CNRS, 29 rue Jeanne Marvig, 31055 Toulouse Cedex 4, France
[3]Ikerbasque, 48011 Bilbao, Spain
a.bittner@nanogune.eu

While microfluidic devices enjoy widespread popularity, the properties of fluids and flow processes at the nanoscale, especially for fluid confinement below 30 nm, are largely unknown. The main experimental hurdle is the design of channels that are chemically and structurally well defined down to (nearly) atomic dimensions.

Tobacco mosaic virus (TMV) is a tube-shaped nanoobject with 4 nm inner diameter, which is indeed structurally and chemically defined [1]. The diffusion of metal ions into TMV has already been used to construct one-dimensional nanostructures [2]. We integrated single TMVs in micro- and nanofluidic devices, with aid of nanofabrication techniques. E.g., electron beam lithography (eBL) was employed to construct hydrophobic barriers to prevent fluid movement on TMV's outer tube surface (Figure 1). Due to TMV's surprising chemical and thermal stability, it is compatible with positive (PMMA) and negative (mrEBL6000.1) eBL resists, both spin-coated from anisole solution (Figure 2).

We conducted dynamic fluidic experiments by NADIS [3] and ESEM [4]. NAnoDISpensing allows placing sub-microscale droplets of non-evaporating liquids from an AFM cantilever. With this technique we deposited droplets of various sizes at both ends of a single TMV tube, and imaged virus and droplets with AFM. The flow speed through the virus was much smaller than expected from related micro- and macroscale systems. On the other hand, environmental SEM (ESEM) allowed us following the flow of liquids with improved time resolution (ca. 1 frame/10s), without much compromise in spatial resolution (tens of nm). We found, however, that beam damage limits the use of ESEM especially for biomolecular systems.

References

[1] A.M. Bittner, Naturwissenschaften, **2** (2005) 51
[2] M. Knez, A.M. Bittner, F. Boes, C. Wege, H. Jeske, E. Maiß, K. Kern, Nano Letters **8** (2003) 1079
[3] A. Fang, E. Dujardin, T. Ondarçuhu, Nano Letters **10** (2006) 2368
[4] A. M. Donald, Nature Materials (2003), 511

Figure 1

Virus nanotube immobilization through negative resist mrEBL6000.1
(fabrication)

Figure 2

TMV particle covered by a rectangular block of polymer resist (mrEBL6000.1). Image size: 3.7x3.4 µm
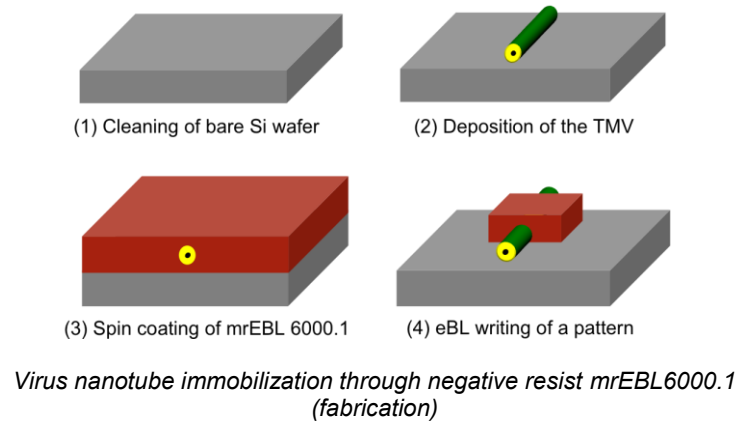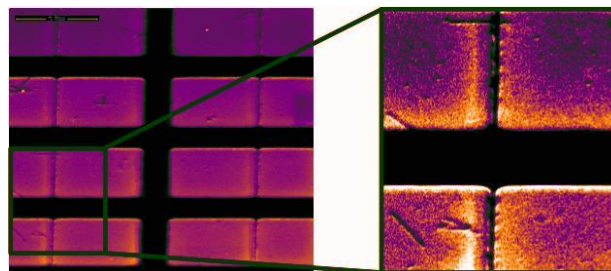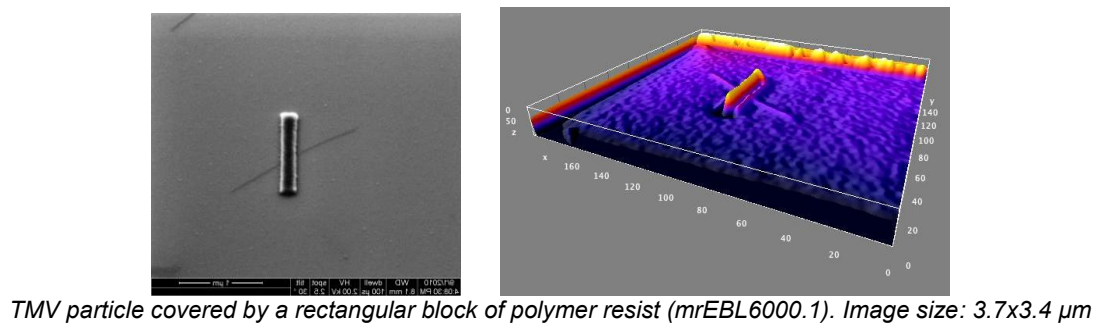
TMV particles inside a polymer resist grid (PMMA). The particle at the bottom can be separately addressed by two liquid containers (left and right). Grid size: 4.1x2 µm

Study of the Layer-by-Layer assembly of PDADMAC/PAA multilayer films as function of pH

T.Alonso, B. Szczupak, J.J.Iturri, S.E.Moya

Laboratory of Biosurfaces, CIC biomaGUNE, Paseo Miramón 182 Edif. Empr. C, 20009, San Sebastián , Spain

talonso@cicbiomagune.es

Polyelectrolyte multilayers (PEMs) fabricated by means of the Layer-by-Layer (LBL) technique are a good example of nanostructured polymer films that can be easily applied for surface modification and device fabrication [1].

PEMs are fabricated by the alternative assembly of polycations and polyanions on charged surfaces that is mainly driven by electrostatic interactions [2]. The stepwise assembly protocol allows obtaining structures with controllable composition at the nanoscale level in the growing direction, which can include multiple functionalities like proteins, nanoparticles, growth factors, lipids, etc. [3].

In this work we studied the assembly of poly(diallyl dimethyl ammonium chloride) (PDADMAC) and poly(acrylic acid) (PAA), which are a strong and a week polyelectrolyte respectively. The charge of PAA depends on the pH and increases with increasing pH [4] [5]. On the other hand, the charge of PDADMAC remains constant and is independent of the pH [6]. Since the main interaction in the build up of polyelectrolyte one would expect that the charging of PAA at high pH would favour the multilayer build up.

The assembly of PDADMAC and PAA in different pH ranging from 3 to 13 was followed in real time by means of the Quartz Microbalance with Dissipation (QCM-D) combined with ellipsometry. It was observed that at low pH, around 3, the assembly follows a supralinear trend and results in film thickness of 480nm. Surprisingly, with increasing the pH and the charge of PAA, the amount of assembled polymer diminishes what results in the film thickness of only 20nm.
In order to understand the interaction between PAA and PDADMAC and their behaviour at different pH, We applied Confocal Raman Microscopy (CRM) and Isothermal Titration Calorimetry (ITC) techniques. CRM allowed us to determine the stoichiometry between the polyelectrolytes and the degree of charge of PAA as a function of pH. By means of ITC it was possible to measure the heat of complexation of PDADMAC/PAA at different pH and establish the thermodynamic basis for the polycation-polyanion interaction.

References

[1] Gero Decher, SCIENCE, **277** ,(1997),1232-1236.

[2] Claudine Porcel, Philippe Lavalle, Vincent Ball, Gero Deher, Berenard Senger, Jean-Claude Voegel and Pierre Schaaf , Langmuir, **22** ,(2006) ,4376-4383.

[3] Gleb B. Sukhorukov , Edwin Donath , Heinz Lichtenfeld , Eberhard Knippel ,
Monika Knippel , Axel Budde , Helmuth Mohwald , Colloids and Surfaces
Physicochemical and Engineering Aspects ,**137,** (1998), 253-266

[4] Philippe Lavalle, Jean-Claude Voegel, Dominique Vautier, Bernard Senger, Pierre Schaaf and Vincent Ball , Advanced Materials,**20,** (2011), 1-31

[5] Steven W. Cranford , Christine Ortiz and Markus J. Buehler, Soft Matter, **6** (2010) 4175-4188

[6] Eduardo Guzman, Hernan Ritacco, Jose E. F. Rubio, Ramon G. Rubio* and Francisco Ortega, Soft Matter, **5**, (2009), 2130–2142

Duty Cycle Effect on Barrier Breakdown in MgO Magnetic Tunnel Junctions

S.Amara[a], R.C. Sousa[a], J. Alvarez-Hérault[b], L.Lombard[b], H.Bea[a], I.L. Prejbeanu[b], K. Mackay[b] and B. Dieny[a]

[a] *Spintec (UMR 8191 CEA/CNRS/UJF), Grenoble, France.*
[b] *Crocus Technology, Grenoble, France.*
selma.amara@cea.fr

Spin-transfer torque magnetoresistive random access memory (STT-MRAM) is a promising memory technology because of its non-volatility, high speed operation, unlimited endurance, high density and compatibility with the standard CMOS process [1]. As the magnetic tunnel junction (MTJ) size shrinks, the MTJ resistance increases compared with the resistance of the selection transistor in a one transistor-one MTJ (1T-1MTJ) design. Hence, a thinner tunnel barrier that does not compromise on reliability is required. Oxide barrier breakdown is one of the key integration and reliability issues for advanced semiconductor memory technology. Notwithstanding its excellent potential, the breakdown mechanism of ultrathin MgO-MTJ has not been completely understood although a thorough understanding is essential for the success of STT-MRAM. In this work, we studied the lifetime of junctions using a time dependent dielectric breakdown (TDDB) [2] technique. Studies of time-dependent dielectric breakdown in magnetic tunnel junctions (MTJ) are usually carried out by applying a DC voltage while recording the time to breakdown [3]. This work reports on the breakdown behaviour of MgO tunnel barriers when submitted to consecutive voltage pulses with different time delays between consecutive pulses.

The studied junctions structure was buffer/ PtMn 20/ CoFe 2/ Ru 0.8/ CoFeB 2/ MgO 1.1/ CoFe 2/ NiFe 3/ cap (thickness in nm) with a plasma oxidised MgO layer. The measured devices were patterned into 200nm circular pillars showing 130% TMR and an R$\times$A value of 30Ω.µm².

The experimental procedure consisted in applying successive pulses of 30ns with constant amplitude (~1.5V) at zero magnetic field until barrier breakdown occurs. The time interval, i.e. the delay, between consecutive pulses was a variable parameter. Experiments were repeated for time delays between pulses from 1ns up to 10µs. The pulse amplitude was 1.48V, corresponding to an electric field of 14 MV/cm. The data are well described by a Weibull distribution with scale parameter η, representing the total cumulated pulses when 63.2% of MTJ have failed.

The value of η is plotted in Fig. 1 as a function of the delay between consecutive pulses in Fig.1. Each point represents the average value for 20-40 junctions. This experiment shows that η has three different regimes.

For short delays <30ns between pulses, there is an increase in barrier lifetime, as the delay between pulses is increasing allowing for some cooling between pulses, which reduces the mean temperature on the cell. For pulse delays between 50ns to approximately 100ns, there is a significant increase in barrier lifetime as the dots completely cool to their pre-pulse temperature. However, this increased lifetime value is not maintained for longer delays. This behavior was observed for both pulse polarities of different amplitudes but it disappears with alternative polarity pulses as represented in the figure. The peak also depends on the pulse amplitude. For 1.48V the maximum lifetime is attained for 100ns delay time between pulses. The difference of behavior between unipolar pulses and alternative pulses excludes the possibility for the effect to be only temperature related. To interpret this result, we assume a model that combines thermal and electric charge-discharge phenomena.

For pulse delays shorter than 30ns, there is not enough time for the cell to return to its initial temperature. The cell temperature undergoes steady oscillations around an average value significantly higher than the ambient temperature. This increased average temperature renders the breakdown event more likely.

The second regime, for pulse delays between 50 and 100ns, corresponds to a significant increase of the barrier lifetime. This is followed by a decrease of barrier lifetime as the delay is further increased. We tentatively associate this intermediate behavior with an electric charge-discharge phenomenon, occurring as charges become trapped in barrier defects. The characteristic time for trapped charge release seems to be around 100ns. Therefore, if the delay between pulses is of the order of 100ns, a steady balance takes place between the amount of additional charges trapped in the barrier at each pulse and the amount of trapped charges released to the electrodes between two successive pulses. The barrier therefore reaches a sort of charged steady state during which the oxide barrier is not too much stressed.

The last regime for delays longer than 100ns can be explained as a second breakdown behavior of structural origin. The lattice dynamics of the magnesium oxide barrier is changed as a result of the electrostatic interactions between charges on traps. Because the charges have enough time to be released from the traps between successive pulses, a strong variable internal stress of electrostatic

origin is exerted within the barrier. This variable stress facilitates the diffusion of metallic species from the metallic electrodes within the barrier especially through dislocations. According to our assumption, the electrostatic interactions between trapped charges can cause lattice vibrations of amplitude approximately 0.2A.

We have studied the duty cycle effect on barrier breakdown in MgO Magnetic Tunnel Junctions.

Three regimes were observed as a function of delay between voltage pulses. The results were interpreted in terms of temperature variation of the tunnel barrier and charge-discharge phenomenon impacting the barrier structure.. Further investigations of these phenomena are in progress on other samples and with other pulses amplitudes in order to further improve the resistance of these ultrathin MgO barriers to electrical breakdown.

References :

[1] M. Hosomi et al., "A novel nonvolatile memory with spin torque transfer magnetization switching: Spin-RAM," *IEDM Tech. Dig.*, pp. 473-476, 2006.

[2] J. Akerman et al., *Reliability of 4Mbit MRAM,* IEEE Int. Symp.Reliability Phyics. Pp.163-167.

[3] J. Åckerman, P. Brown, M. DeHerrera, M. Durlam, E. Fuchs, D. Gajewski, M. Griswold, J. Janesky, J. J. Nahas, and S. Tehrani, IEEE Transactions on Device and Materials Reliability, Vol.4, No.3, September 2004
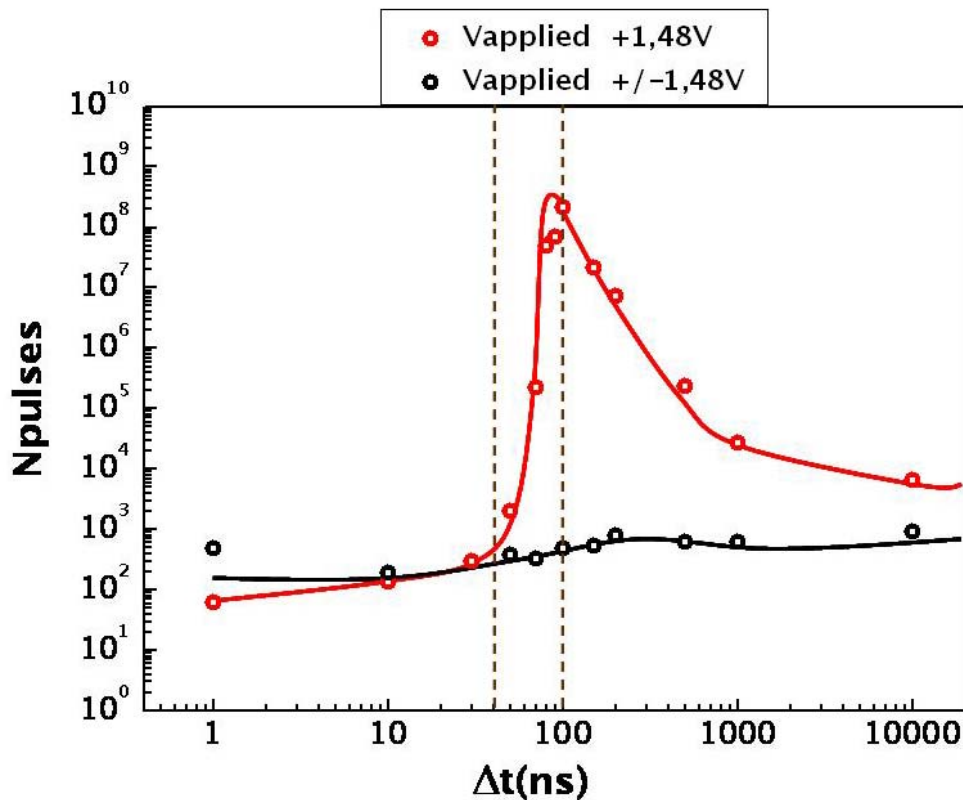
Fig.1: Time dependent barrier breakdown failure in 1.1nm MgO barriers. The stress voltage was applied in pulses of varying time gap between pulses maintaining constant amplitude.

Wetting behavior of sintered nanocrystalline TiO$_2$ by Armco Fe and 22CrNiMoV5-3 steel grade using sessile drop wettability technique

Zuriñe Amondarain, Leiv Kolbeinsen, Jose Luis Arana

Tecnalia Research and Innovation, P. Tecnologico de Bizkaia, Edif.700, 48160, Derio (Bizkaia), Spain

zurine.amondarain@tecnalia.com

The study of the wetting behavior at elevated temperatures constitutes one of the most important scientific aspects of high temperature liquid phase materials processing stimulated by the needs of modern metallurgy and foundry industry. [1]

The wettability of sintered TiO$_2$ nanocrystalline powder by liquid Armco Fe and by 22CrNiMoV5-3 steel grade was studied using sessile drop wettability technique. The liquid deposited on the solid surface under gravity, has tendency to spread until the cohesion (internal forces) of the liquid, the gravity forces and the capillary (surface tension) forces are in balance, and an equilibrium state is reached. [2] The relationship between the contact angle and the respective interfacial tensions acting at the triple point is given in the Young equation [3] which is as follows: $(\gamma_{SG} - \gamma_{LS}) = \gamma_{LG} \cdot \cos\theta$ where θ is the contact angle and $\gamma_{LG}, \gamma_{LS}, \gamma_{SG}$ are the liquid/gas, liquid/solid and solid/gas interfacial tensions respectively.

The nanometric powder was pressed and sintered under different pressures, heating rates and holding times. The later grinding and polishing surface treatments were characterized by infinite focus microscope. The wetting experiments were carried out under pure argon atmosphere in the wettability furnace (Figure 1). A small piece of Armco Fe and steel grade was melted on sintered nano oxides, heating up to 1600ºC with a holding time of 10 minutes for each experiment.

The contact angles were measured (see drop morphological evolution in Figure 2) and chemical analyses were conducted on tested samples to characterize the wetting reactions. The chemical compositions were studied for Electron Probe X-ray microanalysis (EPMA) supported by wavelength dispersive spectroscopy (WDS) It was found that sintered nano TiO$_2$ not only suffered considerable wetting by Armco Fe (Figure 3) and 22CrNiMoV5-3 steel in both cases, but also reacted with the substrate to form ilmenite and pseudobrookite.

From this experiment it is concluded that sintered nano TiO$_2$ shows high and reactive wetting for both low alloyed iron matrix and steel grade matrix. In both cases, a reaction layer formed by Fe-Ti-O solid solutions with various stoichiometries was observed.

The preliminary results of this investigation may help to determine the suitability of the nanoparticle to be added in a liquid iron based matrix in order to influence the microstructure evolution improving mechanical properties by a fine distribution in the metallic alloy.

References

[1] N. Sobczak, M. Singh, and R. Asthana: *Curr Opin Solid State Mater Sci*, 9 (2005), 241.

[2] K.J. Kubiak, M.C.T. Wilson, T.G. Mathia and Ph. Carval: *Wear* Article in Press.

[3] T. Young: *Phil.Trans. R. Soc.Lond.*, 95 (1805), 65.

Figures

Figure 1. Schematic diagram of the experimental set up

Figure 2. Morphologycal evolution of the Armco Iron (top images) and 22-CrNiMoV-5-3 (bottom images) on the TiO$_2$ substrate.

	Atomic ratio			
Element	Point 1	Point 2	Point 3	Point 4
Fe	914.281	188.094	88.211	
Ti		200.468	279.426	328.375
O		576.443	602.453	638.269

Figure 3. (a) The cross section backscattered micrograph of the solidified Armco Iron drop on sintered nano TiO$_2$ substrate and (b) the element distribution of the reaction layer obtained by EPMA. Left table: Atomic ratio of elements in the drop phase (point 1), reaction layer (points 2 and 3) and TiO$_2$ substrate (point 4) in the vicinity of the reaction layer for Armco Fe-sintered nano TiO$_2$ wettability experiment.

Figure caption

Figure 1. Schematic diagram of the experimental set up

Figure 2. Morphologycal evolution of the Armco Iron (top images) and 22-CrNiMoV-5-3 (bottom images) on the TiO$_2$ substrate.

Figure 3. (a) The cross section backscattered micrograph of the solidified Armco Iron drop on sintered nano TiO$_2$ substrate and (b) the element distribution of the reaction layer obtained by EPMA. Left table: Atomic ratio of elements in the drop phase (point 1), reaction layer (points 2 and 3) and TiO$_2$ substrate (point 4) in the vicinity of the reaction layer for Armco Fe-sintered nano TiO$_2$ wettability experiment.

24

Nanocomposites based on carbon nanotubes oxidized by solar energy

M Blanco, M López, E Aranzabe, A Marcaide

Fundación Tekniker, Av Otaola 20, 20600 Eibar Gipuzkoa, Spain
mblanco@tekniker.es

Carbon nanotubes (CNT) have attracted considerable attention in some potential applications due to their remarkable properties, such as mechanical and electrical properties. Therefore, they have been expected to be excellent fillers for polymer composites. In order to obtain nanocomposites with enhanced properties, it is necessary to oxidize or functionalize their surface in order to improve CNT-matrix interaction and CNT dispersion in the matrix. Chemical treatments, above all acid treatments, are being widely employed to oxidize CNT [1]. However, the high consume of solvents and energy required for these oxidation processes and the fact that morphology of carbon nanotubes can be highly damaged during this process point out the necessity of more environmentally friendly processes.

In the present work, the oxidation of CNT by the photoFenton process assisted by solar energy is proved that overcomes main problems associated to conventional processes. The Fenton process consists on the generation of hydroxyl radicals, which have a high oxidation potential, using H_2O_2 as source of OH• radicals and Fe^{2+} salt as catalyser in an aqueous medium (pH=2.7) [2]. When the process rate is enhanced by UV radiation, it is call photoFenton process. The process conditions such as reactive concentration, reactant ratio and time of reaction have been optimized using a parabolic collector (Figure 1) to concentrate solar radiation. The process promotes the generation of carboxylic (-COOH), carbonylic (C=O) and/or hydroxylic (-OH) groups onto CNT surfaces without affecting their structural integrity as was shown by Fourier transform infrared (FTIR) spectroscopy and thermogravimetric analysis (TGA) in Figure 2 and by scanning electron microscopy (SEM). The photoFenton process achieves an increase in the oxidation degree in comparison with a usual oxidation method, the oxidation in HNO_3 concentrated acid.

In a second step, carbon nanotubes (pristine and oxidized by the photoFenton process assisted by solar energy and by HNO_3) were incorporated into a thermoplastic matrix, polyamide 6 (PA 6), by a twin screw corrotating microextruder. SEM micrographs show that a good CNT dispersion into the matrix was obtained with the applied processing conditions for the three types of CNT, as it is shown in Figure 3. The effect of CNT content and CNT oxidation treatment in thermal and mechanical behavior of nanocomposites were analyzed by dynamic mechanical analyzer (DMA), differential scanning calorimetry (DSC) and TGA. The obtained results show a similar performance of nanocomposites based on CNT oxidized by both methods.

In summary, CNT oxidation by the photoFenton process assisted by solar energy is proved a suitable alternative environmentally friendlier and less costly to conventional chemical oxidation processes. Composites obtained by the incorporation of CNT oxidized with the photoFenton process into polyamide 6 show a similar behaviour than the obtained by the incorporation of CNT oxidized with common chemical methods.

References

[1] V. Datsyuk, M. Kalyva, K. Papagelis, J. Parthenios, D. Tasis, A. Siokou, I. Kallitsis, C. Galiotis, Carbon **46** (2008) 833–840
[2] L. Zhang, J. Li, Z. Chen, Y. Tang, Y. Yu, Applied Catalysis A: General **299** (2006) 292–297

Figures
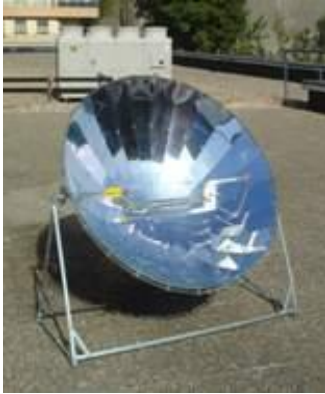
Figure 1. Parabolic collector
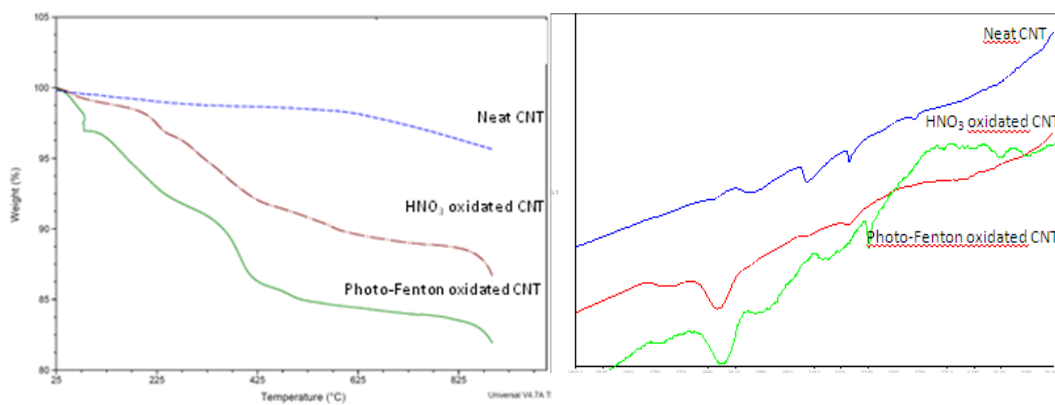
Figure 2. TGA thermograms and FTIR spectra of MWCNT pristine and oxidized with HNO₃ and photoFenton treatment
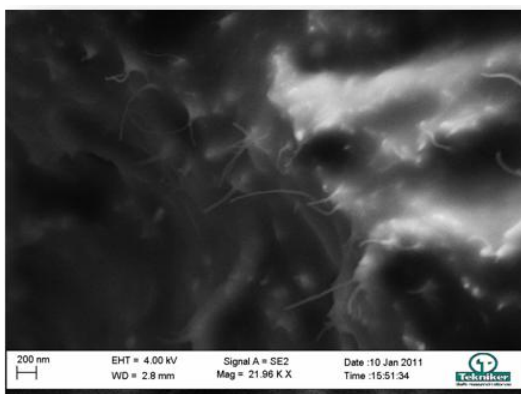
Figure 3. SEM micrograph of photoFenton oxidized CNT in PA 6 matrix.

The Diels-Alder cycloaddition reaction of 1,3-butadiene to MWCNTs

Rui F. Araújo[a], M. F. Proença[a], C. J. R. Silva[a], M. C. Paiva[b]

[a] Centre of Chemistry, Department of Chemistry, University of Minho, Gualtar, 4710-057 Braga, Portugal.
[b] Institute for Polymers and Composites, Department of Polymer Engineering, University of Minho, 4800-058 Guimarães, Portugal
rui.araujo@quimica.uminho.pt

The non-polar nature of carbon nanotubes, favouring their aggregation as bundles, poses a serious limitation to a wide range of potential applications of this strong and flexible material [1]. Grafting of chemical functions on the surface of multiwall carbon nanotubes (MWCNTs) has been widely used to add new properties and improve their dispersion in solvents and/or materials. A number of chemical reactions were reported for the functionalization of the outer layer of MWCNTs, tailoring their properties and widening their applications [2]. Previous studies of Diels-Alder cycloaddition reaction of 1,3-butadiene generated *in situ* from sulfolene with carbon nanofibers showed that can be a good method to obtain high degree of functionalization without significative structural damages.[3].

In this study the funtionalization of MWCNTs with 1,3-butadiene generated *in situ* from solfolene was investigated. The reaction was studded at two different temperatures (100ºC and 150ºC), mass ratios (CNTs:Sulfolene of 1:1 and 1:2) and different time reaction (2, 4 and 7 days). Thermogravimetric analysis (TGA) showed high degree of functionalization in a range of 10 % to 23 % in weight loss at 800 ºC. The acid properties of funtionalized materials were recorded by potentiometric titration that suggests some oxidation during the funtionalization process (Figure 1). In Figure 2 are summarized the results of weight loss obtained by TGA and respective acid properties of functionalized carbon nanotubes. The funtionalization was also evaluated by X-ray photoelectron spectroscopy (XPS) and transmission electron microscopy (TEM).

References

[1] Andreas Hirsch, Angew. Chem. Int. Ed., **41** (2002) No. 11, 1853.
[2] D. Tasis et al, Chem. Rev., **106** (2006) 1105.
[3] M. Fernanda et al, J. Nanosci. Nanotechnol., **vol. 9** (2009), 1.

Figure 1. Possible mechanism of functionalization of MWCNTs by 1,2-butadiene.
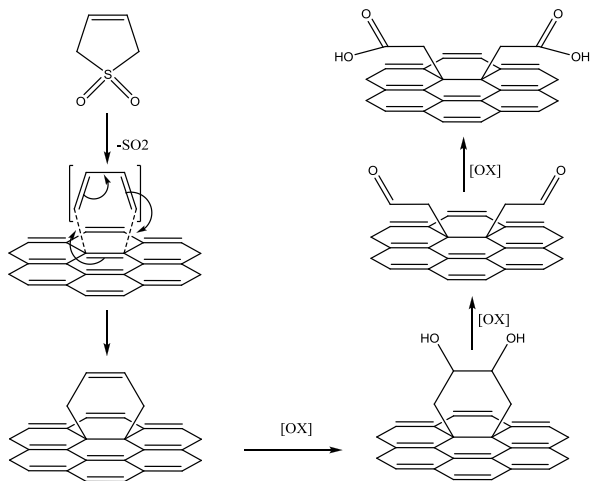
Figure 2. Degree of functinalization (%) (black line) and acidity (mmol) (blue line) of MWCNTs obtained at different conditions of functionalization.
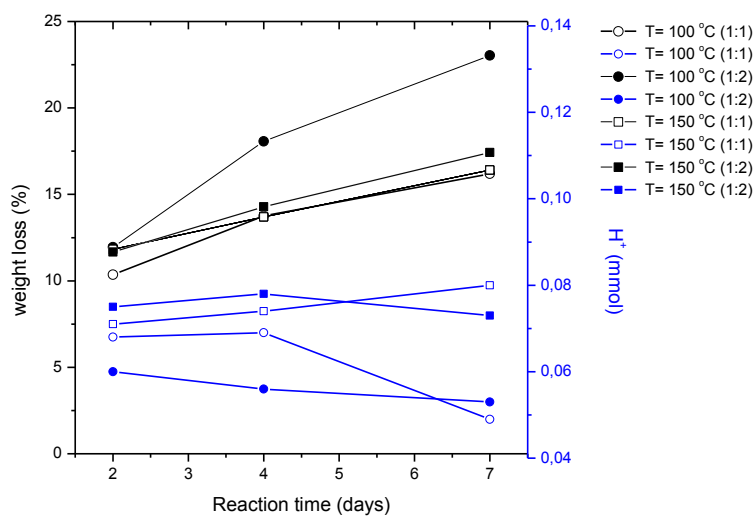
Anisotropy study of Dye Intercalation into 1D Sepiolite clay fibers by Fluorescence Microscopy

Teresa Arbeloa, Virginia Martínez-Martínez, Cecilia Corcostegui, Leire Gartzia, Jorge Bañuelos and Iñigo López Arbeloa.

Departamento de Química Física, Universidad del País Vasco UPV-EHU, Apdo. 644, 48080-Bilbao, Spain
virginia.martinez@ehu.es

The encapsulation of dyes into nanostructured ordered systems is a good tactic to provide new functional materials. On the other hand, a great variety of solid matrices with different 1-, 2- or 3-dimension arrays are suitable to induce an anisotropy orientation on the guest molecules.

In this sense, nanotubes and nanostructured tubular systems with elongated pores can act as a powerful ordering framework in one dimension for the guest species. Sepiolite, Sep, is a very special magnesium silicate clay, with rod-like particles with interior rectangular tunnel-likes pores of 3.6Å x 10.6 Å and external channels along a-axis which offers a large specific area and porosity and is a good hosts to get 1D highly order in suitable dye/clay hybrid functional materials.

In this work, four fluorescent dyes with different molecular dimensions, Rhodamine 6G (R6G), Pyronine Y (PY), Styryl 698 (LDS 698) and Styryl 722 (LDS 722), are encapsulated into Sepiolite clay at low and high loadings.

An study of single dye/Sep fibers was performed by Confocal Fluorescence Microscopy. The combination of Fluorescence Lifetime Imaging (FLIM), polarized fluorescence intensity experiments and spectral resolution shows a straightforward method to study the molecular distribution inside the tunnels and/or at the external channels, the dye orientation (evaluated by the fluorescence dichroic ratio, D) and the formation of different dye species (monomer and aggregates). The ability of the dyes to penetrate into the Sep tunnels is R6G < LDS 698 < PY < LDS 722, analyzed by thermal analysis. As a result the alignment along the main axis of Sep increase in the same order reaching fluorescence dichroic ratios of around 1.5, 6, 8 and 10 respectively for each dye.

In summary, to favor internal over external adsorption in the Sep and therefore the alignment along the fiber direction, dyes with small thickness and long main molecular axis are the best candidates.

Dye/Sep particle by SEM

Dye/Sep by Fluorescence Microscopy Polarized Emission
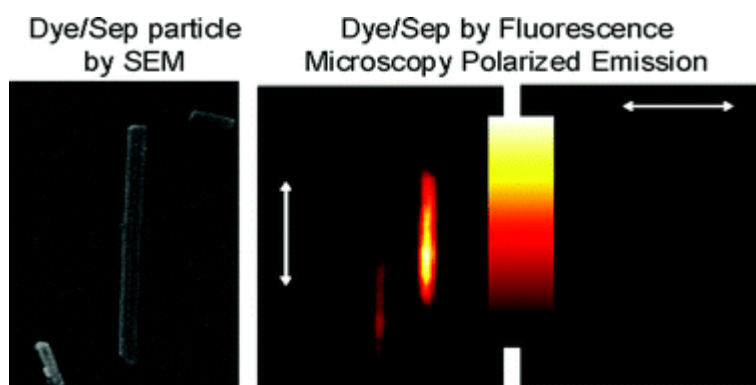
References

[1] Virginia Martínez Martínez, Cecilia Corcósteguia, Jorge Bañuelos Prietoa, Leire Gartzia, Sandra Salleres and Iñigo López Arbeloa, . **J. Mater. Chem.,** 2011, 21, 269-276.

Tunable g-factors in SiGe quantum dots

N. Ares [a], G. Katsaros [a], P. Spathis [a], M. Stoffel [b], F. Fournel [c], M. Mongillo [a], V. Bouchiat [d], F. Lefloch [a], A. Rastelli [b], O. G. Schmidt [b], and S. De Franceschi [a]

a CEA, INAC/SPSMS/LaTEQS, F38054 Grenoble, France
b IFW-Dresden, Institute for Integrative Nanosciences, Dresden, Germany
c CEA, LETI, MINATEC, F38054 Grenoble, France
d Institut Néel, CNRS and Université Joseph Fourier, BP 166, 38042 Grenoble cedex 9, France

natalia.ares1@gmail.com

So far, most of the experimental work on semiconductor spin qubits has focused on GaAs-based single and double quantum dots (QDs) [1-5]. However, the quantum coherence of electron spins in GaAs QDs is lost on relatively short time scales due to hyperfine interaction with the nuclear spins.

Here we investigate an alternative material system: SiGe self-assembled nanocrystals. Si and Ge are attractive materials because in these materials electronic spins can have a long coherence time due to the absence of hyperfine interaction (in isotopically purified crystals) [6]. One further advantage of SiGe nanocrystals is their compatibility with CMOS technology [7].

We have recently reported the first realisation of single-hole transistors based on such individual SiGe nanocrystals [8]. A variety of low-temperature transport regimes depending on the strength of the tunnel coupling to the leads were observed. Transport spectroscopy reveals largely anisotropic hole g-factors. By changing the number of holes localized within the SiGe QDs a clear modulation of the g-factor is observed indicating that the g-factors are linked to the corresponding orbital wavefunctions.

Furthermore, in order to be able to study the effect of an external electric field on the value of the g-factor for the same orbital wave function, i.e. for the same number of holes, we have fabricated dual gate devices with both bottom and top gates. Our measurements demonstrate that the g-factor can be varied for at least a 300% when changing the value of the perpendicular electric field, as it is shown in Fig.1 [9].

The observed tunable g-factors make SiGe self-assembled QDs an interesting material system for performing all-electrical spin coherent manipulations.

Figures

V_bg (mV)
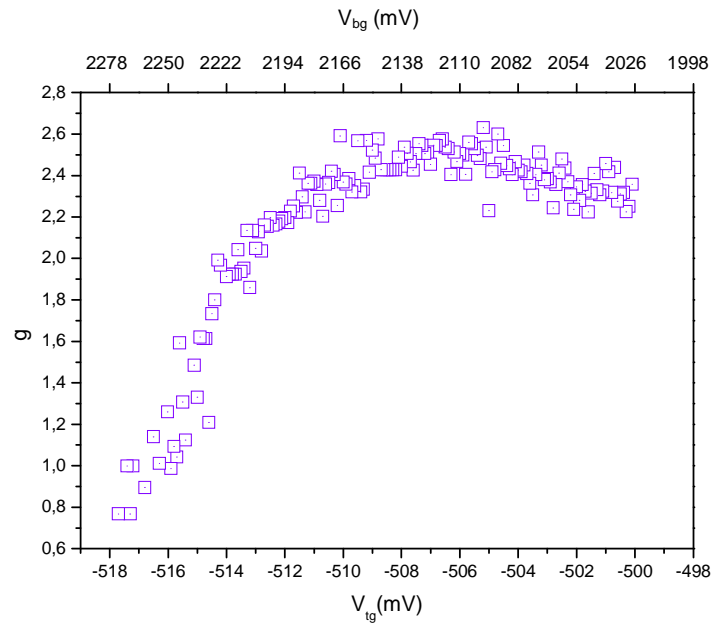
Fig.1. Measured g-factor as a function of the voltage applied to the top gate (V_{tg}) and to the back gate (V_{bg}). A big modulation in g is observed.

References

[1] M. Kroutvar et al., *Nature*, **432** *(*2004) 81.
[2] J. M. Elzerman et al., *Nature*, **430** (2004) 431.
[3] J. R. Petta et al., *Science,* **309** (2005) 2180.
[4] F. H. L. Koppens, *Nature*, **442** (2006) 766.
[5] K. C. Nowack et al., *Science,* **318** (2007) 1430.
[6] A. M. Tyryshkin et al., *Phys. Rev. Lett.,* **94** (2005) 126802.
[7] O. G. Schmidt et al., *IEEE Trans. Electron Devices,* **48** (2001) 1175.
[8] G. Katsaros et al., *Nature Nanotechnology,* **5** (2010) 458.
[9] N. Ares et al., unpublished.

Experimental Study on Chemical Stabilization of Nanofluids Suspension

Maite Aresti, Cecilia Wolluschek

Cemitec, Pol. Mocholi, Plaza Cein 3, 31110 Noain, Spain
maresti@cemitec.com, cwollus@cemitec.com

Heat transfer fluids, such a water, mineral oil and ethylenglicol play a vital role in many industrial proceses. The poor heat transfer properties of these common fluids compared to most solids is a primary obstacle to the high compactness and effectiveness. To improve the energy efficient of these process exist two possibilities: reduce the size of the fluid circulation channels or dramatically increase heat transfer. In the last sense, the nanofluids - suspension of ultrafine particles in a conventional base fluid- tremendously enhance the heat transfer characteristic of the original fluid [1, 2].

The industrial groups that would benefit from such improved heat transfer fluids are quite varied and included solar thermal collectors, transportation, electronics, medical, food and manufacturing.

The use of solid particles suspended in fluids for improving heat transfer of conventional fluids is a technique that has developed over 100 years ago, using millimeter particles. However, in these scales, there are many problems such as abrasion, sedimentation, locking mechanisms, etc. The recent advances in materials technology have made possible the production of nanoparticles (particles between 1 and 100 nm) that could solve some of these problems.

However, there are still many issues for understanding including the explanation of the anomalous increase in thermal conductivity, the stabilization of the nanofluids and other practical issues such as the effect of nanofluids on sedimentation and erosion.

In this study, we focus on the chemistry and preparation of material. Nanofluids require a stable and durable suspension, with low clusters of particles and that does not interact with the fluid changing its chemical composition. Therefore, for the practical applications of the nanofluids at large scales, at a first step it is crucial to develop an adequate chemical method of preparation of nanoparticles and suspensions. In particular, we study the influence of dispersants on nanofluids stabilization .

References

[1] W.Yu, D.M.France, S.U.S. Choi, J.L. Routbort, Review and Assessment of Nanofluid Technology for Transportation and Other Applications, ANL/ESD/07-9, 2007.
[2] J.R.Vazquez Peñas, J.M.Ortiz de Zarate, M- Khayet, "Measurement of the thermal conductivity of nanofluids by the multicurrent hot-wire method", Journal of Applied Physics 104, (2008).

Angular dependent magnetization reversal modes in Co-films with in-plane uniaxial anisotropy

J. A. Arregi, O. Idigoras, P. Vavassori and A. Berger

CIC nanoGUNE Consolider, Tolosa Hiribidea 76, E-20018 Donostia-San Sebastian, Spain
j.arregi@nanogune.eu

Magnetization reversal and the associated phenomenon of hysteresis are key aspects of ferromagnetic materials. The hysteresis property specifically is of great interest in fundamental science but also for modern technology, such as for the application in magnetic storage devices, for instance, that rely on hysteresis as the non-volatile information preservation mechanism. While the significance of the hysteresis phenomenon is mirrored by a vast scientific literature, some features remain still unexplained and are subject to scientific disagreement. One of such topics of active scientific discourse is the existence of criticality upon fine-tuning of magnetic disorder, which has been proposed theoretically [1]. Within this scientific approach, the magnetization M versus field H hysteresis loop itself becomes critical and undergoes a non-equilibrium second order phase transition from a discontinuous $M(H)$ curve with a sample sized magnetization jump to a smooth curve with many intermediate states [1]. It is believed that this kind of criticality has been experimentally observed in thin and therefore effectively two dimensional Co-films [2], even though theoretical predictions indicate that this type of critical point should actually not occur in two dimensional systems.

In this work, we have studied the angular dependence of the magnetization reversal in thin Co-films with in-plane uniaxial anisotropy. The underlying idea of this experiment is that by changing the orientation of the applied field, we change the effectiveness of the magnetic disorder already present in the material due to the partial misalignment of its crystallographic grains. This approach could then allow a continuous tuning of the "effective disorder" in our samples, and hereby provide an alternative experimental pathway to test for criticality of magnetization loop hysteresis in a two dimensional system. In order to grow in-plane uniaxial films with a suitable level of weak crystalline disorder, we have deposited the previously reported [3] epitaxial sequence Ag(110)/Cr(211)/Co(10$\underline{1}$0) on top of Si (110) single crystal substrates by means of ultra high vacuum (UHV) sputter deposition. Certain aspects of magnetization reversal have already been studied in these systems but the angular dependence of magnetization reversal modes and criticality have not been addressed [4].

The experimental characterization of our samples has been done by means of a home-built magneto-optical Kerr effect set up, which allows for a high-resolution of sample alignment with respect to the magnetic field orientation. With this set-up, hysteresis loops where measured for different angles of the applied field in the range from 0º to 60º as measured from the easy axis, with an angular resolution of 0.2º. Furthermore, a high field amplitude resolution of 0.1 Oe was utilized to allow for a very detailed study of the magnetization reversal. In our experiments, no multi-loop signal averaging was done to avoid a smearing out of possibly sharp features in the reversal regime, hereby setting very high requirements for the signal-to-noise ratio of our experimental set-up. Measured $M(H)$–curves demonstrate a clear change of loop shape as one changes the applied field angle θ from the easy axis towards the hard axis. Figure 1 shows a clear distinction between the sharp loop measured at small θ and the continuous curve at higher angles. Figure 2 shows this behavior even more clearly by means of $M(\theta,H)$ color maps for both branches of the loop. For small angles, the magnetization switches from positive saturation to negative saturation, or vice versa, with almost perfect abruptness, indicated by the sharp transition range from red to blue near the coercive field. For larger values of θ, intermediate magnetization states become increasingly more relevant as denoted by the white and yellow areas in both maps.

Moreover, the high resolution of our experiment in field and angle of the applied field will also permit a detailed quantitative determination of the nature of this qualitative behavioral change, an aspect that is currently under investigation.

References

[1] J. P. Sethna, K. Dahmen, S. Kartha, J. A. Krumhansl, B.W. Roberts, and J.D. Shore, Phys. Rev. Lett. **70,** 3347 (1993)
[2] A. Berger, A. Inomata, J.S. Jiang, J. S. Pearson, and S.D. Bader,, Phys. Rev. Lett. **85,** 4176 (2000)
[3] W. Yang, D. N. Lambeth, and D. E. Laughlin, J. Appl. Phys. **85**, 4723 (1999)
[4] O. Idigoras, P. Vavassori, J. M. Porro, and A. Berger, J. Magn. Magn. Mater. **320**, L57-L60 (2010)
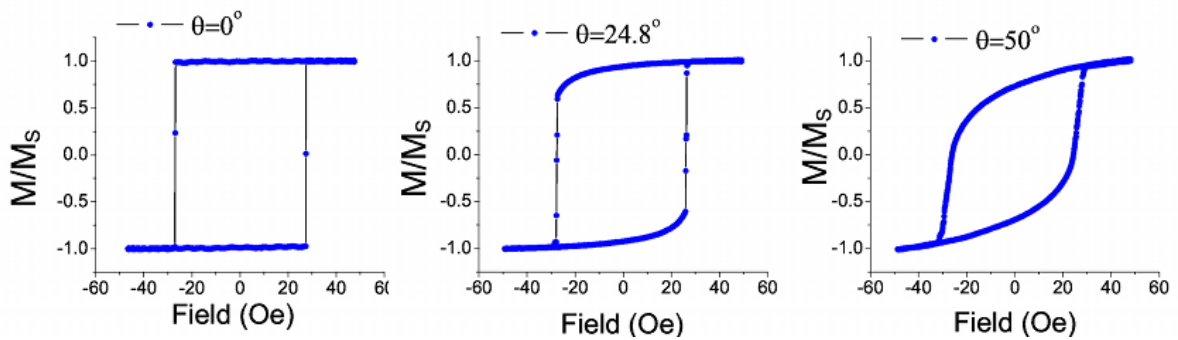
Figures

Figure 1: Hysteresis loop curves for different in-plane orientations of the applied field, as characterized by the angle from the easy axis for θ. While the reversal is very sharp at and near the easy axis, the behavior transitions into a smooth curve as the field orientation moves towards the hard axis.
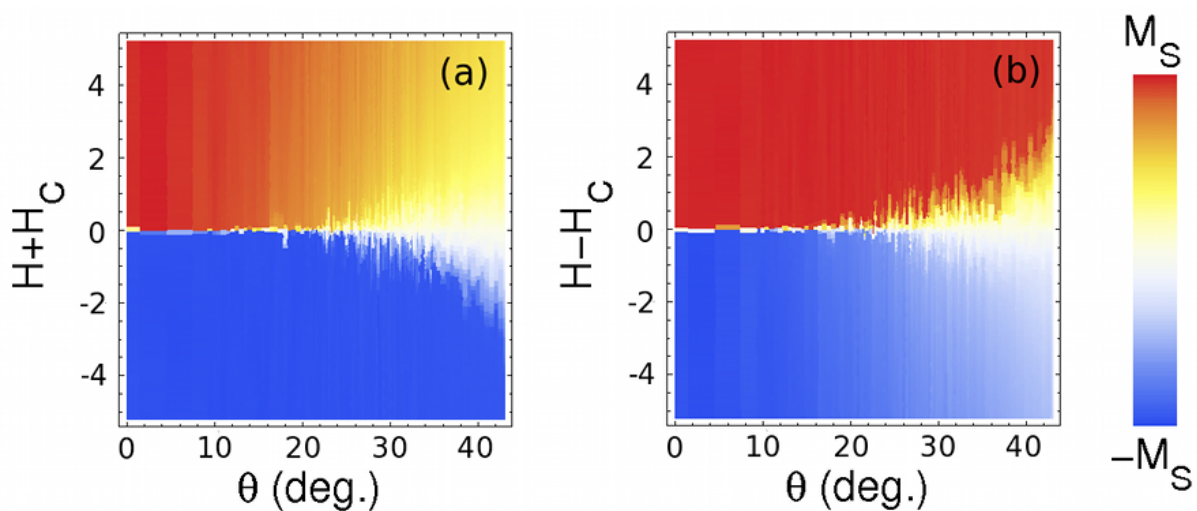
Figure 2: Color-coded magnetization M(θ,H) maps for (a) the decreasing field branch and (b) the increasing field branch of hysteresis loops, measured on a Co-film with in-plane uniaxial anisotropy.

High energy spectroscopy on rare-earth nanowires inside the hollow core of Carbon Nanotubes

Paola Ayala, Hidetsugu Shiozawa, Ryo Kitaura, Hinsanori Shinohara, Thomas Pichler

University of Vienna, Faculty of Physics, Strudlhofgasse 4, A-1090 Wien, Austria
paola.ayala@univie.ac.at

Single wall carbon nanotubes (SWCNTs) are archetypical 1D systems with peculiar electronic properties which can be modified in a controlled manner by various methods. One of these methods takes advantage of the tubular space inside the SWCNTs, which can encapsulate 1D crystals or tiny molecular structures. We aim at explaining how applying thermo-chemical reactions in ultra high vacuum, it is possible to obtain elemental rare earth nanowires still encapsulated in the CNTs. As first example, the case of Er nanowires obtained from the transformation of ErCl3 will be addressed [1]. A second example considers the filling of the hollow core of SWCNTs with $Gd@C_{82}$ metallofullerenes and how subsequent modifications can be induced utilizing the nanotube hollow space as a nano-reactor [2].

The work to be presented focuses on controlling the effective hybridization and charge transfer of rare earths inside the SWCNT nanoreactor. This has been monitored by a combined high resolution photoemission and x-ray absorption study [3]. The hybridization degree and the effective charge changes were directly accessed by across the 4d and 3d edges of Er in the corresponding case. Here, it is found that Er is trivalent but the effective valence is reduced for Er filled tubes. This strongly suggests an increased hybridization between the nanotube π states and the Er 5d orbitals. In the metallofullerene-filling case, from a detailed analysis of the Gd 3d, 4d, and C1s responses, as well as the valence band resonant photoemission, we have been able to elucidate the changes in the bonding environment and charge transfer in these 1D systems. This particular case is very interesting because we observe a clear modification of the low energy electronic properties of the SWCNT transformed partly into double walled tubular structures with encapsulated Gd nanowires.

These results have significant implications for the 1D electronic and magnetic properties of these and similar rare earth nanowire hybrids.

References

[1] Templating rare-earth hybridization via ultrahigh vacuum annealing of $ErCl_3$ nanowires inside carbon nanotubes, P.Ayala, R. Kitaura, R.Nakanishi, H. Shiozawa, R. Kitaura, R. Nakanishi, H. Shiozawa, D.Ogawa, P.Hoffmann, H. Shinohara, and T. Pichler, Phys Rev. B, **83** (2011) 085407.

[2] A resonant photoemission insight the electronic structure of Gd nanowires templated in the hollow core of SWCNTs ,P.Ayala , R.Kitaura, C.Kramberger, H.Shiozawa, N.Imazu, K.Kobayashi, D.J.Mowbray, P.Hoffmann, H.Shinohara, and T. Pichler, , Materials Express (2011) In Press.

[3] Unraveling the electronic properties of metallicity selected Single-Walled Carbon Nanotubes, P.Ayala, Y. Miyata, K. De Blauwe, H. Shiozawa, R. Silva, R. Follath, H. Kataura, C. Kramberger, and T. Pichler, , Phys. Rev. B, **80** (2009) 205427

Photochemical nanomodification of polymer surfaces

Aymerich, E., Casanova, I.

Centre de recerca en nanoenginyeria, Universitat Politècnica de Catalunya (CRnE - UPC),
C. Pascual i Vila, 15. 08028, Barcelona, Spain
edu.f.aymerich@gmail.com

Polymers are, nowadays, one of the most interesting materials because of their huge variety of usages. A large number of investigations are treating with those materials with the objective of giving new properties and usages to polymers.

Polypropylene is becoming one of the most used polymers, because of its good initial characteristics, productivity and cost. For the automotive sector it is also an interesting material for their applications; however it is very difficult to paint, for its neutral chemical surface and its chemical composition, so the objective it's been improve the dyeability of this polymer. All this study is performed inside a project named nAUTO (now in the second stage, named nAUTO[2]) which purpose was to involve nanotechnology capabilities with the automotive needs.

It is studied the effect of high intensity UV light + O_3 on the surface of a polymer (Polypropylene (PP) and Polycarbonate (PC)) with the objective of changing its surface roughness characteristics to increase the dyeability and decrease the reflexivity [1] [2]. This change must be achieved in micro - nano scale, and thus maintaining the same initial appearance at first glance.

If the interaction between the UV/O_3 and the surface is understood and the result is the desired, changes in the roughness at nano or micro level and the surface activation, could become a solution for improving the dyeability characteristics and end up with a paintable polypropylene [3].

The exposition is performed with a high intensity UV lamp, so intense that its rays are able to break the O-O bonds in the air and promote the creation of O_3. During the exposition it was controlled the time and varied the distance between the source and the sample. For the surface analysis, when measuring the surface roughness average before and after the UV treatment, it was used an interferometric microscope and the reflexivity study is done with an UV-Vis-NIR spectrometer.

With the results obtained (figure 1), the change in the surface roughness from 0.77 nm to 1.81 nm in the PP and from 0.094 nm to 0.110 nm in the PC and the enhanced surface activation, it could be said that the proposed UV treatments (figure 2) gives to this PP and PC polymer the necessary modification to increase the surface roughness and the surface activation in such a manner that improves the dyeability tests. This corresponds to an improvement of the coating characteristics of the PP, a polymer very difficult to attach any kind of particle, either chemically or mechanically.

References

[1] Jang, J. and Jeong, Y., Dyes and Pigments, **Nano roughening of PET and PTT fabrics via continuousUV/O3 irradiation** (2006) vol. 69, no. 3, pp. 137-143.

[2] Kumagai, H.; Kusunoki, T.; and Kobayashi, T., Azojomo, **Surface Modification of Polymers by thermal Ozone Treatments**. (2007) vol. 3

[3] Athanassiou, A.; Andreou, E.; Bonarou, A.; Tornari, V.; Anglos, D.; Georgiou, S.; and Fotakis, C., Appl. Surf. Sci. **Examination of chemical and structural modifications in the UV ablation of polymers** (2002) vol. 197-198, pp. 757-763.

Figures

Sample	Mode	Distance (cm)	Time (s)	Ra (um)
PP + 0.0046 nanofluor	PSI 0.8	----------------	---------	2.17
PP CNT MB 5%	PSI 0.2	----------------	---------	2.65
PP	VSI 20.40.7	----------------	---------	0.77
PP	PSI 0.8	9	5	-----
PP	PSI 0.8	17	5	1.81
PP	PSI 0.8	17	10	2.63
PP	PSI 0.8	17	20	-----
PC/PBT	VSI 20.40.7	----------------	---------	0.094
PC/PBT	VSI 20.40.7	17	5	0.110
PC/PBT	VSI 20.40.7	17	10	0.132

Fig.1Summary Table

Sample	Time (s)	Ra (um)	Dose (J/cm^2)
PP	---------	0.77	--------
PP	5	1.81	240
PP	10	2.63	480
PP	20	-----	960
PC/PBT	---------	0.094	--------
PC/PBT	5	0.11	240
PC/PBT	10	0.13	480

Fig. 2 Energetic dose
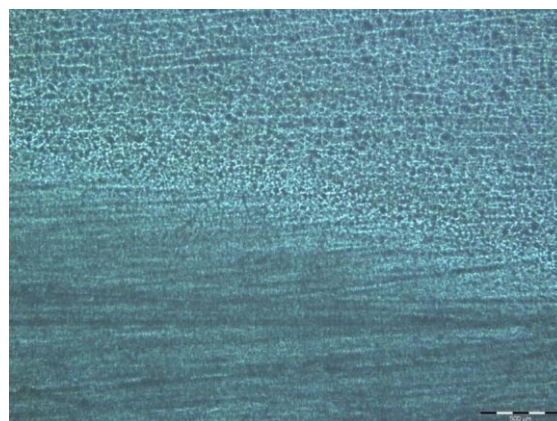
Fig.3 Treated PP part (porous) non treated PP (striped)

Analytical nanochemistry in RECOMOL

Rosana Badía Laíño, Alejandro Simón de Dios, Teresa Díaz-Faes López, María Antonia Escudero Francos, Alfonso Fernández González, Josefa Angela García Calzón, Marta Elena Díaz García

Analytical Group of Molecular Recognition, Department of Physical and Analytical Chemistry, Julián Clavería 8, Oviedo, España
rbadia@uniovi.es

As the properties of the matter at nanoscale differ drastically from those at macro- and microscopic range, complex nanoparticles such as silicon nanotubes, gold nanorods/nanoespheres or materials with tailored-made nanocavities, are attracting much interest from researchers in the field of new materials. The core research lines of the Analytical Group of Molecular Recognition (RECOMOL) are devoted to the preparation of metal nanoparticles (Au, Si) with capabilities to perform different functions and to the synthesis and development of specialized nano-structured materials with improved molecular recognition properties (molecularly imprinted materials)[1-4]. In this communication we present a general overview of relevant aspects and results of our current work on:
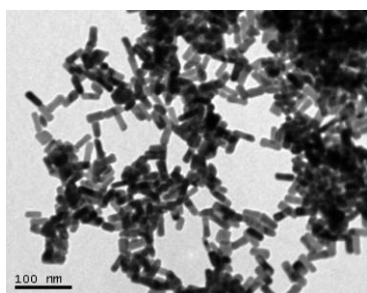
Figure 1. Gold nanorods
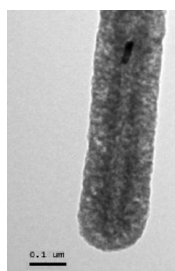
Figure 2. Silica nanotube

1. The synthesis of functional nanoparticles: a) gold nanorods which are synthesized by "seeding" gold nanoparticles (Fig.1), followed by a further functionalization with suitable reagents, thus providing the nanomaterials with capabilities to selectively interact with different target molecules[1,2] and b) Molecularly imprinted silicon nanotubes obtained by Ag nanowire transcription method (Fig.2).

   The new materials are physical, -chemical (adsorption isotherms, TEM, SEM, FTIR and UV-VIS spectroscopy) and analytically characterized. Those nanosystems exhibiting promising analytical potential are applied as nanochemosensors for determination of analytes of clinical/medical and pharmaceutical concern (albumins, amino acids, cancer markers, etc).

2. The development of imprinted materials by using sol-gel approaches against substance P and 5-hydroxyindolacetic acid. We also report our results in blending the chemistry of molecularly imprinted sol-gels with microfluidics applied to the development of smart sensory systems (Figure 3).
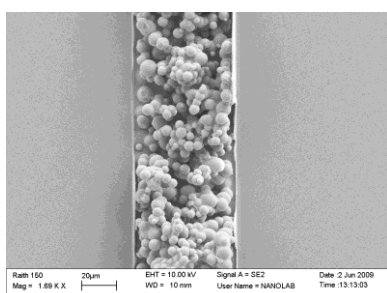
Figure 3. Molecularly imprinted sol-gel modified microchannel

References

[1] A. Cruz Enriquez, I. A. Rivero Espejel, E. Andrés García, M. E. Díaz-García, Anal. Bioanal. Chem., **391** (2008) 807-815.

[2] E. A. Reynoso-Soto, A. Fernández-González, I. Rivero, M.E. Díaz-García. DCM-dye laser dual fluorescence upon interaction with gold nanoparticles: Analytical potential for cyanide sensing. Unpublished results (2010).

[3] L. Guardia, R. Badía Laíño, C. Ania, B. Parra, M.E. Díaz-García, Biosensors & Bioelectronics, **23** (2008) 1101-1108.

[4] A. Fernández-González, A. Simón de Dios, R. Badía-Laíño, M. E. Díaz-García. Insights into the molecular recognition mechanism of 5-hidroxy-indol acetic acid imprinted xero-gel materials through spectroscopy. Unpublished results (2010).

Characterization of Multi-Component Materials on the Sub-Micrometer Scale
A Topographic 3D Raman and AFM Study

E. Bailo, F. Vargas, A. Jauss, T. Dieing and U. Schmidt

WITec GmbH, Lise-Meitner Str. 6, 89081 Ulm, Germany
ute.schmidt@witec.de

Knowledge about the morphology and chemical composition of heterogeneous materials on a sub-micrometer scale is crucial for the development of new material properties for highly specified applications. Such materials can either have mono-atomic flat surfaces or a roughness of several hundred micrometers or millimeter. In the past two decades, AFM (atomic force microscopy) was one of the main techniques used to characterize the morphology of nano-materials spread on nanometer-flat substrates. Fig. 1a shows the high spatial resolution AFM image of carbon nanotubes spread on a silicon wafer. From such images it is possible to gain information about the physical dimensions of the material on the nanometer scale, without additional information about their chemical composition, crystallinity or stress state. On the other hand, Raman spectroscopy is known to be used to unequivocally determine the chemical composition of a material. By combining the chemical sensitive Raman spectroscopy with high resolution confocal optical microscopy, the analyzed material volume can be reduced below 0.02 μm^3, thus leading to the ability to acquire Raman images with diffraction limited resolution from very flat surfaces [1, 2]. The combination of confocal Raman microscopy with Atomic Force Microscopy (AFM) is a breakthrough in microscopy. Using such a combination, the high spatial and topographical resolution obtained with an AFM can be directly linked to the chemical information provided by confocal Raman spectroscopy [3]. Fig. 1b shows the intensity distribution of the G-band obtained from the same sample position as in Fig. 1a using Raman imaging. In this imaging mode a complete Raman spectrum is acquired in every image pixel, leading to a 2D array of single Raman spectra. The evaluation of peak intensity and peak position results in different Raman images, representing various properties of the carbon nanotubes. The Raman spectrum of a SWCNT with its unique Raman bands is shown in Fig. 1 (right side). Characteristic for SWCNT only are the radial breathing modes (RBM), providing information about the diameter of the tube. The position and width of the G-band is used to distinguish between metallic (bright color in Fig. 1c) and semiconducting (bright color in Fig. 1d) CNT and to probe the charge transfer arising from doping CNT`s.

Topographic Raman imaging, a new imaging technique developed for measurements on rough surfaces over large areas, allows confocal Raman imaging guided by the surface topography obtained by an integrated profilometer. Large-area topographic coordinates from the profilometer measurements can be precisely correlated with the large area confocal Raman imaging data. This allows true surface Raman imaging on heavily inclined or rough surfaces, with the true sample surface held in constant focus, while maintaining highest confocality. Fig. 2a shows the topography of a pharmaceutical tablet on the order of several hundred micrometer. In Fig. 2b the true surface Raman image is presented, showing the distribution of the API (red) in the various excipients (green and blue color).

In summary, the combination of confocal Raman microscopy and topographic Raman imaging allows the characterization of materials at high, submicron resolution, as well as on mm-rough surfaces across large areas. Examples from various fields of applications will be presented.

References

[1]   P. Lasch, A. Hermelink. and D. Naumann, *The Analyst*, **1-9**, (2009).
[2]   A. Jungen, V. N. Popov, C. Stampfer, C. Durrer, S. Stoll, and C. Hierold *Physical Review*, 75, 405-410, (2007).
[3]   U. Schmidt, S. Hild, W. Ibach and O. Hollricher, *Macromol. Symp.* 230, 133-143 (2005).
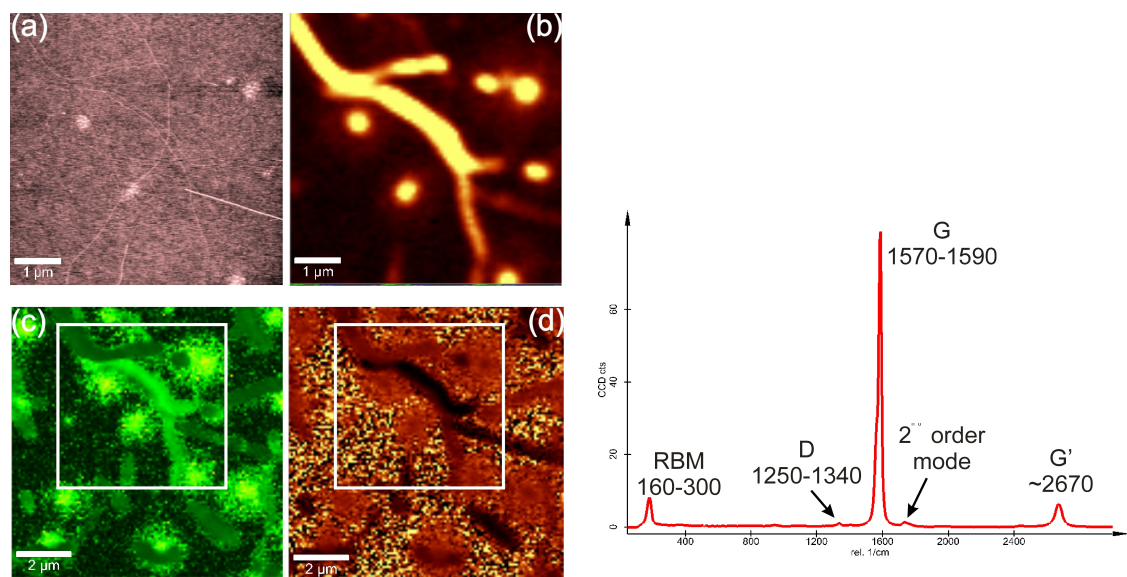
Figure 1: *AFM image of CNT`s spread on a Si substrate (a), confocal Raman image showing the intensity of the G-band, thus the distribution of CNT`s on the Si substrate (b), enlarged scansize confocal Raman images showing the width (c) and center of mass (d) of the G-band revealing crystalline defects and stress states of the different CNT`s.*
Right side: Characteristic Raman spectrum of a SWCNT.
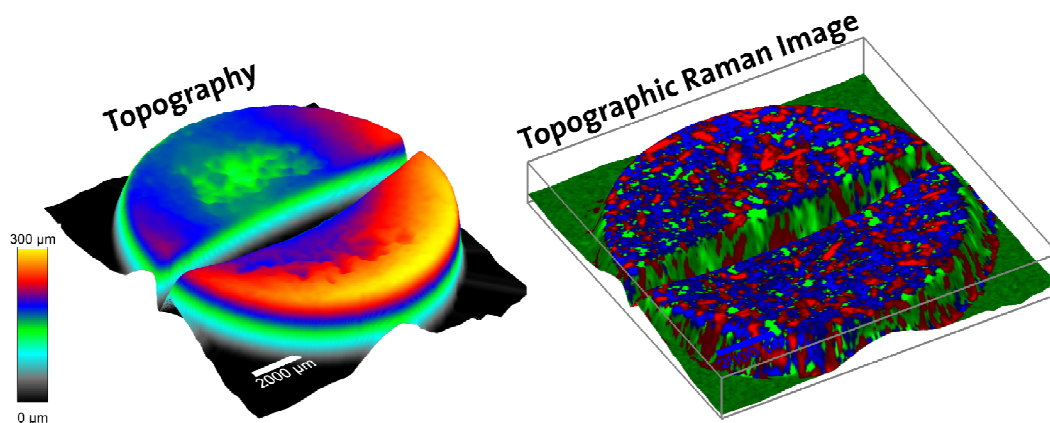
Figure 2: *Topography and True Surface Raman Image of a pharmaceutical tablet.*

Hybrid Nanomaterials based on BODIPY-Functionalized Octasilsesquioxanes

Jorge Bañuelos,[1] M. Eugenia Perez-Ojeda,[2] Jose Luis Chiara,[2] Angel Costela,[3] Iñigo López Arbeloa[1]

[1]Dpto. Química Física, Universidad del País Vasco (UPV-EHU), Aptdo 644, 48080 Bilbao, Spain.
[2]Instituto de Química Orgánica General (CSIC), Juan de la Cierva 3, E-28006 Madrid, Spain.
[3]Dpto Sistemas de Baja Dimensionalidad, Superficies y Materia Condensada, Instituto de Química Física "Rocasolano" (CSIC), Serrano 119, 28006, Madrid, Spain.

jorge.banuelos@ehu.es

Fully condensed polyhedral oligosilsesquioxanes (POSS) are nanometer-sized materials.[1] Their rigid inorganic core ensures a considerable chemical and thermal stability. Moreover, these nanoparticles are well dispersed at the molecular level and can be readily functionalized with different organic molecules, for instead monomers. In this way novel hybrid materials can be obtained with improved homogeneity and transparency. Owing to these properties, currently POSS nanoparticles are widely applied in photonics and electronic devices.

Another possibility never exploited before, is to use these POSS nanoparticles as random materials. Dye molecules grafted to POSS can be adequately dispersed, leading to a homogeneous material. The weak scattering of the POSS cores should provide an extra feedback elongating the light path in the gain media. Such phenomenon is known as incoherent random laser and results in an improvement of the lasing performance. The chosen dye was BoronDiPyrromethene (BODIPY) which nowadays is probably the benchmark in efficiency and photostability in tunable dye lasers.[2]

Therefore, in the present work we show the characterization of the corresponding BODIPY model to be attached to the POSS core, together with mono- and octasubstituted-POSS derivatives (Figure 1). The incorporation of the linking chain at central position of the BODIPY chromophore does not alter its photophysical properties. As result, such spacer is adequate to covalently bound the BODIPY to the POSS core. The photophysical properties of the monosubstituted-POSS are close to those of the free BODIPY indicating that the greafting process has been successful. Even more, the lasing properties of the BODIPY are enhanced by the presence of POSS due to the above commented extra feedback provided by the light scattering of the POSS nanoparticles. However, the octasusbtituted-POSS has no lasing emission and very low fluorescence intensity. The reason of such behavior is the interaction between neighbors BODIPY molecules. The proximity of the BODIPY fluorophores around the POSS core and the flexibility of the linking chain facilitates that the molecules adopt different conformations. Indeed, the absorption spectrum is not the sum of eight BODIPY chromophores and the absorption intensity increase in the shoulder region at higher energies. Such feature indicates the presence of H-type aggregates as is also supported by the theoretical simulated ground state geometry (Figure 1). This kind of association is characterized by an inactive absorption of the light and the fluorescence quenching of the emission coming from the monomer, with the consequent deleterious effect in the lasing emission.

In short, the unique photophysical properties of BODIPY are kept in spite of being linked to POSS. The light scateering of the POSS core ameliorates the lasing efficiency of the BODIPY dye. However, this hold true for the monosusbtituted derivative, since in the octasubstituted one the interaction between the dye molecules (aggregation) drastically decrease both the fluorescence and lasing ability. This work is

the platform for future POSS based systems, where a POSS core is functionalized both with a fluorophore and a bio-recognition element, with potential applications as bioimaging agents.

References

[1] D. B. Cordes, P. D. Lickiss, F. Rataboul, Chem. Rev. **110** (2010) 2081.
[2] M. J. Ortiz, I. Garcia-Moreno, A. R. Agarrabeitia, G. Duran-Sampedro, A. Costela, R. Sastre, F. López Arbeloa, J. Bañuelos, I. López Arbeloa, Phys. Chem. Chem. Phys., **12** (2010) 7804.

Figures
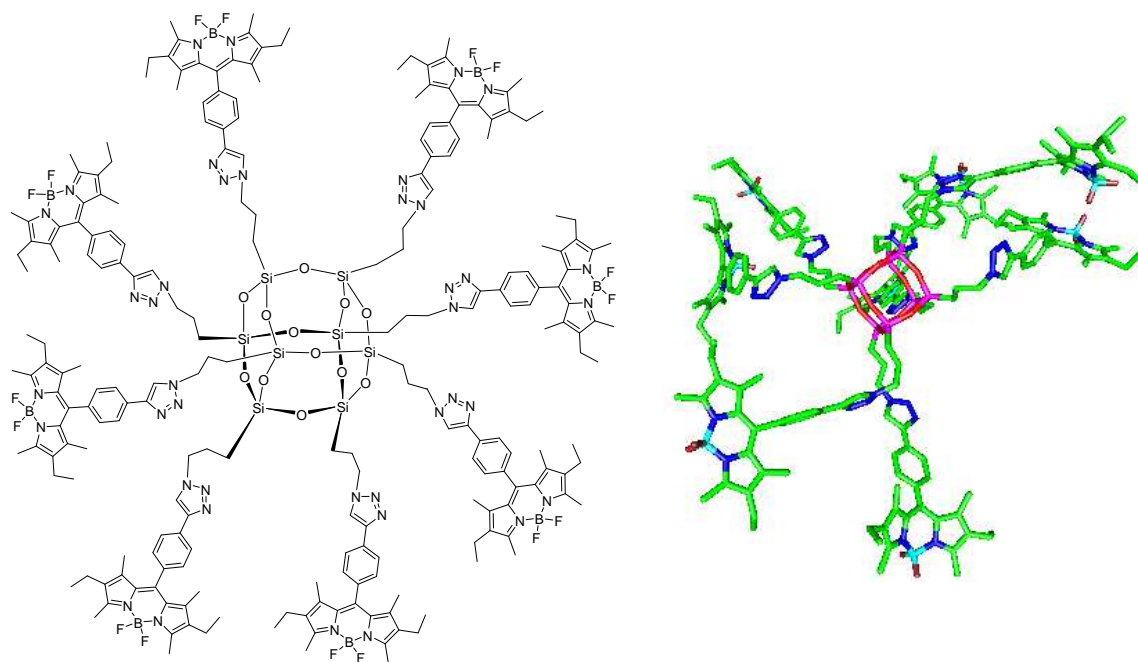
Figure 1. *Molecular structure of the POSS core bearing eight BODIPYs. The corresponding ground state optimized geometry is also depicted.*

Nanoscale Chemical Spectroscopy with the Atomic Force Microscope

Juergen Schluetter[1], Craig B. Prater[2], Debra Cook[2], Roshan Shetty[2] and Kevin Kjoller[2]

[1] LOT-Oriel GmbH & Co. KG, Im Tiefen See 58, Darmstadt, 64293, Germany, schluetter@lot-oriel.de
[2] Anasys Instruments, 25 W. Anapamu Street Suite B, Santa Barbara, CA 93101, USA

The ability to unambiguously identify arbitrary material under the tip of an Atomic Force Microscope (AFM) has been identified as one of the "Holy Grails" of probe microscopy. While the AFM has the ability to measure a range of material properties including mechanical, electrical, magnetic and thermal, the technique has lacked the robust ability to characterize and identify unknown materials. Infrared spectroscopy is a benchmark technique routinely used in a broad range of sciences to characterize and identify materials on the basis of specific vibrational resonances of chemical bonds. Several AFM probe-based techniques have been used to beat the diffraction limit of conventional IR measurements, however, none of these techniques provide readily interpretable broadband IR spectroscopy with nanoscale resolution. We have successfully integrated the capabilities of AFM with IR spectroscopy to allow chemical characterization on the micro and nanoscale. The instrument employs a technique called photothermal induced resonance (PTIR) [1-3] that uses an AFM probe to measure the local thermal expansion from IR light incident upon a sample. This technique enables the ability to obtain a high quality IR spectrum at a selected point in an AFM image and/or automatically map spectra at an array of points on a sample to enable chemical mapping. In this presentation, we will share the details of the measurement technique including application examples on polymer multilayers and blends, along with measurements on plant cells.
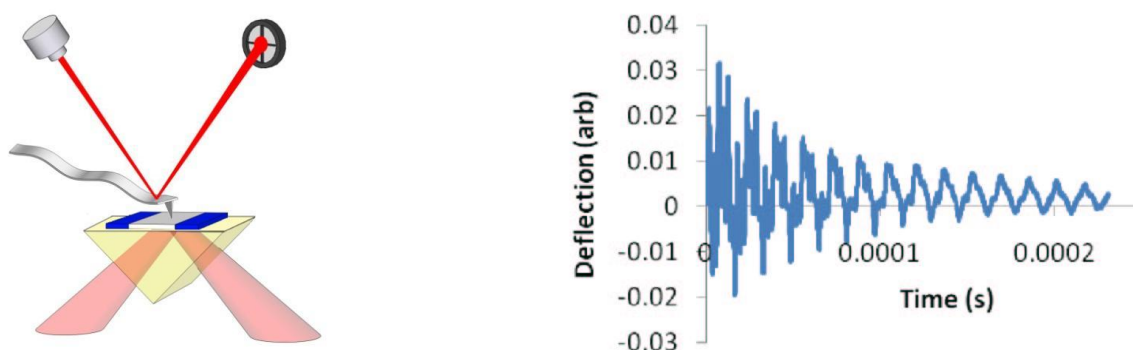
Figure 1. (L) Schematic diagram of PTIR technique for nanoscale IR spectroscopy. A pulse of infrared light from a tunable source is directed at a region on a sample. When the source is tuned to an absorption band of the sample, the absorbed radiation heats up the area, resulting in a rapid thermal expansion of the sample. This rapid thermal expansion excites resonant oscillation modes of the cantilever. (R) Example cantilever ringdown after excitation by sample IR absorption. The amplitude of this ringdown is proportional to the strength of IR absorption under the AFM tip. The PTIR technique also enables complementary and simultaneous mapping of mechanical properties through measurements of the ringdown resonant frequencies.

Topic Area: Nanoscale Materials Characterization-Direct Space Imaging Method

References
[1] A. Dazzi, R. Prazeres, E. Glotin and J. M. Ortega, Optics Letters **30**, 2388-2390 (2005).
[2] A. Dazzi, R. Prazeres, F. Glotin and J. M. Ortega, Ultramicroscopy **107**, 1194-1200 (2007).
[3]. A. Dazzi, R. Prazeres, F. Glotin, J. M. Ortega, M. Al-Sawaftah and M. de Frutos, Ultramicroscopy **108**, 635-641 (2008).

Hydraulic Cement Comprising Amine-functionalized Nanoparticles

Gemma Berriozabal, Yolanda de Miguel

Tecnalia Research and Innovation, Parque Tecnologico de Bizkaia Geldo st 700 48160 Derio , Spain
gberriozabal@labein.es

The performance of cement composites has been traditionally improved by means of reactive additions, such as silica fume,[1] or inert reinforcements, such as steel bars or different types of fibres. This research project focuses on the production of a cement having improved properties, particularly strength, owing to the incorporation of organosilane molecules, and to the uses thereof. For this purpose, in this poster is related a method for obtaining nanoparticles of organosilane, specifically containing amine groups, and the addition thereof to cement in nanoparticle form, yielding an improved hydraulic cement in comparison with conventional Portland cement.

Previously, it was carried out the study and development of novel synthetic methodologies for the obtention of nanoparticles containing amine groups. A convenient single step (one-pot) method based on well-known Sol-Gel methodology,[2] particularly the Stöber method[3] was described for the preparation of these nanoparticles. As a result of this novel method, stable colloidal suspensions of monodisperse silica nanoparticles with pendant amines were successfully obtained; the size of these nanoparticles of 120 nm, as can be observed in the images obtained by Atomic Force Microscopy (AFM) (Fig 1).

The experimental results obtained have shown that nanosilica increases the strength of the cement paste about a 30% in cured samples (Fig 2).[4] At the level of the structure of the C–S–H gel, amine-functionalized silica nanoparticles increase the average length of the silicate chains and reduce their polymerization as calcium dissolves.

In addition, ^{29}Si CP/MAS NMR spectra of cement composites have been obtained (Fig 3). The information obtained provided a general and detailed picture of the nature of the cementitious matrix. This not only served to understand the effect of the use of reactive reinforcements, but it will also contribute to broaden the existing knowledge on the cement matrix.

References

[1] Bjornstrom, J; Martinelly, A; Matic, A; Borjesson, L; Panas, I; Chem. Phys. Lett. **392** (1–3) (2004) 242.
[2] Brinker. C.J.; Scherer G.W. (Eds.), "*Sol-Gel Science. The Physics and Chemistry of Sol-Gel Processing*", Academic Press, San Diego (1990)
[3] Stöber. W.; Fink. A.; Bohn. E.; *J. Colloid Interface Sci.*, **26** *(*1968) *62*.
[4] Berriozabal. G; De Miguel. Y; Porro. A; Patent PCT_ES2008/000808

Figures
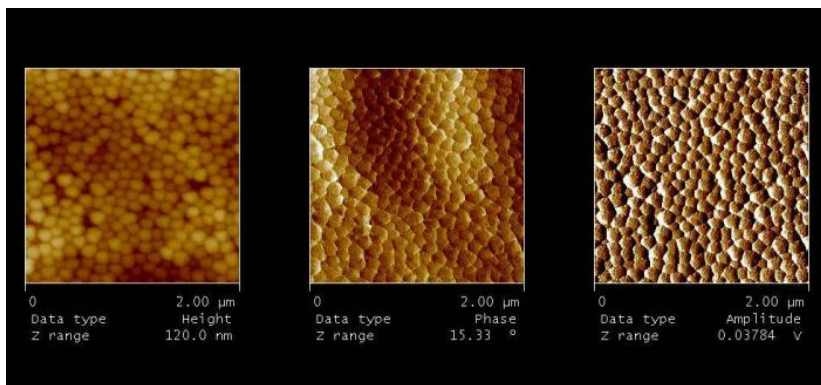
Fig. 1. AFM images of Aminepropyl-functionalized silica nanoparticles
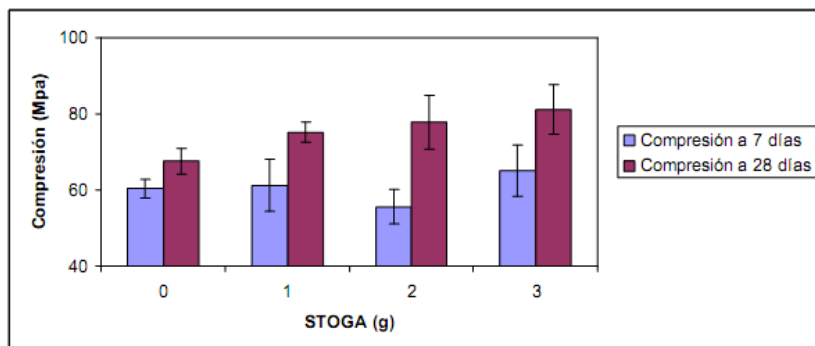
Fig. 2. Mechanical properties as measured by the compression tests.
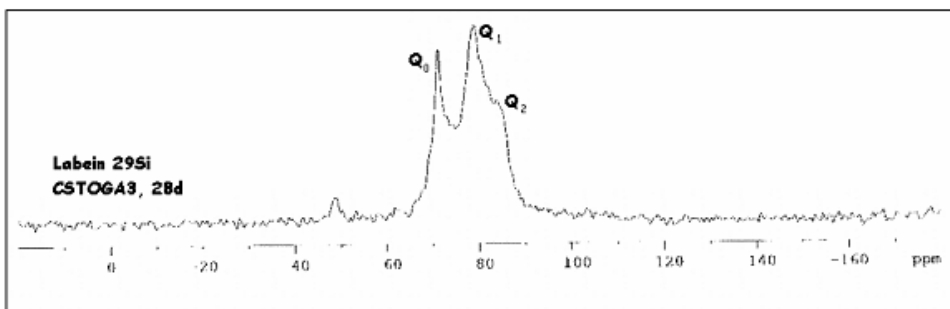
Fig. 3. ^{29}Si CP/MAS NMR spectra of cement composites

Plant viral particles as nano-scaffolds for controlled positioning of enzymes on solid supports

Jane E. Besong[1], Noelle Carette[2], Daniela Cardinale[2], Jocelyne Walters[2], Thierry Michon[2], Kristiina Makinen[1]

[1]Department of Food and Environmental Sciences, Latokartanonkaari 11, P.o Box 27, FI-00014, University of Helsinki - Finland.

[2]INRA-Bordeaux (France)

jane.besong@helsinki.fi

Within the cell, enzymes involved in cascade reactions are precisely positioned in close proximity, the product of the first enzyme becoming substrate for the second. Because it is less diffusion-controlled, this so called "channelling" process allows an increased efficiency of the cascade reaction. VIRUSCAF is a collaborative project between the University of Helsinki, Finland and the Institut de la Recherche Agronomique, Bordeaux, France. This project, launched in November 2009 intends to design a nano platform mimicking the intracellular organisation of enzymes working in cascade. In a first step, the highly ordered surface of virus particles will be used as Enzymes Nano Carriers (ENCs). Using genetic engineering the virus particles will be functionalized in order to evenly distribute various enzymes on its surface. In a second step, these ENCs will be patterned on solid supports (enzymes chips). Our study aims at evaluating the gain of catalysis efficiency of complex reactions. Numerous potentially exciting outcomes in biosensors and nano-reactors technology can be envisaged.

Virus particles are precisely defined nanometer-sized objects formed by the self-association of capsid proteins monomers. Potato virus A (PVA) is being exploited for the first time for nano-technological applications. It forms flexible rod shaped particles of about 2000 capsid protein subunits surrounding a single RNA molecule. PVA virions are about 730 nm long and 15 nm wide, about 90% made up of the capsid protein and 5% the viral RNA. The N-terminus of the capsid protein is exposed to the surface of the particle hence can be engineered to carry functional entities. The constituting capsid protein subunits of PVA virions have been modified by genetic engineering to carry specific peptide linkers as a first approach to functionalize these virus surfaces with enzymes carrying complementary peptide linkers. The peptide linker fused to the N-terminus of the capsid protein has been successfully expressed in *Nicotiana benthamiana* plant leaves. Its ability to form virus-like particles is currently being studied using the electron microscope. A second approach involves the use of PVA specific binding peptides which will be fused to the enzyme of interest. Phage display screening was used to identify peptides specific for PVA and further analysis are being perform to confirm this specificity.

For a successful study and application of these virus-like particles (VLP) in nanotechnology, understanding the assembly process of PVA capsid protein is crucial. As in other viruses, this assembly is initiated by binding of the capsid protein to the viral RNA. Using a reporter based gene expression system, the region in the viral RNA involved in this interaction has been identified and is being studied in detail.

Effect of relative humidity on the microstructure of electrospray deposited polymer thin films

Eszter Bodnar[1], Pavel Kiselev[1], Joan Rosell[1,2]

[1]Departament d'Enginyeria Quimica, Universitat Rovira i Virgili, 43007 Tarragona, Catalunya, Spain
[2]ICREA (Catalan Institution of Research and Advanced Studies), Barcelona, Catalunya, Spain
joan.rosell@urv.cat

Polymer nano-structured thin films have great potential in applications in semiconductor industries [1], as an active component in opto-electronic devices [2], in biotechnology [3], and for coatings that modify surface properties, like stimuli-responsive polymer nanocoatings [3]. With a proper combination of the composition and morphology of the thin film a wide range of film properties and functionalities can be achieved. Microstructure of thin films is highly important for film properties such as super-hydrophobicity [3].

In this study we use electrospray (ES) deposition to create polymer thin films of different microstructures. Unlike to the most popular method for making polymer thin films, spin coating, ES allows to deposit thin films onto complex surfaces, however, it has one significant drawback – low throughput. ES produces highly charged mono-disperse droplets that dry out to become nano- or micro-particles which are attracted to the substrate forming a thin film. Changing the particle size and morphology one can create thin films with different microstructures. It is well-known which parameters control particles size, but to our knowledge the parameters that affect morphology of particles in ES deposition have not been studied. We have found that one important parameter that has a strong effect on the shape and morphology of a polymer particle is the relative humidity of the ambient gas during electrospray deposition.

In this work thin films have been generated from electrosprays of dilute polymer solutions (0.1-1.0 wt%) of ethylcellulose (EC), polystyrene (PS), and poly(methyl methacrylate) (PMMA) in organic solvents with electrolyte added, at various values of RH. Under dry conditions films consisting of compact individual sphere- or disk-like particles were obtained for all polymer solutions (figure 1a-d, left column). The solutions for which an addition of small amount of water causes polymer to precipitate due to an anti-solvent effect of water, e.g. EC in dichloromethane and PS in 2-butanone, produced films made of porous particles at high RH (figure 1a-b, right column). We believe that the following mechanism explains particle porosity. Solvent evaporation from the droplet causes concentration of the polymer at the surface of the droplet as well as cooling and consequent water condensation onto the droplet. The condensed water diffuses into the droplet and causes precipitation of the polymer. Similar mechanism has been proposed to explain the effect of RH on film morphology during spin coating (Breath Figure Formation [4]). For other solutions where large relative amount of water was needed to cause precipitation (EC in butanone and EC in Isopropanol-Acetone), as was determined experimentally, non-porous wrinkled particles were formed for high polymer concentration (1.0 wt%) (figure 1c) while for lower concentration (0.1 wt% EC or PMMA in Isopropanol-Acetone) continuous uniform thin films were formed under high RH (figure 1d).

References

[1] deBoer, B; Facchetti, A, Polymer Reviews, Vol. **48** (2008) 423-431
[2] Ma, H; Liu, MS; Jen, AKY Polymer International, Vol. **58** (2009) 594-619
[3] Kumar, Ch, Nanostructured Thin Films and Surfaces, Wiley-VCH, 2010
[4] Bunz, UHF, Advanced Materials, **18** (2006) 973-989

Figures
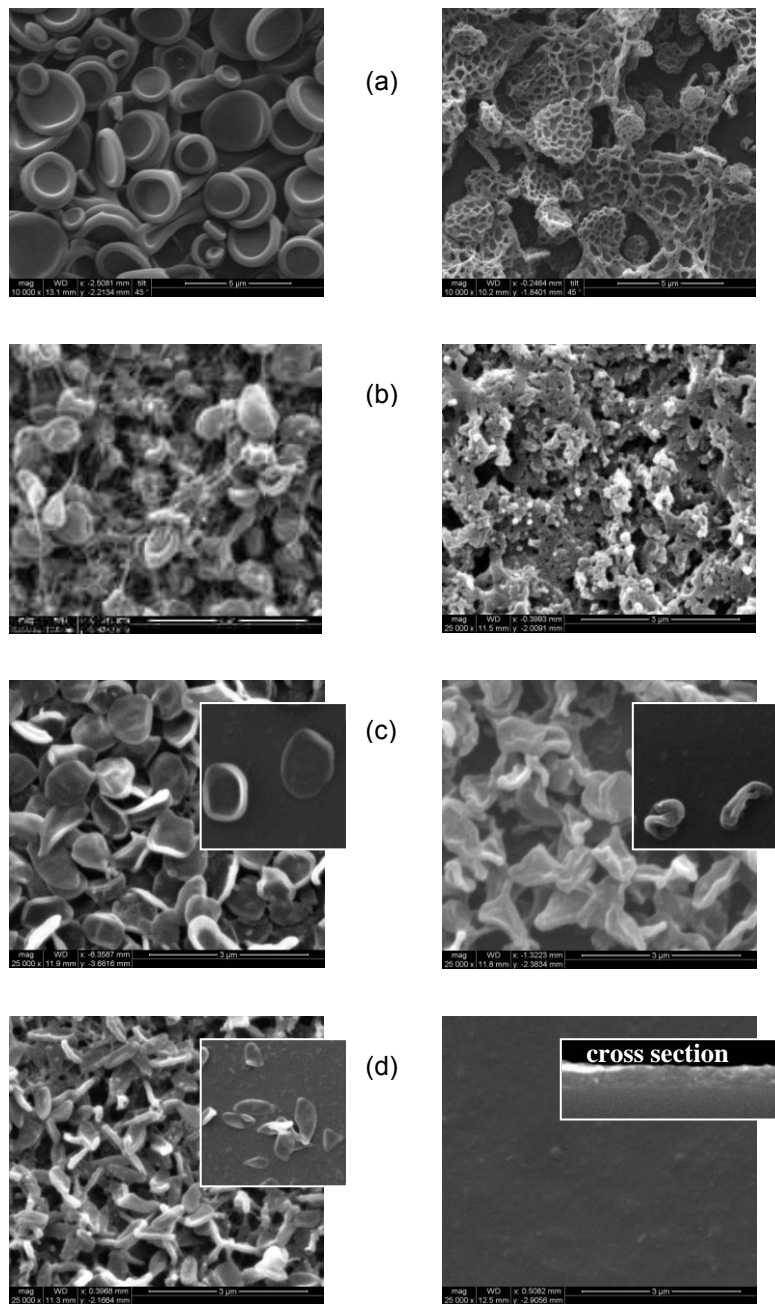
Figure 1. SEM images of polymer thin films deposited by electrospray on silicon wafer under different relative humidity (left column – 10 % RH, right column – 60 % RH); (a) 1.0 wt% EC in DCM; (b), 0.1 wt% PS in 2-butanone; (c) 1.0 wt% EC in IPA-Acetone (50-50 v%); (d) 0.1 wt% EC in IPA-Acetone (50-50 v%)

An electrochemical competitive biosensor for deoxynivalenol based on paramagnetic microparticle beads functionalized with protein A

Laura Bonel[2], Juan C. Vidal[1], Alba Ezquerra[1], **Susana Hernández[2]** and Juan R. Castillo[1]

[1]Institute of Environmental Sciences (IUCA)

Analytical Spectroscopy and Sensors Group (GEAS)

University of Zaragoza. Ciudad Universitaria (50009) ZARAGOZA. Spain

[2]CAPHER IDI S.L, C/Ermesinda de Aragón , 4, c 116, 50012 ZARAGOZA. Spain

E-mail: lbonel@capher.es

The work done so far have been based on the design of an electrochemical competitive aptamer-based biosensor for ochratoxin A (OTA) [1,2]

OTA is one of the most important mycotoxin contaminants of foods, particularly cereals grains (corn, barley, wheat and rye) and cereal products, with strict low regulatory levels (of ppb) in many countries worldwide. The highest OTA concentration in unprocessed cereals and cereal products permissible by the European Community is 3–5 µg kg^{-1} (Commission Regulation No. 1881/2006).

Paramagnetic microparticle beads (MBs) were functionalized with an aptamer specific to OTA, and were allowed to compete with a solution of the mycotoxin conjugated to the enzyme horseradish peroxidase (OTA–HRP) and free OTA. After separation and washing steps helped with magnetic separations, the modified MBs were localized on disposable screen-printed carbon electrodes (SPCEs) under a magnetic field, and the product of the enzymatic reaction with the substrate was detected with differential-pulse voltammetry. In addition to magnetic separation assays, other competitive schemes were preliminary tested, optimized and compared. From all these kind of biosensors for OTA, electrochemical inmunosensors have the advantages of simplicity and sensitivity.

The magnetic aptasensor showed a linear response to OTA in the range 0.78 to 8.74 ng mL^{-1} and a limit of detection of 0.07±0.01 ng mL^{-1}, and was accurately applied to extracts of certified and spiked wheat samples with an RSD lower than about 8% [3].
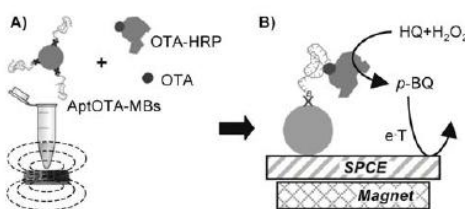
In the present experimental work is to undertake the design of an immunosensor for the detection of deoxynivalenol (DON) in cereals, following the steps carried out for the OTA. The biosensor will be a direct immunosensor (immobilized biorecognition element) and competitive (competitive reaction between the DON and DON-HRP) and mode of detection is performed by a electrochemical technique.

Deoxynivalenol is a mycotoxin produced by Fusarium fungus, one of the most abundant fungi, which are abundant in certain cereals such as wheat, corn, barley, oats, and rye and their processed grains such as malt, beer or bread. DON inhibits the synthesis of DNA and RNA and protein ribosomes. This toxin has a hemolytic effect on erythrocytes. In high doses, DON causes vomiting, and if the concentration taken in the diet is lower growth and reduced food consumption (anorexia).

Maximum permissible concentrations of deoxynivalenol for different foods, are between 200 and 1750 µg/Kg, and the tolerable daily intake is 1 µg/Kg body weight.

The immobilization of anti-DON on paramagnetic beads functionalized with protein A (MBs) is based on the antiDON and protein A interaction. The sample of the antiDON-MBs is mixed in an eppendorf vial with a previously mixed solution containing DON and the conjugate DON–HRP (a fixed concentration).

After of incubating at room temperature, the global reaction is: MBs-protein A+anti-DON + DON + DON-HRP.

A sample of the global reaction is dropped onto the surface of the SPCE. For the specific location of the beads close to/on the electrode surface, a magnetic block is placed just at the bottom of the SPCEs. Then hydroquinone and hydrogen peroxide are deposited in this order onto the SPCE strip, and after 10 minutes at room temperature the enzymatic product (p-BQ) is determined using chronoamperometry.

References

[1] J. C. Vidal, P. Duato, L. Bonel and J. R. Castillo, "Use of polyclonal antibodies to ochratoxin A with a quartz–crystal microbalance for developing real-time mycotoxin piezoelectric immunosensors", *Anal Bioanal Chem* **(2009)** 394, 575–582.

[2] L. Bonel, Juan C. Vidal, P. Duato and Juan R. Castillo, "Ochratoxin A nanostructured electrochemical immunosensors based on polyclonal antibodies and gold nanoparticles coupled to the antigen", *Anal. Methods* **(2010)** 2, 335–341.

[3] Laura Bonel, Juan C. Vidal, Patricia Duato, Juan R. Castillo, "An electrochemical competitive biosensor for ochratoxin A based on a DNA biotinylated aptamer", *Biosensors and Bioelectronics* **(2010)** DOI:10.1016/j.bios.2010.12.036.

size distribution of single walled carbon nanotubes (SWNT) obtained by asymmetric flow field fractionation (AFFF)

Zaira Monasterio[a], Virginia Saez-Martinez[a,b], Leire Bilbao[a], Naiara Azurmendi[a], Izaskun Bustero[a,b]

[a]TECNALIA RESEARCH & INNOVATION, Parque Tecnológico de Miramón,
Mikeletegi Pasealekua 2, E-20009, Donostia-San Sebastián, Spain

[b]Ciber-BBN, Donostia-San Sebastián, Spain

Izaskun.bustero@tecnalia.com

The most accurate geometrical characterization of tubular nanoparticles in suspension is achieved by examining them one-at-a-time within a well defined microscopic field (transmission electron microscopy, atomic force microscopy, etc..). An alternative far easier approach involves separating particles by their size and then measuring them in real time on-line by a Multiangular Light Scattering (MALS) detector.

Asymmetric Flow Field Fractionation (AFFF) separates particles according to their sizes in a manner similar to the separation of molecules within a chromatography column. AFFF has been employed to provide separation and quantification of the size distribution of different samples of single walled carbon nanotubes (SWNT-Nanocyl) that have been previously purified and cut into short lengths by a chemical oxidation process [1].

The size distribution characterization was carried out on an Eclipse AF4 system equipped with the standard channel (25 cm), 350 μm spacer and regenerated cellulose membrane (5 kDa cutoff) (fig.1). For the determination of optimal AF4 separation conditions, different injection volumes and channel flow to crossflow ratios were tested. Immediately after the fractionation, the dimensions of the separated nanotubes were measured sequentially in a MALS (DAWN) coupled with a UV-detector and a refractive index detector. DAWN detector yields an elution curve that directly represents the size distribution of the sample (fig.2).

Figure 3 shows the cumulative weight fraction versus the root mean square (rms) radius of the purified and cut SWNT samples, respectively. The rms radius of purified SWNT ranges from **120 to 584nm** and they are distributed in three ranges. As it was expected, the size range for cut SWNT is shorter and the larger concentration (94%) ranges from **53 to 134nm**. The average size of purified and cut SWNT samples was also calculated at the same run time in both cases (8 min. and 12min). The results confirm again the shorter size of cut SWNT respect to the purified ones.

Run time (min)	Purified SWNT (nm)	Cut SWNT (nm)
8	233.3 ± 18.2 (0.5 ± 0.1)	105.1 ± 5.1 (0.3 ± 0.1)
12	141.8 ± 13.1 (0.1 ± 0)	86.4 ± 15.3 (0 ± 0)

These results show an alternative method to measure nanoparticles with tubular morphology. The AFFF/DAWN combination is a fast separation method suitable for carbon nanotubes size distribution characterization.

References

[1] Liu et al. Science, **280** (1998) 1253-1256.

Figures

Figure 2 Particle size distribution of cut SWNT-Nanocyl samples by AFFF/DAWN analysis

Figure 1. Set-up for a complete FFF-MALS system (Eclipse, DAWN, Optilab, Agilent HPLC)

Purified SWNT
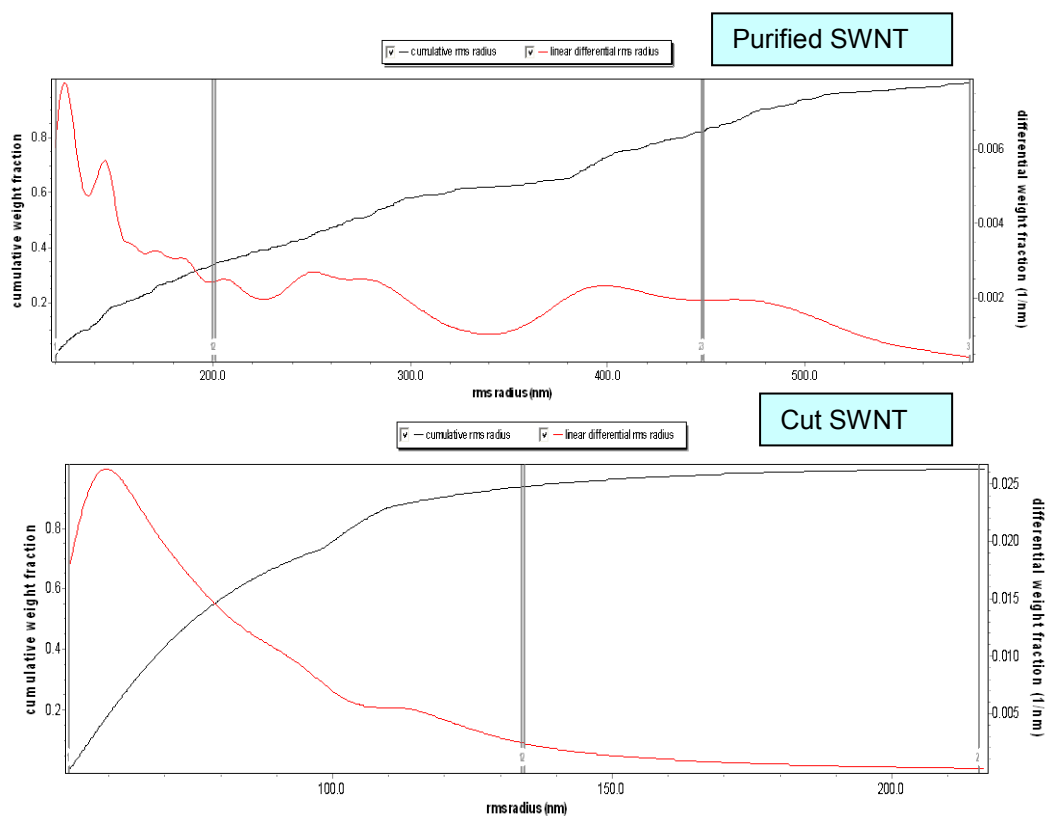
Cut SWNT

Figure 3 Cumulative weight fraction versus rms radius of the purified and cut SWNT samples

SWNT	Name	Type	Start - End	Limits (%)	Cumulative %
	Range 1	rms radius	120.3 - 199.4 nm	0.6 - 33.5	32.9
Purified	Range 2	rms radius	201.1 - 447.6 nm	34.1 - 82.0	47.9
	Range 3	rms radius	448.8 - 583.6 nm	82.2 - 99.7	17.5
Cut	Range 1	rms radius	52.9 - 133.8 nm	0.0 - 93.8	93.8
	Range 2	rms radius	134.4 - 215.5 nm	93.9 - 99.7	5.9

Designing the surface of biomaterials – real-time evaluation using QCM-D

A. Oom

Q-Sense AB, Hängpilsgatan 7, 426 77 Västra Frölunda, Sweden

e-mail: anna.oom@q-sense.com

Introduction

Protein adsorption is of utmost importance when designing new biomaterials, since the introduction of a foreign material into the body will cause a layer of biomolecules on the surface, mainly proteins. The subsequent cellular attachment is therefore in turn mediated by interactions with this protein layer. However, current biomaterials research is limited by the availability of tools for real-time evaluation of such events. Quartz Crystal Microbalance with Dissipation Monitoring (QCM-D) is a versatile instrument that enables real-time studies of processes taking place at a surface. QCM-D simultaneously measures the mass and viscoelastic properties of molecular layers forming on the sensor surface. This provides unique information on the structure of the layer and therefore events such as binding and conformational rearrangements of molecules can easily be tracked. Here we present a number of studies where QCM-D reveals novel insights into how surface modifications affect protein adsorption and cell attachment.

Materials & methods

Protein charge dependence. QCM-D was used to study protein adsorption and correlate the net charge of the protein with the charge density of the surface [1]. Protein adsorption was investigated on PAA (adsorption promoting) and PEO (adsorption resistant) polymer surfaces, using BSA, lysozyme, lactoferrin and fibronectin at pH 4 – 8.5.
Surface morphology. The impact of surface morphology on protein adsorption was investigated in two studies using QCM-D. BSA was adsorbed onto smooth and rough platinum sensor surfaces [2] and fibronectin was adsorbed onto smooth and rough tantalum sensor surfaces [3].
Cell attachment. QCM-D was combined with fluorescence microscopy to monitor cell attachment and spreading onto surfaces preadsorbed with fibronectin, calf serum or albumin [4].

Results & discussion

Protein charge dependence. Each protein exhibited unique adsorption properties, in most cases adsorbed and rearranged in multiple phases, which could be studied in real-time. Fibronectin at pH 4 adsorbed in two phases on PAA and was the only protein to form fibrils in its second phase, most probably due to its unfolded conformation that revealed self-associating domains.

Surface morphology. BSA molecules on the rough surface placed themselves in a more densely packed protein layer and showed a two step adsorption behavior, where the second step involved proteins adsorbing in a more open structure, which was not seen on the smooth surface. The nanoscale roughness induced an increased stiffening of the saturated fibronectin layers. This suggests that the roughness promoted proteins to adsorb in a more spread out rigid conformation which was further supported by differences in antibody adsorption. *Cell attachment.* Depending on the surface coating, the optical image revealed different cell behavior, which was consistent with the QCM-D signal. Interestingly, QCM-D was able to sense events associated with changes in cell-surface contacts and cytoskeleton rearrangements, which were not detectable with microscopy.

Conclusions

QCM-D is a powerful tool for the analysis of protein and cell interactions with surfaces. The real-time analysis enables direct monitoring of the ongoing events in situ. Furthermore, the unique information on viscoelastic properties of adlayers provides valuable insight into protein conformation characteristics and cell behavior phenomena at surfaces, not easily detectable by other methods. Taken together the QCM-D technique is an interesting tool for evaluation of biomolecular structures.

Acknowledgements

References

[1] Belegrinou S, Mannelli I, Lisboa P, Bretagnol F, Valsesia A, Ceccone G, Colpo P, Rossi F (2008) Langmuir, 24, 7251-7261.
[2] Dolatshahi-Pirouz A, Rechendorff K, Hovgaard MB, Chevallier J, Besenbacher F (2008) Colloids and Surfaces B: Biointerfaces, 66, 53-59.
[3] Hovgaard MB, Rechendorff K, Chevallier J, Foss M, Besenbacher F (2008) J. Phys. Chem. B., 112, 8241-8249.

[4] Lord MS, Modin C, Foss M, Duch M, Simmons A, Pedersen FS, Milthorpe BK, Besenbacher F (2006) Biomaterials, 27, 4529-4537.

Water Adsorption on Clean and Oxygen Decorated Metal Substrates

P. Cabrera-Sanfelix,[1,*] S. Maier,[2] I. Stass,[2,3] Byoung-Young Choi,[2] Yu Shi[2,4] A. Arnau,[1,5,6] M. Salmeron[2,4] and D. Sánchez-Portal.[1,6]

[1]Donostia International Physics Center (DIPC), P. Manuel de Lardizabal 4, San Sebastian 20018, Spain

[2]Materials Sciences Division, Lawrence Berkeley National Laboratory, Berkeley, CA 94720, USA

[3]Institut für Experimentalphysik, Freie Universität Berlin, Arnimallee 14, 14195 Berlin, Germany

[4]Dep. of Materials Science and Engineering, Univ. of California Berkeley, Berkeley, CA 94720, USA

[5]Dep. de Física de Materiales UPV/EHU, Fac. de Química, Apdo. 1072, San Sebastian 20080, Spain

[6]Centro de Física de Materiales CSIC-UPV/EHU, Materials Physics Center MPC, P. Manuel de Lardizabal 5, San Sebastian 20018, Spain

swbcasam@sc.ehu.es

Water growth on metal surfaces has been a topic of debate during many years. Nowadays, it is still unclear what are the growth mechanisms and the structures for water layers on many substrates. An important ingredient to understand the self-organization of water in metallic surfaces is the competition between inter-molecular and metal-substrate interactions. This competition determines whether the molecules (i) cluster in a 3D-phase, (ii) wet the surface following a well-ordered 2D-adlayer or even, in a more complicated scenario, (iii) a significant fraction of water molecules in the layer undergo partial dissociation (thus, decomposing into H and OH).[1-3]

Both, the inter-molecular and metal-substrate interactions, are strongly influenced by the substrate itself and by co-adsorbing other adsorbates.[4] In this work we have explored both types of interaction in the adsorption of water on clean Cu(110) and oxygen decorated Ru(0001) surfaces using Density Functional Theory (DFT) calculations motivated by recent scanning tunneling microscopy experiments.

The wetting of Cu(110) has been recently reported. Experimental results showed that at low temperature and coverage water forms one dimensional arrays of side-sharing pentagons on Cu(110).[5, 6] These pentagon row structures can evolve to hexagon row structures as the coverage of water increases beyond 0.2 layers, according to the experimental evidence.[6] It is then proposed that this transformation is mediated by the formation of lobe structure (LS) clusters made of n pentagons connected to a central hexagonal ring (n-LS). These cluster configurations are characterized by the appearance of additional bright spots in the experimental STM images (see Figure 1). The most frequent LS configurations are the 4-LS and they are believed to act as a catalyst for the propagation of H-bond re-orientation along the chain of pentagons and thus, they could be considered the precursors of the transformation to the hexagonal row structure. Using DFT calculations, we compare the structures and energetics of pentagon and hexagon infinite row structures and explore the possible structures for the isolated 4-LS, depending merely on the molecules orientation. Finally, we present the several 4-LS "defects" into the pentagon row structure.[7]

We also present results on the wetting of the oxygen decorated Ru(0001) surface at 0.5 ML oxygen coverage, consistent with the O(2x1)/Ru(0001) surface. We found that the adsorption of water causes a shift of half of the chemisorbed oxygen atoms from hcp sites to fcc sites, creating a (2x2) honeycomb structure. Our calculations show that the energy cost of reconstructing the oxygen overlayer is more than compensated by the adsorption of water on the newly created unbounded Ru atoms. The STM images reveal a (4x2) water super structure, which is due to the existence of two relative orientations of the water molecules. Interestingly, the oxygen honeycomb structure induced by the adsorption of water remains metastable after

water desorption and does not revert to the stable linear 2x1 structure until after temperatures close to 300K.[8]

[1]   P. J. Feibelman, *Sci.* **2002**, *295*, 99.
[2]   A. Michaelides, A. Alavi, D. A. King, *Phys. Rev. B* **2004**, *69*, 113404.
[3]   P. Cabrera-Sanfelix, A. Arnau, A. Mugarza, T. K. Shimizu, M. Salmeron, D. Sanchez-Portal, *Physical Review B* **2008**, *78*.
[4]   P. Cabrera-Sanfelix, D. Sanchez-Portal, A. Mugarza, T. K. Shimizu, M. Salmeron, A. Arnau, *Phys. Rev. B* **2007**, *76*, 205438.
[5]   J. Carrasco, A. Michaelides, M. Forster, S. Haq, R. Raval, A. Hodgson, *Nature Materials* **2009**, *8*, 427.
[6]   B.-Y. Choi, Y. Shi, M. Salmeron, *Submitted* **2010**.
[7]   Cabrera-Sanfelix P et al., *In preparation*.
[8]   S. Maier, P. Cabrera-Sanfelix, I. Stass, D. Sanchez-Portal, A. Arnau, M. Salmeron, *Physical Review B* **2010**, *82*, 075421.
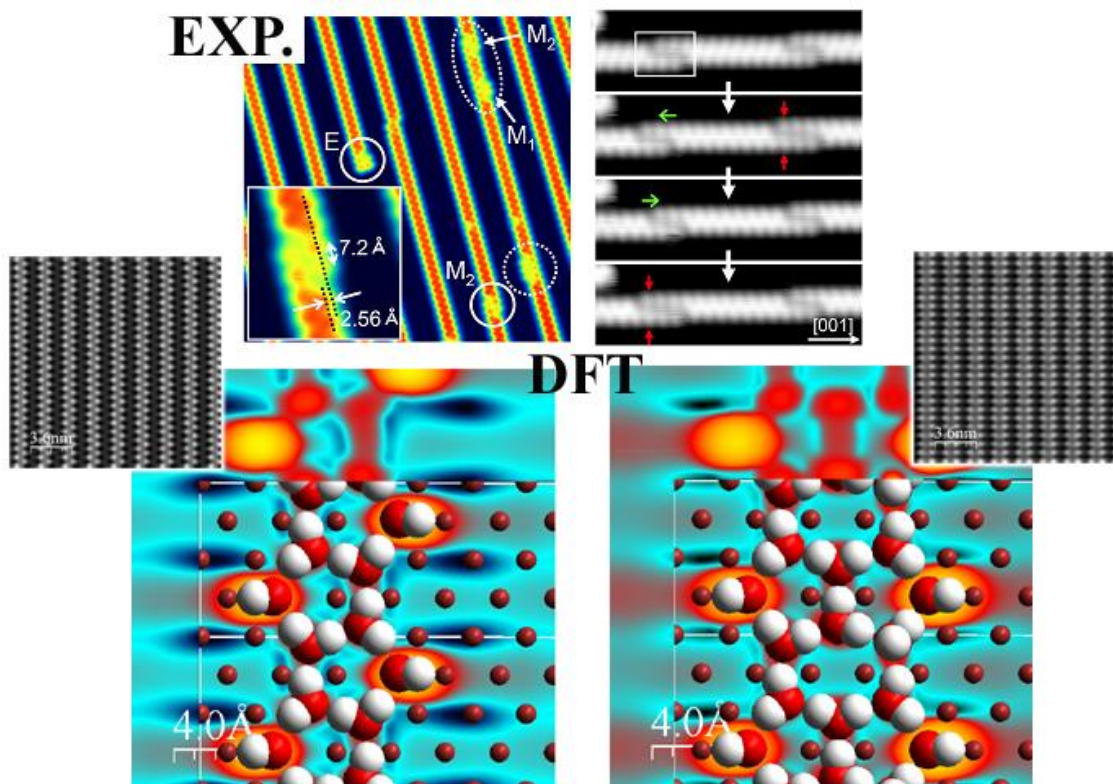
Figure 1. Upper panels correspond to experimental images: on the left STM images (30nm × 30nm) of the Cu(110) surface covered by 0.2 ML water after annealing to 120 K. The peculiar structures (named n-LS) are found in various locations: isolated (I), at the end of chains (E) and in the middle of chains (M_1 and M_2). On the right STM images (5nm × 15nm) of a chain composed of three segments offset by one lattice constant. The first image was obtained at 0.1V and 30pA followed by three successive images at the same bias but higher tunnel current (80, 100 and 120pA). The 4-LS can be displaced right and left along the zigzag chain (green arrows). Downward panels correspond to DFT images for pentagonal row structure, on the left, and, on the right, the proposed hexagonal row structured based on the propagation of 4-LS clusters.

Optimization of CVD processes for the growth of carbon nanotubes with applications in the development of novel polymeric nanocomposites and water purification concepts.

Nuria Campos[1], David Gómez[1], Matías Blanco[2], Patricia Alvarez[2], Rosa Menéndez[2]

[1] ITMA Materials Technology, C/ Calafates 11, 33417, Avilés, Spain
[2] Instituto Nacional del Carbón, CSIC, Apartado 73, 33080, Oviedo, Spain

n.campos@itma.es

1. Introduction

Chemical vapor deposition, is considered the most promising method of synthesis of high-purity, good-quality carbon nanotubes, with the possibility of being upscaled [1]. This technique uses hydrocarbon as a carbon source and transition metals as a catalyst. Albeit many studies on the topic have been released recently, an important effort has to be made to relate slight changes in the process parameters to the final properties of the nanotubes, as industrially fabricated CNTs are still quite non-uniform in morphology and properties.

In present work different processes and catalysts have been evaluated towards the obtaining of tailored carbon nanotubes (CNTs) by means of this technique for applications in the development of nanocomposites and water purification concepts.

2. Fabrication process

2.1. Catalyst preparation

Different alumina-supported iron catalysts have been developed in two different forms on silicon substrates:

- As a liquid suspension of iron nitrate, alumina and a molybdenum salt, spin-coated on a substrate. Iron nitrate is oxidized into iron oxide during heating and is finally reduced in the growth process, alumina acts as a placeholder for iron particles and molybdenum as a growth promoter.

- By the deposition of sputtered thin films (500nm of silica, 10nm of alumina and 5nm of iron). By means of the annealing of the samples in a hydrogen atmosphere, the iron film is nucleated, acting like a seed for the growth of the nanotubes when the hydrocarbon gas is decomposed in a high-temperature process [2].

2.2. CVD process

Two kinds of processes have been developed using ethylene or methane as the carbon source.

- In the first process, there is an initial step in which the sample is soaked in hydrogen at 600ºC. Then, the temperature is elevated to 750ºC and a flow of ethylene is introduced during 1h for the growth of the nanotubes.

- In the second process, the sample is soaked in hydrogen at 900ºC to prepare the catalyst. Afterwards, the growth takes place when methane is introduced at the same temperature during 20min.

3. Results

By the combination of these processes and catalysts (and variations of them), CNTs of different dimensions, purity and morphology have been grown and inspected by field emission scanning electron microscopy (FE-SEM).

Attending to the pursued applications in the development of nanocomposites and water purification systems, a process using ethylene and the thin film catalyst have been selected, leading to high-purity vertically-aligned multi-wall carbon nanotubes, shown in figure 1. This combination produced the largest yield of CNTs per process and unit area of the substrate, as nanotubes of more than 1mm long have been obtained, meeting the requirements in volume for the concerned applications.

By means of transmission electron microscopy, the diameter of carbon nanotubes was determined to be between 10nm and 15nm.

For the optimization of this established process, thermogravimetric analysis (TGA) and Raman spectroscopy were of great help to determine the level of impurities.

TGA (figure 2, left) indicates low concentration of amorphous carbon (which is lost in air at 400ºC), as well as low metal catalyst residues [3], having CNTs with a purity near to 98%.

The time of injection of ethylene was varied between 15min and 2h and it was observed that the length of the nanotubes increased, but after 1h the growth was slower and amorphous carbon appeared. From the Raman measurements (figure 2, right) it can be noted that the amount of the impurities increased with the time of growth, as seen from the relation between the intensity of the peaks D and G [4] for the different samples.

In light of these results, it could be said that the nanotubes obtained as explained above are of very good quality, which makes them be expected to work well as an additive for the fabrication of good properties nanocomposites and also for water purification applications.

4. Application of the obtained CNTs

In the field of the refractory bricks, there is an interest in substituting graphite by CNTs by its inclusion in the precursor resins used for its fabrication, which are expected to improve the durability of the final product. Different kind of carbon nanostructures, including the above described CNTs, have been added to a phenolic resin (Bakelite type) and dispersed with the aid of ultrasounds and mechanical stirrers. Research is at the moment at the stage of comparing the properties and performance of nanocomposites fabricated with commercial CNTs with the ones developed during the project at a lab scale.

Elimination of contaminants in industrial wastewater is another field of interest in which CNTs obtained as explained in this work are being applied. For recalcitrant wastewater purification, carbon nanotubes were oxidized in order to enhance their dispersive properties in water by means of different treatments: i) nitric acid/sulphuric acid, ii) nitric acid/hydrogen peroxide and iii) ammonium hydroxide/hydrogen peroxide. Characterization of the obtained products by TPD and XPS demonstrated the selective introduction of functional groups: carboxilic acid, alcohols and ketones, respectively.

In a similar way, obtained CNTs will be used in different concrete applications of interest to industry, including integrated sensors, ropes and slings, domotic tiles and fire-resistant sandwich panels. These cases of study have been proposed in the framework of NANOCIT, an Alliance of Spanish technological centers created with the aim of promoting collaboration in the field of the development of new materials based on the use of carbon nanostructures.

Acknowledgements

References

[1] C. Zhang, S. Pisana, C.T. Wirth, A. Parvez, C. Ducati, S. Hoffman, J. Robertson, Diamond & Related Materials, 17 (2008), 1447-1451

[2] A. Moisala, A.G. Nasibulin, E.I. Kauppinen, Journal of Physics: Condensed Matter, 15 (2003), S3011-S3035

[3] V. Shanov, Yeo-Heung Yun, M.J. Schulz, Journal of the University Of Chemical Technology and Metallurgy, 41, 4 (2006), 377-390

[4] A. Jorio, E. Kauppinen, Abdou Hassanien, Carbon-Nanotube Metrology, Carbon Nanotubes. Advanced Topics in the Synthesis, Structure, Properties and Applications, Springer (2008), 63-100

Figures
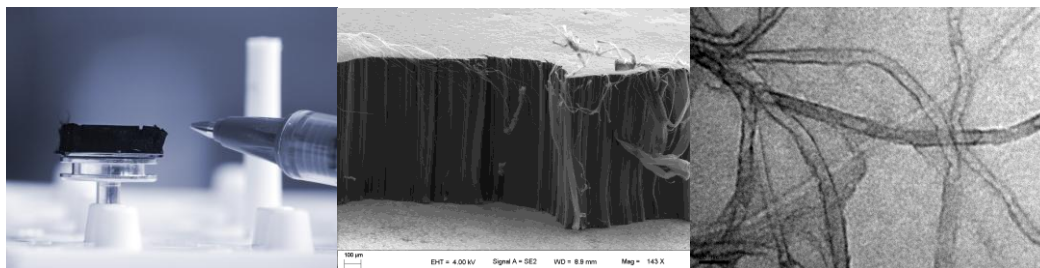
Figure 1. Images of the CNTs obtained at increasing magnification level from left to right. (Photograph, Field Emission Scanning Electron Microscopy and Transmision Electron Microscopy)
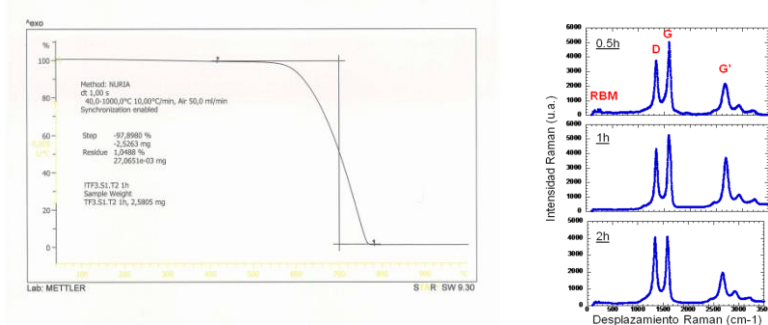
Figure 2. TGA and Raman spectroscopy of the CNTs samples, from which purity was evaluated.

Substitutional doping in MoS$_2$

Xavier Cartoixà, Moisés Yaro, Riccardo Rurali

Departament d'Enginyeria Electrònica, Universitat Autònoma de Barcelona, Bellaterra, Spain
Institut de Ciència de Materials (ICMAB-CSIC), Campus de la UAB, Bellaterra, Spain
Xavier.Cartoixa@uab.es

Planar materials, such as graphene [1,2], have recently raised a great deal of interest due to the exceptional electronic properties, in particular a high electron mobility [3], which render them very attractive as the channel material for a field effect transistor (FET). On the other hand, graphene has a semimetallic character, with the bands crossing at the Fermi point, which causes a residual non-negligible conductivity even in the off state. Thus, great efforts have been made to generate a gap in graphene by the action of external biases, fabrication of bilayered structures, molecular adsorption, strains, etc.; but that has been at a cost to the electronic transport properties [4].

A different approach is to choose a different planar material with a semiconductor character from the onset in order to fabricate an FET channel, such as Radisavljevic *et al.* have recently made [4]. They have used MoS$_2$, which is similar to graphene in the sense that it is a layered hexagonal material with strong covalent intralayer bonding and a weak van der Waals interlayer bonding. This lies at the root of the extremely good properties of MoS$_2$ as an industrial solid lubricant, as well as the facility with which it can be exfoliated into single layers, with a structure shown in Fig. 1. The semiconductor character of the MoS$_2$ single layer is clear in Fig. 2, with a direct GGA band gap of 1.67 eV, comparing to the experimental value of 1.8 eV [5].

Of course, the addition of dopant impurities to a semiconductor is what enables the fabrication of a multitude of interesting devices. We will present first-principles calculations of dopant activation energies of different single substitutional impurities into the MoS$_2$ lattice, in order to identify promising candidates for shallow p- and n-type doping, using a method that we have recently developed [6,7] to correct for the spurious interactions arising from the periodic boundary conditions.

References

[1] A. K. Geim and K. S. Novoselov. Nature Materials **6** (2007) 183.
[2] K. S. Novoselov et al., Science **306** (2004) 666.
[3] K. I. Bolotkin et al., Solid State Commun. **146** (2008) 351.
[4] B. Radisavljevic at al., Nature Nanotechnology **6** (2011) 147.
[5] K. F. Mak et al., Phys. Rev. Lett. **105** (2010) 136805.
[6] R. Rurali and X. Cartoixà, Nano Lett. **9** (2009) 975.
[7] Á. Miranda-Durán, X. Cartoixà, M. Cruz-Irisson and R. Rurali, Nano Lett. **10** (2010) 3590.

Figures
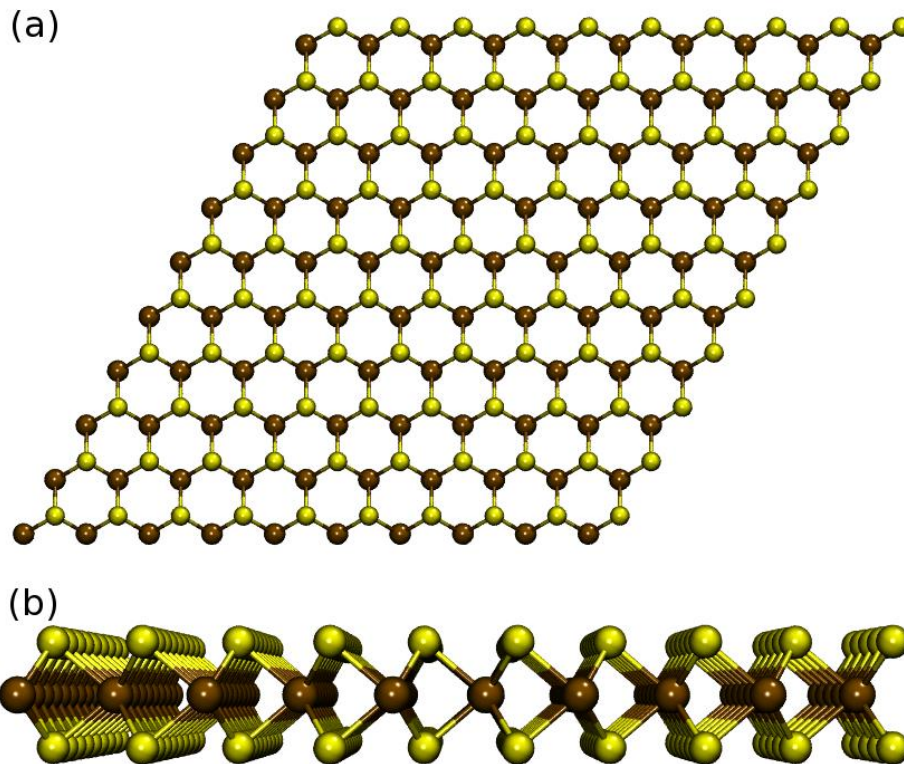
FIG. 1: *(a) Top and (b) side view of a single layer of MoS$_2$.*
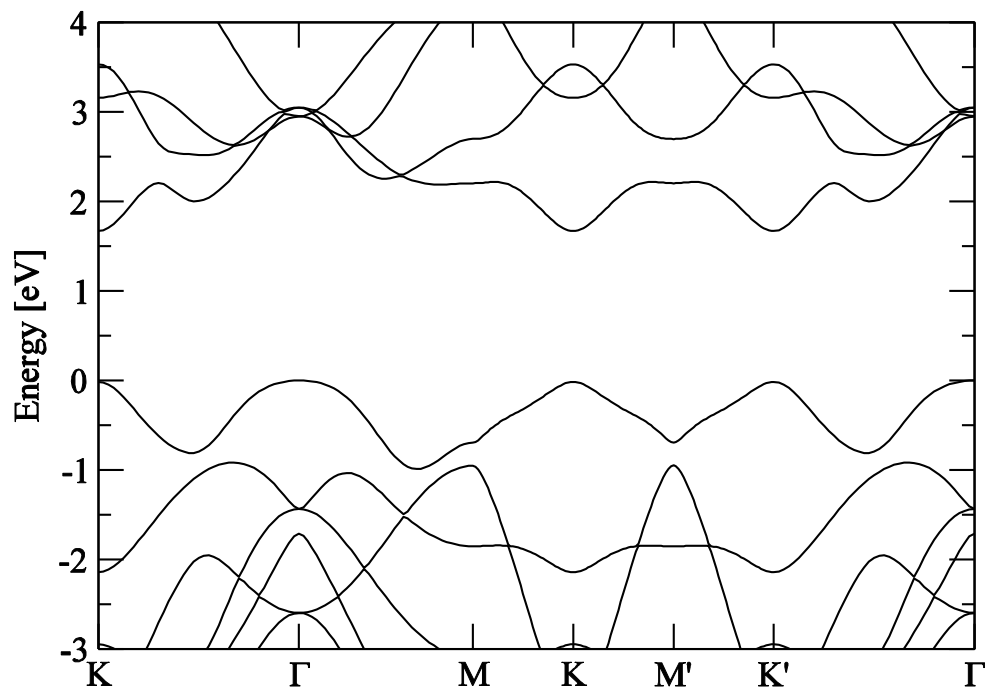
FIG. 2: *Band structure of a single layer of MoS$_2$.*

Influence of n-alkylamine ligands in properties of magnetic palladium nanoparticles

I. Castellanos-Rubio, L. Lezama, M. Insausti, I. Gil de Muro and T. Rojo

Dpto. Química inorgánica, Facultad de Ciencia y Tecnología, UPV/EHU, Bº Sarriena, 48940 Leioa, Spain

Idoia.castellanos@ehu.es

Size confinement to a nanometer scale has induced effects not observed in macroscale. That is the case of magnetic properties, which are often remarkably different from those of their bulk counterparts, in particular in the case of materials that are known to have nonmagnetic or antiferromangetic ground states in bulk [1]. A candidate material for controllable magnetism could be palladium because this metal is nearly ferromagnetic, lying close to a ferromagnetic instability [2]. Consequently, Pd magnetic nanoparticles could play an important role not only in the understanding magnetism at nanoscale, but also in the applications to magnetic devices and especially in biomedical fields because of its good biocompatibility.

In this sense, monodispersed magnetic palladium nanoparticles, between 2 and 4 nm, surrounded by amine ligands have been successfully synthesized and characterized by infrared spectroscopy (IR), X-Ray Diffraction (DRX), thermogravimetry (TG) and Transmission Electron Microscopy (TEM). Finally, the magnetic behaviour has been studied by magnetization measurements. Additionally, the effect of ligand chain length on the particles properties has been analyzed.

Palladium nanoparticles were synthesized following the Brust method [3], which is based on the transfer of $NaPdCl_4$ from an aqueous solution to toluene, using tetraoctylammonium bromide (TOAB) as the phase-transfer reagent. The reduction of the solution, with $NaBH_4$ aqueous solution, in the presence of $CH_3(CH_2)_nNH_2$ (n = 3, 5, 7, 9) ligands yields four kinds of Pd-NR nanoparticles with different chain length. To confirm the attachment of the n-alkylamine ligands to Pd IR spectroscopy was used.

In order to know the stability of the samples and the quantity of organic matter, thermogravimetric measurements were performed. A first mass loss (4-8 %), related to the absorbed solvent, takes place at temperature around 100 ºC. Subsequently, a loss corresponding to the capping agent, above 200 ºC, was observed in the 11% to 28% range depending on the sample.

Size distributions of the nanoparticles are very homegeneous. TEM measurements also indicate that the particle size of each of the four studied systems fluctuate in a specific size range. Furthermore, the particle size decreased with the increase of the carbon chain length of the $CH_3(CH_2)_nNH_2$ ligand. From these measurements together with TG analysis, Pd:N relation on nanoparticle surfaces have been estimated ranging from 6:1 to 1:1, depending on the sample.

The ferromagnetic character of the nanoparticles has been proved by the presence of hysteresis loops in M vs H measurements at 293 K and 5 K. The samples present saturation at low field, around 10 kOe, and coercive fields between 60 and 100 Oe. However, the obtained magnetization values are notoriously variable from one sample to another. Electron magnetic resonance measurements corroborate these results.

References

[1] Crespo, P.; Litrán, Rojas, T.C.; Multigner, M.; de la Fuente, J.M.; Sánchez-López, J.C.; García, M.A. *Phys. Rev. Lett.* **93**, 087204, (2004).
[2] J.F. Janak, *Phys. Rev. B*, **16**, 255, (1977).
[3] Brust, M.; Walker, M.; Bethell, D.; Schiffrin. D.J.; Whyman, R. *J. Chem. Soc., Chem. Commun*. 801, (1994).

Magnetic field sensitive elastic polymeric nanocomposites with tuneable mechanical parameters

M. Castrillon[1], J.G. Meier[1], S. Irusta[2]

Instituto Tecnológico de Aragón (ITA,) C/ María de Luna, nº 7. 50018, Zaragoza, Spain 1.
Instituto de Nanociencia de Aragón, (INA) C/ Mariano Esquillor s/n 500018, Zaragoza, Spain 2.
mcastrillon@ita.es

The identification and characterization of novel materials with enhanced magnetic properties is vital for the development of improved sensors and actuators. In several cases, the identification of new materials can open up innovative applications for magnetic sensors and actuators which were previously not possible[1]. The new generation of magnetic elastomers corresponds to a new type of composites consisting of magnetic nanoparticles dispersed in an elastic polymeric matrix[2]. In comparison with the existing magnetic materials (composed mainly by metals)[3], the polymer technology allows easily components fabrications with diverse forms and mechanical properties. Applications of these nanostructured materials may include force sensors, displacement/positioning devices, torque sensors and field sensors devices[4].

In the present work, magnetic nanocomposites were prepared by both: dispersion and melt-mixing methods[5]. The used elastic polymer matrix was an amorphous thermoplastic elastomer SEBS, characterised by cylindrical phase morphology of the polystyrene blocks in the ethylene-co butylene phase[6,7]. Two types of magnetic nanoparticles were used: 1) Ferromagnetic carbon coated cobalt nanoparticles with average size of 25 nm purchased to Nanoshel[TM] and 2) Superparamagnetic nanoparticles for avoiding strong particle-particle interactions that may result in particles agglomeration. The used superparamagnetic nanoparticles were: A stable dispersion of oleic acid coated magnetite nanoparticles dispersed in chloroform and toluene with average size of 10.5 nm (both purchased to Nanogap)[8], and graphite coated bimetallic FeCo and NiCo nanoparticles synthesised by a solid state chemical vapour deposition method. The nanocomposites were prepared by dispersion and melt-extrusion of magnetic nanoparticles with SEBS polymer using an UP400S ultrasonic processor and a twin-screw microextruder.

The prepared nanocomposites were characterized by transmission electron microscopy (TEM), thermal gravimetric analysis (TGA) and differential scanning calorimetry (DSC). Magnetic properties were evaluated by means of hysteresis loops and ZFC/FC measurements in a superconducting quantum interference device (SQUID). Results showed that with a small content of nanoparticles (<3wt%) a global magnetic response from the composite is achieved.

In order to establish the effect of the external magnetic field on the mechanical behaviour of the resulting composites, they were designed and built two mechanical test assemblies using an electromagnet and neodymium magnets: Shear test with the applied force (Fy) and the direction of the magnetic field (B) perpendicular between them; and a tensile essay (relaxation) with Fy and B parallel between them. A schema of the forces and the external field applied is showed in Fig. 1 for both cases.

It was found that the shear modulus and young modulus are increased by external magnetic field application. The differences in magneto-mechanical response among prepared composites are attributed to the type of used nanoparticles, their magnetic behaviour and magnetization, as well as the nanoparticles real concentration in polymer and the presence of residual solvent in the composites.

Our findings may assist, for example the development of new devices where the mechanical response can be actively controlled in real time by a magnetic field. These concepts would have general implication on the design of specific nanoparticles polymer composites and its processing for dedicated purposes.

References

[1] DC Jiles, CCH Lo, Sensors and Actuators A: Physical. **106** (2003) 3-7.
[2] Z Varga, G Filipcsei, M Zrínyi, Polymer. **47** (2006) 227-233.
[3] RS Popovic, JA Flanagan, PA Besse, Sensors and Actuators A: Physical. **56** (1996) 39-55.
[4] K Singh, A Ohlan, RK Kotnala, AK Bakhshi, SK Dhawan, Mater.Chem.Phys. **112** (2008) 651-658.
[5] G Kickelbick, Progress in Polymer Science. **28** (2003) 83-114.

[6] L Peponi, A Tercjak, L Torre, JM Kenny, I Mondragon, Composites Sci.Technol. **68** (2008) 1631-1636.
[7] MR Bockstaller, RA Mickiewicz, EL Thomas, Adv Mater. **17** (2005) 1331-1349.
[8] W Voit, DK Kim, M Zapke, M Muhammed, KV Rao, Materials research society. **676** (2001).

Figures
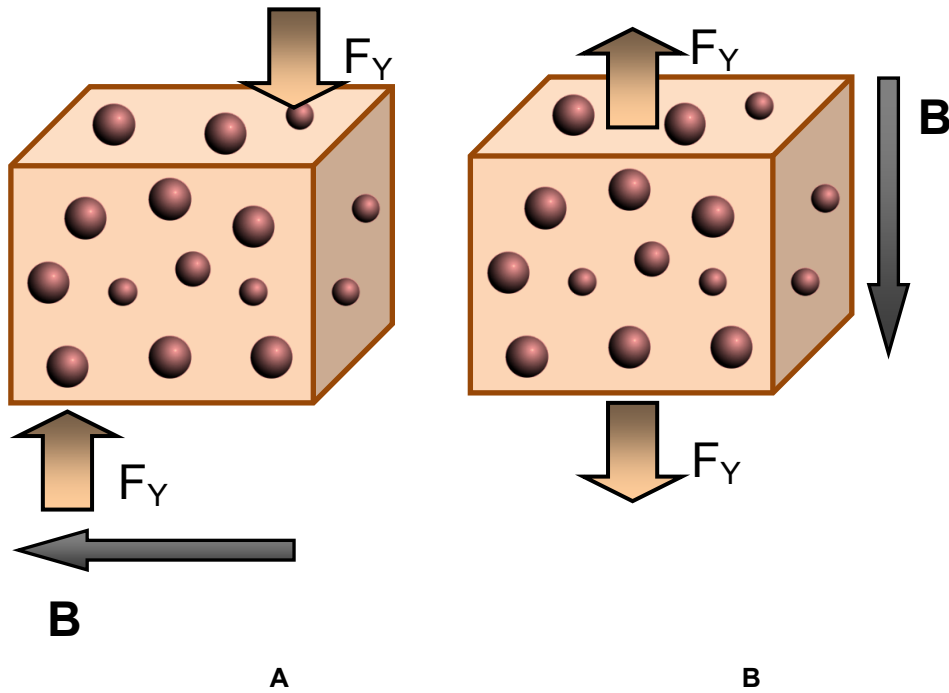
Figure 1. Magneto-mechanical test forces schema. a) Shear test and b)Tensile test (Relaxation).

Transparent and conductive films of carbon nanotubes

Amélie Catheline, Alain Pénicaud

Université de Bordeaux I – CRPP - CNRS, 115 av Schweitzer, Pessac, France
catheline@crpp-bordeaux.cnrs.fr

Transparent and conductive films of carbon nanotubes (CNTs) are under great interest for some years due to the combination of different properties as conductivity, transparency and flexibility. These thin films are investigated to use them as transparent and conductive electrodes in flexible electronic devices.

There are several methods to disperse CNTs such as aqueous dispersion with surfactant, or acid treatment of the CNTs but these techniques tend to damage the nanotubes, reducing the performances of the end material.
In this study, carbon nanotubes were dispersed in an organic solvent by a mild dissolution route[1] : the reduction of CNTs with alkali metals allows dissolution in a solvent without the need of mechanical energy, detrimental to nanotubes. In particular, CNTs are *not* shortened by the mild dissolution process and no additional defects are introduced.

A comparative study was undertaken on films obtained from both dispersions and solutions using single-, few- and multi-walled NTs. Films were obtained by a filtration method and transfer on transparent substrates[2,3]. The transparency of the films has been investigated by UV-visible spectroscopy and linked to the conductivity. Films obtained from solutions show a decrease of one order of magnitude of the surface resistance when compared to dispersions for the same transparency, reaching 105 Ohm/sq at 80% of transmittance for single-walled tubes enriched in metallic NTs.
Our study shows the advantage of the mild dissolution of NTs to prepare transparent and conductive films giving performances close to ITO'ones without any post treatment or any doping of our films.

References

[1] Pénicaud, A.; Poulin, P.; Derré, A.; Anglaret, E.; Petit, P. Journal of the American Chemical Society 2005, 127, 8-9.
[2] Zhou, Y.; Hu, L.; Gruner, G. Appl. Phys. Lett. 2006, 88, 123109-3.
[3] Kong, B.; Yoo, H.; Jung, H. Langmuir 2009, 25, 11008-11013.

Synthesis of Ca(OH)₂ nanoparticles using a renewable feedstock: Medical applications

Leonardo Chávez-Guerrero[1],*, Moisés Hinojosa R[1].

[1]School of Electrical and Mechanical Engineering of the Universidad Autónoma de Nuevo León
Av. Universidad s/n, Cd. Universitaria, C.P. 66451. Nuevo León, México.

*Laboratoire d'électrochimie, chimie des interfaces et modélisation pour l'énergie. Chimie ParisTech.
11, rue Pierre et Marie Curie. 75231 PARIS Cedex 05, France.
E-mail: leonardo.chavezgr@uanl.edu.mx.

The agave bagasse is a byproduct generated in the mezcal and tequila industry (alcoholic beverage). Normally it is burned to reduce its volume, then a byproduct is generated in the form of ash, which can contaminate the water in rivers and lakes near the production places called "mezcaleras". It is known that 15-33 kg of agave are needed to produce one liter of mezcal or tequila [1-2]. Tequila production in the first 6 months of the 2008 was 8254 L per month, this information is given in order to have an idea of the mezcal production and consequently the huge amount of bagasse and ash produced [3].

This report details measurements of the A*gave salmiana* fiber transformation after the burning process in order to obtain $Ca(OH)_2$ nanoparticles. The wasted ash ($CaCO_3$) was heated at 950 ºC to obtain lime (CaO), then it was hydrolyzed to get hydrated lime ($Ca(OH)_2$) in the form of microcrystals and nanoparticles. The compounds were indentified using X-ray diffractrograms [4-5].

The use of calcium hydroxide, was introduced by Hermann in 1920 and has been used within the root canal system for the control of inflammatory root resorption after luxation and avulsion injuries. The high pH and antimicrobial properties of $Ca(OH)_2$, may account for its effectiveness as an intercanal inter-appointment medicament and an inhibitor of inflammatory root resorption [6].

Thermal (TGA), elemental (SEM) and morphological characterization (AFM) of the ash were done. The images obtained by scanning electronic microscope (SEM) showed all the morphological transformations of the samples through the whole process (**Fig. 1**). Experiments showed that 16% of ash was produced in the burning process of agave bagasse (450 ºC), and 66% of the ash remains after heating (950 ºC) in the form of calcium oxide.

In preliminary experiments the $Ca(OH)_2$ nanoparticles were compared with a commercial material used in endodontic procedures (root canal treatment), showing promising results (**Fig. 2**).

We have found calcium hydroxide nanoparticles (cylindrical) in the ash, which measure 800 x 28 nm (**Fig. 3**). These nanoparticles were obtained by taking advantage of the natural structure of A*gave salmiana* that grows in arid lands, which creates an easy way to produce nanoparticles in a sustainable way using renewable feedstock.

References

[1] Jenna Kuttruff et al. Science 281, 72 (1998).
[2] Antonio de León Rodríguez et al. J. Agric. Food Chem. 54 (2006), 1337-1341.
[3] INEGI 2008. National Institute of Statistics and Geography. Bebidas destiladas de agave/tequila/ volumen, México. Access 12/17/2009. <http://dgcnesyp.inegi.org.mx/cgi-win/bdieintsi.exe/>
[4] L. Chávez-Guerrero, J. Flores, B.I Kharissov. Chemosphere 81 (2010), 633-638.
[5] L. Chávez-Guerrero and M. Hinojosa. Fuel 89 (2010) 4049-4052.
[6] Glen E. Doyon,Thom Dumsha, and J. Anthony von Fraunhofer. JOE 31 (2205), 895-897.
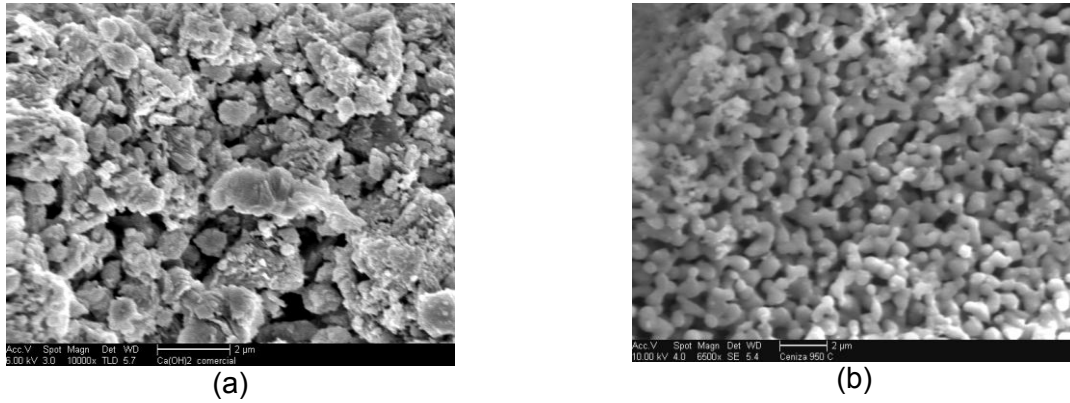
Fig 1.- A sample of commercial Ca(OH)$_2$ is shown in (a) while in (b) the Ca(OH)$_2$ made using ash is showing the structure of one fiber and its natural structure.
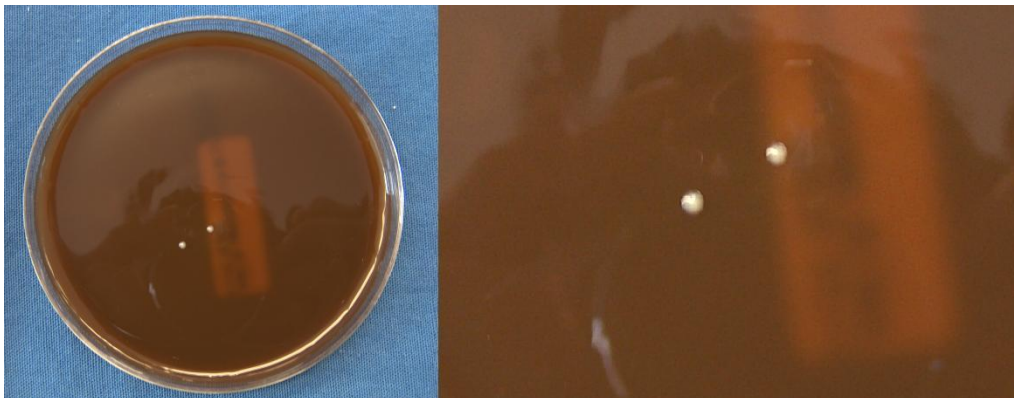
Fig 2.- Preliminary experiments using the Ca(OH)$_2$ nanoparticles in a Petri dish with Enterococcus faecalis.
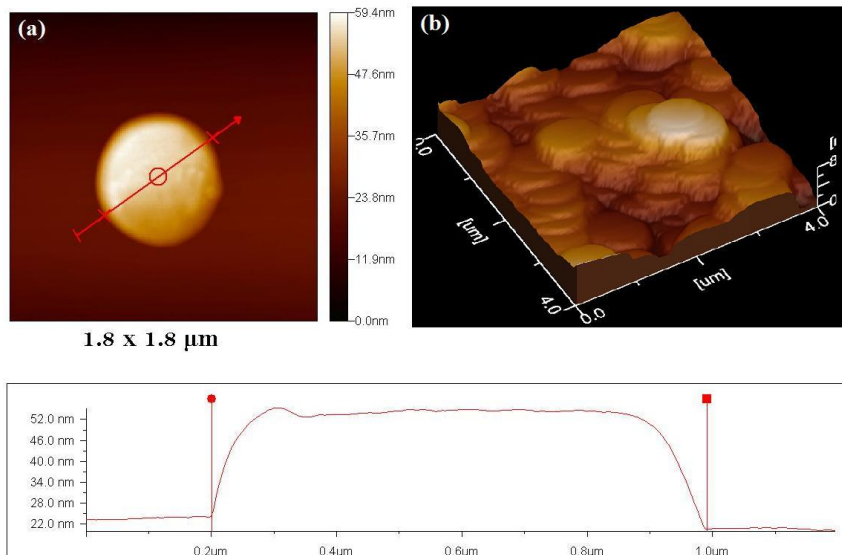
Fig 3.- One isolated nanoparticle is measured using the AFM, where it can be seen the cylindrical form and the dimensions ∅ 800 nm x 28 nm (a). A 3D image of the nanoparticles showing the cylindrical shape (b).

Mechanisms of Perpendicular Magnetic Anisotropy at Fe(001)|MgO(001) Interfaces

H. X. Yang[1], J. H. Lee[1,2], **M. Chshiev[1]**, A. Manchon[1,3], K. H. Shin[2] and B. Dieny[1]

[1]SPINTEC, UMR-8191 CEA/CNRS/UJF Grenoble 1, 38054 Grenoble, France
[2]Korea Institute of Science and Technology, Seoul 136-791, Korea
[3]King Abdullah University of Science and Technology, Thuwal 23955-6900, Saudi Arabia
mair.chshiev@cea.fr

Perpendicular magnetic anisotropy (PMA) at the interface between ferromagnetic (FM) and non-magnetic layers has become of major interest in a view of next generations of magnetic tunnel junction (MTJ) based spintronic devices with increased density and thermal stability. The presence of a heavy non-magnetic layer (Pt, Pd, Au, W, Mo) at the interfaces was believed to be essential to trigger the PMA due to strong spin orbit interaction (SOI) [1] but this yield low spin polarisation and increased Gilbert damping which detrimental for spin transfer torque based devices. However, the PMA with surprisingly large values up to 1 to 2 erg/cm^2 have been first observed at Co(Fe)|MOx interfaces (M=Ta, Mg, Al, Ru etc) [2] despite the weak SOI. Furthermore, large PMA values have been reported for Co|MgO [3] and CoFeB|MgO magnetic tunnel junctions MTJs [4]. The latter have been extensively studied because of Bloch state symmetry based spin filtering phenomenon leading to high tunnel magnetoresistance (TMR) values [5] making them ideally suitable for implementation in hard disk reading heads or as bit cells in magnetic random access memories (MRAM).

Here we investigate the effect of interfacial oxidation conditions on the PMA in Fe(001)|MgO(001) MTJs and elucidate mechanisms responsible for the PMA from first-principles [6]. Two structures have been chosen to model the ideal and overoxidized interfaces as shown in Fig. 1(a) and (b), respectively. These structures be viewed as a model system for FM|MOx interfaces comprising bcc electrodes including Co$_x$Fe$_{(1-x)}$ alloys. Full structural relaxation in shape and volume has been performed. We found very large PMA values up to 2.96erg/cm^2 [7] for MTJs with pure interfaces in agreement with recent experiment [4]. Furthermore, the PMA weakens in case of overoxidized interfaces (see below) indicating that PMA correlates with TMR) in agreement with experiment [8]. In order to understand the correlation between PMA and TMR, in Fig. 1(c) we plot the wave function character of Δ_1 Bloch state as a function of the position across the supercells used for PMA calculations. One can clearly see that the Δ_1 decay rate is strongly enhanced in the case of overoxidized interface compared to the ideal one.

To elucidate the PMA origin at Fe|MgO interfaces, we performed detailed analysis of the impact of SOI on electronic band structure with out-of-plane (d_{z2}, d_{xz}, d_{yz}) and in-plane (d_{x2-y2}, d_{xy}) Fe-3d and O-p_z orbital character. When no SOI is included (middle subcolumns in Fig. 2a), the band level resulting from hybridization between Fe-d_{z2} and O-p_z orbitals is present. The double degenerated bands with Δ_5 symmetry related to minority Fe are also present close to the Fermi level. When spin-orbit interaction is switched on, the degeneracy is lifted and majority Δ_1 and minority Δ_5 are mixed up producing bands with both symmetry characters. As a result, band levels with d_{z2}, d_{xz}, d_{yz} and p_z character split around the Fermi level and this splitting is larger and the lowest band deeper for out-of-plane magnetization orientation as clearly seen in left and right subcolumns in Fig.2(a), respectively. Thus, the lift of degeneracy of d_{xz} and d_{yz} orbitals along with their mixing with Fe-d_{z2} and O-p_z orbitals is at origin of perpendicular magnetic anisotropy for pure Fe|MgO interfaces.

Next, we proceed with the same analysis for overoxidized Fe|MgO interfaces. In this case (Fig.2b), SOI lifts again the degeneracy for states with $d_{xz,yz}$ causing stronger splitting and deeper level position in case of out-of-plane orientation of magnetization compared to the in-plane one. However, these states are not mixed anymore with Fe-d_{z2} and O-p_z orbitals due to local charge redistribution induced by additional oxygen atoms [9]. Since d_{z2} and p_z orbital hybridization which is mainly responsible for PMA is not splitted, the anisotropy is significantly reduced (0.98 erg/cm^2).

References

[1] D. Weller et al, Phys. Rev. B, **49** (1994) 12888; G. Daalderop et al, Phys. Rev. B, **50** (1994) 9989.
[2] S. Monso et al, Appl. Phys. Lett., **80** (2002) 4157; B. Rodmacq et al, J. Appl. Phys., **93** (2003) 7513.
[3] L. E. Nistor et al, Phys. Rev. B, **81** (2010) 220407.
[4] S. Ikeda et al, Nature Mater., **9** (2010) 271.
[5] W. H. Butler et al, Phys. Rev. B, **63** (2001) 054416; J. Mathon et al, Phys. Rev. B, **63** (2001) 220403.
[6] G. Kresse and J. Hafner, Phys. Rev. B 47, 558 (1993); 54, 11169 (1996); Comput. Mater. Sci. 6, 15 (1996).
[7] H. X. Yang et al, arXiv:1011.5667.
[8] L. E. Nistor et al, IEEE Transactions on Magnetics, **46** (2010) 1412.
[9] X.-G. Zhang and W. H. Butler, Phys. Rev. B, **68** (2003) 092402.

Figures
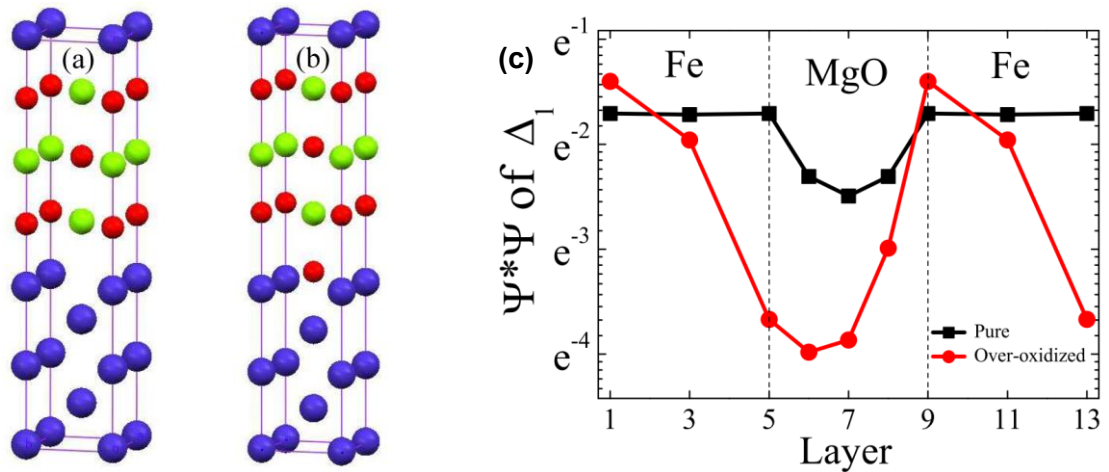
Figure 1. Schematics of the calculated crystalline structures for (a) pure, and (b) over-oxidized Fe(001)| MgO(001) (Fe, Mg and O are represented by blue, green and red balls respectively); (c) Δ_1 Bloch state character at Γ-point around the Fermi level as a function of layer number in pure and over-oxidized interfaces shown in (a) and (b), respectively.
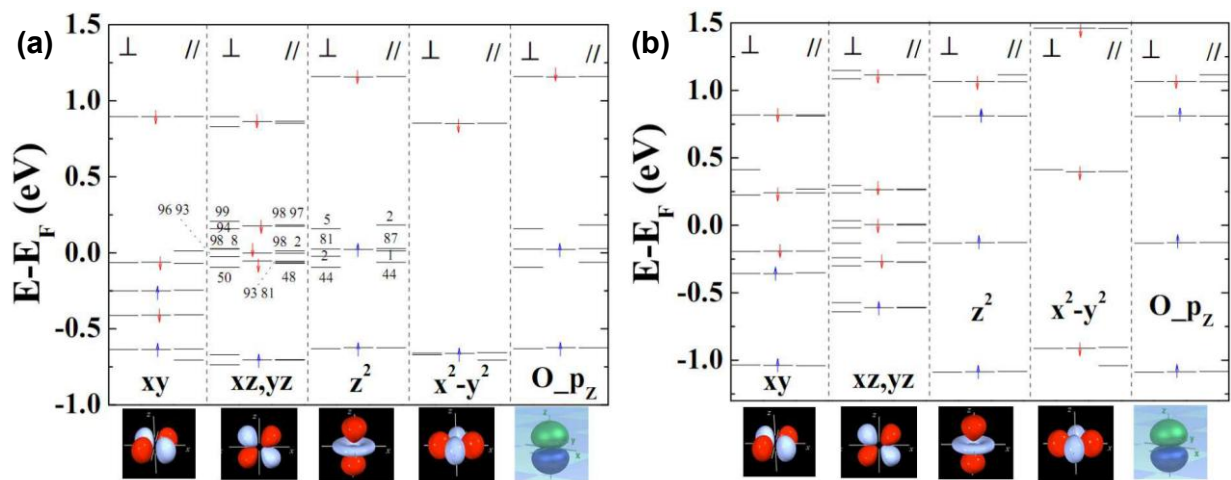
Figure 2. Spin-orbit coupling effects on wave function character at Γ point of interfacial Fe-d and neighbor oxygen p_z orbital for (a) pure and (b) over-oxidized Fe|MgO interfaces. Three subcolumns in each column show the band levels for out-of-plane (left) and in-plane (right) orientation of magnetization as well as for the case with no spin-orbit interaction included(middle), respectively. Numbers are the percentage of the orbital character components within Wigner-Seitz spheres around interfacial atoms.

ENZYME COUPLED GOLD NANOPARTICLES: COMPARISON BETWEEN CARBODIIMIDE AND PHYSICAL ADSORPTION

Paula Ciaurriz[1], Edurne Teiletxea Malda[1,2], Luis Olangua[1], Aaron C. Asensio[1], Jose F. Moran[2]

[1]FideNa, Edificio Jerónimo de Ayanz, C/ Tajonar s/n, 31006 Pamplona, Navarra, Spain
[2]Instituto de Agrobiotecnología, Universidad Pública de Navarra-CSIC-Gobierno de Navarra, Campus de Arrosadia s/n, 31006, Pamplona, Navarra,
paula.ciaurriz@fidena.es

Conjugation of biomolecules with inorganic materials provides access to a variety of functional hybrid systems with applications in biotechnology, medicine and catalysis. Coupling gold nanoparticles (AuNPs) and protein/enzymes allow us to design multifunctional nanocarriers for new therapy and sensing technology [1]. In the case of enzymes, the effective conjugates require the retention of protein structure and function [2].

The aim of this work is to design multifunctional protein nanocarriers. For this purpose a superoxide dismutase (SOD) enzyme (VuFeSOD) is used as a model protein and 15nm AuNPs as a carrier.

SOD is a metallo-enzyme that catalyzes the dismutation of superoxide radicals into hydrogen peroxide and molecular oxygen. These enzymes have great physiological significance and therapeutic potential in the prevention of the oxidative damage from superoxide radicals. The superoxide radical and SOD have been implicated in many disease states including inflammatory diseases, diseases of ischemia and reperfusion, neurodegenerative diseases, and cancer, as well as more subtle roles in cell signaling and perhaps in immune function [3]. FeSOD, a plant superoxide dismutase, is a very stable biomolecule. It contains a Fe atom in a well characterized 3D protein structure [4], which may serve as model for conjugates studies, as well as for developing methods and strategies easily applicable to human SODs.

AuNPs are excellent candidates for protein bioconjugation due to their high surface volume ratio, biocompatibility, and the ability to form functionalized bioconjugates via simple chemistry [5-6].

In this work we present the comparison between covalent conjugation and physical adsorption of FeSOD on 15nm AuNPs. Our approach is based on the utilization of different concentration of mercaptoundecanoic acid (MUA) capped AuNPs for covalent linkage with the protein. The covalent conjugates were obtained by water soluble carbodiimide reactions [sulfo-NHS (N-hydroxysulfo-succinimide) and EDC (1-ethyl3(3-dimethylaminopropyl) carbodiimide hydrochloryde)]. We tested different reaction conditions and measured the biological activity of the conjugates. The results indicated that the enzyme activity is affected by the conjugation method, and the optimal protocol for the conjugation is achieved.

The formation of the conjugates, stability, and activity of the different steps were study by dynamic light scattering (DLS), ζ-potential measurement, UV-VIS spectroscopy, scanning electron microscopy and agarose gel electrophoresis.

Acknowledgements

References

[1] M.Srinivas et al., Advanced drug delivery Reviews **62** (2010) 1080.

[2] M-E Aubin-Tam et al., Biomedical Materials, **3** (2008) 034001.

[3] McCord et al, Biomedicine & Pharmacotherapy, **59** (2005) 139.

[4] Muñoz, I.G., et al., Acta Crystallographica - Section D Biological Crystallography, **59** (2003) 1070.

[5] Angshurman Pal et al., Colloids and Surfaces A: Physicochem. Eng. Aspects, **302** (2007) 51.

[6] Brust, M., et al Colloids Surface A: Physicochem. Eng. Asp, **202** (2002) 17.

Control of the surface chemistry and selectivity of a CO oxidation catalyst by changing the shape of its oxide support nanoparticles

J. C. Conesa, D. Gamarra, A. Martínez-Arias, A. López-Cámara, D. Olea, M. Monte
Instituto de Catálisis y Petroleoquímica, CSIC, Marie Curie 2, 28049 Madrid, Spain
jcconesa@icp.csic.es

In previous works of our laboratory[1], the active species in CuO/CeO_2 catalysts used for mild temperature preferential oxidation of CO by O_2 in presence of H_2 (PROX process) have been found by several experimental techniques to be formed by partially reduced CuO nanoclusters dispersed on the ceria surface. Trying to influence the catalytic properties by tuning the $CuO-CeO_2$ interfacial interaction, CuO (1% by weight) has been deposited on different high surface area nanocrystalline ceria supports made by hydrothermal or precipitation methods, which display specific morphologies exposing different crystal planes of the CeO_2 lattice (Fig. 1).

The ceria material alone shows already different surface chemistry depending on the surface crystal planes exposed. Thus CeO_2 nanocubes exposing mostly (100) faces display in the $CO + O_2$ reaction higher specific rate per surface area than other ceria preparations, while stabilizing a different type of surface carbonates and higher amounts of acidic OH groups as shown by *in situ* IR spectra (Fig. 2).

In the case of the CuO/CeO_2 catalysts made by impregnation on these different ceria materials, different chemistry in the PROX process is also evidenced both by the *in situ* IR spectra and the reaction products analysis. Those spectra display different carbonate groups on the different samples, similarly to what is observed for pure CeO_2 in the $CO + O_2$ reaction; furthermore, they show Cu^+-CO carbonyls in higher amounts on the ceria nanocube-supported sample, in spite of the lower CuO dispersion that could be expected in this sample if one considers simply its lower specific surface area (Fig. 3). It seems thus that the ceria (100) surface stabilizes a higher CuO dispersion or/and a higher surface density of the Cu^+ species that produce these carbonyls.

This nanocube-based sample provides lower reaction rate than the other catalysts in the PROX reaction (Fig. 4a); this may be due to its lower surface area, although if compared with the intensity of the IR peak due Cu^+-CO species (Fig. 4b) it questions previous interpretations about the direct relationship between the amount of these carbonyls and the catalytic activity. However, if reaction contact times are adjusted to give at the same temperature (130 ºC and above) a similar overall CO conversion degree (90% and above), the product analysis shows that the nanocube-supported catalyst gives, for the same conversion level, clearly better selectivities (i.e. it oxidizes less H_2) than the other more active catalysts (Fig. 4). This evidences again that different chemical reactivity patterns are displayed when the type of crystal plane exposed at the surface by the ceria support is different. Efforts to characterize with AFM the CuO species dispersed on nanocube-shaped ceria, as well as DFT quantum modeling of the different situations, have been started to better understand the features of these catalysts.

References

[1] D. Gamarra *et al.*, J. Phys. Chem. C **111** (2007) 11026; and refs. therein

Figures
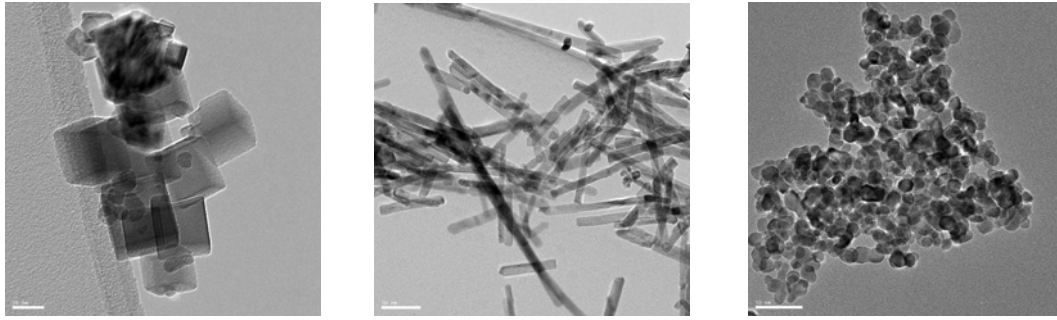
Fig. 1 TEM images of different CeO₂ preparations: nanocubes, nanorods and microspheres
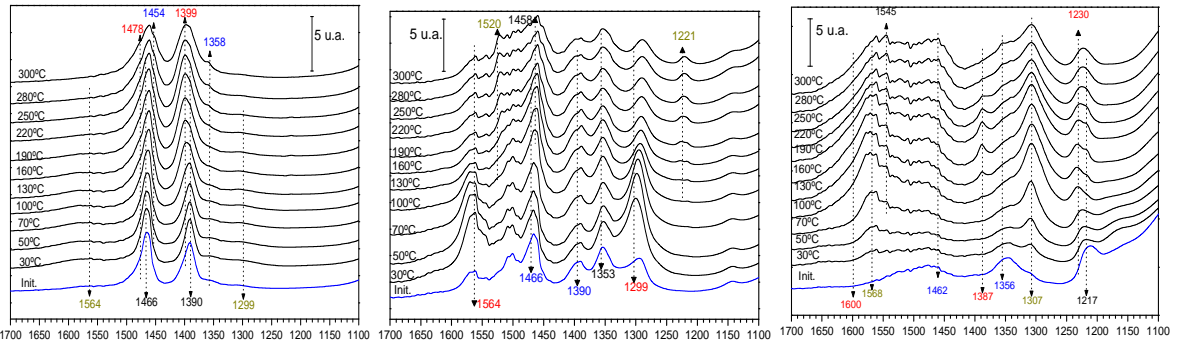
Fig. 2 IR spectra (carbonate range) of differently shaped CeO₂ particles under T-programmed CO + O₂ reaction
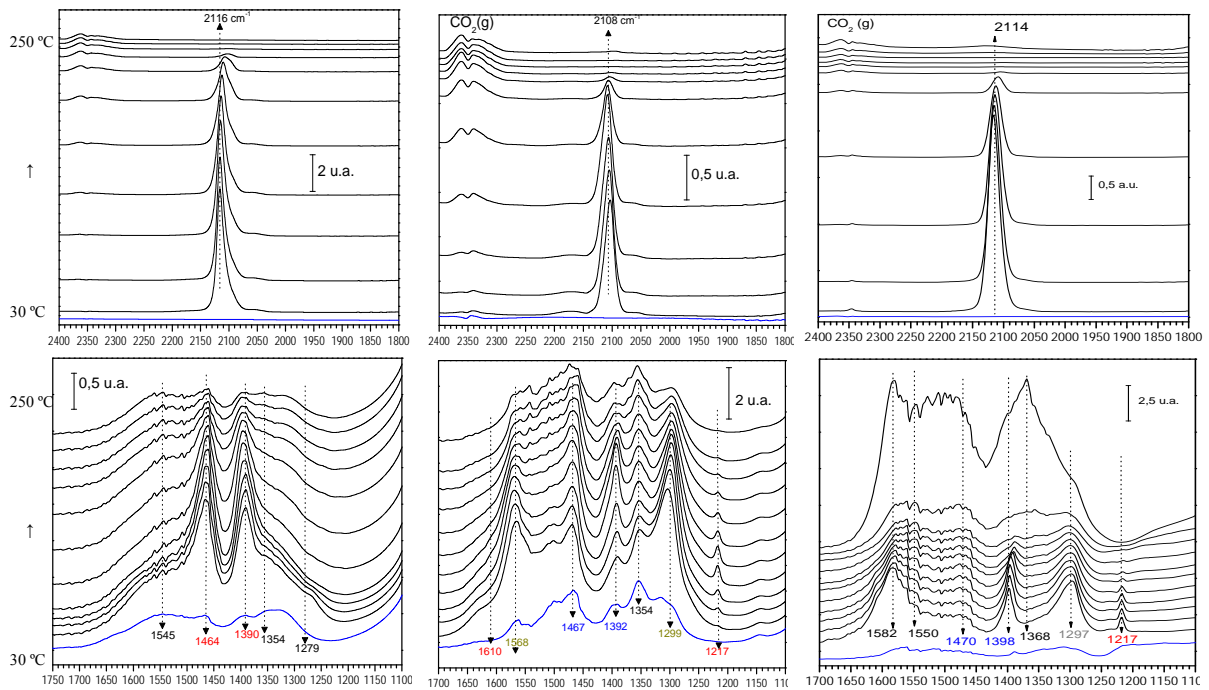
Fig. 3 IR spectra of different CuO/CeO₂ samples under the CO + O₂ + H₂ reaction at increasing temperatures
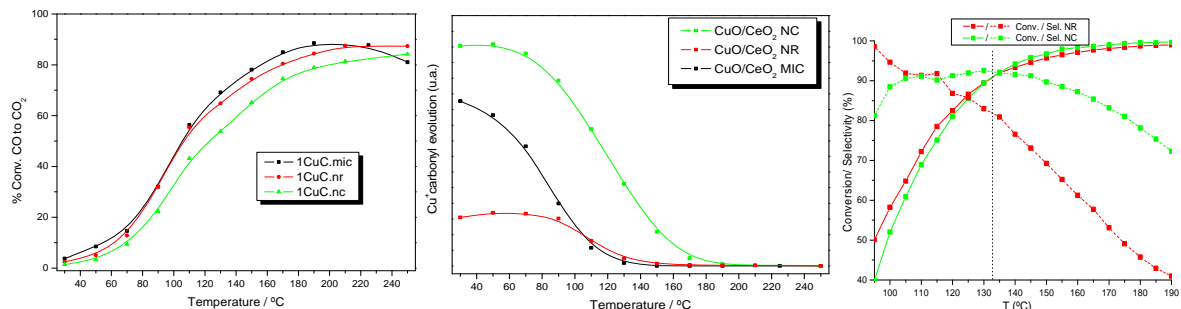
Fig. 4 Data obtained on different CuO/CeO₂ samples under CO + O₂ + H₂ reaction: evolution of a) products and b) Cu⁺-CO IR band; c) activity and selectivity of nanocube- and nanorod-based samples at tuned contact times

A DFT Study of the Interaction of Surfactants Containing a Sulfuric Group with a (5,5) Carbon Nanotube

Nicolas A. Cordero[1,2] and Julio A. Alonso[3,4]

[1] Departamento de Fisica, Universidad de Burgos, C/Villadiego s/n, E-09001 Burgos, Spain
[2] Department of Materials Science and Engineering, University of Pennsylvania,
3231 Walnut St., Philadelphia, PA 19104, USA
[3] Departamento de Fisica Teorica, Atomica y Optica, Universidad de Valladolid,
Prado de la Magdalena, E-47011 Valladolid, Spain,
[4] Departamento de Fisica de Materiales, Universidad del Pais Vasco, and Donostia International
Physics Center (DIPC), Paseo Manuel de Lardizabal 4, E-20018 San Sebastian, Spain

ncordero@ubu.es

The extraordinary mechanical, electronic, and transport properties of single-walled carbon nanotubes (SWCNTs) have led to an enormous interest in them from both fundamental and technological points of view. SWCNTs are produced in bundles held together by van der Waals forces and have to be disentangled in order to separate them by length and chirality. The problem is their insolubility in either water or organic solvents. Both mechanical and chemical methods can be used to disperse SWCNTs in a liquid environment. These can be grouped in three categories: sonication, chemical functionalization, and dispersion with surfactants. Sonication can break the nanotubes, while functionalization can modify the surface of the tubes and affect its electrical, mechanical, and optical properties. The use of surfactants appears then as the most appealing alternative. Among the best surfactant molecules for dispersing SWCNTs are sodium dodecyl sulfate (SDS), sodium dodecylbenzene sulfonate (NaDDBS), and sodium polystyrene sulfonate (NaPSS). All of them have in common a sulfonate head group with a Na atom. Sulfuric acid itself is a good nanotube disperser, the proposed reason being the protonation of SWCNTs by this acid, but surfactants containing a sulfuric head group with a Na atom are better for dispersing carbon nanotubes. Nevertheless, there is no explanation for the importance of the sodium atom in the head group. We have thus studied the interaction between sulfuric acid (H_2SO_4) (see Fig. 1), sodium bisulfate ($NaHSO_4$) (see Fig. 2), and sodium butyl sulfate ($NaSO_4$-C_4H_9 or NaBS) (see Fig. 3) molecules with a (5,5) SWCNT in order to shed some light on this point[1].

We have analyzed the interaction of sulfuric acid, sodium bisulfate, and sodium butyl sulfate molecules with a (5,5) SWCNT using the Density Functional Theory (DFT) and a supercell model. The interaction does not affect the geometrical structure of the nanotube. The binding energies are large enough for the adsorbed molecules to act as surfactants. But these energies are at the same time small enough for the nanotube to be easily cleaned afterwards. There is electronic charge transfer from the nanotube to the adsorbed molecule, but the interaction cannot be completely understood only in terms of the global charge transfer. It is necessary to consider the charge transfer to the atoms close to the tube and the number of oxygen atoms not far from it. When these molecules are adsorbed on the tube there is protonation of the latter. In spite of the curvature, the results for sulfuric acid are similar to those previously obtained for its interaction with graphene[2]. Binding energy and charge transfer are bigger for the cis conformer than for the trans conformer. Besides, the DOS of the tube close to the Fermi energy is not affected by the presence of the acid. In the case of sodium bisulfate three equilibrium configurations have been studied. Once again, there is protonation of the tube and the cis isomer is more tightly bound than the trans isomer, but a new feature appears: The presence of a sodium atom pointing to the tube increases the DOS in the region close to the Fermi energy. This feature also appears in the case of sodium butyl sulfate. When the alkyl tail is pointed to the tube there is no change in the DOS near the Fermi energy but when the molecule head is close to the tube (independently of the molecule orientation) this DOS enhancement is observed. This fact could play a role in molecules with a sodium atom in a sulfonate head being better nanotube surfactants than those with a hydrogen atom in its place. To check if this is so, it will be necessary to include solvent (i.e., water) molecules in the calculations.

References

[1] N.A. Cordero and J.A. Alonso, J. Phys. Chem. C, **114** (2010) 17249.
[2] N.A. Cordero and J.A. Alonso, Nanotechnology, **18** (2007) 485705.

Figures
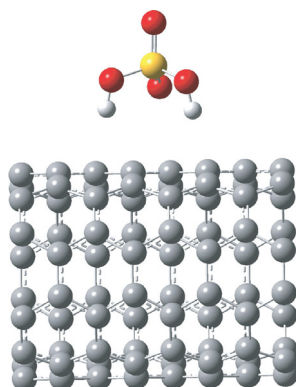
Fig. 1 Equilibrium geometry for a cis-H2SO$_4$ molecule adsorbed on a (5,5) carbon nanotube
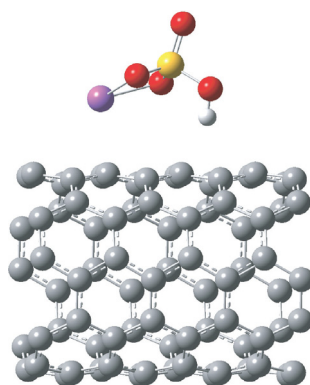
Fig. 2 Equilibrium geometry for a cis-NaHSO$_4$ molecule adsorbed on a (5,5) carbon nanotube.
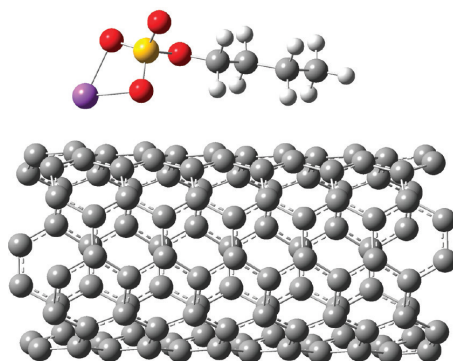
Fig. 3 Equilibrium geometry for a NaSO4-C4H9 molecule aligned with a (5,5) carbon nanotube

W- based superconducting ultranarrow nanowires grown by Focused-Ion-Beam induced deposition

R. Córdoba[1,2], J. Sesé[1,2], M. R. Ibarra[1,2,3], I. Guillamón[4], H. Suderow[4], S. Vieira[4], J. J. Palacios[5] and J. M. De Teresa[2,3]

[1]Instituto de Nanociencia de Aragón, Universidad de Zaragoza, Zaragoza, 50018, Spain
[2]Departamento de Física de la Materia Condensada, Universidad de Zaragoza, Zaragoza, 50009, Spain
[3]Instituto de Ciencia de Materiales de Aragón, Universidad de Zaragoza-CSIC, Zaragoza, 50009, Spain
[4]Laboratorio de Bajas Temperaturas, Departamento de Física de la Materia Condensada, Instituto de Ciencia de Materiales Nicolás Cabrera, Facultad de Ciencias, Universidad Autónoma de Madrid, E-28049, Madrid, Spain
[5]Departamento de Física Teórica de la Materia Condensada, Universidad Autónoma de Madrid, Madrid 28049, Spain

rocorcas@unizar.es

The fabrication of superconducting nanostructures is opening interesting research fields in Nanotechnology [1]. Focused-ion-beam-induced-deposition (FIBID) is a powerful single-step technique that allows the control of the growth of nanostructures on any substrate where precursor gas molecules are adsorbed and dissociated by the focused-ion-beam (FIB) scanning [2]. It was found that FIBID can produce superconducting W-based nanostructures with T_C ~5 K [3]. Recently, it was demonstrated using Scanning Tunnel Microscopy/Spectroscopy (STM/S) techniques that this material follows the BCS theory precisely, allowing for the direct observation of the melting of the two-dimensional vortex lattice, and the motion of vortex bundles with preferential direction [4]. Its technological potential has also been demonstrated for the repair of damaged micro-SQUIDs or the conversion of SQUIDs into highly sensitive SQUID-susceptometers [5].

In the present work, we report the growth of W-FIBID superconducting ultranarrow nanowires (NWs) with the minimum lateral size (~50 nm) achieved so far by means of FIBID (Figure 1). The dependence of resistivity as a function of temperature for the studied samples showed similar behaviour to the one found previously for microwires and wider NWs (Figure 2) [6]. These nanostructures could be relevant in nanoscale superconductivity, as for instance in the topics of one-dimensional superconductivity, SQUID sensors, vortex confinement and pinning, opening a new route to tailor vortex effects in nanometric superconductors.

References

[1] M. Velez et al., J. Magn. Magn. Mater. **320** (2008) 2547.
[2] I. Utke, P. Hoffmann, and J. Melngailis, J. Vac. Sci. Technol. B **26** (2008) 1197.
[3] E. S. Sadki, S. Ooi, and K. Hirata, Appl. Phys. Lett. **85** (2004) 6206.
[4] I. Guillamón et al., New Journal of Physics **10** (2008) 093005; I. Guillamón et al., Nat Phys **5** (2009) 651; I. Guillamón et al., Phys. Rev. Lett. in press.
[5] M. J. Martínez-Pérez et al., Supercond. Sci. Technol. **22** (2009) 125020.
[6] J. M. De Teresa et al., Mater. Res. Soc. Symp. Proc. **1180** (2009) CC04-09.

Figures
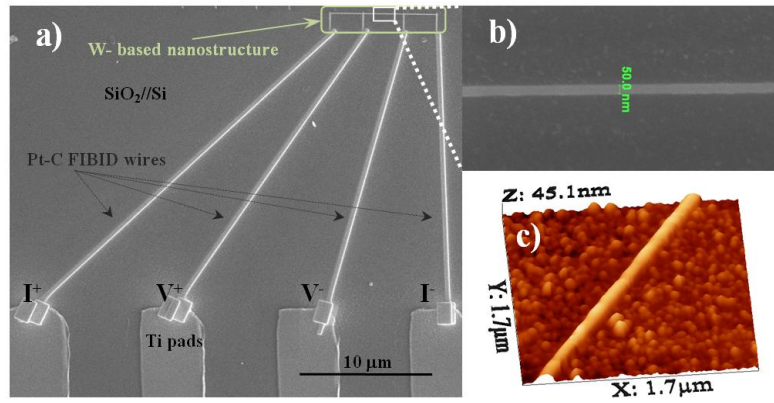
Figure 1: a) SEM image of the experimental configuration for four-wire electrical measurements. b) SEM image of the deposited horizontal NW of W- based nanostructure. c) AFM image of the deposited horizontal NW of W- based nanostructure.
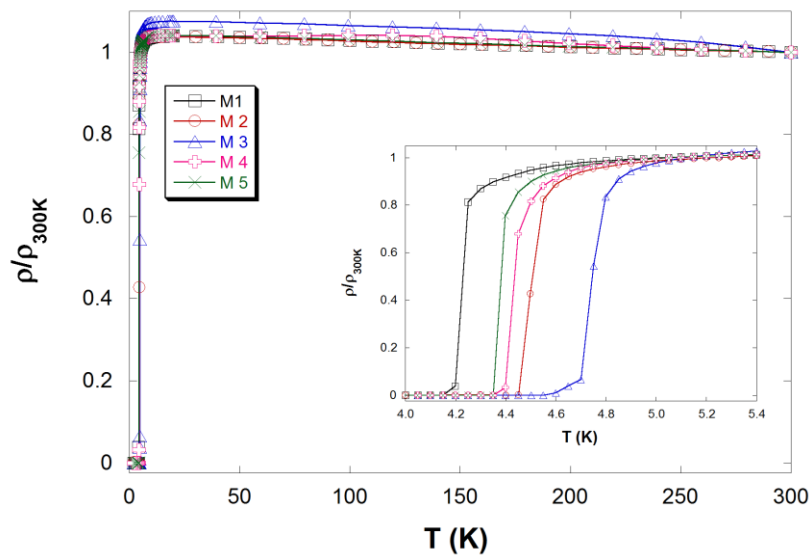
Figure 2: Normalized resistivity of W- based ultranarrow NWs as a function of the temperature. The detailed evolution of the normalized resistivity close to critical temperature is shown in the inset.

LARGE AREA PERIODIC NANOSTRUCTURES: INFLUENCE OF SEVERAL PROCESS PARAMETERS

I. Cornago, S. Domínguez, J. Estella, J. Bravo

FideNa. Edificio Jerónimo de Ayanz (Campus Arrosadía), C/ Tajonar s/n, 31006 Pamplona (Spain)
inaki.cornago@fidena.es

Abstract

Laser Interference Lithography (LIL) is a method to easily pattern large areas (in the range of 10cm diameter) with nanogratings or nanogrids [1]. The tool used for this work is known as "Lloyd's Mirror" and uses the interference of a coherent laser beam (λ = 325nm). The set-up is depicted in Fig. 1. A layer of photoresist is deposited on the substrate (a Si wafer for example), and then is placed 90° with respect to a mirror, in front of the laser beam. Due to the light reflected from the mirror, an interference pattern is created and recorded into the photoresist. The period of this pattern is easily adjusted fixing the angle of the mirror-substrate set, according to the expression $\sin\theta = \lambda / 2P$. This expression shows the theoretical restriction for the minimum period achievable, $\lambda/2$ (162,5nm). Gratings or holes and columns grids can be obtained exposing the substrate once, or twice in different angles.

Lines width or holes and columns diameter can be controlled by adjusting the exposure dose. The exposure dose is defined to be the energy deposited per unit area and it is the power of laser at the substrate per unit area multiplied by the exposure time [2]. A graph of holes diameter vs exposure dose made to this work can be seen in Fig. 2. Similar graphs have been published by other authors using different LIL set-up [3].

The intensity of the laser spot has a Gaussian distribution in the plane perpendicular to the beam direction, which maximum is aligned to the center of the mirror-substrate set [2]. Substrate points farther from the center receive less exposure dose. According to the data showed in Fig. 2, wafers exposed to higher doses will have larger uniform areas. Fig. 3 shows pictures of wafers where zones with different tones in their color can be seen due to the difference in exposure dose. The wafer in Fig. 3.a has received less exposure dose than the other wafer. The right edge of this wafer has received very low dose and the pattern has not been recorded into the photoresist. The wafer in Fig. 3.b has received high exposure dose and features size had a high uniformity. The pink zone on the left side of both wafers is the shadow produced by the mirror.

Once obtained the photoresist pattern, features size of final nanostructure can be adjusted using O_2 Reactive Ion Etching (RIE). Fig. 4 shows a graph that relates hole diameters of a grid with O_2 plasma time, with rf-power 75W and chamber pressure 10mTorr.

Finally, the photoresist pattern is transferred to the substrate using RIE again [4]. All plasma parameters are controlled to obtain different etch depths (gas, flow gas, chamber pressure, rf-power, time, etc.). Images of several nanostructures can be seen in Fig. 5.

References

[1] H.I. Smith, Physica, E 11 (2001), 104-109.
[2] T.B. O'Reilly and H.I. Smith, J. Vac. Sci. Technol. B 26(6) (2008), 2131-2134.
[3] Cheng-Wei Chien, Jyh-Chen and Ju-Yi Lee, Applied Optics, Vol. 45 No.32 (2006), 8278-8287.
[4] J. Bravo, I. Cornago, S. Domínguez and J. Irigoyen. Easy large area Nanopatterning. NanoLitho 2009, Madrid.

Figures
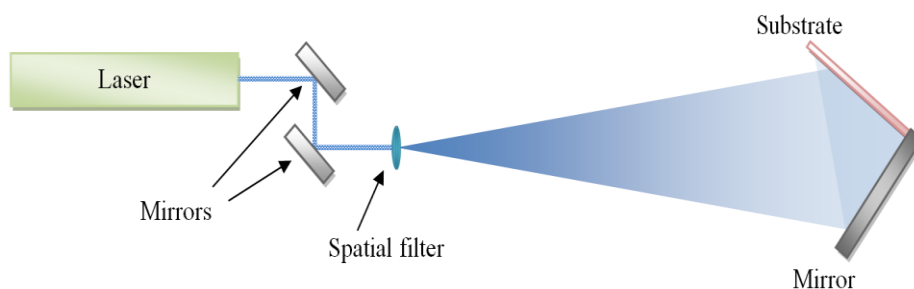
Fig. 1. Lloyd's Mirror set-up
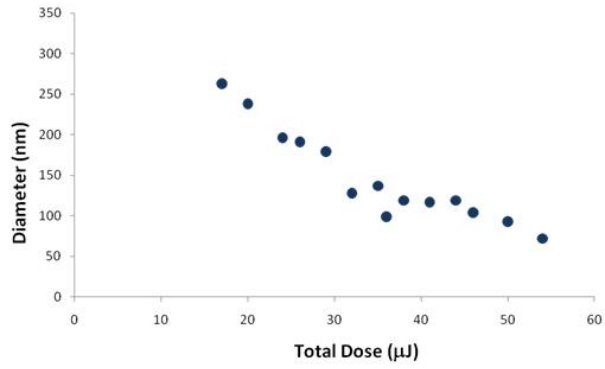
Fig. 2. Relation between holes diameter and exposure dose
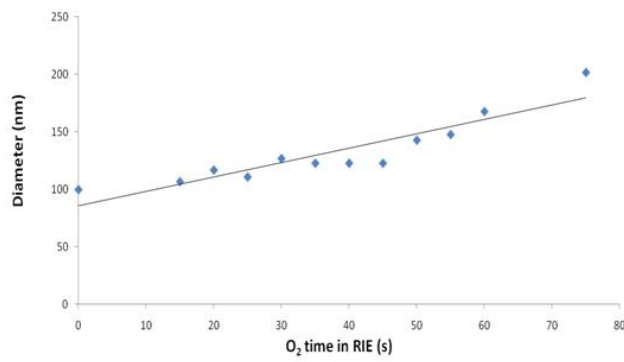
Fig. 4. Relation between holes diameter and O₂ plasma time in RIE

a)

b)
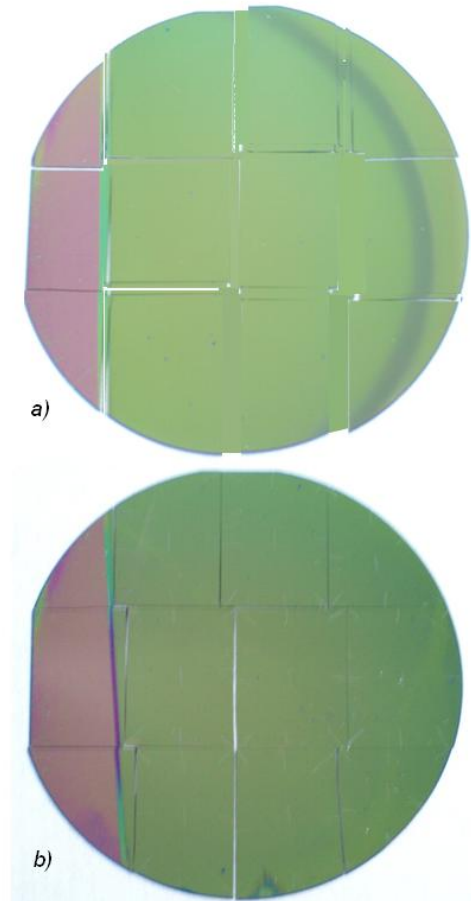
Fig. 3. Wafers exposed with different doses. a) 24µJ; b) 45µJ . They were cleaved for their inspection
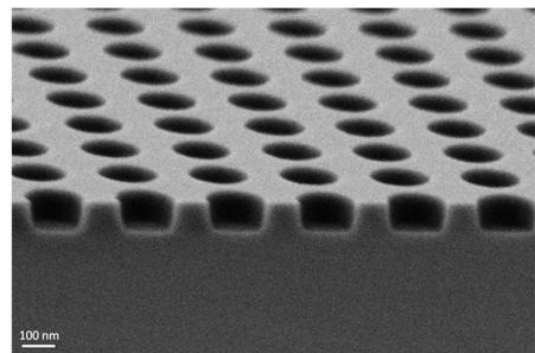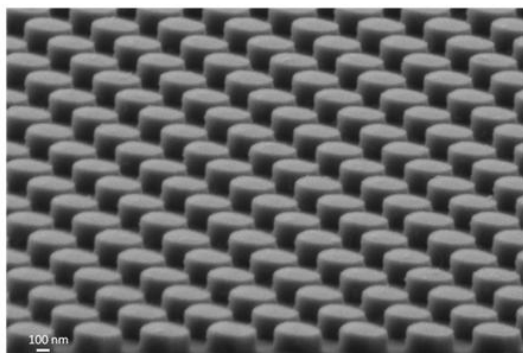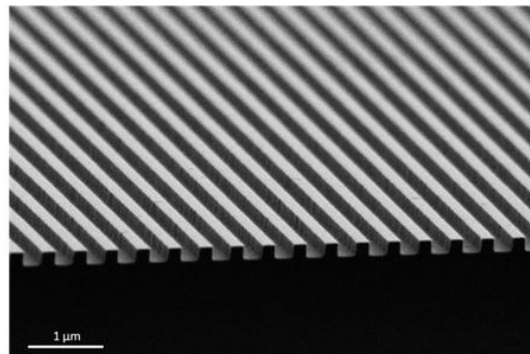
Fig. 5. SEM images of lines, columns and holes nanostructures

Manifold domain structure of double films with perpendicular magnetic anisotropy

Edna C. Corredor, David Coffey, José Luis Diez-Ferrer, José I. Arnaudas, Miguel Ciria,

Instituto de Ciencia de Materiales de Aragón, CSIC.
Instituto de Nanociencia de Aragón, Universidad de Zaragoza.
ednac@unizar.es

Structures made of blocks with competing magnetic anisotropies separated by interleaving layers suitable for large antiferromagnetic coupling are systems where a tiny difference in the energy, tuned by structural parameters, can be favored by a small magnetic field, resulting in a remarkable change of the magnetic configuration [1], suitable for the use as sensor or multiple storage states media [2].

Here we present magnetic force microscopy images in structures with a copper block separating two twin nickel layers with out-of-plane magnetization due to a magnetoelastic (ME) effect. We observe that the number of levels of the MFM signal changes with the thickness of the copper block, and images with two, tree and up to four stable states can be observed (see Figure 1a). Whereas the images with two and three levels are explained as result of dipolar and lineal exchange interaction that keep the magnetization in each Ni block perpendicular to the film plane but parallel or anti-parallel to each other [3], the fourfold contrast suggests the presence of domain structures with in-plane components of **M** in the Ni blocks. For the latter structures, the M-H loops show a plateau during the inversion of the magnetization (see Figure 1c),

To explain the presence and stability of magnetic domains with intermediate contrast we consider the formation of magnetoelastic domains that elude the clamping done by the buffer layer and balance the perpendicular anisotropy and a biquadratic exchange coupling that stabilize a non collinear orientation of **M** in each Ni block. The proposed domain structure is made of domains with in plane components separated by 90 degrees domains wall (see Figure 2). The calculation of the elastic energy shows that the domain configuration releases elastic energy in the Ni film blocks and can balance the effective perpendicular anisotropy, about 90 kJ/m^3 [4], if the average deformation in each domain is ~ -42 10^{-6} a value compatible with the bulk value (-60 10^{-6} [5]). Thus, if the perpendicular anisotropy is balanced out. the biquadratic exchange interaction that favors a orientation of 90 degrees, even being small in absolute value, could play the capital role of stabilizing non-collinear structures and be responsible for the plateaux observed in the MH loops since additional Zeman energy, supplied by increasing the magnetic field, is needed to unlock the non-collinear state. Considering that the energy associated to the area in the M-H loops due to the presence of plateaux [see figure 1(c)] can be assigned to the biquadratic term, a value of ≈ -0.005 mJ/m^2 is obtained for the biquadratic exchange constant.

References

[1] F Yildiz, M Przybylski and J Kirschner Phys. Rev. Lett.,**103** (2009) 147203.

[2] M Albrecht, G Hu, A Moser, O Hellwig, and B D Terris J. Appl. Phys. **97** (2005) 103910.

[3] K Janicka, J D Burton and E Y Tsymbal J. Appl. Phys. **101** (2007) 113921.

[4] E C Corredor, J L Diez-Ferrer, D Coffey, J I Arnaudas and M Ciria J. Phys. Conf. Ser. **200** (2010) 072019.

[5] E W Lee and M A Asgar Proc. R. Soc. Lond. A. **326** (1971) 73.

Figures
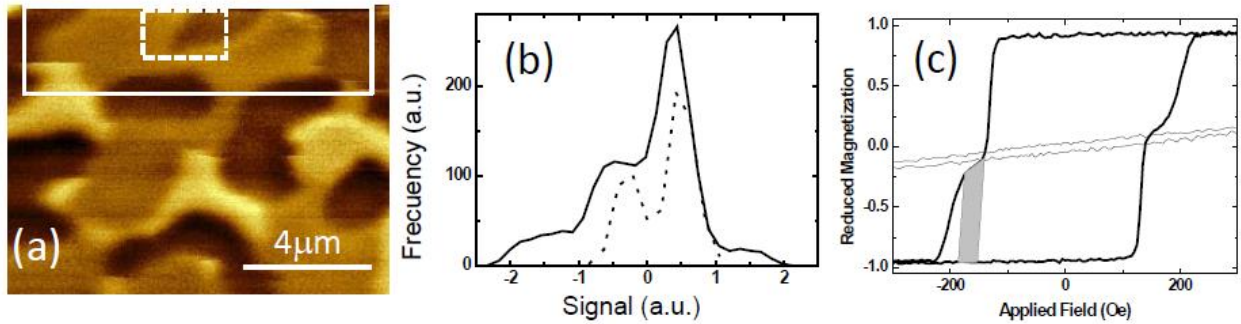
Figure 1(a) Magnetic force microscopy images taken on a Ni(3)/Cu(4.5)/Ni(3) structure. (b) Histograms taken on the areas marked with continuous and dashed lines on the MFM image (c) Detail of the M-H loops with H perpendicular (thick line) and parallel (thin line) to the plane. The grey area in panel is used to estimate the strength of the biquadratic exchange contribution.
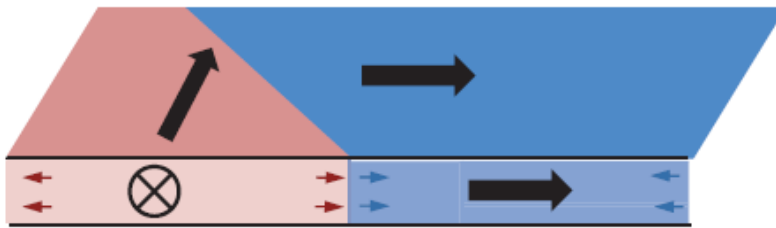
Figure 2 Stress distribution for a film with a 90° domain wall, the thick arrows stand for the magnetization vector. The small arrows indicate the in-plane stress component at a section of the film within each domain for a material with negative magnetostriction.

Optically and catalytically functionalized multiple-cored magnetic nanoparticles

A. B. Dávila-Ibáñez,[1,2] J. Rivas,[2] V. Salgueirino[1]

Universidade de Vigo, Dpto. de Física Aplicada, 36310 Vigo Spain
Universidade de Santiago de Compostela, dptos. de Química Física y Física Aplicada, 15782 Santiago de Compostela Spain

vsalgue@uvigo.es

Nanotechnology has reached the stage of development where the subject of most investigations is not individual nanoparticles but rather systems of much greater complexity. The diversity of the ultimate magnetic functionalities of these complex nanomaterials systems finds place in applications including such far-reaching challenges as bio-related sensors, [1] or catalysts. [2] This fascinating approach of artificial nanostructuring to create completely new ever-progressing magnetic materials and technologies was demonstrated to be directly dependent on the further improvement of the current materials used. The applications underlined will become feasible if previously one can exert control on the magnetism displayed.

With that in mind, two strategies were developed, focusing the synthetic efforts on the creation of multiple-cored magnetic nanoparticles, which tie together the intrinsic properties of the individual constituents (M_S, K_1, etc.) and the collective properties of the final composites (dipolar interactions, grain-boundary or exchange-coupling effects between the subunits forming them).

The first strategy describes the synthesis of relatively large magnetic plasmonic composite particles. Their magnetic characteristics (M_S and H_C) reach sufficiently increased values if compared to other hybrid composites, owing to a compromise between size, percentage of the soft magnetic material, and to a remarkable morphology consisting of inner (smaller) cobalt boride clusters assembled as larger spheres (magnetic interactions) and stabilized with an outer shell of silica. These magnetically stable silica-coated cobalt boride spheres were optically functionalized, acquiring a characteristic SPB (surface plasmon band) (figure 1, left). Outstandingly, due to the silica formation procedure (acid- or acid- and base-catalyzed), silica shells between the optical and magnetic functionalities were proven to undergo chemical and morphological changes translated into an optical response. [1]

To check envisioned activities in fields, such as sensing, or for in vitro applications (in vivo applications are extremely hindered due to the high percent of cobalt in the magnetic core), the magnetic and optically active nanostructures were subjected to the following tests in which controlled fractions (1 and 10 vol %) of water were added to the ethanolic composite solutions, in restricted periods of time. In the presence of water in the solution, the composites with acid-catalyzed silica were subjected to characteristic morphological changes, for example, an increase in the typical thickness and roughness of the silica shell. These morphological changes were simultaneously reflected on the optical signal displayed, revealing dielectric changes near the gold nanoparticles' surface and electromagnetic coupling between them.

The same experiments were also carried out with composites built with silica deposited onto the magnetic cores using successive acid- and base-catalyzed silica condensation steps, but neither gelation nor dissolution of silica took place when the same amounts of water were added. The composites were, after that, transferred to aqueous and phosphate buffered saline (PBS) solutions, keeping the same morphology and optical properties. These results underline therefore these magnetic and optically active composites to be used in bio-related in vitro applications, taking advantage of their strong magnetic signal and SPB displayed.

The second strategy describes the synthesis of highly active and magnetically recoverable colloidal catalysts, synthesized assembling iron oxide and platinum nanoparticles with silica. Conveniently, these composites present multiple magnetic cores gaining special relevance in the catalysts recovery as responding to low magnetic fields. As a proof of concept, they were used to assess the retarded gold reduction in the cetyltrimethylammonium bromide (CTAB) micelles, permitting to tune the gold reduction rate and therefore the production of spherical or anisotropic gold nanostructures. [2]

The platinum-based catalytically active magnetic nanocomposite particles (Pt-MNC) were prepared by a successive combination of the base-catalyzed hydrolysis of tetraethyl orthosilicate (TEOS) onto iron

oxide nanoparticles and the LbL self-assembly. The latter drives Pt nanoparticles onto the surface of the magnetic particles previously coated with silica (see scheme in figure 1, inset on the right).

The Pt-MNC were investigated in terms of their catalytic activity and recyclability monitoring the Au^{3+} reduction in CTAB solution, reaction which is generally used for the synthesis of gold nanorods and becomes very appropriate for catalysis assessment because of its hindered reaction nature. Since the measurement of the SPB during the synthesis of Au nanostructures provides useful information in terms of the kinetics of the reactions, three typical sets of UV-vis spectra were used to monitor their formation (see figure 1b). Although the different experiments were accomplished under the same conditions of concentration of precursors and temperature, a faster reduction of Au^{3+} ions to give metallic gold was found as increasing the concentration of magnetic and catalyst nanocomposites.

The representative sets of data (displaying the exponential type of kinetics in which absorbance values approach a plateau) indicate that the reaction rate was clearly increased in the presence of the Pt-based nanocomposites. Because of the increasingly faster Au^{3+} reduction rate, the synthesis of different gold nanostructures was carried out, thermodynamically favoring the spherical shape. This increase in the reduction rate (from 2.4×10^{-3} s^{-1} to 7.36×10^{-3} s^{-1}) leads to a decrease in nanorods yield and instead, the formation of some spherical particles is observed (much bigger proportion of particles compared to that appearing in a typical gold nanorods synthesis).

This tendency becomes raised as increasing the catalyst concentration in the reaction medium and ends up in the production of gold nanoparticles but no nanorods. Consequently, the UV-vis spectra shown have the SPB located around 520 nm and 800 nm for gold nanorods (for those structures synthesized without catalyts, [Pt-MNC] = 0), located around 520 and 740 nm (in the presence of the Pt-based nanocomposites ([Pt-MNC] = 0.24 mg/mL) (spherical gold nanostructures were also formed so that an increase in the transversal SPB intensity is observed), and just around 540 nm for the highest catalyst concentration ([Pt-MNC] = 0.32 mg/mL]) which inhibits the anisotropic structures formation and forces the system to produce spherical nanoparticles instead.

In summary, magnetic composites optically or catalytically functionalized were synthesized and the assessment of their optical and catalytic activity was carried out in different experiments.

References

[1] A. B. Dávila-Ibáñez, M. A. López-Quintela, J. Rivas, V. Salgueirino J. Phys. Chem. C (2010), 114, 7743-7750.
[2] A. B. Dávila-Ibáñez, M. A. Correa-Duarte, V. Salgueirino J. Mater. Chem. (2010) 20, 326-330.

Figures
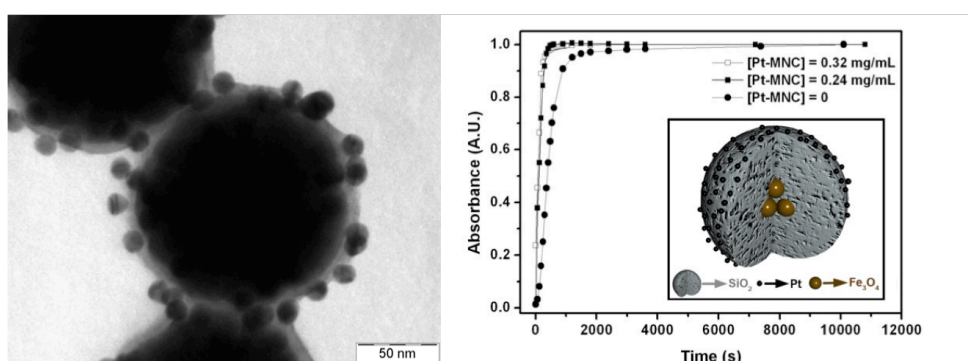
Optically (left) and catalytically (right) functionalized multiple-cored magnetic nanoparticles

Towards Stable Magnetization of Plant Viral Nanorods via Covalent Coupling of Metal Oxide Particles

Sven Degenhard[1,2], Eoin Fox[3], Fania Geiger[4], Fabian Eber[1], Sabine Eiben[1], Jürgen Schmucker[5], Annika Thormann[6], Zhenyu Wu[7], Lapo Bogani[8], Dermot Brougham[3], Joachim Spatz[4], Günter Tovar[5], Andreas Heilmann[6], Carl Krill[7], Martin Dressel[8], Alexander Bittner[2], Holger Jeske[1], Christina Wege[1]

[1] Department of Molecular Biology and Plant Virology, Institute of Biology, Stuttgart University, Stuttgart, Germany
[2] CIC NanoGune, San Sebastian, Spain; Ikerbasque, Bilbao, Spain
[3] School of Chemical Sciences, Dublin City University, Dublin, Ireland
[4] Max Planck Institute for Metals Research, Stuttgart, Germany
[5] Fraunhofer Institute for Interfacial Engineering and Biotechnology, Stuttgart, Germany
[6] Fraunhofer Institute for Mechanics of Materials IWM, Halle, Germany
[7] Institute for Micro- and Nanomaterials, Ulm University, Ulm, Germany
[8] Physical Institute, Stuttgart University, Stuttgart, Germany

sven.degenhard@bio.uni-stuttgart.de; s.degenhard@nanugune.eu

Using biomolecule complexes such as viruses for nanoapplications offers the possibility to take advantage of their unique size and their multivalence. *Tobacco mosaic virus* (TMV), a tube-shaped plant virus self-assembled from one single-stranded RNA and 2130 identical, helically arranged coat proteins is ideal as a scaffold due to its high stability (wide range of the pH value, high temperatures and tolerance to several organic solvents) regarding its biological origin. In addition selective end-modification and fast immobilization has been demonstrated [1], [2]. Adding magnetic functionality is a matter of interest, especially for medical treatment (hyperthermia) and switchable devices (spintronics) as ferrofluids supplemented with TMV derivatives already show dramatic performance enhancement [3], [4]. We therefore intend to achieve stable magnetization of TMV via covalent coupling of magnetic particles carrying a functionalized shell in order to produce virus-scaffolded magnetic nanorods for applicable devices. Upon preparation of different types of TMV-nanoparticle complexes, standard methodology of biochemistry and purification needed adaptation to the exceptionally large hybrid assemblies of organic and inorganic materials. First promising architectures were generated, which are currently being characterized with respect to magnetism and mechanical stability.

References

[1] S. Balci, K. Noda, A.M. Bittner, A. Kadri, C. Wege, H. Jeske, K. Kern; Angew. Chemie Int. Ed. **46** (2007), 3149-3151.
[2] S. Balci, D.M. Leinberger, M. Knez, A.M. Bittner*, F. Boes, A. Kadri, C. Wege, H. Jeske, K. Kern; Adv. Mater. **20** (2008), 2195-2200.
[3] Z. Wu, A. Mueller, S. Degenhard, S. E. Ruff, F. Geiger, A. M. Bittner, C. Wege, C. E. Krill; ACS Nano **4** (2010), 4531-4538.
[4] Z. Wu, R. Zierold, A. Mueller, S. E. Ruff, C. Ma, A. A. Khan, F. Geiger, B. A. Sommer, M. Knez, K. Nielsch, A. M. Bittner, C. Wege, C. E. Krill; Phys. Stat. Sol. B **247** (2010), 2412-2423.

Figure
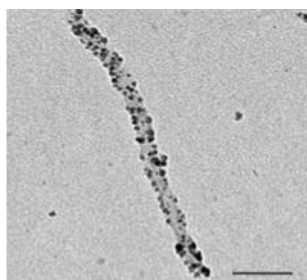
Transmission electron microscopy images of *Tobacco Mosaic Virus* decorated with magnetic nanoparticles. Bar 100 nm.

Prevention of ordered mesopore structure degradation during microporosity generation in nanocasted carbons

M. Enterría, F. Suárez-García, A. Martínez-Alonso, **J.M.D. Tascón**

Instituto Nacional del Carbón, CSIC, Apartado 73, 33080 Oviedo, Spain

tascon@incar.csic.es

Introduction

Emerging applications of porous carbon materials require the development of novel hierarchical carbons with tailored pore sizes. In recent years, a number of reports have been published on the synthesis of ordered mesoporous carbons by "hard templating" with ordered silicas. However, very little knowledge is available to prepare carbons with a controlled bimodal micro-mesopore distribution of pore sizes while avoiding the gradual destruction of the ordered mesostructure. In this work we have investigated the development of microporosity in ordered mesoporous carbons by chemical activation with KOH, comparing the effects of carrying out the activation step in the presence and absence of SBA silica used as template.

Experimental

CMK3-type ordered mesoporous carbon (CMO) was prepared by gas-phase infiltration of carbon in SBA-15 silica (TG results in air at 1000 ºC showed a carbon infiltration degree of 58%) using propylene at 750 ºC for 6 h. The resulting composite (SBA-15-CMO) was divided into two parts: one of them was directly activated with KOH, and the other was washed with HF to remove the silica template and obtain the ordered mesoporous carbon (CMO), which was then activated with KOH as well.

Chemical activation was performed in a horizontal furnace. CMO was mixed with powdered KOH in KOH/carbon ratios (X) of 2:1 and 4:1. The impregnated materials were heated in Ar at 5 ºC/min to either 750 or 850 ºC (T) for 30 min. The resulting activated carbons are denoted as CMMO X:1 T series. SBA-15-CMO composites were activated in the same conditions and are denoted as SiC X:1 T series. The carbons resulting from HF washing the template after activation are denoted as CMMO**B** X: T series.

Results and discussion

Figure 1 shows the N_2 adsorption-desorption isotherms measured at 77 K on a selection of representative samples. All the isotherms belong to Type IV in the BDDT classification and they maintain the shape of the isotherm of the starting mesoporous carbon, which indicates the conservation of the mesoporous character, except for CMMO 4:1 850 sample, which becomes type I. The adsorbed volume at low relative pressures increases gradually with increasing both X and T, which evidences microporosity development upon activation. Several pore textural parameters are compiled in Table 1. All of them increase with increasing either X or T. Thus, the micropore volume [$V_{DR}(N_2)$] goes from 0.13 (CMO) to 0.52 cm^3/g (CMMO**B** 4:1 850). The BET surface area (S_{BET}) increases from 341 (CMO) to a maximum value of 1247 m^2/g (CMMO**B** 4:1 850). The mesopore volume (V_{meso}) remains almost constant (a slight increase being observed due to collapse of adjacent micropores during activation), with the exception of a drastic decrease to 0.16 cm^3/g for sample CMMO 4:1 850, which confirms the destruction of the regular mesopore network.

The materials activated after having removed the template with HF exhibit greater N_2 adsorbed amounts at low relative pressures than those activated in the presence of the template. However, as Figure 2 shows, X-ray diffractograms reveal that the solids directly activated with the template (CMMO**B** series) keep the ordered nanostructure to a much greater extent; note that the characteristic peaks of hexagonal symmetry can be clearly seen in these materials as well as in CMO. However, these diffraction peaks practically disappear following activation in the absence of the template (CMMO series).

Under mild activation conditions (low X and T), microporosity development is greater when the activation is carried out in the absence of the template (Figure 1, Table1), but a slight degradation of the ordered structure occurs upon activation (Figure 2). In the case of strong activation conditions (high X and T) the materials derived from the silica-carbon composite present bigger microporosity development (Figure 1, Table1) along with a substantial preservation of the structural order (Figure 2).

Conclusions

Hierarchical carbons have been obtained by chemical activation with KOH of ordered mesoporous carbons. Under mild activation conditions, better results are obtained for carbons activated without template as a good compromise is obtained in terms of structure preservation/microporosity development. For strong activation conditions (high X and T), greater micropore volumes are obtained for the activation in the presence of the template, and the destruction of the ordered mesoporous structure is avoided to a larger extent.

Figures
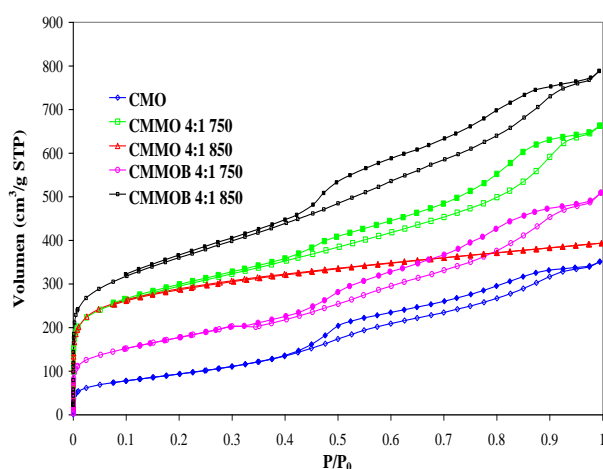
Figure 1. N_2 adsorption-desorption isotherms at 77 K for a selection of activated samples.
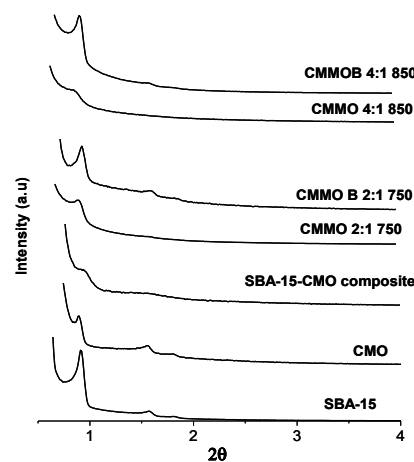
Figure 2.Low-angle X ray diffractograms for a selection of activated samples

Table 1. Porous texture parameters calculated from the N_2 adsorption-desorption isotherms at 77 K.

Sample	S_{BET} (m^2/g)	V_T (cm^3/g)	$V_{DR}(N_2)$ (cm^3/g)	V_{meso} (cm^3/g)
CMO	341	0.53	0.13	0.40
CMMO 2:1 750	726	0.81	0.30	0.51
CMMOB 2:1 750	393	0.62	0.15	0.46
CMMO 4:1 750	1028	1.00	0.42	0.58
CMMOB 4:1 750	634	0.75	0.25	0.51
CMMO 4:1 850	982	0.60	0.44	0.16
CMMOB 4:1 850	1247	1.19	0.52	0.67

Object detection with SNOM making use of humidity

Maysoun Douas, P.A.Serena, M.I.Marqués

[1]*Instituto de Ciencia de Materiales de Madrid, Consejo Superior de Investigaciones Científicas, Campus de Cantoblanco, 28049 Madrid, Spain*
[1]*Departamento de Física de Materiales, Módulo 4, Facultad de Ciencias, Universidad Autónoma de Madrid, 28049, Spain*
Maysoun.douas@icmm.csic.es

Near Field Scanning Optical Microscopy (SNOM) is a hybrid scanning probe-optical technique used for overcoming the diffraction limit of light for optical spectroscopy and high resolution marking of materials [1]. Like most scanning probe techniques, SNOM is affected by geometrical parameters and environmental conditions, such as atmospheric humidity. As hydrophilic materials attract air water molecules, it is important to understand the effect of the condensed water between probe and sample [2]. Nanometric liquid bridges may affect the shear force damping and optical signals achieved with SNOM [3-6]. For that reason, we present a simulation study using two complementary computational techniques: Finite Difference Time Domain (FDTD) calculations for light propagation [7] and Monte Carlo techniques for water condensation [8].

Thus, to show the effect of the water bridge on the optical signal achieved in the transmission mode configuration, we simulate the scan of the SNOM tip above a substrate. Furthermore, we place a hydrophilic buried dielectric inside the substrate, in order to register not only the effect of the water bridge formation but also the change in the refractive index given by the buried dielectric. Three humidity conditions were considered (Figure 1). At low humidity no bridge formation is observed. However, increasing humidity leads to the formation of the bridge between the tip and substrate when the buried dielectric is near the tip, and finally when there is enough humidity the bridge of water turns to a stable droplet during the overall measurement.

In Figure 2, we depict the intensity collected for those scan measurements depicted in Figure (1) (normalized to the case of maximum humidity) and its comparison to measurment without hydrophilic buried dielectric objects. After Figure 2, we conclude that both the presence of hydrophilic patch and atmospheric humidity affect the optical signal, opening the possibility of implementing this technique to detect water meniscus, hydrophilic regions, etc.

[1] J.H.Kim., K.B.Song., Micron, **38** (2007), 409
[2] J.J.Jang.,G.C.Schatz.,M.A.Ratner. Physical Review Letters, **90** (2003), 156104-1
[3] P.J.Moyer.,S.B.K., Applied Physics Letters, **68** (1996), 3380
[4] S.Davi.,M.Spajer.,D.Courjon., Applied Physics Letters, **73** (1998), 2594
[5] F.M.Huang.,F.Culfaz,F.Festy.,D.Richards., Nanotechnology, **18** (2007), 015501
[6] Rod S. Taylor .et.al, Journal of Applied Physics, **107**(2010)
[7]   A.Taflove., S.Hagness, Computational Electrodynamics- the finite difference time-domain method, 2nd ed. Norwood, M.S: Artech House, 2000
[8] P. A. Serena, M. Douas, M. I. Marqués, C. Carrasco, P. J. de Pablo, R. Miranda, J. L. Carrascosa, M. Castellanos, and M. G. Mateu, Physica Status Solidi-C, **6** (2009), 2128
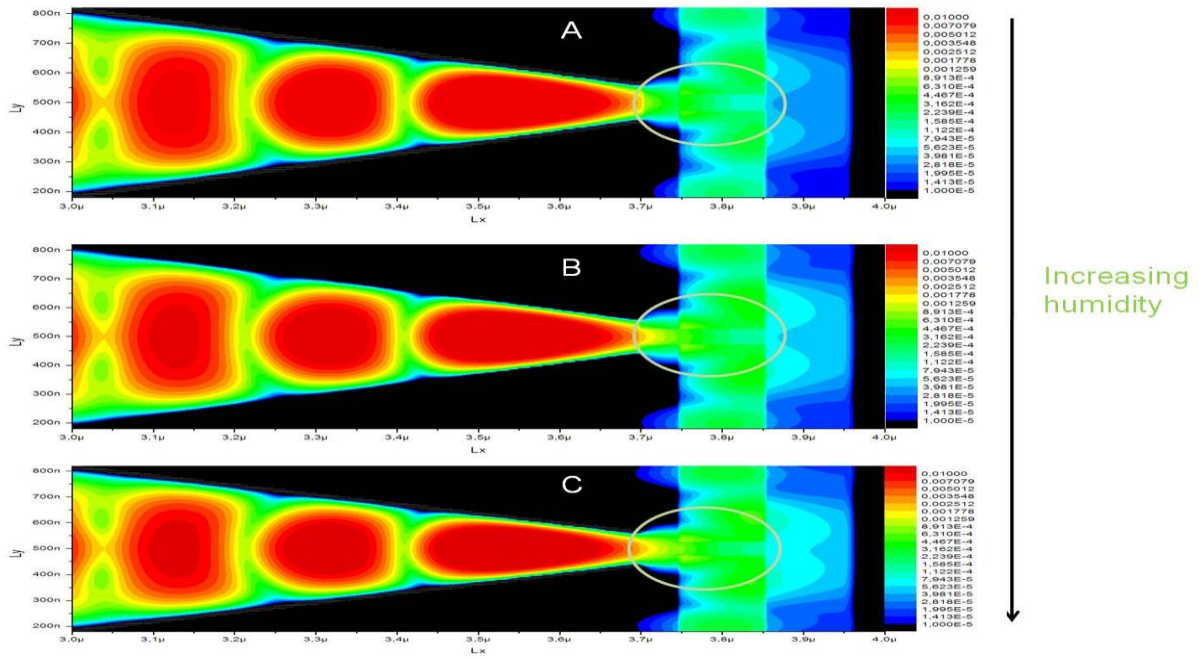
Figure 1. Intensity Color Map in logarithmic scale for the propagation of a TMz mode through the SNOM tip.
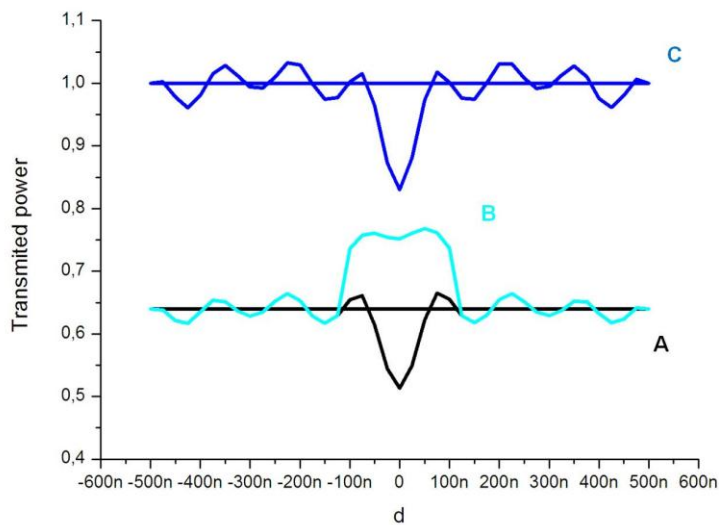
Figure 2. Normalized intensity collected for those scan measurements depicted in Figure (1) compared to measurement without object (straight lines). Liquid bridge formation clearly enhaces the amount of transmitted power (B & C).

Interdigitated micro-and nano-electrodes for DNA hybridization detection using electrochemical techniques

U. Eletxigerra[1,2], I. Alonso[1], R. Bayón[2], J. Martínez-Perdiguero[1], S. Merino[1]

[1]Micro and Nanofabrication Unit, Tekniker, Avda. Otaola 20, 20600 Eibar, Spain
[2]Tribology Unit, Tekniker, Avda. Otaola 20, 20600 Eibar, Spain
ueletxigerra@tekniker.es

Interdigitated gold microelectrodes are widely used as bio-sensors by combining the properties of the electrodes design (fabrication process, number of electrode pairs, electrodes width, length and space, coating properties, etc.) with customized electrochemical techniques that allow to measure and analyze the electrical signal of the electrodes response to specific biological compounds [1-4].

The aim of this work is to develop and characterize a micro sensor based on interdigitated electrodes manufactured by photolithography method able to detect DNA hybridization. Sensors were fabricated on SiO_2 wafers covered with a thin titanium adhesion layer and gold top layer deposited by e-beam PVD-sputtering technique (fig. 1).

Ti/Au microelectrodes with different geometries were exposed to thiolated DNA and then to the complementary DNA chain. Hybridization process is detected by Surface Plasmon Resonance and electrochemical techniques such as impedance spectroscopy and potentiostatic-potentiodynamic measurements in PBS solution.

As a further step to achieve higher sensitivity [1], nanointerdigitated electrodes with submicron widths were also fabricated via nanoimprint lithography. Preliminary fabrication results will be presented (fig. 2).

References

[1] A. Bonanni, I. Fernández-Cuesta, Microchimica Acta, Volume 170 (2010), 275-281.
[2] E. Finot, E. Bourillot, Ultramicroscopy, Volume 97 (2003), 441-450.
[3] P. Van Gerwen, W. Laureyn, et al., Sensors and Actuators B: Chemical, Volume 49(1998), 73-80
[4] M. Varshney, Y.Li, Biosensors and Bioelectronics, Volume 24 (2009), 2951-2960

Figures
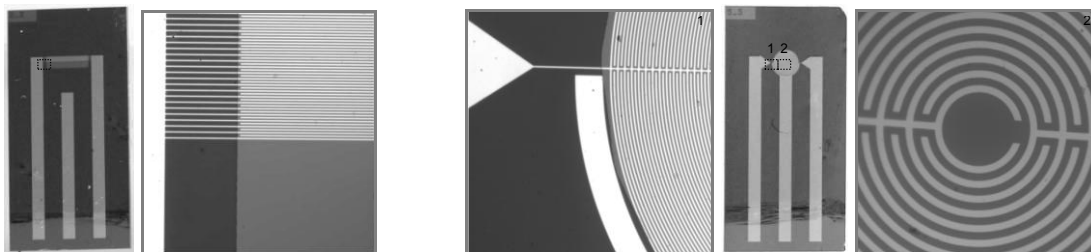
Figure 1. Sample pictures of microelectrodes used in this work: linear geometry (left), 2 μm width and 2 μm gap; and circular geometry (right), 5 μm width and 5 μm gap.
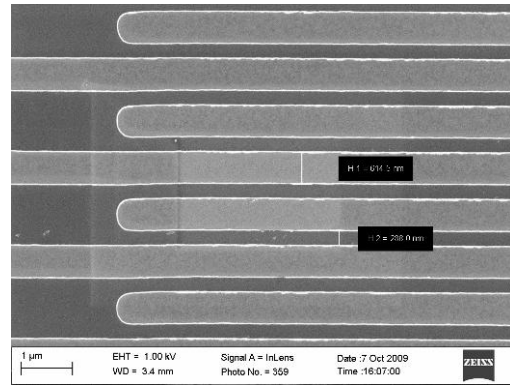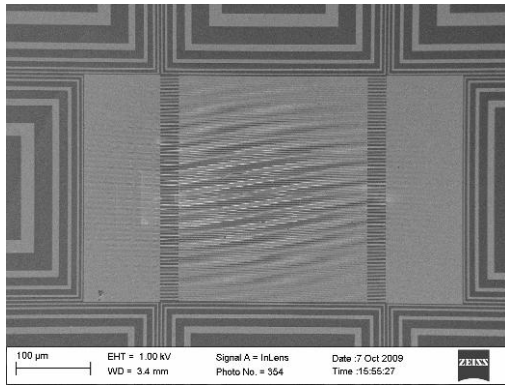
Figure 2. Micrographies obtained by scanning electron microscopy showing the interdigitated nanoelectrodes.

Multifunctional Layers for Safer Aircraft Composites Structures

M. Txapartegi, A. Iriarte, N. Markaide and **C. Elizetxea**

TECNALIA, Plastics and Organic Composites
Mikeletegi Pasealekua 2, E-20009 Donostia-San Sebastian, Spain

The use of composite materials in aeronautics industry has increased constantly over the last 35 years, due mainly to their high specific strength and stiffness combined with the possibility of designing complex geometry components that are more aerodynamically efficient than metals. But due to organic nature of polymeric matrix component, composite materials are electrically and thermally bad conductors and they tend to burn easily, emitting toxic gases and smoke. For that, they require affordable, effective and certifiable protection systems against atmospheric hazards such as icing and erosion, as well as fire and burning not only for accidents prevention, but also for survivability in case of them. Moreover, improved in field inspection techniques for continuous assessment of their structural health are required with the increased use of composite materials.

The limitations of composite structures for thermal, electrical and fire performance have been a drawback to extend it in many applications. Current technologies address those issues separately; ice protection is usually performed by mean of a metal mesh or foil incorporated into the outer ply of fabric on the skin of the structure, fire protection is performed with thermal barrier coatings on the structures and life monitoring, is performed with embedded sensors. All of them add high weight penalty and complexity during the component manufacturing and posterior maintenance even may go against the structural integrity of the component in some cases.

Final objective of the work to be performed consists of developing a multifunctional layer with thermal and electrical conductivity, improved fire performances and sensing capabilities to be incorporated in aircraft composite structures for ice and fire protection, as well as health monitoring. This can be achieved with the developing of a nanocomposite layer consisting of a polymeric matrix doped with fibrous nanomaterials like CNTs (Carbon Nanotubes) or CNFs (Carbon Nanofibres) that afterward will be incorporated in the manufacturing process of composite parts. Low volume additions of those materials (1-5%) provide property enhancements with respect to the neat resin that are comparable to that achieved by conventional loadings of traditional fillers (15-40%), even unique value-added properties not normally possible with traditional fillers are also observed, such as reduced permeability, tailored biodegradability, optical clarity, self-passivation and flammability, oxidation and ablation resistance. In addition, the lower filler percentage facilitates processing and reduces component weight increase.

In the present work, polymer nanocomposite layers have been prepared incorporating different concentrations of MWCNTs into epoxy and benzoxazine resins. Electrical and electro-thermal characterizations have been also performed, and the preliminary electro-thermal tests confirm the heating capacity of the CNT network. The nanocomposites present good heating performance and low electrical resistivity.

Nanowire diodes with semiconductor heterojunctions

Ionut Enculescu[1], Elena Matei[1], Monica Enculescu[1], Maria Eugenia Toimil Molares[2], Jean Philippe Ansermet[3]

[1]National Institute of Materials Physics, Atomistilor 103 bis, Magurele, Romania; [2]GSI Darmstadt, Germany; [3]EPFL, Lausanne
encu@infim.ro

During the last decade the main focus in the field of nanotechnology shifted from the pure knowledge driven research towards more complex, application focused work. Nanowires are quasi – 1 – dimensional nanoparticles with a huge potential of applications ranging from building blocks of tomorrow electronics to active components of ultrasensitive biological detectors. These nanostructures not only allow extreme miniaturization but, based on their unique morphology low dimensionality and high surface to volume ratio, offer new specific functionalities. The template method is one of the most convenient in order to fabricate nanowires or nanotubes [1].

By replicating a nanoporous membrane with cylindrical pores with controlled dimensions, such as polymer ion track membranes or anodic alumina, one is able to obtain nanowires with well controlled morphology and extremely high aspect ratio. Usually the replication of the nanoporous membranes is performed using electrochemical and chemical deposition due to the fact that is more difficult to fill such low diameter pores by employing physical methods. Using this approach metal and semiconductor nanowires were obtained. Further, complex structure nanowires such as multilayered magnetic nanowires with current perpendicular to plane giant magnetoresistance were prepared by a simple electrochemical pulsed deposition [2]. Semiconductor electrodeposition advanced steadily during the last two decades opening the possibility that by template replication to fabricate high quality nanowires. Moreover, the next logical step was to prepare more complex structures, either by pulsed deposition when the electrochemical properties of the system make it possible or in a more complicated manner namely by a sequential approach where the deposition bath is changed as a function of the desired result.

In this paper we present our results related to the fabrication of multisegment nanowires containing semiconductor heterojunctions, by electrochemical deposition in ion track membranes. Scanning electron microscopy, energy dispersive X-ray analysis and optical spectroscopy were employed to characterize the nanostructures.

The first step was to prepare the nanoporous membranes by swift heavy ion irradiation (performed at the UNILAC accelerator of GSI, with heavy ions such as Au or U with specific energy of 11.4 MeV/nucleon) of the polycarbonate foils 30 micrometer thick. The total fluence of irradiation will represent the pore density, taking into account that each ion passing through the sample leaves a defect track. This defect track is further etched with a mixture of an aqueous solution of sodium hydroxide (5M) and 10% methanol at a temperature of 50°C. In these conditions the etching is extremely selective, cylindrical, parallel pores being obtained. The diameter of the pores is controlled by the etching time, a 2 micrometer diameter corresponding to one hour of etching.

The next step of the algorithm was to deposit the working electrode. Thus, a thin layer of gold was deposited onto one face of the membrane and further thickened by electrodeposition of copper. After the metal electrode was prepared, the pores were completely closed on that face of the membrane.

We deposited multisegment nanowires, containing a metal i.e. nickel and a semiconductor heterojunction zinc oxide/cadmium telluride. Nickel electrodeposition was performed using a typical Watts bath containing nickel sulphate and chloride as source of metal ions and boric acid as pH buffer. CdTe was deposited from a solution containing cadmium sulphate, tellurium dioxide as sources of cadmium and tellurium ions. The pH of the solution was approximately 2. Zinc oxide was deposited from a nitrate bath which contains zinc nitrate as the source of zinc ions (see figure).

The structures where characterised from the point of view of composition, morphology, optical and electrical properties.

By this approach we succeeded in fabricating nanowires with high morphological and structural quality. These can be employed in a wide field of applications, most interesting being the biological molecule (DNA, cancer markers, proteins and so on) detectors. Such nanostructures with controlled properties may also be used in optoelectronics, as photodetectors. By further refining the method and improving the quality of the deposited nanowires one can develop ultra miniaturised light emitting diodes or even laser diodes.

References

[1] Martin C. R., Science, , 266, (1994) 1961-1966.
[2] Enculescu I.; Toimil-Molares M.E.; Zet C.; Daub M.; Westerberg L.; Neumann R.; Spohr R. Appl. Phys. A, (2007), **86**, 43 – 47.
[3] I. Enculescu, M. Sima, M. Enculescu, M. Enache, V. Vasile and R. Neumann, Optical Materials, **30**, (2007), 72-75
c

Figure
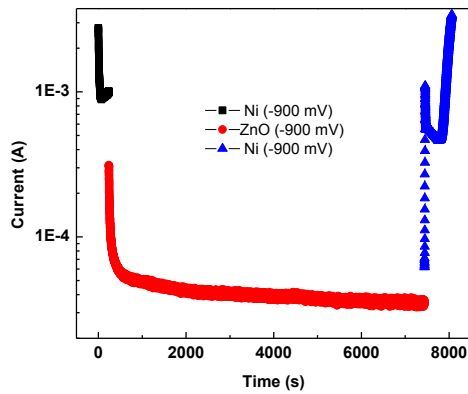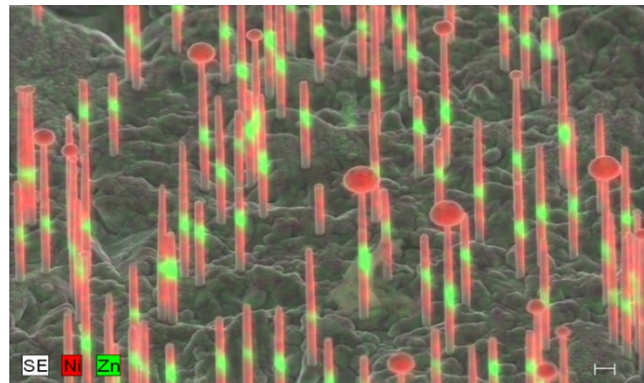
(a)   (b)

Figure caption (a) deposition current for a Ni – ZnO – Ni multisegment array of wires and (b) EDX mapping of an array of multisegment wires.

Encapsulation via sol-gel of different organic compounds and their characterisation

E. Erkizia*, I. Kaltzakorta*, J. M. Laza[#], J. L. Vilas[#], L. M. León[#]

*Tecnalia, Centre for Nanomaterials Applications in Construction (NANOC), Calle Geldo, Edificio 700, Parque Tecnológico de Bizkaia, 48160 Derio, Spain
[#]Departamento de Química Física, Facultad de Ciencia y Tecnología, Universidad del País Vasco, Apartado de correos 644, 48080 Bilbao, Spain
edurne.erkizia@tecnalia.com

Because of its importance in different areas of industry such as agriculture, pharmaceutics medicine and cosmetics there is an extensive research going on the field of encapsulation [1]. Microcapsules can be considered as small containers filled of active compounds that depending on the final application can hold a very wide range of different materials. Often these capsules are made up of organic materials. However, in recent years researchers have been focusing on the synthesis of inorganic capsules, and in particular, silica capsules due to their great chemical resistance, thermal stability, biocompatibility and their non-toxic quality for the environment [2].

Taking all this into account, in the current study silica microcapsules with diameters in the range of nano, micro, and in some cases almost in the millimetre scale containing different organic compounds have been synthesized combining the sol-gel chemistry with the oil in water microemulsion technology [3]. Having final applications possibilities in mind two types of organic compounds have been encapsulated, epoxy materials and phase change materials (PCM).

It has been observed that as well as the sol-gel parameters the viscosity (which in this case ranges from 3 cP to 6000 cP) and the chemical nature of the compounds have an effect on the size and morphology of the microcapsules. Furthermore in the current study the thermal stability of the organic compounds after been encapsulated as well as the phase change performance of the microencapsulated PCMs have been characterised. In particular the phase change performance is an important parameter for the later application of these materials.

References

[1] Authors, Journal, **Issue** (Year) page.
[1] I.van Driescche, S. Hoste in:"Functional Coatings by Polymer Microencapsulation" Ed. by S.K.Ghosh (Wiley-VCH, Weinheim, 2006). Chapter 8.
[2] C.J. Barbé, L. Kong, S. Calleja, J.V. Hannah, E. Drabarek, D.T. Cassidy, M.G. Blackford, J. Sol-Gel Sci. Techn., **46** (2008), 393.
[3] B.Y. Ahn, S.I. Seok, I.C. Baek, S.I: Hong, Chem. Commun., **2** (2006) 189 (2006).

Characterization of nanomechanical biosensors for DNA detection by Scanning Light Analyzer and Fluorescence Microscopy.

Carina Esteves*, Nicolás F. Martínez*****, Oscar Ahumada*****

*MecWins S.L., C/ Santiago Grisolía 2, 28760 Tres Cantos (Spain)

cesteves@mecwins.com

Nanomechanical biosensors are based on the principle that molecular recognition on the surface of a biofunctionalized cantilever, results in its bending by few nanometers (static mode) or in changes in its resonant frequency (dynamic mode). On both modes, the origin of the nanomechanical response is the change of the surface stress due to electrostatic, Van der Waals forces and steric intermolecular interactions on the cantilever's surface. These sensors require covalent chemioadsorption of biomolecules on one side of the cantilever through means of surface chemistry.

Cantilever deflections are monitored as a direct measure of adsorption-induced surface stress. Fast deflection sensing and full 3D characterization of cantilever arrays of any size are possible with a Scanning Light Analyzer (SCALA), a new platform developed by Mecwins [1,2].

We have used SCALA to detect the immobilization of DNA molecules on chemically-modified silicon microcantilever biochips. The biosensing principle, applied as the key application for DNA detection, is based on the role of hydration forces in controlled biolayers [3]. To perform this experiment, the upper surfaces of cantilevers in a silicon chip were chemically-modified to generate a high density of silanol groups. Afterwards, a solution containing fluorecescence marked amine-modified single-stranded (ss) DNA was dropped on one of the modified surface of the cantilever, resulting in the adsorption of amine-modified ssDNA molecules onto the cantilever's surface forming a self-assembled monolayer (SAM). Simultaneously to the characterization done with SCALA, samples were examined by fluorescence microscopy to relate the homogeneity and density of biomolecules with the measured surface stress.

References
[1] N. F. Martínez, P. M. Kosaka, J. Tamayo, J. Ramírez, O. Ahumada, J. Mertens, T. D. Hien, C. V. Rijn, and M. Calleja Rev. Sci. Instrum. **81**, (2010) 125109.
[2] Kosaka P.M., Tamayo J., Gil-Santos E., Mertens J., Pini V., Martínez F.M., Ahumada O., and Calleja M., Journal of Applied Physics, **JR10-6518R** (2011).
[3] Mertens, J., Rogero, C., Calleja, M., Ramos, D., Martín-Gago, J.A., Briones, C. & Tamayo, J., Nature Nanotechnology **3** (2008) 301.

Nanostructure biosensor for fumonisin b1 based on paramagnetic beads and monoclonal antibodies

Laura Bonel[2], Juan C. Vidal[1], **Alba Ezquerra[1]**, Susana Hernández[2] and Juan R. Castillo[1]

[1]Institute of Environmental Sciences (IUCA)

Analytical Spectroscopy and Sensors Group (GEAS)

University of Zaragoza. Ciudad Universitaria (50009) ZARAGOZA. Spain

[2]CAPHER IDI S.L, C/Ermesinda de Aragón , 4, c 116, 50012 ZARAGOZA. Spain

E-mail: lbonel@capher.es

Analytical methods for the determination of mycotoxins are usually based on high pressure liquid chromatography (HPLC) with fluorescence detection (FLD). Many of these methods have been validated by the AOAC (Association of Official Analytical Chemists). The chronoamperometric immunosensor with disposable screen-printed electrodes (SPCEs) are a valuable analytical tool that can be used in portable systems for in situ determination of mycotoxins, with a sensitivity and selectivity comparable or superior to that obtained by traditional ELISA methods but with a much better reagent consumption and less time of determination. Specifically, this immunosensor was successfully developed for the detection of ochratoxin A. In our previous work are explained in detail all the steps necessary to optimize and develop this sensor.

Fumonisin B1 is a mycotoxin produced by several Fusarium fungi, classified as possible human carcinogen by the IARC in Group 2B. Fumonisins are similar structurally to sphingosine therefore interfere and disrupt sphingolipid metabolism, specifically inhibit ceramide synthase. In animals, these mycotoxins cause diseases such as equine leukoencephalomalacia (ELEM) in horses and pulmonary oedema (PE) in pigs. Other toxic effects include carcinogenicity, hepatotoxicity, nephrotoxicity and effects on the immune system. In humans, ingestion of these toxins is linked to high rate of esophageal cancer in areas of South Africa and China. Therefore the European Commission suggests that the maximum tolerable intake of Fumonisin is 2 µg/kg body weight.

We have developed different strategies of immunosensors for Fumonisin B1, using monoclonal antibodies and magnetic particles functionalized with tosyl group, which allows different stages of the immunoassay in solution and SPCE sensor surface allows a good electrochemical detection, avoiding problems of nonspecific adsorption on the electrode or electroactive interference.

Silver and Poly(*tert*-butyl)acrylate Nanocomposites for Molecular Detection by SERS

S. Fateixa, N. Jordão, H. Nogueira and T. Trindade

Department of Chemistry, University of Aveiro, 3810-193 Aveiro, Portugal
e-mail: sarafateixa@ua.pt

Abstract — Nanocomposites of poly(*tert*-butyl)acrylate have been prepared via in situ miniemulsion polymerization in the presence of Ag nanoparticles (NPs) that have been previously prepared by the polyol method. Electron microscopy (SEM/TEM) showed sub-micron polymer composite particles loaded with the metal phase. The nanocomposites were characterized by infrared spectroscopy and thermal analysis, and these results will be discussed. The Ag based nanocomposites were then investigated as new substrates for surface enhanced Raman scattering (SERS) aiming to develop new platforms for (bio)sensing. In this context, the performance of the composite substrates for SERS of distinct analytes (e.g. thiosalycilic acid) will be discussed.

Introduction

Nanotechnology based on novel systems composed by metal particles encapsulated in a polymer matrix open a broad range of new applications for biomedical material [1], optoelectronics and photonics areas [2], as well as biosensors [3].

Following our studies on the effects of inorganic nanoparticles (NPs) on the properties of diverse polymers, this work aims to investigate the influence of Ag NPs in poly(*t*-butylacrylate) (P*t*BA), used here as dispersing medium. Furthermore, the Ag/P*t*BA nanocomposites were investigated in more detail as new SERS substrates using the thiosalicylic acid as model analyte (Figure 1).

Experimental

Silver nanoparticles (NPs) were firstly prepared by an adaptation of the polyol method and employed as fillers to load P*t*BA prepared *in situ*, based on a similar methodology described by us for Au nanocomposites [4]. All the nanomaterials used in this work have been characterized by a number of techniques, which include vibrational spectroscopy, electron microcopies and thermal analysis.

Results and Discussion

The final morphological characteristics of the nanocomposite particles of Ag/P*t*BA depend on several parameters such as the Ag particle size and shape, capping agent and, as expected, on the polymerization conditions.

SEM and TEM analysis of the nanocomposites showed that the polymer is coating each single Ag NP. Thermal analysis showed that the glass transition temperature (T_g) of the nanocomposite decreased in comparison to the T_g of the pure polymer. These results will be discussed taking into account the possible effects of the Ag NPs on the polymer chain interactions.

The Ag/P*t*BA nanocomposites describe above were investigated in more detail as new SERS (Surface-Enhanced Raman Scattering) substrates. These nanocomposites are particularly promising for (bio)molecular detection due to the potential application as substrates in aqueous emulsions or as solid films.

Figure 2 shows the Raman spectrum of a drop of thiosalicylic acid solution (10^{-3} M) on the top of the solid nanocomposite substrate and pure polymer. These results showed an enhancement (see 1500-1600 cm^{-1} region) of the analyte Raman signal when Ag/P*t*BA was used as substrate. For sake of comparison, Fig.2 also shows the conventional Raman spectrum of thiosalicylic acid. Furthermore, we have investigated the dependence of the SERS signal of thiosalicylic acid when deposited onto the nanocomposites and at temperatures lower and higher than T_g.

Conclusions

New Ag/PtBA nanocomposites were prepared by *in situ* miniemulsion polymerization using the respective monomer and organically capped Ag nanoparticles. TEM analysis confirmed the encapsulation of the Ag nanoparticles in the polymer matrix and DSC showed a decrease of the polymer glass transition temperature (T_g) in the nanocomposite. The nanocomposites obtained revealed as new SERS sensitive substrates using thiosalicylic acid as molecular model. These results open new perspectives to develop a new class of Ag based substrates for (bio)molecular detection using Raman spectroscopy.

References

[1] J. J. Mock, S. J. Oldenburg, D. R. Smith, D. A. Schultz, S. Schultz, Nano Lett., 5 (2002) 465.
[2] L. Nicolais, G. Carotenuto (Eds), Wiley Interscience, 2005;
[3] A. J. Haes, D. A. Stuart, S. Nie, R. P. V. Duyne, J. Fluorescence, 14 (2004) 355.
[4] M. A. Martins, S. Fateixa, A. V. Girão, S. S. Pereira, T. Trindade, Langmuir, 26 (2010) 11407.

Figures
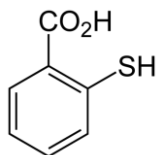
Figure 1
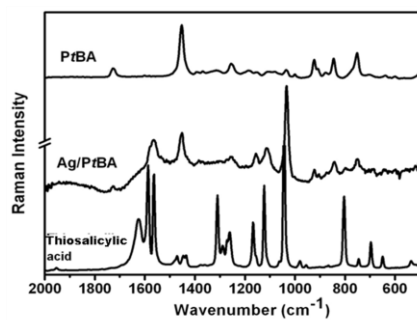
Figure 2

Figure caption

Figure 1: Structural formula for thiosalicylic acid
Figure 2: Conventional Raman spectrum for thiosalicylic acid. SERS spectrum of thiosalicilyc acid solution (10-3 M) dropped in Ag/PtBA solid film and the corresponding Raman spectrum when pure PtBA was used as substrate.

Role of interface in the interparticle magnetic interactions in Fe_xAg_{100-x} ($20 \leq x \leq 55$) granular thin films

Alonso, Javier[1]; **Fdez-Gubieda, Mª Luisa[1]**; García Prieto, Ana[1]; Fernández Barquín, Luis[2]; Alba Venero, Diego[2]; Meneghini, Carlo[4]; Neisius, Thomas[5]; Fauth, Francois[6]; Ruffoni, Matt[6]; Orue, Iñaki[3]; Svalov, Andrey[1]

1. Electricity and Electronics, UPV/EHU, Leioa, Vizcaya, Spain.
2. CITIMAC, Universidad de Cantabria, Santander, Spain.
3. SGIker, UPV/EHU, Leioa, Spain.
4. Dipartamento di Fisica "E. Amaldi", Università di Roma Tré, Roma, Italy.
5. Institut Matériaux Microelectronique Nanosciences, Universités paul Cézanne, Marseille, France.
6. ESRF, Grenoble, France.

jalonsomasa@gmail.com

Nanogranular solids present a rich variety of magnetic states, which are related to, among other factors, the magnetic interactions. These interactions depend on the size and the separation of the magnetic nanoparticles, but also on the nature of the nanoparticles/matrix interface, as seen in Fe-Ag and Co-Cu granular thin films [1-3]. In order to study the role of this interface, we have prepared Fe-Ag thin films ($\sim$100-200 nm) in the range of 20-50 at. % Fe by pulsed laser deposition technique (PLD). These films have been deposited at 300 K onto Si(100) substrates, and coated with $\sim$10 nm of Ag. Their compositions have been determined by energy dispersive X-ray analysis (EDX) and the structure has been studied by X-Ray Diffraction (XRD), High Resolution Transmission Electron Microscopy (HRTEM), Grazing Incidence Small Angle X-Ray Scattering (GISAXS) and X-Ray Absorption Spectroscopy (XAS). DC and AC zero-field-cooled/field-cooled (ZFC-FC) curves have been measured, using SQUID and PPMS magnetometers, as a function of temperature (5-350 K) and the applied magnetic field (5-100 Oe).

Structure analysis has revealed that Fe_xAg_{100-x} are basically composed of small bcc Fe nanoparticles ($\sim$2-3 nm) inside a granular Ag fcc matrix ($\sim$10 nm). For the $Fe_{50}Ag_{50}$ sample, together with these crystalline nanoparticles, an interparticle amorphous $Fe_{50}Ag_{50}$ alloy has been found, with a variable thickness of a few nm, as revealed by ultra-HRTEM micrographs (see figure 1, left). This interface occupies around a 25 % of the sample, as indicated by EXAFS fittings. As the Fe concentration decreases, the system becomes more amorphous like.

Concerning the magnetic behaviour, $Fe_{50}Ag_{50}$ sample shows two magnetic transitions at high and low temperatures (see figure 1, right). We have determined that these transitions are mediated by the magnetic ordering/disordering of the amorphous interface.

At low temperatures ($T < 65$ K), this interface is in a spin glass like state, as corroborated by the presence of an exchange bias phenomenon in the hysteresis cycles $M(H)$. Consequently, the amorphous interface disables the transmission of the direct exchange interactions between the Fe nanoparticles. This makes the global magnetization decrease, and the system enters into a superspin glass (SSG) state, mediated by the dipolar interactions, the intraparticle anisotropies, and the inherent structural disorder. If the magnetic field increases, the spin glass disorder is rapidly overcome. Using a modified random anisotropy model [4], we have estimated that the effective anisotropy of the Fe nanoparticles is $K = 0.9.10^5$ J/m^3, while the average distance for the correlated magnetic fluctuations is $L_0 = 48$ nm.

At intermediate temperatures, $70 < T < 205$ K, the amorphous interface is ferromagnetically ordered, coupling the Fe nanoparticles by direct exchange interaction. Therefore, the system reaches a very stable long range ferromagnetic (FM) order and the global magnetization increases. By increasing the field, an increasingly stable ferromagnetic behaviour is observed.

At high temperatures ($T > 210$ K), the amorphous interface becomes paramagnetic, as previously observed by Chien *et al.* [5] and, therefore, the direct exchange between the nanoparticles is again disabled, and the magnetization of the system decreases. As a result, the correlation length among the

nanoparticles decreases, as corroborated by a sudden increase in the coercive field with T, and the system enters into superparamagnetic like (SPM) state.

Very similar magnetic behaviours have been obtained in reentrant spin glass systems, such as nanocrystalline alloys with small nanograins of Fe growth from an amorphous matrix [6]. In this kind of materials, the interactions among the Fe nanograins are highly influenced by the nature of the interface between them and the matrix.

For the Fe_xAg_{100-x} thin films with $x < 50$, both the $M(T)$ and $M(H)$ curves indicate a predominantly amorphous nature, even if some small Fe nanoparticles are present.

References

[1] A. García Prieto, M.L. Fdez-Gubieda, C. Meneghini, A. García Arribas, and S. Mobilio *Phys. Rev.* B **67** (2003) 224415

[2] A. García Prieto, M.L. Fdez-Gubieda, J. Chaboy, M.A. Laguna-Marco, T. Muro, and T. Nakamura *Phys. Rev.*B **72** (2005) 212403

[3] J. Alonso, M.L. Fdez-Gubieda, J.M. Barandiarán, A. Svalov, L. Fernández Barquín, D. Alba Venero, and I. Orue, *Phys. Rev.* B **82** (2010) 054406

[4] W.C. Nunes, L.M. Socolovsky, J.C. Denardin, F. Cebollada, A.L. Brandl, and M. Knobel *Phys. Rev.* B **72** (2005) 212413

[5] C.L. Chien and K.M. Unruh *Phys. Rev.* B **28** (1983) 1214

[6] J. Arcas, A. Hernando, J.M. Barandiarán, C. Prados, M. Vázquez, P. Marín, and A. Neuweiler *Phys. Rev. B* **58** (1998) 5193

Figures
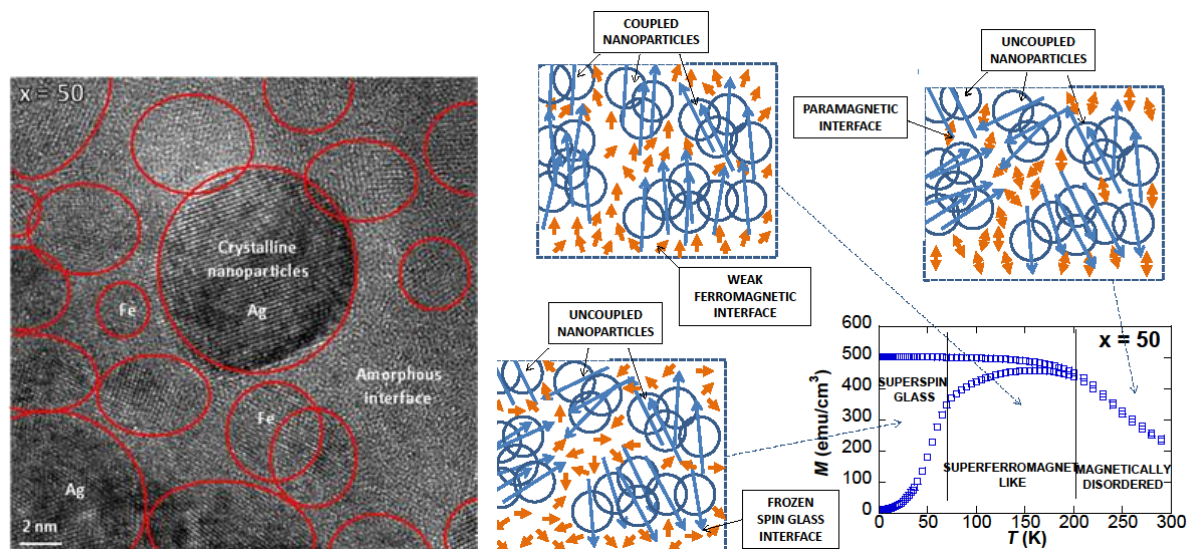
FIG1: (left) High resolution transmission electron micrograph obtained for a $Fe_{50}Ag_{50}$ sample deposited by PLD. Ellipsoids mark the positions of some crystalline nanoparticles. (right) Picture of the thermal evolution of the magnetic structure for a $Fe_{50}Ag_{50}$ thin film. Simplified pictures of the magnetic moments configurations in three ranges of temperatures are also included.

Enhanced adherence of ALD TiO$_2$ nanocoatings in polymeric substrates

O. Prieto, J. Fermoso, I. Segura, I. Lungoci, M. Acebes, R. Irusta and A. Lorenzana

Fundación CARTIF, Parque Tecnológico de Boecillo Par. 205, Boecillo (Valladolid), España.
olgpri@cartif.es

TiO$_2$ self-cleaning coatings are finding increasing applications in several fields, i.e. windows´ glasses, buildings´ materials, pavements of roads, automobiles´ components, etc. Such an interest is due to the capability of those coatings, to add decontamination and self-cleaning properties to the substrates in which are deposited. The coatings are generally layers of around 200 nm thickness, which can be obtained by several techniques. Atomic layer deposition (ALD) is a method for thin film deposition where the solid material is formed as a result of subsequent self-limited surface reactions [1]. The deposition occurs sub-monolayer by sub-monolayer, giving an accurate control over film thickness and composition. Furthermore, the self-limiting growth mechanism enables the deposition of uniform films on large areas and complex-shaped surfaces. ALD nucleation usually requires that the substrate has reactive surface groups with which the precursor molecules can react to initiate ALD growth. Hydroxyl groups on oxide surfaces are typical examples of such reactive groups. In that case, the deposited thin film is chemically bonded to the underlying substrate, and will therefore usually have a good adhesion.

Polymers are very important as substrate materials for self-cleaning coatings. Polymeric substrates include paints, plastic sheets and laminates. A problem in coating polymers by oxide materials is the low surface energy of polymers, and the lack of proper binding sites on the surface, which result in low adhesion and weak mechanical properties. Various surface treatments have been suggested for increasing the surface energy of polymers, including ion-beam irradiation, plasma modification, laser treatment, UV irradiation and chemical treatment [2]. Increasing surface energy enhances the wettability and improves coating uniformity and adhesion [3].

This work presents the results of a thorough study which main objective was the surface modification of polymer substrates to enhance the adherence of TiO$_2$ nanocoatings obtained by ALD tool (figure 1) Two polymeric substrates where considered (PMMA and PC), and were subjected to physical (UV irradiation) and chemical (immersion under sulphocromic solution). These methods cause the C–C chains to break down and form polar groups such as carbonyl, carboxyl and alkoxy, thus changing the wettability characteristic of the surface from hydrophobic to hydrophilic. The samples were characterised to evaluate the characteristics of the modified surfaces, by conducting FT-IR, and surface energy measurements. Spectroscopic results allow to monitor photochemical changes in PMMA surface. ATR-FTIR spectra of unirradiated and UV-irradiated PMMA are shown in figure 2. The hydroxyl/hydroperoxide (absorbing at 3000–3600 cm^{-1} range) and carbonyl groups (absorbing at 1600–1800 cm^{-1}) are mainly responsible for the increase of sample wettability upon UV. The broadening of the whole carbonyl band indicates that new oxidized groups are formed resulting of photochemical reactions. Furthermore, the roughness of the surfaces was measured by nanoindentation. Samples from the surface-treated and sound polymers were TiO$_2$ coated by ALD (5000 cycles, 100ºC). The adherence of the coatings was measured by using the cross-sectional nanoindentation technique, as well as scratch analyses [4], obtaining both quantitative and qualitative measurements of the coatings adherence.

References

[1] M. Leskelä, M. Kemell, K. Kukli, V. Pore, E. Santala, M. Ritala, J. Lu., Materials Science and Engineering C 27 (2007) 1504

[2] M. Ozdemir, C. U. Yurteri, and H. Sadikoglu. Critical Reviews in Food Science and Nutrition 39 (1999) 457.

[3] C. Li, K. Jordens, G.L. Wilkes, Wear 242 (2000) 152.

[4] J.M. Sánchez, S. El-Mansy, B. Sun, T. Scherban, N. Fang, D. Pantuso, W. Ford, M.R. Elizalde, J.M. Martínez-Esnaola, A. Martín-Meizoso, J. Gil-Sevillano, M. Fuentes, J. Maiz. Materialia 47 (1999) 4405.

Figures

Figure 1. Atomic Layer Deposition equipment used to obtain nanocoatings
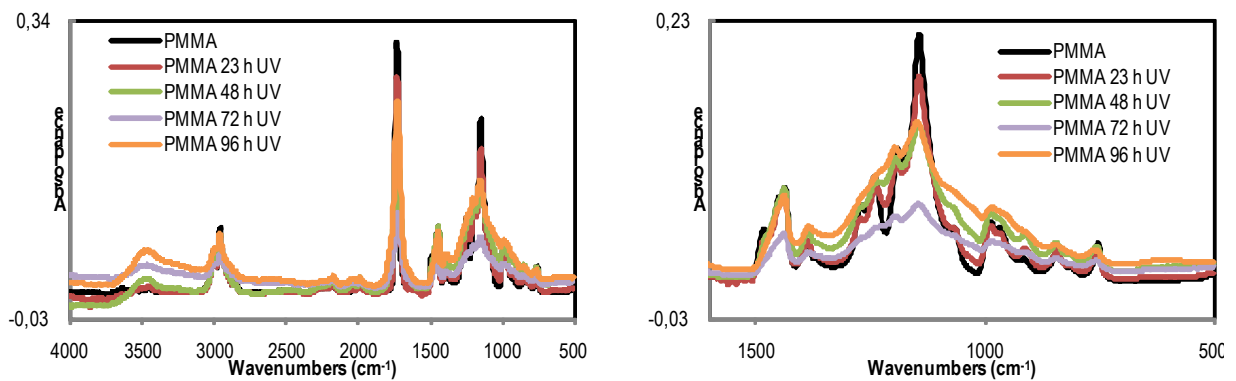
Figure 2.ATR- FTIR spectra of PMMA with UV treatment.

Phonon softening on the specific heat of nanocrystalline metals

L. Fernández Barquín, D. P. Rojas, J. Rodríguez Fernández, L. Rodriguez Fernández , J. Gonzalez and C. Echevarria-Bonet

University of Cantabria, av. de los Castros s/n. 39005, Santander, Spain
barquinl@unican.es

In nanocrystalline (nc) metals with particle sizes below 5 nm and $T \leq \Delta$ (Δ is the average electronic level spacing), the quantum electronic effects seem to strongly influence the thermodynamic properties at low temperatures [1]. However, at higher temperatures for $T >> \Delta$ and/or sizes above 5 nm, the level distribution becomes irrelevant and the influence of size effects on the specific heat can be basically attributed to phonons. It is expected that at the surface of particles the loss of bonding of atoms leads to a modification of the phonon modes, affecting the thermodynamic properties, such as the specific heat.

In this sense, specific heat measurements in the temperature range between 150 and 300 K on nc-Pd (6 nm) and Cu (8 nm) have revealed higher values than in the polycrystalline state, which was attributed to the contribution of the interface [2].

It is worth commenting that the experimental results reported in nc-metals have been constrained to this enhancement above 150 K, and no experimental evidences about a low temperature anomaly, which has only been described theoretically [3], were reported before our results [4,5]. Our first step towards the understanding of this issue was addressed very recently in the study of the influence of size effects on the physical properties of the $YbAl_3$ intermediate valence material [4]. In particular, a low temperature peak around 40 K in the specific heat was derived from the analysis of changes on the magnetic contribution of nanosized samples. However, this last result may be affected by the complicated electronic structure of these alloys.

For this reason, we have extended our studies to more simple systems as common metals Cu, Fe and Ni in order to give a full description of the behaviour of the specific heat in all temperature ranges [5].

The results of measurements in bulk and nc-Fe, Cu, Ni and $LaAl_2$ alloy have shown an excess specific heat in the nanosized samples. In addition to a slope increase at high temperatures (T > 150 K), already reported in some nc-metals, a peak at low temperatures between 20 and 65 K is clearly observed. The analysis of the specific heat curves indicates that the experimental data are in good agreement with a model which considers contributions from the grain boundary and core atoms in the nanoparticles. This model is supported by Raman spectroscopy measurements, indicating the presence of a softening of phonon modes at the surface in the nc-samples associated with a size reduction and increase of the atomic disorder.

References

[1] Halperin W P, Rev. Mod. Phys. 58 (1986) 533; Volokitin Y, Sinzig J, de Jongh L J, Schmid G, Vargaftik M N and Moiseev I I, Nature 384 (1996)621.

[2] Rupp J and Birringer R Phys. Rev. B 36 (1987) 7888

[3] Wolf D, Wang J, Phillpot S R and Gleiter H, Phys. Rev. Lett. 74 (1995) 4686

[4] Rojas D P, Fernández Barquín L, Espeso J I, Rodríguez Fernández J and Chaboy J, Phys. Rev. B 78 (2008) 094412

[5] Rojas D P, Fernández Barquín L, Rodríguez Fernández J, Rodríguez Fernández L, Gonzalez J, Nanotechnology 21 (2010) 445702

Figure 1
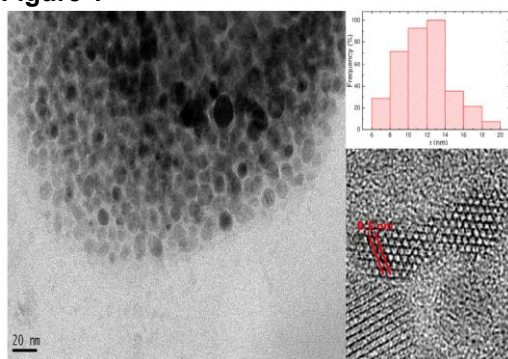
TEM image of nc-LaAl$_2$ showing nanoparticles with a mean size of 12 nm. In the insets, details of the distribution of the particle sizes (above right) and high resolution TEM images of a particle (below right) are given. The interatomic distance between lattice planes inside a particle is around 0.5 nm.

Figure 2
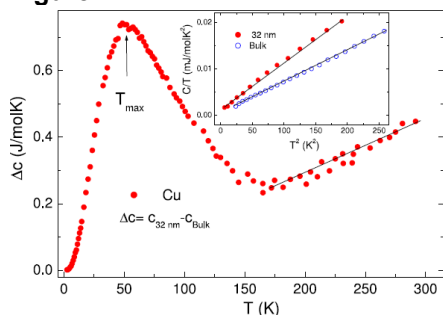
Temperature dependence of the difference of the specific heat between the bulk and nc-Cu (32 nm). A peak at 50 K and a contribution (slope increase) above 150 K are observed. In the inset, the plot of c/T versus T^2 evidencing the change in the slope, and therefore in θ_D, is presented. Lines are just guides for the eyes.

Figure 3
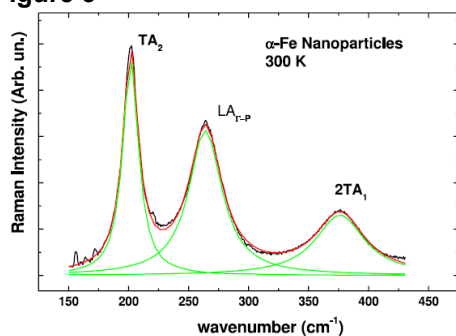
Raman spectrum of nc-Fe (20 nm) at 300 K showing overtones of acoustic phonons (TA1 and TA2) in the $\Gamma-N$ direction and LA in the $\Gamma-P$ ones. The solid lines are the result of the fitting of the peaks with Lorentzian functions.

Advanced large-scale production of high-purity small-sized nanoparticles, dispersions, ready for use nanoproducts with industrial applications

TECNAN
TECNOLOGÍA NAVARRA DE NANOPRODUCTOS SL
Perguita Industrial Area, A street, 1
Los Arcos (Navarre), Spain
tecnan@tecnan-nanomat.es

These days, the importance of nanotechnology is continuously increasing not only for the incredible future prospects, but also for current applications. Regarding this idea, solid projects in order to take advantage of the present possibilities will be the pillars for the next stage. Among all the synthesis techniques available, it is worth highlighting the advanced technology used in TECNAN (developed in L'UREDERRA Technological Centre) for a large-scale production of a wide variety of nanoparticles; resulting in extremely innovative nano-products with a very competitive price.

Nanoparticles of simple nano-oxides such as CeO_2, TiO_2 and ZnO have been synthesised by the pyrolytic dry-oxidation/pyrolysis of various precursors commercially available. This method is advantageous as many step processes of wet chemistry are not involved; resulting in high-purity nano-products after completing a process of outstanding simplicity. Furthermore, the procedure is environmentally friendly (the emission of nanoparticles into the air is carefully controlled) and no by-products are generated. The innovative process used in TECNAN starts solving the precursor in an organic solvent (e.g. toluene) under stirring in a reactor; this resulting solution is then exposed to pyrolysis in sophisticated equipment. Synthesised nano-powders are deposited in some filters and after several shakes the product is collected. Some details are confidential due to a patent.

Moreover, a detailed research has been made in order to achieve an appropriate methodology for industrial scale. The innovative technology developed enables high production rates, from grams to tonnes (lab. & industrial orders). In fact, when working at full capacity, a kilogram per hour can be obtained. For the obtaining of each nano-product, different specific procedure has been followed considering parameters such as solvent proportion, temperature, etc; based on the same method typology. Besides the basic production of those nano-oxides, the flexibility of the method makes possible new complex synthesis in such a large scale as well. Several variations are also being introduced in order to improve size-control and dispersity.

BET measurements were made to the described nanoproducts in order to obtain precise information related to the specific surface area of each material In addition, the nanoparticles have also been characterised by TEM technique, showing relative/acceptable dispersity. The obtained nano-powders have soft colours (white, yellowish white...) and show great stability; they are packed in plastic bags and containers and stored in a warehouse at room temperature.

Another technical advantage that TECNAN has, is that TECNAN can produce complex and simple oxides with the same easiness, using the same procedure for both, with high quality

standards, high purity, stability at a very competitive price, in a flexible and environmentally friendly way, since no waste or by-products are generated. Production in only one step results in important savings in time, energy and cost. The flexibility of this methodology enables the preparation of a wide range of nanoproducts. TECNAN has 4 product range categories:

1- Nano-powders: Using advanced synthesis techniques, TECNAN produces and commercialises at industrial scale nano-oxides of more than 60 elements of the Periodic System in a clean and environmentally friendly way, obtaining products with high quality and purity, very small size (7-25 nm) and with multisectoral applications.

2- Dispersions: All the nano-powders produced by TECNAN are available dispersed in different media such as water, alcohols and other solvents, both in standard concentrations and in ad-hoc conditions according to the client's demands.

3- Tecnadis "ready for use nanoproducts": With it's know-how in nanotechnology, TECNAN has developed a range of exclusive references based in advanced nanoparticle. These innovative products are completely ready to be applied directly on different substrates.

4- Masterbatches: TECNAN is highly skilled regarding incorporation of diverse nanofillers into polymeric matrices in order to obtain optimised properties for a broad spectrum of plastic materials such as polyethylene, both high and low density, polypropylene, EVA, rubber, etc.

TECNAN nanomaterials have applications in very different sectors, e.g. automotive catalysts, energy sector, construction of gas and pollutant sensors, photo-catalysts, electronic and photovoltaic materials, cosmetic, paint and varnish, etc. helping to establish TECNAN as one of the most competitive suppliers of these new materials worldwide.

Wet-chemistry methods for the synthesis of anisotropic nanoparticles with different magnetic order

Nerio Fontaiña-Troitiño,[1] Michael Farle,[2] Veronica Salgueirino[1]

[1]Universidade de Vigo, Dpto. de Física Aplicada, 36310 Vigo Spain
[2]Universität Duisburg-Essen, Fakultät fur Physik and CENIDE, Duisburg, Germany
vsalgue@uvigo.es

In the last decade interesting magnetic properties have been reported for nano-crystalline magnetic particles for which the importance of size and shape is well known. These materials have been widely used in the electronics industry for the fabrication of components, in ferrofluids, sensors and biomedical applications.

We propose two wet-chemistry processes that allow the synthesis of anistropic magnetic nanoparticles of very different materials that therefore offer different magnetic properties.

Ferrimagnetic ferrite nanostructures (MFe_2O_4, M: Mn, Fe, Co, Ni, Zn) with cubic shapes can be synthesized following a new wet-chemistry method based on the thermal decomposition of metal precursors [1] and on the growth of the nanostructures controlled by amines. Before studying their magnetic properties control over their size, shape (cubooctahedral in the left TEM image) and polydispersity has been achieved by means of the synthesis conditions.

Antiferromagnetic Cr_2O_3 nanoparticles can be synthesized by means of the calcination of the chromium hydroxide precursor $Cr(OH)_3$, previously obtained by precipitation in the presence of sodium hydroxide.[2] The final nanoparticle shape (mainly cubic but also hexagonal in the right TEM image) can be controlled by changing the ligands in the initial solution during the coprecipitation.

References

[1] B. Yuhas, D. Zitoun, P. J. Pauzauskie, R. He, P. Yang, Angew. Chem. Int. Ed., **45** (2006) 420.
[2] M. Bañobre-López, C. Vázquez-Vázquez, M. A. López-Quintela, J. Rivas, Nanotech. **14** (2003) 318.

Figures
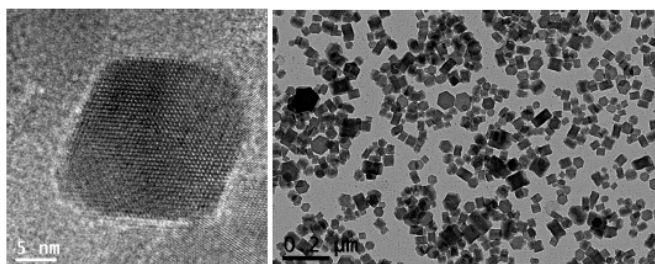
(HR)TEM images of $ZnFe_2O_4$ (left) and Cr_2O_3 (right).

Effect of different couplings on the relaxation time of a magnetic dimer

A. F. Franco, J. M. Martinez, J. L. Dejardin, and H. Kachkachi

LAMPS, Université de Perpignan Via Domitia, 52 Avenue Paul Alduy, 66860 Perpignan Cedex, France
andres.franco@univ-perp.fr

An issue of great interest to the community of magnetism today is the dynamics of coupled magnetic films and their applications in MRAM technology. It has been shown [1] that these structures, and among them the so-called Magnetic Tunnel Junctions (MTJ), provide promising features for efficient magnetic recording. The dynamics of such systems strongly depends on many physical parameters related with the films material properties and, in particular, on the coupling between the magnetic films.

In this work we investigate the effect of exchange (EI) and dipole-dipole (DDI) coupling on the dynamics of a magnetic dimer (MD) composed of two magnetic layers coupled via a nonmagnetic spacer. We use the kinetic theory of Langer to obtain (semi-)analytical expressions [2, 3] for the relaxation time of the MD coupled by either EI or DDI and compare their efficiency in the MD reversal.

Each magnetic layer is modeled by a macroscopic magnetic moment of fixed magnitude and with uniaxial anisotropy pointing in an arbitrary direction with respect to the applied field (Fig. 1). In the case of DDI, three different anisotropy configurations have been studied: longitudinal anisotropy (both easy axes are parallel to the MD bond), transverse anisotropy (both easy axes perpendicular to the MD bond) and mixed anisotropy (one parallel and one perpendicular to the MD bond). In the case of the longitudinal anisotropy the DDI has been compared to EI.

The results are shown in Fig. 2 where the (reduced) relaxation time is plotted as a function of $\sigma = \dfrac{KV}{k_B T}$,

which is the anisotropy-energy (reduced) barrier in the absence of interactions. Here K is the anisotropy constant of the material, taken to be the same for both magnetic layers; V is the volume of the magnetic slabs; T the temperature; and k_B the Boltzman constant. $\tau_0 \sim 10^{-9}$ is the (characteristic) free-diffusion time. In order to compare the effects of these two interactions, which lead to different switching mechanisms, we have considered the switching of the MD from the same initial state into the same final state, the initial state being with both magnetic moments pointing upwards out of plane; the final state being with them pointing downwards out of plane. The switching path followed by the two magnetic moments, which determines the switching mechanism of the MD, depends on the type of coupling and intensity of the latter.

Apart from the fact that the relaxation time obviously increases with σ (or with decreasing temperature) for both EI-MD and DDI-MD, we see that for both coupling regimes there is a critical value σ_c at which the relaxation times corresponding to EI and DDI intersect each other. This means that below σ_c the MD switches faster via one coupling than via the other; the order in which this happens depends on the coupling regime.

In the strong coupling regime it is the DDI that leads to the shortest switching time below σ_c and then the situation reverses beyond σ_c . In this regime the EI energy barrier is constant (owing to saturation) while that of DDI continues to grow. So, below σ_c the prefactor of the relaxation time prevails and the

DDI is more favorable for a fast switching. However, as σ_c is exceeded, the energy barrier prevails over the prefactor and thereby the ever growing DDI energy barrier leads to a longer switching than via EI.

In the WC regime the situation is different since the MD switching operates via the fanning mode (a two-step process) passing through an intermediate state and crosses two saddle points. For EI the ratio of the relaxation rate of the second step to that of the first step implies that for small values of σ (high temperature), namely $\sigma \leq \sigma_c$, the second step is slower than the first. However, in the case of DDI the second step is always faster than the first. Therefore, for small σ the EI leads to a faster switching, whereas above some critical value of σ , or equivalently below some critical temperature, the lower energy barrier of DDI leads to a shorter switching time.

In conclusion, at low temperature, the EI-MD switches faster than DDI-MD in the SC regime, while at high temperature, EI-MD switches faster than DDI-MD in the WC regime.

References

[1] S.S.P. Parkin et al., J. Appl. Phys. 85 (1999) 5828.

[2] J.S. Langer, Phys. Rev. Lett. 21 (1968) 973; Ann. Phys (N. Y.) 54 (1969) 258

[3] H. Kachkachi, Europhys. Lett. 62 (2003) 650; J. Molec. Liquids 114 (2004) 113 ; Phys. Rev. B 72 (2005) 134425.

Figures
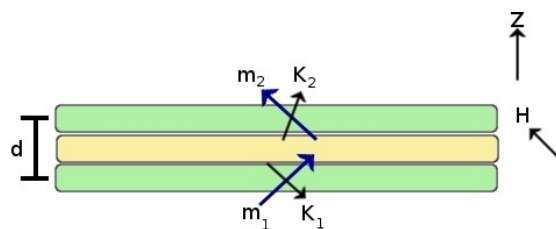
Figure 1: Scheme of an MTJ
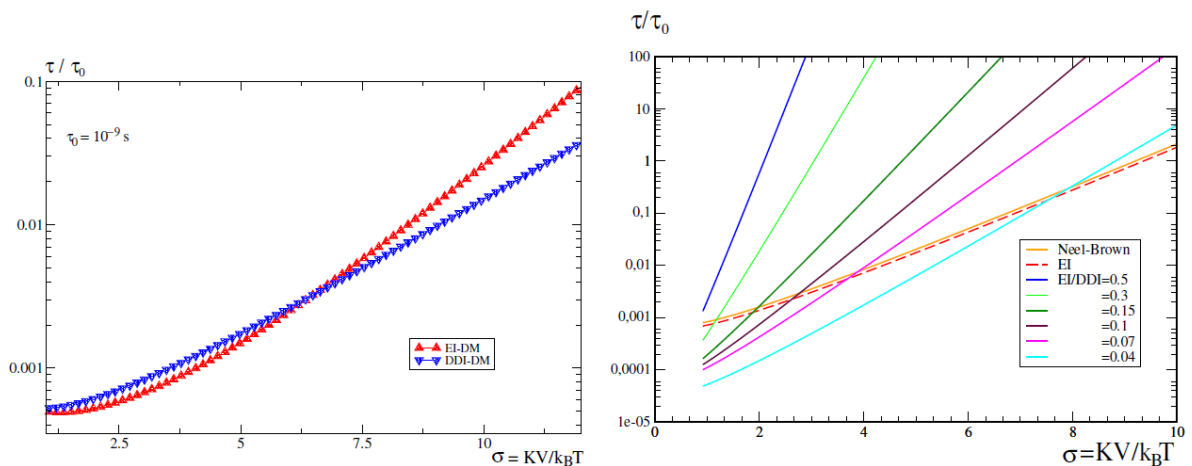
Figure 2: Reduced relaxation time, τ/τ_0 , versus $\sigma = \dfrac{KV}{k_B T}$ for the EI- and DDI-MD, in the absence of the magnetic field, for weak-coupling regime (left) and strong-coupling regime (right). The Néel-Brown result coincides with EI (j=10)

Electron-phonon interactions and magnetism in Fe-based superconductors

Thomas Frederiksen,[1] Bruno Rousseau,[2] Felix Yndurain[1,3]

1) DIPC – Donostia International Physics Center, Paseo Manuel de Lardizabal 4,
20018 Donostia-San Sebastián, Spain
2) Centro de Física de Materiales, CSIC-UPV/EHU, 20018 Donostia-San Sebastián, Spa in
3) Departamento de Física de la Materia Condensada, Universidad Autónoma de Madrid, Cantoblanco,
28049 Madrid, Spain.

Email: thomas_frederiksen@ehu.es

Since the recent discovery of superconductivity in layered Fe-based materials [1,2], with transition temperatures up to 55 K, enormous research efforts have been devoted to characterizing this new class of compounds. One of the most fundamental questions, namely the nature of the Cooper pairing mechanism responsible for superconductivity, is still intensely debated [3]. The coexistence of antiferromagnetic, non-superconducting phases and non-magnetic, superconducting phases depending on chemical doping have lead to theoretical studies exploring the importance of magnetic moments coupled to phonons for superconductivy [4,5,6].

Here we present a first-principles study of electron-phonon interactions and magnetism in $LaFeAsO_{1-x}F_x$ compounds. Our calculations are based on density functional theory as implemented in the SIESTA code [7]. We perform calculations using the virtual crystal approximation (VCA) as well as supercell calculations with F substitutional impurity atoms, and determine the electronic structure as a function of doping. Within a finite difference scheme [8] we further calculate the phonon properties and corresponding electron-phonon couplings to arrive at estimates for the effective electron-phonon coupling strength, conventionally labeled λ, as an average over the Fermi surface. By comparing trends for both non-magnetic and magnetic calculations we are able to quantify the importance of the detailed interplay between electron-phonon coupling and magnetism, as well as their role in superconductivity.

References

[1] Y. Kamihara, H. Hirmatsu, M. Hirano, R. Kawamura, H. Yanagi, T. Kamiya, and H. Hosono, J. Am. Chem. Soc. **128**, 10012 (2006).
[2] Y. Kamihara, T. Watanable, M. Hirano, and H. Hosono, J. Am. Chem. Soc. **130**, 3296 (2008).
[3] J. Paglione and R. Greene, Nature Physics **6**, 645 (2010).
[4] F. Yndurain and J. M. Soler, Phys. Rev. B **79**, 134506 (2009).
[5] L. Boeri, M. Calandra, I. I. Mazin, O. V. Dolgov, and F. Mauri, Phys. Rev. B **82**, 020506(R) (2010).
[6] F. Yndurain, arXiv:1009.4909.
[7] J. Soler, E. Artacho, J. Gale, A. Garcia, J. Junquera, P. Ordejon, and D. Sanchez-Portal, J. Phys.: Condens. Matter **14**, 2745 (2002).
[8] T. Frederiksen, M. Paulsson, M. Brandbyge, A.-P. Jauho, Phys. Rev. B **75**, 205413 (2007).

Conductance distributions in doped single wall Carbon nanotubes: full ab-initio calculations versus macroscopic models.

Luis S. Froufe-Pérez[(1,3)], Alejandro López-Bezanilla[(2)], J. J. Sáenz[(3)]

(1) ICMM-CSIC. Sor Juana Inés de la Cruz, Cantoblanco, 28049 Madrid. Spain.
(2) Oak Ridge National Laboratory, One Bethel Valley Road, Tennessee, USA.
(3) Condensed Matter dept. UAM, Av. Tomás y Valiente. Cantoblanco, 28049 Madrid. Spain.

Luis.froufe@uam.es

In low dimensional systems, the effect of coherent multiple scattering of charge carriers plays a crucial role in transport properties[1]. The disorder inherent to many systems leads to fascinating statistical transport properties, such as Universal Conductance Fluctuations (UCF) [2] or Anderson Localization [3]. Different statistical descriptions of electronic transport through low dimensional systems have evolved over time.

On the one hand, macroscopic approaches, often based on random matrix theory (RMT) [4], consider the scattering matrix of the system as an statistical variable from which relevant transport coefficients can be obtained through the use of Landauer-Büttiker formalism for two probe systems. One of the most celebrated such theoretical frameworks is the DMPK equation [5], it describes the evolution of transport coefficients statistics as a function of the system length. In DMPK, all statistical transport properties depend on a single scaling parameter, namely the length of the system normalized by the transport mean free path.

On the other hand, accurate and realistic first principle models have acquired enough efficiency to deal with large systems. For instance, calculations of conductance as a function of energy, length and functional groups concentration in functionalized single wall carbon nanotubes (SWCNT) [6] can be performed up to micrometer lengths and coverages of hundreds of functional groups.

Only recently both theoretical approaches has been partially compared for rather realistic systems. For instance in [7], first principles modeling of transport through doped Silicon nanowires has confirmed the one-parameter scaling hypothesis comparing conductance averages, and its fluctuations, as a function of system length in the diffusive regime.

Nevertheless, several questions are still open. It is known [8] that surface and bulk disorder can lead to different shapes in the statistical conductance distributions even though they present similar behavior of the first moments of the distribution in the diffusive regime. The comparison of the above mentioned theoretical descriptions all the way from the quasi-balistic regime to the deep localized one has not been done. Interestingly, If the system under consideration is a SWCNT with some kind of scattering sources, it is not clear whether the statistical signatures of disorder will correspond to surface or bulk disorder. It is the purpose of this work shedding light on these questions.

To do so, we study charge transport through metallic SWCNT's with random distribution of phenyl groups attached to the tube surface. The attachment of this functional groups allows us to introduce a defect in the surface of the nanotubes which has consequences in the potential distribution around the grafting sites. Our results describe how the nanotube conductance is perturbed as a function of incident electron energy and functional groups coverage density. To cope with this task an efficient numerical method is crucial. We use a hybrid scheme where we resort to both first principles calculations, to obtain a suitable parametrization of the electronic structure, and a real space renormalization procedure to reduce the size of the system and, then, to solve for the transport problem of large and disordered systems [6]. The quantum transport modeling is based on the Green's function formalism, combining an

iterative scheme for the calculation of transmission coeficients with the Landauer-Büttiker formula for the coherent conductance.

We then compare the results obtained by first-principles calculations with the DMPK equation predictions. The input parameters for the DMPK equation are the number of channels, two in the case of a SWCN, and its average conductance. Using these data we perform a Monte Carlo integration of the joint probability distribution function of the transport eigenvalues in order to obtain the conductance distribution for the current ensemble of functionalized SWCN's.

In Fig.1 we compare both first-principles and DMPK conductance distributions. It can be seen that the full conductance distributions coincide to a large extent within the numerical accuracy of DFT calculations. Furthermore it can be shown that this agreement remains valid at all transport regimes, from quasi-balistic to localized ones.

This fact implies that transport in doped SWCN's is controlled by a single scaling parameter (the averaged conductance) and that the macroscopic transport properties can be obtained through the properties of a single scatterer. Hence, these properties can be predicted for arbitrarily large systems.

On the other hand, the validity of the DMPK signals the bulk nature of the scattering induced by disorder in contrast to surface disorder.

It is worth emphasizing that there is no fitting parameter, the whole conductance distributions are obtained once the average value is fixed.

This quantitative agreement between DMKP and ab-initio descriptions might be extended to more comprehensive descriptions based on RMT [9] able to describe systems where bulk and surface disorder play different roles [10].

References

[1] B.L. Al'tshuler, P.A. Lee and R.A Webb. "Mesoscopic phenomena in solids". North Holland, Amsterdam (1991).
[2] B.L. Al'tshuler, Pis'ma Zh. Eksp. Teor. Fiz. [JETP Lett.] **41**[41] (1985) 530[648]; P. A. Lee and A. D. Stone, Phys. Rev. Lett. 55 (1985) 1622.
[3] P. W. Anderson, Phys. Rev. **109** (1958) 1492.
[4] C. W. J. Beenakker, Rev. Mod. Phys. **69** (1997) 731.
[5]O. N. Dorokhov: JETP Lett. **36** (1982) 318; P. A. Mello, P. Pereyra and N. Kumar: Ann. Phys. (N.Y.) **181** (1988) 290.
[6] A. López-Bezanilla, F. Triozon, S. Latil, X. blasé and S. Roche
, Nano Lett. **9** (2009) 940.
[7] T. Markussen, R. Rurali, A.-P. Jauho and M. Brandbyge, Phys. Rev. Lett. **99** (2007) 076803.
[8] L. S. Froufe-Perez, P. Garcıa-Mochales, P. A. Serena, P. A. Mello and J. J. Saenz, Phys. Rev. Lett. **89** (2002) 246403.
[9] L. S. Froufe-Pérez, M. Yépez, P. A. Mello and J. J. Sáenz, Phys. Rev. E **75** (2007) 031113.
[10] T. Markussen, R. Rurali, M. Brandbyge and A.-P. Jauho, Phys. Rev. B. **74** (2006) 245313.

Figures
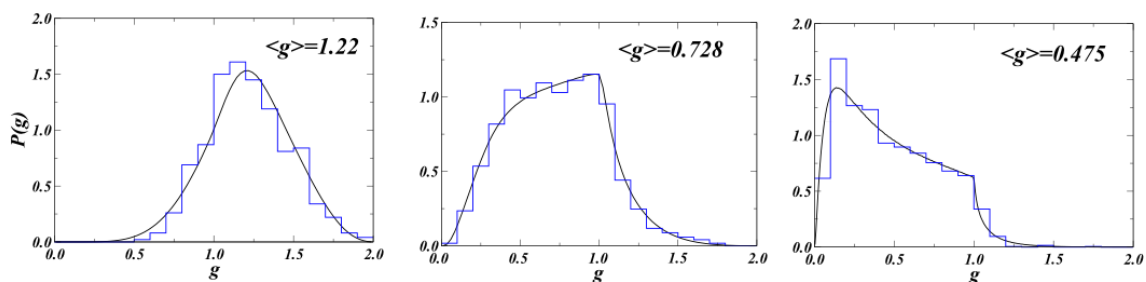
Figure 1: Conductance distributions for different ensembles of functionalized SWCNT's labeled by its averaged conductance. Histograms corresponds to DFT simulations and lines to the DMPK distributions.

Inclusion of Pironine Y in AlPO-5

Raquel Garcia[1], Virginia Martínez-Martínez[2], Cecilia Corcóstegui[2], Joaquin Pérez-Pariente[1], Iñigo López Arbeloa[2]

[1]Instituto de Catálisis y Petroleoquímica (CSIC), C/Marie Curie 2, 28049, Cantoblanco, Madrid, Spain.
[2]Departamento de Química Física, Universidad del País Vasco UPV-EHU, Apdo. 644, 48080-Bilbao, Spain
rgs@icp.csic.es

Abstract

The encapsulation of dyes in different inorganic hosts results in composite materials with interesting optical properties. The ordering of the solid matrix imposes the way of aggregation and ordering of the included dye molecule and, therefore, influences the photophysical properties the composite material [1]. The open nature of the structure of zeolites and zeotypes made them very interesting as host materials. The structure of these solids is built by a three-dimensional arrange of corner-sharing tetrahedra characterized by the presence of channels and/or cavities of molecular dimensions, where different molecules can be encapsulated. These materials are usually prepared using organic compounds which are denominated structure directing agents (SDAs) that remain occluded within the structure at the end of crystallization. As dye molecules are not very different to typical SDAs used in zeolite synthesis, this gives the opportunity to study the in situ incorporation of the dye during synthesis of the material. In particular in this work, we have studied the inclusion directly during crystallization of Pironine Y (PY) within AlPO-5 (AFI structure-type material) focusing on the influence of different paremeters.
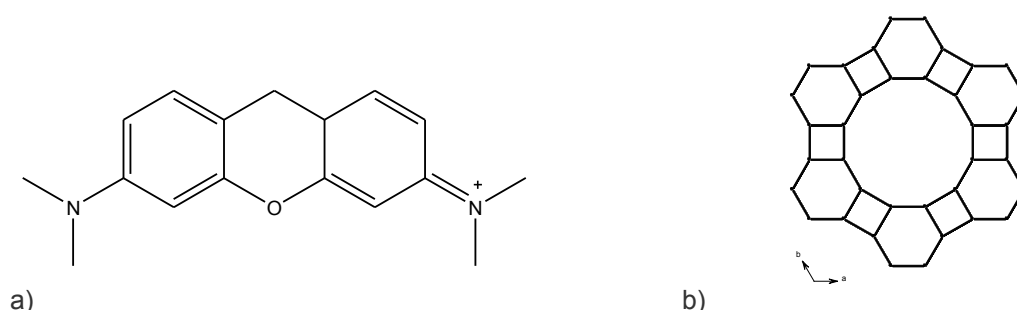
Figure 1 *a) Molecule of Pironine Y and b) channel of AlPO-5*

The big pore material AlPO-5 (AFI) possesses a structure with channels running along one direction (the *c* axes of the structure). The windows that give access to the pore system are delimited by twelve tetrahedra and the dimensions of the channel system are 7.3x7.3 Å

Initially, magnesium aluminophosphate materials were prepared with different SDA as for example triethylamine or tripropylamine, with and without the addition of the dye molecules. Various synthesis parameters were studied as the amount of magnesium and SDA added to the gel. The products obtained were characterized by XRD, TGA, CHN analysis. In the presence of the PY dye, slightly pink in colour AlPO-5 needle-like crystals were obtained as the main product of crystallization with morphology and crystal size similar to those obtained for those prepared in the absence of dye molecules.

Incorporation of the dye in the materials was assessed by fluorescence microscopy. By polarization experiments the adsorption of dye molecules into the internal channels of the aluminophosphate material are checked. Due to the constraints imposed by the framework, the dye molecules should be internally adsorbed mainly along the direction of the main axis of the AlPO needles.

Analysis of the fluorescence of the crystals indicates that the fluorescence is not homogeneous along the particles but is concentrated in the center of the crystals and decreases towards the ends. This result suggests that the dye molecules are preferentially incorporated during the early stages of crystallization and as the concentration of the dye is reduced in the synthesis medium, the dye incorporation in the crystals is gradually decreased. This has been previously observed for a related system [2] and indicates a certain competition between the structure directing agent and the dye molecules.
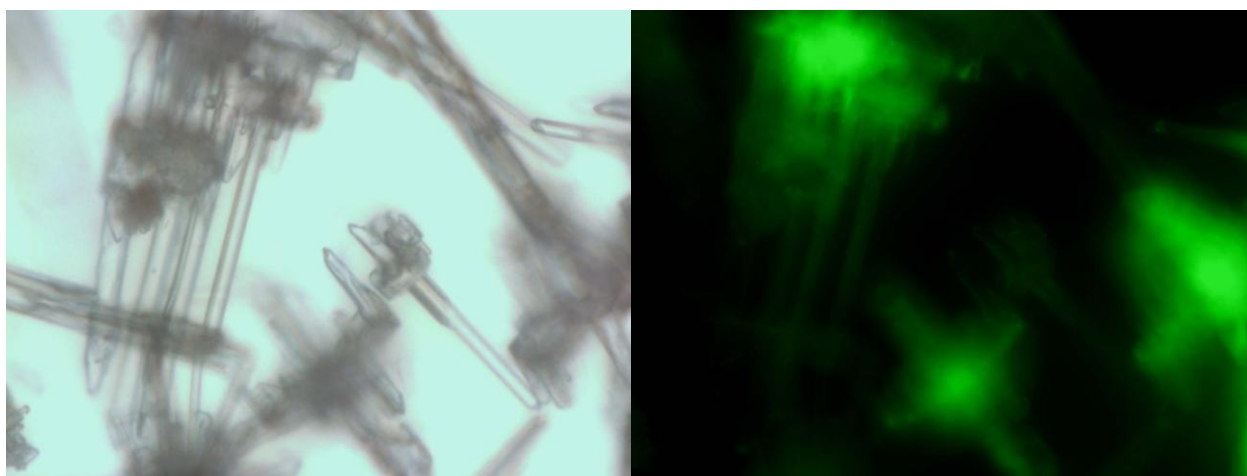
Figure 2. Fluorescence images of MgAPO-5 with PY included..

References

[1] N. Gfeller, and G. Calzaferri, J. Phys. Chem. B**, 101** (1997) 1396.

[2] Ö.Weiβ, J. Loerke, U. Wüstefeld, F. Marlow, and F. Schüth, Journal of Solid State Chemistry, **167**, (2002) 302.

Great improvement of Magneto-Impedance in FeNi-based multilayers by adding Ti spacers of nanometric thickness

E. Fernández, A. V. Svalov, G. V. Kurlyandskaya, J. M. Barandiarán and A. García-Arribas

Departamento de Electricidad y Electrónica, Universidad del País Vasco, Apartado 644, 48080 Bilbao, Spain
alf@we.lc.ehu.es

Soft magnetic thin films with high permeability are being actively studied in several fields such as magnetoelectronics (based on domain wall dynamics, for instance), spin polarized transport, flux concentrators for microdevices and materials for high sensitivity magnetic field sensors, among others. In some of these fields, basic research is exploring amazing possibilities, but still far from real applications. In some others, oriented investigations are trying to enhance the properties of the materials to improve the performance of the devices.

Soft ferromagnetic materials exhibit the Magneto-Impedance (MI) effect manifested by a great change of their electrical impedance under the influence of a magnetic field. If is basically a consequence of the reduction of the effective section for current flow due to the skin effect, and is controlled by the changes of the material permeability due to the applied magnetic field. The relative change in impedance can reach 800% with huge sensitivities to small fields, up to changes of about 500% per Oesterd [1,2]. These extraordinary figures are not approximated at low fields by any other room-temperature magnetic field sensor. Cobalt-based amorphous wires are used in commercial magnetic field sensors that are utilized, for instance, in electronic compasses to detect the Earth magnetic field [3].

In fact, magnetic field sensors are earning an exceptional prominence for multiple applications such as personal electronics (entertainment gadgets, smart phones and related devices, sports, etc.), automotive and transportation (driving aids and autonomous vehicles, high speed trains, aerospace, etc) and bio-medicine (quick and self-diagnosis, targeted drug dosing, localized cancer treatment, etc.). New, competitive sensors must combine high performance with small size (microsensors) and smooth interfacing with conditioning electronic circuitry. Thin film-based MI sensors are well-adapted candidates to fulfill those requirements.

Permalloy ($Fe_{20}Ni_{80}$) thin films can be easily fabricated by evaporation or sputtering (which is preferred for mass production). For MI, a small, well-defined transverse anisotropy (anisotropy field of 1 to 5 Oe) is desired. This can be accomplished by applying a magnetic field during deposition and can be improved by an after-deposition magnetic field annealing. On the other hand, MI is dominated by the skin effect, which is noticeable when the penetration depth is comparable to the thickness of the film. For good results at 1 GHz, 1μm thick films are needed. However, thick sputtered FeNi films develop a columnar structure that takes the anisotropy out of the plane and ruins the magnetic softness. The Argon pressure during the sputtering process determines the energy of the atoms arriving at the surface and the structure of the deposit. After a systematic study of these dependences we succeeded in obtaining 170 nm thick films with optimum magnetic properties deposited at room temperature with an Ar pressure of 4×10^{-3} mbar [4].

In order to further increase the overall thickness of the MI material we have explored a multilayered approach using thin Ti layers to frustrate the tendency of FeNi layers to develop the columnar structure. We have determined that a 6 nm thick Ti layer is sufficient to accomplish that, and have produced multilayered samples of the type [FeNi(170nm)/Ti(6nm)]$_n$/FeNi(170nm) up to n=5, which sums up about 1 μm thin sample [5].

Best MI results are obtained when the Magneto-Inductive effect (reactive part of the impedance) is enhanced. This can be done using a trilayer structure with the magnetic layers enclosing a non-magnetic conducting layer (gold, silver or copper, for instance). We have prepared and tested a series of [FeNi/Ti]$_n$/Cu(t)/[FeNi/Ti]$_n$ multilayered structures with n from 1 to 6 and central Cu layer thicknesses (t) from 10 to 500 nm (figure 1). The samples were deposited onto either rigid glass or flexible polymeric substrates by rf-sputtering, using metallic masks for patterning the samples in the form of 10 mm long and 1 mm wide stripes. Figures 2 shows the MI at 35 MHz (at which the maximum sensitivity is achieved). Figure 3 displays the frequency dependence of the MI ratio and the MI sensitivity of a sample with $n = 3$ and $t = 500$ nm deposited onto a glass substrate. The measurements were performed in a network analyzer using a microstrip line test fixture. The MI ratio $\Delta Z/Z$ for the absolute value of the impedance is defined with respect to the value at the maximum applied field (150 Oe). The MI sensitivity is defined by S (%/Oe) = $(\Delta Z/Z)/\Delta H$, with $\Delta H = 0.1$ Oe. The values of MI (210 %) and S (110 %/Oe) are extremely competitive and promising for applications.

References

[1] M. Vázquez, J. Magn. Magn. Matter., **226-230** (2001) 693.

[2] G. V. Kurlyandskaya, H. Yakabchuk, E. Kisker, N. G. Bebenin, H. García-Miquel, M. Vázquez, V. O. Vas´kovskiy, J. Appl. Phys., **90** (2001) 6280.

[3] Y. Nakamura, T. Uchiyama, C. M. Cai, and K. Mohri, IEEE Trans. Magn., **44**, (2008) 3981.

[4] A. V. Svalov, I. R. Aseguinolaza, A. García-Arribas, I. Orue, J. M. Barandiaran, J. Alonso, M. L. Fernández-Gubieda, and G. V. Kurlyandskaya, IEEE Trans. Magn. **46** (2010) 333.

[5] G. V. Kurlyandskaya, A. V. Svalov, E. Fernández, A. García-Arribas, and J. M. Barandiaran, J. Appl. Phys. **107** (2010) 09C502.

Figures
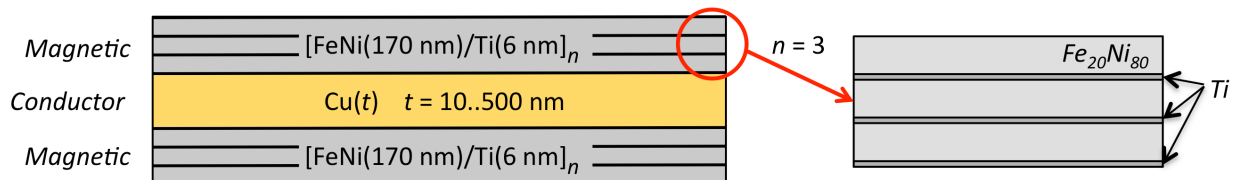
Figure 1. Scheme of the structure of the multilayered $[FeNi/Ti]_n/Cu(t)/[FeNi/Ti]_n$ samples.
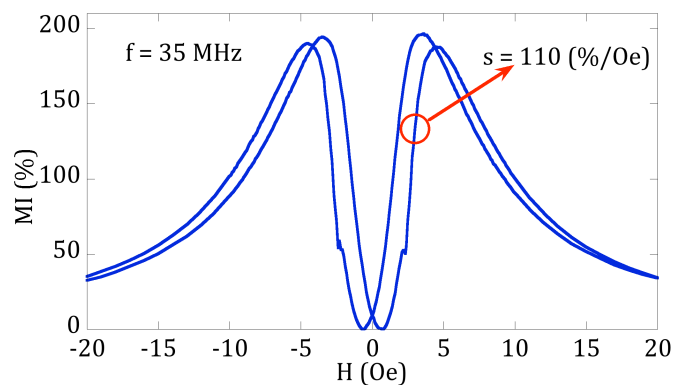
Figure 2. Low field detail of the Magneto-Impedance curve ($\Delta Z/Z$) for a multilayered $[FeNi/Ti]_5/Cu/[FeNi/Ti]_5$ sample with a central Cu layer thickness of 500 nm, measured at the frequency at which the sensitivity is maximum.
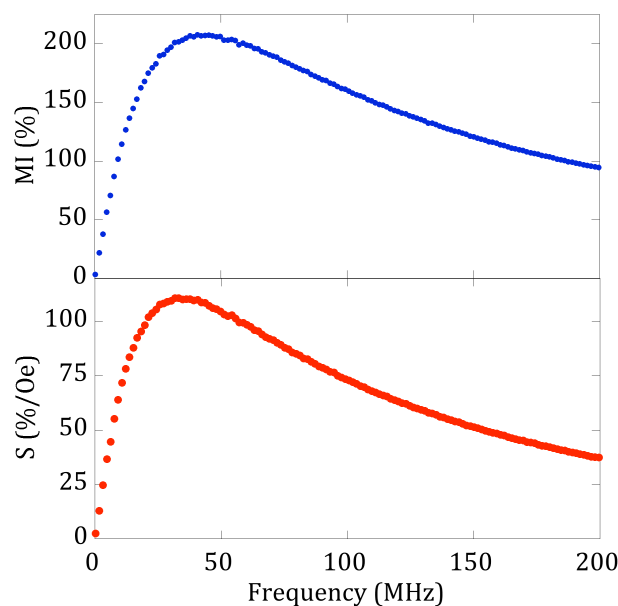
Figure 3. Frequency dependence of: (top) the maximum value of the Magneto-Impedance ratio and (bottom) of the maximum value of the sensitivity for a multilayered $[FeNi/Ti]_5/Cu/[FeNi/Ti]_5$ sample with a central Cu layer thickness of 500 nm.

Dimer-covering RVB treatment of single-walled zigzag carbon nanotubes

M.A. Garcia-Bach

Departament de Física Fonamental, Facultat de Física
and Institut de Química Teòrica i computacional,
Universitat de Barcelona,
Diagonal 647, 08028-Barcelona, Catalonia, Spain.
m.angels.garcia_bach@ub.edu

Single-walled zigzag carbon nanotubes (CNTs) with h hexagons around the carbon nanotube, h ranging from 3 to 19, have been investigated from a resonating-valence-bond point of view. These values of h include realistic CNTs with diameters ranging from 0.5 to 1.5 nm, which correspond to $h \sim 6$ and $h \sim 19$, respectively.

Long-range spin-pairing order (LRSPO) [1,2,3] allows to separate the set of VB configurations in $h+1$ different subsets or phases. The parameter associated with the LRSPO, p, can take the relevant values $p = 0, 1, \cdots , h$.

We have obtained the Heisenberg energy, in units of J per carbon atom, $\varepsilon_p(h)$, and also per polyene ring for zigzag single-walled CNTs with $h= 3, 4, \cdots , 19$ and $p= 0, 1, 2, \cdots , h$, witin a dimer-covering counting approximation [4,5,6]. First, the ground-state energy per carbon atom is obtained when the phase, which we design as p_0, is the integer closest to $h/3$. See, for instance, Figure 1.

From the difference in energy per polyene ring, $\Delta(h)$, in units of J, between the two lowest-lying phases, p_0 and p_1 it is noted that degeneracy between the two lowest-lying phases occurs when $(h +1)/3$ is an integer. Therefore, de-confined low-energy topological spin defects would occur, and these carbon nanotubes should be conductors, in analogy to polyacethylene. See, for instance, Figure 2, where $\Delta(h)$ is represented as a function of h for $h= 3n$-1, $3n$, $3n+1$. In clear contrast, no such degeneracy is observed for either, $h= 3n+1$ or $h= 3n$, so bound pairs of topological spin defects are expected to occur in these cases.

References:

[1] M.A. Garcia-Bach, Eur. Phys. J. B **14** (2000), 439.
[2] M.A. Garcia-Bach, ``Many-body VB ansätze. From polymers and ladder materials to the square lattice'' in *Valence Bond Theory*, Elsevier, New York, 2002, pp. 729-768.
[3] M.A. Garcia-Bach, Phys. Rev. B **72** (2005), 024530.
[4] W.A. Seitz, D.J. Klein, T.G. Schmalz, and M.A. Garcia-Bach, Chem. Phys. Lett. **115** (1985), 139; **118** (1985), 110E.
[5] D.J. Klein, G. E. Hite, and T. G. Schmalz, J. Comput. Chem. **7** (1986), 443.
[6] T.P. \v{Z}ivkovi\'c, B.L. Sandleback, T.G. Schmalz, and D.J. Klein, Phys. Rev. B **41** (1990), 2249.

Figures:
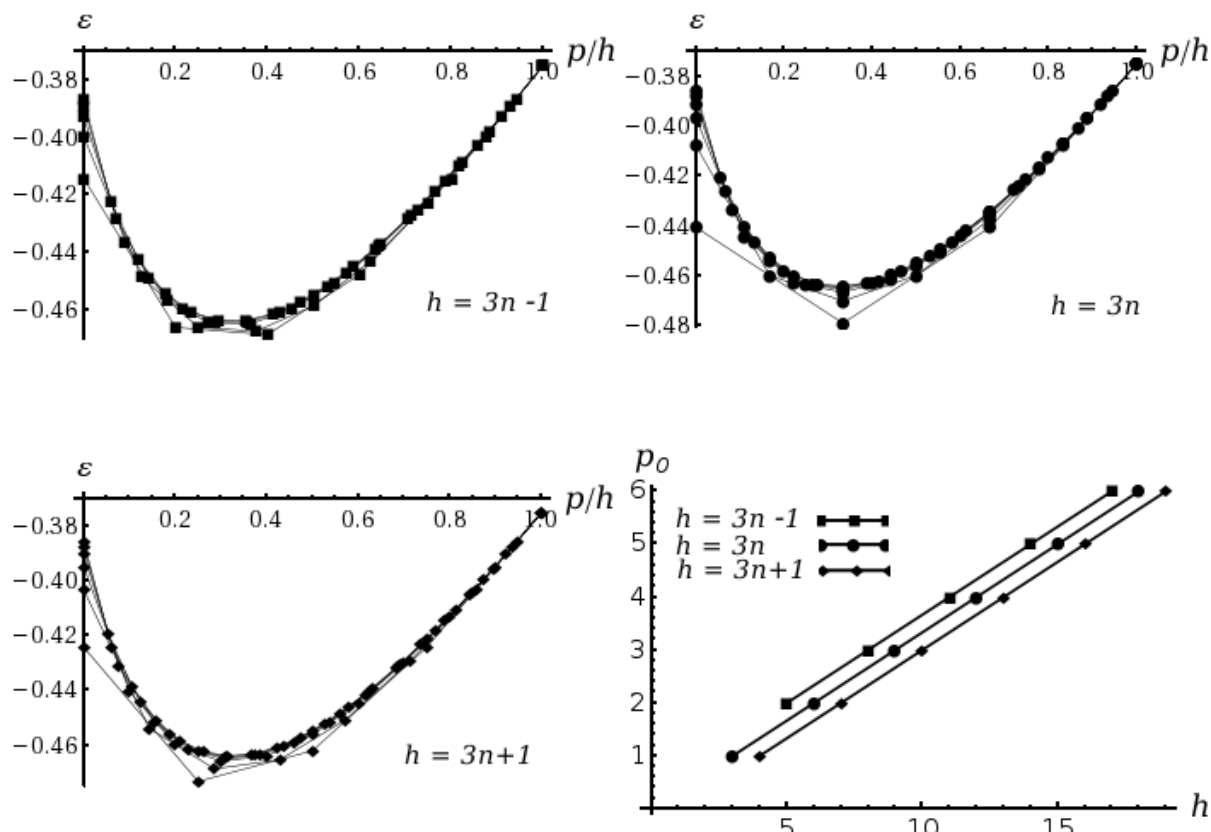
Figure 1.
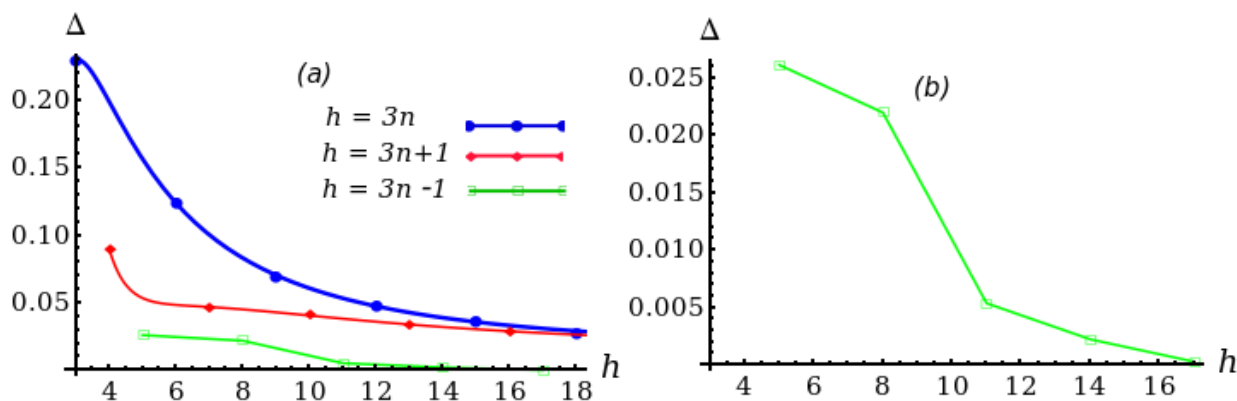
Figure 2.

Figure caption

Figure 1. The energy per carbon atom, $\varepsilon_p(h)$, as a function of p/h: $h = 3n-1$ (■), $h = 3n$ (●), $h = 3n+1$ (◆), with n = integer and h decreasing from top to bottom. Bottom right: The value of the phase p_0 yielding the lowest-lying energy per polyene ring, for $h=3n$ (●), $h=3n+1$ (◆), and $h=3n-1$ (■).

Figure 2. *(a)* Diference in energy per polyene ring, $\Delta(h)$, in units of J between the two lowest-lying phases, p_0 and p_1, as a function of the number of hexagons around the CNT. De continuous lines, from top to bottom, correspond to $h = 3n$ (●), $h = 3n+1$ (◆), and $h = 3n-1$ (□), respectively. The top two continuous lines are obtained by fitting the Δ values by a power series on *1/h, and tend asymptotically to* 0.0125907 and 0.0123187, respectively. The bottom continuous line is obtained by simply joining the calculated values of Δ. *(b)* Δ for $h = 3n-1$, *for $n = 2, \cdots, 6$.*

Apparition of burning phenomenon during the self-ordering of anodic nanoporous alumina

E. García-Lecina[a], B. Gastón-García[a], J.A. Díez[a], M. Belenguer[b], C. Müller[b]

[a] Surface Finishing Department, CIDETEC-iK4, Pº Miramón 196, E-20009 San Sebastián, Spain
[b] ELECTRODEP, Departament de Química Física, Facultat de Química, Universitat de Barcelona, C/Martí i Franquès 1, E-08028 Barcelona, Spain

egarcia@cidetec.es

In the last decades nanostructured surfaces have drawn attention for potential applications in several fields as medical, biological, electrical, optical and micromechanical. One of the promising candidates is anodic aluminium oxide (AAO) with self-organized hexagonal arrays of uniform parallel nanopores, formed by electrochemical oxidation of aluminum (i.e. anodizing process) [1]. These AAO films have recently been proposed as templates for the growth of nano-materials (nano-dots, nano-wires, nano-tubes, etc.), as micro/nano-structures itself (photonic-crystal, nano-composite structures, membranes for bio-separation, etc.) and as reservoir for solid lubricants to form self-lubricating structures [2].

Although aluminum anodic oxidation is a technique used to fabricate highly ordered array structures at a nanometer scale, the conditions under which self-organization occurs are limited and depend on the acid species of the electrolyte. Thus, each electrolyte has an individually specified self-ordering voltage, for example: sulfuric acid at 25 V, oxalic acid at 40 V and phosphoric acid at 195 V, giving 63, 100 and 500 nm pore intervals, respectively [3-5]. When the anodic voltage deviates outside the self-organization regime, the order of nanopores becomes poorer. Therefore, voltage is a crucial parameter to control the self-ordering and for this reason anodizing applying a constant voltage is the most standard method to fabricate highly ordered AAO films. It should be noted that the self-ordering voltage induces high current density, conditions close to the apparition of burning [6,7] (phenomenon that occurs at extremely high current flow concentrated at the local points of the aluminum surface leading to the local film thickening [8,9]). This suggests that the condition inducing film growth under high current density, i.e. the high electric field, is the key factor determining the self-ordering. Consequently, anodizing at constant current is also an interesting procedure because it allows a more uniform oxide growth and a better control of local catastrophic phenomena as burning or cracking.

In the present work, the development of burning during the formation of nanoporous AAO films in a sulphuric acid anodizing process was investigated. The study focused mainly on the AA1050 aluminum anodizing in galvanostatic conditions and the comparison with voltage control conditions. Within this context, the effect of different variables as temperature, electrolyte concentration, current density-voltage, etc. were analyzed. Additionally, the application of a two-step anodizing and the utilization of high purity (99.998%) aluminum as substrate were studied. The characterization of the AAO films consisted in assessing their appearance, thickness, morphology (OM, FE-SEM), composition (EDS, EPMA) and microhardness.

References

[1] P.G. Sheasby and R. Pinner, *The Surface Treatment and Finishing of Aluminum and Its Alloys*, 6th ed., Vol. 1, Finishing Publications Ltd. with ASM International, 2001.
[2] A. Eftekhari, *Nanostructured Materials in Electrochemistry*, WILEY-VCH, 2008.
[3] H. Masuda and K. Fukuda, Science 268 (1995) 1466.
[4] H. Masuda, F. Hasegwa and S. Ono, J. Electrochem. Soc. 144 (1997) L127.
[5] H. Masuda, K. Yada and A. Osaka, Jpn. J. Appl. Phys. 37 (1998) L1340.
[6] S. Ono, M. Saito and H. Asoh, Electrochem. Solid-State Lett., 7 (2004) B21.
[7] S. Ono, M. Saito, M. Ishiguro and H. Asoh, J. Electrochem. Soc., 151 (2004) B473.
[8] T. Aerts, I.D. Graeve and H. Terryn, Electrochim. Acta 54 (2008) 270.
[9] T. Aerts, I.D. Graeve and H. Terryn, Surf. Coat. Technol. 204 (2010) 2754.

Figures
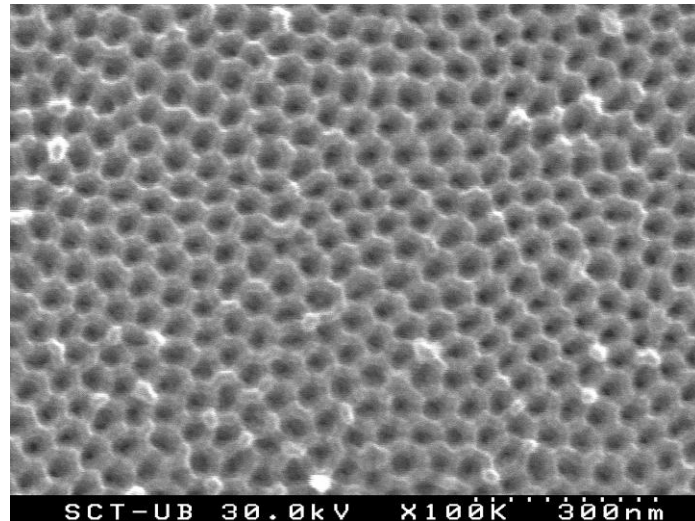
Fig.1. On-bottom FE-SEM image of an AAO film obtained after a two-step anodizing process in sulphuric acid electrolyte.

Transverse magneto-optical effects in Fe antidot arrays

J. F. Torrado[1], E. Th. Papaioannou[2], G. Ctistis[3], P. Patoka[4], M. Giersig [4],G Armelles[1] and
A. Garcia-Martin[1]

[1]Instituto de Microelectrónica de Madrid (IMM-CNM-CSIC), Isaac newton 8, Tres Cantos,
28770 Madrid, Spain
[2] Department of Physics and Astronomy, Uppsala University, 75121 Uppsala, Sweden
[3] Complex Photonic Systems (COPS), MESA+ Institute for Nanotechnology, University of Twente, The
Netherlands
[4] Helmholtz-Zentrum Berlin fur Materialien und Energie GmbH, 14109 Berlin, Germany

antonio@imm.cnm.csic.es

During the last decade, an increasing interest has been devoted to the analysis of the interplay between plasmon resonances and magneto-optical (MO) effects [1], since the plasmon resonances can be used to enhance the MO response [2-4] and the MO effect can be used to control the plasmon propagation [5].

A great number of the studies of the MO enhancement due to plasmon excitation have been carried out in the so-called Polar Kerr configuration for MO active nanostructures (either dots or antidots) [2] or when metal nanostructures have been put into contact with continuous films of MO active material [3]. However, in the Transverse Kerr configuration the studies focus on metallic nanostructures over continuous films [4].

Here we cover that gap and study the Transverse Kerr Magneto-Optical Effect (TMOKE) of iron hexagonally perforated films (470nm pitch, 100nm thickness and radii of 248nm and 297nm respectively) [6]. We observe a large enhancement of the TKOME signal with respect to that of the continuous film, and relate that frequencies to the possibility of surface plasmon excitations.

Apart from the orientation of the magnetic field the TMOKE differs from the Polar configuration in the angle of incidence of the light beam: the Polar effect is studied at normal incidence, whereas the TMOKE needs to be off normal, since the signal is zero otherwise. This means that when the nanostructuration is realized in a periodic fashion (see Fig. 1) there is an additional parameter to take into account: the azimuth (in-plane) angle. We will also analyze the TMOKE enhancement as a function of the orientation of the sample plane with respect to the incident light beam as shown in the experimental TMOKE spectra in Fig 1.
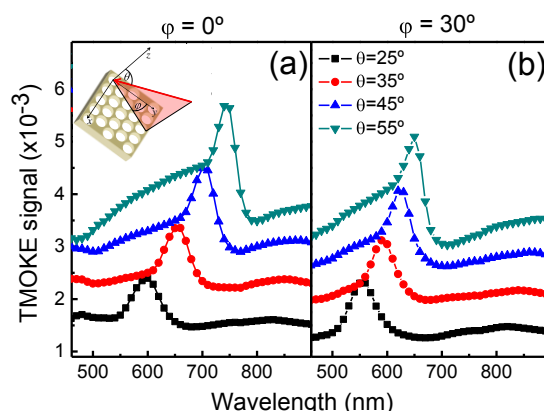
Fig. 1: Schematic representation of the system, and TMOKE signal for a Fe membrane along $\phi = 0°$ and $\phi = 30°$.

References

[1] G. Armelles, et al., J. Opt. A: Pure Appl. Opt. **11** (2009) 114023.

[2] J.B.González-Díaz, et al., Adv.Mater. **19**, (2007) 2643; Small **4**, (2008) 202; G. Ctistis et al., Nano Lett. **9**, (2009) 1; J.B. González-Díaz, et al., Appl. Phys. Lett. **94**, (2009) 263101; E. Th. Papaioannou, et al., Phys. Rev B **81**, (2010) 054424.

[3] A.B. Khanikaev, et al., Opt. Express **15**, (2007) 6612; V. I. Belotelov, et al., Phys. Rev. Lett. **98**, (2007) 077401; G.A. Wurtz, et al., New J. of Phys. **10** (2008) 105012; G.Armelles, et al, Opt. Express **16**, (2008) 16104.

[4] V.I. Belotelov, et al., J. Opt. Soc. Am. B, **26** (2009) 1594;

[5] J.B. González-Diaz, et al. Phys. Rev. B. **76**, (2007) 153402; E. Ferreiro-Vila, et al., Phys. Rev. B **80**, (2009) 125132; V.V. Temnov, et al. Nature Photonics **4**, (2010) 107.

[6] J.F. Torrado, et al, PSS-rrl, **4**, (2010) 271.

Effect of nano-sized Al_2O_3 particles on the electrodeposition and properties of Ni/Al_2O_3 nanocomposite coatings

I. García-Urrutia[a], E. García-Lecina[a], A. Salicio[a], P. Indyka[b], J.A. Díez[a], J. Morgiel[b]

[a]Surface Finishing Department, CIDETEC, Pº Miramón 196, 20009 Donostia-San Sebastián, Spain
[b]Institute of Metallurgy and Materials Science, Polish Academy of Science, ul. Reymonta 25, 30-059 Krakow, Poland
igarcia@cidetec.es

Composite electrodeposition is a method of codepositing micrometer or nanometer-sized particles of metallic, non-metallic compounds or polymers in an electrodeposited metal matrix in order to improve material properties such as wear resistance, lubrication or corrosion resistance. In this sense, the codeposition of ceramic particles gives exceptional advantages in terms of mechanical properties (hardness, chemical inertia, good frictional behaviour) as compared to alloy and pure metal electroplating [1-3].

One of the most widely applied composite coatings is the Ni/Al_2O_3 system [4-6]. They have good tribological properties and have quite good anticorrosion properties. Due to their properties, they find application as coatings of engine cylinders, high-pressure valves and dies and in the production of musical instruments, drill fittings, car accessories and small aircraft and electrotechnical parts [7].

Most of the studies in this field have been focused on the use of micrometric particles, but with the emergence of nanotechnologies, interest on the codeposition of nanometer-sized particles have increased in the last years. Some studies have demonstrated that a decrease in the size of the particles from micro- to nano-scale can improve mechanical and tribological properties of electrochemically deposited composite coatings. However, first attempts showed that the percentage of nanoparticles incorporation was low and that the particles tend to form agglomerates in the electrolyte bath. To confirm this behavior, in previous studies developed in CIDETEC the Al_2O_3 nanoparticles suspended in a nickel Watts baths were analyzed using electroacoustics method in order to determine particle size. In this sense, it was observed that the nano-alumina particles were easily agglomerated into larger particles in the electrochemical electrolyte. In order to avoid this agglomeration, the use of different physical (pulse plating, ultrasounds) and chemical (additives) methods are currently being investigated by different research groups [8-10].

In the present work, Ni/Al_2O_3 composite coatings were electrodeposited galvanostatically from a Ni Watts electrolyte to which γ-Al_2O_3 nanoparticles (d_m = 50 nm) were added. The effect of physical (agitation by means of an ultrasonic horn) and chemical (addition of a cationic surfactant) dispersion methods on the electrodeposition of Ni/Al_2O_3 nanocomposite coatings and on the composite properties was analyzed.

The Ni/Al_2O_3 nanocomposite coatings obtained were characterized from the compositional (EDX), morphological (SEM) and structural (TEM) points of view. As the mechanical behavior of these systems is very important from the viewpoint of practical applications, some mechanical properties like hardness and wear resistance were also evaluated.

The results showed that both methods (ultrasonic agitation and additive addition) lead to an increase on the codeposition of Al_2O_3 particles, modify the morphology and structure of the composite coatings and improve their mechanical (hardness and wear resistance) properties. The dispersion effect was more pronounced in the case of electrodeposition under ultrasonic field.

References

[1] C. Kerr, D. Barker, F.Walsh, J. Archer, Trans. IMF **78** (2000) 171.
[2] J. Fransaer, J.P. Celis, J.R. Roos, J. Electrochem. Soc. **139** (1992) 413.
[3] C. Buelens, J.P. Celis, J.R. Roos, J. Appl. Electrochem. **13** (1983) 541.
[4] A. Bund, D. Thiemig, Surf. Coat. Technol. **201** (2007) 7092
[5] Q. Feng, T. Li, H. Yue, K. Qi, F. Bai, J. Jin, App. Surf. Sci. **254** (2008) 2262
[6] B. Szczygiel, M. kolodzieg, Electrochim. Acta, **50** (2005) 4188
[7] S. Steinhauser, B. Wielage, Surf. Eng. **13** (1997) 289
[8] L. Chen, L. Wang, Z. Zeng, J. Zhang, Mat. Sci. Eng. A, **434** (2006) 319

[9] S-L. Kuo, Y-C. Chen, M-D. Ger, W-H. Hwu, Mat. Chem. Phys., **86** (2004) 5
[10] L. Chen, L. Wang, Z. Zeng, T. Xu, Surf. Coat. Technol., **201** (2006) 599

Figures
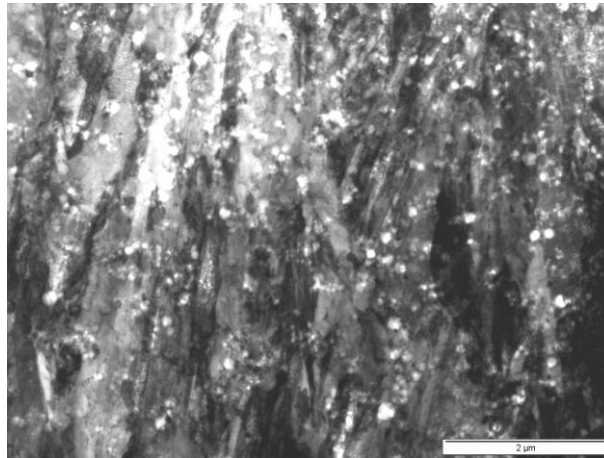
Figure 1. TEM micrograph of a cross section of a Ni/Al$_2$O$_3$ composite coating obtained under ultrasonic agitation.

Photoactive Nanomaterials based on Zeolite L doped with BODIPY

Leire Gartzia Rivero, Jorge Bañuelos, Iñigo López Arbeloa

Dpto Química Física, Facultad de Ciencia y Tecnología, Universidad del País Vasco (UPV-EHU), Aptdo 644, 48080 Bilbao, Spain
leire.gartzia@ehu.es

The incorporation of organic photoactive molecules into nanostructured solid host is an active area of research.[1] Such materials offer many advantages for the development of new versatile optoelectronic devices. On one hand, the rigid environment of the solid host protects the organic molecule against chemical or photochemical attacks and increases its thermal resistance. Moreover, such constrained framework can modulate the electronic and optical properties of the organic guest. On the other hand, the organic molecule can act as a fluorescent sensor to monitor the physicochemical characteristics of the surrounding solid environment of the fluorophore.

To this aim laser dyes are adequate guest molecules. Among the different laser dye families covering the ultraviolet and visible region, recently Boron DiPyrromethene (BODIPY) fluorophores are becoming one of the most used molecules in tunable lasers, fluorescent sensors, antenna systems or fluorescent markers in biochemical systems (Figure 1).[2] This is due to their unique photophyscial properties. BODIPY laser dyes present strong absorption and fluorescence bands characterized by very high fluorescence quantum yields. Besides, the emission region and even their photophysical properties can be modulated by the adequate substitution pattern. Taking all these features into account we decide to incorporate this fluorophore into a nanostructured host with a channel architecture. In this sense zeolite L fulfill of these requirements.[3] Zeolite L is an aluminosillicated with one-dimensional channels running along the crystal with a pore diameter of about 7.1 Å (Fig. 1). Both commercial zeolite L (Lucidot) and ourself synthesized zeolite L by the hydrothermal method assisted by microwave energy, have been employed.

Therefore, the present work is focused on the incorporation of BODIPY dyes into the nanochannels of zeolite L and the spectroscopic and microscopic characterization of the resulting material. The dye doped zeolite has been successfully achieved by gas adsorption at high temperatures after sublimation at vacuum of the BODIPY. Thus, a highly fluorescence material is obtained since the BODIPY is adsorbed into the pores exclusively in the monomeric form. The photophysical properties of the dye doped zeolyte remind to those recorded in diluted dye solutions in spite of the high number and proximity of the dye molecules in the channels. In this way, the presence of aggregates is avoided, which damage the fluorescent ability of the dye. Polarized light confocal microscopy ensures that the BODIPY is only present in the inner space and not in the outer surface of the zeolite. Moreover, the anisotropy response of the material indicates that the geometrical restrictions of the channels orient the dye with its transition moment parallel to the main axis of the channel (Figure 2).

Summing up, we have obtained zeolite L crystals doped with a high amount of BODIPY dye without sign of aggregation. Consequently, a highly fluorescent and ordered material is obtained. Moreover, the cage-protecting effect of the zeolite improves the thermostability of the dye. Such requirements are essential in order to be successfully applied in optoelectronic devices. Further work is in progress in our laboratory to explore the possibilities of these novel hybrid materials.

References

[1] M. Ogawa, K. Kuroda, Chem. Rev., **95** (1995) 399.
[2] F. López Arbeloa, J. Bañuelos, V. Martínez, T. Arbeloa, I. López Arbeloa, Int. Rev. Phys. Chem. **24** (2005) 339.
[3] G. Calzaferri, S. Huber, H. Maas, C. Minkowski, Angew. Chem., **42** (2004) 3732.

Figures
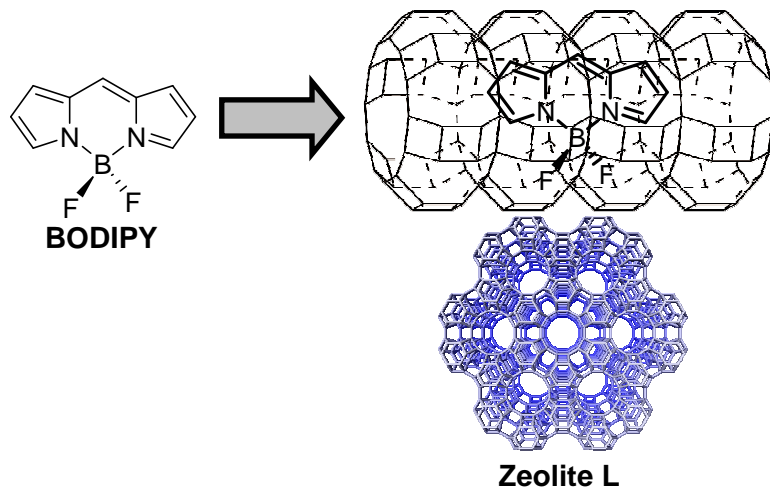
Figure 1. *Boron DiPyrromethene (BODIPY) molecular structure and view of the channel framework of zeolite L.*
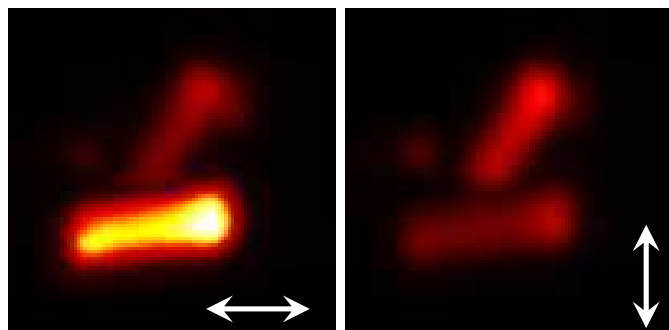
Figure 2. *Fluorescence confocal microscope images of micrometer-size zeolite L doped with BODIPY with horizontal and vertical polarized light.*

Scaling Pentacene organic field-effect transistors down to the 20 nm regime

F. Golmar[*1], F. Marchesin[1], M. Gobbi[1], R. Llopis[1], F. Casanova[1,2], and L. E. Hueso[1,2]

[1] CIC nanoGUNE Consolider, Tolosa Hiribidea 76, E-20018 San Sebastian, Spain
[2] IKERBASQUE, Basque Foundation for Science, E-48011 Bilbao, Spain
* On leave from CONICET, Argentina
e-mail: fgolmar@nanogune.eu

Currently, there is significant interest in organic thin-film transistors (OTFT) due to their potential application in inexpensive, large-area electronics. However, carrier mobilities are typically low (<1cm^2/V s) and, to increase the OTFT drive current per unit area, there is a need for short-channel devices (below 10 μm).

Here, we report on the fabrication and electrical properties of short-channel OTFT. Palladium (Pd) source and drain electrodes were formed by e-beam lithography and lift-off, in order to obtain channel lengths down to the sub-20 nm range. Our selected organic semiconductor (Pentacene, Pc) was deposited from a Knudsen cell in a ultra-high vacuum evaporation system. Pc morphology has been optimized by varying both the evaporation and substrate temperatures. We have fabricated working devices with channel lengths from 10 μm down to 20 nm (see Fig. 1), covering 3 orders of magnitude in the channel length. The fabrication process has been optimized resulting in high (90%) yield of working devices. OTFT that employ Pc as the semiconducting layer work as p- channel accumulation- mode devices (see Fig. 2).

Similar transistors have also been fabricated using Permalloy (NiFe) electrodes. These ferromagnetic electrodes will allow us to explore spin-polarized currents in organic materials.

Figures
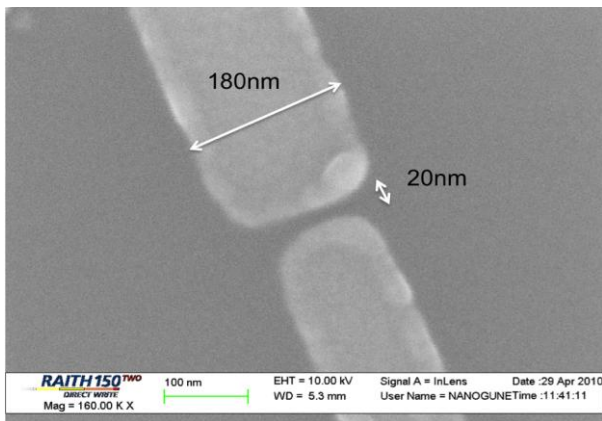
Figure 1: Palladium drain and source electrodes separated by a 20 nm gap.
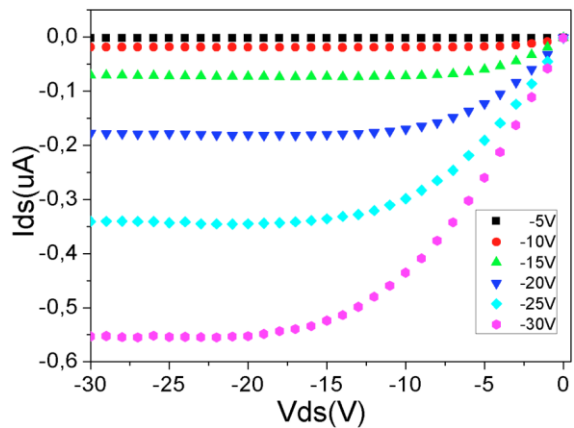
Figure 2: Drain-Source currents of a Palladium-Pentacene device, as a function of the Drain-Source voltage for different Gate-Source voltage from -5V to -30V.

Improving hydrophobicity of ZnO surfaces by combining nanoimprint lithography and sol-gel technology

Estíbaliz Gómez, Mª Carmen Márquez, Amaia Martínez, Estíbaliz Aranzabe

Fundación Tekniker, Avda Otaola, 20, Eibar, Spain
egomez@tekniker.es

In recent years, the wetting properties of solid surfaces have attracted much attention, partly inspired by the natural lotus effect resulting from a kind of natural surface with very high water repellency. In addition to naturally occurring micro- and nanostructures, the fabrication of artificial structures on a solid surface can render the surface with tunable wetting characteristics.

The wetting property is deeply influenced by the surface free energy and the surface roughness. The preparation of hydrophobic surfaces, can then be achieved mainly by several physical and chemical methods [1]. Some typical examples of chemical methods include the surface modification by materials with low surface free energy, e.g., fluorination, the fabrication of aligned nanorods or nanowires, and the construction of hierarchical porous structure. On the other hand physical methods to increase surface roughness include mechanical abrasion, etching, anode oxidation, molding, lithography, etc. [2]

ZnO is an inexpensive material that is receiving attention because of its high conductance, chemical and thermal stability as well as its optical properties, with interesting applications such as thin film gas sensors, photo-detectors and light emitting diodes especially for UV region [3].

Most of the work focused on obtaining hydrophobic ZnO surfaces has relied upon surface roughness modification with regular patterns. This is due to the inherent hydrophilicity of ZnO surfaces that difficult to obtain surfaces with lower free surface energy.

Patterning of ZnO thin film usually requires at least three processes: deposition of ZnO layer, lithography and etching of ZnO. Compared to photolithography, nanoimprint lithography (NIL) can effectively fabricate nano-scale patterns with simple process, high throughput and relatively low cost [4]. By using the imprinting technique with the sol–gel process, the number of process steps can be decreased and the expensive processes such as photolithography and reactive ion etching steps can be skipped. Therefore, ZnO nano-patterns can be made inexpensively and various kinds of ZnO-based nano-devices can be realized using sol–gel nano-imprinting [5].

The direct patterning of gel film developed by sol-gel technology shows great advantages for cost-effective mass production [6]. There are a rich variety of techniques about the preparation of ZnO thin films including sputtering, chemical vapor deposition (CVD), spray pyrolysis, and sol–gel process [7]. The sol-gel method has some merits, such as the easy control of chemical components, good homogeneity, low processing temperature, large area coatings, good optical properties and fabrication of thin film at a low cost [8]. Particularly, the sol–gel processes are efficient in producing thin, transparent, multi-component oxide layers of many compositions on various substrates [9].

A combination of nanoimprinting of ZnO sol–gel films and thermal nanoimprint lithography technique is used to prepare nanostructured ZnO films with hydrophobic properties. This is a very simple and relatively inexpensive method to produce a high quality patterned film. . The phenomenon of the OH absorption on the surface of ZnO gel-films results in the hydrophlilicity and the nanopatterns on the surface enhance the hydrophobocity of ZnO gel film. The thermal imprint process is developed by using a poly-dimethylsiloxane (PDMS)-based polymer mold, chosen due to its capability to absorb the solvent without deformation, and when temperature is raised the organic solvent in the ZnO-sol solution is removed by diffusion through PDMS polymeric mold and the formed nanostructures of ZnO-gel are stable, thus further enhancing the hydrophobocity of ZnO gel film (Figure 1). As a result of the increased surface roughness, composite surfaces demonstrate a CA enhancement from 30º to 100º.

References

[1] C.Y. Kuan, M.H. Hon, J.M. Chou, I.C. Leu, J. Electrochem. Soc. 156 (2009) 32-36.

[2] B. Ding, T. Ogawa, J. Kim, K. Fujimoto, S. Shiratori, Thin Solid Films 516 (2008) 2495

[3] D. Raoufi, T. Raoufi, Appl. Surf. Sci. 255 (2009) 5812–5817

[4] S.Y. Chou, P.R. Krauss, W. Zhang, L. Guo, L. Zhuang, J. Vac. Sci. Technol. B 15 (1997) 2897

[5] K.Y. Yang, K. Yoon, K.C.H. Lee, Microelec. Engin. 86 (2009) 2228-2231

[6] M. Li, H. Tan, L. Chen, J. Wang, and S. Y. Chou, J. Vac. Sci. Technol. B, 21 (2003) 660

[7] Z. Liu, Z. Jin, W. Li, J. Qiu, Mat. Let. 59 (2005) 3620 – 3625

[8] S. Ilican, Y. Caglar, M. Caglar, J. Optoelectr. Adv. Mat. 10 (2008) 2578 – 2583

[9] M. Dutta, S. Mridha, D. Basak, Appl. Surf. Sci. 254 (2008) 2743–2747

Figures
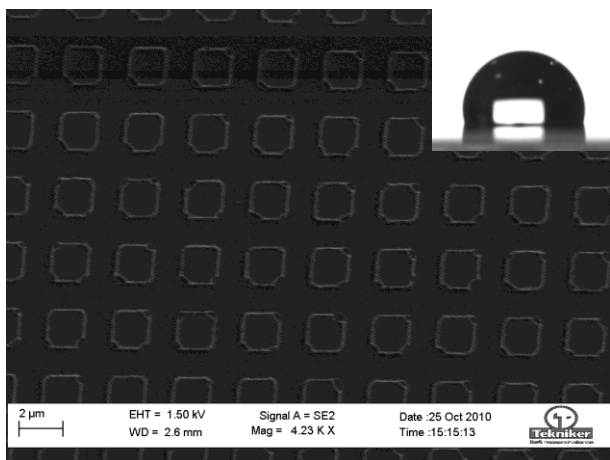
Figure 1.- SEM micrographs of ZnO-gel patterns

Synthesize and investigation of magnetic properties of Ca-Zr doped Bi-YIG nano powders via mechano chemical processing method

Ahmad Hasanpour[1], Narges Faridnia,[1] and Mohammad Niyaifar[1]

1 Department of physics, Science and Research Branch, Islamic Azad University, Khuzestan- Iran

Hasanpour88@gmail.com

Calcium- zirconium-substituted Bismuth-yttrium iron garnetnanoparticles with composition of ($BiY_{2-x}Ca_xFe_{5-x}Zr_xO_{12}$) were prepared by mechano chemical processing and subsequent heating treatment. X varied from 0 to 1.25 by step 0.25. The effect of Zr mol ratuo on Phase formation

and crystalline structure were investigated by X-ray diffraction(XRD, IR spectroscopy and scaning electron microscopy(SEM) .The magnetization and susceptibility of samples was studied by AGFM and . The experimental results show that the Zr substitution lowers the phase formation and sintering temperature. This results show that single-phase powders can be obtained at temperature lower than 850°C

which is much lower than an undoped sample Y3Fe5O12(900°C)[1].

Key words:Ca,Zr, Bi substitutedYttrium iron garnet, Nanoparticles, mechano chemical processing

Electric and magnetic optical forces on submicron dielectric particles

R. Gómez-Medina[1,2], M. Nieto-Vesperinas[1], J. J. Sáenz[2]

[1] Instituto de Ciencia de Materiales de Madrid,
Consejo Superior de Investigaciones Científicas (CSIC),
Campus de Cantoblanco, Madrid 28049, Spain.
[2] Departamento Física de la Materia Condensada
Universidad Autónoma de Madrid, Madrid 28049, Spain

rgomezmedina@icmm.csic.es

The understanding and control of particle transport and diffusion properties is a most relevant issue in fields ranging from biophysics to material science and chemical processing, with countless applications which include particle mixing, diffusive separation of particles, microrhelogy, intracellular transport or drug delivery, to mention a few[1-3].

The advances in sculpting optical wavefronts and light intensity profiles, make optical tools ideal for both imaging and manipulation of particles. Optical fields are easily tunable in general and affect any polarizable object, from atoms to microscopic colloidal particles [4, 5]. These fields can be used to arrange, guide or deflect particles in appropriate light pattern geometries [6-10].Intense optical waves can also induce significant forces between particles [11-14].

Light forces on small dielectric particles are traditionally described as the sum of two terms: the dipole or gradient force and the radiation pressure or scattering force proportional to the Poynting vector [15-17]. A non-conservative scattering curl force appears when the spatial distribution of the field polarization is not uniform [18]. For magnetodielectric particles [19-21], the force presents both electric and magnetic gradient and scattering contributions together with an additional term due to the electric-magnetic dipolar interaction, that contributes to both the scattering force and to the gradient force [20,22]. The main purpose of this work is to illustrate the relevance of this additional contribution.

In free space, the calculation of optical forces acting on small (Rayleigh) dipolar particles is relatively simple, allowing analytical treatment of the problem [15, 18, 23]. However, when the particle size is of the order of or larger than the internal wavelength, in the so-called "Mie" regime, it is difficult to obtain systematic predictions and most theoretical work in this regime is based on a numerical approach [24]. An analytical approach for the optical forces on particles far beyond the Rayleigh limit is still possible provide the scattering can be described by the first two electric and magnetic Mie coefficients [20-22, 25-26]. We will discuss the strong magnetic and electric optical forces on submicron dielectric particles with unusual scattering effects [20-22, 26]. As we will show, the electric-magnetic dipolar interaction plays an active role in spinning the particles either in or out of the whirls sites of the interference pattern, leading to trapping or diffusion [22]. This may permit the exploration of new forms of controlled atom motion in optical lattices [27, 28] and may be used to separate and sort small particles with slightly different optical characteristics [9, 10].

References

[1] P. Reiman, Phys. Rep**. 361** (2002) 57. T. G. Mason *et. al.* Phys. Rev. Lett. **79** (1997) 3282.

[2] F. Scheffold, and P. Schurtenberg, Soft Mater **1**, (2003) 139.

[3] V. M. Rotello, Adv. Drug Delivery Rev. **60**, (2008) 1255.

[4] A. Ashkin, Proc. Natl. Acad. Sci. USA **94**, (1997) 4853.

[5] J. E. Curtis, B.A. Koss, and D.G. Grier, Opt.Comm. **207** (2002)169.

[6] M. M. Burns, J.-M. Fournier, and J.A. Golovchenko, Science **249** (1990) 749.

[7] M. I. Antonoyiannakis, and J. B. Pendry, Europhys. Lett**. 40** (1997) 613.

[8] R. Gómez-Medina, et. al. Phys. Rev. Lett. **86** (2001) 4275.

[9] P. T. Korda, M. B. Taylor, and D. G. Grier, Phys. Rev. Lett. **89** (2002) 128301.

[10] M. P. MacDonald, G. C. Spalding, K. Dholakia, Nature **426** (2003) 421.

[11] M. M. Burns, J.-M. Fournier, and J.A. Golovchenko, Phys. Rev. Lett. **63** (1989) 1233.

[12] S. A. Tatarkova, W. Sibbett, and K. Dholakia, Phys. Rev. Lett. **91** (2003) 038101.

[13] R. Gómez-Medina, and J.J. Sáenz, Phys. Rev. Lett. **93** (2004) 243602.

[14] M. Guillon, O. Moine, and B. Stout, Phys. Rev. Lett. **96** (2006) 143902. S. Gaugiran *et. al.*, Opt. Express **15** (2007) 8146. K. Dholakia, and P. Zemanek, Rev. Mod. Phys. **82** (2010) 1767.

[15] P. C. Chaumet and M. Nieto-Vesperinas, Phys. Rev. B **61** (2000) 14119; P. C. Chaumet, A. Rahmani, and M. Nieto-Vesperinas, Phys. Rev. Lett. **88** (2002) 123601; M. Nieto-Vesperinas, P.C. Chaumet, and A. Rahmani, Phil. Trans. R. Soc. Lond. A **362** (2004) 719.

[16] M. Mansuripur, Opt. Express **12** (2004) 5375.

[17] B. A. Kemp, T. M. Grzegorczyk, and J. A. Kong, Phys. Rev. Lett. **97** (2006) 133902.

[18] S. Albaladejo, M. I. Marques, M. Laroche, and J. J. Sáenz, Phys. Rev. Lett. **102** (2009) 113602.

[19] P.C. Chaumet, and A. Rahmani, Opt. Express **17** (2009) 2224.

[20] M. Nieto-Vesperinas, J. J. Sáenz, R. Gómez-Medina, and L. Chantada, Opt. Express **18** (2010) 11428.

[21] M. Nieto-Vesperinas, R. Gómez-Medina and J. J. Sáenz, J. Opt. Soc. Am. A **28** (20111) 54.

[22] R. Gómez-Medina, M. Nieto-Vesperinas and J. J. Sáenz, Phys. Rev. A (submitted 2010).

[23] P. Zemanek, V. Karasek, and A. Sasso, Opt. Commun., **240** (2004) 401. S. Albaladejo *et al.*, Nano Lett. **9** (2009) 3527. I. Zapata *et al.*, Phys. Rev. Lett. **103** (2009) 130601.

[24] P. Zemanek, M. Siler, V. Karasek, and T. Cizmar, Proc. SPIE Int. Soc. Opt. Eng. **5930** (2005) 59301N.

[25] A. García-Etxarri *et al,* ArXiv:1005.5446v1, Opt. Express (submitted 2010).

[26] R. Gómez-Medina *et al,* J. Eur. Opt. Soc, Rapid Publ. (submitted 2011).

[27] A. Hemmerich, and T. W. Hänsch, Phys. Rev. Lett. **68** (1992) 1492.

[28] G. Grynberg *et. al.*, Phys. Rev. Lett. **70** (1993) 2249.

Figures
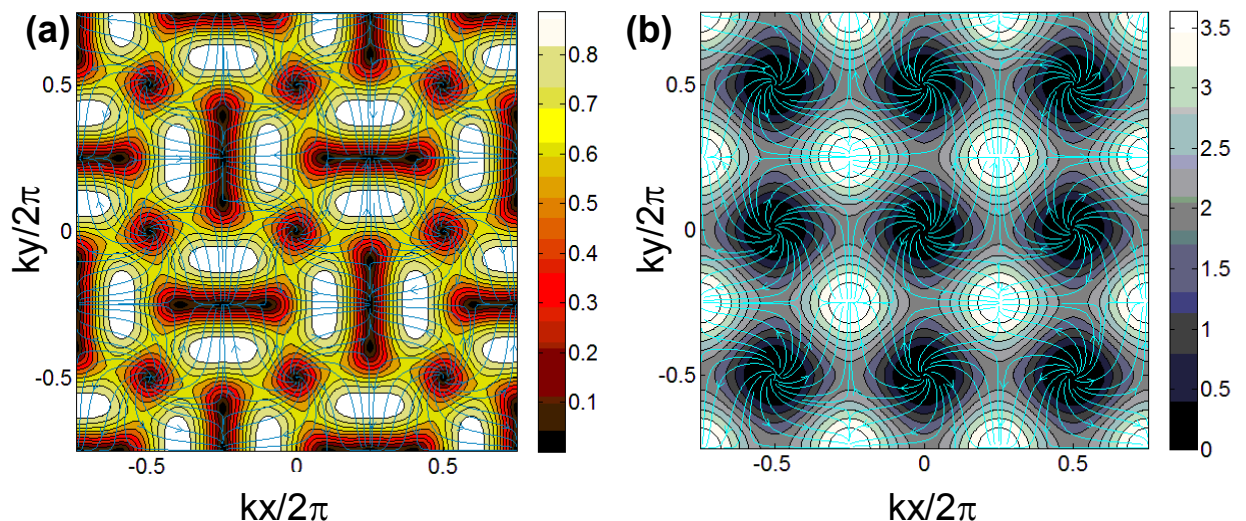
Nonconservative forces on a Si sphere of radius a = 230nm placed in the intersection region of two standing waves with a dephasing ϕ=1/2 in a medium with ϵ =1. (a) Contour intensity maps of the normalized total force, $<|\mathbf{F}|>/F_0$ with $F_0=|\mathbf{E_o}^2|/ka^3$, (b) Contour intensity maps of the normalized electric field intensity $|\mathbf{E}|/|\mathbf{E_0}|^2$. The light field wavelength, λ = 1600nm, slightly below (blue-shifted) the magnetic dipolar resonance. Equilibrium (zero force) positions correspond to electric field maxima.

Controlled synthesis system for production of crystalline ZnO nanobelts and nanowires
*B. González Rolón, L. A. Vera Salas
*FIMEE Universidad de Guanajuato, Campus Salamanca Km 3.5 +1.8 de la carretera Salamanca-Valle de Santiago CP 36885, Comunidad Palo Blanco, Salamanca Gto. México
E-mail barbara@salamanca.ugto.mx

Interest in nanotechnology has greatly increased over the past years because of its wide implementation in technology, biotechnology and energy production. However the nature of these applications demands a very accurate and detailed manufacture method. Recently, industrialization of the ZnO has gained a lot of interest as an optoelectronic material due to its properties in the range of UV. Its energy gap is 3.37 eV, making this material suitable to insulate an electric field. The high electrical resistivity, which is derived from the previously mentioned energy gap, prevents current leakage. Alongside, the ZnO display another two key properties, its piezoelectric characteristics and the changes shown in its morphological configurations. Here we report the development of an automatized method to produce ZnO nanobelts and nanowires with a digitalized control of the reactor's temperature and pressure in a simple vapor transport system. Using this method we have successfully obtained nanobelts and nanowires with specific characteristics. The structural properties and composition of the samples were studied by X-ray diffraction (XRD) and the results demonstrated the formation of ZnO phase. Morphology of as-prepared products was characterized by scanning electron microscopy (SEM, LEO 1200).

The synthesis is based on thermal evaporation of ZnO powder (purity of 99.99% and melting point of 1975ºC). The oxide was placed in the middle of an alumina tube that was inserted in a horizontal tube furnace, where the temperature, pressure, and evaporation time were digitally controlled. In our research, except for the evaporation temperature, which was determined assuming the ZnO, we kept the following parameters constant: evaporation time of two hours, pressure of 300 torr and Argon flowing rate of 50 standard cubic centimeters per minute. Products were deposited onto a platinum plate, placed at the downstream end of the alumina tube. We have discovered that production of different nanostructures of ZnO can be made through the control of the process of synthesis. Figure 1 shows a diagram of how this method is controlled. As shown in figure 2, two types of one-dimensional ZnO nanostructure were identified on the basis of morphology. The product is observed as entangled, and in a place of the fiber changes the trajectory of its growth. It is bi-dimensional and the length of these nanostructures was in the range of several micrometers (about 3m- 0 2mm) and their diameters normally range from 50 to 120 nm. Beside, this shows another typical morphology of ZnO nanostructure, of which there are some straight wire-like products which all they have high yield and hardness.

Figures
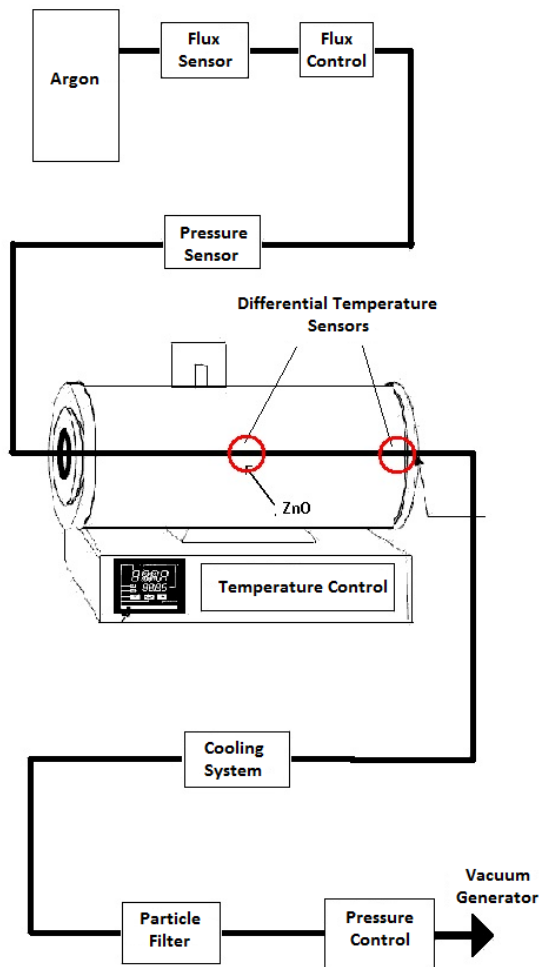
Figure1. Diagram of the automated production method for ZnO nanobelts and nanowires.
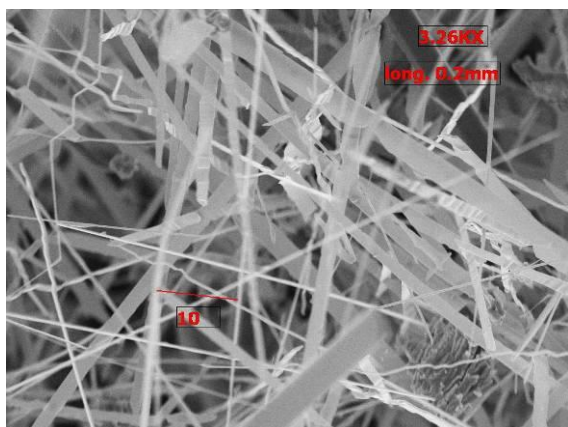
Figure2. SEM of obtained ZnO nanobelts and nanowires.

[1] Dehspandey. "Evaporation Process": Semiconductors and Semimetals". Academic Press. 1991.
[2] N. R. Franklin, Y. Li, R. J. Chen, A. Javey, and H. Dai, Appl. Phys. Lett. 79, 4571s2001d.

Pressure dependence of Raman modes in double wall carbon nanotubes filled with amorphous selenium

E. Belandria[1], J. M. Broto[2], E. Flahaut[3], F. Rodríguez[4], R. Valiente[5], E. del Corro[6], M. Taravillo[6], V. G. Baonza[6] and **J. Gonzalez[4,7]**

[1]Centro de Estudios Avanzados en Óptica, Universidad de los Andes, 5201 Mérida, Venezuela,[2]Laboratoire National des Champs Magnétiques Intenses (LNCMI) - CNRS UPR 3228,Université de Toulouse, 143 Avenue de Rangueil, 31400 Toulouse, France [3]CIRIMAT, Université de Toulouse, F-31400 Toulouse, France,[4]DCITIMAC-Malta Consolider Team, Universidad de Cantabria, 69005 Santander, Spain,[5]Dto de Fisica Aplicada- Malta Consolider Team, Universidad de Cantabria, 69005 Santander, Spain [6] MALTA-Consolider Team, Departamento de Quimica Fisica I, Facultad de Ciencias, Universidad Complutense de Madrid, Plaza de Ciencias 3, 28040- Madrid, Spain,[7] Centro de Estudios de Semiconductores, Universidad de los Andes, Mérida 5201,Venezuela.

jesusantonio.gonzalez@unican.es

The synthesis of mono-dimensional nanocrystals is complex due to the lack of stability of such structures. One way to stabilize them is to prepare them within a container, such as carbon nanotubes (CNTs). CNTs are good candidates for this application due to their inner diameter in the nanometer range, as well as their good chemical and thermal stability. Selenium, which is a p-type semiconductor, exhibits both photovoltaic and photoconductive properties. It is utilised in many devices ranging from solar cells to rectifiers and xerography [1]. Trigonal selenium (hexagonal) is the most stable allotrope under normal temperature and pressure. Selenium has also monoclinic allotropes although it is generally commercially available in the amorphous state. The confinement of Se inside CNT was only scarcely studied but Chancolon et al. [2] proposed a method for filling CNT in the vapour phase and performed a comprehensive study of the structure of Se within the CNT by X-Ray diffraction and X-ray absorption spectroscopy. They found that the Se present inside the CNT was mainly amorphous in their synthesis conditions. Earlier studies have revealed that the space available within CNT may play an important role on the crystal structure of the confined material, especially in the case of narrow DWCNT where materials are often found in amorphous state even if they crystallise in singlewalled CNT of similar inner diameter [3]. The samples are characterized by high resolution transmission electronic microscopy and Raman spectroscopy.

A systematic analysis of TEM images reveals that samples produced by this method contain approximately 77% of double wall carbon nanotubes (DWCNTs), the high proportion of DWCNTs was also confirmed by electron diffraction with a small admixture of about 18% single-wall CNTs (SWCNTs), and roughly 5% triple-wall CNTs . The inner and outer diameters range from 0.53 to 2.53 nm and from 1.23 to 3.23 nm, respectively. The median inner diameter is 1.2 nm and the median outer diameter is 1.9 nm [4,5,6]. They were filled using a high filling yield capillary wetting technique [6]. Filling yield was roughly estimated to be *ca*. 50%, straight from transmission electronic microscopy (TEM) observation, presented in Figure 1.In order to investigate their structural stability and unravel the differences induced by intershell interactions, unpolarized room temperature Raman spectra of radial and tangential modes of DWCNTs filled with 1D nanocrystalline Se excited with 514 nm were studied at high pressures (figure 2). Up to 12 GPa we found a pressure coefficient of 4.9 $cm^{-1}GPa^{-1}$ for the internal tube and 7.5 $cm^{-1}GPa^{-1}$ for the external one. In addition, the tangential band of the external and internal tubes broadens and decreases in amplitude. Under pressure, we note that the pressure coefficient of the G-bands of the internal and external CNTs filled with amorphous Se are larger than the pressure coefficients of empty CNTs and this has been attributed to the effect of charge transfer from the Selenium nanowires to the CNTs. Finally, we unravel that the outer tubes act as a protection shield for the inner tubes (figure 3).

References

[1] H. Fana, Z. Wanga, X. Liua, W. Zhenga, F,Guoa, Y. Qian,Solid State Communications **135**, (2005).319.

[2] W. C. Cooper, R. A Westbury, *Selenium,* 87-147, (1974).

[3] J. Chancolon, F. Archaimbault, S. Bonnamy, A.Traverse, L. Olivi, G. Vlaic, Journal of Non-Crystalline Solids **352**, (2006) 99.

[4] José Jorge, E. Flahaut, F. González- Jiménez, Gema González, J. González, E. Belandria,J.M.Broto, B. Raquet, Chemical Physics Letters, **457**, (2008) 347.

[5] E. del Corro, J. Gonzalez, M. Taravillo, E. Flahaut and V. G. Baonza, *Nano Lett.*, **8** (8), (2008) 2215

[6] E. Belandria, M. Millot, J.M. Broto, E. Flahaut, F. Rodriguez , R. Valiente , J. Gonzalez, Carbon, **48**, (2010) 2566.

Figures
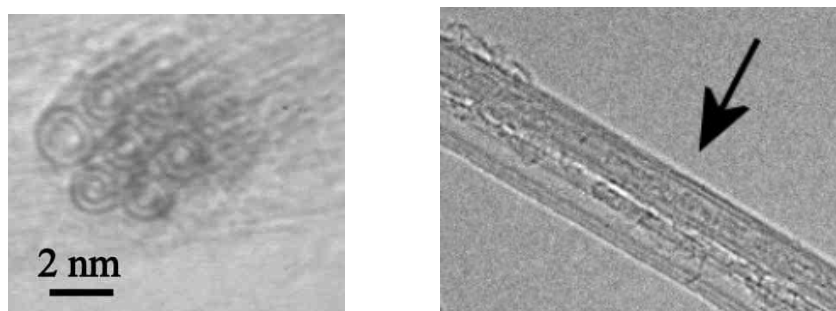
Figure 1: HRTEM images of Se@DWCNT
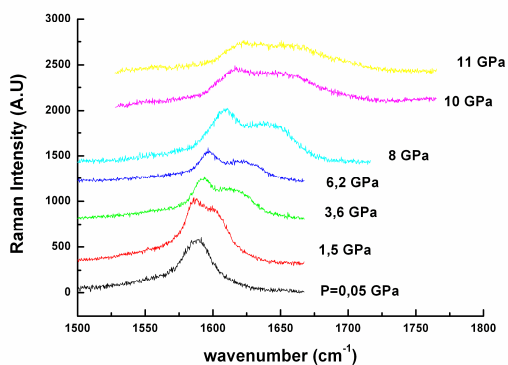
Figure 2: Raman spectra at different pressures in the upstroke of Se@DWCNTs
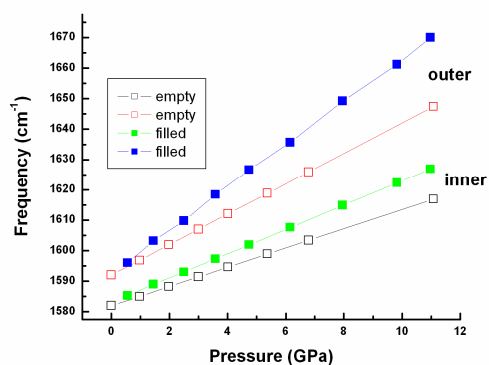
Figure 3: Pressure dependence of tangential modes of DWCNT@Se for the inner and outer tubes.

A Brownian Dynamic study on the formation of cementitious Calcium-Silicate-Hydrate (C-S-H) nanostructure

Raquel González-Teresa, P. Achutha, J. C. Gimel, J. S. Dolado

Tecnalia, Parque Tecnologico de Bizkaia Geldo st 700 48160 Derio , Spain
teresa.gonzalez@tecnalia.com

The Calcium Silicate Hydrate (C-S-H) gel is the most important hydration product present in cementitious materials. Thanks to recent advanced nanoindentation experiments [1,2], there is now evidence that in terms of its mechanical properties the C-S-H gel can present itself either in a low stiffness and Low Density variety (called LD C-S-H gel) or in a variety with a high stiffness and High Density (called HD C-S-H gel). This dissimilar bearing capacity is indeed much more pronounced in their resistance to osteoporosis-like degradation processes. Along their life-service, cementitious materials, akin to human bones, may lose calcium (the so called calcium leaching). This is a slow and long-term process, but it leads to a significant loss of strength/stiffness and impermeability, reduces the concrete's capacity to passivate the steel and ultimately causes the material to become significantly stress sensitive, which may eventually impair the structural integrity.

The existence of two dissimilar varieties of C-S-H gel fits well with the current colloidal conception of the C-S-H gel, i.e. the Jennings model (see figure) [3,4]. According to this model ~5nm sized globular Basic Building Blocks (BBB) exist and pack themselves together to form LD and HD C-S-H forms depending on ad-hoc packing factors (see figure 1). Although this ad-hoc model has rationalized much of the information available at this scale it is clear that this description is an oversimplification. In fact, several nagging questions persist. On the one hand, numerous TEM and SEM analysis have shown that C-S-H gel effectively presents itself in two varieties, but not in globular ones. It is usual for TEM microscopists to differentiate between the morphologies close to the cement grains (called Inner Product) with respect to those found in the outer free space (called Outer Product (OP)) (figure 2)[5]. As can be seen from the annexed figure the Inner product (IP) turns to be dense and made of tiny globular-like particles, whereas the Outer Product is loose (or at least looser than the IP) and made of strands of aligned particles. These dissimilar morphologies can not be easily accounted for by the Jennings model. On the other hand, the Jennings model neglects the underlying chemistry by assuming a granular nature for the assemblage of C-S-H particles. Under this assumption the aggregation of the basic C-S-H particles (or BBBs) is merely described as coming from isotropic Hard Sphere (HS) aggregations [6,7]. It is clear that OP morphologies can not be explained in such terms. By the contrary, it is fair to assume that they require both directional long-range interactions to "align" the particles and short range forces to bond the particles.

In this scenario, the employment of computational means to describe the aggregation of nanoparticles is appealing. Aggregating systems can be considered from two different viewpoints. Either we speak of concentration fluctuations of individual particles governed by inter-particle forces derived from a potential (MD simulation) or we speak of aggregates, which form and break-up continuously i.e. the approach developed in BCD simulations. Both techniques are strictly equivalent but the main advantage of BCD simulations is that they are able to monitor the kinetics, the dynamics and the statics over longer time and for bigger systems compared with classical MD simulations. In this study we have studied the relaxation of the system by cooperative cluster motion and also the effect and bond rigidity. With our computational scheme we have monitored gel formation, phase separation, glass formation, crystallization, etc.. It is clear that this computational framework can help us to achieve a better understanding of the colloidal behavior of the C-S-H nanoparticles. This knowledge might allow us in a future to control the aggregation in order to improve the cohesion in cementitious materials.

References

[1] Constantinedes, G.and F.J. Ulm, Cement and Concrete Research, "The effect of two types of C-S-H on the elasticity of cement based materials: results from nanoidentation and micromechanical modelling". 2004.34(1): p.67-80.
[2] Constantinedes, G.and F.J. Ulm, Journal of the Mechanics and Physics of Solids,"The nanogranular nature of C-S-H". 2007.55(1): p. 64-90.

[3] Jennings, H.M. Cement and Concrete Research "A model for the microstructure of calcium silicate hydrate in cement paste" ., 2000.30:p.101-116.
[4] Jennings, H.M. Cement and Concrete Research "Refinements to colloid model of C-S-H in cement: CM-II" , 2008.38:p.275-289.

[5] I.G. Richardson,Cement and Concrete Research, "Tobermorite/jennite- and tobermorite/calcium hydroxide-based models for the structure of C-S-H: applicability to hardened pastes of tricalcium silicate, beta-dicalcium silicate, Portland cement, and blends of Portland cement with blast-fumace slag, metakaolin, or silica fume". 2004 34(9):p.1733-1777.

[6] V. Morales-Florez, N. de la Rosa-Fox, M. Pinero, L. Esquivias. Journal of Sol-Gel Science and Technology,"The Cluster Model: A Simulation of the Aerogel Structure as a Hierarchically-Ordered Arrangement of Randomly Packed Spheres". (2005).**35**,p: 203-210

[7] M. D. Rintoul and S. Torquato Journal of Chemical Physics. "Computer simulations of dense hard-sphere Systems". 1996 105(20):p.9258–9265.

Figures
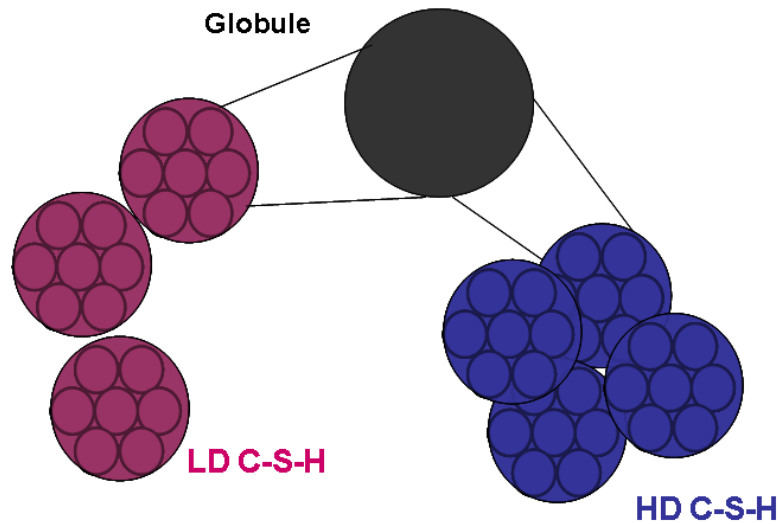
Figure 1: Schematic representation of the colloidal model I of Jennings
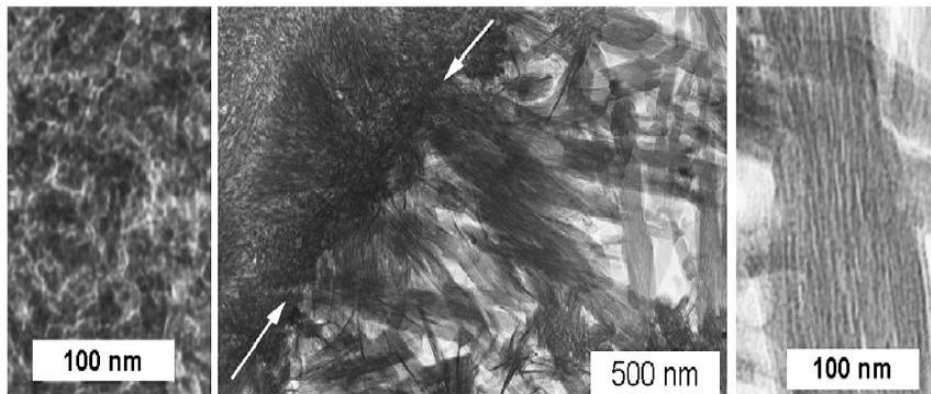
Figure 2: TEM picture of the structure of the C-S-H gel .On the left the inner product and on the right the outer product. [5]

Spin excitations of nanomagnets over a non-uniform magnetization ground state: Topological gauge field approach

Konstantin Y. Guslienko[1,2], Gloria R. Aranda[3], and Julian M. Gonzalez[1]

[1]Dpto. Física de Materiales, Universidad del Pais Vasco, M. Lardizabal, 3, San Sebastian 20018, Spain
[2]IKERBASQUE, the Basque Foundation for Science, Alameda Urquijo, 36-5, Plaza Bizkaia, Bilbao 48011, Spain
[3]Centro de Física de Materiales UPV/EHU-CSIC, M. de Lardizabal, 5, San Sebastián 20018, Spain
Contact@E-mail: sckguslk@ehu.es

We developed a general approach to description of the small spin wave (SW) excitations of a non-uniform moving magnetization background in magnetic nanostructures [1]. We introduced a topological gauge vector potential which influences the SW excitation spectra over arbitrary non-uniform, slowly moving magnetization background. To describe magnetization (**M**) dynamics we used the Lagrangian Λ corresponding to the Landau-Lifshitz equation of motion of the reduced magnetization $\mathbf{m} = \mathbf{M}/M_s$:

$$\Lambda = \int d^3\mathbf{r}\lambda(\mathbf{r},t), \qquad \lambda = \mathbf{D}(\mathbf{m})\cdot\dot{\mathbf{m}} - w(\mathbf{m},\partial_\alpha\mathbf{m}), \qquad (1)$$

where $\mathbf{D}(\mathbf{m}) = (M_s/\gamma)(1+\mathbf{m}\cdot\mathbf{n})^{-1}[\mathbf{n}\times\mathbf{m}]$, **n** is the unit vector in arbitrary direction, γ is the gyromagnetic ratio, the dot over symbol means derivative with respect to time (*t*), *w* is the magnetic energy density $w = A(\partial_\alpha\mathbf{m})^2 + w_m + w_H$ (α= *x, y, z*), $w_m = -M_s\mathbf{m}\cdot\mathbf{H}_m/2$ is the magnetostatic energy density, $w_H = -M_s\mathbf{m}\cdot\mathbf{H}$ is the Zeeman energy density, *A* is the exchange stiffness, $M_s = |\mathbf{M}|$, $\mathbf{H}_m$ and **H** are the magnetostatic and external fields, respectively.

We express the magnetization field **m** as a sum $\mathbf{m} = \mathbf{m}_\upsilon + \mathbf{m}_s$ of the slow moving magnetization (υ) and spin wave (s) contributions. The components of $\mathbf{m}_s$ are the simplest in a moving coordinate frame *x'y'z'*, where the axis *Oz'* (quantization axis) is directed along the instant local direction of $\mathbf{m}_\upsilon$. We perform a rotation of the initial *xyz* coordinate system to the direction of $\mathbf{m}_\upsilon$. The corresponding 3x3 rotation matrix $R(\Theta_\upsilon,\Phi_\upsilon) = \exp(i\Phi_\upsilon J_z)\exp(i\Theta_\upsilon J_y)$ is defined by the spherical angles of $\mathbf{m}_\upsilon(\Theta_\upsilon,\Phi_\upsilon)$, and the magnetization components in the *x'y'z'* frame are $\mathbf{m}'_s = R\mathbf{m}_s$, $\mathbf{m}'_\upsilon = (0,0,1)$. Here J_α are the angular momentum components for *J*=1 in the Cartesian basis representation. To preserve the Lagrangian (1) in the same form after the transformation $\mathbf{m} \to \mathbf{m}' = R\mathbf{m}$ we introduce covariant derivatives $(\partial_\mu - A_\mu)$ instead of ∂_μ, where A_μ is a gauge vector potential (the index μ = 0, α denotes the time and space coordinates $x_\mu = t, x, y, z$, and $\partial_\mu = \partial/\partial x_\mu$). The A_μ components are transformed as $A_\mu \to A'_\mu = RA_\mu R^{-1} + \partial_\mu R \cdot R^{-1}$. The term $\partial_\mu R \cdot R^{-1}$ has sense of a topological contribution to the vector potential. We denote it as $\hat{A}_\mu = \partial_\mu R \cdot R^{-1}$ and put $A_\mu = 0$ in the laboratory coordinate system *xyz*. The gauge vector potential $\hat{A}_\mu$ represented by time and spatial derivatives of $\mathbf{m}_\upsilon$ describes a "minimal" interaction between the υ- and *s*-subsystems and can be applied to a wide class of problems related to excitation of the SW in the non-uniform magnetization ground state. There is a simple equation $\hat{A}_\mu\mathbf{m} = \mathbf{A}_\mu \times \mathbf{m}$ for arbitrary vector **m**, where $\mathbf{A}_\mu = (\sin\Phi_\upsilon\partial_\mu\Theta_\upsilon, -\cos\Phi_\upsilon\partial_\mu\Theta_\upsilon, -\partial_\mu\Phi_\upsilon)$. The Lagrangian (1) can be rewritten in the form $\Lambda = \Lambda_\upsilon + \Lambda_{sw} + \Lambda_{int}$, where Λ_υ and Λ_{sw} are contributions of the slowly moving non-uniform magnetization and spin waves. An interaction term Λ_{int} described by the density $\lambda_{int} = -\mathbf{D}' \cdot \hat{A}_0\mathbf{m}'_s$ corresponds to the dynamic υ – SW interaction. *I.e.*, the time-component of the potential $\hat{A}_0(\mathbf{r},t)$ plays an important role in the magnetization dynamics of typical nanostructures.

As an example, we consider spin eigenmodes excited in the vortex state cylindrical magnetic dots. The

excited mainly outside the vortex core SW modes are described by integers (n, m), which indicate number of nodes in the dynamic magnetization along radial (n) and azimuthal (m) directions. The vortex – SW interaction is described as a consequence of the gauge field arising due to the moving vortex magnetization and represented by the components $A_\mu^z = -\partial_\mu \Phi_\upsilon$. There is the most essential contribution to the SW motion due to the variable vortex phase $\dot{\Phi}_\upsilon = -A_0^z$. The approach yields a giant frequency splitting (1-2 GHz) of the azimuthal spin waves with the indices m=+1/-1 having non-zero overlapping with the vortex gyrotropic mode (Fig. 1) as well as a renormalization of the vortex background motion due to appearance of the vortex profile distortion and a finite vortex mass of dynamical origin. The frequency splitting was measured experimentally for the modes with n=0 and n=1 by using precise broadband ferromagnetic resonance technique [2, 3]. The vortex mass is calculated as $M_\upsilon \approx (3/2)L/\gamma^2$ and is about of 10^{-20} g (L is the dot thickness). The renormalized vortex gyrotropic frequency can be represented in the form $\omega_0 = 20\gamma M_s \beta[1 - 4\beta/3]/9$ at small $\beta \le 0.2$ (β=L/R is the dot aspect ratio - thickness/radius (R)). The moving vortex core distortion and the frequency renormalization can be represented as a result of the hybridization of the gyrotropic mode with the azimuthal SW (n, m=+1/-1). The vortex core reversal can be achieved by a.c. magnetic field pumping at the frequency close to the eigenfrequencies of the azimuthal SW. Increasing amplitude of the azimuthal spin waves leads to appearance of instability of the vortex background in the form of the vortex core polarization reversal. Recent measurements of the spin eigenfrequencies in the vortex state permalloy cylindrical dots [2, 3] can be explained by the developed approach. Other dynamic magnetic nano-structures, *e.g.*, moving domain walls in nanostripes (rings) can be considered within the approach.

References

[1] K. Y. Guslienko, G. R. Aranda, and J. Gonzalez, *Phys. Rev.* B **81** (2010) 014414.
[2] F. G. Aliev et al., *Phys Rev.* B **79** (2009) 174433.
[3] A. A. Awad et al., *Appl. Phys. Lett.* **96** (2010) 012503.

Figures
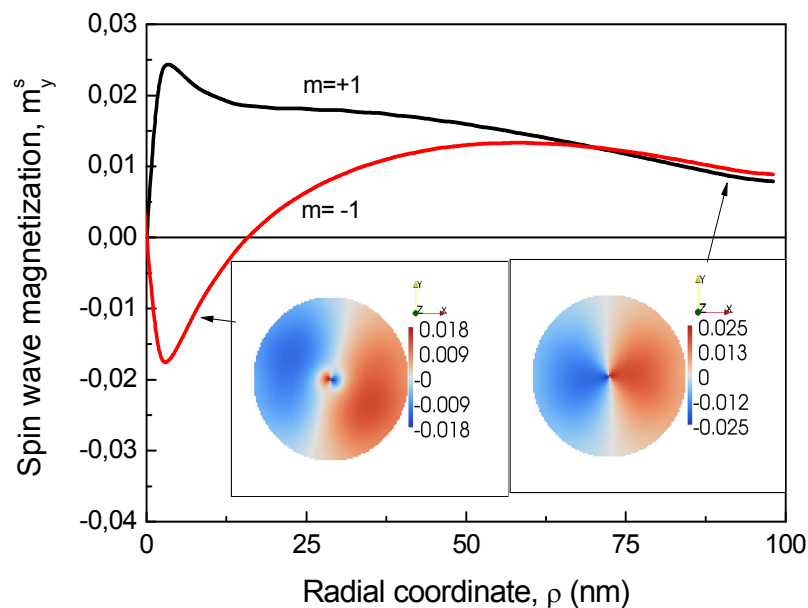
Figure 1. The calculated radial profiles of the main (the radial index n=0) azimuthal spin waves in the vortex state cylindrical dot made from permalloy. The eigenmode frequencies are ω0,+1/2π =8.98 GHz and ω0,-1/2π = 10.44 GHz for the SW azimuthal indices m=+1 and m=-1, respectively. Inset: snapshots of the dot dynamic in-plane my^s - magnetization component. The dot thickness is 10 nm, the dot radius is 100 nm, the dot saturation magnetization is Ms = 800 G, and other parameters are as in Ref. 1.

Conductive properties of hybrid TiO₂/bacterial cellulose fibres by electrostatic force microscopy

Junkal Gutierrez, Aloña Retegi, Itxaso Algar, Gurutz Mondragon,
Agnieszka Tercjak and Iñaki Mondragon

"Materials + Technologies' Group, Department of Chemical and Environmental Engineering
University of the Basque Country, Plaza Europa 1, 20018 Donostia/San Sebastián, Spain
juncal.gutierrez@ehu.es

Nowadays new research area focused on hybrid inorganic/organic fibres materials based on bacterial cellulose and inorganic nanoparticles paid attention of many researches. It is well known that homogeneously dispersed nanoscale inorganic particles in a polymer matrix improve the mechanical properties of the resulting nanocomposites. Hybrid materials containing metal or semiconductor nanoparticles are interesting from the point of view of nanotechnology due to inorganic-organic composites gather together typical advantages of organic polymers like flexibility, formability, toughness with the ones displayed by typical inorganic nanoparticles like optical, magnetic and electrical properties, luminescence, ionic conductivity and selectivity, as well as chemical or biochemical activity.

Instead of the typical polymeric matrix we propose bacterial cellulose to be used as template for preparation of novel hybrid inorganic-organic composites. Bacterial cellulose can be produced by Gram-negative, acetic acid bacteria *Gluconobacter xylinus*. The formation of cellulose by laboratory bacterial cultures is an interesting and attractive biomimetic access to obtain pure cellulose with excellent properties such as good biocompatibility, high tensile strength, high water retention capability, high hydrophilicity and high crystallinity. Additionally, the chance to obtain cellulose by laboratory bacterial cultures allow us to control the molar mass, molar mass distribution and the supramolecular structure by selecting the substrates, cultivation conditions, various additives, and finally the bacterial strain.

In this work, we used sol-gel method to synthesize titanium dioxide (TiO₂) nanoparticles based on titanium isopropoxide precursor. It should be pointed out, that a good-dispersion of nanoparticles is the key issue to take fully advantage of nanoparticles. From this point of view it is essential to develop a processing method to uniformly disperse nanoparticles in the polymer matrices with high particle loadings in order to maximize their effects. The sol-gel method allows the preparation of hybrid inorganic/organic materials due to the in-situ generation of inorganic particles, which are uniformly dispersed at the nanometer scale as a result of hydrogen or covalent bonds. Thus, using titanium isopropoxide as sol-gel precursor, inorganic network having hydroxyl groups on the surface can be generated. These inorganic networks surrounded by hydroxyl groups can interact with hydrophilic bacterial cellulose.

The aim of the present work was focused on the study of the conductive properties of both bacterial cellulose and generated hybrid TiO₂/BC fibres by electrostatic force microscopy (EFM) measurements. This technique allows to measuring qualitatively the electric field gradient distribution above the sample surface, which consequently allows distinguishing different conductive parts of the sample. Different voltages have been applied to check conductive properties of designed systems. Additionally, the influence of the sign (positive or negative) of the applied voltage on the response of the samples has been also investigated.

References

[1] A. Retegi, N. Gabilondo, C. Peña, R. Zuluaga, C. Castro, P. Gañan, K. de la Caba, I. Mondragon, Cellulose **17** (2010) 661.
[2] S. Ifuku, M. Tsuji, M. Morimoto, H. Saimoto, H. Yano, Biomacromolecules **10** (2009) 2714.
[3] P. A. A. P. Marques, T. Trindade, C. P. Neto, Comp. Sci Technol. **66** (2006) 1038.
[4] R. T. Olsson, M. A. S. Azizi Samir, G. Salazar-Alvarez, L. Belova, V. Ström, L. A. Berglund, O. Ikkala, J. Nogués, U. W. Gedde, Nature Nanotechnol. **5** (2010) 584.

Nano-structured fibre-to-chip grating coupler for bio-sensing applications

R. Halir[1], P. Cheben[2], J. H. Schmid[2], R. Ma[2], S. Janz[2], D.-X. Xu[2], A. Densmore[2], J. Lapointe[2], and Í. Molina-Fernández[1]

[1]Departamento Ingeniería de Comunicaciones, Universidad de Málaga, Málaga, Spain
[2]Institute for Microstructural Sciences, National Research Council of Canada, Ottawa, Canada
robert.halir@ic.uma.es

Direct monitoring of molecular reactions in real-time is key to many aspects of biochemical research. Intermediate labeling steps hamper detection reliability, which is why optical biosensors, which enable label-free monitoring, are advantageous. The most established optical monitoring method is surface plasmon resonance, which is based on probing the material with a lightwave travelling along a metal surface. However, the precision of this method is fundamentally limited by the short propagation length (~30 μm) along the metal surface [1]. Due to their low propagation loss (~3 dB/cm), dielectric based, integrated optical sensors do not suffer from this limitation [2]. Use of the high index contrast silicon-on-insulator platform furthermore allows for drastic sensor size miniaturization, thus enabling parallel probing of several samples in a single device [3]. Detection limits of 0.5 pg/mm^2 have been reported for devices with a sensing area smaller than 130 μm x 130 μm in the silicon platform, yielding a minimum detectable mass of 0.5 fg [3], thus readily competing with commercial surface plasmon resonance techniques. The operation of these photonic biosensors is based on evanescent field sensing: part of the waveguide mode travels outside the actual guiding region and thus experiences different phase velocities depending on the refractive index of the material that is deposited on the waveguide surface. This phase velocity change can be exploited for biosensing by defining Mach-Zehnder interferometers or ring resonators with these waveguides [2-4]. Both configurations produce strong intensity variations at their outputs as a result of refractive index changes on the waveguide surface, which can be measured with photodetectors. Fig. 1 shows the fundamental TM (vertically polarized) mode of a silicon wire waveguide. The substantial evanescent tails make this polarization highly sensitive to changes of the refractive index of the material on the waveguide, and thus particularly suitable for biosensing [5].

Practical photonic biosensing chips must be compatible with large scale, low cost fabrication, and should present efficient and robust light coupling interfaces with standard optical fibres. In Si-wire waveguides the latter is especially challenging because of the large size mismatch between optical fibres (8 μm core size) and the miniaturized waveguides (~ 250 nm x 450 nm core size). Diffractive grating couplers, as shown on the left of Fig. 2, are widely used for coupling TE (horizontally polarized) light into these waveguides. However, this solution is not directly applicable to biosensors, not only because the TM polarization is not injected efficiently, but mainly because the gratings are etched only ~70 nm into the waveguide layer. This shallow etch is necessary to reduce the discontinuity between the alternating strips of the grating, thereby matching the large fiber mode to the field diffracted by the coupler. However, the second etch step, added to the full etch needed for waveguide definition, increases fabrication costs. Here we present our latest findings on a novel fibre-to-chip coupler that can be fabricated in a single etch step and offers efficient light coupling for TM polarization. The coupler uses nano-structures to synthesize effective materials, which are used to optimize coupling efficiency [6,7].

A schematic view of the proposed coupler is shown on the right of Fig. 2, with the optical fibre positioned above it, and the polarization states indicated with arrows. The device couples light coming from the optical fibre into the waveguide along the *z* axis, and into the vertical (*y* direction) polarization state, as required for biosensing. The fully etched, periodic nano-structures along the *x* axis have a pitch of 450 nm, which is small enough to create an equivalent homogenous medium at the operation wavelength of 1550 nm. By tuning the width of the silicon tooth in the sub-wavelength structure, effective media with refractive indexes ranging from air (no silicon tooth) to silicon (no air gap) can besynthesized. Specifically, if the size of the silicon tooth is set to 185 nm, an effective medium with a refractive index of 2.73 is created. For a uniform grating, this intermediate refractive index provides a near optimum match of the diffracted field and the fiber mode. Furthermore, it is readily fabricated, since the 185 nm minimum feature size is fully compatible with large volume deep ultraviolet lithography.

Fig. 3 shows a scanning electron microscope image of a fabricated, uniform coupler, with the diffractive grating along the *z*-direction and the stripes of effective media along the *x*-direction. By coupling light into the waveguide through one grating, and extracting it with an identical grating, the coupling efficiency of the grating can be determined. As shown on the right hand side of Fig. 3, an experimental peak coupling efficiency of 4 dB is achieved, which exceeds the coupling efficiency of traditional dual etch gratings by almost 1 dB [8].

Simulations show that using an apodized design, i.e., by varying the refractive index of the effective medium along the grating, coupling efficiencies of up to 3 dB can be achieved.

In summary, we present a novel fibre-to-chip grating coupler optimized for bionsensing applications, that is fabricated in a single etch step and fully compatible with high volume production. Using nano-structure effective media, this coupler achieves an experimental coupling efficiency of 4 dB.

References
[1] Homola, J.; Yee, S. S. & Gauglitz, G, Sensors and Actuators B: Chemical, **54** (1999), 3-15
[2] Laura M. Lechuga, et al, SPIE Newsroom, December 2008
[3] Densmore, A, *et al*, Opt. Lett., **34** (2009), 3598-3600
[4] Xu, D.-X., *et al*, Opt. Express, *16* (2008), 15137-1514
[5] Densmore, A., *et al*, IEEE Photonics Technol. Lett., **18** (2006), 2520-2522
[6] Halir, R., *et al*, Opt. Lett., **34** (2009), 1408-1410
[7] Halir, R., *et al,* Opt. Lett., **35** (2010), 3243-3245
[8] Roelkens, G., *et al,* IEEE J. Sel. Top. Quantum Electron. (2010), forthcoming

Figure 1
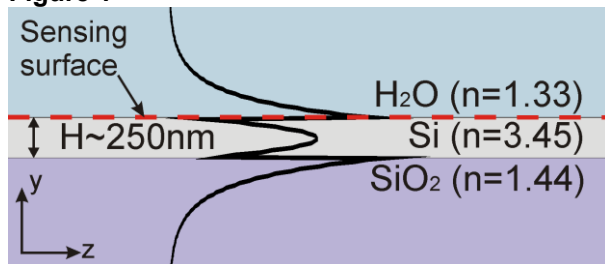
Electrical field (E$_y$) of the fundamental TM (vertically polarized) mode of a silicon-wire waveguide. Refractive indexes are given at λ=1.55µm.
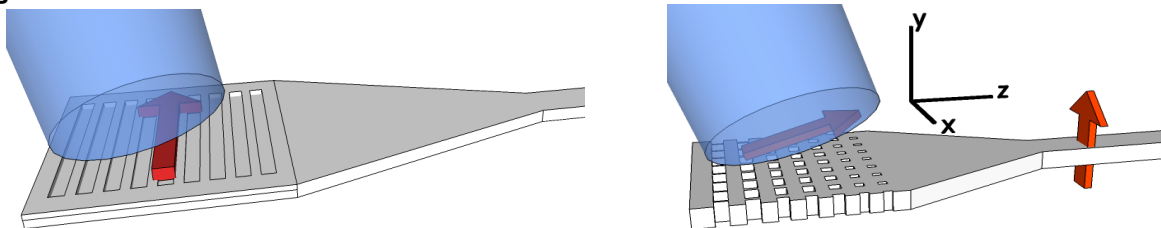
Figure 2

Left: Schematic view of traditional fibre-to-chip grating coupler. Right: Proposed coupler. In both figures the arrows indicate the polarization state.

Figure 3
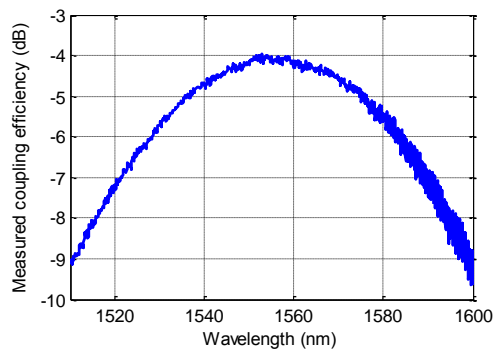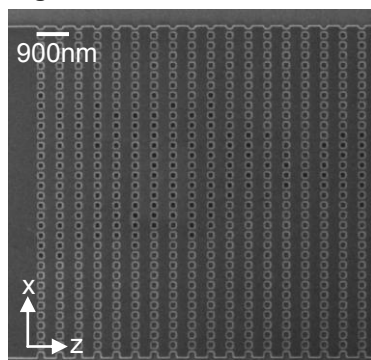
Left: Scanning electron microscope structure of the fabricated structure. Right: Measured coupling efficiency.

Design and test of ionization gas sensors based on single metal oxide nanowires

Francisco Hernandez-Ramirez,[1,2] Juan Daniel Prades,[2] Angelika Hackner,[3] Thomas Fischer,[4] Gerhard Mueller,[3] Sanjay Mathur[4] and Joan Ramon Morante [1,2]

1. Catalonia Institute for Energy Research (IREC), Barcelona, Spain
2. Department of Electronics, University of Barcelona, Barcelona, Spain
3. EADS Innovation Works, Munich, Germany
4. Institute of Inorganic Chemistry, University of Cologne, Cologne, Germany

fhernandez@irec.cat, fhernandez@gmail.com

Gas detection experiments were performed with individual tin dioxide (SnO_2) nanowires specifically configured to observe surface ion (SI) emission response towards representative analyte species. These devices were found to work at much lower temperatures (T=280ºC) and bias voltages (V=2V) than their micro-counterparts, thereby demonstrating the inherent potential of individual nanostructures in building functional nanodevices [1]. High selectivity of our miniaturized sensors emerges from the dissimilar sensing mechanisms of those typical of standard resistive-type sensors (RES). Therefore, by employing this detection principle (SI) together with RES measurements, better selectivity than that observed in standard metal oxide sensors could be demonstrated. Simplicity and specificity of the gas detection as well as low-power consumption make these single nanowire devices promising technological alternatives to overcome the major drawbacks of solid-state sensor technologies. In this contribution, the fundamentals of this new line of research and experimental data will be presented and discussed [2].

References

[1] A. Hackner, A. Habauzit and G. Müller, Sensors and Actuators B, **146** (2010) 433.
[2] F. Hernandez-Ramirez, J.D. Prades, A. Hackner, T. Fischer, G. Mueller, S. Mathur and J.R.Morante, Nanoscale (2011) DOI: 10.1039/C0NR00528B

Figures
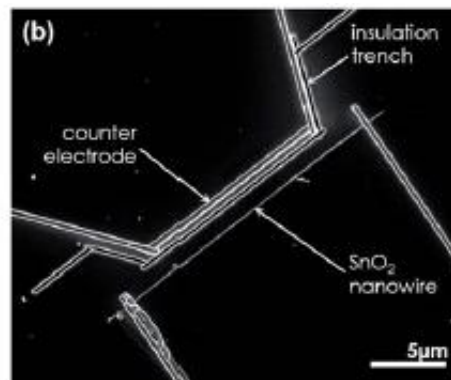
SEM Image of a surface ionization gas sensor based on a single metal oxide nanowire and fabricated with FIB lithography
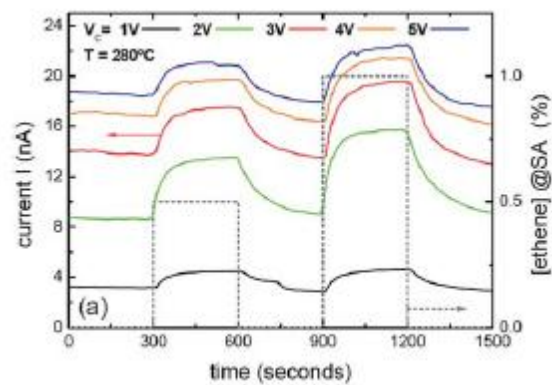
For the device shown in the previous figure, SI response towards two different concentrations of ethane (0,5% and 1%) diluted in synthetic air at an operation temperature of 280ºC and different working conditions

Towards new ammonia sensors based on individual metal oxide nanowires

F. Hernandez-Ramirez[1,2], F. Shao[1], J.D. Prades[2], J.R. Morante[1,2]

1. Catalonia Institute for Energy Research (IREC), Barcelona, Spain
2. Department of Electronics, University of Barcelona, Barcelona, Spain

fhernandez@irec.cat, fhernandez@gmail.com

Solid state devices based on metal oxides are amongst the most popular types of gas sensors for monitoring toxic species, such as carbon monoxide (CO) and nitrogen oxides (NOx) [1]. In the last years, significant research efforts have been devoted to extend their fabrication to the nanoscale, due to the excellent sensing properties of nanowires, related to the high surface-to-volume ratio. In general, the exclusive properties of nanostructured materials in respect to bulk materials have attracted research efforts because of their potential applications in electronic devices [2].

The feasibility of having gas and optical sensors based on individual nanowires has been demonstrated, and the integration of nanowires in prototypes devices has been validated [3]. Nevertheless, the fabrication of electrical contacts with high stability, low contact resistances and ohmic behavior remains a challenge. Focused Ion Beam (FIB) lithography is a powerful fabrication technique for prototypes with dimensions in the range of the nanoscale [4]. Using this technique, electrical contacts are fabricated over the nanowire with electron beam assisted deposition while ion beam assisted deposition can be used to extent these contacts to large metal electrodes, giving macroscopic access to the electrical response of the nanowire while preserving the nanowire from ion damage. The resulting devices provide an excellent opportunity to study the electrical, optical and gas sensing properties of individual metal oxide nanowires.

In this work, we report the fabrication of individual metal oxide nanowire-based sensors using FIB lithography (see attached image) and their characterization as ammonia sensors. Ammonia (NH3) is normally considered a dangerous pollutant classified as "dangerous for the environment" by EU and US regulations. Their performances and the possibility of integrating them in autonomous systems powered by energy harvesters will be shown and discussed.

References

[1] B. Hoffheins, in: R.F. Taylor, J.S. Schultz (Eds.), Handbook of Chemical and Biological Sensors, IOP Publishing, Bristol, (1996) 371.
[2] Xing-Jiu Huang and Yang-Kyu Choi Sensors Actuators B, 122 (2007) 659.
[3] A. Kolmakov and M. Moskovits, Annu. Rev. Mater. Res, 34 (2004) 151.
[4] F. Hernandez-Ramirez, A. Tarancon, O. Casals, J. Rodriguez, A. Romano-Rodriguez, J. R. Morante, S. Barth, S. Mathur, T. Y. Choi, D. Poulikakos, V. Callegari and P. M. Nellen, Nanotechnology, 17 (2006) 5577.

Figures
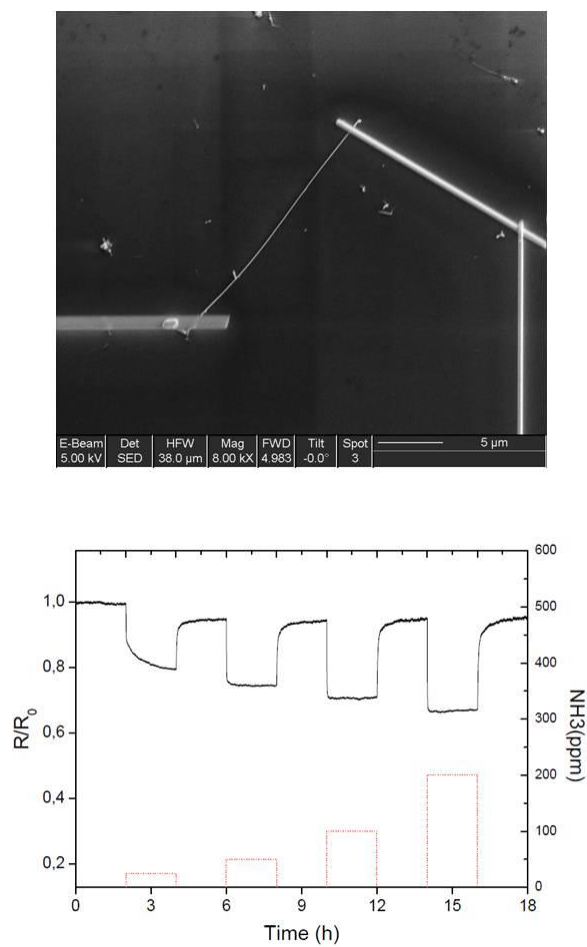
Fig.1. (a) SEM image of a SnO2 nanowire electrically contacted with FIB nanolithography techniques. (b) Response of a SnO2 nanowire towards different ammonia concentrations. Reproducible, reversible and stable responses are observed.

Nanostructural Analysis of Nanofeatures in Semiconductors

J. Hernández-Saz[1]**,** M. Herrera[1] and S. I. Molina[1]

[1]Departamento de Ciencia de los Materiales e I.M. y Q.I., Universidad de Cádiz,
11510 Puerto Real (Cádiz), Spain.
jesus.hernandez@uca.es

The swift developments in nanotechnology and the miniaturization of devices raise the need for detailed bi and three-dimensional characterization of nanostructures. Transmission Electron Microscopy (TEM) is a basic tool to study the structure of materials at nanometric scale. Within TEM techniques, electron tomography (ET) is standing as one of the techniques that allows obtaining three-dimensional information. Sample preparation is a key step in TEM and the ideal geometry of a specimen to be studied by ET is one where the thickness remains invariant along tilting series. Nowadays, the advances in focused ion beam equipment allow making progress in this essential stage, obtaining right quality and good geometry of the samples. The ideal geometry of such samples has been achieved with the needle-shape sample preparation using focused ion beam (FIB) of a dual-beam FIB/Scanning EM system [1].

In this communication, we study by ET a number of semiconductor nanostructures inside electron-transparent needle-shape samples. We demonstrate the capacity of FIB to prepare needle-shape samples with nanostructures inside the needles, which is not possible by using conventional TEM preparation methods. We also present the usefulness of the ET combined with Z-contrast scanning transmission electron microscopy imaging to obtain 3D information of nanofeatures in semiconductors materials.

Our sample preparation procedure consists of sculpting nanofeatures containing the volume of interest, a particular semiconductor nanostructure in our case, in the FIB instrument. FIB conditions are selected in such a way that the prepared needles have a good quality for ET studies, that is, a small diameter (some tens of nanometers) and a minimum thickness of amorphous layer at its surface. For this, a lamella is fabricated and needles are milled by Annular Milling Method from it. Figure 1 shows an example of a series of nano-needles prepared by this procedure.

References

[1] Larson, D. J., Foord, D. T., Petford-Long, A. K., Liew, H., Blamire, M. G., Cerezo, A. and Smith, G. D. W., Ultramicroscopy, **79** (1999) 287.

Figures
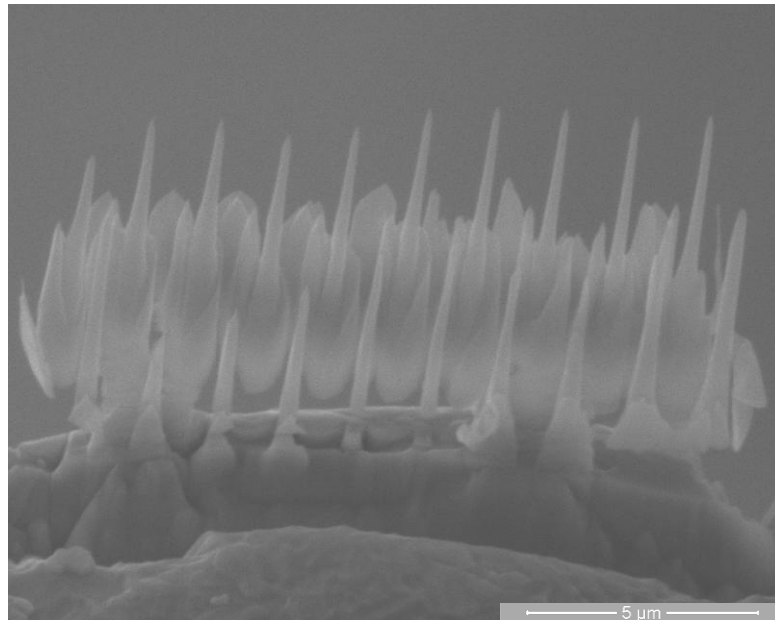
Figure 1. SEM image of a series of needles fabricated by Annular Milling Method with a FIB equipment.

"Quantitative High Resolution Electron Microscopy of III-V semiconductor nanostructures "

D. Hernández-Maldonado[a)], M. Herrera[a)], D. L. Sales[a)], P. Alonso-González[b)], D. Fuster[b)], Y. González[b)], L. González[b)], J. Gazquez[c)], M. Varela[c)], S. J. Pennycook[c)],J. Pizarro[d)], P. L. Galindo[d)] and S. I. Molina[a)]

[a)]Departamento de Ciencia de los Materiales e I.M. y Q.I., Facultad de Ciencias, Universidad de Cádiz, Campus Río San Pedro, s/n, 11510 Puerto Real, Cádiz, Spain.

[b)]Instituto de Microelectrónica de Madrid (CNM-CSIC), Isaac Newton 8 (PTM), 28760-Tres Cantos (Madrid) Spain.

[c)]Materials Science and Technology Division, Oak Ridge National Laboratory, Oak Ridge, Tennessee 37831, USA.

[d)]Departamento de Lenguajes y Sistemas Informáticos, CASEM, Universidad de Cádiz, Campus Río San Pedro, s/n, 11510 Puerto Real, Cádiz, Spain.

david.hernandez@uca.es

The introduction of aberration correctors in Scanning Transmission Electron Microscopy (STEM) has represented a great advance in the field of microscopy and materials science, allowing nanostructures to be analyzed with sub-Angstrom spatial resolution [1]. We present here a methodology developed in our group to extract quantitative compositional information with atomic-column resolution from high resolution High Annular Angular Dark Field (HAADF) images [2]. This analysis contributes to the characterization of the shape, size and composition distribution of nanostructures. This is an important issue because functional properties of nanostructures depend on these characteristics.

The method is based on the local integration of intensities around atomic columns positions of aberration corrected HAADF-STEM images. These intensities are normalized with respect to an area of the sample of known composition; the resultant quotient between the intensity of each atomic column in a selected area, with respect to the intensity in the area of reference is called the normalized intensity ratio, and it is denoted as R. It has been demonstrated that R is almost independent of thickness and has a simple dependence on the material composition. Hence, the determination of the parameter R of each atomic column leads quite straightforwardly to quantify column-by-column the chemical composition. The method was originally developed for $InAs_xP_{1-x}$ alloys, but it has been extended to other ternary semiconductor alloys like $In_xGa_{1-x}As$ and $GaAs_xSb_{1-x}$ [3], and has been applied to a different number of materials and nanostructures [4, 5]. Fig. 1 shows a high-resolution HAADF-STEM image of an InAs/InP nanowire and the corresponding integrated intensity map around each atomic column. For this example, red colour corresponds to InAs-rich zones whereas the blue colour represents pure InP.

We have to notice that the direct application of this method allows quantifying composition in bulk or heteroepitaxial layers; on the other hand, composition of strained nanostructures can be estimated combining this method with image simulations from supercells representing the nanostructures [6]. Results obtained from this and other high resolution techniques, such as strain distribution determined from High Resolution Transmission Electron Microscopy (HRTEM) images in phase contrast mode [7], give valuable information to improve our understanding of nucleation of nanostructures. We review in this communication the application of these methods to a number of semiconductor nanostructures with telecommunication, photonic and photovoltaic applications.

References

[1] Nellist P.D., Chisholm M.F., Dellby N., Krivanek O.L., Murfitt M.F., Szilagyi Z.S., Lupini A.R., Borisevich A., Sides Jr, W.H., Pennycook S.J., Science, **305** (2004) 1741

[2] Molina S. I, Sales D. L., Galindo P. L., Fuster D., González Y., Alén B., González L., Varela M. and Pennycook S. J., Ultramicroscopy, **109** (2009) 172

[3] Molina, S. I., Guerrero, M. P., Galindo, P. L., Sales, D. L., Varela, M., Pennycook, S. J., *J. Electron Microsc.* , in press.

[4] Molina S. I., Varela M., Ben T., Sales D. L., Pizarro J., Galindo P. L., Fuster D., González Y.,González L. and Pennycook S. J., *J. NanoSci. Nanotechnol.* **8** (2008) 3422

[5] Molina S. I., Beltrán A. M., Ben T., Galindo P. L., Guerrero E., Taboada A. G., Ripalda J. M. and Chisholm M. F., *Appl. Phys. Lett.* **94** (2009) 043114

[6] Pizarro, J., Galindo, P. L., Guerrero, E., Yáñez, A., Guerrero, M. P., Rosenauer, A., Sales, D. L., Molina, S. I., *Appl. Phys. Lett.* **93** (15) (2008) 153107

[7] Galindo, P. L., Kret, S., Sanchez, A. M., Laval, J.-Y., Yañez, A., Pizarro, J., Guerrero, E., Ben, T., Molina, S. I., *Ultramicroscopy* **107** (2007) 1186
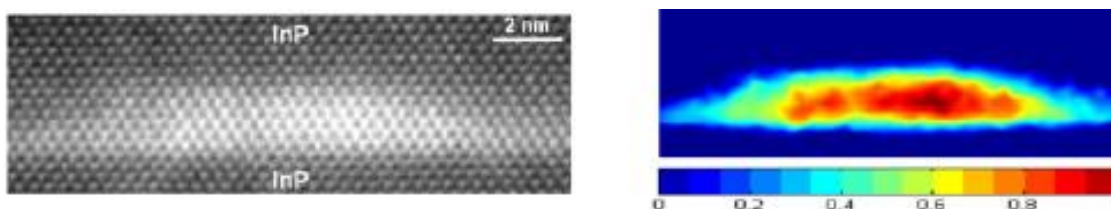
Figure 1. *High resolution HAADF-STEM image of an InAs/InP quantum wire and its corresponding normalized integration intensity maps (reproduced from [4] with the permission of the copyright owner).*

Functionalization and characerization of CNTs by means of water plasma

Shahzad Hussain, Eric Jover, Roger Amade, Enric Bertran
FEMAN Group, IN2UB, Department of Applied Physics and Optics,
Universitat de Barcelona, c/Martí i Franquès 1,E-08028, Barcelona
Sha.awan@hotmail.com

Carbon nanotubes (CNTs) produced by Plasma Enhanced Chemical Vapor Deposition (PECVD) show particular structural and morphological characteristics suitable for different applications like energy and charge storage , environment, biomedicine, electrochemistry or photonics [1].

In order to modify their physical and chemical properties, the surface of the nanotubes can be functionalized with chemical groups, expanding their potential application in the energy and environmental fields. The easiest way to covalently attach chemical groups like, e.g., carboxylic groups, is by oxidation such as acid oxidation, air oxygen oxidation, ozone oxidation, and plasma oxidation, resulting in the formation of hydroxyl, carbonyl and carboxyl groups on the surfaces of the nanotubes. However, due to the rather harsh conditions involved, most oxidation reactions result in the opening of the nanotube tips, detrimental damage of their sidewalls, or both [2].

In this work, vertically aligned carbon nanotubes (VACNTs) were prepared by means of PECVD and functionalized with water plasma treatments [3] (Figure 1). The oxidation process was optimized adopting a Box-Wilson experimental design using the pressure and plasma power as the operational parameters. The water-plasma treated CNTs were characterized by SEM, TEM, Raman Spectroscopy, XPS and contact angle. The results allow us to describe the functionalization process as a function of water pressure and plasma power.

References

[1] M. Paradise, T. Goswami, Materials and Design, 28, 1477–1489, 2007.
[2] C. Chen, A. Ogino, X. Wang, M. Nagatsu, Applied Physics Letters, 96, 131504 (1-3), 2010.
[3] F. Javier del Campo, J. García-Céspedes, F. Xavier Muñoz, E. Bertrán, Electrochemistry Communications, 10, 1242–1245, 2008.

Figure
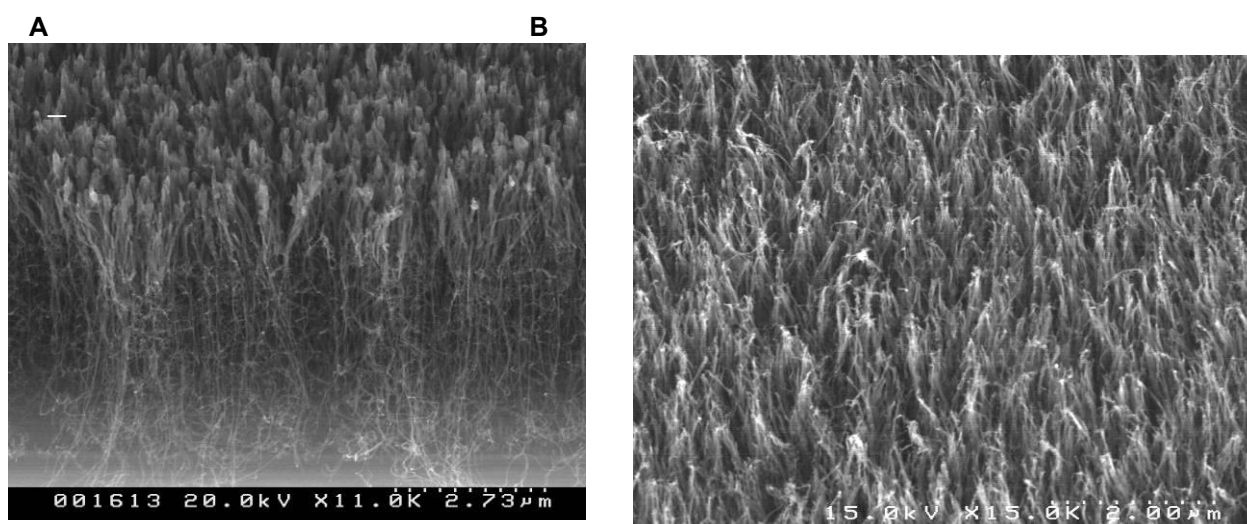
Figure 1 A. CNTs grown by PECVD without water plasma treatment. B. CNTs grown by PECVD after water plasma treatment.

Coercivity, morphology and anionic defects in Fe/NiO layers on nanoporous Al$_2$O$_3$ membranes

M. Iglesias,[1] G. Domínguez-Cañizáres,[2] E. Navarro,[1] E. Paz,[1] D. Díaz Fernández,[2] A. Gutiérrez,[2] L. Soriano,[2] M. Alonso,[1] F. Soria,[1] F. Cebollada,[3] J. M. González[4] and F.J. Palomares*[1]

[1] Instituto de Ciencia de Materiales de Madrid (ICMM-CSIC), Cantoblanco, E-28049 Madrid, Spain.
[2] Dpto.Física Aplicada, Univ. Autónoma de Madrid (UAM), Cantoblanco, E-28049, Madrid, Spain
[3] POEMMA, Dpto.Física Aplicada a las T.I., Universidad Politécnica de Madrid, E-28031 Madrid, Spain
[4] Unidad Asociada ICMM-CSIC / IMA-UCM, Cantoblanco, E-28049 Madrid, Spain
fjp@icmm.csic.es

We report on the morphological and magnetic properties of two Au(capping)/ Fe/ NiO series of samples, grown on top of Si substrates (series 1) and Al$_2$O$_3$ nanoporous membranes (series 2), respectively. The NiO layers in both series were prepared by magnetron sputtering of a NiO target in an argon-oxygen atmosphere with different O$_2$/Ar ratios. The presence of oxygen in the deposition plasma produces a density of interstitial anionic defects whose magnitude is known to increase with the increase of the oxygen pressure. The aim of our work is to examine the influence of i) the antidot-type morphology and ii) the properties of the antiferromagnetic layer, on the hysteretic behavior of the metallic-ferromagnetic/oxide-antiferromagnetic, exchange coupled layers.
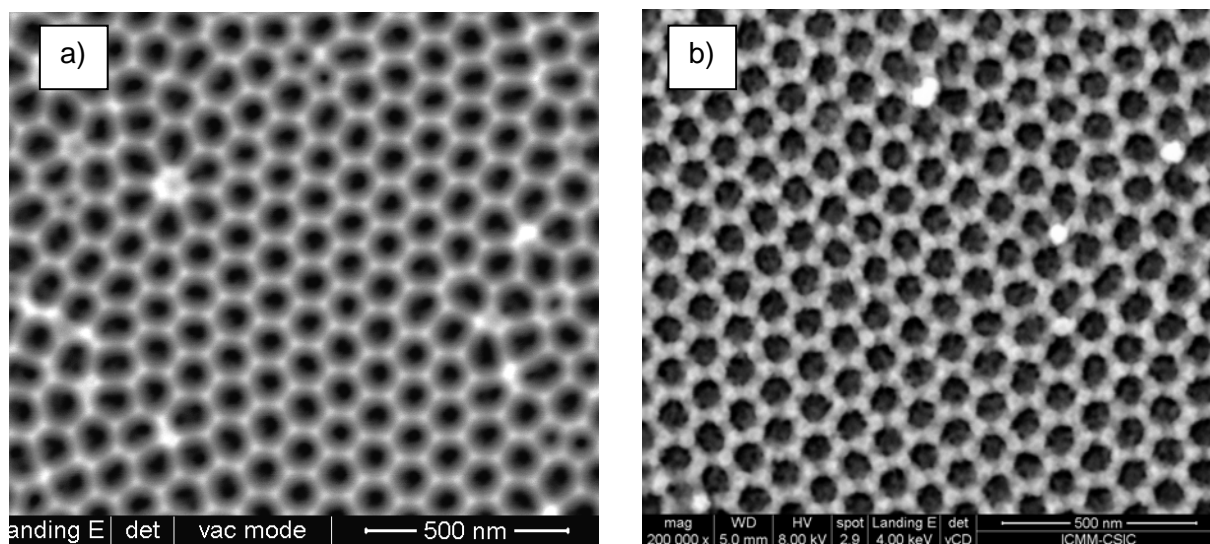
Figure 1. *Field emission scanning electron micrographs (FE-SEM) taken in: a) Al$_2$O$_3$ membrane substrate; b) Au(5 nm)/ Fe(5 nm)/ NiO(160 nm)/ Al$_2$O$_3$ sample (series 2).*

Samples were prepared by magnetron sputtering (NiO layers, 160-200 nm), pulsed laser ablation (Fe layers, 5 and 20 nm) and molecular beam epitaxy (Au capping layers, 5 nm). Analysis of the sample surface morphology by means of atomic force microcopy and field emission scanning electron microscopy (FE-SEM) evidenced that: i) a continuous film was formed in series 1 (Si substrate), and ii) the nanoporous morphology of the Al$_2$O$_3$ membranes was preserved in series 2 (see Figure 1). Nevertheless, FE-SEM reveals significant differences from sample to sample in series 2, depending on the Fe layer thickness and the growth parameters of the NiO layer. Originally, the Al$_2$O$_3$ membranes exhibited a hexagonal lattice with average pore diameter of 45 nm and inter-pore distance of ca.100 nm.

The magnetic characterization of the samples included the measurement of the temperature dependence of the low field magnetization measured after zero field cooling and field cooling the samples, and that of the temperature dependence of saturated hysteresis loops recorded after field cooling the samples.

In Figure 2 we have plotted the hysteresis loops measured at 290 K for series 2 samples with 10 nm-Fe layers and different plasma oxygen concentrations during NiO growth. From the figure it is evident that the coercivity in these samples increases with the increase of the oxygen partial pressure (up to a value of 160 Oe measured in the sample deposited with a 70% oxygen partial pressure). A similar trend is observed for samples with thicker (20 nm) Fe layers, whereas for thinner (5 nm) Fe layers the highest coercivity (240 Oe) corresponds to samples grown without oxygen in the plasma. A distinctly different behavior is found in series 1 (Si substrate) samples, where the presence of oxygen significantly deteriorates sample coercivity, independently of the Fe layer thickness.
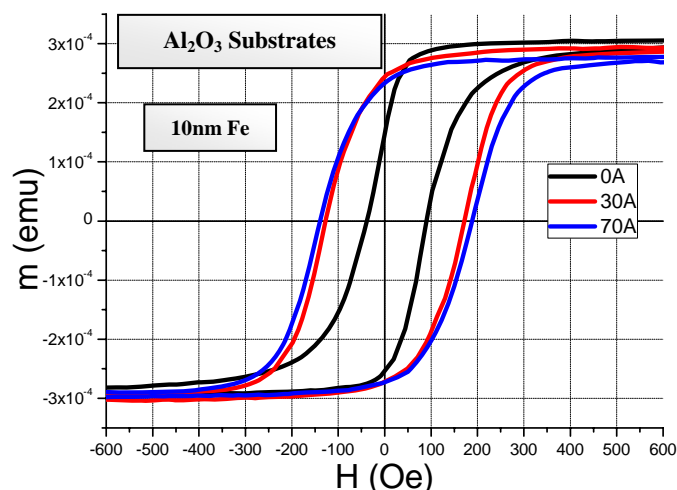
Figure 2. *Hysteresis loops measured at 290 K in series 2 samples for 10 nm-Fe layers; sample labeled OA was grown without oxygen in the Ar plasma (NiO growth); samples 30A and 70A were grown under 30% and 70% oxygen partial pressure, respectively.*

Figure 3 presents the temperature dependence of the loop displacement measured in the samples with 20 nm Fe layers after cooling them down to the measuring temperature under a field of 1000 Oe (all the displacements are opposite to the saturating field). As it is clear from the figure, the loop displacements are larger in series 1 than in series 2, and the same occurs for 10 nm Fe layers. Note, however, that the displacement in series 1 decreases with the oxygen pressure increase, whereas in series 2 and thick (10-20 nm) Fe layers, samples grown with oxygen exhibit larger displacements than those without it.
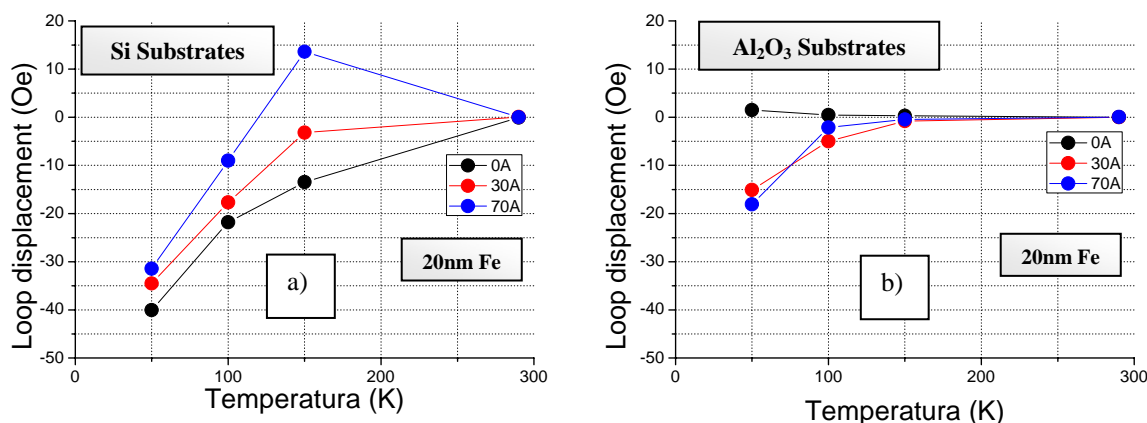
Figure 3. *Temperature dependencies of the loops displacements measured after field cooling the sample in the case of 20 nm-Fe layers; a) series 1; b) series 2.*

These results are discussed in terms of i) the amount of anionic defects present in the NiO layer and ii) the lateral limit to the size of the locally coupled regions associated to the nanoporous morphology. We conclude that it is possible to maximize the coercivity of Fe films grown onto NiO layers by preparing them under large oxygen partial pressures and using nanoporous Al_2O_3 membranes as substrates.

Quantification of Critical Magnetic Fields and Local Hysteresis Loops in Individual Nanostructures

O. Iglesias Freire[1], M. Jaafar[1,2], A. Awad[2], F. G. Aliev[2], L. Serrano[3], J. M. de Teresa[3], A. Fernández-Pacheco[3,4], R. Córdoba[5], M. Ibarra[3,5] and A. Asenjo[1]

[1] Instituto de Ciencia de Materiales de Madrid, Cantoblanco, 28049, Madrid, Spain
[2] Dpto. Física de la Materia Condensada, Universidad Autónoma de Madrid, 28049, Madrid, Spain
[3] Instituto de Ciencia de Materiales de Aragón, 50009, Zaragoza, Spain
[4] Imperial College London, South Kensington Campus, London, United Kingdom
[5] Instituto de Nanociencia de Aragón, 50009, Zaragoza, Spain

oiglesias@icmm.csic.es

Nanomagnetism is a research area of growing interest focused on phenomena related to the low dimensionality of magnetic elements. Besides its interest from a fundamental point of view, these magnetic nanostructures are of great technological importance in a wide variety of applications such as magnetic recording, sensors, biomagnetism, etc. For the development of such fields it becomes necessary not only the use of fabrication techniques which allow us to obtain patterned nanostructures but also access to characterization methods with suitable spatial resolution and sensitivity in order to study domain configurations and magnetization reversal processes on the nanoscale. In the last years, new alternatives based on magnetic nanostructures have emerged to the current electronic devices and information storage systems. Remarkable are new research lines based on the domain wall control in magnetic nanostripes (as racetrack memories [1] and domain wall logic [2]) or on the control of both the chirality and polarity of magnetic vortices [3], [4].

In this work we are able to quantify the critical fields in individual magnetic nanostructures. By means of a Variable Field Magnetic Force Microscope (VF-MFM) [5] and utilizing the so-called 3D Modes [6], the switching fields of individual cobalt nanostripes and the nucleation-annihilation fields of magnetic vortices in permalloy dots were obtained. Furthermore, a local hysteresis loop at every specific point of the nanostructure can be measured, providing an advantage over other magnetometer systems.

VF-MFM allows high quality imaging of magnetic nanostructures with high mechanical stability under a variable external magnetic field that can be applied both along in-plane and out-of-plane directions. In the 3D Modes, the MFM tip continuously scans over the same region as the external magnetic field is varied with the aim of performing a hysteresis loop.

References

[1] – Stuart S. P. Parkin et al., Science **320**, (2008) 190
[2] – D. A. Allwood et al., Science **309**, (2005) 1688
[3] – R. P. Cowburn, Nature Materials **6**, (2007) 255
[4] – M. Jaafar et al., Physical Review B **5**, (2010) 054439
[5] – M. Jaafar et al., Ultramicroscopy **6**, (2009) 693
[6] – M. Jaafar et al., Submitted (2011)
[7] – F. G. Aliev et al., IEEE Xplore (2010), 160

Figures
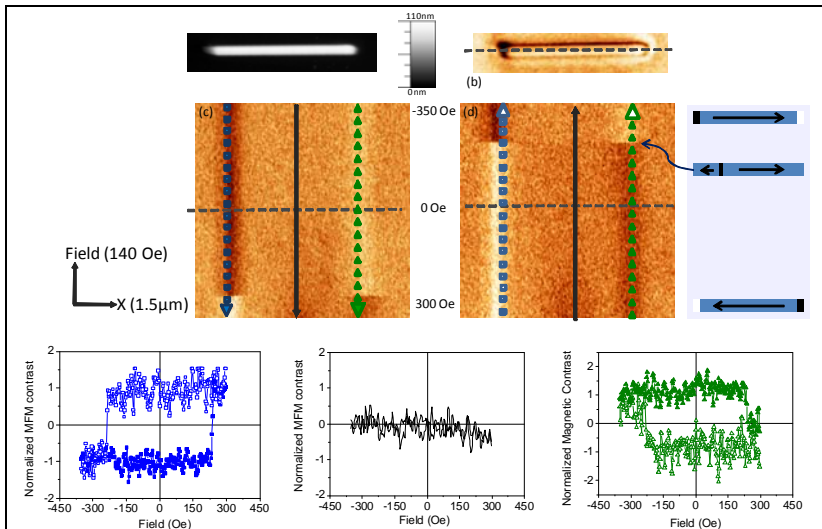
Figure 1. (a) Topography and **(b)** MFM images of a cobalt nanostripe of dimensions 250 nm x 5 µm. **(c)** and **(d)** MFM images using the *3D-Modes* (X vs Magnetic field), where and abrupt change in the nanostripe's magnetization can be clearly observed. **(e)** By plotting vertical profiles on images (c) and (d), local hysteresis loops are obtained (blue/black/green curves).
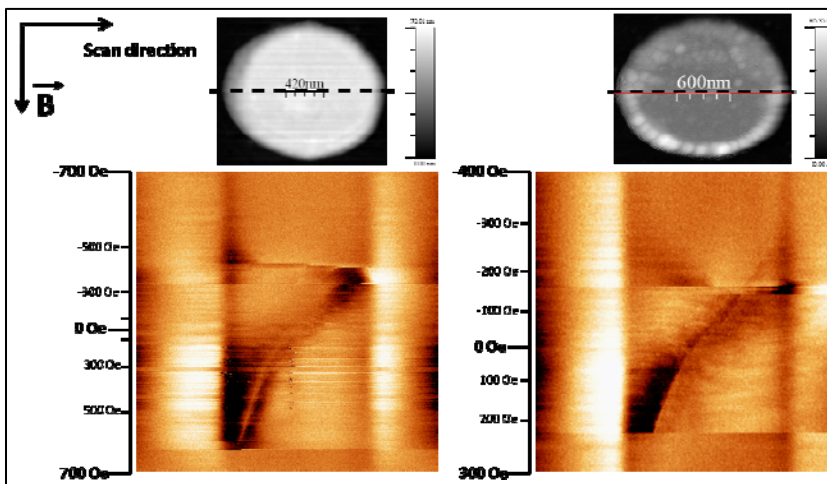
Figure 2. Topographic images of permalloy ($Ni_{80}Fe_{20}$) dots with a diameter of 1 µm and **(a)** 50 nm and **(b)** 20 nm thick. **(c)** and **(d)** MFM images obtained utilizing the 3D Modes (X vs. Magnetic field), both critical fields related to vortex nucleation-annihilation can be quantitative determined. Furthermore, it is indeed possible to observe a double-vortex metastable state on (d), as predicted in **[7]**.

Magnetoresistance Of Granular Cu-Co Alloys Prepared In The Form Of The Glass-covered Microwires

M. Ilyn[1], A. Granovsky[2], V. Zhukova[1], J. Gonzalez[1] and A. Zhukov[1]

[1]Department of Materials Physics, University of Basque Country UPV/EHU, 20080 Plaza Europa 1, San Sebastian, Spain
[2]Department of Physics, Moscow State University, 119992 GSP-1 Leninskye Gory, Moscow, Russia
maxim.ilin@ehu.es

Heterogeneous metallic systems consisted of magnetic nanoparticles embedded in the non-magnetic metallic matrixes were found to posses large magnetoresistance [1]. One of the techniques suitable for producing of such systems is an activation of heating-induced precipitation in the supersaturated non-equilibrium alloys of immiscible elements. Cu-Co, Cu-Fe, Ag-Co, Fe-Ni-Ag systems prepared using different methods like a co-sputtering, co-evaporation, mechanical alloying and melt-spinning followed by annealing have been already investigated [2].

Rather distinct magnetoresistance behavior has been found in granular $Cu_{90}Co_{10}$ alloy prepared in the form of the glass-covered microwires with various geometric parameters [3]. The reason for this difference is probably concerned with incomplete precipitation of Co during the preparation of the microwires.

This work is aimed to check the variation of the magnetoresistance in the Cu-Co glass-covered microwires with the stoichiometry and geometric parameters. Glass-covered microwires with metallic thread made of $Cu_{1-x}Co_x$ (5<x<30) granular alloys and different diameters of the metallic cores and glass layers have been manufactured. Magnetization and magnetoresistance have been measured in the range of temperatures from 5 to 305 K and magnetic fields up to 5 T. Except the common negative magnetoresistance originated from the spin-dependent scattering, positive magnetoresistance have been observed in moderate fields in the samples with highest concentration of Co (Fig 1, 2). In the samples with the lowest concentration of Co field dependent growth of resistivity with cooling below certain characteristics temperature was observed.

References

[1] J. R. Childress, C. L. Chien, "Reentrant magnetic behavior in fcc Co-Cu alloys", Phys. Rev. B **43** (1991), 8089-8093
[2] R. H. Yu, X. X. Zhang, J. Tejada, M. Knobel, P. Tiberto, P. Allia, "Magnetic properties and giant magnetoresistance in melt spun Co15Cu85 alloys", J. Phys. Condes. Matter **7** (1995), 4081-4093
[3] A. P. Zhukov, J. L. Martines, V. A. Zhukova, J. Palomares, J. Gonzalez, J. J. del Val, M. Vazquez, "Magnetoresistance in granular Co-Cu glass-coated microwires", IEEE Trans. Magn. **40** (2004), 2254-2256.

Figures
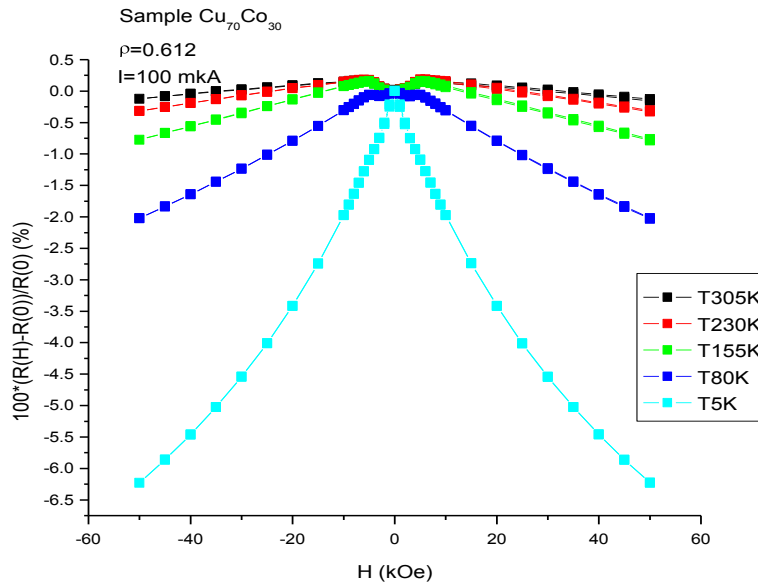
Fig. 1 Magnetoresistance of the sample with the highest in the series content of Co
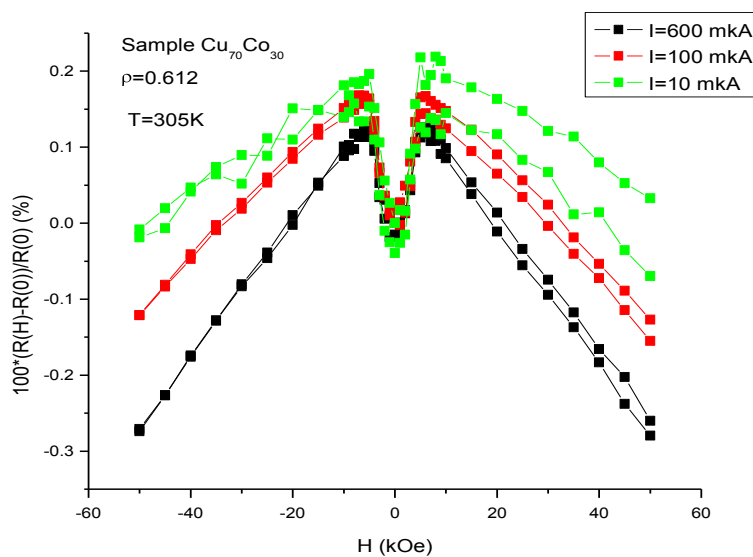
Fig. 2 Pronounced positive magnetoresistance easily seen in moderate fields

176

Characterization of Fe$_3$O$_4$ nanoparticles by Electron Magnetic Resonance Spectroscopy: Relation between synthetic parameters and magnetic behaviour

M. Insausti, J. Salado, L. Lezama, I. Gil de Muro, T. Rojo

Dpto. Química inorgánica, Facultad de Ciencia y Tecnología, UPV/EHU, Bº Sarriena, 48940 Leioa, Spain
maite.insausti@ehu.es

Magnetic nanoparticles have attracted importance in the biological area due to different applications such as contrast agents for magnetic resonance imaging [1], magnetic carriers for drug delivery [2] or hyperthermia [3]. Among the myriad of materials with high magnetic response, magnetite has been widely used because of its active surface chemical functionality, biocompatibility and low cost. Nevertheless for medical purposes it is necessary to control not only the size and the size distribution, but also the synthesis method must also provide a way to avoid particle aggregation and protect the surface from oxidation. In this sense, we present a comparative study of the synthetic parameters that affect the size and the content of matter surrounding magnetite nanoparticles smaller than 7 nm. What's more, in this kind of magnetic nanoparticles, different effects like surface effects or aggregations yield contradictory results for the same kind of nanoparticles. In order to discriminate these contributions, electron magnetic resonance spectroscopy has been employed.

For the preparation of Fe$_3$O$_4$ nanoparticles, reduction of iron(III) acetylacetonate by hexadecanediol in the presence of oleylamine and oleic acid was performed. Variations in the concentrations of the reagent and the stirring method yielded monodisperse nanoparticles between 3.5(5) to 7.1(9) nm. The content of organic ligands attached to the surface was calculated from thermogravimetric measurements. The weight loss was associated to oleic acid and differs remarkably among studied samples, ranging from 16.1 % to 40.9 %. Although the higher organic content corresponds to samples with smallest particle size, it has been observed that reagents concentrations also affect the organic content.

Electron magnetic resonance spectra of solid nanoparticles show an intense and slightly asymmetric line. The position of the main resonance field, H$_r$,, as well as the peak to peak linewidth, ΔH_{pp}, vary depending on the sample. The signal broads and shifts to the left from the position at g$_{efec}$ = 2.0, corresponding to samples with ideal superparamagnetic behaviour, with decreasing organic content. Nevertheless, it was verified a dependence of the shape and position of the signal with the sample handling in the RPE experiments. In this sense, a measurement method has been optimized in order to get reproducible results, that is the samples were either embedded in a piece of paper or deposited in a polymer film forming a monolayer. The angular dependence of the signal on these deposited nanoparticles was studied when the sample was placed in the perpendicular (θ = 90º) and parallel (θ = 0º) orientations. It has been observed that the shifting between 0 and 90º (Δg$_{efec}$) is more related with the organic content surrounding the NP than with the diameter in the studied size range. Finally, the thermal evolution of the resonance signal was also measured for two samples with two different Δg$_{efec}$ values related to superparamagnetic and ferromagnetic behaviours, respectively.

References

[1] Y.-M. Huh, Y.-W. Jun, H.-T. Song, S. Kim, J.-S. Choi, J.-H. Lee, S. Yoon, K.-S. Kim, J.-S. Shin, J.-S. Suh, J Cheon, *J. Am. Chem. Soc.*, **127**, 2005, 12387.
[2] J. Dobson, *Drug. Develop. Res.*, **67**, 2006, 55.
[3] A. Jordan, R. Scholz, K. Maier-Hauf, M. Johannsen, P. Wust, J. Nadobny, H. Schirra, H. Schmidt, S. Deger, S. Loening, W. Lanksch, R. Felix, *J. Magn. Magn. Mater.*, **225**, 2001, 118.

Lithium Ion Battery Cathodes Using Hollow Co_3O_4 Nanoparticles

Mohammad A. Islam

Department of Physics, American University of Sharjah, P.O. Box 26666, Sharjah, United Arab Emirates

Energy Materials Center at Cornell, Cornell University, Ithaca, New York

mislam@aus.edu

In spite of the ubiquitous use of the lithium ion batteries (LIB) in consumer electronics, these batteries are still in their infancy and significant amount of research is still left to bring out the full potential of the LIBs [1]. The electrode materials of the current state of the art LIBs are mostly dense laminates of tens to hundreds of μm in thickness, composed of electrochemically active materials few μm in size, conductive additives, and polymeric binders. These "bulk materials" experience kinetic limitations that hinder the diffusion of mobile charge carriers and lowers energy delivery rate, or power. In addition to the rate limitation, LIBs suffer from significant longevity issue due to the inability of bulk material's to accommodate Li insertion/deinsertion during discharging and charging of the batteries [2].

We propose to alleviate many of these problems by using electrophoretically deposited hollow Co_3O_4 nanoparticles thin films as the cathode [3.4]. Preliminary results show that these systems do have significant advantages over the current state of the art, as shown in figure 1 below. We believe these are due to three main advantages inherent to ordered and interconnected microporous geometry: first, the 3D interconnected pore structures facilitates mass transport through the electrodes, providing mobile species ready access to active material; second, short diffusion lengths, typically few nms, offer high rate performance; and third, the porous architecture creates relatively large specific areas that provide more exposed sites readily available to react with diffusing mobile species.

References

[1] U. Kasavajjula, C. Wang, A. Appleby, J. Power Sources **163** (2007), 1003-1009.

[2] J. Ryu, J. Kim, Y. Sung, S. Oh, Electrochem. Solid-State Lett**. 7** (2004), A306-A309.

[3] P. Piozot, S. Laruelle, S. Grugeon, L. Dupont, J. Tarascon, Nature **407** (2000), 496.

[4] W. Y. Li, L. N. Xu, J. Chen, Adv. Funct. Mater. **15** (2005), 851-857.

Figure 1: Left: Cyclic voltammograms of the battery and Right: Discharging and charging capacity of the battery.
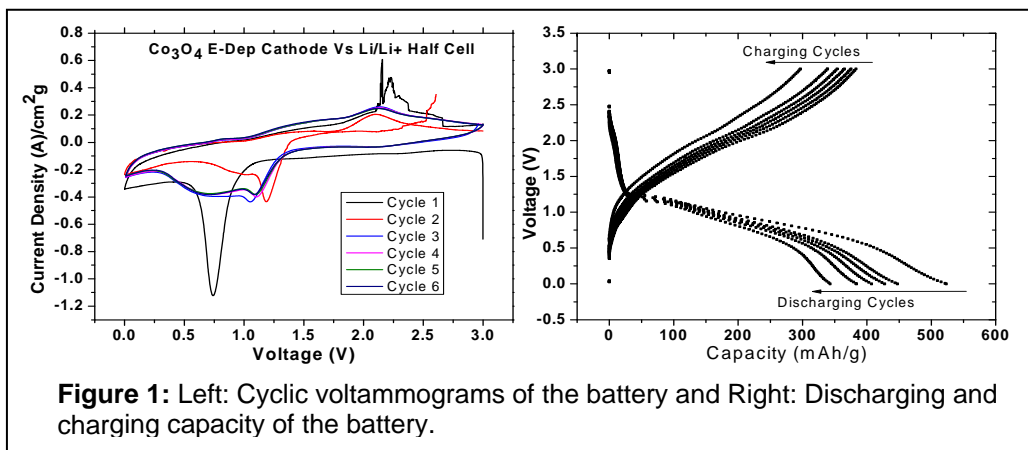
The Supercontinuum Laser as a Flexible Source for Quasi-Steady State and Time Resolved Fluorescence Studies

Roger Fenske[1,2]**, Dirk U. Näther**[1]**, Richard B. Dennis**[1] **John Clowes**[3]

[1]Edinburgh Instruments Ltd, 2 Bain Square, Kirkton Campus, Livingston, EH54 7DQ, UK.
[2]Heriot Watt University, Edinburgh, Scotland, EH14 4AS, UK
[3] Fianium, 20 Compass Point, Ensign Way, Southampton, SO31 4RA UK
E-mail: roger.fenske@edinst.com

Commercial Fluorescence Lifetime Spectrometers have long suffered from the lack of a simple, compact and relatively inexpensive broad spectral band light source that can be flexibly employed for both quasi-steady state and time resolved measurements (using both Time Correlated Single Photon Counting (TCSPC) and Multi-Channel Scaling (MCS) techniques).

This paper reports the integration of an optically pumped, photonic crystal fiber, supercontinuum source[1] with a pulse picker (Fianium model SC400PP) as a light source in a combined Steady State and Fluorescence Lifetime Spectrometer (Edinburgh Instruments model FLS920), with double excitation and emission monochromators and with single photon counting detectors (micro-channel plate photomultiplier and a near-infra-red photomultiplier) covering the UV to NIR range.

The spectrally corrected output from the supercontinuum laser (repetition rate selectable up to 20MHz) has been measured over the range 375-1700nm and shown to have the same order of higher spectral brightness as a 450W Xenon lamp over the majority of the range. The pulse height distribution and leading edge jitter of the output pulses has been measured and the performance optimised.

Alternative methods to select the emission wavelength and bandwidth from the supercontinuum output will be reported. These include using a tunable acousto-optic filter with up to 16 channels, which can be superimposed to provide a variable bandwidth, or the novel use of two motorised linear variable wedge interference filters, one low pass and the other high pass. Performance will be contrasted and compared.

Although the master oscillator within the supercontinuum laser has a short pulse width of ca 6ps it is known that the output pulse is significantly broadened by dispersion in the optical fibre. A key parameter which controls the precision of a TCSPC measurement is the Instrumental Response Function (IRF), which has been measured and shown to be <150ps over the majority of the tuning range.

The "Proof of Concept" of using the supercontinuum laser as a source for TCSPC measurements has been shown by measuring several known materials. A sample of antrathcene in cyclohexane (5×10^{-5}M) was studied as this is one of the most documented standards of fluorescence lifetime spectroscopy with a lifetime of 5.1ns when degassed. However, the excitation spectrum has a longest wavelength peak at 375nm with no absorption above ca 390nm. This showed the supercontinuum laser can be used at these short wavelengths. More challenging applications to measure shorter lifetimes of erythrosine B in water (lifetime ca 88ps) and pinacyanol chloride (lifetime ca 13ps) with excellent "Goodness of Fit" parameter will be shown.

By varying the repetition rate with the pulse picker, the supercontinuum laser is capable of measuring fluorescence lifetimes up to 50µs using the TCSPC. The possibility of using bursts of pulses in a variable envelope as a longer pulse width source for phosphorescence lifetime measurements in the micro- and milli-second range using the MCS technique will be discussed.

In conclusion, the supercontinuum laser offers the possibility of measuring fluorescence lifetimes down to a few 10's of picoseconds with the advantages of broadband tunability. The use of new supercontinuum sources with output further into the UV spectral region will be discussed.

References: [1] J.M. Stone, J.C. Knight Opt. Express 16 (2008) 2670-2675

Integration of Gallium Oxide Nanowires in Electronic Devices for Gas Sensing and UV Photodetection

Román Jiménez-Díaz[1], Iñaki López[2], Emilio Nogales[2], Bianchi Méndez[2], Javier Piqueras[2], J. Daniel Prades[1], Francisco Hernández-Ramírez[3], Albert Romano-Rodriguez[1]

[1] MIND-IN2UB, Departament d'Electrònica, Universitat de Barcelona, Barcelona 08028, Spain
[2] Departamento de Física de Materiales, Universidad Complutense de Madrid, Madrid 28040, Spain
[3] IREC, Catalonia Institute for Energy Research, E-08019, Barcelona, Spain
rjimenez@el.ub.es

Solid state devices based on metal oxides are amongst the most popular types of gas sensors for monitoring toxic species, such as carbon monoxide (CO) and nitrogen oxides (NOx) [1]. In the last years, significant research efforts have been devoted to extend their fabrication to the nanoscale, due to the excellent sensing properties of nanowires, related to the high surface-to-volume ratio. In general, the exclusive properties of nanostructured materials in respect to bulk materials have attracted research efforts because of their potential applications in electronic devices [2]. Although great advances have been achieved in synthesis, characterization of the fundamental properties and sensing mechanism of the materials, the fabrication of reliable and reproducible sensors based on these structures is still scarce due to the difficulties of the manipulation and characterization of the sensors [3].

Gas and optical sensors based on individual nanowires have been demonstrated and integration of nanowires in prototypes devices has proven its feasibility [4]. Nevertheless, the fabrication of electrical contacts with high stability, low contact resistances and ohmic behavior remains a challenge. Focused Ion Beam (FIB) lithography is a powerful fabrication technique for prototypes with dimensions in the range of the nanoscale [5]. Using this technique, electrical contacts are fabricated over the nanowire with electron beam assisted deposition while ion beam assisted deposition can be used to extent these contacts to large metal electrodes, giving macroscopic access to the electrical response of the nanowire while preserving the nanowire from ion damage (see Figure 1). The resulting devices provide an excellent opportunity to study the electrical, optical and gas sensing properties of individual metal oxide nanowires [6].

Gallium Oxide Nanowires are synthesized by the controlled thermal annealing of metallic gallium under argon flow, at temperatures between 1100ºC and 1300 ºC. Gallium oxide compacted powders were used as substrates. The growth mechanism of the nanowires is based in a vapor-solid process avoiding the use of a foreign catalyst [7]. The nanowires obtained exhibit a high crystal quality, which has been demonstrated by Transmission Electron Microscopy (TEM) techniques.

These Gallium Oxide Nanowires are contacted electrically by using FIB techniques and their electrical characteristics are studied in detail. The electrical response of these devices can be measured in different gas atmospheres studying the effect of surrounding gas in the electrical conduction of the nanomaterials. Finally the photoconductivity properties inherent to metal oxides can be exploited in the form of nanowires by the use of these devices also as photodetectors.

The potential of these metal oxide nanowires for their integration in sensing devices and the possibility of developing highly efficient future sensors will be discussed.

References:

[1] B. Hoffheins, in: R.F. Taylor, J.S. Schultz (Eds.), Handbook of Chemical and Biological Sensors, IOP Publishing, Bristol, (1996) 371.

[2] Xing-Jiu Huang and Yang-Kyu Choi Sensors Actuators B, **122** (2007) 659.

[3] Y. Chen, C. Zhu, M. Cao, T. Wang, Nanotenology, **18 (**2007) 285502.

[4] A. Kolmakov and M. Moskovits, Annu. Rev. Mater. Res, **34** (2004) 151.

[5] F. Hernandez-Ramirez, A. Tarancon, O. Casals, J. Rodriguez, A. Romano-Rodriguez, J. R. Morante, S. Barth, S. Mathur, T. Y. Choi, D. Poulikakos, V. Callegari and P. M. Nellen, Nanotechnology, **17** (2006) 5577.

[6] F. Hernandez-Ramirez, J. Rodriguez, O. Casals, E. Russinyol, A. Vila, A. Romano-Rodriguez, J.R. Morante and M. Abid Sensors and Actuators B, **118** (2006) 198.

[7] E. Nogales, B. Méndez, J. Piqueras and J. A. García, Nanotechnology, **11** (2009) 115201.

Figures
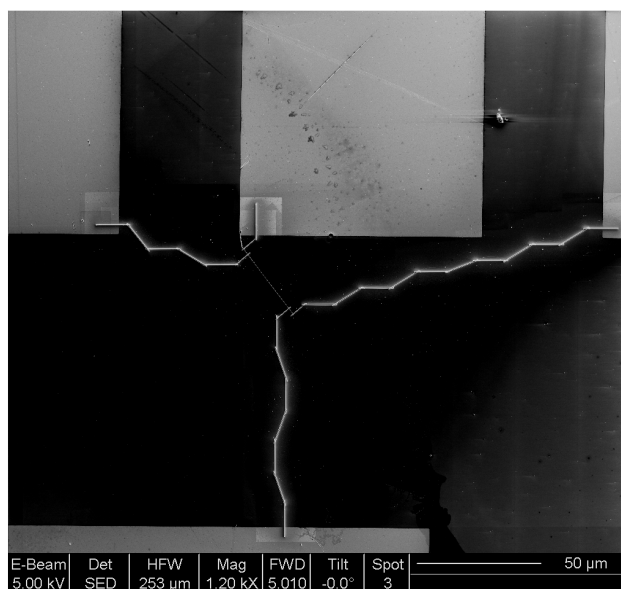
Figure 1. Gallium Oxide Nanowire contacted to four electrodes by FIB techniques.

Nonlinear Fluctuation Relations in a Spin Diode System

Jong Soo Lim [(1)], Rosa López [(1,2)], David Sánchez [(1,2)], Jan Martinek [(3)]

[1]*Departament de Física, Universitat de les Illes Balears, E-07122 Palma de Mallorca, Spain*
[2]*Institut de Física Interdisciplinar i Sistemes Complexos IFISC (CSIC-UIB), E-07122 Palma de Mallorca, Spain*
[3]*Institute of Molecular Physics, Polish Academy of Sciences, 60-179 Poznań, Poland*

email: lim.jongsoo@gmail.com

The linear fluctuation dissipation theorem (Kubo formula) and Onsager's reciprocity relation have been useful tools in analyzing linear transport of mesoscopic systems. For steady state transport, there have been several attempts to extend the linear relations into higher-order relations when a mesoscopic system is driven out of equilibrium. In order to derive such a nonlinear fluctuation relation, one of those attempts extends the microreversibility principle even into a nonequilibrium regime [1], while the other theoretical approach employs the microreversibility principle only at equilibrium [2]. It has been shown that two approaches yield the same results when the system under consideration respects the microreversibility. It is thus quite interesting to investigate the nonlinear fluctuation relations in the situation when the mircoreversibility is broken.
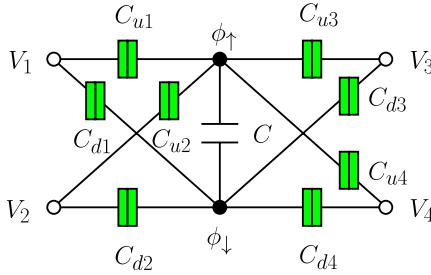
Fig. 1 Capacitively coupled model representation of a spin diode.

When the microreversibility is explicitly broken, the nonlinear fluctuation relations were theoretically tested using mesoscopic Coulomb drag effects [3]. But, a study for the relations in the presence of a magnetic field is still missing. In this work, we examine the nonlinear relations in the absence of the microreversibility and in the presence of a magnetic field. We study a quantum dot coupled to normal and ferromagnetic leads (spin diode). In order to break the microreversibility, we introduce incoherent spin-flip relaxation dynamics between up and down spins in a quantum dot. Also, to ensure gauge invariance we consider a capacitively coupled model shown in Fig. 1. Using full counting statistics [4] and Markovian master equation, the higher-order transport coefficients with respect to the bias voltage are then analyzed.

First, we check the linear fluctuation relations and verify they are exactly satisfied. Next, we proceed to examine second-order relations. Figure 2 shows second-order current and first-order noise transport coefficients with respect to the bias voltage as a function of incoherent spin-flip relation rate γ_{sf} and left lead polarization p_L in the presence of a magnetic field. We observe that the green and red lines perfectively overlap and this implies a second-order fluctuation is exactly satisfied for various parameters. It can be proven that our model system is an irreversible Markov chain and this means the microreversibility is broken. Our result confirms that there exist higher-order fluctuation relations even when the microreversibility is broken in the presence of a magnetic field.
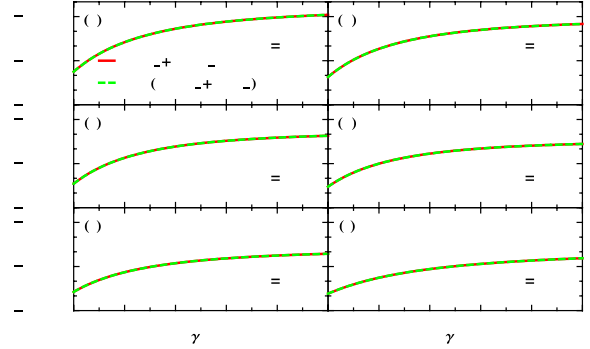
Fig. 2. Second-order fluctuation relations in the presence of a magnetic field.

References

[1] Keiji Saito and Yashuhiro Ustumi, Phys. Rev. B **78**, 115429 (2008).
[2] H. Förster and M. Büttiker, Phys. Rev. Lett. **101**, 136805 (2008).
[3] R. Sánchez and R. López, D. Sánchez, and M. Büttiker, Phys. Rev. Lett. **104**, 076801 (2010).
[4] C. Flindt, T. Novotny, A. Braggio, M. Sassetti, and A.-P. Jauho, Phys. Rev. Lett. **100**, 150601 (2008).
[5] J. S. Lim, R. López, D. Sánchez, and J. Martinek, in preparation (2011).

Calibrated nanoscale capacitance and dopant profile measurements using a scanning microwave microscope

[1]Gerald Kada, [1]Matthias A. Fenner, [2]Hans-Peter Huber, [3]Hassan Tanbakuchi, [1]Manuel Moertelmaier, [4]Pavel Kabos, [5]Juergen Smoliner, [2]Peter Hinterdorfer, [1]Ferry Kienberger

[1]Agilent Technologies Austria, Mooslackengasse 17, 1190 Vienna, Austria
[2]JKU University of Linz, Institute for Biophysics, Altenbergerstr. 69, 4040 Linz, Austria
[3]Agilent Technologies Inc., NanoDivision, 4330 W. Chandler Blvd., Chandler, AZ 85226, USA
[4]National Institute for Standards and Technology (NIST), Electromagnetic Division, Boulder, CO, USA
[5]Technical University of Vienna, Institute for Solid State Electronics, Floragasse 7, 1040 Vienna, Austria
Gerald_Kada@Agilent.com

A scanning microwave microscope (SMM) for spatially resolved capacitance measurements in the attoFarad-to-femtoFarad regime is presented. The system is based on the combination of an atomic force microscope (AFM) and a performance network analyzer (PNA).

For the determination of absolute capacitance values from PNA reflection amplitudes, a calibration sample of conductive gold pads of various sizes on a SiO_2 staircase structure was used (figure 1). The thickness of the dielectric SiO_2 staircase ranged from 10 nm to 200 nm. The quantitative capacitance values determined from the PNA reflection amplitude were compared to control measurements using an external capacitance bridge. Depending on the area of the gold top electrode and the SiO_2 step height, the corresponding capacitance values, as measured with the SMM, ranged from 0.1 fF to 22 fF at a noise level of ~2 aF and a relative accuracy of 20%.

For dopant profiling, n- and p-doped reference samples with densities between 10^{14} and 10^{19} atoms/cm^3 in 1.5 micron-wide regions were imaged in dC/dV modulation mode (figure 2). A calibration curve relating signal levels and dopant densities was established.

Possible applications of an SMM range from quality control of ICs, solar cells, and other semiconductor devices to materials science, (e.g. measurements of quantum dot dielectric constants), and to bioscience (e.g. the detection of viruses, and thickness measurements of protein layers). Examples shown will include capacitance and dielectric measurements on organic thin films, graphene, nanotubes and naowires as well as magnetic bacteria.

References

[1] H.P. Huber, M. Moertelmaier, T.M. Wallis, C.J. Chiang, M. Hochleitner, A. Imtiaz, Y.J. Oh, K. Schilcher, M. Dieudonne, J. Smoliner, P. Hinterdorfer, S.J. Rosner, H. Tanbakuchi, P.Kabos, F. Kienberger, Rev Sci Instrum, **81** (2010) 113701.

[2] J. Smoliner, H.-P. Huber, M. Hochleitner, M. Moertelmaier, F. Kienberger, J Appl Phys, **108** (2010) 064315.
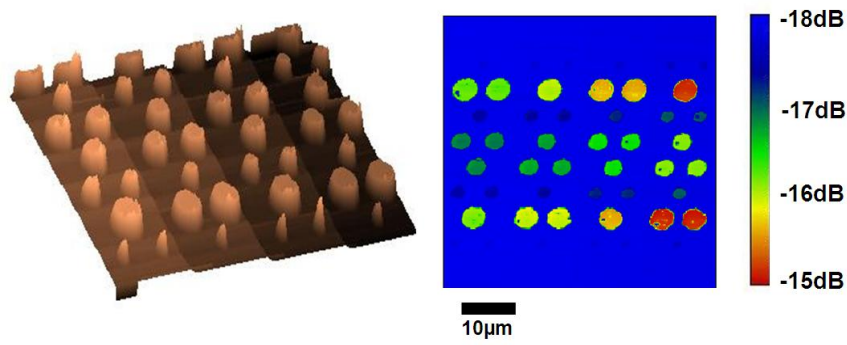
Figure 1. SiO$_2$ staircase in 3D-topography view (left) and corresponding PNA amplitude signal (right) used for calibrated capacitance measurements
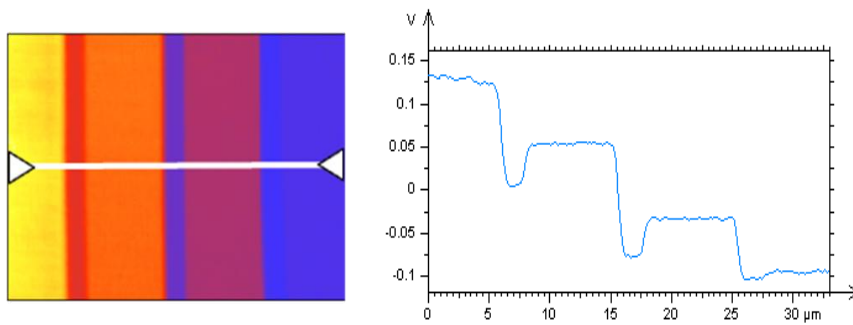
Figure 2. Dopant density calibration test sample (IMEC, Belgium) with densities ranging from 10^{14} (left) to 10^{19} atoms (right), measured in dC/dV mode.

Biodistribution of Microemulsion and Solution Containing Technetium-99m Labelled Aprotinin in Rats

H. Yeşim Karasulu[1], Derya İlem[2], Neslihan Üstündağ Okur[1], Nevin Oruç[3], Hayal Özkılıç[4], Makbule Aşıkoğlu[2], İ. Eren Akçiçek[3], Zeynep Ay Şenyiğit[1], Funda Yılmaz[5], Tamer Güneri[1], Ömer Özütemiz[3]

[1]Department of Pharmaceutical Technology, Faculty of Pharmacy, University of Ege, Izmir, Turkey
[2]Department of Radiopharmacy, Faculty of Pharmacy, University of Ege, Izmir, Turkey
[3]Department of Gastroenterology, Faculty of Medicine, University of Ege, Izmir, Turkey
[4]Nuclear Medicine, Faculty of Medicine, Ege University, Izmir, Turkey
[5]Department of Pathology, Faculty of Medicine, University of Ege, Izmir, Turkey
yesim.karasulu@ege.edu.tr

Abstract

The purpose of the present study is to evaluate aprotinin microemulsion biodistribution by gamma scintigraphy in rats.

For scintigraphic studies, aprotinin was directly labeled by ^{99m}Tc with small modification on previously described methods (1-2). Both ^{99m}Tc-aprotinin solution and ^{99m}Tc-aprotinin loaded microemulsion were administered Wistar albino rats (200–250 g) via tail vein under anesthetize. Serial static images were acquired with a gamma camera at different time intervals.

For evaluation of [99m]Tc- Aprotinin uptake regions of interest were drawn around the interested organs and uptake was calculated dividing by the ratio of decay corrected counts per pixel in the region of target to ratio of decay corrected counts per pixel in the region of soft tissue.

For biodistribution study the rats were sacrificed, abdominal cavity was opened and interested organs radioactivity was determined as count per gram by NaI-Tl gamma scintillation detector.

Aprotinin was radiolabeled by ^{99m}Tc with a high labeling efficiency greater than 95% and the complex is stable at room temperature up to 6 h. According to the scintigraphic and biodistribution studies, i.v. administration of [99m]Tc- Aprotinin-microemulsion had high uptake in liver and spleen while [99m]Tc- Aprotinin solution distributed mostly in kidneys and bladder (Figure 1).

a   b
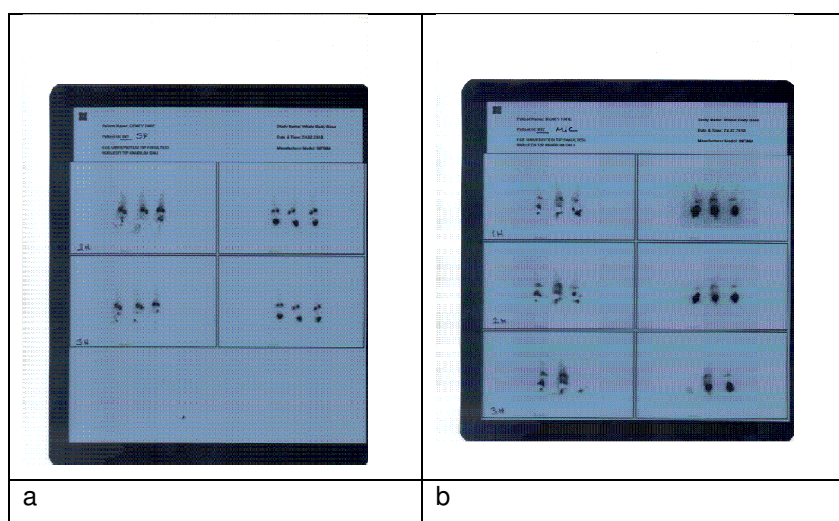
Figure 1:(a) ^{99m}Tc aprotinin loaded serum physgologic at 120 and 180 minutes **(b),** [99m]Tc loaded microemulsion at 60, 120 and 180 minutes

This comparative study indicates that; both formulations have totally different biodistribution in rats. Kidney uptake of microemulsion was slower and less than [99m]Tc- Aprotinin solution. In the literature knowledge aprotinin solution application has serious complications for kidney and also cause deadly heart problems and brain disease. Therefore, aprotinin loaded microemulsion may be use more safety than serum physiologic solution.

Acknowledgements

References

1. Douglas R. Smyth, Chris Tsopelas, An improved ^{99m}Tc-aprotinin kit formulation: quality control analysis of radiotracer stability and cold kit shelf life, Nuclear Medicine and Biology 885-89 (32), 2005.
2. Bente K. Schaa, Helle W. Hendel,Peter Gimsing, Viggo Jønsson, Heidi Pedersen, Bpharm, Birger Hesse, 99mTc-Aprotinin Scintigraphy in Amyloidosis, J Nucl Med 2003; 44:177–183

Materials, processes and quality inspection methods for photonic and bio related applications

N. Kehagias[1], T. Kehoe[1], M. Chouiki[2], M. Sa1aün[2], M. Zelsmann[2]and C. M. Sotomayor Torres[1,3,4]

[1]*Catalan Institute of Nanotechnology (CIN2-CSIC), Campus Bellaterra - Edifici CM3, 08193-Bellaterra (Barcelona), Spain*
[2]*LTM-CNRS, CEA-LETI-MINATEC, 17 rue des Martyrs 38000, Grenoble, France*
[3]*ICREA, Institució Catalana de Recerca i Estudis Avançats, 08010 Barcelona, Spain,*
[4]*Dept. Physics, Universitat Autònoma de Barcelona, de la UAB, 08193 Bellaterra (Barcelona), Spain*
Email: nikolaos.kehagias.icn@uab.es

Nanoimprint lithography (NIL) has proven to be a low cost and ownership "free" nanofabrication method suitable for medium scale production lines. Moreover nanoimprint lithography based methods have found more and more users in academic research laboratories which have taken the opportunity to explore (mainly the IC industry) various (potential) application. Towards this step new materials and alternative processes have driven NIL to a technological level which favors flexible and low cost device production at high throughput. In association to device manufacturing, non destructive inspection methods for quality control, have become essential.

In this paper we discuss the synthesis of novel resists suitable for UV based nanoimprint lithography which have opened new fields of applications such as graphoepitaxy, permanent photonic applications and bio compatible surfaces. In particular low-viscosity hybrid organic / inorganic UV-NIL resists based on polyhedral silsesquioxane (SSQ) functionalized with photo-polymerizable aliphatic epoxy groups have been synthesized [1]. These materials are very attractive because they present a high thermal and mechanical resistance. We discuss the properties of two similar materials but with different surface free energy (SFE) values. SSQ-Epoxy with a SFE value of 52.3 mJ/cm^2 (water contact angle 54.8^o) and SSQ-C6$_3$F$_5$, a fluorinated product (epoxy and fluorinated ligands are grafted on the SSQ T8 cage) with a SFE value of 18.9 (water contact angle 100.1^o). Figure 1 illustrates two scanning electron microscope (SEM) images of SSQ-C6$_3$F$_5$ and SSQ-Epoxy resists imprinted at room temperature, with a pressure of 4 bar for 1 min and exposed to UV light for 2 min. Such surfaces have been used as templates on which block copolymer (BCP) systems are deposited. By controlling the surface energy we managed to form micro-droplet periodic arrangements with sub-50 nm hexagonally arranged domains (figure 2).

The adoption of nanoimprint lithography as a widely used fabrication technique depends upon the use of suitable, reliable and cost-effective metrology techniques. We have developed a nanometrology technique based on sub-wavelength diffraction [2] which allows us to detect non-destructively sub wavelength polymer features. We compare our theoretical and experiments results showing that sub-wavelength diffraction is sensitive enough to changes of the line shape below 10 nm (figure 3), including rounding, induced by thermal relaxation, and that it is possible to accurately simulate the optical signal produced from complex three-dimensional profiles.
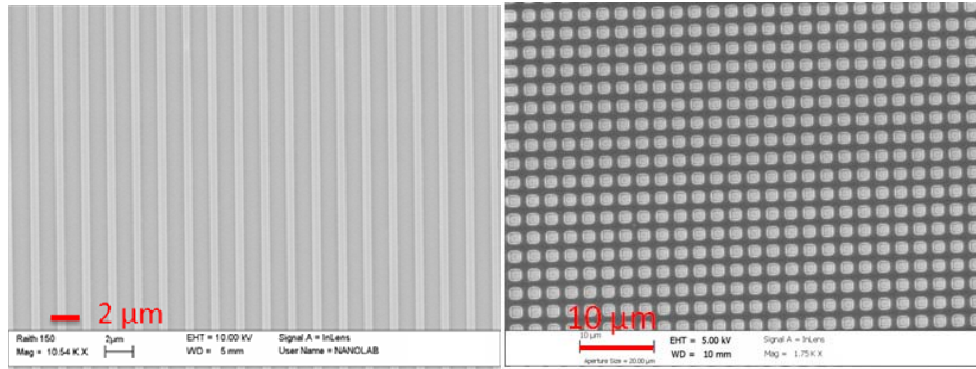
Figure 1 *(left) Top view SEM image of 500 nm SSQ-C6$_3$F$_5$ gratings imprinted by means of UV assisted NIL, (right) Top view SEM image of 1.3 µm square structures imprinted in SSQ-Epoxy*
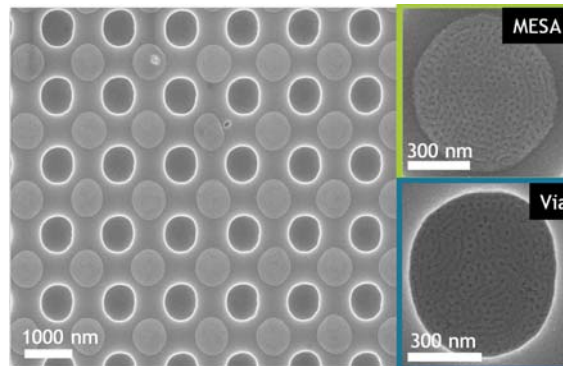
Figure 2 *SEM images of a regular array of ~675 nm microdroplets formed on top of the diagonal mesas between the 600 nm via-holes as a result of dewetting processes for a 1% wt PS-PMMA (46-21 kg/mol) solution; (insert) SEM images of microphase separation within the microdroplet on the mesa and within the via-hole (reservoir) taken from image*
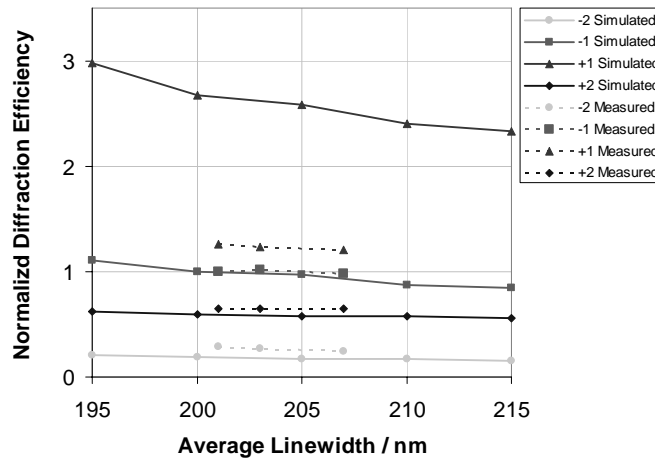
Figure 3 *Measured and simulated diffraction efficiencies, as a function of average grating line-width.*

References
[1] N. Kehagias, V. Reboud, J. De Girolamo, M. Chouiki, M. Zelsmann,J. Boussey, C.M. Sotomayor Torres, Microelectronic Engineering 86 (2009) 776–778.
[2] T Kehoe, V Reboud, C M Sotomayor Torres, Microelectronic Engineering 86, 1036–1039 (2009)

Synthesis of iron oxide nanotubes using TMV as a biotemplate.

Abid Ali Khan[1], Sachin Shah[1], Wiwat Nuansing[1], Andre Chuvilin[1], Christina Wege[2], Mariana Ungureanu[3] and Alexander Michael Bittner[1,4]

[1] CIC nanoGUNE Consolider, Tolosa Hiribidea 76, 20018 Donostia – San Sebastian, Spain
[2] Institute of Biology, University of Stuttgart, Pfaffenwaldring 57, 70569 Stuttgart, Germany
[3] CIC BiomaGUNE, Parque Tecnologico de San Sebastian, Edificio Empresarial C, Paseo Miramon 182, Donostia-San Sebastian, Spain
[4] IKERBASQUE, Basque Foundation for Science, 48011 Bilbao, Spain
a.khan@nanogune.eu

Tobacco mosaic virus (TMV) is a rod shaped plant virus containing RNA and 2100 identical coat proteins. It has a length of 300nm and a diameter 18nm [1]. TMV often aligns to linear oligomers of 600nm, 900nm, 1200nm in length. The exterior surface is highly polar and contains OH and COOH groups, the latter mainly deprotonated [2]. The synthesis of iron oxide on TMV involves simple wet chemistry under mild conditions. A mixture of aqueous Fe^{2+} and Fe^{3+} salts was used form iron oxide on the carboxylate covered exterior protein surface of TMV [3]. SEM shows plant viruses covered by a thin layer of iron oxide (5-7nm). Local EDX analysis pointed out clear peaks for Fe and O, proving the presence of iron oxide on the external protein surface.

XPS was used for a more detailed chemical analysis. In fact the iron oxide coating is a mixture of magnetite (Fe_3O_4) and maghemite (γ-Fe_2O_3). While magnetite is synthesized, it oxidizes and gives rise to maghemite on its surface. XRD showed no peaks, which could correspond to either magnetite or maghemite. Hence it is concluded that iron oxide coating on the TMV external surface is predominantly amorphous. Mineralized plant viral particles were also tested for their magnetic properties in a SQUID-VSM at 300K. The magnetic moment of mineralized TMV has a magnetization saturation of 0.00082emu/g [4,5]. However, the high coercivity value of 0.04T is due to the ferrimagnetic nature of the oxide and tubular structure of our iron oxide nanotubes [5,6].

References:

1. G. Stubbs. *Semin. Virol.* **1990**, 1, 405.
2. S. Balci, A.M. Bittner, M. Schirra, K. Thonke, R. Sauer, K. Hahn, A. Kadri, C. Wege, H. Jeske, K. Kern, *Electrochim. Acta.* **2009,** 54, 5149-5154.
3. W. Shenton, T. Douglas, M. Young, G. Stubbs and S. Mann. *Adv. Mater.* **1999**, 11:253-256.
4. Z. Wu, R. Zierold, A. Mueller, S.E. Ruff, C. Ma, A.A. Khan, F. Geiger, B.A. Sommer, M. Knez, K. Nielsch, A.M. Bittner, C. Wege, C.E. Krill III, *Phys. Status Solidi B.* **2010**, 10, 2412-2423.
5. YC. Zhang, JY. Tang, and XY. Hu. *J. Alloys Comp.* **2008**, 462(1-2):24.28.
6. B. Geng, F. Zhan, H. Jiang, Y. Guo and Z. Xing. *Chem. Comm.* **2010**, 5774.
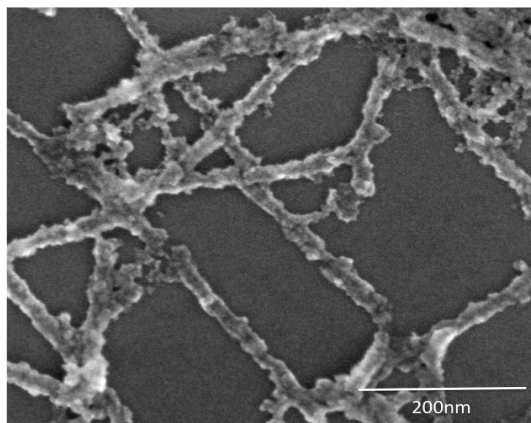
Figure 1. SEM of iron oxide-coated TMV nanotubes.
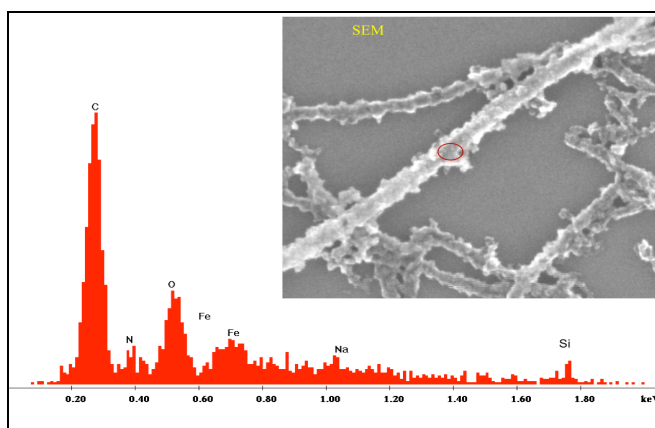
Figure 2. EDX spectrum of a single spot on iron oxide-covered TMV. Inset: SEM, spot area marked.
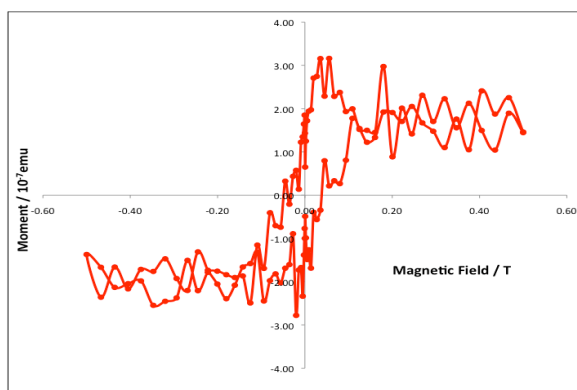
Figure 3. Magnetic field vs moment of mineralized TMV particles at 300K. Although the amount of material is very small, a ferrimagnetism hysteresis is found.

Nanofluid, Molecular Clusters and Cluster Self-Assembled Thin Films

Ramesh Jagannathan
New York University, Abu Dhabi
Tel: + 971 (0) 567 52 1309, email: rj31@nyu.edu

In this presentation we will describe unique, supercritical CO_2 based processes to prepare organic nanoparticles, which are essentially molecular clusters. The clusters exhibit novel phase and optical properties such as, room temperature liquid-like behavior, spontaneous self-assembling tendencies, process dependant photoluminescence and super hydrophobicity.

We will present evidence for a novel nanostructured fluid, composed of molecular clusters of a polar organic dye and surfactant. These are **not** nanoparticles dispersed in a solvent and there are no solvent molecules present. These materials, which are solids under ambient conditions, are non-reactively precipitated from a compressed CO_2 solution resulting in a liquid-like material, which we call nanofluid. The precipitated dye-surfactant clusters are 1-4nm in size and exhibit intense luminescent signatures, which are significantly blue-shifted with respect to the dye powder or a solution of it. The X-ray diffraction pattern did not show any structure in the low-angle regime. We believe that the ultra fast and controlled precipitation from compressed CO_2 preserves the electrostatic coupling and promotes a structured molecular cluster.

We also demonstrate the strong tendency of compressed CO_2 precipitated organic nanoparticles to rapidly self-assemble into highly aligned super-lattices at room temperature, when solution-cast from dispersions or spray-coated directly onto various substrates. The nanoparticles dispersions are stable for years. The novel precipitation process used is believed to result in molecular distances and alignments in the nanoparticles, which are not normally possible. Self-assembled thin films of these novel materials exhibit lamellar structures and coatings on cloth and stainless steel have been found to be superhydrophobic in nature.

Functional OLEDs - which have the same host-dopant emissive material combination as their vacuum fabricated checks- with process tunable electro luminescence, have been built with these nanoparticles, indicating the presence of novel nanostructures. For example, only changing the conditions of the precipitation process changes the OLED emission from green light to yellow.

Biomedical and Nanomaterials Capabilities at ATIC Innovation Center

Pavel Kiselev, Ciara O'Sullivan, Ioanis Katakis, Robert Rallo, Francesc Castells, Joan Rosell, Olivier Henry, Alex Fragoso, Pablo Lozano, Valerio Beni, Joan Sans, Isabela Butnar

Centre ATIC, Universitat Rovira i Virgili, Avda. Països Catalans 18, 43007 Tarragona, Spain
pavel.kiselev@urv.cat

We describe the research and development activities in Nanotechnology at the Advanced Technology and Innovation Center, ATIC, of the Universitat Rovira i Virgili of Tarragona:

BIOTECHNOLOGY and ENVIRONMENT: Surface modification of surfaces via electrodeposition of modified nanoparticles (NPs) for micro-systems applications in biotechnology, health, environment, etc. Size controlled in situ deposition of Au, Pd and mixed Au-Pd NPs for enhanced catalysis. Surface immobilized NPs for a more environmental friendly oxidation of primary alcohols to aldehydes, and for CO oxidation to CO2.

HEALTH: Biosensor arrays housed within integrated microsystems for the early detection of disease. Example 1: Low cost microsystem for use at the point-of-care for the biopsy free diagnosis & monitoring of celiac disease via combined HLA-typing and serology measurement, with automated actuation and assay time under 15 minutes. Example 2: In post-surgery/radio/chemo-therapy, circulating rare cancer cells are isolated from blood for an early detection of metastasis, moving towards theranostics and individualized medicine according to the patient's RNA expression profile. Example 3: Nanoliposomes for targeted drug delivery to cancer cells, functionalized with specific antibodies.

BIOINFORMATICS: The characterization and modeling of the potential toxic effects of nanoparticles requires the use of advanced computational techniques. Our expertise in the application of data mining schemes and machine learning to analyze nanoparticle data is applicable a variety of industrial processes as well as in environmental monitoring of nanoparticle effects.

FLUIDS TECHNOLOGIES: Electrospinning, electrospray and other liquid atomization / spraying methods are used to produce pharmaceutical NPs and for their controlled deposition, to synthesize thin films and powders of polymers, oxides, pharmaceutics etc. Electrospun fibers can be used for filtration, or as templates for tissue engineering.

Relationship between atomistic arrangement and internal nanocrystal superstructure ordering within PbS-organic mesocrystals

L. Liebscher[a], W. Carrillo-Cabrera[b], E. Rosseeva[b], P. Simon[b], S. G. Hickey[a], A. Eychmüller[a]

[a] Physical Chemistry, TU Dresden, Bergstraße 66b, 01062 Dresden, Germany
L.Liebscher@chemie.tu-dresden.de

[b] Max Planck Institute for Chemical Physics of Solids, Nöthnitzer Straße 40 ,01187 Dresden, Germany

Nanoscale materials show behavior which is intermediate between the properties of single molecules or atoms and the properties of bulk materials. Therefore by controlling the dimensions of materials in the nanometer size regime a number of material properties which demonstrate size dependence can be tuned. For example semiconductor nanocrystals (NC) show size-dependent optical-properties, magnetic NCs show size-dependent magnetic-properties (superparamagnetism), including transitions from paramagnetism to ferromagnetism and noble-metal NCs possess size-tunable plasmonic resonances. [1] Through the development of new optimized synthesis strategies highly monodisperse NCs can be produced, which have potential applications in optical, magnetic or electronic devices.

2D and 3D arrangements of NCs combine the properties of individual NCs with new features that derive from the unique collective properties of arrays of ordered particles. These particle arrangements have further promising applications as light emitting devices, photodetectors, thermoelectric heat-to-electricity converters and solar cells[2]. Because of the potential locked within these new material sets the field of interest is shifting away from the synthesis of the nanoparticles as building blocks to the assembly of these small units into hierarchical structures.

In this contribution we present a novel method, using the gas phase diffusion technique (Figure 1), for the formation of hierarchal architectures (mesocrystals, superstructures) with spherical lead chalcogenide NCs as building blocks. The mesocrystal dimensions are increased by up to six times (300µm) using this new destabilization technique as compared to the technique employed by Podsiadlo *et al* [1]. After thinning the mesocrystals using FIB, the inner crystallographic arrangement of the building blocks and the 3D arrangement of the NCs could be visualized. TEM analyses (Figure 2) have shown the relationship of the superstructure crystal arrangement to the crystal structure of the individual NCs and their facets and simulations provide insights into the superlattice packing. Electron holography studies demonstrate that the NCs in the superstructure arrangement are of the same size and morphology as before the destabilization process.

References

[1] P. Podsiadlo *et al.*, Nano Lett., Article ASAP, DOI: 10.1021/nl103587u
[2] S. M. Rupich *et al.*, JACS **132** (2010) 289.

Figures
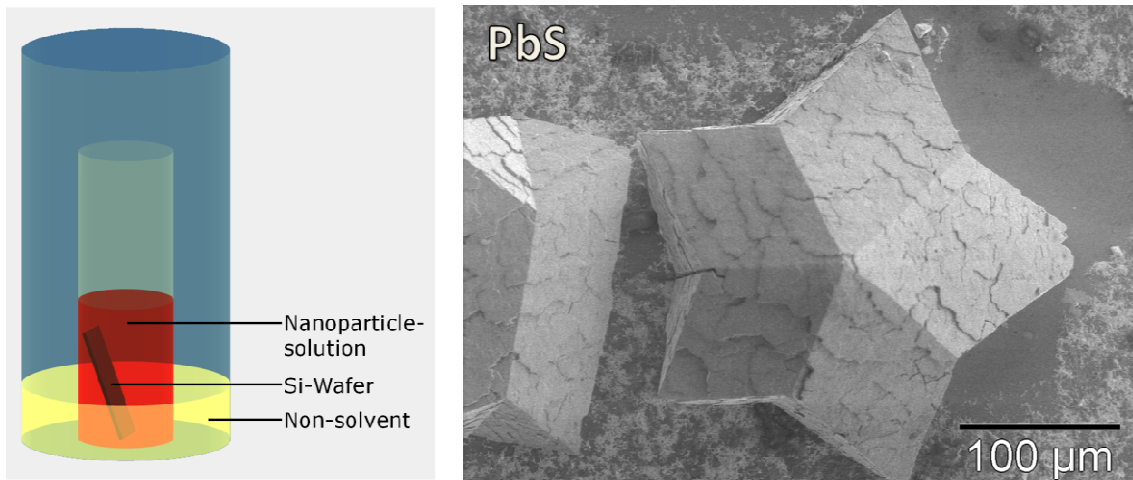
Figure 1: Gas phase diffusion technique and PbS-mesocrystal.
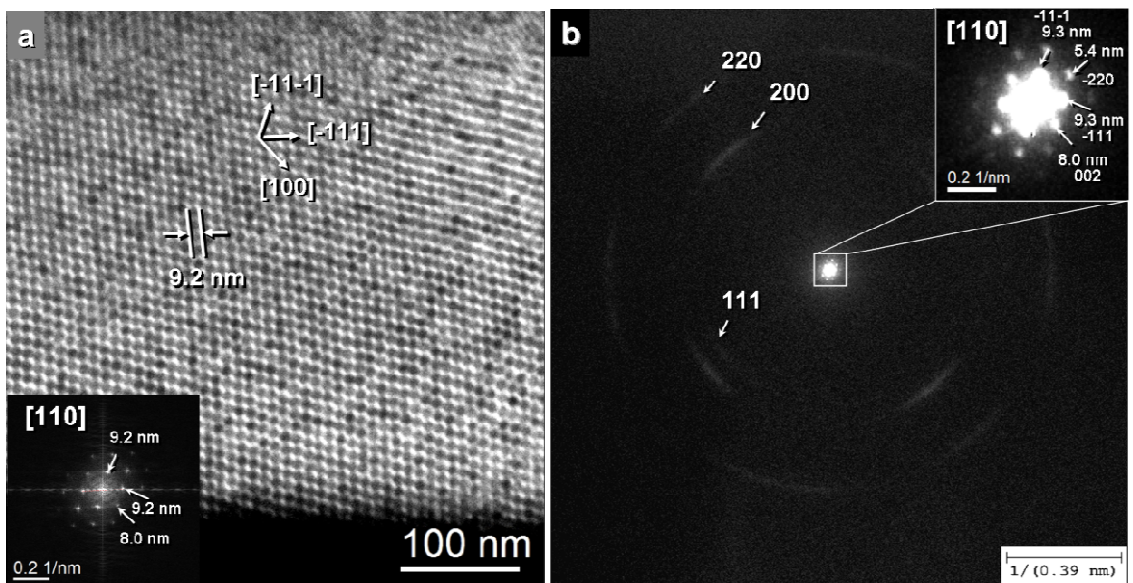
Figure 2: (a) Overview TEM image of FIB-cut with corresponding fast Fourier transform (FFT) inset, showing the superstructure ordering of the nanoparticles. (b) Electron diffraction from the same area visualizing relationship between superstructure (inset - zoomed small angle area) and PbS (galena) nanocrystals reflections

Liquid friction acting on solid surfaces probed by second harmonic generation spectroscopy

Dan Lis[1], Sung Chul Bae[2], Steve Granick[2]

[1]*Laser and Spectroscopy Laboratory, Research Centre in Physics of Matter and Radiation, University of Namur (FUNDP), Belgium*
[2] *Departments of Materials Science and Engineering, Chemistry, and Physics, University of Illinois*
dan.lis@fundp.ac.be

This work aims to investigate the friction acting on a solid surface and resulting from a fluid motion against it. Indeed, although the no-slip condition is known to be violated at micrometric scale in many systems, the liquid slip phenomenon occurring at the very surface is still far to be fully understood [1].

To better understand how fluids may behave very close to solid surfaces in a non confined environment, we used dye molecules physisorbed at the interface as local sensors. We chose second harmonic generation (SHG) spectroscopy to obtain orientational informations on the molecular system. SHG is indeed very well suited to probe buried interfacial regions thanks to its high sensitivity to non-centrosymmetric environments [2,3]. Moreover, it allows retrieving accurate information on molecular conformations through a polarized study [4].

In detail, we worked at the quartz-water (or water-glycerol mixture) interface. The SHG spectroscopy is executed in the total internal reflection configuration (see Figure 1). First, we performed a characterization of the dye orientation in static condition, that is with no liquid flow. Thereafter, the liquid flow is switched on and important SHG signal modifications are observed, those latter being attributed to dye re-orientation. By using different fluid viscosities and debits, we retrieved the correlation between shear rate and surface stress.

References
[1] S. Granick, H. Lee, Y. Zhu, Nature Materials, **2** (2003), 221-227
[2] Y. R. Shen, *Annu. Rev. Phys. Chem.,* **40** (1989), 327-350.
[3] K. B. Eisenthal, Chemical Reviews, **96** (1996), 1343-1360.
[4] T. Kikteva, D. Star, Z. Zhao, T. L. Baisley, G. W. Leach, J. Phys. Chem. B, **103** (1999), 1124-1133.
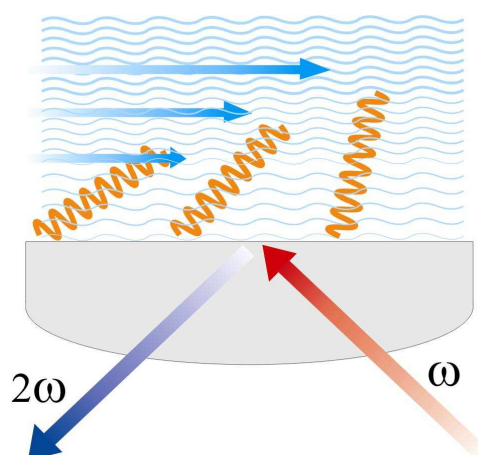
Figure 1. Second harmonic generation spectroscopy is used to probe how a solid surface responds to a liquid flowing over it. This is achieved through the analysis of the molecular re-orientation induced at the interface.

Optical detection of proteins using gold nanoparticles

C. Nietzold, F. Lisdat

Biosystems Technology, Technical University Wildau,
Bahnhofstrasse 1, 15745 Wildau, Germany
flisdat@th-wildau.de

In this study we describe the development of a detection system for the sensitive and fast analysis of proteins. The immunological method uses gold nanoparticles to detect proteins at the nanogram level, as is required for clinical diagnosis.

Gold nanoparticles are characterised by their intensive light absorption which is caused by excitation of collective oscillations of valence band electrons, the so called plasmon resonance. The plasmon resonance wavelength is, amongst others, a function of the direct particle environment so that changes therein can be monitored spectroscopically.

Subject of this work is the surface modification, functionalization and bioconjugation of this kind of nanoparticles with a diameter in the range 20-60 nm. First we used as a test system, the protein ovalbumin and a specific antibody.

Bioconjugates of the gold nanoparticles and antibodies are produced in solution and characterised. The formation of antigen-gold nanoparticle conjugates is detected by an increase in hydrodynamic diameter as determined by dynamic light scattering (DLS). An analysis time of 10 minutes is sufficient to detect the immune complex formation. This is accompanied by a change in the absorption properties of the nanoparticles. Using UV/Vis spectroscopy this can be monitored and it is possible to quantify the shift of the plasmon resonance wavelength. The system is sensitive in the concentration range 0.06-0.25µg/ml. When the size dependence of this diameter increase is analysed, the larger particles result in a higher relative change as compared to the small (20 nm) particles.

The test system is then adopted to the detection of alpha-fetoprotein. This protein is a relevant tumor marker. Sensitivity can be provided here in the relevant concentration range of 0.15-0.5µg/ml.

[1] Bellino, M.G., Calvo, E.J. and Gordillo G., Phys.Chem.Chem.Phys., **6** (2004), 424-428.
[2] Chen, S. and Kimura, K., Langmuir, **15** (1999), 1075-1082.
[3] Pieper-Fürst U., Kleuser, U., Stöcklein, W.F.M., Warsinke, A. and Scheller F. W.,
   Analytical Biochemistry, **332** (2004), 160–167.

Rhodamine 6G Confined in Polymeric Nanoparticles as Active Media of Tunable Lasers

Jorge Bañuelos,[1] Eduardo Enciso,[2] Virginia Martin,[3] Inmaculada Garcia-Moreno,[3] **Iñigo López Arbeloa**,[1]

[1]Dpto Química Física, Universidad del País Vasco (UPV-EHU), Aptdo 644, 48080 Bilbao, Spain.
[2]Dpto Química Física I, Universidad Complutense, Ciudad Universitaria, 28040 Madrid, Spain.
[3]Dpto Sistemas de Baja Dimensionalidad, Superficies y Materia Condensada, Instituto de Química Física "Rocasolano" (CSIC), Serrano 119, 28006, Madrid, Spain.

inigo.lopezarbeloa@ehu.es

Fluorescent dyes are usually applied in signalling, imaging and sensing different process of interest or molecular events. To this aim, the fluorophore should be stable in different environments, small enough to ensure a good compatibility with the biochemical systems and highly fluorescence. However, sometimes the fluorophores are affected by the surrounding environment properties. For example, extreme acid or basic conditions could damage the dye causing a loss of the sensing ability of the dye. In other cases, the environment might induce interactions between dye molecules causing the aggregation and hence the quenching of the fluorescence signal.[1]

One way to circumvent this problem is to encapsulate the fluorescence label into a nano-sized organic or inorganic particle. Thus, the dye is protected against external factors increasing its photo and thermal stability. That is why we decide to encapsulate Rhodamine 6G (Rh6G) laser dye into latex polymeric nanoparticles. The obtained dye-doped materials are small enough and show a random distribution in solution. Consequently the transparency is not affected and these systems could be applied as the active media of tunable lasers. Even more, the lasing action of rhodamine 6G is enhanced in the latex framework by the non-resonant feedback of the emission by multiple scattering.[2] The dye doped latex nanoparticles act as scattering centers, which, instead of being detrimental for the laser action, improve the lasing efficiency of the dye.

In the present work, we have studied in detail the photophysical and lasing properties of aqueous suspensions of Rh6G encapsulated in latex nanoparticles.[3] The influence of the dye concentration, composition of the latex and morphology of the polymeric nanoparticle have been taking into account looking for the best conditions to optimized the optical properties of these systems. This is possible since the size, polarity and viscoelasticity of the surrounding environment of the dye can be controlled by carefully changing the latex composition.

The small size of the latex nanoparticles makes possible to obtain stable aqueous suspensions. Dye aggregation is one of the mayor drawbacks of tunable dye lasers. Their inactive absorption and their fluorescence quenching effect drastically decrease the lasing efficiency. Instead, Rh6G has tendency to self-associate in concentrated media, which are required for the lasing action. However, this problem is overcome with the dye encapsulation. No sign of aggregation has been observed up to dye concentrations around 10^{-2} M inside the latex, obtaining highly fluorescence emissions and hence improved lasing signals.

While the latex polymeric composition has minor effect onto the photophysical properties of Rh6G the size of the nanoparticle is a key factor. For small enough particles (diameter lower than 70 nm) the fluorescent efficiency is unaltered. Due to the incoherent random lasing, the weak scattering of the

emission elongates the light path inside the gain media providing extra feedback and improving the lasing efficiency of Rh6G with regard to liquid solutions. However, for big nanoparticles the fluorescence is quenched and no lasing emission is detected. In these conditions the scatter effect is so high that increases the losses in the resonator cavity.

Summarizing, the encapsulation of Rh6G in latex nanoparticle lads to a highly fluorescent system, even at high concentrations, and ameliorates the lasing properties of the dye due to the weak scatter of the light, which provide an extra non-resonant feedback of the emission. Besides, the dye is protected against photobleaching. However, big nanoparticles damage the fluorescence and laser emission owing to the too high light scattering probability.

References

[1] F. López Arbeloa, T. Arbeloa, I. López Arbeloa, in Handbook of Advanced Electronic and Photonic Materials and Devices, **7** (2001) 209.
[2] A. Costela, I. García-Moreno, L. Cerdan, V. Martin, O. Garcia, R. Sastre, Adv. Mater. **21** (2009) 4163.
[3] V. Martin, J. Bañuelos, E. Enciso, I. López Arbeloa, A. Costela, I. García-Moreno, J. Phys. Chem. C (in press).

Figures
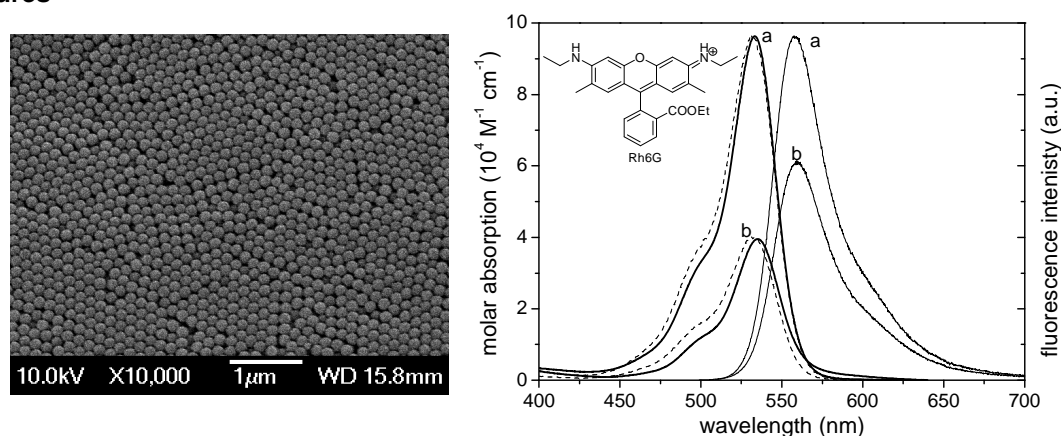
Figure 1. *Scanning Electron Microscopic (SEM) image of the latex nanoparticles and absorption, excitation (dashed) and fluorescence spectra of rhodamine 6G (Rh6G) inside small (a, diameter 20nm) and big (b, diameter 166 nm) polymeric nanoparticles.*

SERS analysis of a bioactive isomer of pyridinecarboxamide: picolinamide

M.R. Lopez-Ramirez, J.L. Castro, J.F. Arenas, J.C. Otero

Department of Physical Chemistry, Faculty of Science, University of Málaga, E-29071 Málaga, Spain.
mrlopez@uma.es

SERS phenomenon (Surface-enhanced Raman scattering) has been widely used to study the adsorption on some metallic roughed surfaces, mainly of Ag, Cu and Au, of many organic molecules. The high sensitivity of this effect allows an accurate structural study of adsorbates at very low concentrations. This technique can be used to gain information concerning the adsorbed species and the functional groups which are in contact with the metal surface and in many cases, concerning the conformation of the adsorbate [1,2].

In this work we have recorded the Raman and SERS spectra of picolinamide (PIA) recorded on silver colloids. PIA is one of the three bioactive isomers of pyridinecarboxamide and it shows an important biological activity with the NAD coenzyme (nicotinamide adenine dinucleotide) [3] which plays important roles in more than 200 aminoacid and carbohydrate metabolic reactions [4].

Raman and SERS spectra were recorded with a Jobin-Yvon U-1000 double monocromator spectrometer fitted with a cooled Hamamatsu R943-02 photomultiplier, using the 514.5 nm exciting line from a Spectra Physics 2020 Ar^+ gas laser. In the case of liquid samples a quartz cell with a 1cm path length was used, whilst a glass capillary was used for the microcrystalline solids. Colloidal silver solutions have been prepared in deionized and triply distilled water according to the method described by Creighton et al.[5].

Fig.1.a shows the Raman spectrum of solid crystalline PIA and Fig.1.b the SERS spectrum of a 10^{-4} M solution of PIA adsorbed on silver colloids, both in the range 100-1800 cm^{-1}.

EXPERIMENTAL WAVENUMBERS			
Mode	Solid	SERS	$\Delta\nu$ (cm^{-1})
Amide I	1662	1636	-26
Amide III	1406	1416	+10
ν (CX)	1175	1230	+55
1; ν_{ring}	787	836	+49
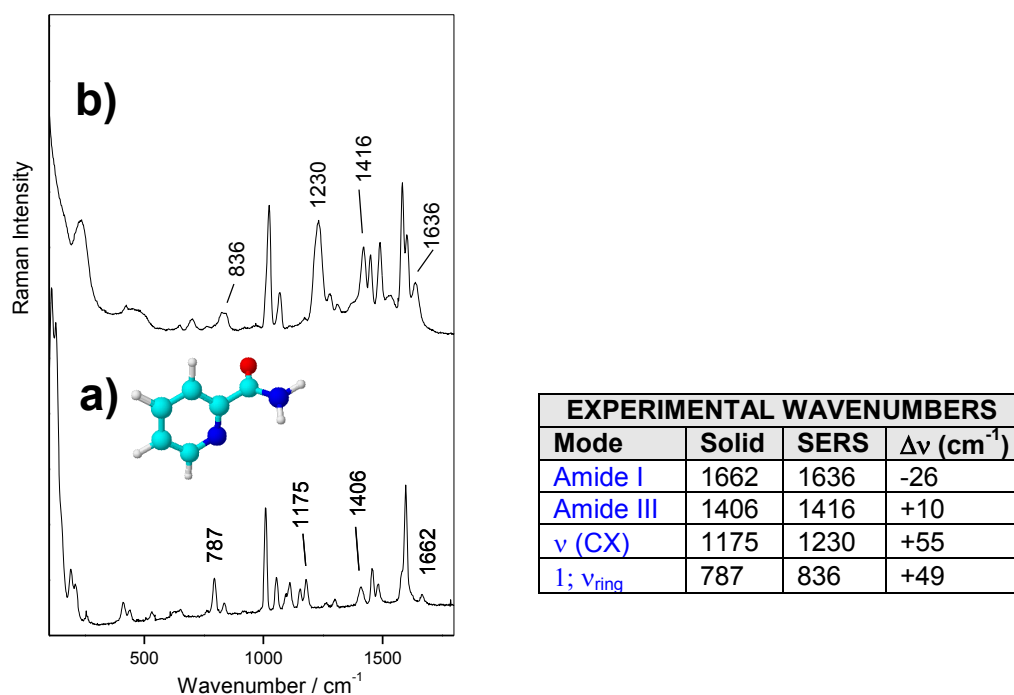
Fig. 1. a) Raman spectrum of solid PIA; b) SERS spectrum of a 10^{-4} M solution of PIA. Table: Experimental wavenumbers of the Raman and SERS spectra of PIA and wavenumber shifts between them.

This region of the Raman spectrum of the solid (Fig. 1.a) is dominated by two very strong bands at 1004 and 1594 cm^{-1}. These bands are assigned to the 12; δ_{ring} and 8a; ν_{ring} modes, respectively, and they don't experiment important changes in the SERS spectra. However there are some characteristic bands of this molecule associate with the amide and aromatic functional group that undergo significant wavenumber shifts in the SERS spectra. Therefore the Raman vibrational modes related to the amide I, amide III, ν(CX) and 1;ν_{ring} recorded at 1662, 1406, 1175 and 787 cm^{-1}, respectively, undergo important wavenumber shifts of -26, +10, +55 and +49 cm^{-1} when PIA is adsorbed on the nanostructures. The shift undergone by the mode 1;ν_{ring} is very similar to that observed in the SERS spectra of aromatic molecules as benzamide which indicates the adsorption on silver nanoparticles as azanions linking to the metal through both the nitrogen and the oxygen atoms of the ionized carboxamide group. The delocalization of the negative charge in the whole molecule originates changes in the molecular structure affecting to these vibrational modes.

Finally, the enhancement of the SERS bands attributed to amide I, amide III and ν(CX) vibrations is due to the fact that PIA interacts to the metal through both the nitrogen and the oxygen atoms of carboxamide group and the aromatic ring is orientated approximately perpendicular to the mentioned surface.

References
[1] J.L. Castro, J.F. Arenas, M.R. López-Ramírez, J.C. Otero, Biopolymers **82** (2006) 379.
[2] J.L. Castro, J.F. Arenas, M.R. López-Ramírez, D. Peláez, J.C. Otero, J. Colloid Interf.Sci. **332**, (2009) 130.
[3] R.A. Olsen, L. Liu, N. Ghaderi, A. Johns, M.E. Hatcher and L.J. Mueller, J. Am. Chem. Soc. **125** (2003), 10125.
[4] Food and Nutrition Board, Institute of Medicine, Thiamin, Riboflavin, Niacin, Vitamin B-6, Vitamin B-12, Pantothenic Acid, Biotin and Cholin, National Academy Press, Washington, DC (1998) pp. 123–149.
[5] J.A. Creighton, C.G. Blatchford, M.G. Albrecht, J. Chem. Soc. Faraday Trans. II **75** (1979) 790.

Novel polymer-metal based nanostructures.

Jon Maiz*, Helmut Schäfer[&], Javier Sacristán*, Brigitte Hartmann[&], Martin Steinhart[&], Markus Haase[&], Carmen Mijangos*

* Instituto de Ciencia y Tecnología de Polímeros, CSIC, c/ Juan de la Cierva 3, 28006 Madrid, Spain
[&] Institut für Chemie, Universität Osnabrück, Barbarastr. 7, D-46069 Osnabrück, Germany
jon@ictp.csic.es

During the last few years there has been tremendous interest in template-based synthesis of nanomaterials for numerous nanotechnology applications. Anodic Aluminium Oxide (AAO) is a suitable template for the preparation of 1D polymeric nanostructure by "template synthesis" due to its relatively low cost, good quality architecture with long-range order, adjustable length and diameter and uniform nanopores with hexagonal symmetry. Tailored polymer-metal nanotubes and nanofibers can be prepared by choosing the suitable AAO template, and the appropriate infiltration method and conditions [1-4].

Moreover, the extraordinary mechanical properties of SWCNT make them suitable additives for a new generation of polymer nanocomposites. Incorporating SWCNT into polymers has the potential to radically improve the properties of the polymer matrix in terms of strength, toughness, electrical conductivity, thermal conductivity and/or flame retardancy [5]. In addition, the Brust-Schiffrin method for Au nanoparticles synthesis has had a considerable impact on the overall field in less than a decade, because it allowed the facile synthesis of thermally stable and air-stable Au nanoparticles of reduced dispersity and controlled size for the first time (ranging in diameter between 1.5 and 5.2 nm). Indeed, these Au nanoparticles can be repeatedly isolated and redissolved in common organic solvents without irreversible aggregation or decomposition, and they can be easily handled and functionalized just as stable organic and molecular compounds (Fig.1). Gold presents advantages mainly on the basis of more robust chemical stability, which guarantees a long-term preservation of the optical features [6].

In relation with this, the aim of the present work is to prepare novel nanostructured polymer based composites. For that, we will embed single-wall carbon nanotubes (SWCNT) and gold (Au) nanoparticles in different polymers.

In the present work we have prepared new polymer-metal based nanostructures, in particular polyvinylidene fluoride (PVDF) – SWCNTs and polyethylene – Au nanoparticles. In order to achieve these composites we have developed; (i) different infiltration methods, either for polymeric fluids or polymer based composites fluids into the alumina template cavities; (ii) different anodization conditions in order to obtain both hollow and solid one dimensional nanostructures with tailored dimensions; (iii) characterization process by Raman Confocal Spectroscopy of the SWCNTs all along PVDF nanorods (Fig. 2) [7]; (iv) finally, we have studied the crystallization process of PE and PE/Au nanorods under confinement conditions, by differential scanning calorimetry (DSC) and X-ray diffraction (XRD) [8].

References

[1] Martin, C. R. Science **1994**, 266, 1961.

[2] Martin, J; Krutyeva, M; Monkenbush, M; Arbe, A; Allgaier, J; Radulescu, A; Falus, P; Maiz, J; Mijangos, C; Colmenero, J; Richter, D. Physical Review Letters, **2010**, 104, 197801

[3] Martín, J; Mijangos, C. Langmuir **2009**, 25, 1181.

[4] Steinhart, M; Wendorff, J. H; Greiner, A; Wehrspohn, R. B; Nielsch, K; Schilling, J; Choi, J; Gösele, U. Science **2002**, 296.

[5] Calvert, P. D. Nature **1999**, 210.

[6] Brust, M; Walker, M; Bethell, D; Schiffrin, D. J; Whyman, R. J. Chem. Soc., Chem. Commun., **1994**, 801.

[7] Maiz, J; Sacristán, J; Mijangos, C. Chemical Physics Letters **2010**,484, 290.

[8] Maiz, J; Schäfer, H; Hartmann, B; Steinhart, M; Haase, M; Mijangos, C. in preparation, **2011**

Figures
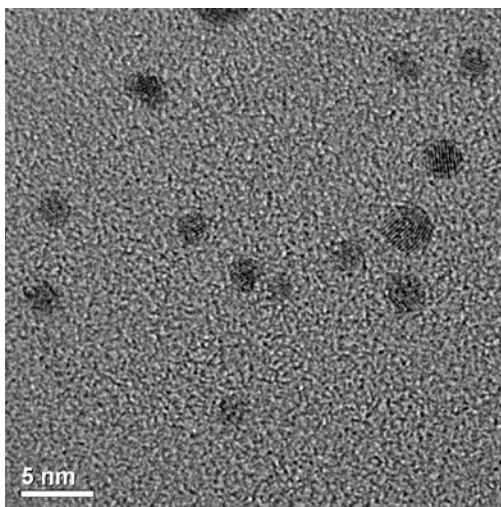
Figure 1. TEM picture of the thiol derivatised gold nanoparticles.
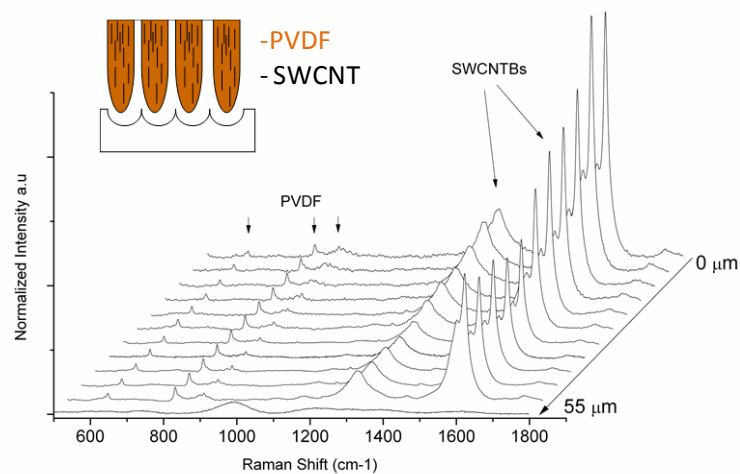
Figure 2. Depth profile Raman spectra of PVDF/SWCNT nanorods.

High-pressure study of YVO$_4$ nanoboxes

F.J. Manjón[1], O. Gomis[2], S. Ray[1], S. F. León-Luis[3], U.R. Rodríguez-Mendoza[3], V. Lavín[3], A. Segura[4], D. Martínez-García[4], and Ch. Ferrer-Roca[4]

[1] Instituto de Diseño para la Fabricación y Producción Automatizada, MALTA Consolider Team, Universitat Politècnica de València, Camí de Vera s/n, 46022 València (Spain)
[2] Centro de Tecnologías Físicas, MALTA Consolider Team, Universitat Politècnica de València, Camí de Vera s/n, 46022 València (Spain)
[3] MALTA Consolider Team and Departamento de Física Fundamental y Experimental, Electrónica y Sistemas, Universidad de La Laguna, E-38200 San Cristóbal de La Laguna, Santa Cruz de Tenerife (Spain)
[4] Instituto de Ciencia de Materiales de la Universidad de Valencia, MALTA Consolider Team, Universitat de València, C/. Dr. Moliner 50, 46100 Burjassot, València (Spain)

fjmanjon@fis.upv.es

YVO$_4$ is a very interesting material which finds an extensive use in material science and technology due to its outstanding optical properties. YVO$_4$:Nd^{3+} is used in industrial diode pumped solid state lasers [1]. The improvement of luminescence properties in nanosized and pressure-treated materials has opened an enormous working field in phosphors [2] and the study of rare-earth ions in the nano-environment of ABO$_4$ compounds is important for the development of phosphors with enhanced luminescence efficiency by combining the promising optical properties of rare-earth ions and nanoparticles [3,4].

Bulk YVO$_4$ crystallizes in the zircon structure (space group S.G. #141) and it undergoes two pressure-induced phase transitions: a first one towards the scheelite structure (S.G. #81) above 7.5 GPa [5,6] and a second one towards the fergusonite structure (S.G. #15) above 23 GPa [7]. Knowing the phase transitions in nanocrystals could give a better insight into the relation between compositional, structural and optical properties in order to design better phosphors or even provide novel nanocrystal phases which could be retained in metastable way, like diamond, at ambient conditions with enhanced optical properties with respect to parent materials.

We have synthesized Eu-doped YVO$_4$ nanoboxes with zircon structure and 25 ± 5 nm lateral size. Nanoboxes have been characterized by X-ray diffraction, Raman scattering, and photoluminescence under pressure up to 18 GPa. The pressure behaviour of nanocrystals has been compared to that of bulk material [2,5-7]. We have found that the zircon-to-scheelite phase transition occurs at a much higher pressure in nanocrystals as compared to the bulk. Additionally, a possible intermediate monoclinic phase between zircon and scheelite could be present in nanocrystals unlike in the bulk as recently suggested to occur in zircon-type chromates [8].

References

[1] W. Koechner, Solid-state Laser Engineering, Springer, New York, 2006.
[2] G. Chen, N.A. Stump, R.G. Haire, J.R. Peterson, M.M. Abraham, J. Phys. Chem. Solids **53** (1992) 1253.
[3] A.J. Silversmith, W. Lenth, R.M. Macfarlane, Appl. Phys. Lett. **51** (1987) 1977.
[4] A. Patra, C.S. Friend, R. Kapoor, P.N. Prasad, Appl. Phys. Lett. **83** (2003) 284.
[5] A. Jayaraman, G. A. Kourouklis, G. P. Espinosa, A. S. Cooper, and L. G. Van Uitert, J. Phys. Chem. Solids **48** (1987) 755.
[6] X. Wang, I. Loa, K. Syassen, M. Hanfland, and B. Ferrand, Phys. Rev. B **70** (2004) 064109.
[7] F.J. Manjón, P. Rodríguez-Hernández, A. Muñoz, A. H. Romero, D. Errandonea, and K. Syassen, Phys. Rev. B **81** (2010) 075205.
[8] A.K. Mishra, N.Garg, K.K. Pandey, K.V. Shanavas, A.K. Tyagi, and S.M. Sharma, Phys. Rev. B **81** (2010) 104109.

A virtual nanomanipulator coupling with a multi-sensorial interface: a serious interactive game for the 'grand public' and students to explore the nanoworld

Florence Marchi[1], J. Chevrier[1], J.L Florens[2], A. Luciani[2]

[1]Institut Néel CNRS/UJF, Grenoble, France; [2]ICA-ACROE, Grenoble INP, France
Contact@E-mail

Nanosciences and nanotechnology constitute a research field with two complementary objectives: (1) to study and to characterize the physical and chemical properties of the materials and structures at the nanoscopic scale, (2) to take advantage of these specific properties to develop smart applications in key areas of our daily life as medicine or computer and communication technology...

As these potential smart applications should impact strongly our daily life, it is crucial that the general public understand their interest in order to be able to evaluate objectively their positive and negative impacts. In this frame, the large audience should understand the key points of the chemical and physical behavior of material and object at the nanoscale. To face this challenge, we have developed a virtual nanomanipulator coupling with a multi-sensorial interface (haptic, visual and sound rendering) to illustrate the notion of the contact at the macro and the nanoscale (figure 1). This virtual and interactive nanomanipulator is an original output of scientific research carried out by a group of physicist specialist in nanophysics and using scanning probe microscopy and a group of engineers working in the field of virtual reality and haptic system.

Thanks to the general public version of the force feedback virtual nanomanipulator, every person can experiment and compares the notion of contact between the macroscopic and the nanoscopic scale in few minutes. Indeed in the virtual macro-scene, the person manipulates thanks to a force feedback system (a joystick), a soft stick to hit a piece of wood; during the manipulation the person feels in his/her hand the force and at the same time hears the sound induced by the impact of the stick on the surface and sees the movement of the stick on the screen. In this condition, the person experiments with the classical hard contact happening in the daily life. In the nanoscene, the person performs the same task with a nano-stick (an Atomic Force Microscope probe) to interact with the atomic structure of a nanosurface. During the manipulation, the person feels in his/her hand the Lennard-Jones force: an attractive force then the repulsive one. To improve the person immersion in the virtual scenes, sound and visual renderings are implemented; they are produced directly by the physical model and amplified.

This general audience version of the virtual and multi-sensorial nanomanipulator has been one of the more appreciated module of the exhibition show on Nanotechnology developed by the scientific museum Grenoble (CCSTI: Centre de Culture Scientifique Technique et Industrielle), more than 200 000 persons have used it in France and around Europe.

Based on this success we have developed an educative version of the virtual and multi-sensorial nanomanipulator called the Nanolearner. Scientific students from first years of university to Master level use the Nanolearner during practical work dealing with scanning probe microscopie.

Three complementary virtual nanoscenes are available on the Nanolearner. All the virtual nanoscenes deal with the AFM in contact mode probing a sample where several parameters as the spring constant of the cantilever, the sample stiffness or the type of tip-surface interaction, can be adjusted via a specific interface. The first nanoscene is dedicated to the force curve, a well-known mode in AFM technique to study in one dimension (1D) the evolution of the tip-sample interaction according the tip-sample distance. Thanks to the specific interface, the student can explore in less than one hour, several classical configurations as probing hard or soft materials with short or long range interactions with a soft or rigid cantilever. Students explore the impact of these various configurations with their perception

senses but also they could record several signals during the manipulations to plot them in order to obtain formal representation as with a standard and real AFM instrument.

The second nanoscene representes a surface in 2D where students can map the surface in different points and feel the well known stick and slip effect. In addition student can spot what is happening when an AFM tip probes a soft membraneby chosing suitable parameters. This configuration constitutes a relevant case for biological applications.

The third virtual nanoscene is in 2 Dimensions and deals with the manipulation (push or pull) of an nano-object on a surface with the AFM tip. This nanoscene underlines that the manipulation process at the nanoscale relies on surface effect rather than on the volume effect leading students to think about basic manipulation strategy for grabbing and depositing an object at the nanoscale.

Thanks to these three nanoscenes, students can explore in less than 4 hours most of the working situations that appears in AFM techniques. This could not be performing with a classic AFM instrument during a 4 hours practical work. The impact of each rendering (haptic, visual and sound) in the learning process of the students has been carried on in details [1].

From a more general point of view, the Nanolearner system is part of the emergent field of "serious games" whose one of the goals is to get comprehensible complex phenomenon that are not easy to transmit through classical pedagogical media (images or formal equations). In this frame our research group is developing some other serious games as example one dedicated to Brownian motion where its effect is translated into a force in the hand of the serious gamer. We believe that the development of serious games constitutes a pedagogical innovation to improve the interest of scientific and non scientific students for physics.

During the ImagineNano conference experts and large audience will have the opportunity to test the NanoLearner instrument and the Brownian motion serious game on the Grenoble stand of the Nanosociety session.
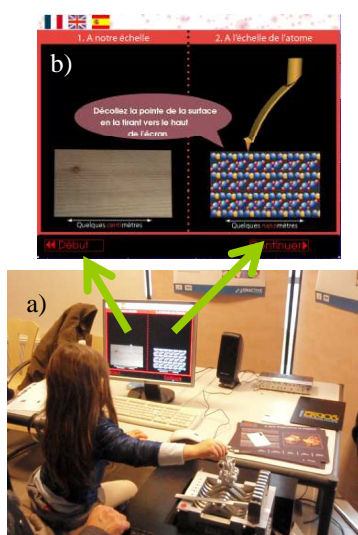
Figure 1: a) the whole virtual nanomanipulator platform with the loudspeaker, the screen and the force feedback system manipulated by a child; b) Zoom on the visual representation displayed on the screen.

[1] "An Augmented Reality Nanomanipulator for Learning Nanophysics: The NanoLearner Platform", F.Marchi, S. Marliere, J.L. Florens, A Luciani and J. Chevrier, Transactions on Edutainment IV, LNCS 6250, Springer, pp. 157–175, 2010.

Synthesis and functionalitation of nanoparticles for bio-applications

M.A. Meabe[1], A. Cruz[1], M. Pascual[1], J.L. Vilas[2], J.R. Marin[1]

[1] Gaiker Technological Center, Parque Tecnológico, Edificio 202, Zamudio, Spain
[2] UPV/EHU, Barrio Sarriena S/N, Leioa, Spain

meabe@gaiker.es

Inmobilized antibodies have a broad variety of uses in areas as immunoassays or biosensors due to their high sensitivity and high specificity. For that, it is very important to know how the antibodies are attached to the surface to be used as a support, in order to determine if the antibody binding sites are accessible to the antigen that is willing to join. In the present work is aimed to develop a system for the immobilization of the biorecognition molecule using as support nanoparticles. Specifically, we have synthesized silver nanoparticles [1, 2], which have joined antibodies by passive adsorption. Modifications of the optical properties as consequence to specific ligand attachment are of great interest in the development of biosensors for biomolecules.

Specifically, silver nanoparticles have been synthesized by chemical reduction [3]. In order to meet their morphology they were characterized by Transmission Electron Microscopy (TEM) and UV-Visible spectroscopy. TEM images show that nanoparticles obtained by hydride reduction method have a spherical morphology with an average diameter of 35 nm. The UV-Visible spectra shows an absorption band at 400 nm, which corresponds to the absorption by surface plasmon resonance [4]. This band confirms the presence of silver nanoparticles. Also, it is noticed the existence of a single peak, indicating that the nanoparticles have a spherical morphology.[5]

After the characterization of nanoparticles, the immobilization of biorecognition molecules is carried out, designing a system for the immunochemical detection of rabbit immunoglobulin [6-9]. It also analyzes the specificity of the union for real sample.

The verification of the union has been carried out by immunochemical tests with colorimetric signal through the use of secondary antibodies conjugated to enzyme peroxidase. The technique used here is based in the conventional ELISA procedures [10]. It can be concluded that the biomolecule immobilization on the surface of silver nanoparticles is generally effective, enabling the development of a system for the detection of rabbit immunoglobulin samples with a high specificity.

References

[1] K. J. Klabunde, Nanoscale Materials in Chemistry. John Wiley and Sons, Inc.: (2001).
[2] J. H. Fendler, Chemistry of Materials, **8** (1996) 1616-1624
[3] A. Roucoux, J. Schulz, H. Patin, Chemical Reviews, **10 (**2002) 3757-3778.
[4] T. Klar, M. Perner, S. Grosse, G. von Plessen, W. Spirkl, J. Feldmann, Physical Review Letters, **80** (1998) 4249-4252.
[5] S. Link, M.A. El-Sayed, J. Phys. Chem. B, **21** (1999) 4212-4217.
[6] M. Nisnevitch, M. A. Firer, J. Biochem Biophys Methods, **1-3** (2001) 467- 480.
[7] J. Buijs, J. W. T. Lichtenbelt, W. Norde, J. Lyklema, Colloids and Surfaces B: Biointerfaces, **4 – 5** (1995) 239 – 249.
[8] S. Chen, S. Jiang, L. Liu, J. Zhai, Langmuir, **7** (2003) 2859 – 2864.
[9] C. A. J. Janeway, P. Travers, M. Walport, J. D. Capra, (Eds.). Masson, S.A. (2000).
[10] M. P. Marco, S. Gee, B. D. Hammeck, Trends in Analytical Chemistry, **7** (1995) 341 – 350.

Figures
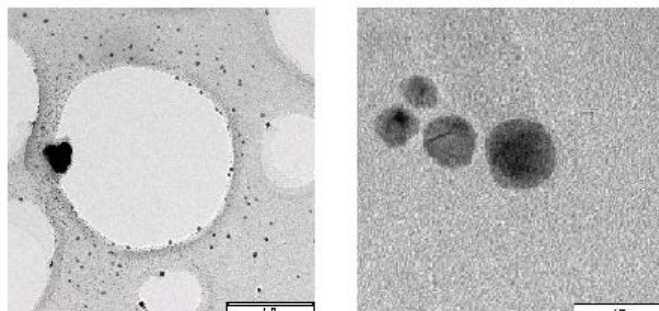
Figure 1. *TEM images of silver nanoparticles. The scale bar corresponds to 300 nm and the right one to 30 nm.*
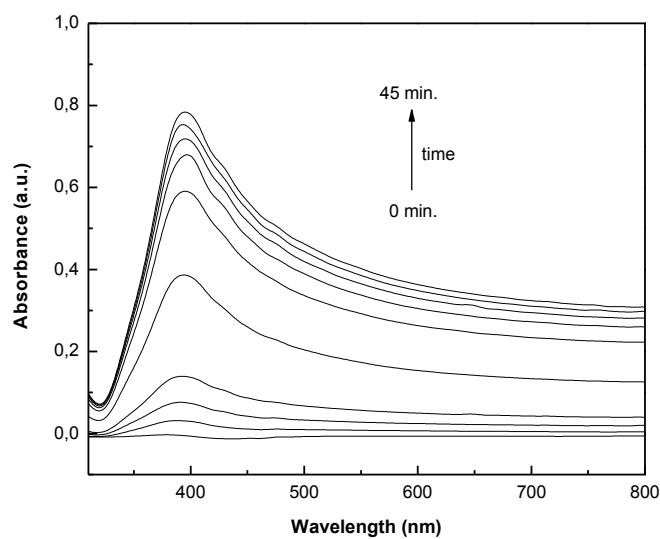
Figure 2. *UV-Visible spectra of silver nanoparticles.*
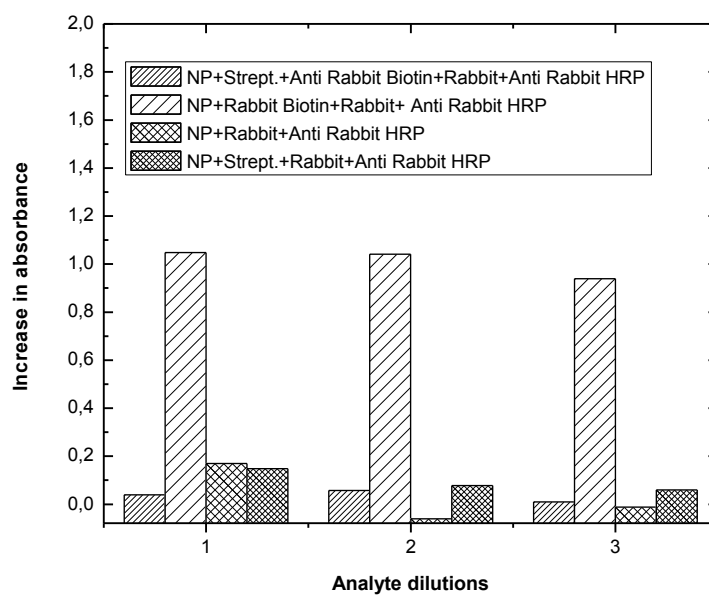
Figure 3. *Absorbance values for four systems consisting of silver nanoparticles and different biomolecules. Stock dilution of the analyte to 1 mg · ml^{-1}. 1. Dilution 1:50, 2. 1:100 dilution, 3. 1:200 dilution.*

Surface modification and patterning of proteins on photocrosslinkable glycosaminoglycans

M. Carmen Márquez-Posadas[1], Jorge Ramiro[1], Santos Merino[1], Jana Becher[2], Albrecht Berg[2], Ralf Wyrwa[2], Matthias Schnabelrauch[2]

[1] TEKNIKER-IK4 Departamento de Micro y Nanotecnologías, Avd. Otaola 20, 20600 Eibar, Spain
[2] INNOVENT e.V., Biomaterials Department, Prüssingstraße 27 B D-07745 Jena, Germany
smerino@tekniker.es

Natural polymers such as polysaccharides might have advantages for biological samples and cell-based devices because they are natural components of the *in vivo* microenvironment [1]. A method combining natural photocrosslinkable polymers such as hyaluronic acid (HA) with micromolding approaches was presented and characterized in order to fabricate hydrogels able to immobilize cells.

Recently, photolithography and soft lithography have been used to encapsulate live cells within microscale polymeric hydrogels (i.e. microgels) anchored onto two-dimensional (2D) surfaces. This offers great potential for diagnostics and cell screening applications. Yeh et al. [2] presented a micromolding approach to generate cell-encapsulating 3D hydrogels of controlled shapes and sizes in the form of harvestable free units. Cells were suspended in a hydrogel precursor solution containing photoinitiator, deposited onto hydrophilic poly(dimethylsiloxane) (PDMS) patterns, crosslinked under UV radiation, and retrieved upon hydration. Two common photocrosslinkable hydrogel materials, methacrylated hyaluronic acid (MeHA) and poly(ethylene glycol) diacrylate (PEGDA), were tested using this technique, yielding shape controlled microgels with homogeneous cell distribution at various viable cell densities.

In this work, two glycosaminoglycans (GAGs), MeHA and chondrotin sulfate methacrylate, were synthesized and microstructured combining soft lithography and UV crosslinking, initiated by addition of an ultraviolet photoinitiator, Irgacure 369 (kindly supplied by Ciba). Solutions of these GAGs were deposited on silicon substrates treated with 3-(trimethoxysilyl) propyl methacrylate [1]. PDMS stamps were moulded using silicon masters previously fabricated by conventional UV-Lithography and deep ultraviolet (DUV) optical lithography (λ = 248nm) and etched by a SF_6/C_4F_8 and $Cl_2/HBr/O_2$ gases combination, respectively. The PDMS stamp microstructures were transferred to the GAGs substrates using an EVG620 mask-aligner curing with UV light (Figure 1).

We have also studied the localized anchorage of proteins (for a subsequent study with human mesenchymal stem cells) over these materials by microcontact printing of poly(OEGMA-co-MA) [3], amino-PEG and PLL-g_PEG, so that areas that avoid the adhesion of proteins can be created, giving rise to well-defined patterns (Figure 2).

References

[1] Khademhosseini, A., Eng, G., Yeh, J., Fukuda, J., Blumling, J., Langer, R., and Burdick, J.A. J Biomed Mater Res A **79A (2006)** 522.

[2] Yeh J., Ling Y., Karp J.M., Gantz J., Chandawarkar A., Eng G., Blumling III J., Langer R. and Khademhosseini A. Biomaterials **27** (2006) 5391.

[3] Lin C.C, Co C. C. and Ho C.C. Biomaterials **26** (2005) 3655

Figures
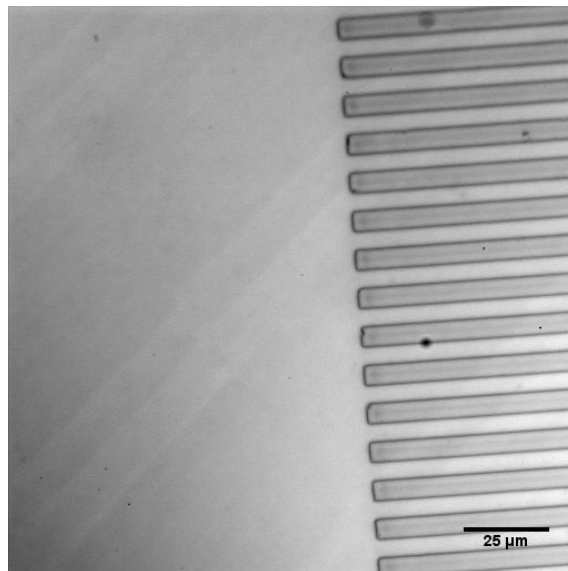
Figure 1. Methacrylated hyaluronic acid microstructures. Period = 11.3µm
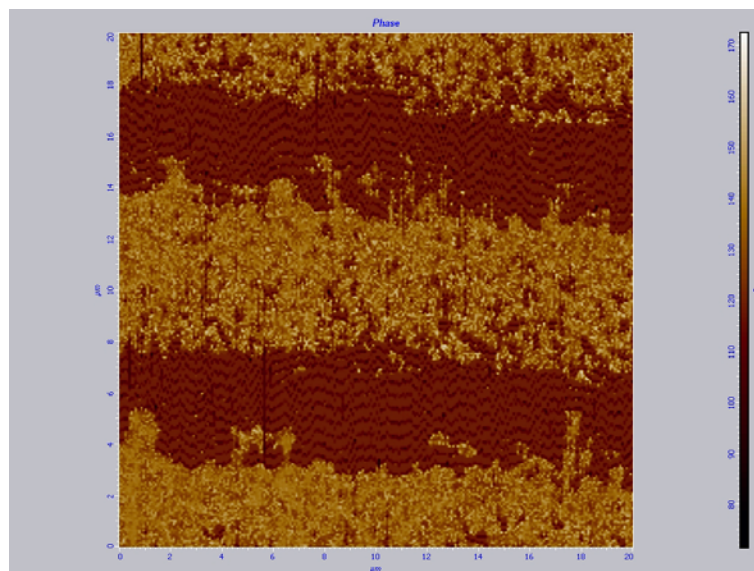
Figure 2. AFM - change of phase image showing microcontact printed P(OEGMA-co-MA) over a chondroitin sulfate methacrylate substrate. Period ~ 10µm

Modification of AFM tips by depositing nanoparticles with an Ion Cluster Source. Enhancement of the aspect-ratio and lateral resolution.

L. Martínez[1], M. Tello[2], M. Díaz[1], E. Román[1], R. García[2] and Y. Huttel[1]

[1]Instituto de Ciencia de Materiales de Madrid, Consejo Superior de Investigaciones Científicas (ICMM-CSIC), C/ Sor Juana Inés de la Cruz, 3 28049 Madrid, Spain.
[2]Instituto de Microelectrónica de Madrid-IMM (CNM-CSIC), Isaac Newton 8 (PTM), 28760 Tres Cantos, Madrid, Spain.
lidia.martinez@icmm.csic.es

The use of Atomic Force Microscopy (AFM) for imaging nanostructures has become a fundamental tool nowadays. However, as the forefront technology fabricates systems with more and more reduced dimensions, the spatial resolution of these systems with AFM is limited fundamentally by the physical size of the probe. In this talk we present a new method to reduce the final radius of the scanning probe microscopies (SPM) tips, by depositing nanoclusters on standard silicon tips. The modified tips present an enhanced resolution, which can be competitive with sharp tips with high aspect ratios. We will explain the modification process of the AFM tips [1] and present some examples comparing images acquired with standard silicon tips and the same tips modified with the deposition of nanoparticles of different sizes [2]. The use of an Ion Cluster Source (ICS) to deposit the nanoparticles, offers the possibility to tune the chemical composition of the deposited nanoparticles. This implies that, in addition to the enhancement of the aspect ratio, this technique can be extended for specific measurements in other force microscopy techniques such as magnetic force microscopy.

Some examples of AFM measurements on zero dimensional, one dimensional and two dimensional structures will be presented. The figure below displays AFM images of a single wall carbon nanotube (SWCNT) deposited on a flat silicon Si(100) substrate, measured with a standard silicon tip (a) and a modified tip covered with 2-3 nm nanoparticles (b). It can be observed a reduction in the feature size and increase of the in-plane contrast and resolution with the modified tip. The increase in the lateral resolution was evaluated by fitting the profiles of the features present in the AFM images. The fit were performed using Gaussian functions and a reduction between 30 % and 50 % of the full width at half maximum (FWHM) of the profiles of the features was determined.

In resume, the use of those tips leads to atomic force microscopy images of higher aspect ratios and spatial resolution. The presented tips modification method represents an alternative for the generation of high-aspect ratio tips for high-resolution measurements. It should be mentioned that the modification of the tips by deposition of nanoclusters is a "one step process" that does not need any additional chemical of physical processes. More information about the process and modification of tips could be found in [3].

References

[1] Spanish patent number P201030059, Elisa L. Román García, Lidia Martínez Orellana, Mercedes Díaz Lagos, Yves Huttel.

[2] L. Martínez, M. Tello, M. Díaz, E. Román, R. Garcia, and Y. Huttel, Review of Scientific Instruments, accepted paper.

[3] http://www.icmm.csic.es/yveshuttel/WebPageYves.html

Figure
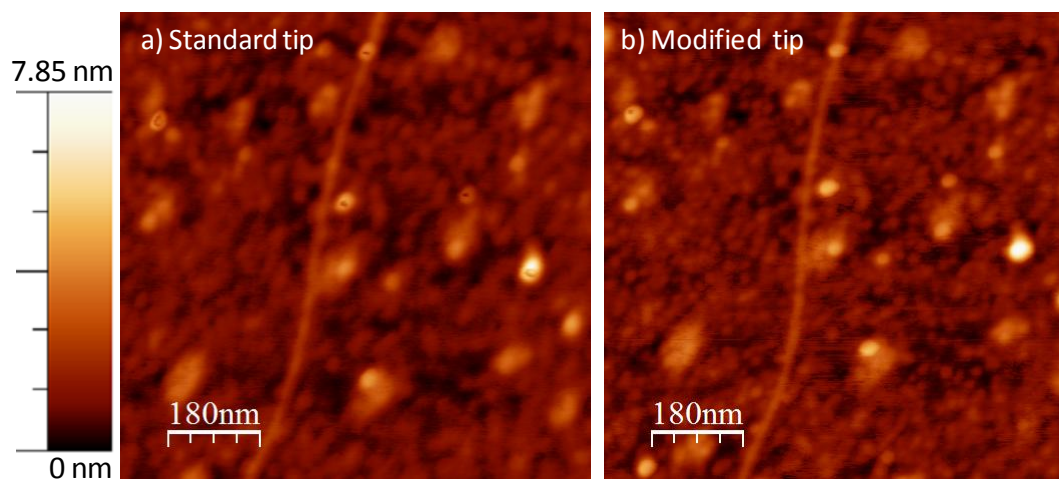
AFM images of SWCNT deposited on a silicon wafer. a) AFM image recorded by using a standard silicon AFM tip; b) AFM image recorded by using a standard silicon AFM tip covered with 2-3 nm nanoparticles.

Size effects on the fluorescence efficiency of biocompatible CdTe quantum dots.

L. Martínez Maestro[1,*] D. Jaque[1], C. Jacinto[2], U.R. Silva[2], and J. García Solé[1].

[1]*Fluorescence Imaging Group, Departamento de Física de Materiales, Universidad Autónoma de Madrid, Madrid, 28049, Spain.*
[2]*Grupo de Fotônica e Fluidos Complexos, Instituto de Física, Universidade Federal de Alagoas, 57072-970, Maceió, AL, Brazil.*

lm.maestro@uam.es

In the last years, semiconductor nanocrystals, usually called Quantum Dots (QDs), have attracted intense attention due to their desirable properties, such as a wide absorption band, high emission yield, good chemical stability and possibility of multi-photon excitation [1]. As a consequence of all the outstanding properties, QDs have been already used in numerous applications such as biological labelling and imaging, and photovoltaic and optoelectronic devices [2].

Because of quantum size effects, their optical properties can be tuned just by changing their particle size. This fact has been already used to tailor the emitted colour. Of particular interest is the use of QDs for biomedical fluorescence imaging. These dots should be easily dispersed in biological fluids and so in water. As different QD sizes can be in principle used it is of primordial importance to investigate the size effects on the QDs fluorescence efficiency.

In this work we have investigated in detail how the fluorescence quantum efficiency of CdTe-QDs (which are commonly used for optical bioimaging) depends on the QD size by means of Thermal Lens (TL) spectroscopy. The non-monotonous variation of the fluorescence quantum efficiency with the dot size has been tentatively explained in terms of surface effects that enhance the non- radiative rate for small QDs.

The CdTe-QDs investigated in this work were provided by Plasmachem Inc. Six different CdTe-QDs were used with nominal emission peak wavelengths at 510, 550, 615, 660, 680 and 710 nm, corresponding to sizes of 1.2, 2.3, 3.6, 3.8, 4.3 and 4.7 nm, respectively. The QDs (0.3% in mass) were dispersed in distilled water with no evidence of precipitation. TL measurements were made by using the same experimental set up as in ref [3].

Figure 1, shows a typical TL transient signal for the CdTe-QDs/water solutions, in this case for those emitting at 660 nm (3.8 nm diameter). From the best fit to the theoretically expected TL transient decay (solid line) [1], the so called TL induced phase shift, θ, and the thermal diffusivity are straightforwardly obtained. Then the quantum efficiency, η, is calculated from the Equation 1. In this equation λ_{exc} is the excitation wavelength, $\langle \lambda_{em} \rangle$ is the average emission wavelength, C is a constant related to the host liquid (C=279 W^{-1} in our case), and $\Theta = \theta / P_{abs}$ (P_{abs} being the absorbed pump power).

$$\eta = \left[1 - \frac{\Theta}{C} \right] \frac{\langle \lambda_{em} \rangle}{\lambda_{exc}} \tag{1}$$

For the particular case of the 3.8 nm, Θ =182 W^{-1}, and considering the excitation (488 nm) and emission (660 nm) wavelengths, a fluorescence quantum efficiency of 0.47 was determined. Then, by analyzing the TL transient signals of CdTe-QDs of the different sizes, we have determined their quantum efficiencies. Figure 2 shows a plot of the quantum efficiency as a function of dot diameter. An

inspection of this plot reveals two different trends: the quantum efficiency rises with decreasing QD size down up to 3.8 nm where a maximum in the quantum efficiency is obtained. Then this trend is reversed so that decreasing sizes produce a decrease in the quantum efficiency. Then, the obtained results indicate that dots of about 4 nm would be the most indicated to be used as luminescent probes for high resolution biomedical fluorescence imaging.

The observed quantum efficiency decrease for dots smaller than about 4 nm indicates that surface effects are playing an important role in the non radiative rate.

References

[1] R. A. Cruz, V. Pilla and T. Catunda. Journal of Applyed Physics **107**, 083504 (2010)

[2] L. Martínez Maestro, Emma Martin Rodriguez, F. Sanz Rodriguez, M.C. Iglesias-de la Cruz, A. Juarranz, R. Naccache, F. Vetrone, D.Jaque, J. A. Capobianco, and J. García Solé. Nano Letters, **10** (2010), p.5109-5115

[3] C. Jacinto, D. N. Messias, A. A. Andrade, S. M. Lima, M. L. Baesso and T. Catunda, *J. Non-Cryst. Solids* **352** (2006), p. 3582

Figures
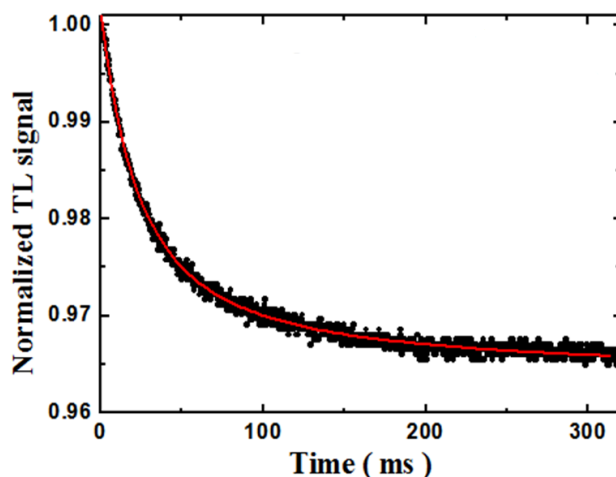
Figure 1. Normalized transient TL signal for CdTe-3.8 nm QDs at room temperature, excitation at 488 nm with a pump power of 0.42 mW. The solid line is the best fit using to the TL theoretical transient decay [1].
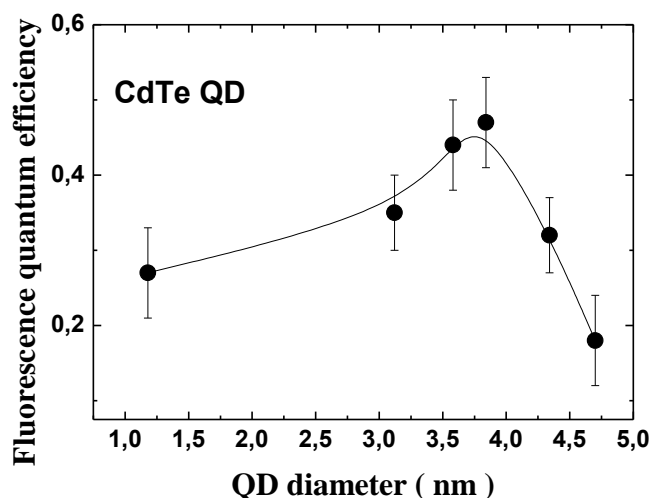
Figure 2. Fluorescence quantum efficiency versus size for the CdTe-QDs (room temperature and 488 nm excitation wavelength).

Influence of the deposition conditions on the properties of Co and Ni nanowires

Elena Matei[1], Victor Kuncser[1], Nicoleta Preda[1], Maria Eugenia Toimil Molares[2], Jean Philippe Ansermet[3], Ionut Enculescu[1]

[1]National Institute of Materials Physics, Atomistilor 103 bis, Magurele, Romania; [2]GSI Darmstadt, Germany; [3]EPFL, Lausanne
elena.matei@infim.ro

Magnetic nanowires are extremely interesting at this moment due to the potential applications in data storage or in other fields of information technology or communications. A large number of methods for preparing such metallic nanostructures were developed during the last decade. These methods are based on a variety of techniques, both physical and chemical.

Electrochemical deposition in nanoporous membranes, the so called template method, represents a convenient method to prepare such nanowires with desired characteristics [1]. One can use membranes with pores with desired shape and dimensions. By this approach one can tune the properties of the deposited material such as composition, structure, optical, magnetic or electric characteristics. Moreover, one can prepare complex structures such as multilayers and multisegment nanowires by pulsed or by sequential deposition [2,3]. The most employed porous membranes used as templates are anodic alumina and ion track polymer membranes. The polymer membranes obtained by swift heavy ion irradiation and subsequent etching contain pore densities ranging from 1 pore sample to 10^9 pores per square centimeter. The characteristics of these templates are quite adequate for studies of magnetic nanowires since one can tune the pore density i.e. the density of nanowires and their dimensions independently.

In the present paper we report our results regarding the influence of the templates and of the deposition conditions on the structural, morphological and magnetic properties of Ni and Co arrays of nanowires prepared by template replication by electrodeposition.

Polycarbonate foils, 30 micrometer thick, were irradiated with swift heavy ions (e.g. Au with 11.4 MeV/nucleon) in GSI's UNILAC accelerator. Further, this defect track is selectively etched by submersing the samples into an aqueous solution of 5M NaOH and 10% vol methanol at 50°C. In these conditions cylindrical pores are obtained, the etching rate being in this case 2 micrometers / hour. The electrochemical deposition was performed from baths containing the metal ions. Thus Ni electrodeposition was performed from a Watts bath containing Ni sulfate and Ni chloride and boric acid. To this "classical" composition we added polyvinylpyrrolidone (PVP) in order to increase the pore wetting and in this way to increase the pore filling efficiency. A similar bath was used for the deposition of Co, namely containing Co sulfate as source of Co ions, boric acid and PVP.

The electrochemical deposition process was performed on samples containing pores with different diameters and with different surface densities. In figure 1 the scanning electron microscopy image of arrays of nickel and cobalt wires deposited in membranes with different pore diameters and at different deposition potentials are presented.

X ray diffraction measurements show that the structural properties of the deposited nanowire arrays depend on the deposition potential. An analysis of the texture coefficient for both Ni and Co show different growth planes for low and high rate deposition of the nanowires.

Magnetic measurements were performed for the nanowire arrays in two geometries namely with the applied field perpendicular and parallel to the nanowire. The measurements evidence the strong shape anisotropy of the magnetic quasi-one-dimensional structures, the interaction of nanowires in an array and the influence of the growth parameters through the structure i.e. crystalline magnetic anisotropy.

References

[1] Enculescu, I.; Matei, E.; Sima, M.; Neumann, R.; Granville, S.; Ansermet, J. – Ph.; IEEE Trans. On Magn. (2008), **44**, 2678-2680

[2] Enculescu I.; Toimil-Molares M.E.; Zet C.; Daub M.; Westerberg L.; Neumann R.; Spohr R. Appl. Phys. A, (2007), **86**, 43 – 47.

[3] Matei E., Ion L., Antohe S., Neumann R., Enculescu I., Nanotechnology, (2010), **21**, 105202

Figures

Figure caption: Arrays of metallic nanowires with magnetic properties deposited in membranes with different pore size: (a) Ni wires with 800 nm diameter, (b) Ni wires with 100 nm diameter; (c) cobalt wires 800 nm in diameter; (d) Co nanowires 100 nm diameter.
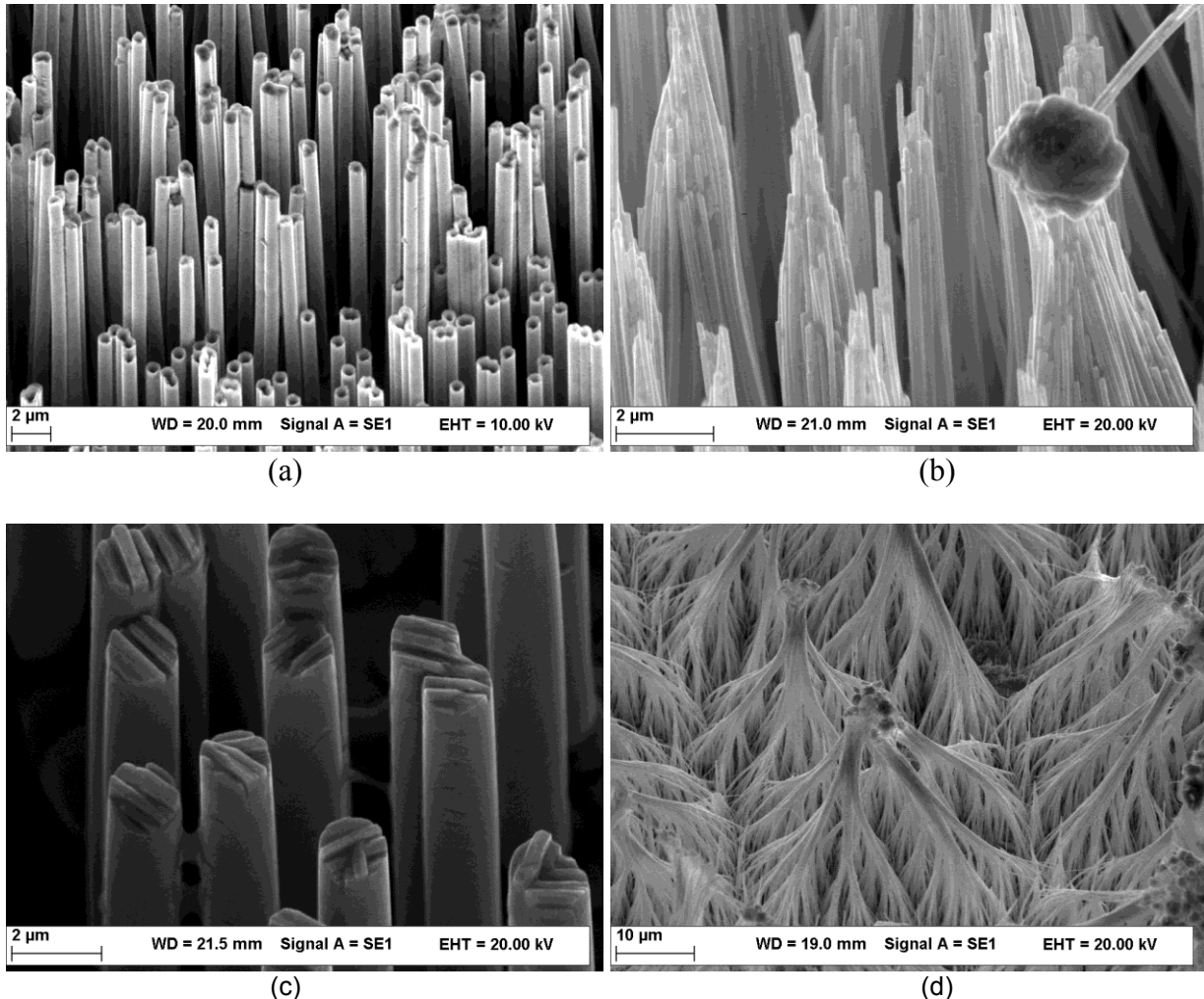
Ordered Vacancy Network Induced by the Growth of Epitaxial Graphene on Pt(111)

G. Otero,[1] C. Gonzalez,[1] A.L. Pinardi,[1] P. Merino,[2] S. Gardonio,[3] S. Lizzit,[3] M. Blanco-Rey,[4] K. Van de Ruit,[5] C.F.J. Flipse,[5] **J. Méndez,**[1] P.L. de Andres,[1] and J.A. Martın-Gago[1,2]

[1]Instituto Ciencia de Materiales de Madrid (CSIC), C. Sor Juana Ines de la Cruz 3, 28049-Madrid, Spain

[2] Centro de Astrobiologıa, INTA-CSIC, Torrejon de Ardoz, 28850 Madrid. Spain

[3] Sincrotrone Trieste SCpA, Strada Statale 14, Km. 163.5, 34149 Trieste, Italy

[4]Department of Chemistry, University of Cambridge, Cambridge CB2 1EW, United Kingdom

[5]Department of Applied Physics, Eindhoven University of Technology, P.O. box 513, 5600 MB Eindhoven, The Netherlands

jmendez@icmm.csic.es

The strength and the nature of the interaction of epitaxial graphene with metallic substrates is still widely discussed in the literature. In order to give additional contribution to this topic we have studied large areas of $(\sqrt{3} \times \sqrt{3})R30°$ graphene commensurate with a Pt(111) structure [1]. Experimental evidence carefully combined with density functional theory calculations led us to the conclusion that this structure causes a reconstruction on the Pt surface which consists of an ordered vacancy network formed in the outermost Pt layer, and a graphene layer covalently bond to the Pt substrate.

References

[1] G. Otero et al., Physical Review Letters, **105** (2010) 216102.

Figures
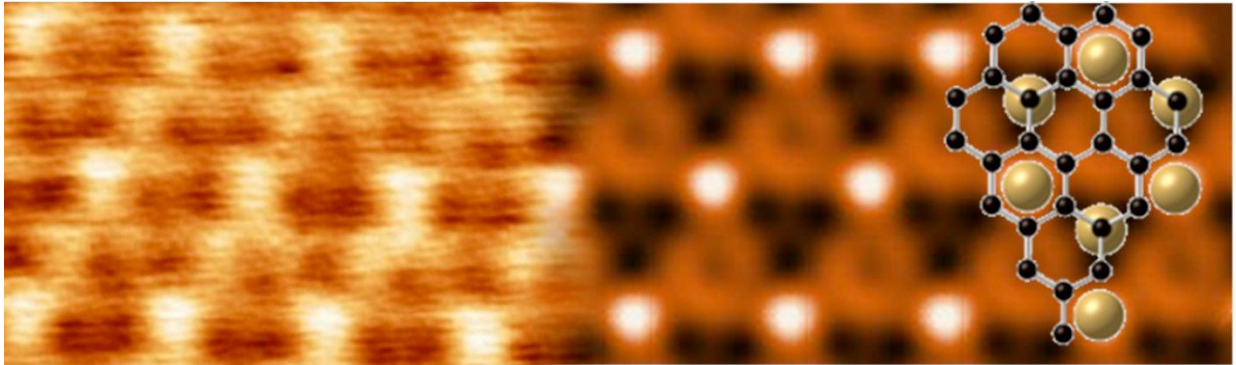
Figure caption. STM image (left) and DFT simulation (right) of the proposed vacancy model (overlaid).

226

1-D Structures of Metal Oxides Templated via Electro-Hydrodynamic Micro-Flows (EHµFs)

Luis B. Modesto-López[a], Joan Rosell-Llompart[a,b]

[a]Universitat Rovira i Virgili, DEW Research Group, Av. Paisos Catalans, 26, 43007, Tarragona, Spain
[b] ICREA (Catalan Institution for Research and Advanced Studies), Barcelona, Spain
luis.modesto@urv.cat

Electro-hydrodynamic micro-flows (EHµFs) of highly viscous liquids (i.e., polymer melts or solutions), also known as electrospinning, are commonly used as templates to form solid 1-D nanostructures, such as nanofibers and nanoribbons. EHµFs have been applied to template 1-D structures of a wide variety of materials ranging from metal oxides (MOs) to organic/inorganic composites. Because of their extensive technological applications in sensors and photocatalysis with UV light, 1-D mats of TiO_2, ZnO, and SnO_2 are the metal oxides most commonly templated via EHµFs. In comparison with, for instance, a nanocrystalline porous film, a 1-D structure has the advantage of a faster electron transport rate while maintaining a relatively high surface area for chemical reactions [1]. Nevertheless, other materials such as *copper oxide*, with *semiconducting properties* and *light absorption in the visible regime*, are being investigated for applications in sensors, batteries, and photocatalytic processes using sunlight. As some works suggest, there is vast room for the investigation and improvement of the physicochemical properties of copper oxide 1-D nanostructures with a high length/diameter ratio ($\geq 10^5$) [2, 3].

EHµFs are formed upon the application of a high voltage (typically kilovolts) to a liquid flowing out of a capillary tube. At a given voltage, the viscous liquid forms a conical shape, a "Taylor cone", and emits a charged liquid jet. As the jet elongates, driven by electrostatic forces towards a collector surface, the jet solidifies and can form various *highly monodisperse* 1-D structures, depending on the solution physicochemical properties and process parameters. Because of the inherent high-charge state of the 1-D structures, their trajectory can be controlled using electric fields and/or by mechanical methods, to form patterns onto either conductive or insulating substrates [4]. Furthermore, one can produce mats made of either uniaxially aligned or randomly oriented 1-D structures through manipulation of the collection process and the electric field intensity[5].

Here we report the application an EHµF technique to produce fiber mats of polymer/CuAc (copper acetate) composites made of (i) long (up to 5 cm), highly aligned and (ii) randomly oriented fibers (Figures 1a-c). The high alignment of the composite fibers was achieved through simultaneous focusing the liquid jet by electrostatic means using a "back electrode" and pulling the jet mechanically with a rotating cylinder collector [5]. Randomly oriented composite fibers were readily obtained by collecting the fibers on a static collector. The MO 1-D structures are obtained after calcination of the polymer matrix and simultaneous decomposition of the MO precursor, followed by nucleation and growth of the MO phase. The polymer tested as template materials were PVAc [Polyvinyl acetate; M_w 100 kDa], PMMA [Poly(methyl methacrylate); M_w 350 kDa], PAN [Poly(acrylonitrile); M_w 150 kDa], and a blend of PVA [Polyvinyl alcohol, M_w 31-50 kDa] and PEO [Poly(ethylene oxide); M_w 5000 kDa]. Although all the electrospun polymer/CuAc solutions had a polymer concentration greater than 10 wt % (suitable for electrospinning), high fiber alignment was only possible for the PVAc/CuAc and PMMA/CuAc solutions. EHµFs of the PVA/PEO/CuAc and PAN/CuAc solutions resulted in randomly oriented fiber mats even at high both electric field intensity and cylinder rotation speed. Subsequent calcination at 500 ºC or higher temperatures of the polymer/CuAc composite fibers formed 1-D nanostructures of copper oxide. Randomly oriented fiber mats of *pristine copper oxide,* as demonstrated by electron dispersive spectroscopic (EDS) analyses, with fiber diameters in the nanometric range, were obtained from

PVA/PEO/CuAc composite fibers (Figure 2a). Conversely, calcination of the 1-D structures of PMMA/CuAc composites on a mica substrate resulted in uniaxially aligned copper oxide 1-D structures (Figure 2b); however, they were cracked in several places along the length of the structures, possibly caused by mechanical stresses during sample manipulation post-calcination. In the case of PAN/CuAc composite fibers "ribbon-like" structures were observed post-calcination. Furthermore, uniaxially aligned fibers of PMMA/CuAc collected on a Si wafer led to collapsed copper oxide 1-D patterns (Figure 2c). A similar phenomenon was observed for the PVAc/CuAc solution. The low melting point of PMMA (~160 ºC) and PVAc (less than 100 ºC) may have played a role in the formation of these 1-D patterns.

The current work presents a methodology for producing fiber mats of copper oxide with various morphologies, depending on the EHμF conditions and the polymer template. The technique can be extended to other MOs by appropriate selection of uniformly mixed polymer/MO precursor solutions. The formation of 1-D patterns of semiconductor materials onto both, conductive and insulating substrates have implications in key technological areas such as solar energy harvesting and storage, nanopatterning, and nanoimprinting.

References

[1] Gonzalez-Valls I, Lira-Cantu M, Energy Environ. Sci., **2** (2009) 19-34.
[2] Bognitzki M et al., Adv. Mater., **18** (2006) 2384-2386.
[3] Guan H et al., Inorg. Chem. Comm., **6** (2003) 1409-1411.
[4] Uecker JC, Tepper GC, Rosell-Llompart J, Polymer, **51** (2010) 5221-5228.
[5] Kiselev P, Rosell-Llompart J, 8th NanoSpain Conference (2011).

Figures
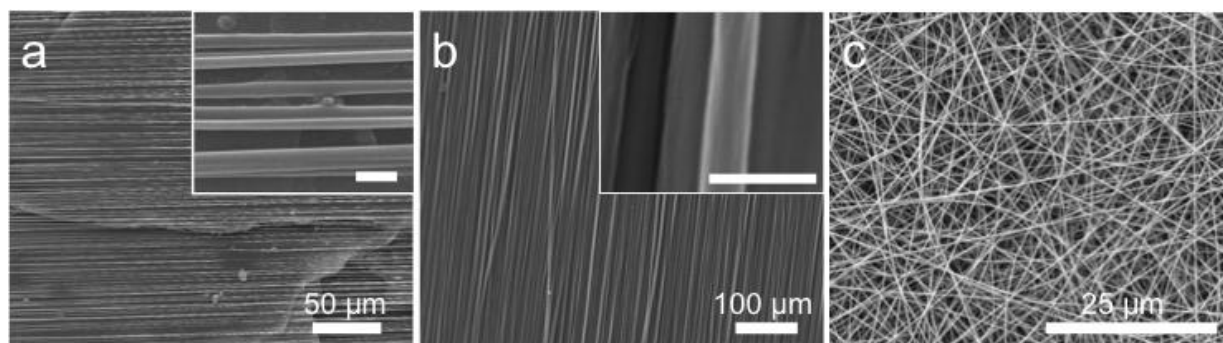
Figure 1. Highly aligned fiber mats (as collected) of *a*) PVAc/CuAc on a mica substrate and *b*) PMMA/CuAc on Al foil, and *c*) randomly oriented fiber mats of PVA/PEO/CuAc on Al foil. The white bar in the insets represents 2 μm.
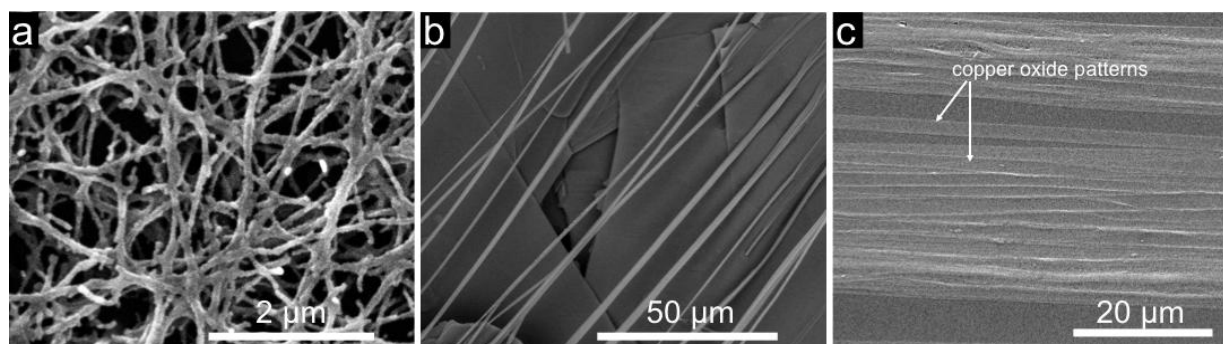
Figure 2. *a*) Randomly oriented fibers of copper oxide on Al foil, *b*) aligned fibers of copper oxide on a mica substrate, and *c*) collapsed copper oxide patterns on Si wafer formed by of calcination of the polymer 1-D template.

Structural, electronic and magnetic study of a single ultra-thin maghemite island.

M. Monti[1], B. Santos[1], O. Mentes[2], M.A. Niño[2], A. Mascaraque[3], O. Rodríguez[3], K.F. McCarty[4], A. Locatelli[2], J.F. Marco[1] and J. de la Figuera[1]

[1]Instituto de Química Física "Rocasolano", CSIC, 28006 Madrid, Spain
[2]Sincrotrone Trieste S.C.p.A, Basovizza, Trieste 34149, Italy
[3]Universidad Complutense de Madrid, 28040 Madrid, Spain
[4]Sandía National Laboratories, Livermore, CA, USA

mmonti@iqfr.csic.es

Iron oxides continue to fascinate us after nearly century of "modern" science devoted to their growth properties, and structures [1]. Recently, a revival of research has been spurred by the multiferroic character of maghemite, or its predicted half-metal character both interesting for spintronic applications. The possibility to fabricate oxides in metal films through hetero-epitaxy is helpful in several ways, first because a suite of standard surface science techniques is available for in-situ characterization, and second because epitaxy opens the door to tailoring materials properties through epitaxial strain, nano-scale self assembly, etc.
How the magnetic structure and electronic properties of iron oxides can be modified, or enhanced, in ultra-thin film form is the fundamental motivation behind this work.

We grow flat islands of maghemite on Ru(0001) by two step oxidation process. In the first step we perform the iron deposition in oxygen atmosphere in order to obtain magnetite triangle islands surrounded by a wüstite wetting layer [2]. The second step consists in the film exposition to a NO_2 pressure to promote the oxidation reaction [3]. This second process allows the oxidation of magnetite islands into maghemite while the wüstite wetting layer changes to hematite.

The islands growth has been followed by low-energy electron microscopy (LEEM). The maghemite islands, together with magnetite islands, have been characterized locally by X-ray photoemission (XPS) and absorption (XAS) in order to describe the electronic state and to study the oxidation reaction. The structure of the islands and the wetting layer has been identified by electron diffraction (LEED). Finally, X-ray circular dichroism has been performed in order to get information about the magnetic properties. All the analyses have been carried out on a single island using a synchrotron-based photoemission electron microscopy (XPEEM)

References

[1] R.Cornell and U. Schwertmann, *The Iron Oxides* (John Wiley & Sons Ltd, 1997), ISBN 3527285768.
[2] S. Santos, E. Loginova, A. Mascaraque, A. Schmid, K. McCarty, and J. de la Figuera, J. Phys. Cond. Matt. 21 (2009).
[3] X. Deng and C. Matranga, Selective growth of Fe2O3 nanoparticles and islands on Au(111), J. Phys. Chem. C 2009, 113, 11104-11109.

Figures
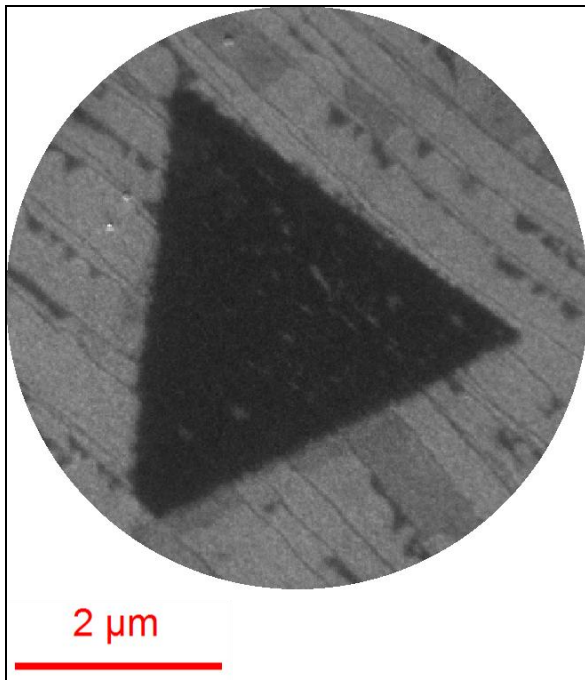
Real space image of a single maghemite island. LEEM image 24eV.
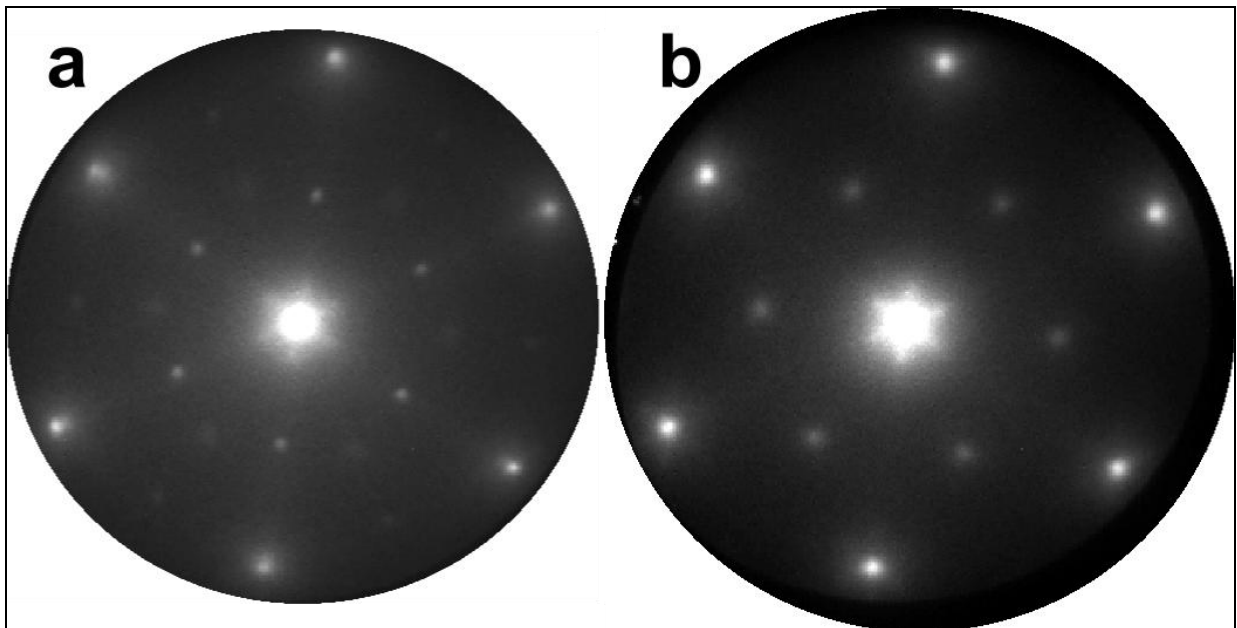
Different reciprocal space images (30eV) of maghemite island (a) and hematite wetting layer (b).

Electrospray deposition of inorganic and organic nanoparticles and biological macromolecules

Eladio Montoya, Esther Hontañón

Ramem, SA
C/ Sámbara, 33 28027 Madrid SPAIN
emontoya@ramem.com

Electrospray deposition is a user-friendly, cheap and fast way to spray and deposit inorganic or organic nanoparticles and biological macromolecules from liquid dispersions [1-3], although it is not known by the vast majority of the scientific community for whom it may be useful.

Electrospray deposition is based on the electrostatic atomization of a conductive liquid. The field can polarize and sharpen the surface of the liquid, generating a cone (Taylor cone) that emits a jet. This jet is broken by surface tension into drops that shrink in size if the solvent is volatile enough. Since these drops are electrically charged, when repulsive electrostatic forces in the surface overcome cohesive surface tension, Coulomb explosion occurs in order to reaccommodate surface charge. The subsequent iteration of this process can give rise to an aerosol composed of the charged solid residue. If the starting conductive sample is a dispersion of nanoparticles, this residue is the charged nanoparticles. It is very easy therefore to use this effect to deposit nanoparticles with diverse origins (inorganic, organic, biological) onto conductive or isolating substrates. Moreover, since the particles are charged, they tend not to agglomerate, avoiding typical artefacts from liquid phase methods (spin coating, dip coating) than can hidden the nanometric nature of the particles. Electrospray deposition can be used at any pressure, does not require expensive instrumentation and typical deposition times are in the order of minutes. In this communication we show several examples of deposition of inorganic, organic and biological nanoparticles.

As an example of inorganic nanoparticles, Fe_3O_4 superparamagnetic nanoparticles with a diameter below 10nm are of large interest for biosensors, medical diagnosis and NMR imaging techniques. We have studied the feasibility of using electrospray techniques to deposit magnetic nanoparticles directly from a diluted suspension in water is analyzed on to an ultraflat mica surface. Characterization is done by means of Atomic Force Microscopy

As an example of organic nanoparticles, Polystyrene latex (PSL) nanoparticles are one of the most common nanoparticle standards for calibration purposes. Commercial PSL nanoparticles were diluted in ethanol (1%) and sprayed on an Al foil for times varying between 1 minute and 1 hour. Scanning Electron Microscopy was used to characterize the deposit. In short deposition times, non-agglomerated deposits can be obtained. At longer times, typical cabbage-like patterns appear.

As an example of biological nanoparticles, DNA solution (100μM) in ethanol was electrosprayed, easily obtaining stable cone-jet operation. The DNA was deposited onto a silicon wafer. After several minutes on working, AFM images were obtained on the silicon wafer.

References

1. A. Jaworek J Mater Sci **42** (2007) 266-297
2. O. Wilhelm, L. Madler, S.E. Pratsinis Aerosol Science **34** (2003) 815-836
3. M. Danek, K.F. Jensen, C.B. Murray, M.G. Bawendi Journal of Crystal Growth **145** (1994) 714-720

X-ray scattering – a tool for the characterization of nano-structured materials

M.Gateshki

PANalytical BV
Lelyweg 1
7602 EA Almelo. The Netherlands
Tel: +31 546 534 444
milen.gateshki@panalytical.com

Nano-structured and advanced thin-layered materials show novel, controllable optical, mechanical and transport properties that enable the design of new electronic, optical, mechanical and energy devices. Typical materials involved are nano-sized powders, semiconductors, metal alloys, dielectrics and also polymers. The necessary scaling of the applied structures challenges the synthesis and processing as well as the characterization tools. A detailed knowledge of the material properties is important for its application and crucial for further development and improvements.

X-ray techniques provide great potential not only in the research and development phase, but also offer unique options for process development and monitoring. A variety of X-ray scattering methods, including X-ray diffraction (XRD) and Small Angle X-ray Scattering (SAXS) have been successively used for material characterization and structural analysis. From X-ray scattering data structural information is extracted to identify and quantify phases, to determine composition and strain profiles, thickness, roughness, density, grain size, residual stress and preferred orientation.

This presentation will give an overview on the experimental aspects, including recent hardware developments and evaluation processes of X-ray scattering methods. Examples of technologically relevant materials will be used to demonstrate the high potential of X-ray techniques.

Author Profile

Dr Milen Gateshki is a Senior Application Specialist X-Ray Diffraction at the Applications Competence Centre of PANalytical BV in Almelo, the Netherlands.

His expertise includes X-ray and neutron diffraction, Rietveld refinement and pair distribution function (PDF) analysis, structural studies of nanocrystalline and highly disordered materials, phase transitions, crystallographic symmetry, microstructure analysis, structure modeling, sample preparation and thermal properties.

Milen received his M.S. degree in Solid State Physics from Sofia University (1995) with a thesis on thermal properties of ternary chalcogenide glasses. His PhD in Materials Science and Technology (2003) is from the **Department of Applied Physics of the University of the Basque Country** - home of the Bilbao Crystallographic Server. Milen's thesis was dedicated to the experimental and theoretical study of the structural phase transitions occurring in a number of double perovskite oxides. After finishing his PhD he joined the Department of Physics of Central Michigan University as a postdoctoral associate (2004-2007). During this period his research was dedicated to structural studies of nanocrystalline materials with applications in electrochemical power sources, catalysts, functional ceramics, and others.

Microstructure and magnetic properties of Co/Ag superlattices grown by MBE on MgO(001)

Enrique Navarro[1], Ana Ruiz[1,] Daniel Margineda[1], María Alonso[1], Pilar Ferrer[2],
F. Javier Palomares[1], Federico Cebollada[3], Jesús Mª González[4]

[1] Instituto de Ciencia de Materiales de Madrid-CSIC. Cantoblanco. E28049-Madrid. Spain.
[2] SpLine-ESRF. 6, Rue Jules Horowitz. BP 220. F38043 Grenoble Cedex 09. France.
[3] Dpto. Física Aplicada a las Tecnol Inform., Universidad Politécnica. E-28031Madrid. Spain.
[4] Unidad Asociada ICMM-CSIC / IMA-UCM, Cantoblanco, 28049 Madrid, Spain.
anaruiz@icmm.csic.es

The renovated interest in the Co/Ag system is not only related to properties like giant magnetoresistance or perpendicular magnetic anisotropy, but also to spin-transfer torque effects and magneto-plasmonic applications. Previous works in the literature have shown the singular and still controversial behavior of the Co/Ag system as compared to other metallic multilayers. An example is that perpendicular magnetic anisotropy and oscillations of the magnetoresistance and exchange coupling have only been reported for samples in which the Co layers thickness lies below 1nm. Microstructure seems to play a relevant role on the magnetic behaviour of Co/Ag multilayers. The formation of a granular system has been suggested to arise when Co layers are extremely thin, in order to explain some of the magnetic results.

We report here on the microstructure and magnetic properties of molecular beam epitaxy (MBE) grown samples consisting of a periodic repetition of Co/Ag layers on MgO(001) substrates. Substrate preparation by Ar+ ion bombardment and annealing is performed prior to growth, so as to obtain clean and ordered surfaces. Growth takes place at room temperature under moderate Co and Ag fluxes (r_g<0.5 Å/s) and is monitored by reflection high-energy electron diffraction (RHEED). Several series of samples have been prepared, changing the Co/Ag ratio per period while maintaining the total Co content within a similar range for all the samples. The thickness of the Co layers in a period is restricted to the 1-12 Å range, and Ag layers are 5 to 40 Å thick. In order to compare results on different substrates and orientations, as well as *with* and *without* buffer layers, selected structures have been simultaneously grown on MgO(111) substrates mounted side by side, or have been deposited with a buffer layer (Ag, 40 nm thick) on clean MgO(001) and Si(111)-7x7 surfaces.
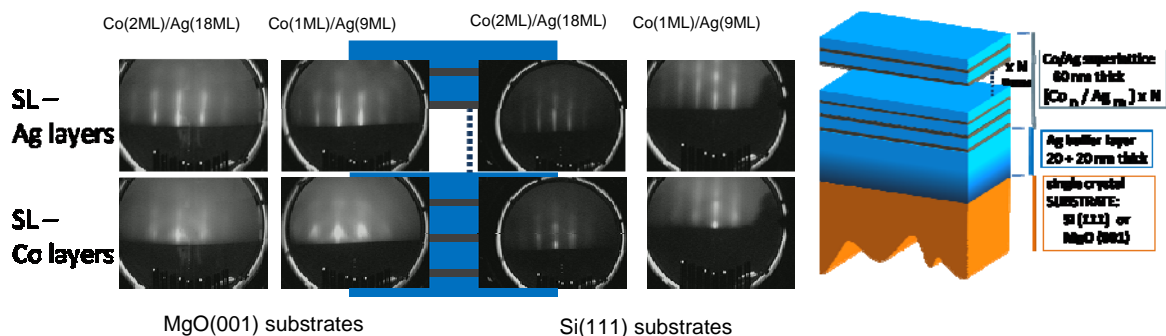
Figure 1*: RHEED patterns during the MBE growth of Co and Ag layers of different superlattice (SL) samples, all of them with extremely thin Co layers per period (about 1 or 2 atomic monolayers, ML). Results for similar layer structures grown either on Mg(001) or 7x7-Si(111) substrate surfaces are shown. In both cases the SL was grown on top of a 40 nm thick Ag buffer layer. Rigth panel: sample sketch for the multilayers of Figs. 1-3.*

Besides RHEED (Fig. 1), several techniques such as low energy electron diffraction (LEED) and Auger electron spectroscopy (AES) were used *in-situ* to assess the crystallinity and composition of the samples after growth. The microstructure and periodicity of the layers was studied by X-ray diffraction, X-ray reflectometry and reciprocal space mapping using conventional sources and synchrotron radiation (Fig. 2). Field emission scanning electron (SEM) and atomic force (AFM) microscopies were employed to investigate surface sample morphology.
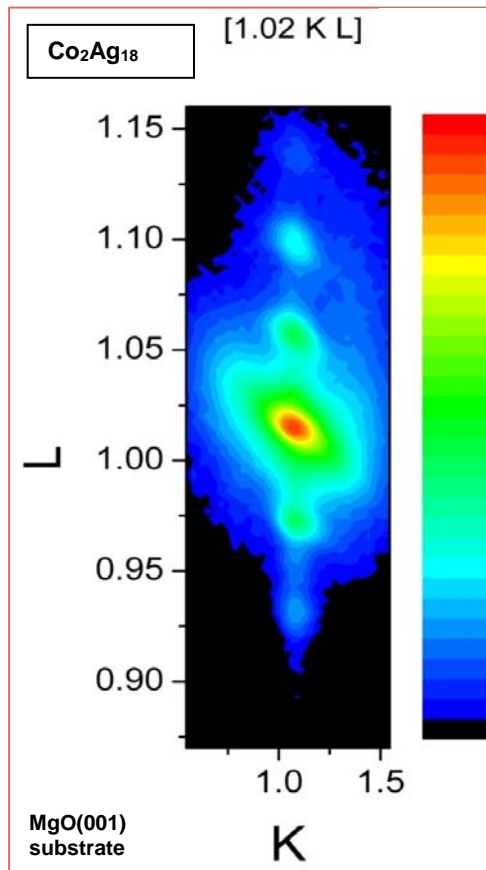
Figure 2. *Reciprocal space map measured with synchrotron radiation (E= 15 keV, λ= 0.82657 Å) around Ag(111) for a multilayer [Co(2ML)/Ag(18ML)]x15 grown on MgO(001). The superlattice extra-spots (L-2, L-1, L+1, L+2, L+3) along L direction can be clearly distinguished.*
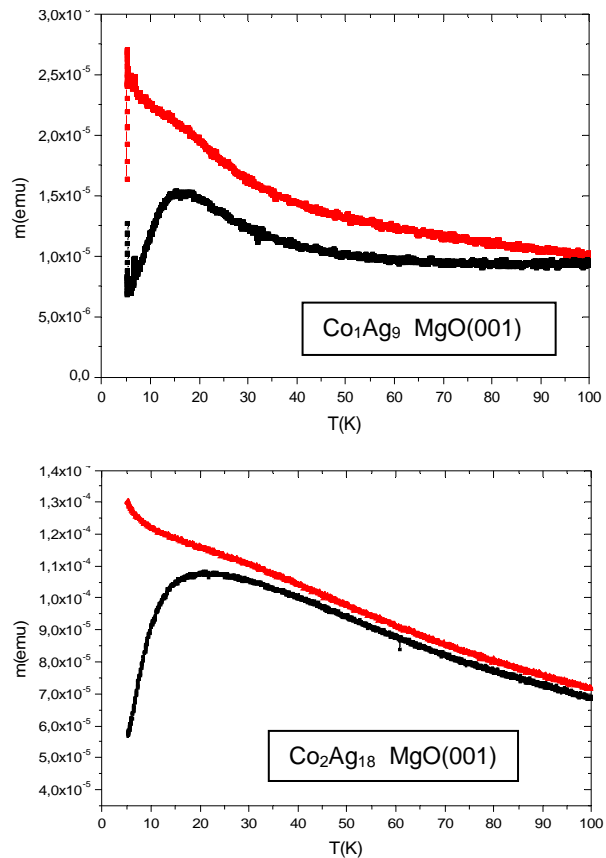
Figure 3: *Low field temperature dependence of the magnetization, measured after zero field cooling (ZFC) and field cooling (FC) the samples, for two MBE-Co/Ag multilayers on MgO (001), both of them with very thin Co layers (1 or 2 ML).*

The magnetic properties (magnetization and hysteretic parameters) were measured versus temperature, down to 5 K, by means of a vibrating sample magnetometer (VSM). Results obtained for the low field temperature dependence of the magnetization, measured after zero field cooling (ZFC) and field cooling (FC) the samples, are also presented (Fig. 3).

Samples with extremely thin Co layers (in the range of 1-2 atomic monolayers per period) exhibit magnetic order up to room temperature (confirmed through the measurement of the thermal dependencies of the remanence and the coercive force). Interestingly, they also show blocking-like temperatures in the range of 15 to 35 K (Fig. 3), being such behavior observed for all the substrate materials and orientations here investigated. Moreover, and in contrast to most of the previous reports for this thickness range, our MBE samples generally display superlattice features (Fig. 2), which are remarkably clear for films grown on the MgO(001) substrates. Magnetic results are discussed in relation to sample growth details and the morphological/structural analysis.

Mechanical Haptic Nanotweezers

Antoine Niguès[1,2], N. Venant[1,2,3], F. Marchi[1,2], M.S. Rodrigues[1], F. Comin[1], J-L. Florens[3] & J. Chevrier[2]

[1]ESRF, 6 rue Jules Horowitz, Grenoble, France, [2]Institut Néel et Université Joseph Fourier, [3]ICA
florence.marchi@grenoble.cnrs.fr

Scanning probes microscopies have been intensively used to study the physical and chemical properties of a wide range individual nanostructure in interaction with a surface; in parallel SPM have demonstrated their capability of nanotools to manipulate and fabricate nano-object. More recently, scientists working in biophysics have combined AFM with optical technique (as fluorescence) to obtain on the same part of the sample a morphological characterization coupled to a classical biological characterization[1]. However, these working configurations do not permit to distinguish between the intrinsic properties of the nanostructure from the ones due to its interaction with the surface substrate and real manipulation in three dimensions are restricted to specific nano-objects. To overcome this limitation, several group have developed mechanical micro-grippers based on MEMS technology to work in vacuum, in air or in water[2]. Thanks to these micro-grippers, full 3D manipulations of submicronic and nanoscopic object have been successfully performed. Nevertheless, to exceed the strong limitations imposed by classic mechanical micro-grippers, namely approximate control of the applied forces and necessity of working under Scanning Electron Microscopes for visual guidance, we developed nano-tweezers based on two independent Scanning Force probes and controlled via a haptic multi-sensorial interface (figure 1a).

Pioneer works on the development of a dual SPM probe head to perform 3D manipulation of micronic objects with a permanent force measurement relied on the two standard AFM probes with a classical optical detection of the cantilever movements [3]. This first design of mechanical nanotweezers is not compact leading to strong difficulties to combine it with an other analyzing technique as X-ray or laser beams. In addition due to the cantilever compliance leading to mechanical instabilities, the operator can not set the working force in the full range of the tip-object interaction. As the ultimate goal of our mechanical nanotweezers is to nanomanipulate object in 3D under a X-ray beam, we selected quartz tuning forks provided with etched tungsten tips as nanofingers (figure 1a).The high quality factor of the tuning forks (Q~10000) and its strong stiffness (*20-40 kN/m*) offers high signal and spatial stability and high sensitivity in the detection of the tip-surface interactions. In addition, this kind of AFM probe have been already successfully implemented on a X-ray beamline to perform AFM imaging and indentation on Ge microdot in order to measure dot Young modulus [4] .

Each finger of the nanotweezers head is mounted on a 3D (XYZ) towels with two open-loop stages, one dedicated to rough displacements and the second a minitritor to the fine displacements (figure 1b). Thanks to a dual specific electronics module from SPEC connected to the nanotweezers head, each nanoprobe can perform classic planar AFM imaging. They have been also used to explore each other in 3D thus providing spatial localisation of their apex. This result opens the way to real «two-finger» nano-tweezers actions as manipulation at the (sub)micron scale. To test the capabilities of our device, a polystyrene sphere of 1 micron of diameter has been manipulated in 3D. Nevertheless these 3D manipulations tend to be hardly reproducible due to the lack of real-time force feedback control and the tip position shifts induced by the open loop displacement stage. Based on this observation and in order to perform efficient manipulations the electronics module of the nano-tweezers has been coupled with a haptic interface to get real-time control of the probe positions and of the strengths applied on objects. A master joystick guides the movement of each slave tip while the frequency shift induced by the tip/sample interaction is directly translated back as a force through the haptic device to the experimentalist.

In this configuration, experiments in 1D have been carried out on different kind of surfaces (PDMS membrane, silicon surfaces) to haptically feel and evaluate the perception of elasticity and hardness [5]. In addition a sub-micron sphere of a 400 nm diameter has been haptically localized and reconstructed in 3D in reproducible manner using a force feedback (Figure 2a). Thanks to this haptic interface, the operator can perform complex tasks like following, at constant height, the contour of the 400nm sphere(fig 2b), this task is required to select the gripping points for future 3D manipulation with the two nanofingers.

Figure1
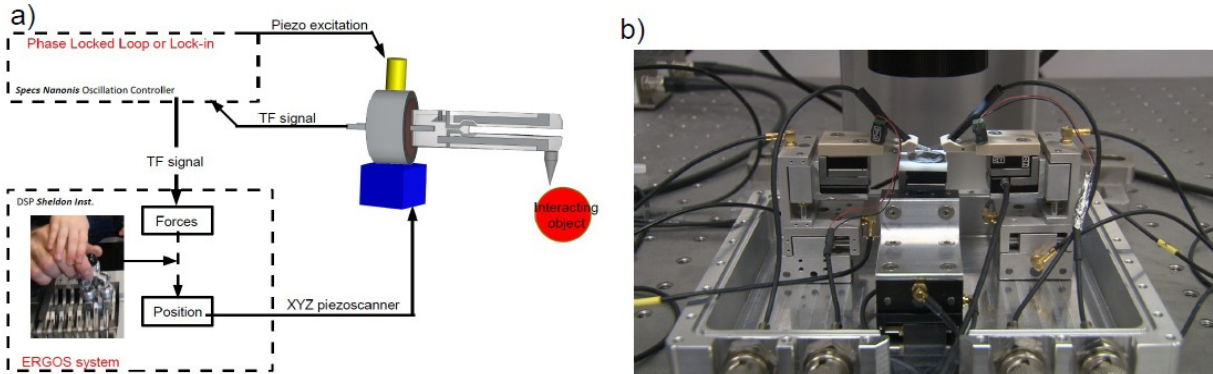
a) Direct teleoperation configuration where the user controls the tip position via the force feedback system. b) System configuration of the nanotweezers. The two nanotweezers fingers and the sample holder are controlled by the same set of devices: Three inertial XYZ motors and a microscanner.

Figure2
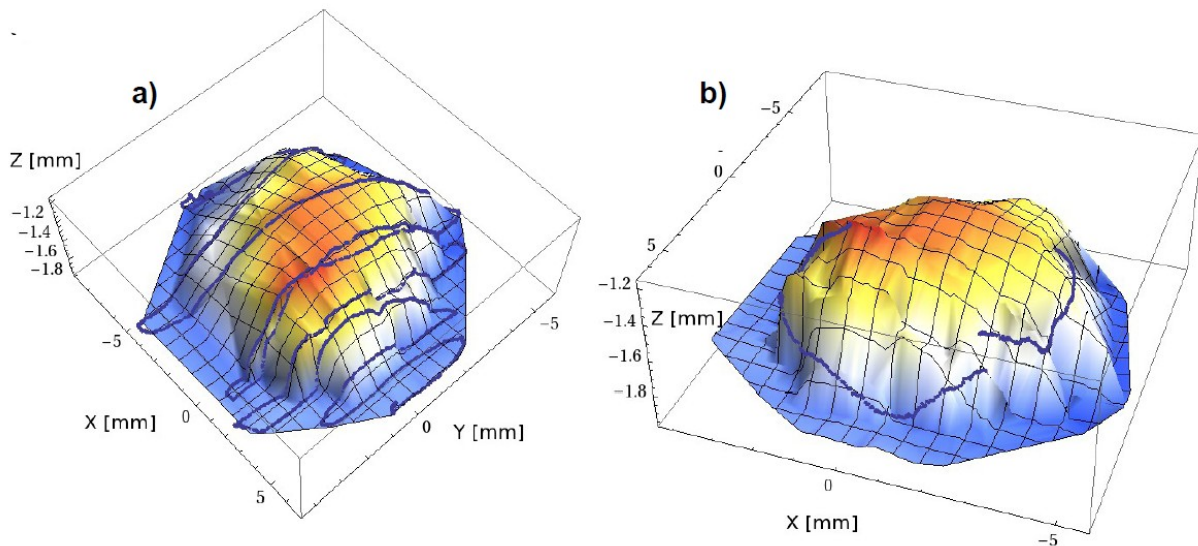
Haptic Recognition performed (a) a view of the sample (1mm corresponding to 100nm in real space) topography is obtained following the tip trajectory (blue line) during the user XY scanning. In this case, the user could feel a virtual relief computed via the height of the tip while he is moving in the XY directions. (b) After the sample exploration, the user had to follow the contour of the sphere. His trajectory during the task has been drawn (blue line) over the reconstructed sample view. The scale on the picture refers to the joystick coordinates and belong to the macroscale.

References

[1] P.P. Lehenkari, Ultramicroscopy, **82** (2000) 289-295

[2] K. Molhave and al., Nanotechnology, **17** (2006) p. 2434-2441.

[3] H. Xie, Nanotechnology, **20** (2009) 215301.

[4] T. Scheler, M.S. Rodrigues, T.W. Cornelius, C. Mocuta, A. Malachias, R. Magalhes-Paniago, F. Comin, J. Chevrier and T.H. Metzger, Appl. Phys. Lett. **94**, 023109 (2009).

[5] N. Venant, A.Niguès, F. Marchi, M. Hrouzek, F. Comin, J. Chevrier and J-L. Florens, Eurohaptics proceedings, Part I, pp35-42, (2010).

Microliter-Electrospinning: A novel technique to produce micro and nanofibers from biomolecules

W. Nuansing[(1)], A. Rebollo[(1)], A.M. Bittner[(1,2)]

[(1)] CIC nanoGUNE Consolider, Tolosa Hiribidea 76, E-20018 San Sebastián, Spain.
[(2)] IKERBASQUE, Basque Foundation for Science, E-48011 Bilbao, Spain.
w.nuansing@nanogune.eu

Conventional electrospinning requires highly concentrated solutions of self-assembling molecular units, and also a certain solution volume. The minimum amount of material is thus in the range of 100 mg. However, many biomolecules, especially peptides and proteins, are only available in μg amounts. In order to assess fiber formation potential even from such molecules, or in fact from any other substance, we developed a microliter-electrospinning system, based on an electrified wire. Figure 1.(a) shows the standard system, where ml volumes are fed from a syringe to an electrified metal needle, controlled by a syringe pump or by air pressure. When the electric field between the needle and a flat collector reaches a critical value, a charged jet of solution is ejected from the tip of the needle and undergoes a series of bending instabilities during its passage to the collector. In addition, evaporation of the solvent reduces the diameter of the traveling solution jet and dries the fiber. Figure 1.(b) shows the microliter setup, where the voltage is applied to a platinum (Pt) wire of 0.27 mm diameter, onto which the solution is directly dropped from a micropipette. Building on the same physical processes, the droplet attached to the wire is stretched, causing the formation of a fiber (see figure 2.).

We tested our system with the self-assembling short aromatic peptides diphenylalanine (Phe-Phe) and Gly-Phe, which we already master well [1,2]. Peptides pose a special challenge since the required highly concentrated solutions demand careful selection of solvents. Only then we can achieve entanglement or at least strong interaction, and a stable fiber is formed. We were able to use amounts as small as 5 μl, which even at concentrations of 10 wt% contain merely 500 micrograms of material. Of course our system is equally compatible with standard polymer fiber spinning, as shown for polyacrylonitrile (PAN) and other polymers, again from microliter droplets.

Optical microscopy revealed extremely long peptide fibers (see figure 3.), which can only be produced by our method. Raman and infrared spectra [3] provide information on molecular vibrations, and were compared to simulation results of single molecules and of dimers (see figure 4.). The comparison shows that changes in O-H and N-H stretching vibrations are due to hydrogen bonding in the fibers. However, the aromatic residues in the peptide cause π–stacking of the molecules [2,4]. This additional interaction supports assembly to fibers when electrospinning assists the molecular alignment.

References

[1] W. Nuansing, A. Rebollo, D. Sedaghat, A.M. Bittner, in prep.
[2] G. Singh, A.M. Bittner, S. Loscher, N. Malinowski, K. Kern, Adv. Mater., **20** (2008) 2332.
[3] W. Nuansing, A.M. Bittner, in prep.
[4] E. Gazit, Prion., **1** (2007) 32.

Figures
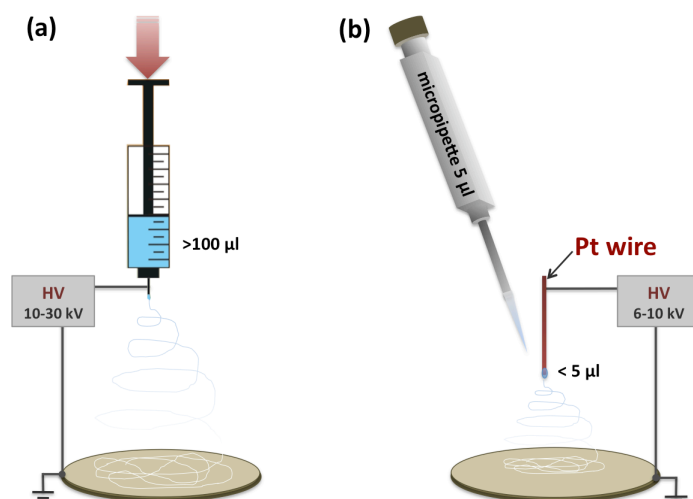
Figure 1. *Schematic of the electrospinning system; (a) conventional and (b) microliter-electrospinning.*
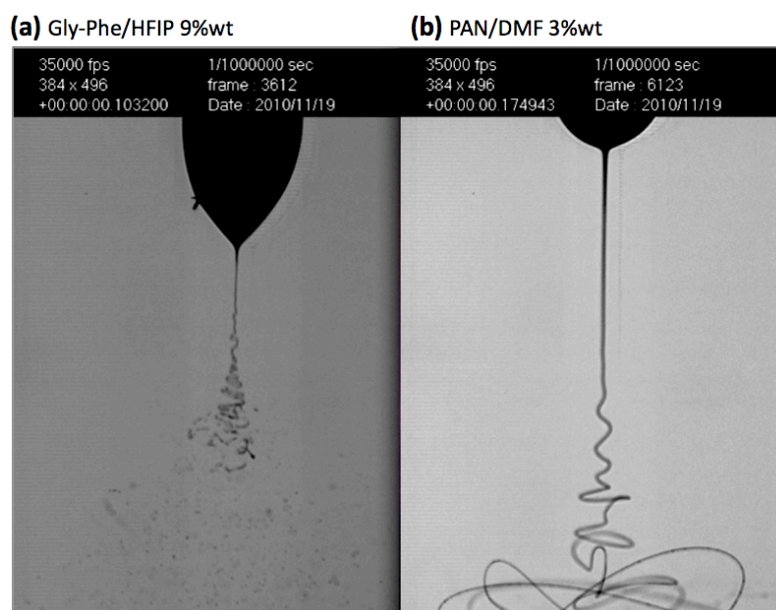
Figure 2. *High-speed photography of the fiber formation during microliter-electrospinning (HFIP = Hexafluoroisopropanol, DMF = N, N-dimethylformamide).*
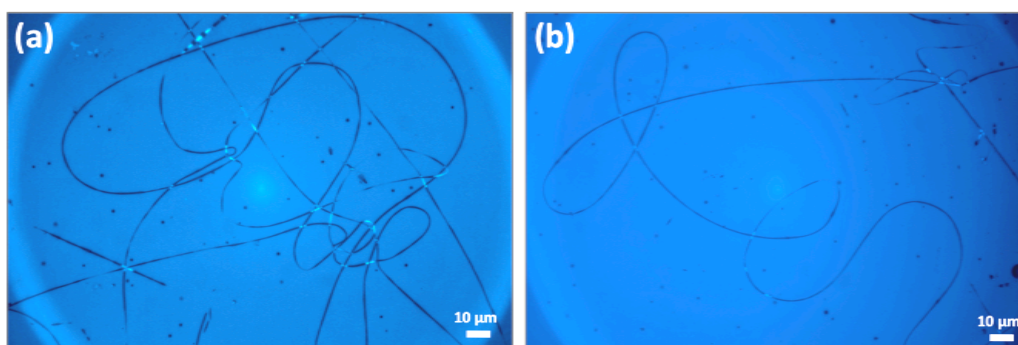
Figure 3. *Optical microscopic images of fibers obtained by microliter-electrospinning (a) Phe-Phe and (b) Gly-Phe.*
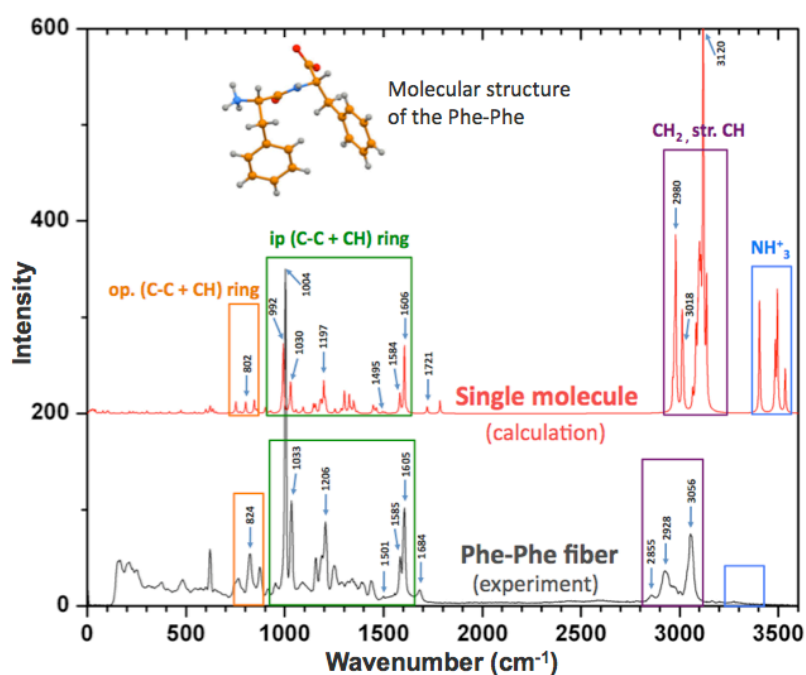
Figure 4. *Raman spectra of a Phe-Phe fiber compared to the calculation result of a single molecule.*

3D nanopatterning of photosensitive hydrogels

Obieta, I[1]; Bilbao, L[1]; Corres, A[3]; Khokhar, AZ[2], Gadegaard, N[2]

[1] Tecnalia, Transport Unit, Parque Tecnológico, E-20009 San Sebastián
[2]. Glasgow University
[3] Polymat

Isabel.obieta@tecnalia.com

Hydrogels are crosslinked polymers that swell in water forming soft and elastic materials. The length and flexibility of the polymeric chains can be controlled and their deformation allows the entry and retention of solutes into the 3D-network. Hydrogels are indispensable for many chemical and biological applications, especially in sensing and actuating devices [1, 2, 3]. The ability to pattern the topologies of gels at the micro and nanoscale is desirable in these applications especially to develop optical devices based on this sensitive nano and micropatterned surfaces. We have previously reported on the development of a new library of hydrogels modified in order to be photocurable and optimally nanoimprinted [4].

The work described is based on a tert-polymer PEGDMA-NIPAAm-AA: poly(ethylene glycol dimethacrylate-co-N-Isopropylacrylamide-co-acrylic acid). This stimulus-responsive or "intelligent" hydrogel shows promising applications, as it is sensitive to pH and to temperature. This tert-polymer **(PEG-co-NIPAAm-co-AA)** is obtained by combining the photoinitiator, IRGACURE 819 (Bis(2,4,6-trimethylbenzoyl) – phenylphosphineoxide) in a concentration of 0.1% w/w with the crosslinker **EGDMA: Etilenglicol dimetacrilato**, in 5% w/w. The NIPAAm is dissolved in the AA-PEGDMA solution, avoiding the introduction of another solvent. The minimum residual layer was obtained with the following combination: **10:40:50 P30** meaning a dilution in ethanol at 30%w.

We have developed a UV-NIL process to obtain 3D nanopatterns with this material. The optimization of the imprinting and etching processes was performed by Tecnalia with a 3D master-stamp developed at UG and replicated in Ormostamp in Tecnalia.

The 3D quartz stamp was fabricated using e-beam lithography. PMMA was used as a mask. Patterns from the PMMA mask were etched into quartz. Oxford 80+ RIE dry-etch tool was used for this purpose. CHF_3 gas was used to etch the quartz. Fabrication was done in two steps. In the first step 1 – 5 μm grating were fabricated on the quartz substrate and in the second step 100 – 500 nm grating were fabricated on 1 – 5 μm gratings. The result is a 1 – 5 μm gratings written on 300 μm x 300 μm patterns as shown in the fig 1. 100 – 500 nm gratings were also written in a 300 μm x 300 μm patterns on the top of 1 – 5 μm gratings. The Qz stamp was replicated in Ormostamp with good pattern fidelity as it can be observed on Fig.1
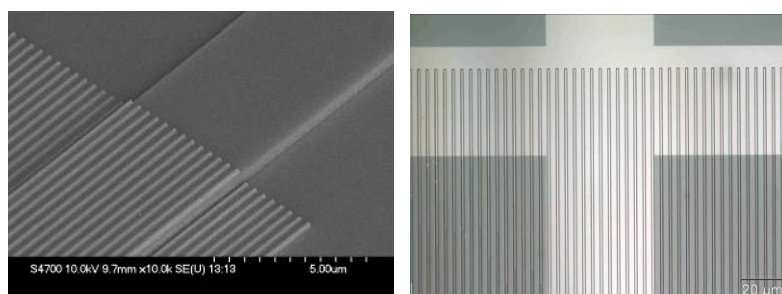
Fig 1. a) Qz 3D stamp and b) replication in Ormostamp

In order to avoid the adhesion between the sample and the stamp, a SAM ($F_{13}TCS$) is deposited over the stamp surface. TPM (3-(Trichlorosilyl)propyl methacrylate) is diluted in a solution of heptane:CCl4 (4:1) and the substrates are kept at room temperature for 5min under N_2 atmosphere in order to obtain good adhesion of the hydrogel on the oxidized silicon.

Table 1 describes the optimized process for 3D nanopatterning in an EVG620 mask aligner.

Materials	Substrate	Silicon oxide + TPM
	Resist	PEGDMA-co-NIPAAm-co-AA
	UMaster	OMS nanometer stamp
3µL drop		
Printing process	Proccess	UV NIL
	Contact mode	vacuum
	Applied pressure during exposure	600mbar
	Delay	10 min
	Exposition time	600seg

Complete filling was obtained as it can be observed on Fig 2.
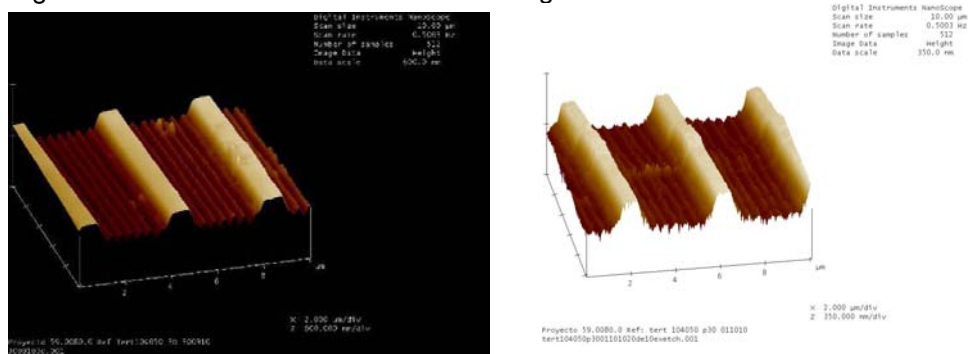
Figure 2. AFM images of the 3D topographies of the tert-polymer a) before and b) after etching

Fluorescein entrapment in the hydrogel after washing, was used in order to verify the complete etching of the residual layer. Hydrogel imprint materials before and after etching were observed under an optical and fluorescence microscope. In all cases, hydrogel imprint materials presented high fluorescence signal as it can be observed on Fig 3 a) optical and b) fluorescence.
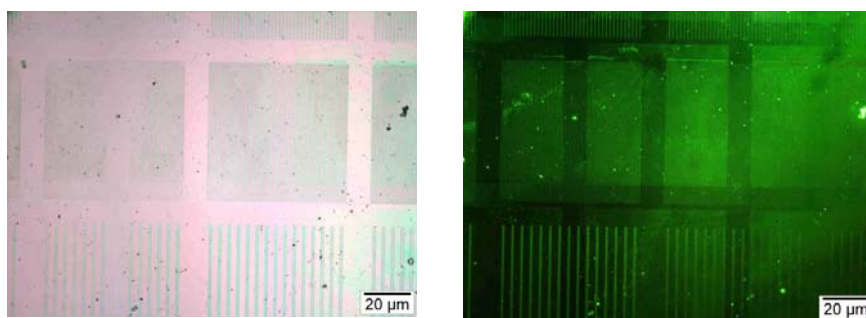
Fig.3. a) Optical and b) Fluorescence imaging of the 3D imprinted hydrogel after etching and posterior fluorescence adsorption.

References:
[1] S. Chaterji et al, "Smart polymeric gels: redefining the limits of biomedical devices", Prog. Polym Sci, 32 (2007) 1083-1122
[2] G. Ye, X. Wang: "Polymer diffraction gratings on stimuli-responsive surfaces: Soft-lithographic fabrication and optical sensing properties" Sensors and Actuators B 147 (2010) 707–713
[3] A. Richter, G. Paschew, S. Klatt, J. Lienig, K.-F. Arndt and H.-J. P. Adler. Sensors, 8, (2008), 561-581
[4] Ainhoa Gaston, Ali Z. Khokhar, Leire Bilbao, Virginia Sáez-Martínez, Ana Corres, Isabel Obieta, Nikolaj Gadegaard, "Nanopatterned UV curable hydrogels for biomedical applications" Microelectronic Engineering, Volume 87, Issues 5-8, May-August 2010, Pages 1057-1061

Chemical functionalization and dispersion of carbon nanofibers in waterborne polyurethane adhesives

Elena Orgilés-Calpena, Francisca Arán-Aís, Ana M. Torró-Palau, César Orgilés-Barceló

INESCOP. Innovation and Technology Center.

Industrial Zone Campo Alto. 03600 Elda, Alicante (Spain).

eorgiles@inescop.es

Carbon nanofibers (CNFs) are considered as ideal reinforcing fibers for polymer matrices in many technological applications due to their unique structure and properties: high aspect ratio, high Young's modulus, excellent mechanical strength and good thermal conductivity. They are excellent nanofillers in polyurethane matrices originating a new polymeric material, exhibiting the same chemical properties as organic polymers, whereas the rheological and thermal properties may be greatly improved.

However, the incorporation of carbon nanofibers to waterborne polyurethanes implies a great difficulty because of their tendency to form aggregates, which sometimes prevents an efficient dispersion [1]. This instability is related to: (i) the Van der Waals interactions between the nanofibers. (ii) the weak nanofiber-polymer interaction. (iii) the huge aspect ratio (length/diameter) in the carbon nanofibers [2]. In this sense, it is necessary to insert functional groups on the surface of the nanofibers, either to induce a repulsive force between the particles or to improve their interaction with the polymer, thus obtaining a stable dispersion [3,4]. Therefore, to improve the dispersion of nanofibers in the polymer, they must undergo a pre-oxidation, thus increasing the number of surface functional groups with oxygen, such as $C=O$, $COOH$, OH, NH_2, etc. and also raising the surface negative charge.

In this sense, several waterborne polyurethane adhesives (WBPU) containing carbon nanofibers were prepared by previous chemical functionalization. Thanks to the chemical treatment, the nanofibers oxidation is produced, the incompatibility between the polymer matrix and the nanofiber is improved and stability of the carbon nanofibers in the dispersion is achieved (Fig. 1).

From the primal polyurethane dispersion, four adhesives were prepared with a different amount of carbon nanofibers (0.10 wt%, 0.25 wt%, 0.50 wt% and 1 wt%). The kinetics of crystallisation was monitored by Differential Scanning Calorimetry (Fig. 2). The maximum of the curve obtained is considered as the crystallization time (t_c) of the polyurethane. Whereas the WBPU without carbon nanofibers reaches the highest crystallization rate of the soft segments at 13 minutes, the addition of the CNFs decelerates the crystallization of the polyurethane in a greater extent by increasing its content, until 21 minutes in case of WBPU/1%CNF. Therefore, although the addition of the carbon nanofibers does not affect the segmented structure of the WBPU, the kinetics of crystallization of the soft segments is decelerated [6], indicating the formation of a reinforced structure, being more noticeable as the content of the carbon nanofiber increases.

The rheological properties were determined using a controlled stress rheometer with a parallel plate shear system (Fig. 3). The addition of the carbon nanofibers produces a noticeable increase in both elastic and viscous moduli of the WBPU, indicating the existence of nanofiber-polyurethane interactions again. This increase is more pronounced as the content of the nanofiber increases [7], due to the existence of a great number of CNFs-polyurethane interactions.

Furthermore, the viscoelastic properties were determined by dynamic-mechanic analysis (DMA), using the two point bending system (single cantilever). According to Fig. 4, the polyurethane which shows the highest moduli values is the one it has the greatest contain in carbon nanofibers (1 wt%), indicating again the existence of polyurethane–CNFs interactions and suggesting a more enhanced structure, in agreement with DSC and plate–plate rheometry results.

References

[1] J. Ryszkowska, M. Jurczyk-Kowalska, T. Szymborski, K. J. Kurzydlowski. Physica E , **39** (2007) 124.

[2] E. Devaux, V. Koncar, B. Kim, C. Campagne, C. Roux, M. Rochery y D. Saihi. Transactions of the Institute of Measurement and Control, **29 ¾** (2007) 355.

[3] T. G Kim, D. Ragupathy, A. I. Gopalan, K. P. Lee. Nanotechnology, **21** (2010) 1.

[4] S. Bose, R. A. Khareb, P. Moldenaersa. Polymer **51, 5** (2010) 975.

[5] W. Chen, X. Tao, Y. Liu. Composites Science and Technology, **66** (2006) 3029.

[6] C.X. Zhao, W.D. Zhang, D.C. Sun. Polymer Composites (2008). DOI 10.1002/pc.

[7] M. Chapartegui, N. Markaide, S. Florez, C. Elizetxea, M. Fernandez, A. Santamaría. Composites Science and Technology **70, 5** (2010) 879.

Figures
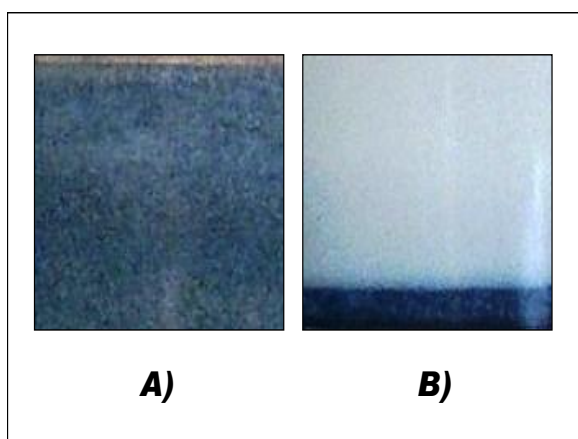
Fig. 1. Stability of the WBPU dispersion after the addition of carbon nanofibers:
A) with chemical treatment of functionalization.
B) without chemical treatment functionalization.
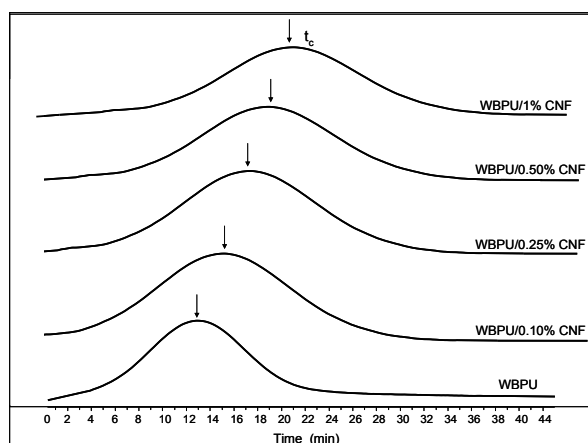
Fig. 2. DSC curves of kinetics of crystallization at 25ºC of the WBPU with different content of carbon nanofibers.
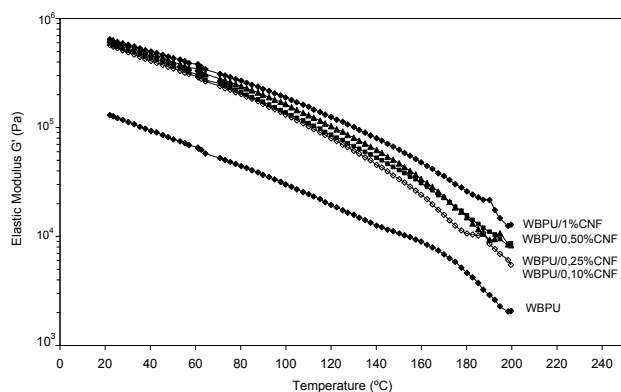
Fig. 3. Variation of the storage (G') modulus as a function of the temperature of the WBPU with different content of carbon nanofibers.
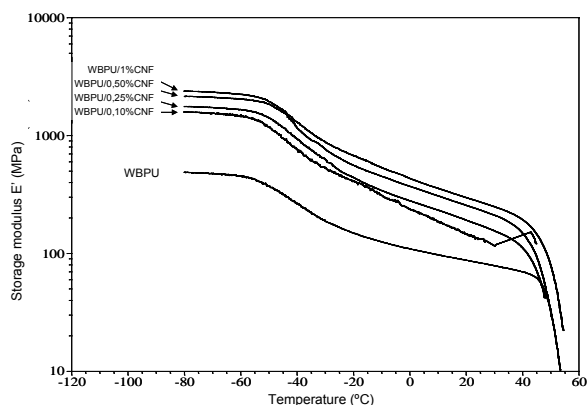
Fig. 4. Variation of the storage (E') modulus as a function of the temperature of the WBPU with different content of carbon nanofibers.

244

Low temperature scanning probe microscopy at high magnetic fields and precise nanopositioning tools for extreme environments

Martin Zech, Florian Otto

attocube systems AG, Koeniginstrasse 11a (Rgb), 80539 Muenchen, Germany
martin.zech@attocube.com

attocube systems, the world-leader in low temperature scanning probe microscopy at high magnetic fields, manufactures and provides ultra-high precision spatial positioning systems and complete probing tools, which are particularly suitable for extreme environmental conditions such as cryogenic temperatures (10 mK – 300 K), high magnetic fields (+31 T) and ultra high vacuum environments (up to 5x10-11 mbar).

The patented, ultra-compact, nano-precise positioning devices specifically designed for extreme environments provide linear, rotational or tilt movement of samples or probes with a sub-nm precision over large travel ranges of up to 20 mm. They are offered in different sizes and out of a variety of materials, and feature an unprecedented variety of applications. This presents a revolutionary advancement for the positioning market, leading to new research in many areas.

The low temperature Scanning Probe Microscopes (LT-SPM) product line comprises an unmatched variety of different probe techniques such as AFM, MFM, SHPM, CFM, Raman, SNOM and STM, and a whole variety of complete cryogenic systems with base temperatures down to 10 mK and magnetic fields of up to 16 T, including e.g. the only proven low vibration pulse-tube cooler based cryostat on the market specifically designed for LT-SPM. Based on our reliable positioning devices, the SPMs allow for in-situ coarse and fine positioning, smooth scanning or automatically focusing of any samples with respect to any probes at low temperatures, high magnetic fields and under high vacuum conditions.

In addition, we offer customized solutions and special products like the world's smallest interferometric displacement sensor (head size only 6 mm x 3 mm) with a stunning resolution of up to 30 pm even over large distances (> 10 cm), while offering sampling rates as high as 12.5 MHz and an absolute accuracy of ±0.5 ppm. These capabilities combined with the compactness are unheard of in industrial metrology and drive new applications in interferometric displacement and vibrometry measurements under harsh conditions in research and industry. With applications ranging from closed-loop scanning to square-foot manufacturing and displacement detection in turboshaft- and gas engines, attocube is creating today's solutions for tomorrow's problems.

In view of the paramount importance of nanotechnology in many areas of today's research as well as industry, attocube's products provide a broad range of ideal products for the growing demand of nano-precise tools for investigation of materials down to the atomic level.

For further technical information concerning attocube systems' products, please visit our website www.attocube.com.

Figures
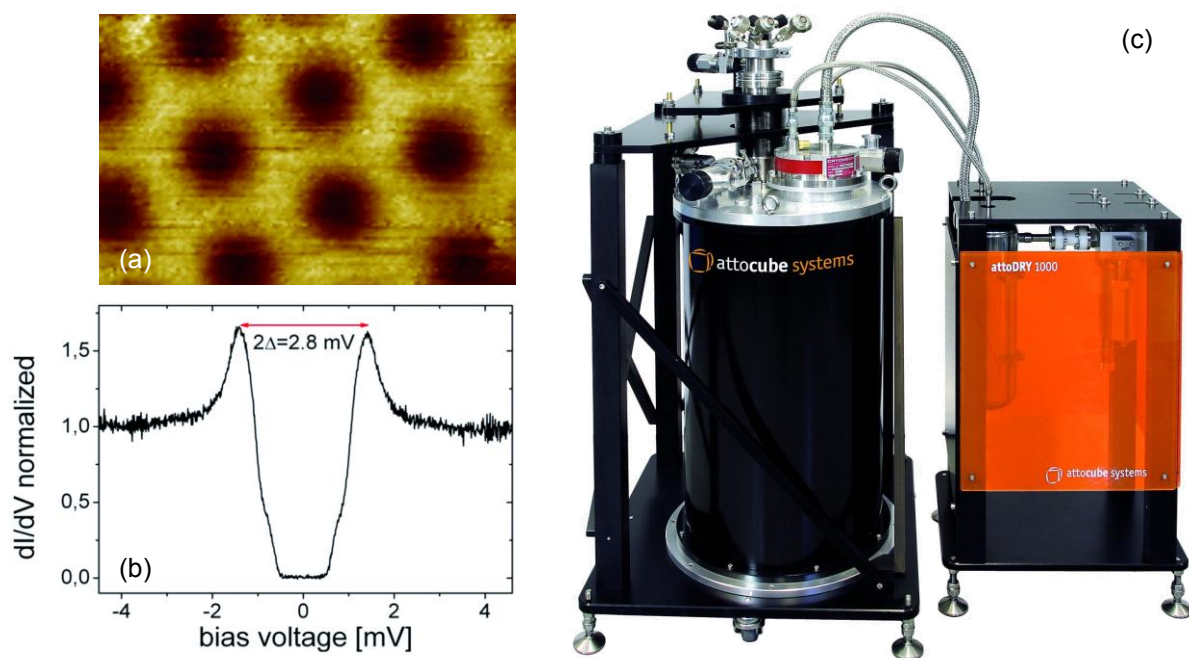
Figure caption: (a) Scanning tunneling spectroscopy (STS) vortex imaging on NbSe$_2$ (Sample courtesy of R. Kramer, Leuven University, Belgium) at 315 mK and 1 T magnetic field. The image was recorded at a bias voltage of 1.4 mV (attocube application labs, 2009). (b) dI/dV spectrum of NbSe$_2$ revealing a local superconducting gap with 2Δ equal to 2.8 mV. (c) The attoDRY1000, a cryogen-free cooling system specifically designed to provide an ultra-low vibration measurement platform for cryogenic scanning probe experiments, without the need for liquid helium.

Metrological SPM for quantitative traced measurements in the nanoscale

M. Ozaita, L.Carcedo, E. Prieto

Centro Español de Metrología (CEM), Alfar 2, Tres Cantos, 28760-Madrid, Spain
mmozaita@cem.mityc.es

The development of new technologies such as microelectronics, nanomedicine or NEMS where the size of the structures under study is decreasing continuously demands high resolution measurements with uncertainties in the nanometer range and below. Scanning Probe Microscopes (SPM) have been widely used to characterize surface properties in research and development institutions, and nowadays it is becoming important also in industrial fabrication and inspection.

These instruments, as many others where quantitative analysis is important, should not only be accurate but also metrologically traceable, [1] i.e. a measurement result should be related to a reference (the definition of the metre in the case of CDs) through a documented unbroken chain of calibrations, each contributing to the measurement uncertainty. In conventional SPMs in which the position is determined from the electrical voltage applied to the piezo scanner, the calibration relies on physical standards. Other metrologically [2] more advanced systems use a variety of sensors (such as strain gauges, capacitive or inductive sensors) to measure position, in an active way not only to measure but also to control position (closed-loop configuration). The calibration of these systems is done either by temporarily connecting laser interferometers to the device or by measuring on high quality standards.

The system that the Centro Español de Metrología (CEM) has just installed in its Micro and Nanometrology Lab. is a reference system with integrated laser interferometers allowing direct traceability to the SI length unit, the metre, via the wavelength of the lasers. This Metrological SPM (MSPM) combines a high precision and large range 3D nanopositioning and nanomeasuring machine (NMM-1 from SIOS) [3] with a resolution of 0.1 nm over a range of (25 x 25 x 5) mm with a versatile scanning probe microscope Dualscope DS-95-50-E from DME and a laser focus sensor from SIOS.

The MSPM is supported by a thermally stable metrology frame and installed within an acoustic chamber. The intersection of the three measuring beams at contact point of the probe sensor allows the system to have a three dimensional Abbe offset free design. The sample under study is placed on a base plate of a corner mirror structure (three mirrors built as a solid corner mirror) reflecting the beams of the interferometers. In addition, the angular position of the corner mirror is controlled by two angular sensors and moved by a 3D stage operated in a close loop controlled by the interferometric system.

The MSPM is intended for the calibration and certification of physical transfer standards (step heights, lateral 1D and 2D standards) used in turn to calibrate other SPM systems and other instruments such as contact profilers and different types of microscopes (interference, holographic or confocal microscopes).

References

[1] Nanoscale Metrology, Editorial, Meas. Sci. Technol. **18** (2007).
[2] VDI/VDE 2656 –Part 1: Chapter 4.2 (pp. 10/11)

[3] SIOS Messtechnik GmbH, "Nanopositioning and Nanomeasuring machine, NMM-1" product brochure. http://www.sios.de/ENGLISCH/PRODUKTE/NMM_E.HTM as of 03/2011

Figures

Basic set-up of the NMM machine:
1 x-interferometer, 2 y-interferometer, 3 z-interferometer, 4 Zerodur® frame,
5 Roll and yaw angle sensor, 6 Pitch and yaw sensor, 7 probe system,
8 Measuring object, 9 Corner mirror, 10 Foundation, guide-drive systems
of the 11 x-axis, 12 y-axis 13 z-axis

Fig. 1: Schematics of the NMM-SIOS system

Fig. 2: Arrangement of Measurement Devices
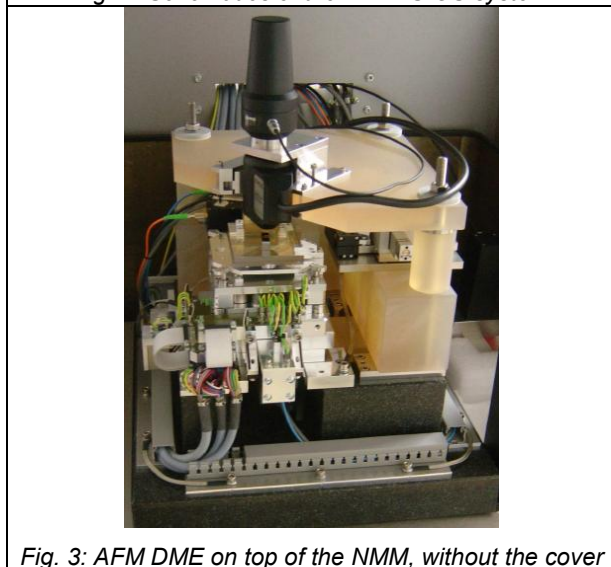
Fig. 3: AFM DME on top of the NMM, without the cover

Fig. 4: Metrological SPM at CEM

Effective synthesis of carbon nanofibers at low temperature

Pacheco, A., Llorca, J.

Centre for Research in NanoEngineering (CRnE). Technical University of Catalonia.
C. Pascual i Vila, 15. 08028 Barcelona, Spain
jordi.llorca@upc.edu

Carbon nanofibers (CNFs) have drawn lots of attention for their potential application as improvement materials for thermal, electrical, optical, frequency shielding, and mechanical properties [1]. They are currently being utilized in different composite formulations thanks to their exceptional properties and low cost. CNFs consist of grapheme layers rolled into cylindrical shape in which carbon atoms are arranged in a hexagonal way. Depending on the degree of coiling and the ordering of the layers, nanofibers of different diameter and different internal geometry are obtained [2].

In this work, CNFs have been synthesized by catalytic chemical vapor deposition (CVD) using alcohol as the source of carbon. Stainless steel plates measuring 50x20x1 mm were used as a catalyst support. Several Fe-, Co- and Ni-based catalyst films were deposited on the metal plates and implemented in a microreactor machined in stainless steel in two differentiated halves. Each reactor halve comprised a 0.5 mm-height rectangular cavity which constituted the flow channel. The catalytic plate was sandwiched between the two halves, except at one of the ends where a window communicated upper and lower flow channels; by these means, the reacting mixture flowed axially along both sides of the plate. The lower part of the reactor comprised distribution and preheating facilities. A gas chamber offered an enhancement of the residence time of the incoming feed to achieve the desired reaction temperature. Six equidistant bores (0.5 mm diameter) were implemented between the preheating chamber and the lower flow channel to assure a uniform distribution of the feed on the channel width. The microreactor was disposed inside an electrical furnace to reach the reaction temperature. A K-type thermocouple ($\pm$0.5 K) was placed in contact with the microreactor to control the furnace temperature. Alcohol mixtures were supplied both as vapor mixtures balanced with inert gas or directly with a liquid pump and passed through the reactor at different flow rates. CNFs were grown at atmospheric pressure in the temperature range 673-873 K for 6 hours.

We have studied the effect of catalyst, reaction temperature and alcohol load on the properties of the CNFs synthesized in order to establish a correspondence between these preparation parameters and the geometrical properties of the CNFs. Nanofiber diameters between 10 nm and 0.1 µm have been obtained by choosing the appropriate preparation parameters. Regarding nanofiber length, values between 0.2 and 3 µm have been attained. It is interesting to note that these values are rarely obtained at temperatures lower than 873 K. Figure 1 shows scanning electron microscopy (SEM) images of various CNFs prepared. Catalyst nanoparticles are located at the tip of the nanofibers, as expected from the CVD method. High resolution transmission electron microscopy (HRTEM) revealed that the CNFs synthesized in this work are cylindric nanostructures with graphene layers arranged as poorly-defined plates. Our method constitutes a simple way to prepare CNFs with geometric properties that are easy to tune. Also, the use of alcohol mixtures as a source of carbon at atmospheric pressure and low temperature allows an easy and safe implementation of the method for the preparation of CNFs at large scale.

All this study is performed inside a project named nAUTO (now in the second stage, named nAUTO[2]) which purpose was to involve nanotechnology capabilities with the automotive needs.

References

[1] J. Coleman, U. Khan, W. Blau and Y. Gun'ko, Carbon 44, 9 (2006) 1624-1652.
[2] S. Iijima, Nature 354, 6348 (1991) 56-58.

Figures
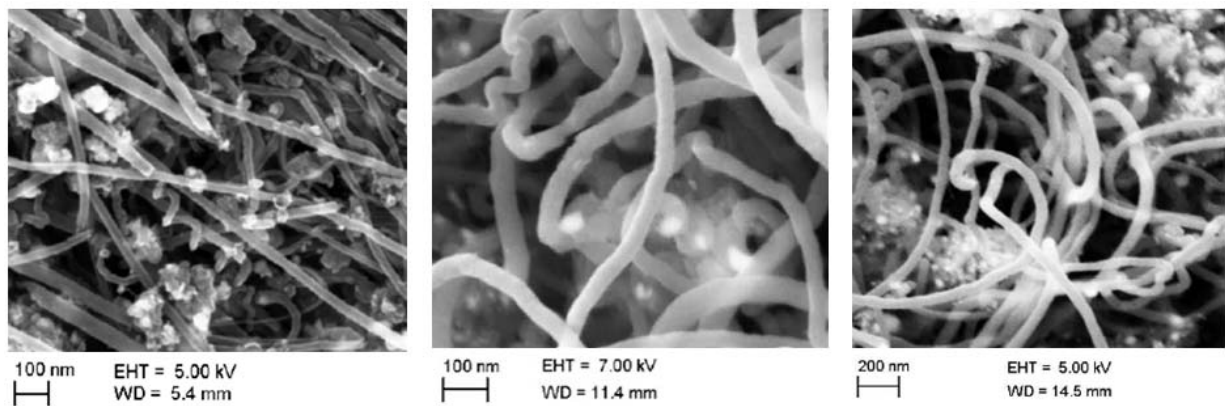
Fig. 1. SEM images of various carbon nanofibers prepared.

Non linear stress-strain response in ultrathin metallic nanowires.
Dependence on the axial orientation.

Samuel Peláez, Pedro A. Serena

Instituto de Ciencia de Materiales de Madrid (ICMM)
Consejo Superior de Investigaciones Científicas (CSIC),
C/Sor Juana Inés de la Cruz 3, 28049-Madrid, Spain
spelaez@icmm.csic.es

Metallic nanowires are a very interesting system from a basic point of view as well as within the context of future nanoelectronics and sensors industry[1]. The mechanical behavior of metallic nanowires under stress has been intensively studied in order to understand their deformation and fracture mechanisms [2-5]. More recently, several studies have focused on the non-linear dependence of stress vs strain in ultra-thin metallic nanowires[6-8]. In this work we examine how non-linear effects depend on the nanowire radius R, its cross-section shape and its crystallographic orientation.

We have performed intensive computer simulations to study the stress response (upon both compressive and tensile strain) of Al, Cu and Ni nanowires. The Embedded Atom Method (EAM) potential [9] is used to describe the interatomic interactions. Periodic boundary conditions are used to simulate infinite nanowires. For each nanowire under study we have carried out a Molecular Dynamics (MD) simulation with a stepwise increasing/decreasing strain. At every strain situation we monitor and average the time evolution of the nanowire stress along its axial direction. From the stress vs. strain curve we determine the Young's modulus E of the nanowire.

We have considered nine different sets (or families) of fcc nanowires. Each family is characterized by a particular cross sectional shape (rectangular, hexagonal or octagonal) and its main axis orientation (parallel to the [100], [110] or [111] crystallographic direction). Each of these sets contains nanowires of different radii, in order to explore size effects of the mechanical response.

We present results on the distribution of the stress inside the nanowire. These results show that surfaces, and specially edges, accumulate a high tensile stress when compared with bulk regions. Additionally we have observed that nanowires in a relaxed state (stress equal to zero) are slightly shorter along their axial direction compared to the original fcc structure. This contraction of nanowires respect to bulk is stronger for thinner nanowires. Regarding the Young's modulus E of nanowires, we have observed the expected trend towards the expected bulk limit value in the corresponding axial orientation when the nanowire cross-section area is larger. However interesting size effects are observed for thinner nanowires. We have observed that the Young's modulus E of the nanowires deviates from the corresponding bulk value as thinner nanowires are observed. Whether this deviation is positive or negative is given by the nanowire axial orientation. In this work we explain this size dependence as the result of the non-linear stress-strain behavior of bulk monocrystals, combined with the strong axial contraction that these nanowires experience as thinner nanowires are considered.

The change of the elastic constants when modifying the nanowire radius opens a way to tailor mechanical properties of future nanoscale devices.

References

[1] N. Agraït, A. Levy-Yeyati and J.-M. van Ruitenbeek, Phys. Rep. **277**, 81 (2002).

[2] I.-L. Chang, and Y.-C. Chen, Nanotech. **18,** 315701 (2007).

[3] A. Hasmy, E. Medina, and P. A. Serena, Phys. Rev. Lett. **86,** 5574 (2001).

[4] P. García-Mochales, S.Peláez, P. A. Serena, E. Medina, and A. Hasmy, Appl. Phys. A **81,** 1545 (2005).

[5] J. Diao, K. Gall, M. L. Dunn, J. Mech. Phys. Sol. **52,** 1935 (2004).

[6] Liang et al. Phys. Rev. B **71**, 241403(R) (2005).

[7] Wen et al. Solid State Comm. **146,** 253 (2008).

[8] McDowell et al. Nanoletters **8,** 11, 3613 (2008).

[9] Y. Mishin, D. Farkas, M. J. Mehl, and D. A. Papaconstantopoulos, Phys. Rev. B **59**, 2292 (1999).

Figures

Aluminum

Copper

Nickel
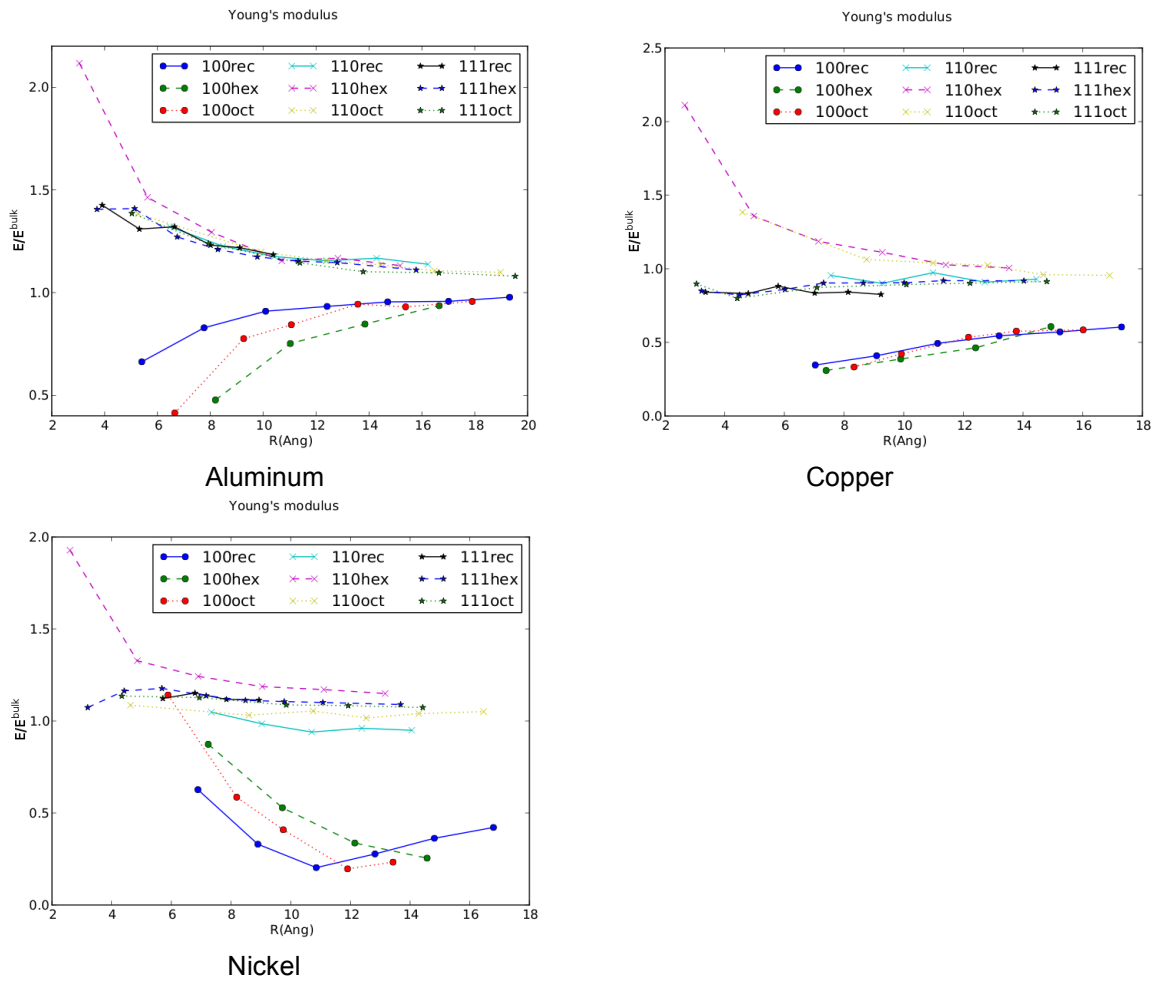
Young's modulus E of Al, Cu and Ni nanowires as a function of the nanowire radius R. For every nanowire orientation E is plotted in units of E^{bulk} of the corresponding orientation. As R increases, E/E^{bulk} tends to 1. However, some nanowires orientations exhibit a Young's modulus stronger than the corresponding bulk. The case of Ni along the [100] direction is particularly weird, since the expected trend is not observed.

Synthesis of inorganic nanoparticles via a novel o/w microemulsion reaction method with fluorescent properties and their dispersion

Kelly Pemartin[1], Conxita Solans[1], Margarita Sanchez-Dominguez[2]

[1]Instituto de química avanzada de Cataluña (IQAC), Consejo Superior de Investigaciones Científicas (CSIC), CIBER en Biotecnología, Biomateriales y Nanomedicina (CIBER BBN), Jordi Girona 18-26, 08034 Barcelona, Spain.
[2]Centro de Investigación en Materiales Avanzados (CIMAV), Unidad Monterrey, CONACYT, Alianza Norte 202, Parque de Investigación e Innovación Tecnológica, 66600 Apodaca, Nuevo León, México
kelnqb@iqac.csic.es

A novel method for the synthesis of inorganic nanoparticles, based on oil-in-water microemulsions has been recently developed [1]. The method consists in the use of organometallic precursors dissolved in nanometric oil droplets, stabilized by surfactant, and dispersed in a continuous water phase (Figure 1). Contrary to the conventional method based on water-in-oil microemulsions (w/o), the advantage of this new approach is the use of water as the external phase; hence the main component is water instead of organic solvents. Therefore, it represents a major advantage for the environment as well as for economic reasons. In addition, the synthesis of nanoparticles via w/o and o/w microemulsion reaction method allows for the preparation of various types of materials with a high control of the nanoparticle size using soft reaction conditions (room temperature, atmospheric pressure) [2, 3].

In our previous studies, the method was applied successfully to the synthesis of a variety of metallic (Pt, Rh, and Pd) [1] as well a metal oxide nanoparticles (CeO_2 and several transition metal oxides) [1, 4]. In the present study, this method is used for the synthesis of inorganic nanoparticles containing Cu and Zn in a 1/1 ratio.

First, a preliminary phase behaviour study was carried out in order to find the appropriate conditions for o/w microemulsion formation. The synthesis was carried out by increasing pH up to specific values. In this one-pot reaction, the synthesis of various types of nanoparticles can be performed according to the pH value. At lower pH, the blue $ZnO/Cu(OH)_2$ nanoparticles are synthesized whereas at higher pH, the brown ZnO/CuO nanoparticles are obtained. The nanoparticles were characterized by Dynamic Light Scattering (DLS), X-Ray Diffraction (XRD), High Resolution Transmission Electron Microscopy (HRTEM) and Fluorescence Spectroscopy. Indeed, the structure of $ZnO/Cu(OH)_2$ is crystalline. ZnO nanoparticles are elongated with a diameter of ~10 nm and ~40 nm of length. $Cu(OH)_2$ nanoparticles have a globular shape with an approximate diameter of 7 nm. In order to explore potential applications, a study was carried out to disperse the nanoparticles in organic solvents; this was achieved in tetrahydrofurane by addition of an anionic surfactant (Figure 2). In addition, fluorescence spectroscopy measurements of the nanoparticle dispersion revealed the fluorescent nature of the nanoparticles (figure 3) which is likely linked to the ZnO nanoparticles [5]. The results obtained demonstrate the versatility of the novel oil-in-water microemulsion method for the preparation of nanoparticles with interesting and varied potential applications.

References

[1] M. Sánchez-Domínguez, M. Boutonnet, C. Solans, **J. Nanoparticle Research** (2009), 11, 1823-1829.

[2] M.A. López-Quintela, C. Tojo, M.C. Blanco, L. Garcia Rio, J.R. Leis, **Curr. Opin. Colloid Interface**

Sci. (2004) 264.

[3] Eastoe J., Hollamby M. J., Judson L. **Adv. Colloid and Interface Sci.** 2006, 5, 128-130.

[4] M. Sanchez-Dominguez, L. F. Liotta, G. D. Carlo, G. Pantaleo, A. M. Venezia, C.Solans, M. Boutonnet, **Catalysis Today** (2010*), 158, 35-46.

[5]Y. Khana, S.K.Durrani, M. Mehmood, J. Ahmada, M.R. Khan, S. Firdous, **Applied Surface Science**, (2010) *in press*.

Figures
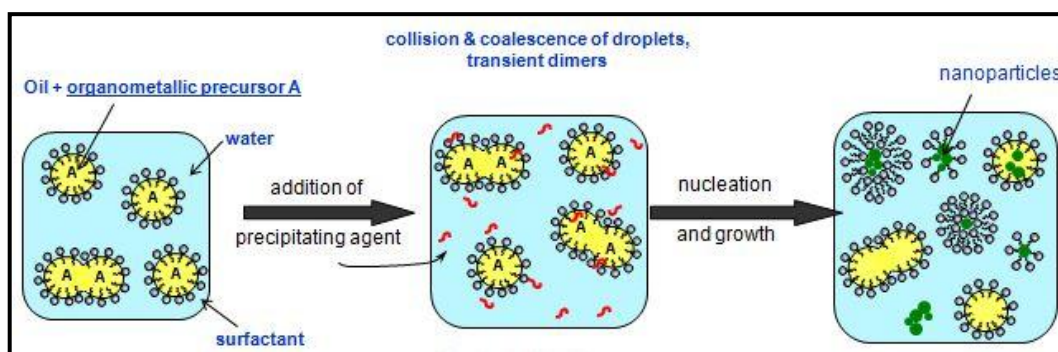
Figure 1: Procedure of the synthesis of nanoparticles via an oil-in-water microemulsion reaction mehod

wt% dried NPs	0.96%	1.45%	2.21%	2.69%	3.43%
wt% AOT	0.8%	0.6%	0.6%	0.7%	0.6
Aspects					

Figure 2: Aspect of dispersion of ZnO/Cu(OH)$_2$ in THF using an anionic surfactant (AOT)
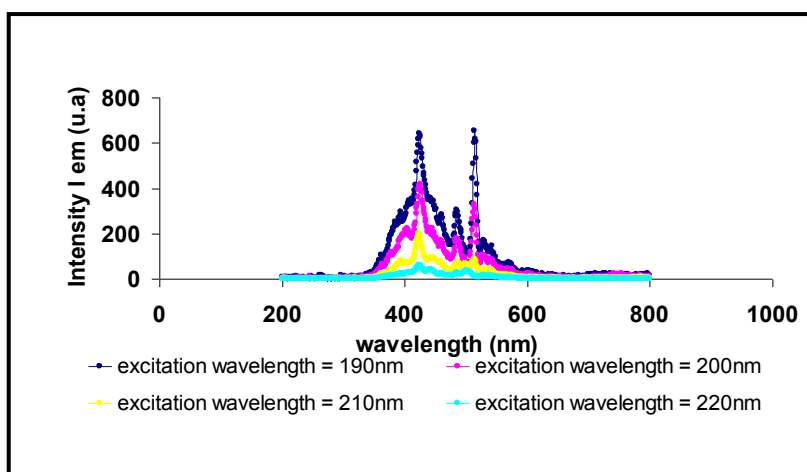
Figure 3: Fluorescent emission spectra of ZnO/Cu(OH)$_2$ nanoparticles (3.43 wt%) dispersed in THF at various excitation wavelengths.

Loaded polymeric nanoparticles for drug delivery

Peres I., Rocha S., Pereira M.C., Coelho M.

LEPAE, Chemical Engineering Department, Faculty of Engineering, University of Porto, Rua Roberto Frias, 4200-465 Porto, Portugal

dce06013@fe.up.pt

Free radicals and oxidative stress are related to cancer, cardiovascular disease, diabetes, autoimmune disorders and neurological disorders (*1*). Epidemiological studies have shown that a diet enriched in antioxidants is associated with reduced risk of such disorders (*2*). Antioxidants, such as catechins from green tea, show a wide range of biological activities including antithrombotic, vasodilatory and anticarcinogenic effects, as well as anti-inflammatory, antiallergic, antiulcer, and antimicrobial properties (*3*). Catechins act as free radical scavengers and chelators of metal ions (*4*). Oral administration is the most efficient delivery system of antioxidants, however oral bioavailability of tea catechins is very low, less than 2-5% and their systemic clearance is also high (*5*). Encapsulation of catechins in carbohydrate nanoparticles (*6*) or other pre-formed materials (*7*), represents a solution to increase the antioxidant's efficacy of therapy. Spray-drying technology is widely used for drying biomolecules or colloidal particles and is based on a fast (~10 sec) convective drying process, in which hot air provides energy for evaporation of solvent (water) from liquid drops formed by atomization. Mixtures of gum arabic and maltodextrin have shown promise as high solid carriers, giving acceptable viscosity in studies on microencapsulation of cardamom oil by spray-drying (*8*). In this work, gum arabic-maltodextrin particles loaded with EGCG (EGCG/P) were successfully produced by homogenization and spray-drying, with an EGCG loading efficiency of 96±3%. Spray-dried particles are spherical or corrugated and polydisperse. The particles in aqueous suspension by dynamic light scattering (DLS) revealed two main populations, with mean average diameters of 40 nm and 400 nm (Figure 1). Transmission electron microscopy (TEM) images (Figure 2) corroborate de DLS measurements. Attenuated total reflection-infrared spectroscopy (ATR-IR) confirmed that EGCG was incorporated in the carbohydrate matrix by intermolecular interactions, maintaining its chemical integrity. Atomic force microscopy imaging proved the particle spherical shape, size and resistance to mechanical strength (up to 8 MPa). Nuclear Magnetic Resonance spectroscopy (NMR) experiments, have been performed to determine the structure of the epigallocatechin gallate-polysaccharide conjugates and to clarify the mechanisms of drug immobilization into the polymer matrix (Table 1). The results suggest the entrapment of EGCG into the polysaccharide matrix of maltodextrin/gum arabic (MD/GA) and support the potential of these vehicles for their sustained delivery and release. This study highlights the use of polysaccharide nanoparticles in chemoprevention as they can be used to deliver natural antioxidants capable of inhibiting steps of the tumorigenesis process in prostate cancer cell lines (Du 145). The results achieved, demonstrate that the carbohydrate matrix is able to preserve EGCG antioxidant properties, as proof of concept to be used as polymeric drug carrier.

References

1. B. A. Warden, L. S. Smith, G. R. Beecher, D. A. Balentine, B. A. Clevidence, *The journal of Nutrition* 131, 1731 (2001).
2. D. V. Ratnam, D. D. Ankola, V. Bhardwaj, D. K. Sahana, M. N. V. R. Kumar, *Journal of Controlled Release* 113, 189 (2006).
3. P. Anand *et al.*, *Pharmaceutical Research* 25, 2097 (2008).
4. C. Kandaswami, E. Middleton, *Adv Exp Med Biol* 366, 351 (1994).
5. Y. Cai, N. D. Anavy, H. H. S. Chow, *Drug Metab Dispos* 30, 1246 (Nov, 2002).
6. S. L. Kosaraju, L. D'ath, A. Lawrence, *Carbohyd Polym* 64, 163 (May 11, 2006).
7. G. R. Shi *et al.*, *Int J Pharm* 349, 83 (Feb 12, 2008).
8. B. Sankarikutty, M. M. Sreekumar, C. S. Narayanan, A. G. Mathew, *J Food Sci Tech Mys* 25, 352 (Nov-Dec, 1988).

Figures
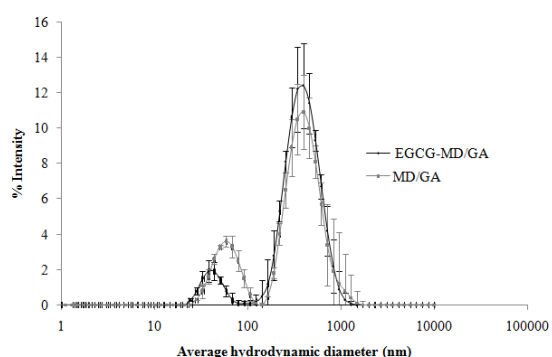
Figure 1. Average hydrodynamic diameter distribution of EGCG-loaded particles and unloaded (MD/GA) nanoparticles.
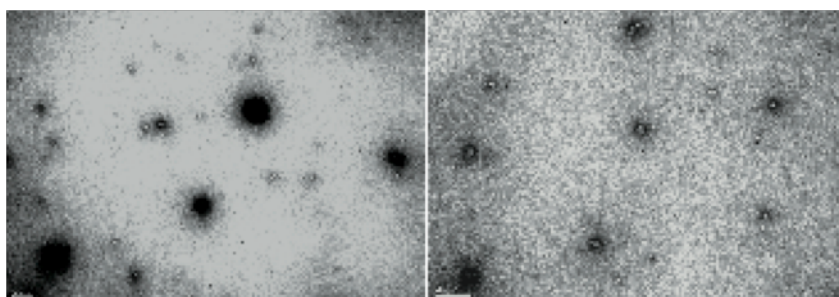
Figure 2. Transmission electron microscopy images of polysaccharide nanoparticles. The scale bar is 200 nm.

Table 1. Relative diffusion coefficients (related to TSP), with calculated standard deviations (in italics) of EGCG and MD/GA in D_2O at 30 °C for the samples studied.

Sample	EGCG (δ, ppm)	MD and GA (δ, ppm)					
	7.03	5.42	5.25	4.1-3.5	3.43	3.3	1.28
EGCG	0.62						
	0.01						
MD/GA		0.40	0.55	0.28	0.37	0.52	0.04
		0.04	*0.01*	*0.03*	*0.02*	*0.02*	*0.03*
EGCG-MD/GA	0.45	0.37	0.52	0.30	0.37	0.50	0.06
	0.03	*0.04*	*0.05*	*0.05*	*0.06*	*0.04*	*0.03*

COMPUTATIONAL APPROACHES FOR DETERMINATION OF THE MELTING TEMPERATURE OF SUSPENDED METALLIC NANOWIRES.

J. A. Pérez Finol[1], S. Peláez[1], P. García-Mochales[2] and P. A. Serena[1].

[1]Consejo Superior de Investigaciones Científicas (CSIC), Instituto de Ciencia de Materiales de Madrid (ICMM), C/Sor Juana Inés de la Cruz 3, 28049-Madrid, Spain
[2]Departamento de Física de la Materia Condensada, Universidad Autónoma de Madrid (UAM)

japerezfinol@icmm.csic.es

During the last two decades, the study of the properties of nanowires has been one of the keystones in the development of nanotechnology, since these nano-objects exhibit electrical and mechanical properties of interest in fundamental knowledge as well as technological applications. In particular, the formation of ultra-thin metallic nanowires from the breaking of nanocontacts has been subject of many experimental and theoretical studies. For instance, the formation of linear atomic chains (LAC) has been observed in both scanning tunneling microscopy (STM) and mechanically controllable break junction (MCBJ) experiments on different metallic species [1]. By means electron beam irradiation of thin Au films long nanowires of helical structures can be obtained [2]. Moreover, theoretical works have shown the formation of a great variety of weird nanowires which present a higher stability than the a priori expected fcc/bcc crystalline nanowires [3].

A few years ago, it has been suggested that icosahedral (a.k.a. pentagonal) nanowires are formed spontaneously in MCBJ ruptures of Cu nanocontacts[4]. In a recent work we have reported Molecular Dynamics (MD) simulations of the breaking process of Al, Ni and Cu nanowires in which these icosahedral nanowires are observed [5]. We have shown that these structures are long, very stable and are formed at relatively high temperatures compared to the corresponding bulk melting temperature. Indeed there is an optimal temperature at which the probability of formation of pentagonal nanowires is highest. The existence of this optimal temperature is the result of a balance between two phenomena. On one hand a high temperature favors the formation of a disordered region in the narrowest section of the nanowire. It is from this disordered region that atoms diffuse to form pentagonal rings. On the other hand, a too high temperature induces the melting of the narrowest section of the nanowire, and the breaking of the contact.

In the present work we are interested in the temperature dependence of the stability of suspended icosahedral nanowires. We use MD simulations to study the dynamical evolution of the nanowires as the temperature increases. In order to have a more consistent methodology different heating rates υ are tested. Infinite pentagonal nanowires are simulated by using periodic boundary conditions along the nanowire axis. Different sizes of the unit cell along the nanowire axis direction are tested, in order to identify size effects in our simulations. Interatomic interactions are modeled using a parameterization of the Embedded Atom Method (EAM). Temperature is controlled by a Nosè-Hover chain algorithm. We have checked that the thermal expansion coefficients in these systems are negligible and were not considered in the simulations.

Here we report the melting temperature T_m of the icosahedral nanowire structures for three metallic species: Al, Ni and Cu. This T_m is determined from a statistical analysis of many MD simulations at different heating rates. For every simulation we monitor the total cohesive energy E_C, Lindemann coefficient, axial component of the stress and angular and radial distribution functions. An abrupt change in these observables indicates that the nanowire has abandoned its pentagonal structure due to thermal diffusion. Massive repetitions of the simulation gives rise to a statistical distribution of temperature values at which this transformation takes place. From this distribution an average melting temperature $<T_m>$ can be obtained. It has been observed that after the pentagonal structure is altered, the nanowire is distorted and becomes a nearly-spherical cluster (see figure 1).

We have observed that the calculated average T_m ($<T_m>$) decreases when the number of atoms N_a used in the simulation unit cell are increased. On the other hand a decrease in $<T_m>$ is observed when lowering the heating rate υ. We expect that the dependence of T_m with both the υ and N_a should converge to a constant value in the limit of slowest υ and largest N_a.

References

[1] N. Agraït, A. Levy-Yeyati, and J.M. van Ruitenbeek, Phys. Rep. **377**, 81 (2003).
[2] K. Kondo and K. Takayanagi, Science **289**, 606 (2000).
[3] O. Gülseren, F. Ercolessi and E. Tosatti, Phys. Rev. Lett. **80**, 3775 (1998).
[4] J.C. González, V. Rodrigues, J. Bettini, L. G. C. Rego, A. R. Rocha, P. Z. Coura, S. O. Dantas, F. Sato, D. S. Galvão, D. Ugarte. Phys. Rev. Lett. **93** 126103-1 (2004)
[5] S. Peláez et al. Current Nanoscience. (2010). (Accepted for publication).
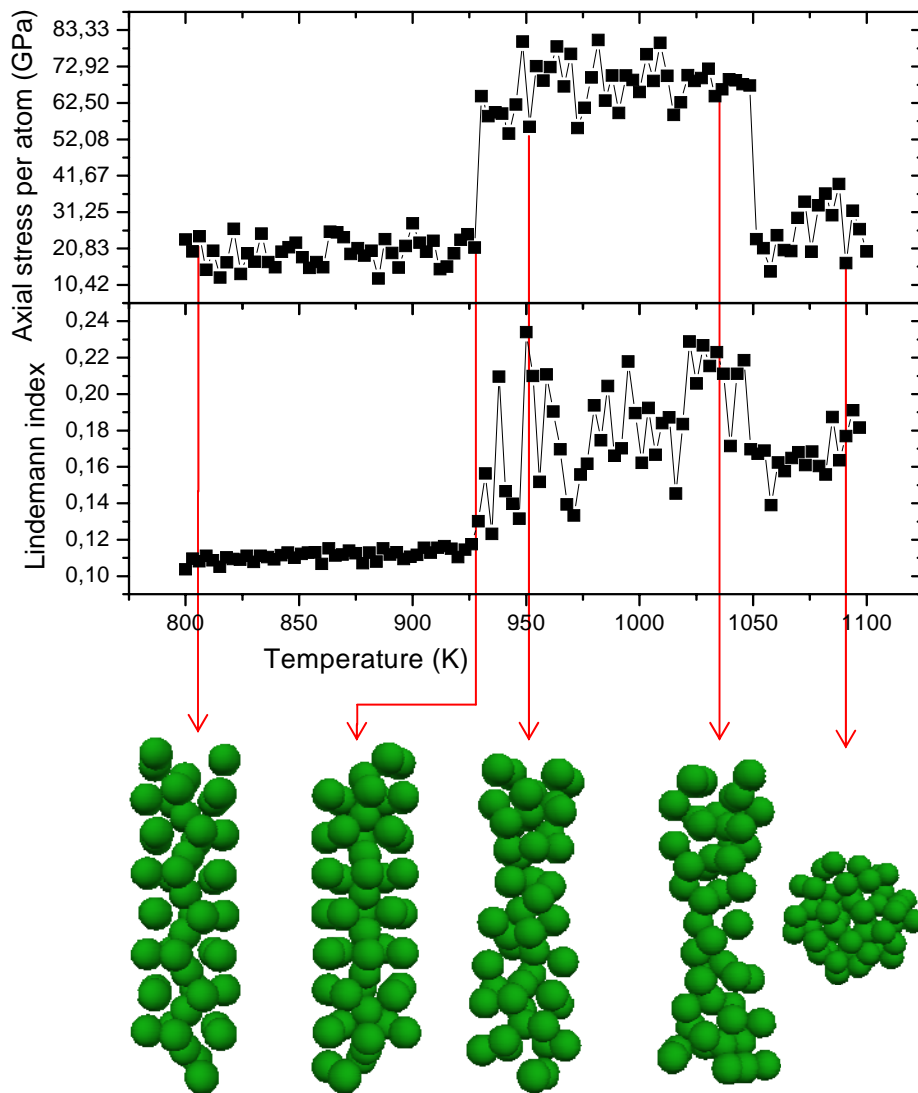
Figures

Figure 1. Melting process of a pentagonal nanowire. An abrupt change in both the axial component of the stress or the Lindemann index corresponds to a diffusive distortion of the nanowire's structure. Later, the nanowire breaks and collapses into a cluster.

Polymer coated iron nanoparticles for biological applications

N. Pérez, J.L. Vilas, J.M. Laza, L.M. León

Laboratorio de Química Macromolecular (Labquimac), Dpto. Química-Física, Facultad de Ciencia y Tecnología, Universidad del País Vasco (UPV/EHU), Apdo. 644 48080 Bilbao (España)

nagore.perez@ehu.es

Magnetic nanoparticles have numerous applications in biotechnology and biomedicine. Iron oxide nanoparticles such as magnetite (Fe_3O_4) or its oxidized form maghemite (γ-Fe_2O_3) are by far the most commonly employed in biomedical applications since their biocompatibility has been proven. They can be used as magnetic carrier for drugs, antibodies or cells, they can be heated up by alternating magnetic fields and potentially kill the cancerous cells by hyperthermia or be used as contrast agents for MRI [1]. This study aimed at the synthesis and surface modification of magnetic nanoparticles.

At present there is a big effort in synthesizing biocompatible magnetic nanoparticles with high susceptibility in order to improve the attraction and actuation of the particles by external magnetic fields. Magnetic nanoparticles are usually modified through the formation of few atomic layers of polymer/surfactant or inorganic metallic or oxide surfaces which are suitable for further functionalization by attachment of various biomolecules. It has synthesized iron nanoparticles coated in a polymer. The role of the polymer coating is twofold: on one hand it prevents the iron from oxidizing and on the other hand it allows the functionalization of the particles and minimizes the direct exposure of the iron nanoparticles surfaces to the biological environment. The polymer coated iron nanoparticles have been synthesized by a microemulsion method in two steps [2].

The water-in-oil microemulsion has been widely used to synthesize uniform size nanoparticles of various kinds, including magnetic materials, and has become a powerful tool. The water nanodroplets (nanoreactor) containing reagents undergo rapid coalescence that allows mixing, precipitation reaction, and aggregation processes for the synthesis of magnetic nanoparticles. The water-in-oil microemulsion has been prepared using nonionic surfactants.

The nonionic surfactant nonylphenol pentaethoxylate (NP5) forms reverse micelles in hydrocarbon oils, and has been successfully employed to synthesize iron nanoparticles [3]. The aim of this study is to introduce another surfactant, the poly (ethylene glycol) (PEG), that acts as a co-surfactant and investigate the influence of PEG surface active coating on the magnetic properties of the iron nanoparticles [4].

Furthermore, we have synthesized iron nanoparticles only coated by PEG with the same technique. The aim is to modify this coating in order to allow the subsequent functionalization of the nanoparticles.

The particles have been characterised by means of X-ray diffraction (XRD) and transmission electron microscopy (TEM). XRD shows a clear Fe_{bcc} phase and no presence of Fe oxides can be detected. The average nanoparticle size of the core-shell structure is about 9-11 nm, with about 3-5 nm diameter core and 3 nm shell.The magnetic properties have been studied by means of the 300 K hysteresis loop performed in a high field vibrating sample magnetometer (VSM). [57]Fe Mössbauer spectroscopy measurements were carried out at room temperature in transmission geometry using a conventional spectrometer with a [57]Co-Rh source.

In conclusion, in this study it is reported the preparation of polymer coated iron nanoparticles by microemulsion technique. We have been able to synthesize high susceptibility Fe nanoparticles of sizes between 10-15 nm coated by a polymer.

References

[1] Q.A. Pankhurst, J. Connolly, S.K. Jones, J. Dobson, J. Appl. Phys. D **36** (2003) R167.

[2] W.L. Zhou, E.E. Carpenter, J. Lin, A. Kumbhar, J. Sims, C.J. O'Connor, Eur. Phys. J. D. **16** (2001) 289.

[3] S. Santra, R. Tapec, N. Theodoropoulou, J. Dobson, A. Hebard, W. Tan, Langmuir **17** (2001) 2900.

[4] A. Skumiel, A. Józefczak, T. Hornowski, Journal of Physics Conference Series **149** (2009) 01211.
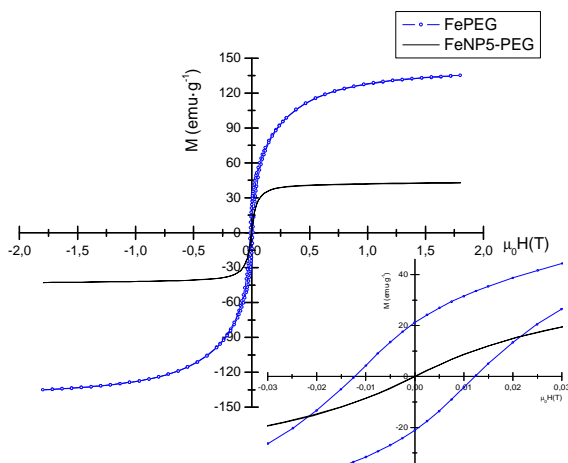
Figures

Figure 1: Hysteresis loop at 300 K. The inset shows the region at low fields to highlight the presence of coercivity and remanence.
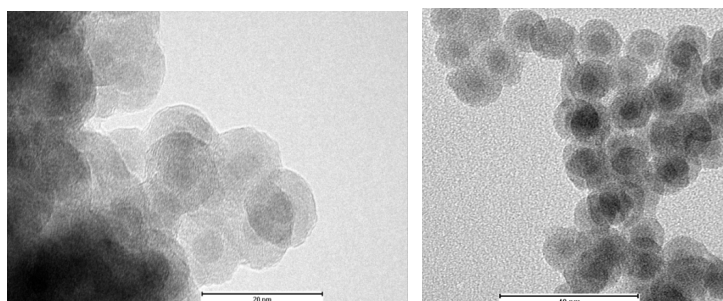

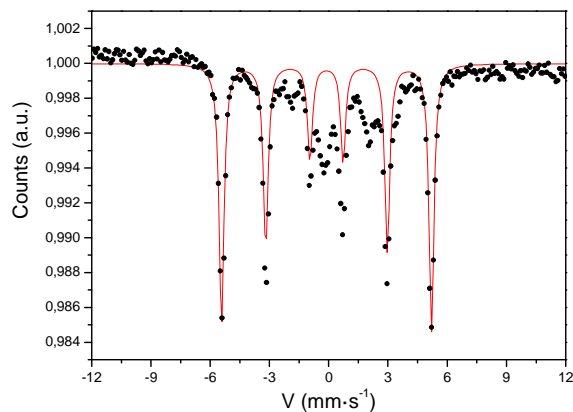*Figure 2: TEM micrographs of iron coated nanoparticles.*

Figure 3: Room temperature Mössbauer spectra.

Multifunctional nanoplatform for in vivo and in vitro biomedical applications

R. Piñol[1], L. Gabilondo[1], J.L. Murillo[1], N.J.O. Silva[2], R. Bustamante[1], L. Mohamed[1], V. Sorribas[3], M. Gutierrez[4], R. Cornudella[4], J. A. Moreno[4], A. Millan[1], F. Palacio[1].

[1] Instituto de Ciencia de Materiales de Aragón. CSIC - Universidad de Zaragoza, and Departamento de Física de la Materia Condensada. Facultad de Ciencias, 50009 Zaragoza, Spain.

[2] Departamento de Física and CICECO. Universidade de Aveiro, 3810-193 Aveiro. Portugal.

[3] Departmento de Toxicologia, Facultad de Veterinaria, Universidad de Zaragoza, 50009 Zaragoza, Spain.

[4] Departamento de Hematologia, Facultad de Medicina, Universidad de Zaragoza, 50009 Zaragoza. Spain.

pinol@unizar.es

Nanotechnology offers clear advantages with respect to conventional techniques that is resulting in a real breakthrough in biomedical research and health care. One of the best chances along this direction would come from the development of multipurpose nanometric systems incorporating several physical (magnetic, optical) and biological functionalities in a single unit that could perform simultaneously a variety of different operations such as driving, sensing, imaging and therapy. Here, we present a core-shell multifunctional nanoplatform containing magnetic nanoparticles, luminescent centres, anchoring sites for biological active molecules and potentially a molecular thermometer[1]. This study involves a variety of research fields and includes researchers from various specialities: chemists, physicists, biology, toxicology and clinical medicine. The magnetic properties of the nanoplatform (magnetic moment, susceptibility, blocking temperature, relaxivity, etc) can be tuned up in the whole superparamagnetic range by changing the size of the magnetic nanoparticles from 2 to 25 nm.[2] The synthesis is based in a polymeric route, in which polymers play multiple role: a) as templates for the control of inorganic nuclei production; b) as a matrix for the encapsulation of the nuclei; c) as a coating containing hydrophilic residues to achieve stabilitization of the nanoparticles in biological media; and d) for the incorporation of inorganic and organic functionalities. Surface functionalization of the magnetic nanoparticles is achieved by Michael addition chemistry between α,β-unsaturated electrophiles and amine based polymers in aqueous solution at different pH conditions and room temperature to moderated temperatures.[3] Michael addition chemistry in water as medium benefits from mild reaction conditions, no by products, high functional tolerance, high conversion and favourable reaction times, non-toxicity and non-hazardous to the environment isolation purification. All the components are biocompatible. The whole particle size, which account for the magnetic nanoparticles and their polymeric multicoating, can be varied from 30 to 150 nm. As it will be shown in this presentation, the nanoplatform is highly stable in biological fluids, shows low toxicity[4], capability of cell internalization, excellent hematocompatibility, anticoagulation properties, and excellent performance in magnetic resonance imaging[5] and hyperthermia, substantially better than commercial standards.

References

[1] C. D. S. Brites, P. P. Lima, N. J. O. Silva, A. Millán, V. S. Amaral, F. Palacio, L. D. Carlos, Advanced Materials, **22** (2010) 4499-4504.

[2] A. Millan, F. Palacio, A. Falqui, E. Snoeck, V. Serin, A. Bhattacharjee, V. Ksenofontov, P. Gütlich and I. Gilbert, Acta Materialia, **55**, (2007), 2201-2209.

[3] R. Piñol, A. Millán, F. Palacio, L. Gabilondo, Spanish Patent no. P201031493 submitted to the Spanish Patent and Trademark Office (07-10-2010).

[4] R.Villa-Bellosta, G. Ibarz, A. Millan, R. Piñol, A. Ferrer-Dufol, F. Palacio, V. Sorribas, Toxicology Letters, **180**, (2008) S221-S221.

[5] H. Amiri, R. Bustamante, A. Millán, N. Silva, R. Pinol, L. Gabilondo, F. Palacio, P. Arosio, M. Corti, A. Lascialfari, "Multifunctional Polymer-based Nanostructured Bio-ferrofluids as MRI Contrast Agents" submitted to Magnetic Resonance in Medicine.

Figures
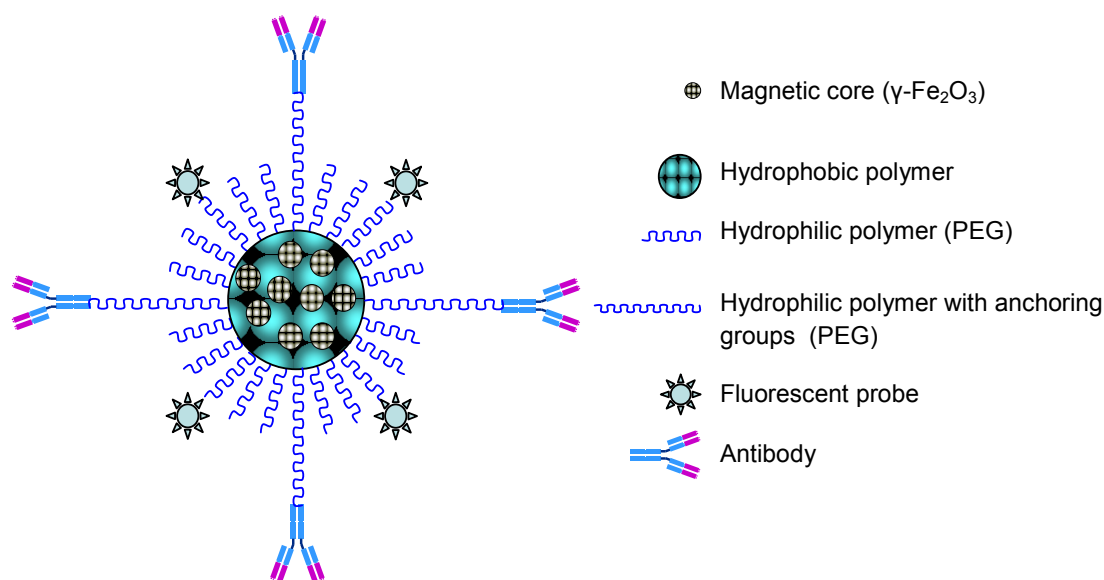
Scheme of core-shell multifunctional nanoplatform containing magnetic nanoparticles

Breakdown of Ising-like behavior of ferromagnetic nano-islands in artificial spin-ice structures driven by asymmetric dipolar interactions

J.M.Porro[(1)], M.Grimsditch[(1)(2)], V.Metlushko[(3)], A.Berger[(1)], P.Vavassori[(1) (4)]

[(1)] *CIC nanoGUNE Consolider, Tolosa Hiribidea 76, E-20018, Donostia-San Sebastián*
[(2)] *Materials Science Division, Argonne Natl. Lab., 9700 South Cass Ave., Argonne, IL 60439*
[(3)] *Department of Electrical and Computer Engineering,University of Illinois at Chicago,Chicago IL 60607*
[(4)] *Ikerbasque, Basque Science Foundation, E-48011, Bilbao*

t.porro@nanogune.eu

Systems governed by competing interactions producing frustration phenomena are being intensively investigated since their study can lead to an improved understanding of the basic physics of disordered states of matter. In general, disordered states are so overwhelmingly complicated that they do not yield a clear picture at the microscopic scale of the forces that lead to frustration. Arrays of lithographically fabricated interacting nano-scale single-domain magnets arranged to produce frustration, the so-called artificial spin-ice structures, have been used to construct particularly simple model systems for the investigation of fundamental physics aspects related to frustration [1]. Understanding the interactions between closely spaced nano-magnets is also crucial for present and future applications such as, ultrahigh density memories for data storage applications and magnetic quantum-dot cellular automata, which are networks of dipole-coupled nano-magnets designed for digital computation [2].

In artificial spin-ice systems, ferromagnetic nano-islands are assumed to behave like single dipoles showing Ising-like properties; i.e., a bi-stable magnetization reversal behavior. Such behavior is normally ensured via shape anisotropy of each island (the self-energy of the island's magnetic moment, which is controlled by its shape), which is used to force the magnetic moment to align along its long axis. This assumption neglects crucial aspects of the physics involved: the dipolar field coupling between adjacent islands is not uniform over the whole island and it might not be spatially symmetric.

We show in this study that the non uniform distribution of the dipolar interaction field can induce formation of non-uniform magnetization distributions during system remagnetization even in magnetic nano-islands that are stable in the single-domain state when isolated, thus leading to a breakdown of the basic assumption of Ising-like behavior. This is shown in Figs. 1, 2 and 3 that display magnetic force microscopy images of the remnant magnetic state, after saturation in a magnetic field H applied as indicated, of chiral artificial spin-ice structures made of elongated Permalloy (FeNi 20/80 alloy) ferromagnetic nano-islands of different aspect ratios, fabricated by electron-beam lithography. Despite of the high aspect ratio, viz., shape anisotropy, non-uniform magnetization vortex states are observed in some of the nano-islands. We demonstrate that the observed breakdown of the expected Ising-like behavior that leads to the nucleation of vortex states of well defined chirality is determined by the interplay between competing asymmetric dipolar interactions and magnetization dynamics of the individual nano-elements.

From a different point of view, our study demonstrates that localized magnetic field sources can be used to actively induce and finely control the magnetization states and reversal paths of nano-magnets, and that such localized field sources can be easily facilitated within the appropriate array structure.

References

[1] R. F. Wang et al., Nature 439, 303 (2006)
[2] A.Imre et al., Science 311, 205(2006)

Figures

Fig.1: AFM topography image (center) of a checkerboard array of ferromagnetic nanoislands arranged in square units with vertical and horizontal bars of 700nm length (AR=4) flanked by micromagnetic simulations and MFM images of single-domain (right) and multidomain (vortex) (left) magnetization states on the vertical nanoislands.
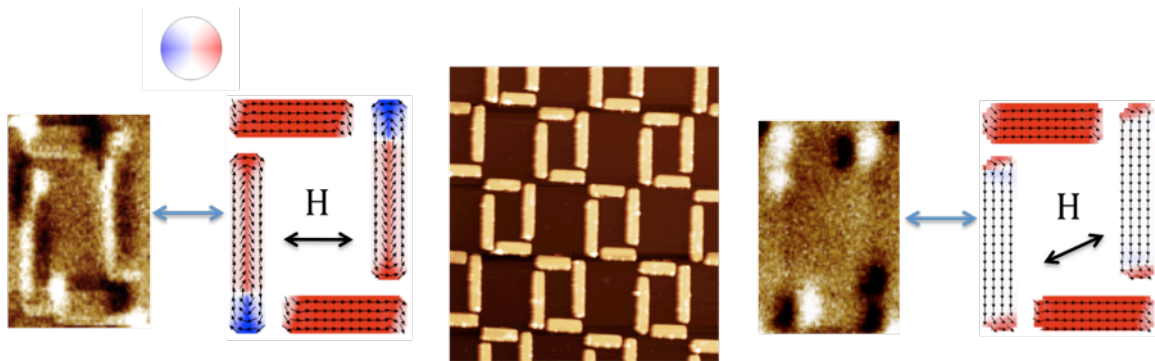
Fig.2: AFM topography image (center) of a checkerboard array of ferromagnetic nanoislands arranged in rectangular units with vertical bars of $1\mu m$ length (AR=6) and horizontal bars of 700nm length (AR=4), flanked by micromagnetic simulations and MFM images of single-domain (right) and multidomain (vortex) (left) magnetization states on the vertical nanoislands.
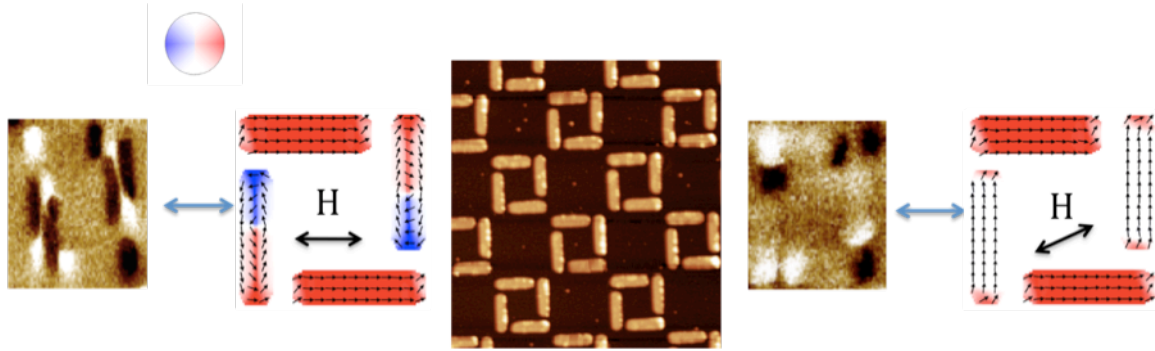

Fig.3: AFM topography image (center) of a checkerboard array of ferromagnetic nanoislands arranged in rectangular units with vertical bars of $1.4\mu m$ length (AR=8) and horizontal bars of 700nm length (AR=4), flanked by micromagnetic simulations and MFM images of single-domain (right) and multidomain (vortex) (left) magnetization states on the vertical nanoislands.
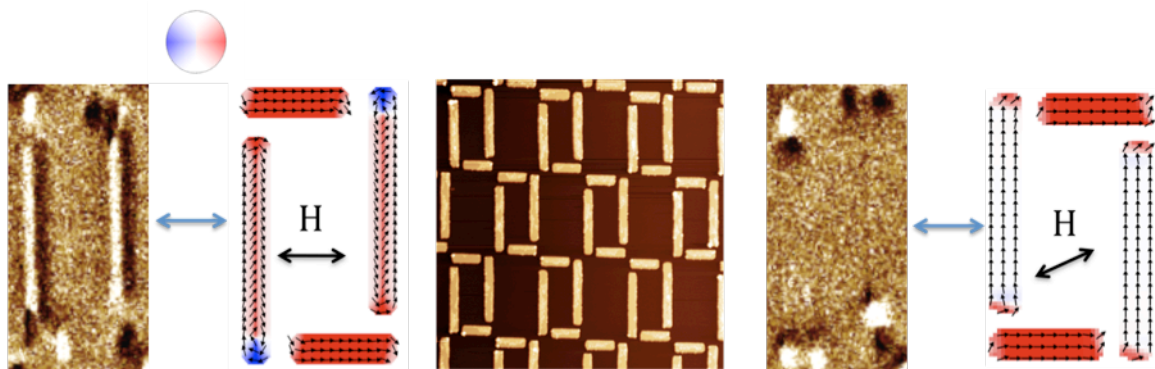
Impact of the polycrystallization of high-k dielectrics on the nanoscale and device level electrical properties of MOS capacitors

V. Iglesias, A. Bayerl, M. Lanza, M.Porti, M.Nafria, X.Aymerich

Dept. Eng. Electrònica, Edifici Q, Campus UAB, 08193 Bellaterra, Barcelona, Spain
vanessa.iglesias@uab.es

High-k dielectrics have been introduced in MOS devices to reduce gate leakage currents [1]. However, their crystallization [2] can affect the electrical properties and reliability of scaled devices [3]. In this work, a Conductive Atomic Force Microscope (CAFM) [4-5] has been combined with standard electrical characterization techniques at wafer level to investigate how the polycrystallization of a high-k layer affects its nanoscale morphological and electrical properties [6] and how such nanoscale properties affect the electrical characteristics of fully processed devices.

When CAFM works on bare (dielectric) surfaces, the conductive tip of the microscope plays the role of the metal gate of a MOS capacitor with an area that is the contact area between the tip and the sample (~100 nm²), so that a nanometer resolution can be achieved. Using this technique, the impact of the polycrystallization after thermal annealing on the nanoscale properties of high-k dielectrics was studied, first, on 5nm thick polycrystalline HfO_2 films. Fig. 1 shows a (a) topographical and (b) current image obtained with the CAFM at 6.5V. Note that a granular structure can be distinguished in (a), which has been attributed to the polycrystallization of the high-k layer: grains in the image correspond to individual randomly oriented nanocrystals separated by grain boundaries (GBs, depressions in the image). The high-k polycrystallization effect on its electrical properties was investigated from the current image (Fig.1.b). In this image, brighter areas correspond to larger currents. A granular current pattern which overlaps with that of the topographical image is observed: leaky sites and breakdown spots are mainly located at GBs. Therefore, these results show that polycrystallization of the HfO_2 layer affects, not only the morphological, but also the electrical properties of the gate stack, increasing the leakage current and the inhomogeneity of its conductivity. Amorphous layers do not show any pattern, neither on topography nor on current, which suggests larger nanoscale homogeneity of the film.

The impact of the nanoscale device inhomogeneities on the global electrical characteristics of MOS devices has been analyzed from I-V characteristics measured on fully processed MOS devices (i.e., with metal gate electrode). Fig. 2 shows I-V curves obtained on MOS capacitors based on an amorphous (squares) and polycrystalline (triangles) 3nm thick HfO_2 layer as gate dielectric. The I-V curve in circles corresponds to a typical post-BD characteristic. Note that two clear different behaviours can be identified. In the amorphous structures (squares), before BD, the I-V curves follow a Fowler-Norheim behaviour with a very small dispersion between samples. However, in polycrystalline samples (triangles), at low fields, the gate conduction is larger than in amorphous gate dielectrics, with a very erratic and non-stable behaviour, suggesting different conduction modes, which can change from sample to sample. At high fields, current increases even more, showing the typical post-BD behaviour. The higher pre-BD currents observed in polycrystalline gate stacks could be related to the gate current that flows through the GBs, which have been shown to be more conductive (Fig. 1).

The impact of an electrical stress on the electrical conduction and charge trapping of amorphous and polycrystalline 10 nm Al_2O_3 layers has been also investigated from the measurement of sequences of current images on the same area. Figure 3 shows sequences of three images measured on the amorphous (a-c) and polycrystalline (d-f) Al_2O_3 layer. First a 500x500nm² area (a and d) was scanned by applying a large enough constant voltage to induce degradation. Afterwards two zooms out were done, and larger areas which include the previously scanned smaller regions where imaged. A quantitative analysis of Fig. 3 demonstrates that, although crystals (in polycrystalline structures) are more resistive and less weak (from an electrical point of view) than amorphous oxides, the GBs in the polycrystalline samples seem to be more sensitive to an electrical stress than non-crystallized structures: GBs would favor a faster generation of defects leading to charge trapping. These results suggest that the presence of GBs in polycrystalline structures strongly contributes to the inhomogeneity increase of the conduction and trapping properties of the stacks.

To conclude, the results show that polycrystallization of high-k dielectrics affects the homogeneity of their nanoscale properties (surface morphology and conductivity), which has a clear impact on the global electrical properties of MOS devices, since a larger sample-to-sample variability is measured.

Moreover, the presence of grain boundaries on polycrystalline dielectrics could also reduce significantly the reliability of MOS devices due to their lower robustness.

References

[1] J. Robertson. Reports on Progress in Physics, 69 (2006), pp. 327-396.
[2] V. Yanev et al, Applied Physics Letters, 92 (2008), pp. 252910.
[3] A. Asenov, IEEE Symposium on VLSI Technology, 2007, pp. 86-87.
[4] W. Frammelsberger et al., Applied Surface Science, 252 (2006), pp. 2375-2388.
[5] YL. Wu et. al., IEEE Transactions on Device and Materials Reliability, 8 (2008), pp. 352-357.
[6] M. Lanza et al., IEEE Trans. on Nanotech. (online published), 2010.

Figures

Fig. 1
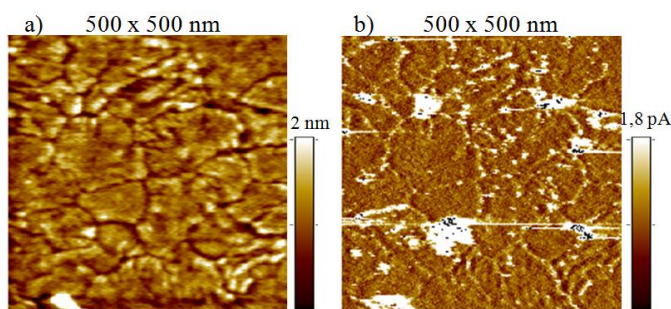
Fig. 2
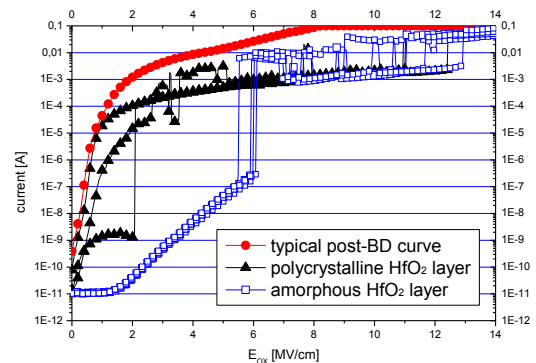
Fig. 3
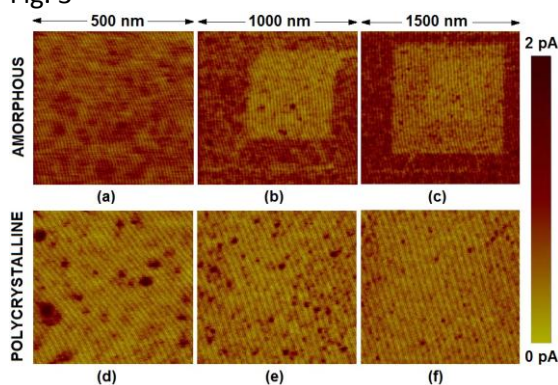
Figure caption

Fig.1. (a) Topographical and (b) current images obtained at 6.5V in a polycrystalline HfO_2 layer (5nm thick). In (a), depressions can be related to grain boundaries between nanocrystals. In (b), brighter areas are concentrated at grain boundaries.

Fig.2. Sets of IV curves obtained at device level on MOS capacitors (area 3µm x 3µm) based on HfO_2 as gate dielectric. Squares/triangles were obtained on fresh structures with an amorphous/polycrystalline HfO_2 layer. Circles correspond to a typical post-BD I-V curve, as reference.

Fig.3. First scans (a and d) and two consecutive zooms out (b/e and c/f) obtained on an amorphous (a, b and c) and polycrystalline (d, e and f) Al_2O_3 layer. Their sizes are (a and d) 500 nm x 500 nm, (b and e) 1µm x 1µm and (c and f) 1,5 µm x 1,5 µm. The applied voltage was 11.5 V in all cases.

Size and surface effects on the magnetic properties of NiO nanoparticles

Mariana P. Proença[a,b], Célia T. Sousa[a], André M. Pereira[a], Pedro B. Tavares[c], João Ventura[a], Manuel Vázquez[b], João P. Araújo[a]

[a] IFIMUP and IN – Institute of Nanoscience and Nanotechnology and Dep. Física e Astronomia, Univ. Porto, Rua do Campo Alegre 687, 4169-007 Porto, Portugal
[b] Instituto de Ciencias Materiales de Madrid, CSIC, 28049 Madrid, Spain
[c] Dep. Química e CQ-VR, Univ. Trás-os-Montes e Alto Douro, 5001-801 Vila Real, Portugal
mippro@gmail.com

NiO nanoparticles (NPs) were prepared by a sol-gel process using the citrate route. The sol-gel parameters were tuned to obtain samples with different average particle sizes, ranging from 12 to 70 nm. Magnetic characterization revealed an increase in the blocking temperature with the diameter of the NPs and an increase in the effective magnetic anisotropy (K_{eff}) with decreasing particle size [1]. The magnetic moment per particle was calculated for all samples using the susceptibility value at T=300 K. The number of uncompensated spins per NP was found to be proportional to $n_S^{1/3}$ (n_S = total number of spins), indicating that they are randomly distributed on the NP surface [2]. For small diameters (<30 nm) the surface anisotropy constant was estimated, using, for NiO NPs, a recent model describing the evolution of K_{eff} with particle size [3]. Hysteretic loops performed at low temperatures after field cooling displayed loop shifts (~6.5 kOe in the field axis and ~0.18 emu g^{-1} vertically), coercive field enhancement (H_C~4.8 kOe) and training effects for the smaller NPs. The sample with NPs of larger diameters presented magnetic properties close to those of bulk NiO.

References

[1] M. P. Proenca, C. T. Sousa, A. M. Pereira, P. B. Tavares, J. Ventura, M. Vazquez and J. P. Araujo, *submitted*.
[2] L. Neel, Compt. Rend., **252** (1961) 4075.
[3] D. Tobia, E. De Biasi, M. Granada, H. E. Troiani, G. Zampieri, E. Winckler and R. D. Zysler, J. Appl. Phys., **108** (2010) 104303.

Figures
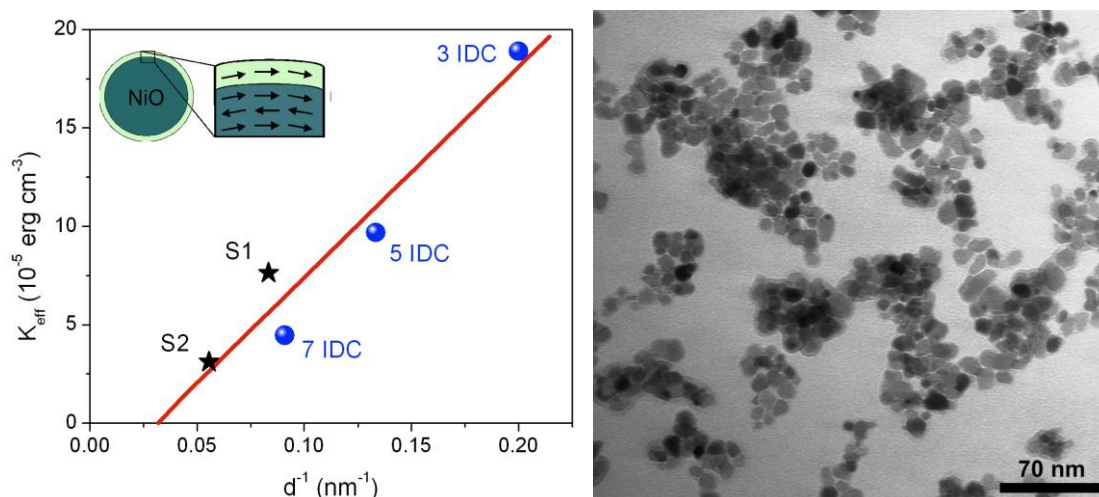
On the left: Variation of the effective magnetic anisotropy with the inverse diameter of small NiO nanoparticles. Inset scheme illustrates the NiO nanoparticle formed by a shell of uncompensated spins with ferromagnetic correlations and an antiferromagnetic core. On the right: TEM image of NiO nanoparticles.

Local semiconducting transition in armchair carbon nanotubes

M.J. Hashemi, K. Sääskilahti, and **M.J. Puska**

Department of Applied Physics, Aalto University, B.O.Box 11100, FI-00076 AALTO, Finland
martti.puska@tkk.fi

Assuming the possibility of chirality-sensitive selection of single wall carbon nanotubes (SWCNT) the next step towards single-SWCNT nanoelectronic devices is the creation of rectifying metal-semiconductor junctions. Occasionally, this kind of junctions are realized due to pentagon-heptagon defects making a seamless junction between nanotubes of different chiralities [1] Another route could be to modify the electronic bandstructure of a single SWCNT spatially by functionalization with defects, adatoms, or molecules. [2,3] We have studied recently how periodic bi-site perturbations on the metallic armchair SWCN turn them locally semiconducting. [4]

We have performed bandstructure and electronic transport calculations within the density functional theory (DFT) implemented in SIESTA [5] and Transiesta [6] programs and within the basic tight-binding method for an armchair SWCNT with periodically adsorbed hydrogen clusters (Figure 1). Figure 2 shows that for infinitely repeated clusters a bandgap opens when the distances $\vec{R}$ between adjacent bi-site perturbations fulfill the condition

$$\vec{R} = p\vec{a} + q\vec{b}, \qquad p - q = 3M, \qquad M \in Z,$$

where $\vec{a}$ and $\vec{b}$ are unit vectors given in Figure 1. Figure 3 shows how the electron transmission coefficient for $M = 6$ ($M = 5$) decays (saturates to the ideal value) at the Fermi level as the length (N) of the periodically decorated section of the armchair SWCNT increases. The opening of the band gap and the decay of the transmission can be understood as the result of the folding of the band intersection point to the Γ point with periodic perturbations or as the constructive interference of backscattered electrons when the distance between the perturbations along the tube axis is a multiple of half of the Fermi wavelength.

We have studied also the robustness of the band gap opening against variations in the types and positions of perturbing cluster species. The gap opening phenomenon is proposed as a means for creating single-SWCNT electronic devices.

References

[1] Z. Yao, H.W.C. Postma, L. Balents, and C. Dekker, Nature, **402** (1999) 273.
[2] O. Gülseren, T. Yildirim, and S, Ciraci, Phys. Rev. B, **68** (2003) 115419.
[3] A. Wall, and M.S. Ferreira, J. Phys.: Condens. Matter, **19** (2007) 406227.
[4] M.J. Hashemi, K. Sääskilahti, and M.J. Puska, Phys. Rev. B in print, cond-mat 1101.0519.
[5] J.M. Soler, E. Artacho, J.D. Gale, A. García, J. Junquera, P. Ordejón, and D. Sánchez-Portal, J. Phys.: Condens. Matter, **14** (2002) 2745.
[6] M. Brandbyge, J.-L. Mozos, P. Ordejón, J. Taylor, and K. Stokbro, Phys. Rev. B, **65** (2002) 165401.
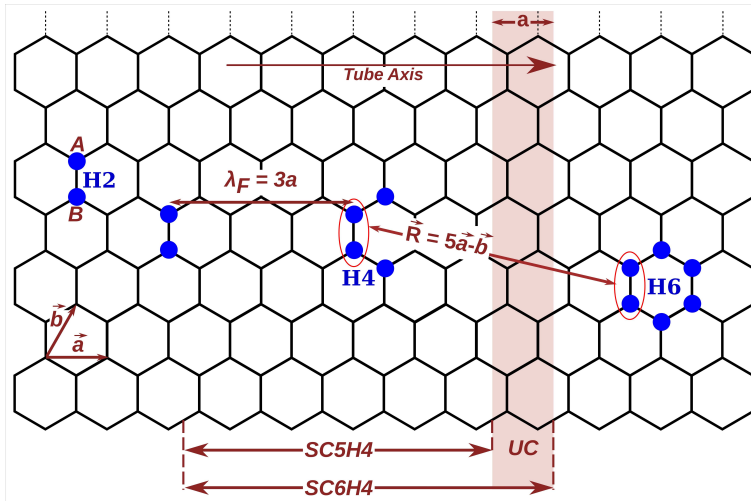
Figure 1. Hydrogen clusters H2, H4, and H6 on an (8,8) armchair SWCNT. The unit cell UC of the pristine tube and the supercells SC5H4 and SC6H4 are defined.
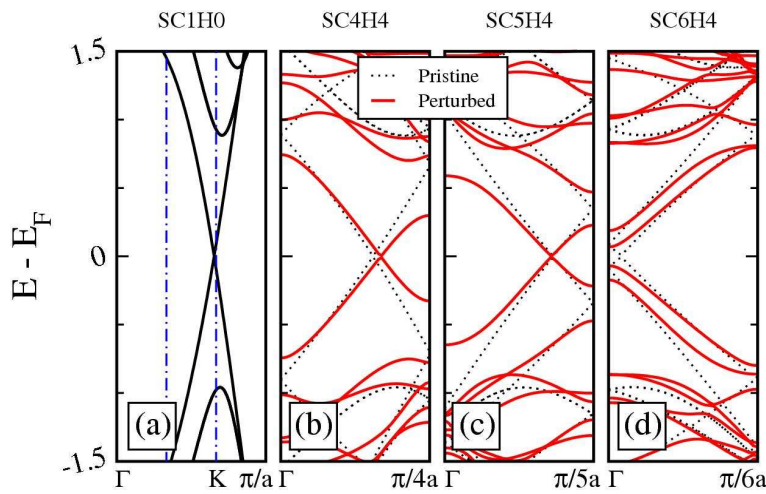
Figure 2. Bandstructures of a pristine armchair SWCNT (SC1H0) and tubes with periodically adsorbed hydrogen clusters (SC4H4, SC5H4, SC6H4).
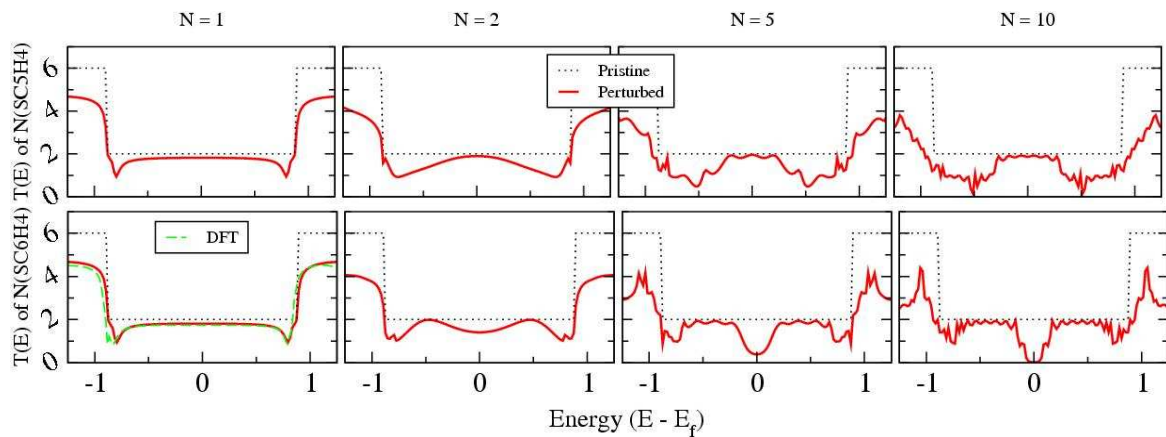
Figure 3. Transmission coefficient of an armchair SWCNT containing a section periodically decorated with H4 clusters. The upper and lower panels correspond to the SC5H4 and SC6H4 supercells, respectively. The length of the decorated section increases from one (N=1) to ten (N=10) supercells.

Nano Grinding in Stirred Media Mills

NETZSCH

Real Grinding

Fused corundum
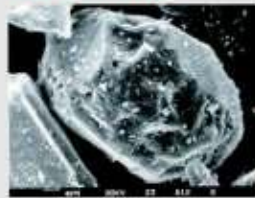
SEM Image before grinding
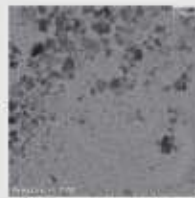
TEM Image after grinding

$$E_m \propto SN \cdot SE_{GM}$$

$$SE_{GM} \propto d_{GM}^3 \cdot \rho_{GM} \cdot v_t^2$$

YTZ 0.3 mm
Zirconox 0.7 - 1.2 mm

YTZ 2 mm
Zirconox 0.4 - 0.7 mm

Coarse disperse particles

Operating parameter
Grinding media size, Density of the grinding media, Stirrer tip speed

Stress energy
Stress number

Dispersion & Grinding media wear

Continuous phase
pH-value
Concentration of electrolyte, surfactants and dispersing agents

Particle size distribution
State of agglomeration

Disperse phase
Surface charge
Morphology
Solid concentration

Viscosity
Conductivity

ζ-potential

Formulation Stabilization

Influence of the grinding media size and the stirrer tip speed

GM: $ZrO_2(Y_2O_3)$
$v_t = 12$ m/s
$c_m = 0.2$
pH 5

- $d_{GM} = 1.3$ mm
- $d_{GM} = 1.1$ mm
- $d_{GM} = 0.8$ mm
- $d_{GM} = 0.5$ mm
- $d_{GM} = 0.4$ mm
- $d_{GM} = 0.2$ mm

$c_m = 0.2$
pH 5

1×10^3 kJ/kg
2×10^3 kJ/kg
5×10^3 kJ/kg
10×10^3 kJ/kg
20×10^3 kJ/kg

GM: $ZrO_2(Y_2O_3)$
$d_{GM} = 100$-1300 μm
$v_t = 6$-15 m/s
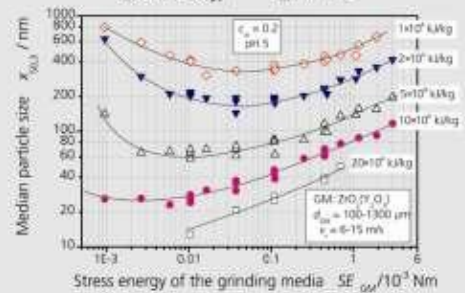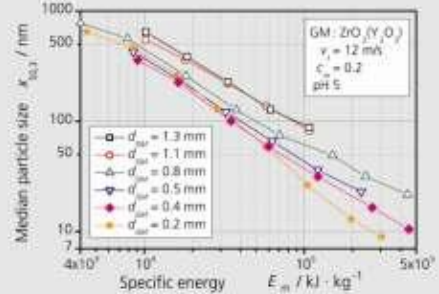
ZETA® RS

This mill is specially designed for real grinding and mild dispersion down to the nanometer size range

Type	Zeta® RS 2	Zeta® RS 4	Zeta® RS 10	Zeta® RS 25
Drive power [kW]	7.5	15	25	45
Speed [min-1]	400 - 3300	350 - 2500	300 - 2000	250 - 1500
Batch sizes [l]	10 - 50	20 - 200	100 - 1000	500 - 2000
Grinding chamber volume [l]	2	4	10	25
Grinding media diameter [μm]	50 - 300			

PE agitator shaft

- The Zeta® RS can alternatively be driven with rotating screen or ODC (Open Dynamic Classifier) system.
- The Zeta® RS is available in steel, ZrO_2, SiC / Si_3N_4, PU.

Zeta® RS 2

filling

operation

emptying

Zeta® RS 10
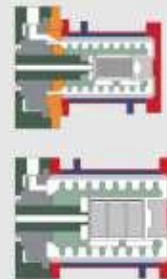
Easy handling by swiveling grinding tank

ZrO_2 agitator shaft

Mild Dispersion

Dispersion of TiO_2 particles for photo catalysts with very good dispersion progress

Change from a crystalline to an amorphous structure

Therefore, smooth conditions are necessary

Operation mode: circulation
Product batch: 3 liter
Primary particle size: 6 nm

GM: $ZrO_2(Y_2O_3)$
$\rho_{GM} = 0.9$
$d_{GM} = 0.1$ mm
$c_m = 0.05$

- = 4 m/s
- = 6 m/s
- = 10 m/s
- = 13 m/s

X-ray diffraction (XRD)
TiO_2-dispersion
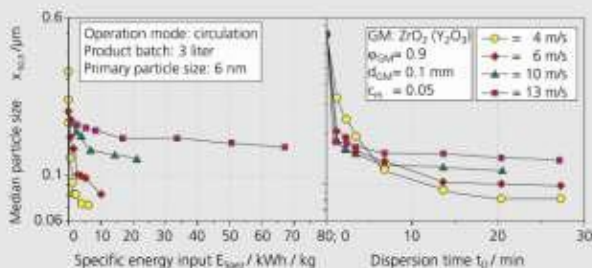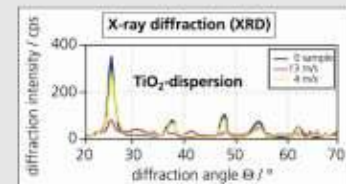
High stirrer tip speed

Small stirrer tip speed

$\sqrt{7} \times \sqrt{3}$ Indium on Si(111): one or two indium layers?

S. Rigamonti[1], A. Arnau[1], T. Nagao[2] and D. Sánchez-Portal[1]

[1]Donostia International Physics Center (DIPC) and Centro-Mixto CSIC-UPV/EHU, San Sebastián, Spain
[2]National Institute for Materials Science, Tsukuba, Japan
santiago_rigamonti@ehu.es

Indium self-assembled overlayers on Si(111) are among the most studied metal-semiconductor surface nano-structures: A tremendously rich and complex structural phase diagram with more than 10 different overlayer reconstructions for up to two In monolayers (ML), as well as a wealth of structural and electronic phase transitions (e.g. the temperature driven $8 \times 2 \Leftrightarrow 4 \times 1$, the deposition driven $\sqrt{3} \times \sqrt{3} \Leftrightarrow 2 \times 2 \Leftrightarrow \sqrt{7} \times \sqrt{3}$, the field induced $\sqrt{3} \times \sqrt{3} \Leftrightarrow 2 \times 2$)[1], have rised great interest in these surfaces.

At around one monolayer (ML) coverage, a commonly observed structure is the $\sqrt{7} \times \sqrt{3}$ reconstruction. This structure has been the subject of many experimental studies[2-5] that shed light on some fascinating structural and electronic properties, e.g., a Fermi surface strikingly close to the ideal two dimensional (2D) electron gas [4] or the recent discovery of superconductivity in this extreme 2D metal [5].

In spite of the accumulated experimental data, no general consensus has been reached to date on the number of In layers comprising the $\sqrt{7} \times \sqrt{3}$ nanostructure. Some experiments point to a single In overlayer model (SL), with In atoms arranged in a quasi-rectangular (-rec) or quasi-hexagonal (-hex) fashion with coverages of 1.2ML and 1.0ML respectively [2], while others support a double-layer (DL) model instead, with 2~3ML coverage [3]. Nonetheless, a precise determination of the overlayer structure at the atomic scale is the prerequisite for understanding its phenomenology.

In this contribution, we report ab-initio density functional theory (DFT) calculations for different In/Si(111) reconstructions (some of them shown in Fig. 1).[6] Our calculations were performed with the SIESTA code[7] within the local density approximation. We show that the Fermi surface (FS) and band-structure calculated for the SL-rec model of Kraft et al.[2] disagree with the experiments in Ref.[4]. We propose a DL structural model with 2.4ML coverage and find excelent agreement with experiments. For both the SL and the DL models the charge transfer from Si dangling bonds to the two dimensional gas is found to be negligible. We also show that the In-In interaction dominates over In-Si bonding.

References

[1] C. Kumpf et al., Phys. Rev. Lett **85** (2000) 4916; A. Saranin, Surf. Sci. **388** (1997) 299; A. A. Saranin, et al., Phys. Rev. B **56** (1997) 7449.

[2] J. Kraft, M. G. Ramsey, and F. P. Netzer, Physical Review B **55** (1997) 5384; S.W.Cho, et al., Physical Review B **67** (2003) 035414; A. A. Saranin, et al., Physical Review B **74** (2006) 035436.

[3] S. Takeda, et al., Surface Science **415** (1998) 264; A. Pavlovska, E. Bauer, and M. Giessen, J. Vac. Sci. Technol. B **20** (2002) 2478.

[4] E. Rotenberg, et al, Physical Review Letters **91** (2003) 246404.

[5] Tong Zhang et al., Nature Physics **6** (2010) 104.

[6] S. Rigamonti, A. Arnau, T. Nagao and D. Sánchez-Portal, unpublished.

[7] J.M. Soler et al., J. Phys.: Condens. Matter **14** (2002) 2745-2779.
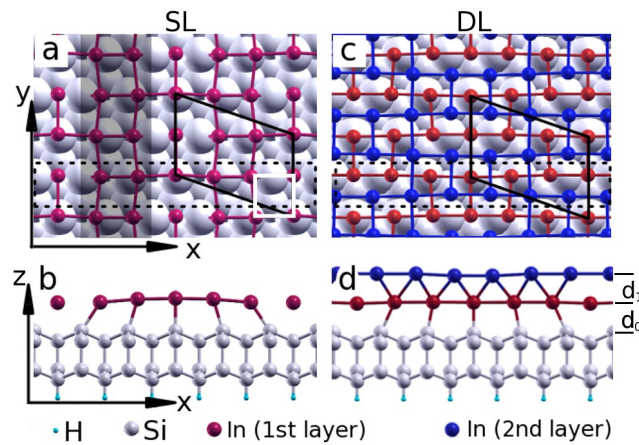
Figures

Figure 1: Left*: SL-rec model. **Right**: DL-rec model. **a** and **c**: top views, **b** and **d**: side views of the structures.*

Single dopant and single electron effects in CMOS devices

Benoît Roche[1], Benoît Voisin[1], Romain Wacquez[2], Mathieu Pierre[1], Xavier Jehl[1], Maud Vinet[2], Marc Sanquer[1]

[1] CEA INAC, 17 rue des Martyrs, 38054 Grenoble Cedex 9, France
[2] CEA LETI, 17 rue des Martyrs, 38054 Grenoble Cedex 9, France
marc.sanquer@cea.fr

For the first time a state-of-the-art CMOS foundry (CEA-LETI-MINATEC) has been used to design silicon nanostructures with single or multiple gates dedicated to the study of single electron effects. The nanofabrication uses two e-beam lithography steps to define an active region formed by silicon-on-insulator (SOI) nanowires of cross section down to 20 nm×10 nm and polysilicon gates of lengths down to 20 nm. The pitch at the gate level (distance between centers of the successive gates) is as small as 70 nm. Several technological splits (SOI thickness, channel doping, LDD doping, nitride spacer's length, trimming of active layer) have been made to compare devices differing only by one crucial parameter. Several dozen of designs have been introduced in the e-beam database to analyse the impact of key geometrical parameters. As a whole few 10,000 samples have been fabricated and several hundreds of them have been studied electrically, mostly at low temperature. Some of them are described in this contribution which focuses i) on ultra scaled Ultra-thin SOI nanowire MOSFET ii) on controlled MOS-SET.

Single dopant effects in UT SOI MOSFET [1, 6]

We have fabricated nanoscale n-type SOI MOSFET with an effective gate length down to 10 nm (see figure 1, right panel). For that dimension current below the threshold can be dominated by transport through a single isolated dopant orbital, which has diffused from source and drain [1]. In that case we show that up to room temperature transport below the threshold is dominated by thermally broadened resonant tunneling via this single dopant coupled to a source and a drain.
We show that the ionization of such a single isolated dopant is strongly affected by its dielectric environment [6], namely the proximity of the BOX of our SOI wafer. This "so-called dielectric confinement" effect was predicted a few years ago [4] and can be a source of large dispersion of dopants ionization energies. This dispersion induces a large sub-threshold variability for ultra scaled FETs. Performing low temperature transport spectroscopy, we are able to detect the filling of the first dopant (see figure 1, left panel). The gate voltage where this occurs is a direct measure of the ionization energy of this dopant. Compared to the bulk case (54meV) we find a strongly enhanced value (up to 108 meV) for a dopant close to the buried oxide. By applying a substrate bias we have a new way to control the sub-threshold SD tunnelling rates thru this buried donor.

Controlled MOS-SETs [2, 3]
By using self aligned spacers and a so-called underlap Source-Gate geometry it is possible to fabricate controlled MOS-SET [2]. We have extended this well controlled technique to fabricate two dots in series are created below two top gates overlapping a silicon nanowire (see figure 2, right panel). The coupling between dots is controlled by gate voltages.

References

[1] M. Pierre, R. Wacquez, X. Jehl, M. Sanquer, M. Vinet and O. Cueto, Nature Nanotechnology, **5** (2009) 133.
[2] M. Hofheinz, X. Jehl, M. Sanquer, G. Molas, M. Vinet and S. Deleonibus, Applied Physics Letters, **89** (2006) 143504.
[3] M. Pierre, R. Wacquez, B. Roche, X. Jehl, M. Sanquer, M. Vinet, E. Prati, M. Belli, and M. Fanciulli, Applied Physics Letters, **95** (2009) 242107.
[4] Diarra, M. and al, Phys. Rev. B, **75** (2007) 045301.
[5] S. J. Shin, C. S. Jeong, B. J. Park, T. K. Yoon, J. J. Lee, S. J. Kim, J. B. Choi, Y. Takahashi and D. G. Hasko, Applied Physics Letters, **97** (2010) 103101.
[6] R Wacquez, M. Vinet and al., IEEE VLSI Symp. Tech. Dig. (2010) 193–194.

Figures
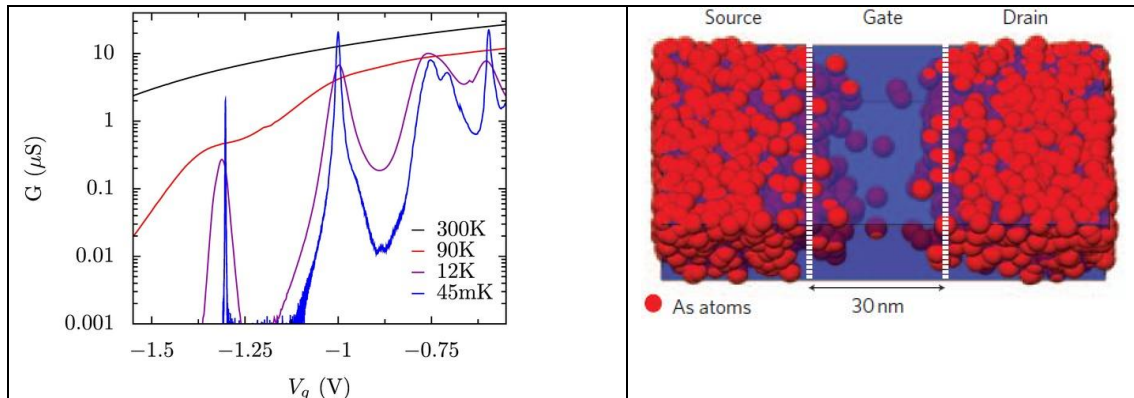
Figure 1
Left panel: Source –drain conductance versus gate voltage for a L*W*Ts$_i$ = 10*50*20 nm^3 at different temperature. The first sharp resonance around Vg = -1.27 V is due to resonant tunnelling through the As+ ➔ As0 transition when the electronic ground state of the first As donor is aligned with the Fermi level in the source (and drain). The associated ionization energy is 108 meV. The resonating donor is centred in the channel but close to the BOX. The second resonance near Vg=-1.0 V is due to a second distinct As donor. The associated ionization energy is 50 meV. The donor is centred in the channel but closer to the gate. The third resonance is due to the double occupation of the second donor, as explained in ref. [1]. Resonance at larger gate voltage are close or above to the threshold voltage which is -0.5V.
Right panel: Process simulation of a typical random arrangement of the As donors in the studied device.
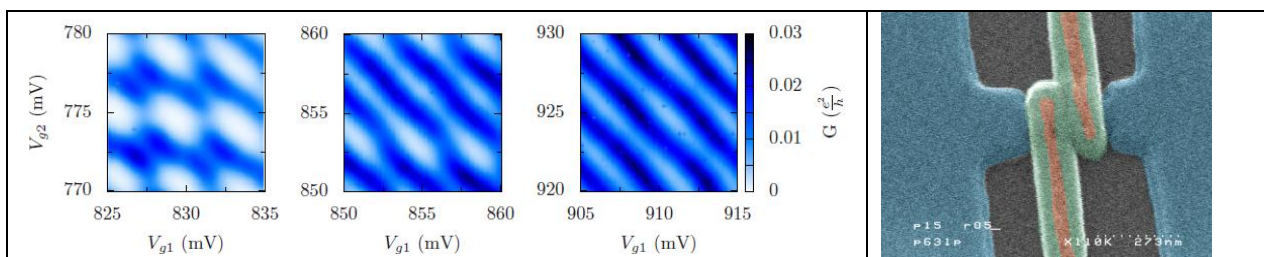
Figure 2
Left panel: The source-drain conductance in quantum units as function of the two gate voltages. The data are recorded at T=1K. For this sample the gate length is 60nm, the spacing between gates is 40nm and the nitride spacers are 40 nm thick. The SOI cross section is 20nm×60nm. At low gate voltage (left panel) the two MOS-SET below the gates are capacitively coupled. The pattern exhibits a typical honeycomb structure. At large gate voltage (right panel) the two MOS-SETs are tunnel coupled by the accumulation channel created in the central region: the two MOS-SETs merge as a single island and an anti diagonal pattern appears. The central panel describes an intermediate situation (from ref. [3]).
Right panel: coloured SEM view of the sample (SOI in blue, PolySiGate in red and SiN spacers in green).

276

Supercritical antisolvent (sas) co-precipitation of ethyl cellulose and rosemary essential oil in SC-CO$_2$

Pocheville, A., Garay, I., Hernando, I.

Gaiker Technology Centre, Parque Tecnológico Edif. 202, 48170, Zamudio, Spain
pocheville@gaiker.es

Essential oils, which are widely known for their antimicrobial, antifungal and/or antioxidant properties, are aromatic, volatile and labile liquids obtained from plants or vegetables. The food industry is considering consumers claim for substitution of chemical additives (preservatives, antioxidants or flavours) with natural extracts/essential oils in food products and packaging coatings [1]. Because of essential oils instability, a great researching effort is being made for improving their thermal and chemical stability and for facilitating their handling when processing. Looking for solutions, different ways of microencapsulation have been described [2], but the impregnation of these compounds in polymeric matrices is another way of incorporating these active compounds in packaging devices.

The objective of this work has been the co-precipitation of the coating material *Ethyl Cellulose (EC)* and the active compound *Rosemary Essential Oil (RO)* using the Supercritical Antisolvent (SAS) precipitation technique with supercritical carbon dioxide (SC-CO$_2$), in order to obtain active microparticles. EC is a hydrophobic material used in different fields such as medicine, cosmetics, food products and pharmacology. It has been widely used for controlled delivery systems, sustained release, tablet drug packaging material, long-acting formulations, taste masking or coatings [2]. RO is characterized for its variety of properties, and it is commonly used in food industry, cosmetics, herbal care, aromatherapy and pharmacology.

Supercritical fluids technology, which is considered a green technology, has been studied for different applications in the last decades. In SAS precipitation, SC-CO$_2$ acts as the antisolvent, so that, when a solution containing the compounds of interest reaches the supercritical medium, the SC-CO$_2$ dissolves the solvent and the compounds of interest co-precipitate in form of microparticles. A supercritical fluid equipment Thar R100 System with a SAS-50 vessel has been used for the co-precipitation of EC and RO, and different parameters have been studied: pressure, EC:RO rate, flow rate (QCO$_2$:Qsolution) or solution concentration. The morphology and size of the obtained precipitates were analyzed by scanning electron microscopy (SEM) and the RO impregnation rate was quantified by extraction and further GC-FID analysis. EC agglomerated microparticles (1-4μm) have been precipitated with a very low RO impregnation rate (%ROimpregnation<0.5%). According to the results, the flow rate (QCO$_2$:Qsolution) is essential for microparticles formation, and particle size increases when a higher Qsolution is used. No noticeable changes in particle size have been observed when increasing operation pressure. Although the obtained RO impregnation rate has been very low, Supercritical Antisolvent (SAS) precipitation using SC-CO$_2$ is an alternative technique for nano-microparticles precipitation or compounds micronization, with application in different fields (e.g: food industry, cosmetics, pharmacology or materials).

References

[1] European Patent Application EP 1 657 181 A1, (2006).
[2] B. Voncina, et al., Textile and Polymer Journal, Vol. 1, No. 1 (2009) 13-19.
[3] Ana Rita C. Duarte, et al., International Journal of Pharmaceutics, 308 (2006) 168-174.

Evaluation of the induction heating of magnetic nanoparticles synthesized by different chemical methods.

C. Rodriguez, P. Bilbao, and J.M. Cuevas
GAIKER Technology Center. Parque Tecnológico, Edificio 202**,**
48170, Zamudio (Spain)
rodriguezc@gaiker.es

Magnetic nanoparticles have already been proved successfully in different biomedical applications (MRI, separation cells, drug delivery…). This work has focused on the development of this kind of particles considering its potential application for hyperthermia.

Several magnetite nanoparticles Fe_3O_4 (**S6,S8, S10**) have been synthesized by two methods of synthesis: the co-precipitation method for the S6 sample and the poliol method for the S8 and S10 samples. Between these last samples, the precursor concentration (iron chloride) was varied.

After the synthesis, these samples were coated with citric acid as dispersant agent (named: **S6-AC**, **S8-AC** and **S10-AC**), for comparing the heating of the particles with and without coating.

It was carried out the evaluation of the size (by transmission electron microscopy), magnetic properties (measured in an electromagnet) and composition (by X-Ray Diffraction) of these magnetic nanoparticles. To study the induction heating of these materials, preliminary tests were done in an industrial equipment. Considering a higher heating capacity of the samples coated with citric acid dispersant, these samples were selected for an accurate study in a specific equipment for hyperthermia.

The particle size was found to be approximately the same for all the samples, between 8 -12 nm. Also, the saturation magnetization values were similar (57-67 emu/g), obtaining values slightly higher for the samples with the citric acid dispersant agent.

The X-Ray diffractograms of the S6-AC and S8-AC samples show identical compositions (magnetite) for both samples. However the S6-AC shows a double heating rate than the corresponding to the S8-AC. Figure 1.

On the other hand, using the same synthesis method but changing the conditions, the particles obtained can be different. This difference is clearly observed in the heating capacity. In the X-Ray diffractogram of the S10-AC sample, in addition to the peaks related to the magnetite, it appears several peaks corresponding to iron metallic nanoparticles. S10-AC particles heat up to 10 times quicker than the S8. Figure 2.

All our particle dispersions have shown capacity to get 70ºC in less than 3 minutes, when heated by exposition to an AC magnetic field with the frequency of 441 kHz.
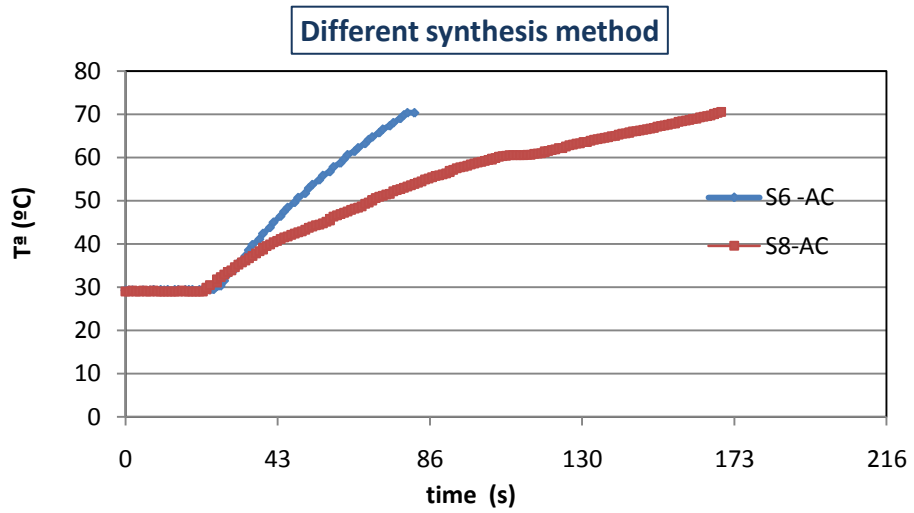
Figure 1. Induction heating for the S6-AC and S8-AC samples.
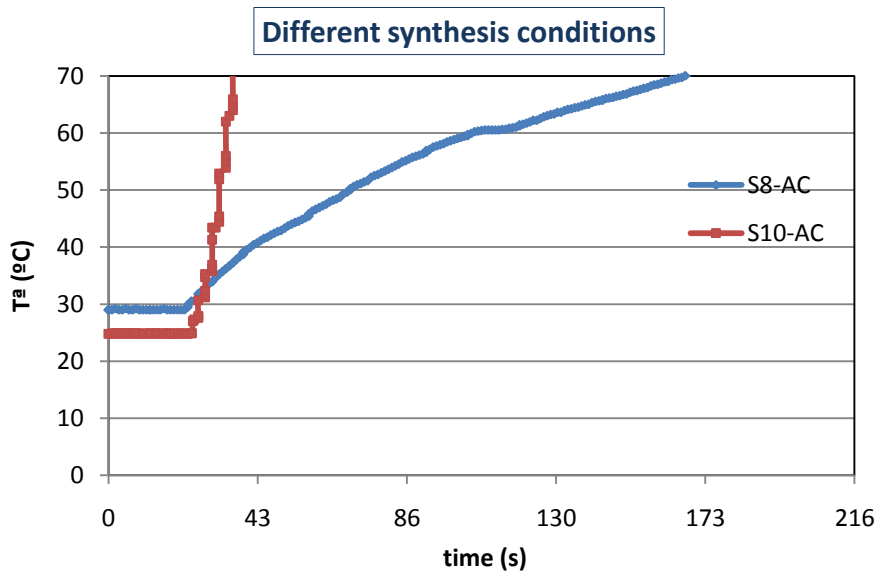
Figure 2. Induction heating for the S8-AC and S10-AC samples.

Control of nanoparticles agglomeration state

J.J. Romero, I. Lorite, A. del Campo, J.F. Fernandez

Instituto de Cerámica y Vidrio, CSIC; C/Kelsen 5, 28049-Madrid, Spain
jjromero@icv.csic.es

Nanoparticles are currently among the most actives field of research due to the novel properties they present. Nevertheless, there are still problems and questions that remain unresolved. One of these problems is the high tendency the particles present to agglomerate on the solid state. Some techniques have been proposed to avoid this agglomeration, but most of them are based on the use of different surfactants, that can modify the nanoparticles properties in an uncontrolled way.

In this work we present a dispersion method, free of surfactants and capping agents, which allow us to obtain isolated nanoparticles or agglomerates of controlled size. The method does not alter the nanoparticles size or properties. The possibility to control the agglomeration of the nanoparticles opens the possibility to study the proximity effects that can exist on these materials.

Producing Highly Aligned Nanofibers by Electrospinning without Whipping Motion

Pavel Kiselev[a], **Joan Rosell-Llompart**[a,b]

[a] Departament d'Enginyeria Quimica, Universitat Rovira i Virgili, Av. Paisos Catalans 26, 43007 Tarragona, Spain
[b] ICREA (Catalan Institution for Research and Advanced Studies), Barcelona, Spain
joan.rosell@urv.cat

Electrospinning is a fast-developing method for production of polymeric and composite nanofibers with diameters ranging from few micro-meters down to tens of nanometers. It is based on applying a high electrostatic potential (typically kilo-volts) on a polymer solution or a polymer melt as it flows out of a nozzle (typically a capillary tube). High charge density on the electrospun jet leads to extensive stretching, which is responsible for such low final diameters, and also believed to be responsible for the unstable trajectory and development of semi-chaotic motion called *whipping instability* (also, bending instability). This work shows how elimination of the whipping motion of electrospinning fibers leads to nearly perfect alignment of fibers.

The whipping motion is eliminated by (i) using more uniform electrical fields (by means of a "back electrode", a planar electrode place slightly upstream of the nozzle) and (ii) by pulling the fiber mechanically by a fast-rotating cylindrical collector. This process is demonstrated for two types of polymeric fibers, solid fibers of poly(ethylene oxide) and porous fibers of polystyrene. They were collected at collector surface speeds ranging from 2 to 15 m/s. Over this range, a transition is observed in the arrangement of the collected fibers: from either non-aligned or wavy fibers at the lower collector speeds, to straight fibers with nearly perfect alignment at an intermediate speed of about 6 m/s (over 95% of the fibers within 1º and 100% within 4º). At the highest collection speeds the electrospun jet developed flailing motion, apparently due to the air turbulence created by the cylinder rotation, which led to worsening of alignment.

The degree of fiber stretching has been quantified as a function of the collector surface speed. A 50% decrease in average diameter was measured for PEO fibers, while in porous PS fibers it decreased by less than 30% for the same change in collection speed.

Figures
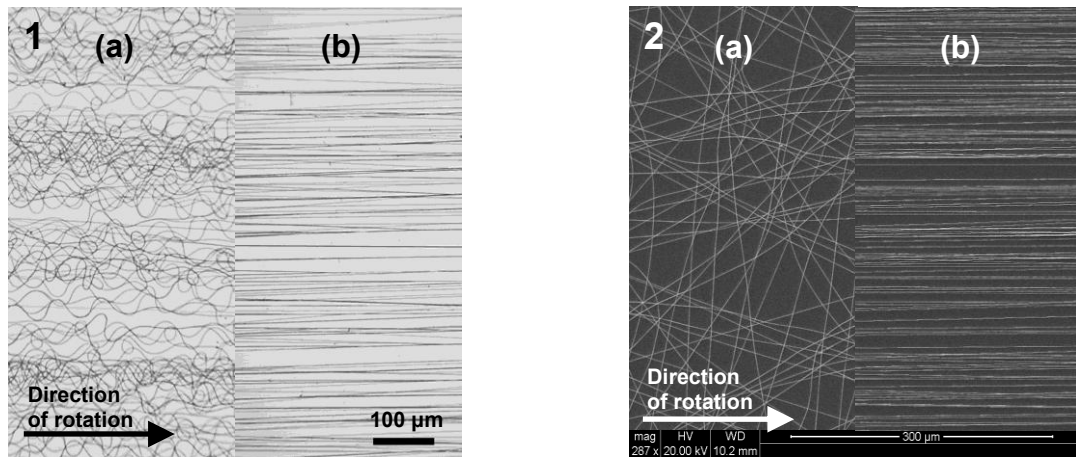
1 – Optical images of PEO fibers collected on 3 cm cylinder at collector surface speeds of (a) 2.07 m/s and (b) 4.71 m/s; 2 – SEM images of PS fibers collected at collector surface speeds of (a) 2.0 m/s and (b) 6.5 m/s

Computing the non-interacting electronic response function using Wannier interpolation: applications to magnons

Bruno Rousseau, Asier Eiguren, Aitor Bergara

Centro de Física de Materiales, Pº Manuel de Lardizabal 5, Donostia - San Sebastián, Spain
Organization, Address, City, Country

rousseau.bruno@gmail.com

Obtaining the non-interacting electronic response function of bulk systems or surfaces is a key step in describing their collective electronic excitations.

Computing this response function from ab initio can be an extremely demanding numerical task because the necessary sum over the first Brillouin zone must be performed on a dense mesh; this is especially true when studying low frequency features.

We propose a novel method for computing the response function which utilizes maximally localized Wannier functions [1,2]. While their construction requires the ab initio eigenvalues and wavefunctions on a relatively coarse reciprocal space "k" mesh, they can be used to interpolate the necessary input to the response calculation on a very dense "k" mesh. The numerical cost of this procedure is but a small fraction of the cost of performing a full non-self consistent ab initio calculation.

In this talk we will also present results when the method is applied to various systems of interest and particularly the computation of magnon dispersions in ferromagnets.

References

[1] Marzari, Nicola and Vanderbilt, David, Phys. Rev. B, **56** (1997) 12847
[2] Souza, Ivo and Marzari, Nicola and Vanderbilt, David, Phys. Rev. B, **65** (2001) 035109

Flexible transparent single-walled carbon nanotube electrodes: applications in electrochromic windows and dye solar cells

Virginia Ruiz[1], G. Cabañero[1], R. Malavé[2], K. Aitola[2], J. Halme[2], E.I. Kauppinen[2], P.D. Lund[2]

[1]Department of New Materials, CIDETEC-IK4, Paseo Miramón 196, 20009 San Sebastián, Spain
[2]Department of Applied Physics, Aalto University, P.O.Box 15100, FI-00076 Aalto, Finland
vruiz@cidetec.es

Single-walled carbon nanotube (SWCNT) networks have emerged as very promising alternative to conventional transparent conducting oxides (TCO) for optically transparent electrodes, exhibiting comparable sheet resistance and optical transmittance but outperforming TCO in terms of mechanical and chemical robustness. Here the advantages of SWCNT films over conventional indium-tin oxide (ITO) on flexible polyethylene terephthalate (PET) as transparent electrodes will be illustrated for applications in two types of electrochemical devices, namely electrochromic windows and dye solar cells (DSC). Apart from their role as transparent conducting layer, the SWCNT film imparts additional functionality in both cases: electrocatalytic properties for the redox couple (as DSC counter electrode) and better resistance to flexure, improved adhesion and higher porosity for the electrochromic layer (in electrochromic films). SWCNTs were synthesized in a laminar flow aerosol reactor by a floating catalyst CVD method using carbon monoxide and ferrocene as carbon source and catalyst precursor respectively. SWCNT films were collected directly from the gas phase downstream of the reactor by filtering through nitrocellulose filters and transferred from the filter to PET by a simple room-temperature dry transfer process [1].

For applications in electrochromic windows, SWCNT-based electrodes act as a high surface area template for electrochemical deposition of the electrochromic material, resulting in nanostructured wire-like porous architectures that facilitate rapid ion uptake during the electrochromic switching. As a result, faster switching response, without sacrificing coloration and color contrast, has been attained for two types of electrochromic materials, a conjugated polymer and an inorganic oxide, electrodeposited on SWCNT/PET electrodes compared to films on TCO/PET. In addition to the improved electrochromic properties (higher coloration efficiency and faster switching time), the presence of the SWCNT skeleton imparts better adhesion of the electroactive layer to the plastic substrate, higher electrochemical/electrochromic stability and resistance to flexure when compared to films on TCO-based flexible electrodes [2].

For applications in photovoltaic devices, we demonstrate that very thin (~100 nm) SWCNT films on PET are very promising counter electrode in Pt-free flexible DSC, acting both as the conducting layer and catalyst toward the tri-iodide reduction reaction. The concept has been illustrated for low-intensity DSC applications, with a solar cell efficiency of 2.5% reached at 8 mW/cm^2 white light illumination [3]. Photocurrent generation of the cells was found to decrease when as-grown SWCNT films (containing iron catalyst particles from the synthesis) were used whereas electrochemical etching of the iron catalyst from the CNT films [4] stabilized the performance of the DSC. Further work is in progress to improve the catalytic properties and conductivity of the films and to reduce the residual iron content.

References

[1] A. Heras, A. Colina, J. López-Palacios, A. Kaskela, A.G. Nasibulin, V. Ruiz, E.I. Kauppinen, Electrochem. Commun. **11** (2009) 442.

[2] R. Malavé Osuna, V. Hernández, J. T. López Navarrete, E. I. Kauppinen, V.Ruiz, J. Phys. Chem. Lett **1** (2010) 1367.

[3] K. Aitola, A. Kaskela, J. Halme, V. Ruiz, A. G. Nasibulin, E. I. Kauppinen, P. D. Lund, J. Electrochem. Soc. **157** (2010) B1831.

[4] A. Heras, A. Colina, J. López-Palacios, P. Ayala, J. Sainio, V. Ruiz, E. I. Kauppinen, Electrochem. Commun. **11** (2009) 1535.

Figures
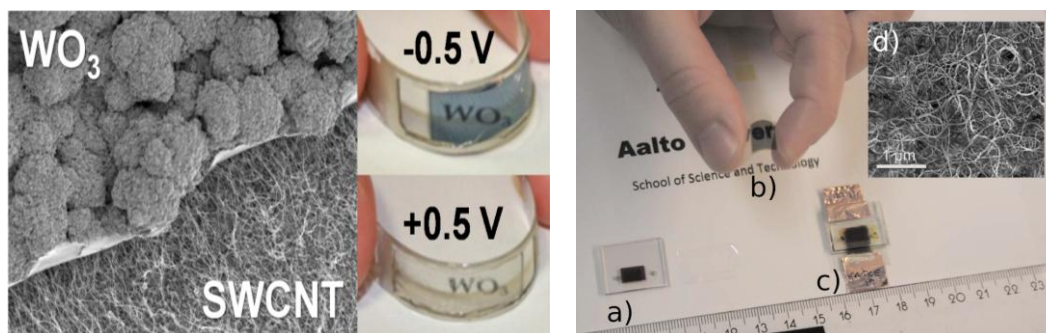
Left- Electrochromic films: SEM image and photograph in the colored and bleached states of a WO₃ on a SWCNT/PET electrode. Right- Photograph of the flexible, transparent SWCNT/PET counter electrode and other cell components: a) Photoelectrode, b) SWCNT film on PET counter electrode, c) Complete dye solar cell, d) SEM image of the SWCNT film.

Assembly of Nanoscale Building Blocks to control the Collective Magnetic Behavior

V. Salgueirino, A. B. Dávila-Ibáñez, N. Fontaíña-Troitiño

Universidade de Vigo, Dpto. de Física Aplicada, 36310 Vigo Spain
vsalgue@uvigo.es

Not long ago, controlled synthesis of nanoparticles with a new composition was considered a substantial advance in nanoscale science. Nanotechnology however has reached the stage of development where the subject of most investigations is not individual nanoparticles or nanowires but rather systems of much greater complexity. [1] In magnetic systems, the focus of synthetic efforts appears to be shifting to creation of secondary structures of nanocrystals, in order to tie together the intrinsic properties of the individual constituents (M_S, K_1, etc.) and the collective properties of the final composites (dipolar interactions, grain-boundary or exchange-coupling effects between the subunits forming them), as both aspects play important roles.

Thus, the concept of a collective behavior of nanoparticles and hybrid nanoscale systems is transitioning from pioneering studies to "proof of concept" applications. We will go through several examples that demonstrate the assembly of nanoscale building blocks to exert the control of the final collective magnetic behavior [2] and the possible diversity of the ultimate functionalities of these complex nanomaterial systems. This fascinating approach of artificial nanostructuring permits to create completely new ever-progressing magnetic materials. These applications include such far-reaching challenges as biological sensors [3] or catalysts. [4]

References

[1] V. Salgueiriño-Maceira, M. A. Correa-Duarte, Advanced Materials, **19** (2007), 4131-4144.
[2] M. Sanlés-Sobrido, M. Bañobre-López, V. Salgueirino, M. A. Correa-Duarte, B. Rodríguez-González, J. Rivas, L. M. Liz-Marzán, J. Mater. Chem. **20** (2010), 7360-7365.
[3] A. B. Dávila-Ibáñez, M. A. López-Quintela, J. Rivas, V. Salgueirino J. Phys. Chem. C **114** (2010), 7743-7750.
[4] A. B. Dávila-Ibáñez, M. A. Correa-Duarte, V. Salgueirino J. Mater. Chem. **20** (2010), 326-330.

Figures
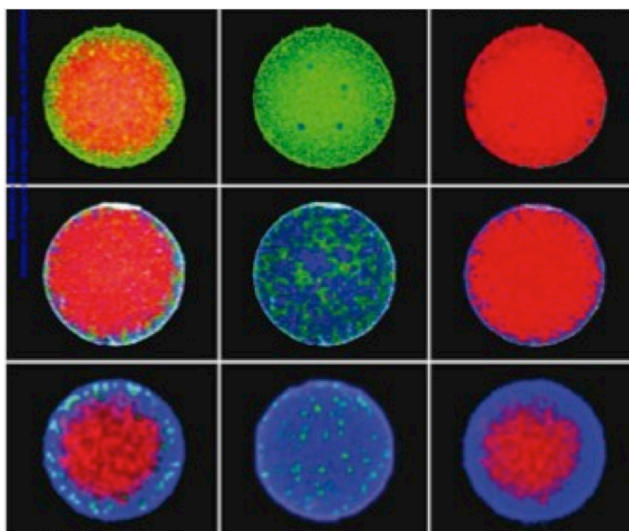
STEM elemental mapping through XEDS analysis for PS/Pt/Ni composite particles with different magnetic content.

Shape Memory and Superelasticity at Nano-scale

J. San Juan [1], M.L. Nó [2]

[1] Dpt. Física Materia Condensada, Facultad de Ciencia y Tecnología, Universidad del Pais Vasco, Aptdo. 644, 48080 Bilbao, Spain.

[2] Dpt. Física Aplicada II, Facultad de Ciencia y Tecnología, Universidad del Pais Vasco, Aptdo. 644, 48080 Bilbao, Spain.

jose.sanjuan@ehu.es

The thermoelastic martensitic transformation is responsible for the thermo-mechanical properties of Shape Memory Alloys (SMA), which are widely used for practical applications as sensors and actuators and in particular they are good candidates to be incorporated in Micro Electro-Mechanical Systems (MEMS). However, the characterization of the shape memory and superelastic behavior at micro and nano scale requires new experimental methodologies.

First, the study of nucleation of martensite plates has been observed at nano-scale by in-situ transmission electron microscopy (TEM), and in particular the nucleation of martensite on the core of the dislocations was reported [1]. New dynamic experiments showing the stress-induced transformation during superelastic in-situ tests at TEM will be presented.

In addition, in the present work we present a new experimental approach for the mechanical characterization of the superelastic behavior by using an instrumented nano indenter to perform nano-compression tests on micro and nano pillars milled by focused ion beam (FIB). Superelastic behavior has been demonstrated along hundred of cycles with a recovery resolution in the range of the nanometer, and shape memory has been also reported in simple devices as nano pillars of about 400 nm diameter.

Some previous results [2,3] in Cu-Al-Ni micro and nano pillars milled by FIB on single crystals will be overviewed, and new results concerning the evolution of the mechanical behavior during compression cycling at nano scale will be presented. In addition these micro pillars exhibit an anomalous ultra-high damping at nano scale, which could be very useful to damp vibrations in MEMS, improving its reliability. We finally discuss the observed behavior, which evidences the existence of size-effects at nano scale on the superelastic behavior, and in general on the martensitic transformation.

In order to understand the martensitic transformation at small scale, in-situ transmission electron microscopy superelastic tests [4], on similar samples, have also been performed to follow the evolution of the martensites nucleation. These experiments also evidence a size-effect on the selection rules for martensite nucleation, which exhibits a different behavior at nano scale than in bulk materials. Finally, a general discussion on the martensitic transformation behavior at nano scale will be addressed.

References

[1] A. Ibarra, D. Caillard, J. San Juan, M.L. Nó. Applied Physics Letters 90, 101907 (2007).

[2] J. San Juan, M.L. Nó, C.A. Schuh. Advanced Materials 20, 272 (2008).

[3] J. San Juan, M.L. Nó, C.A. Schuh. Nature Nanotechnology 4, 415 (2009).

[4] M.L. Nó, A. Ibarra, D. Caillard, J. San Juan. Acta Materialia 58, 6181 (2010).
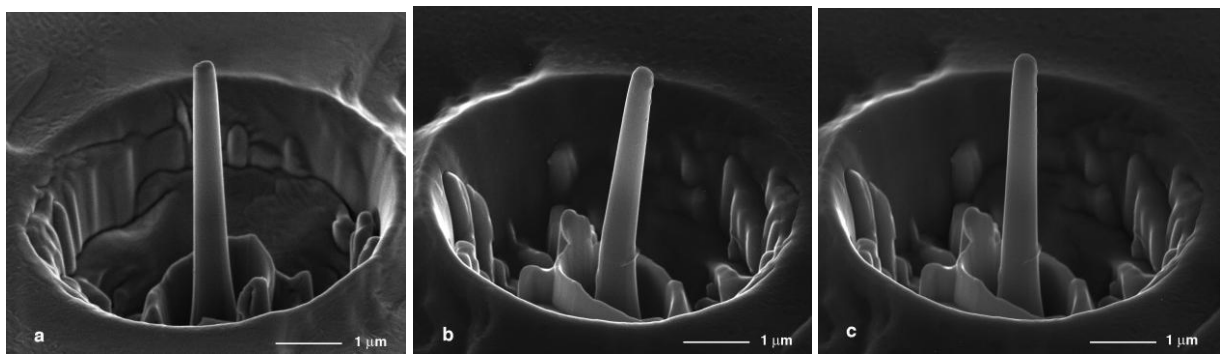
Figures

Figure 1: Shape Memory behavior of a nano-pillar. a) Image of a nano–pillar with ~400 nm diameter, from sample SM. b) The same nano-pillar deformed in bending by off-axis compression at the nano indenter. c) Shape recovery of the nano-pillar by in situ heating [2].
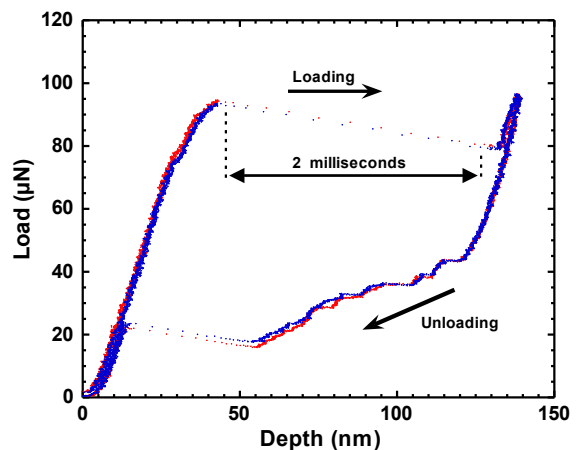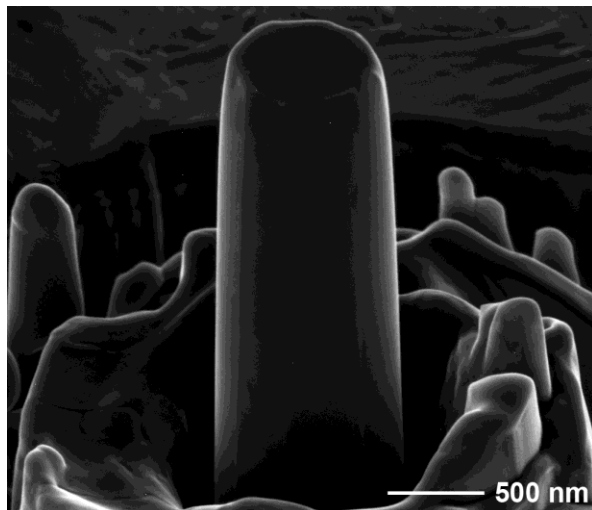
Figure 2: a) Scanning electron microscope image of the sub-micrometer pillar milled by FIB on a Cu-Al-Ni [001] oriented single crystal. It shows a slightly tapered shape with a diameter of about 750 nm at the top, a mean diameter of 900 nm over the bottom part and 3.8 mm height. b) Two consecutive nano-compression tests (in red and blue) obtained after ten prior mechanical cycles on the sub-micrometer pillar [3].

Oil nanocapsules with antimicrobial activity

M. M. Sánchez Navarro, N. Cuesta Garrote, F. Arán Aís, C. Orgilés Barceló

INESCOP. Innovation and Technology Center. Pol. Ind. Campo Alto 03600 Elda Alicante Spain
msanchez@inescop.es

Nanoencapsulation technology presents a new option for the shoe industry as its application can transform traditionally used materials or products into smart ones capable of interacting with feet. For instance, they can improve quality of life by incorporating products for foot care such as properly dosed essential oils. The nanoencapsulation of active substances to be incorporated in different footwear components in order to obtain an "active shoe" presents an opening up of a new way of innovation.

Aromatics plants have traditionally been used in folk medicine as well as to extend the shelf life of foods, showing inhibition against bacteria, fungi and yeasts. Most of their properties are due to essential oils produced by their secondary metabolism. Some essential oils and extracts from several plant species are able to control microorganisms related to skin, dental caries, and food spoilage, including Gram-negative and Gram-positive bacteria. In recent years, interest in natural medicinal products, essential oils and other botanicals, has grown in response to the ever increasing incidence of adverse side effects associated with conventional drugs, and the emergence of resistance to antibiotics, synthetic disinfectants and germicides. Among the wide offer of essential oils, there are some that have recognized their antimicrobial activity such as tea tree oil, lemon or salvia essential oil, for example.

The *in situ* polymerization allows the formation of micro and nanocapsules containing a water-immiscible dispersed phase, with improved mechanical properties and thermal stability. The properties of the membrane depend not only on its chemical structure but also on all the synthesis conditions. The polycondensation of the amino resin occurs in the continuous phase, and the phase separation is linked to the pH and the melamine-formaldehyde resin molar ratio.

In this study a series of melamine-formaldehyde (MF) nanocapsules containing essential oils was prepared by *in situ* polymerization (O/W) method to be applied to footwear materials (lining, insoles, etc…) as antimicrobial agent and their physicochemical properties have been characterized by different experimental techniques.

Experimental

Synthesis of melamine-formaldehyde microcapsules containing antimicrobial oil. First of all, a melamine-formaldehyde (MF) resin to be used as microcapsules shell was prepared from the monomers, melamine and formaldehyde. After that, an O/W emulsion was prepared. The oil phase was composed of the active substance, and the aqueous phase was constituted of distilled water and sodium dodecyl sulfate (SDS) as surfactant. Next is added the above prepared prepolymer and adjust the pH, which causes coagulation of the polymeric shell around the oil droplets. Subsequently, hardening of the polymeric membrane by raising the temperature occurs. Finally, it was allowed to cool down to room temperature and the pH was adjusted to basic. In this study, microcapsules with four different MF/oil ratios were synthesized and characterized.

Characterization of microcapsules. Physicochemical properties of the synthesized nanocapsules containing antimicrobial oils have been characterized by different experimental techniques. The size of the nanocapsules was determined using a particle size meter Coulter LS 230, the chemical structure of the oils and the nanocapsules obtained was analyzed by Fourier transform infrared spectroscopy, (FTIR). Finally, the incorporation of nanocapsules to footwear materials was analyzed by scanning electron microscopy (SEM).

Results and Discussion

Oil antimicrobial activity study.

The antimicrobial activity of TTO against different microorganisms typically found in used footwear (*E. coli, B. subtilis, K. pneumoniae, S. aureus*) was analyzed by in vitro test. Agar Petri dishes were prepared in order to evaluate the antimicrobial activity by measuring the inhibitory halo. The evaluation was carried out in two media: growth in liquid media for 24 h and measurement of inhibition diffusion halos in agar for 24 h.

Nanocapsules characterization.

Figure 1 shows the average particle size distribution in number for the different nanocapsules emulsion synthesized. Nanocapsules containing antimicrobial oil showed a narrow particle size distribution in number with a medium particle size around 100 nm.

FTIR spectra of the nanocapsules containing oils obtained after freeze-dried proved to be the combination of the characteristic bands of the MF resin and the oils. So the intensity of the bands corresponding to the resin decreases as the resin/oil ratio in the nanocapsules decreases. Therefore, there was no evidence of the chemical interactions between the core oil and the polymeric shell of the nanocapsules.

Finally, nanocapsules containing the active substances were incorporated to some materials used as footwear components such as linen and foams to evaluate the feasibility of this technology. Figure 2 shows SEM image of the nanocapsules anchored to the fabric fibers of a lining material.

Conclusions

Some essential oils have shown adequate antimicrobial activity against four microorganisms typically found in used footwear (*E. coli, B. subtilis, K. pneumoniae, S. aureus*).in order to be applied in footwear materials they have been encapsulated for a controlled release

The nanocapsules obtained containing antimicrobial essential oils, the relationship between the resin mass that forms the shell and the active substance contained in the core largely determines the efficiency of the nanoencapsulation process, the morphology of the nanocapsules and the particle size distribution thereof. The results obtained from the incorporation of microcapsules in fabrics and foams demonstrated the feasibility of this technology to achieve the concept of active shoe for footcare.

References

[1] Kunicka-Styczynska A. et al. J. Appl. Microbiol., **107** (6) (2009) 1903.
[2] Reuter J. et al. Am. J. Clin. Dermatol **11**(4) (2010) 247
[3] Luo W et al Polym. Degrad. Stabil. **92**(7): (2007). 1359.
[4] Fabien Salaün et al.. European Polymer Journal **44** (2008) 849.
[5] Li Wei et al. Materials Chemistry and Physics **106** (2007)437.
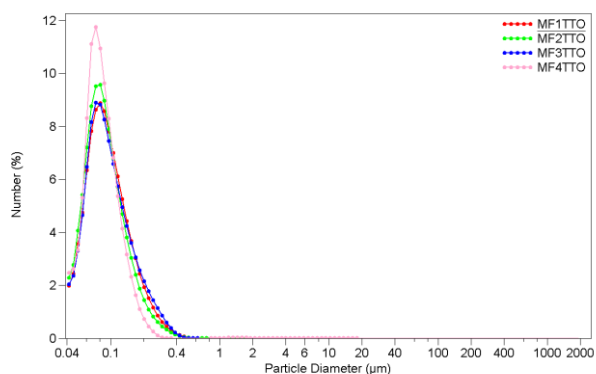
Figures:

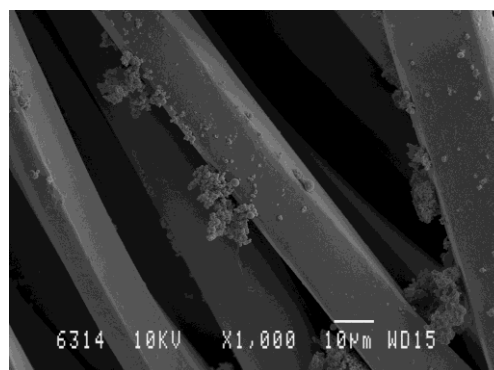**Figure 1:** *Antimicrobial oil microcapsules size distributions*.

Figure 2: *Essential oil microcapsules incorporated to a fabric used as a footwear component.*

Doxorubicin Loaded Magnetic Polymersomes:
Theranostic Nanocarriers for MR Imaging and Magneto-Chemotherapy

Olivier Sandre, Charles Sanson, Odile Diou, Julie Thévenot, Emmanuel Ibarboure, Alain Soum, Annie Brûlet, Sylvain Miraux, Eric Thiaudière, Sisareuth Tan, Alain Brisson and Sébastien Lecommandoux

Laboratoire de Chimie des Polymères Organiques (LCPO)
UMR5629 Université de Bordeaux / CNRS / Institut Polytechnique de Bordeaux,
ENSCBP – 16 avenue Pey Berland, 33600 Pessac, France
olivier.sandre@ipb.fr

Hydrophobically modified maghemite (γ-Fe2O3) nanoparticles were encapsulated within the membrane of poly(trimethylene carbonate)-*b*-poly(L-glutamic acid) (PTMC-*b*-PGA) block copolymer vesicles using a nanoprecipitation process. This formation method gives a simple access to highly magnetic nanoparticles (MNPs) (loaded up to 70 wt %) together with a good control over the vesicles size (100 to 400 nm). The simultaneous loading of maghemite nanoparticles and doxorubicin was also achieved by nanoprecipitation. The deformation of the vesicle membrane under an applied magnetic field has been evidenced by small angle neutron scattering. These superparamagnetic hybrid self-assemblies display enhanced contrast properties that open potential applications for Magnetic Resonance Imaging. They can also be guided in a magnetic field gradient. The feasibility of controlled drug release by radio-frequency magnetic hyperthermia was demonstrated in the case of encapsulated doxorubicin molecules, showing the viability of the concept of magneto-chemotherapy. These magnetic polymersomes can be used as efficient multifunctional nano-carriers for combined therapy and imaging.

References

[1] S. Lecommandoux, O. Sandre, F. Chécot, J. Rodriguez-Hernandez, R. Perzynski, Adv. Mat, **17** (2005), 712-718.

[2] S. Lecommandoux, O. Sandre, F. Chécot, J. Rodriguez-Hernandez, R. Perzynski, Journal of Magnetism and Magnetic Materials **300** (2006), 71-74.

[3] S. Lecommandoux, O. Sandre, F. Chécot, R. Perzynski, Progress in Solid State Chemistry, **34** (2006), 171-179.

[4] C. Sanson, J-F. Le Meins, C. Schatz, A. Soum, S. Lecommandoux, Soft Matter, **6** (2010), 1722-1730

[5] C. Sanson, C. Schatz, J-F. Le Meins, A. Brûlet, A. Soum, S. Lecommandoux, Langmuir **26** (2010), 2751-2760.

[6] C. Sanson, C. Schatz, J-F. Meins, A. Soum, E. Garanger, J. Thévenot, S. Lecommandoux. Journal of Controlled Release, **147** (2010), 428-435.

[7] C. Sanson, O. Diou, J. Thévenot, E. Ibarboure, A. Soum, A. Brûlet, S. Miraux, E. Thiaudière, S. Tan, A. Brisson, V. Dupuis, O. Sandre, S. Lecommandoux, ACS Nano, **Published online** (2011), doi: 10.1021/nn102762f.

Figures
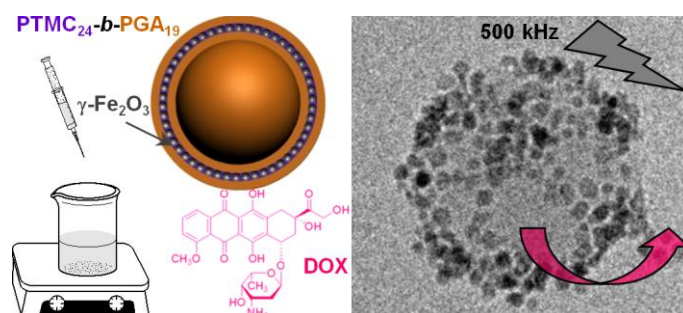
Left: Sketch of dually-loaded vesicles prepared by addition of an aqueous buffer into a mixture of PTMC-b-PGA copolymer, hydrophobically coated magnetic nanoparticles and doxorucin drug.
Right: Cryo-TEM image of vesicle showing the dense mantle of MNPs, which excitation by a radiofrequency magnetic field transmits heat locally to membrane and accelerates the DOX release.

Controlling the magnetic anisotropy in the cobalt bilayer with hydrogen

Benito Santos[1], L. Vergara[1], A. Mascaraque[2], Kevin F. McCarty[3], A. K. Schmid[4]. A. Quesada[4]. A. T. N'Diaye[4] and J. de la figuera[1]

1-Instituto de química-física "Rocasolano", Serrano 119, Madrid, Spain
2-Universidad complutense de Madrid, Spain
3-Sandia national laboratories California, Livermore, USA
4-Lawrence Berkeley national laboratory, Berkeley, CA, USA
benitosantos001@gmail.com

The control of magnetic anisotropy in thin films opens the way to a variety of applications[1]. Thus, research efforts have been devoted to the study of systems where the interplay of roughness, thickness and strain can be revealed. Cobalt or cobalt alloys is widely used in industrial applications[2]. Cobalt is a prototypical ferromagnet with two different crystal structures in bulk, hcp for low temperatures and fcc for temperatures >700K. The magnetic properties of Co thin films on Ru(0001) are determined by the number of the layers. The magnetic easy-axis is in-plane for one layer films or films with three layers or more; on the other hand, the second layer presents perpendicular magnetic anisotropy, i.e. the easy axis is perpendicular to the film plane [2]. This fact makes this system a good model for the study of spin reorientation transitions(SRT).

In this work we present a characterization of the growth and the magnetism of thin Co films on Ru(0001) at two different temperatures. We also study the change in the magnetization of the films upon hydrogen exposure in both cases. The structural characterization was done by low energy electron microscope (LEEM) [3], low energy electron diffraction (LEED) and scanning tunneling microscope (STM). The magnetism of the films and their response to the hydrogen were studied by spin polarized low energy electron microscope (SPLEEM). This microscope allows to determine the magnetization direction of the sample in real time with a lateral resolution of 15nm.

Our results show that the islands of the first and second layer of Co/Ru(0001) grown at room temperature (RT) present a triangular shape with a unique stacking sequence in each terrace. For three or more layers, Co islands present two different stacking sequences in the same terrace. Likewise films grown at 550 K present larger triangular islands with two stacking sequences in the same terrace from the third layer as shown in figure 1. The same interlayer spacing for the Co layers was obtained in both cases.

Cobalt thin films present different magnetic signals depending on the growth mode. For the case of films grown at RT, we did not obtain any magnetic contrast in-plane or out-the-plane for the first two layers. Only for three or more layers of cobalt, a magnetic signal (in-plane) was obtained. This is shown in figure 2(a). This contrast with the films grown at 550 K, where the second layer presents a perpendicular magnetization for temperatures below 400 K. Three layer or more films grown at 550 K always present in-plane magnetization.

On the other hand the second layer of Co on Ru(0001) presents in-plane magnetization when it is grown at RT on Ru(0001) presaturated with hydrogen [figure 2(b)]. This in-plane magnetization of the cobalt bilayer can be also obtained if hydrogen is dosed on the second layer of cobalt grown at 550K. When the hydrogen is bonded to Co it induces a spin reorientation transition of the easy axis, from perpendicular to in-plane magnetization. This change is very sensitive to the hydrogen concentration. By monitoring the change in the anisotropy we could be able to use this system as a gas sensor [patent WO/2010/129390].

STM data confirms that there is no significant changes in the morphology of the Co islands grown on Ru(0001) or on H-Ru(0001). LEED-IV data also do not show changes in the interlayer spacing of layers. Ab-initio calculations showed that the change in the anisotropy of the cobalt is due to electronic effects.

References

[1]*Geoffrey Bate, Journal of Magnetism and Magnetic Materials*, *Vol. 100, Issues 1-3*, 1991

[2]R.D.W. Kemmitt, D.R. RussellComprehensive Organometallic Chemistry, Chapter 34, Pages 1-276, 1982

[2] F. El gabaly, S. Gallego et all New J of physics 9, 80,2006

[3] E. Bauer, *Rep. Prog. Phys.* **57**: 895–938, 1994

Figures
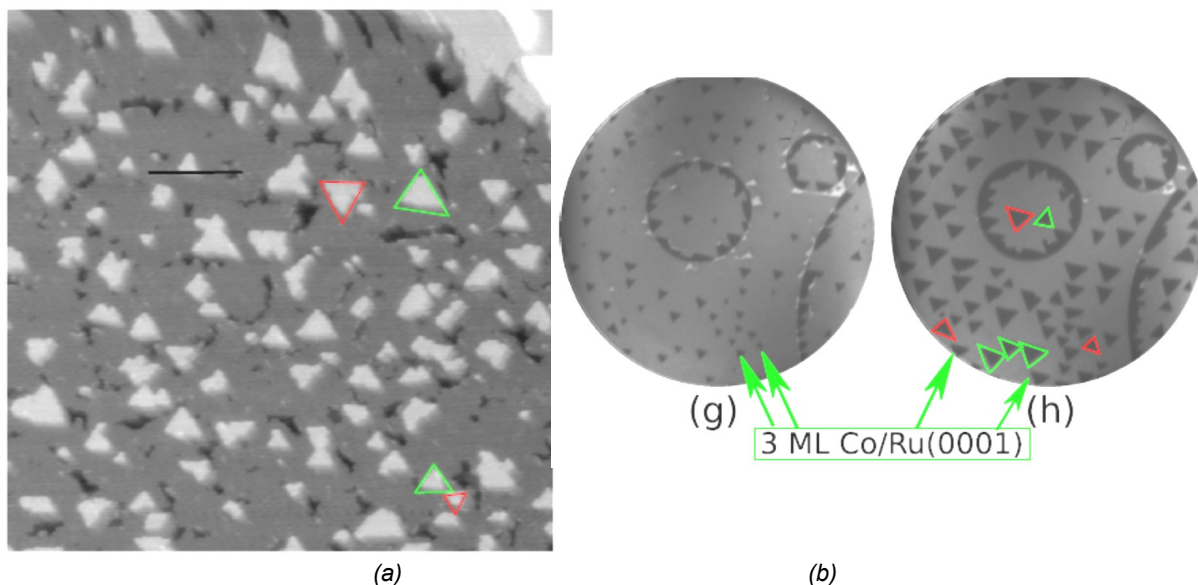
Figure 1: (a)STM image of 2,5ML of Co/Ru(0001) grown at RT, 200nmx200nm (b) LEEM image of 2.5 ML of Co/Ru(0001) grown at 550 K. Field of view was 8 µm. In both cases the triangular islands of Co show two different orientations in the same terrace.
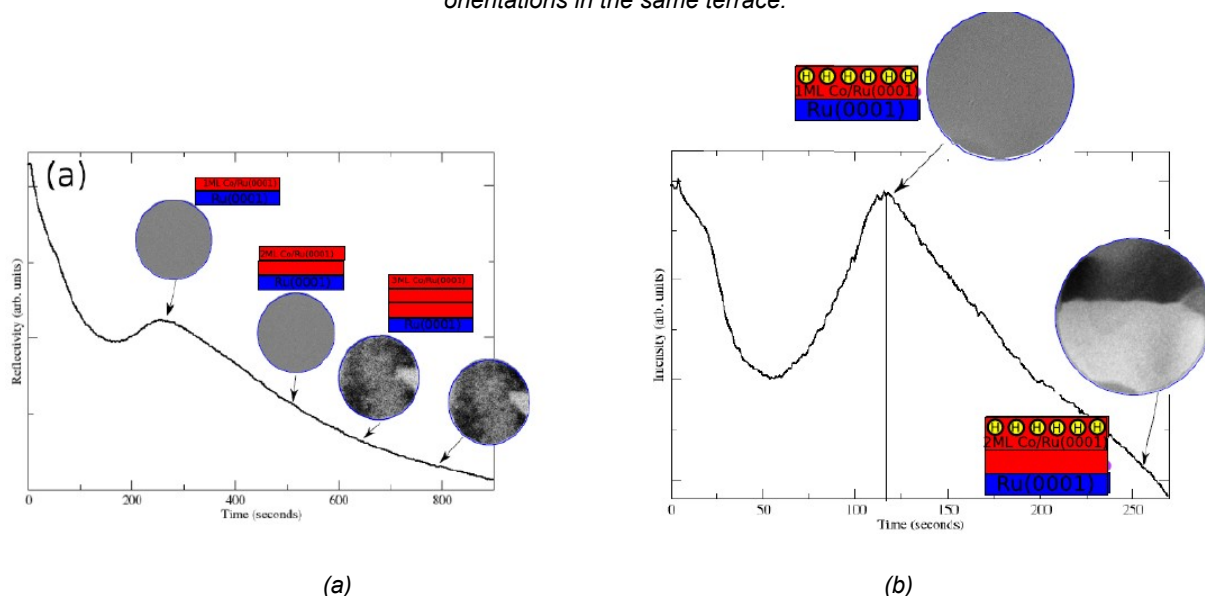
Figure 2: Reflectivity curves acquired while the Co films were grown. The magnetic signal of each film is shown. Field of view was 8 µm in both cases (a) for films grown at RT on clean Ru(0001) (b) for films grown on Ru(0001) saturated with hydrogen.

Electrical Study of 2D Carbon Nanotube Thin Films

G.Sassine, F.Martinez, F.Pascal, A.Hoffmann
Institut d'Electronique du Sud, UMR 5214, Place E. Bataillon, Université Montpellier II,
34095 Montpellier Cedex 5, France.
sassine@ies.univ-montp2.fr

Because of their unique electronic, thermal, optical and mechanical properties [1,2], Carbon Nanotubes (CNTs) have been considered as serious contenders for leading the future of nanosciences. Moreover 2D CNTs films have uniform physical and electronic properties which make them a promising candidate for low cost electronics [3,4]. Here we present a study of 2D CNTs films where a theoretical model and electrical characterization will be presented.

In order to get a microscopic understanding of the transport and noise phenomena, we have developed a model based on the charge transport. In this model, two transport mechanisms are considered: the transport along NTs themselves and the transport between crossed NTs. Considering the large mean free path in CNTs and the weak coupling between NTs, we assume that the contacts between NTs dominate the transport through the film [5]. Using these assumptions, NTs are set randomly on a surface using a Monte-Carlo algorithm, then wide electrodes are defined to form source and drain with a low contact resistance. An equivalent electrical circuit has been drawn where NTs are wire of constant potential and each junction between two tubes in contact is modeled as a dipole with a dynamic resistance. In junction, the hopping from a tube to another is modeled as a perturbation in the transmission probability $T(E)$ in the framework of Landauer formalism. $T(E)$ depends on the CNT charge ρ and on the energy barriers between NTs. Charge inside a tube is calculated using Poisson equation and the density of states $D(E)$. The energy barrier is obtained by a first neighbor tight-binding calculation. The transmission probability is obtained by WKB approximation and the tubes potential are computed using a modified nodal analysis MNA. Figure 1 shows the used algorithm for conductivity and noise simulations.

For a macroscopic validation of the model, high purified HELIX SWCNTs were suspended in aqueous solutions with Sodium Dodecyl Sulfate "SDS" or Bile Salt "BS" with different concentrations. The dispersion of CNTs in the different solutions was studied by MACRO RAMAN, where the spectra are represented in Figure 2. More the RAMAN shift is broad, more the solution is homogeneous.

2D CNTs films with different density of tubes, which is equivalent to different number of deposited layer N_c, are fabricated by spin coating on SiO2/Si substrates. Each film layer was deposited with the same spin-coating parameters. 2D films electrical parameters depend on the homogeneity of the deposited layer.

Conductivity measurements for films deposited with the two kinds of surfactants were extracted using Transmission Length Measurements structures. The results obtained with "BS" show a large conductivity improvement in comparison to the results obtained with "SDS" (Figure 3). In the same way, the contact resistance which is associated to electrodes-NT junctions presents a lower value with "BS". This variations show clearly that films fabricated with "BS" have higher homogeneity in accordance to Raman spectroscopy. Noise measurements were carried out using an HP89410A dynamic signal analyzer with an EGG5182 low noise amplifier. The spectra present 1/f noise, which obeys to the classical equation $K=Si.f/I^2$ [6] for the two kind of surfactants (Figure 4), where Si is the noise current power spectral density PSD, K is the noise amplitude coefficient, f is the frequency, and I is the average current through the sample. The noise is due to fluctuations involving a large number of NT-NT and NT-electrodes junctions. An increase in the density of NTs or a higher homogeneity in the films implies a

decrease in 1/f excess noise. Conductivity ($\sigma \propto (Nc-Nc0)^{tc}$) and 1/f noise ($K \propto (Nc-Nc0)^{-k}$) can be fitted by the classical power laws where tc and k are the critical exponents. N_{c0} is the percolation threshold value.

In summary we have clearly shown the impact of fabrication process of the devices on the conductivity and on 1/f noise level. Percolation theory is used to describe conduction and noise measurements in 2D-CNT films. The developed model, based on NT properties, on NT-NT junction, and NT-electrodes confirm the experimental results and show that these junctions remains a limiting factor for electrical application.

References:
[1] Treacy MMJ, Ebbesen TW, Gibson JM, Nature, **Exceptionally high Young's modulus observed for individual carbon nanotubes,** (1996) 381: 678–80.
[2] Tans SJ, Devoret MH, Dai HJ, Thess A, Smalley RE, Geerligs LJ, et al. Nature, **Individual single-wall carbon nanotubes as quantum wires,** (1997) 386:474–7.
[3] S. Soliveres, J. Gyani, C. Delseny, A. Hoffmann, F. Pascal, Appl. Phys. Lett. 90, **1/f Noise and Percolation in Carbon Nanotube Random Networks,** (2007) 082107.
[4] A. Benham, G. Bosman, A. Ural, Phys. Rev. B 78, Percolation Scaling of 1/f Noise in Single-Walled Carbon Nanotube Films, (2008) 085431.
[5] S. Soliveres, F. Martinez, A. Hoffmann, F. Pascal, **Journal of Physics: Conference Series, Simulation of transport and 1/f noise in carbon nanotube films,** (2009) 193: 012117.
[6] Ashkan Behnam, Amlan Biswas, Gijs Bosman, and Ant Ural, Phys. Rev. B 81, **Temperature-dependent transport and 1/ f noise mechanisms in single-walled carbon nanotube Films**, (2010), 125407.
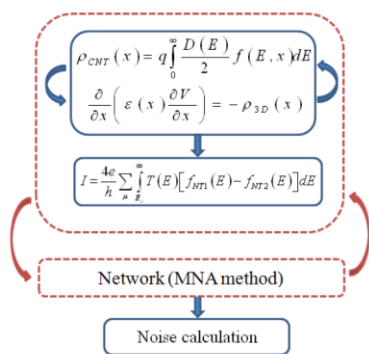
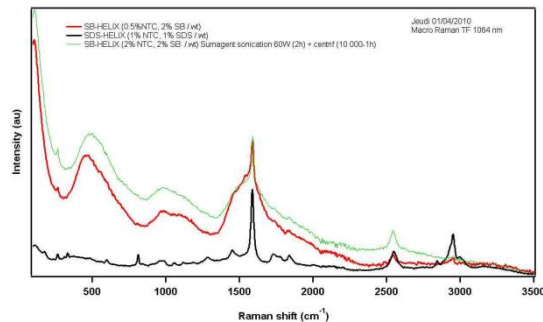Figure 1: General algorithm.

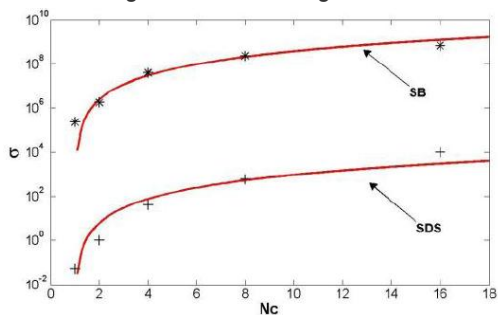
Figure 2: Raman spectra for the different solutions.

Figure 3: Measured conductivity ($\Omega^{-1} m^{-1}$) and power law versus the number of deposited layer (-).
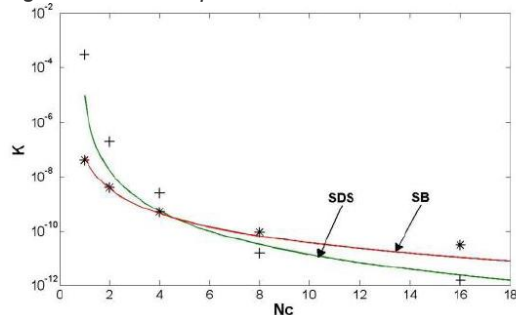

Figure 4: Measured K and power law versus the number of deposited layer (-).

Gold and Silicon Microheaters for Nanotube and Graphene Applications

Marianna Sledzinska*, Neus Sabate**, Marc Salleras**, Pablo Jimenez***, Ana Benito***, Wolfgang Maser***, Adrian Bachtold*

* CIN2 (ICN-CSIC), Campus Universidad Autónoma de Barcelona 08193, Bellaterra (Barcelona), Spain
**Centro Nacional de Microelectrónica (CNM), Campus Universidad Autónoma de Barcelona. 08193 Bellaterra (Barcelona), Spain
***Instituto de Carboquímica de Zaragoza (CSIC), Departamento de Nanotecnologia, Zaragoza, Spain

marianna.sledzinska@cin2.es

We present progress in the fabrication of microheaters, designed for possible applications with carbon-based nanomaterials, such as carbon nanotubes (CNTs) and graphene.

The first type of heaters we fabricate, which we call gold heaters, is schematically shown in Fig. 1 (a, b). It consists of a thin gold layer (70nm), on a suspended, non-conductive 350 nm silicon beam. Joule heating is induced upon passing large currents. At the same time the temperature is monitored by measuring the resistance (and using the measured resistance-temperature coefficient of the system). We achieve temperatures up to 600 C. The limit is given by the maximum current density that can be passed through the gold wire (about $0{,}5*10^9$ A/m2).

For the other type of heaters, which we call silicon heaters, the device consists of a highly doped silicon beam covered by an insulating layer of oxide and a thin platinum layer (Fig.2). High current is passed through the silicon to induce heating. The temperature is measured by probing the resistance of the platinum. The advantage of this layout is that Si is mechanically very stable and can sustain high current densities. Also, since it is not suspended, we avoid possible bending of the structure.

The heaters can be integrated with graphene and nanotubes. Using the microheaters it is possible to introduce controlled temperature gradients in suspended nanotubes or graphene. This will be useful for various applications, for instance in nano electromecanical systems (NEMS). As it was reported in the work of Barreiro et al. [1] thermal gradients can induce motion of objects. The movement direction is from the hot to the cold spot. The heaters will also be used to study heat transport and dissipation.
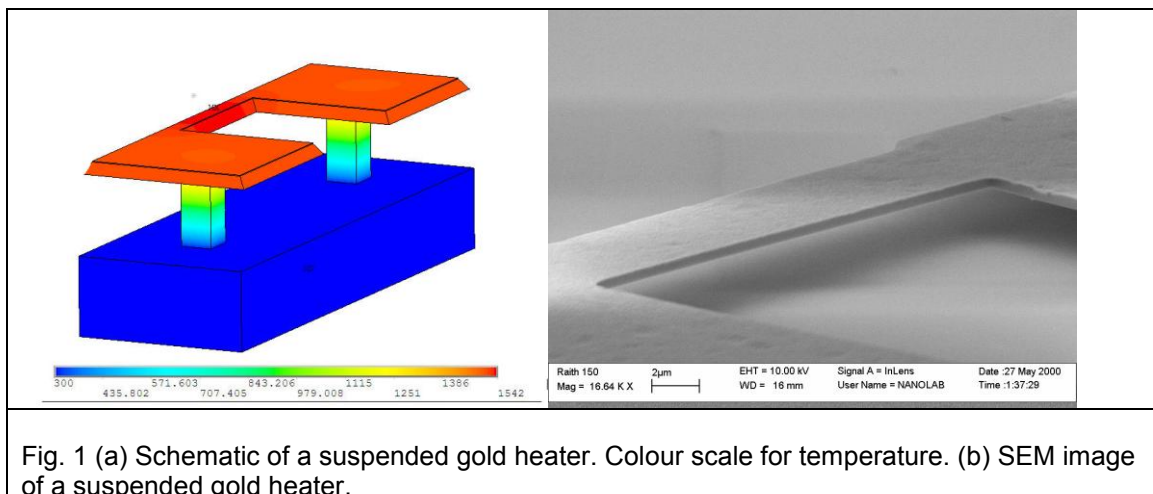

Fig. 1 (a) Schematic of a suspended gold heater. Colour scale for temperature. (b) SEM image of a suspended gold heater.
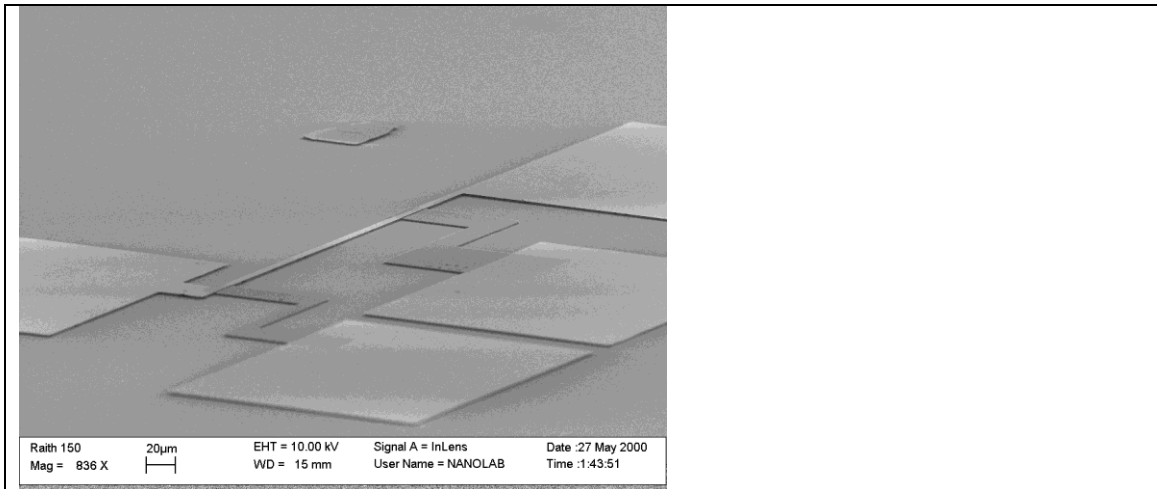
Fig. 2 SEM image of a silicon heater

References
[1] Barreiro et al., Science **320** *(5877) 775*

Study of sensitivity as a function of waist length in nanocoated tapered optical fibers

A. B. Socorro, I. Del Villar, J. M. Corres

Public University of Navarre (UPNA), Campus de Arrosadía s/n, Pamplona – Navarre, Spain
ab.socorro@unavarra.es

Tapered single-mode optical fiber (TSMF) can be designed to be high sensitive structures with the adequate geometry of the waist zone. The spectra of light transmitted by the taper was studied as a function of coating thickness for different waist lengths, which permitted to observe that the design of TSMF based sensors can be optimized by an adequate selection of the waist length.

Layer-by-layer (LbL) electrostatic self Assembly [3], was used to coat the TSMF. Polyallylamine hydrochloride (PAH) mixed with Neutral Red (NR) was used for the positive solution and Poly acrylic acid (PAA) for the negative solution, all purchased from Sigma. LbL technique permits a nanometric control of bilayer thickness, which allowed observing the evolution of transmitted spectra as a function of the coating thickness.

The construction was monitorized with the set up of Fig. 1. Two standard single mode optical fibers were tapered by heating a section of the fiber with a little flame and pulling the fiber's ends. The waist lengths of the fibers were 10 and 20 mm respectively. The waist diameter was 30 μm for both cases. Then, the TSMF were connected to a white-light source at one side and to an optical spectrum analyzer at the opposite size in order to get a transmission configuration. The transmission spectrum was monitorized after the deposition of each bilayer.

In figure 2 a resonance centered at 20 bilayers can be observed for all cases. Moreover, the resonance depth of the 20 mm TSMF increased to that point that the power detected moved below the sensing threshold of the spectrometer. The reason is that light propagates more distance along an area with reduced diameter and so, the evanescent field can escape easier than in the case in which the stretched area is shorter. The maximum sensitivity of both TSMF was studied for different wavelengths in figure 3, where an improvement of a factor of 3 was observed.

To conclude, the device can be used as detector based on coating thickness changes. Its maximum sensitivity can be controlled by choosing and adequate waist length. By stopping the deposition at a thickness were a maximum sensitivity is obtained, optimized pH sensors [3], and biological immunosensors could be obtained.

References

[1] R Jarzebinska, C S Cheung, SW James and R P Tatam, Measurement Science and Technology, **Response of the transmission spectrum of tapered optical fibres to the deposition of a nanostructured coating** (2009) Meas. Sci. Technol. 20. (6pp).
[2] I Del Villar, C R Zamarreño, P Sanchez, M Hernaez, C F Valdivielso, F J Arregui and I R Matias, Journal of Optics, **Generation of lossy mode resonances by deposition of high-refractive-index coatings on uncladded multimode optical fibers** (2010) J. Opt. 12. (7pp).
[3] Jesus M. Corres, Javier Bravo, Ignacio R. Matias and Francisco J. Arregui, IEEE Photonics Technology Letters, Vol. 18, No 8, **Nonadiabatic Tapered Single-Mode Fiber Coated With Humidity Sensitive Nanofilms** (2006) 935-937.
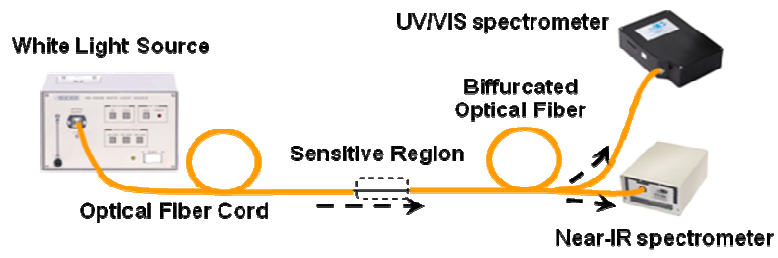
Figures

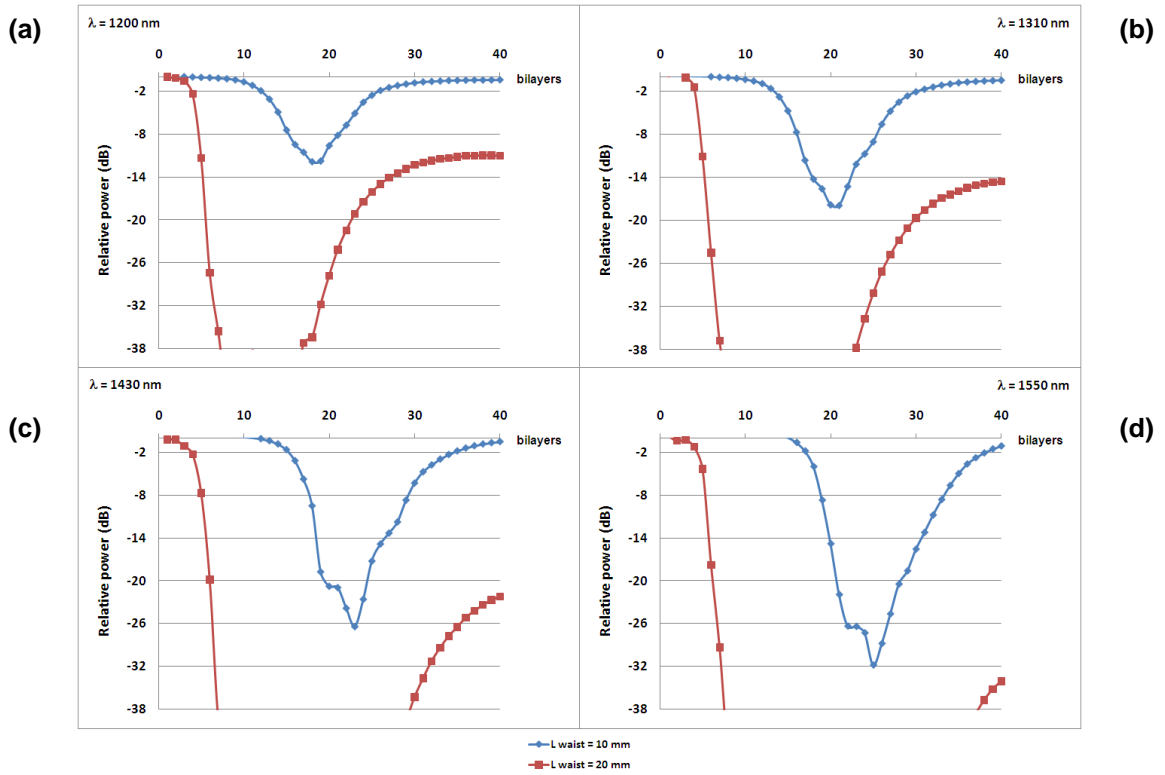
Fig. 1. Set-up of the construction.

Fig. 2. Comparative of the attenuation of the analyzed tapers at (a) 1200nm, (b) 1310, (c) 1430 and (d) 1550 nm.
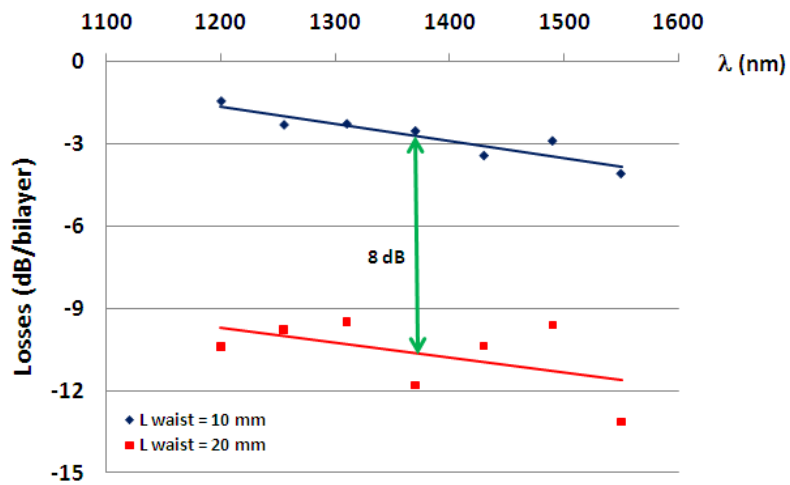

Fig. 3. Resonance sensitivity at different wavelengths.

Unusually photoresistant fluorescence in gold nanoshells with liquid cores

Soraya Zaiba[1,4], Fréderic Lerouge[2], Jean Lermé[3], Stéphane Parola[2], Patrice L. Baldeck[4]

1 Laboratoire d'Electronique Quantique, Faculte de Physique, USTHB,Algerie-Departement de physique –Faculté des sciences –Université M'Hamed Bouguera Boumerdes-Algerie

2 Université de Lyon - Laboratoire de Chimie, CNRS, ENS-Lyon , France.

3Laboratoire des Multimatériaux et Interfaces, CNRS 5615, Université Claude Bernard Lyon 1, Université de Lyon , France.

4 LaboratoierIinterdisciplinaire de Physique, CNRS UMR 5588, Université Joseph Fourier Grenoble, France.

szaiba@liphy.ujf-grenoble.fr

Numerous research works are investigating the possibility of using the light interaction with metallic nanoparticles to improve the fluorescence properties of nearby molecules. But few works have considered the encapsulation of molecules in metallic cavities. In this paper we will present the properties of a new kind of hybrid nanoparticles. We describe an original process allowing the preparation of hollow spheres using fast mechanical stirring stabilized emulsions without surfactants containing an organic dye in their cores [1]. We present the optical and fluorescence properties of liquid core gold nanoshells. Microspectroscopy of unique nanoparticles demonstrates that extinction spectra are in good agreement with Mie's theory. Finite Difference Time Domain (FDTD) calculations show that excitation and emission radiations are efficiently transmitted through the thin gold nanoshells. Thus, they can be considered as transparent nano-containers for molecules located in the shell core. In agreement with FDTD calculations, measurements show that fluorophores encapsulated in gold nanoshells keep their brightness, but they have fluorescence lifetimes an order of magnitude shorter. As a salient consequence, the photoresistance of encapsulated organic dyes is also improved by an order of magnitude. This unusual photoresistance results from the reduced probability of triplet-singlet conversion that eventually expose dyes to singlet oxygen photodegradation.

References

[1] : François Lux and al, Nanotechnoloy, 20, (2009), 355603

Figures
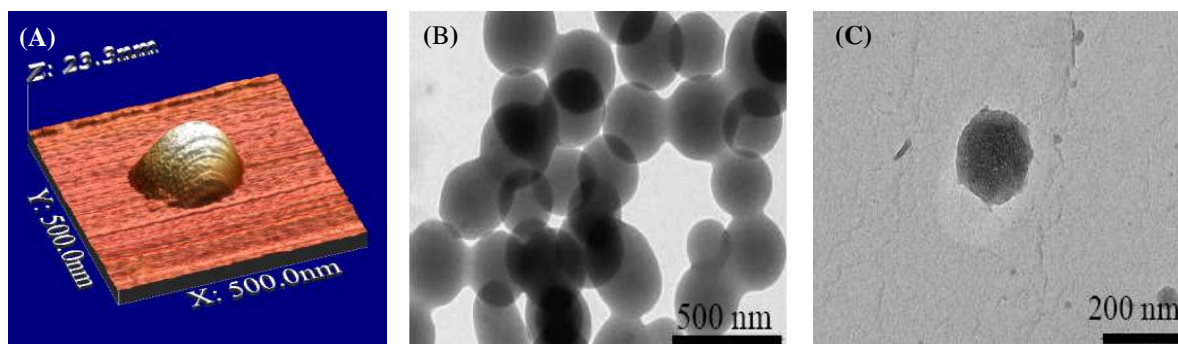
Figure1
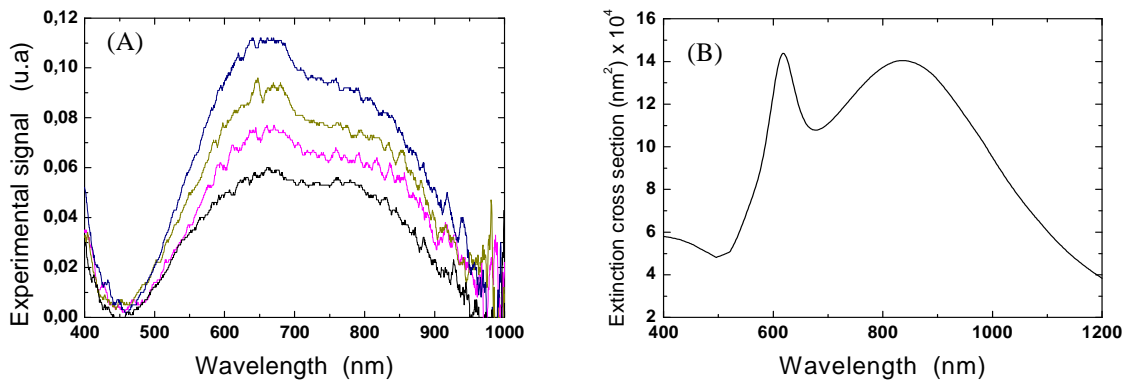
Figure2
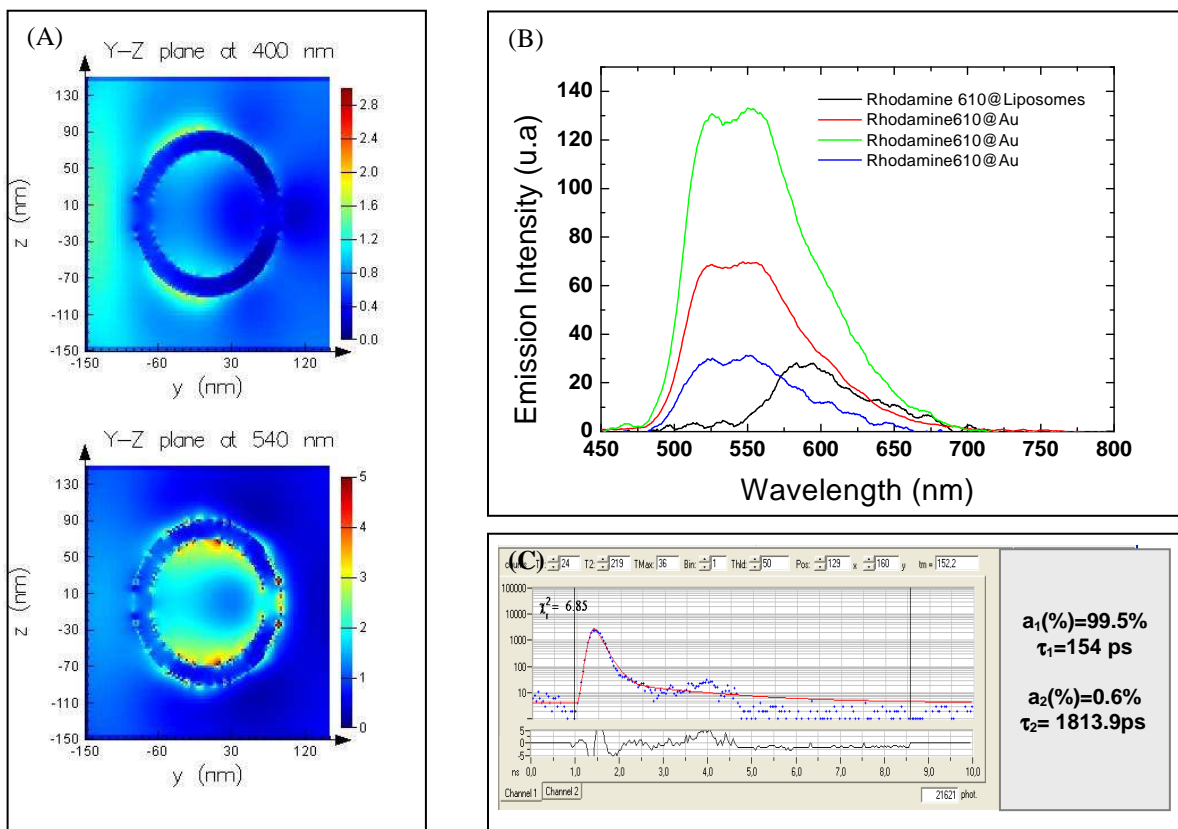
Figure3

Figure caption

Figure 1: (A) AFM image (B), (C) TEM images of hollow gold nanoshells

Figure 2: (A) (A) Measured extinction spectra of Rhodamine 610@Au shells of different sizes in BSA (B) Theoretical extinction cross-section (Mie calculation) of a single water-core gold nanoshell in BSA.

Figure 3: (A) FDTD calculations of field intensity distributions around and inside the metallic shell at the excitation (top) emission wavelengths of Rhodamine 610 (bottom). (B) Typical emission spectra of different Rhodamine 610@Au nanoshells with water cores (colored curves) under the same excitation conditions. Black curve correspond to the emission of Rhodamine 610 in liposomes. (C) Fluorescence Lifetime imaging microscopy measurement.

Silica nanotubes: From the preparation to Drug loading and controlled release

C.T. Sousa[1]*,C. Nunes[2], M. Lúcio[2], M.P. Proença[1], D.C. Leitão[1], J.L.C. Lima[2], S. Reis[2], J.P. Araújo[1]

[1]IN-IFIMUP and Dep. Física, Rua do Campo Alegre 687, 4169-007 Porto, Portugal
[2]REQUIMTE, Serviço de Química-física, Faculdade de Farmácia, Porto, Portugal.
celiasousa@fc.up.pt

Effective disease targeting represents an enormous biomedical challenge in the treatment of several diseases such as cancer because the lack of selectivity of current therapeutic agents results in numerous severe side effects. Thus, it becomes increasingly important to develop drug delivery systems that can efficiently target based on subtle molecular alterations that distinguish specifically injured cells. High aspect ratio nanoparticles, such as nanotubes and nanowires, are inorganic hollow structures that constitute potential candidates for drug delivery since their dimensions are easily varied and a wide range of functionality can be conferred to them [1].

In this work, we provide evidence that our silica nanotubes (SNTs) synthesis method has the advantage of forming Si-O-H chemical bonds at the nanotube's surface, allowing direct aminosilane functionalization [2]. However, the number of OH groups was found to decrease with the increase of calcination temperature. An optimum calcination temperature around 220°C was found that compromises nanotube mechanical stability and OH group availability. Then, among the three tested aminosilane molecules (APTES) showed to have the most effective attachment to the inner surface of the nanotubes. Finally, using the efficient functionalization with amino-silane, the inner void of SNTs was used to control the release of a non-steroidal anti-inflammatory (naproxen) promoted by a polycationic surface drug loading.

References
[1] S. J. Son, et al., Drug Discovery Today (2007), 12, 650.
[2] Corine Tourné-Péteilh, et al., NJC Letters (2003), 27, 1415.

Figures

Figure1. Scheme of drug loading in inner surface of silica nanotubes.

High Resolution KPFM investigation of nanoscale phase segregated organic heterojunctions

Evan Spadafora[a], R. Demadrille[a], B. Ratier[b], and B. Grévin[a]

a UMR 5819 SPrAM CEA-CNRS University Joseph Fourier, Grenoble, France
b XLIM UMR 6172 University Limoges/CNRS, Limoges, France
Evan.Spadafora@cea.fr

A comprehensive high resolution Kelvin probe force microscopy (KPFM) investigation was performed on the active layer of an organic solar cell (OSC), a 100 nm bulk hetero-junction (BHJ) blend of poly(3-hexylthiophene) (P3HT) and phenyl-C61-butyric acid methyl ester (PCBM). This P3HT/PCBM blend has been optimized for use as an OSC with an overall power conversion efficiency of 4.25%[1]. Chemical phase separation of the P3HT clusters is shown to be on the order of the exciton diffusion length, ~10 nm, as seen using non-contact atomic force microscopy under UHV in the frequency modulation mode[2]. KPFM measurements were performed in dark and under illumination at 532 nm. Local surface contact potential measurements are recorded with a resolution of a few nm. In dark, a clear contrast (~100 mV) of the local surface potential between P3HT and PCBM is seen. However, under illumination, there is a global negative shift of the local surface potential and the difference between P3HT and PCBM is significantly reduced. Furthermore, analysis of the surface photovoltage, obtained from contact potential images, reveals a spatial resolution of the space charge region, where exciton dissociation takes place, at the donor/acceptor interfaces to be no more than ~3 nm. The resolution achieved in this work demonstrates that electrical properties can be directly visualized in highly efficient organic BHJ blends at the true nanometer scale by KPFM[3]. In addition, new results on OSC's composed of novel BHJ blends will also be presented.

[1] R. Radbeh, E. Parbaile, J. Bouclé, C. Di Bin, A. Moliton, V. Coudert, F. Rossignol and B. Ratier, *Nanotechnology*, **21** (2010) 035201
[2] B. Grévin, R. Demadrille, M. Linares, R. Lazzaroni, and P. Leclére, *Adv. Mater*, **21** (2009) 4124-4129
[3] E. J. Spadafora, R. Demadrille, B. Ratier, B. Grévin, *Nano Letters,* **10 (9)**, (2010) 3337-3342
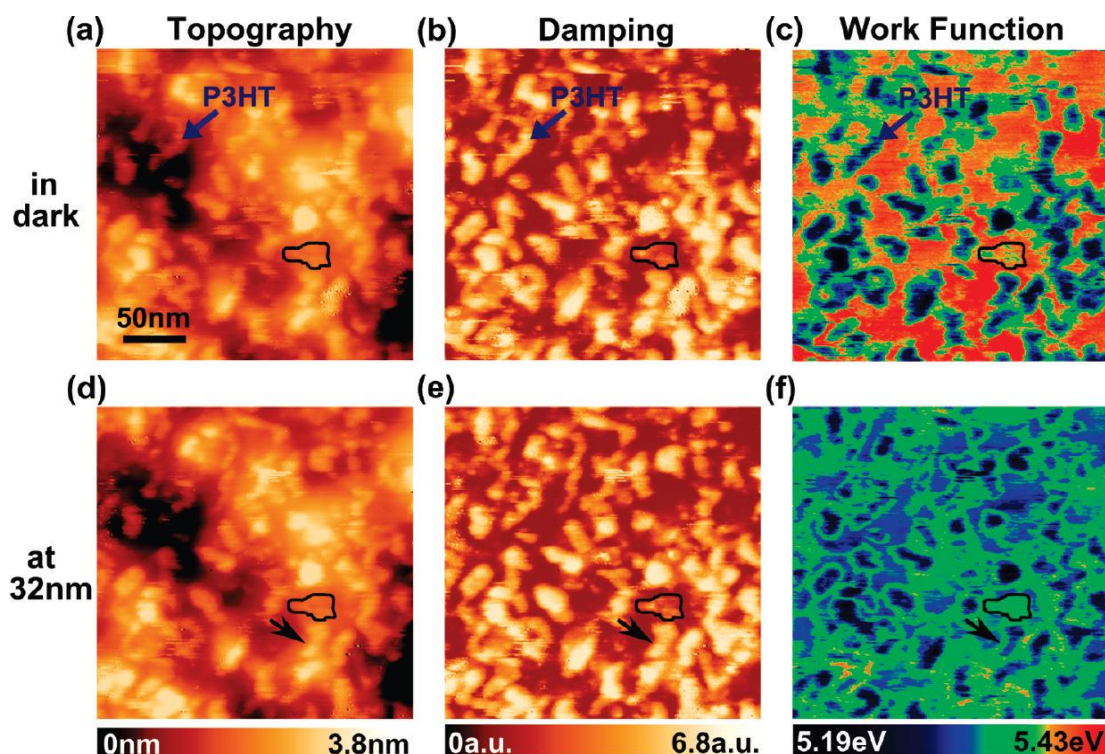
FIGURE 1. (a-f) FM-AFM (UHV, 300K) 2D images (250 nm x 250 nm, 300 x 300 pixels, Δf = -19 Hz, Avib = 44 nm, scan speed = 50 ms per pixel) of the P3HT-PCBM sample recorded in dark (a-c) and under illumination at 532 nm (d-f). (a,d) topography, (b,e) damping, and (c,f)work function calculated from the Kelvin compensation potential. For a direct comparison, the z-values have been coded by using the same color scales in (a,d), (b,e), and (c,f). The dark-blue arrows in (a-c) indicate a P3HT crystallite. The dark arrows in (d-f) pinpoint the interface between an emerging P3HT crystallite and the surrounding PCBM. A nearly buried P3HT crystallite (partially or totally covered by a ultrathin layer of PCBM) is outlined in black.

Mid-infrared detection of 10000 chemical bonds by near-field spectroscopy

Johannes M. Stiegler[1], Yohannes Abate[2], Antonija Cvitkovic[3], Rainer Hillenbrand[1,4]

[1] CIC nanoGUNE Consolider, Avenida Tolosa 76, Donostia – San Sebastian, Spain
[2] California State University, 1250 Bellflower Blvd., Long Beach, USA
[3] Neaspec GmbH, Bunsenstr. 5, Martinsried, Germany
[4] IKERBASQUE, Alameda Urquijo 36-5, Bilbao, Spain
j.stiegler@nanogune.eu

The analysis of chemical composition and structure of substances is a major topic in chemical, physical and biological sciences. A powerful and widely used tool is infrared absorption spectroscopy, because of its ability to identify materials by their vibrational mode fingerprint. It can, however, not be applied to study nanoparticles and/or molecules, owing to the extremely small infrared absorption cross-sections and the diffraction limited spatial resolution.

With the help of scattering-type scanning near-field optical microscopy (s-SNOM) [1], the diffraction-limited spatial resolution can be overcome by orders of magnitude. Nanoscale resolved infrared imaging of particles as small as 10 nm has been already demonstrated [2,3], providing information on the dielectric properties of the particles at single wavelengths.

Here we demonstrate spectroscopic infrared imaging of nanopartices and show that the spectral phase contrast in s-SNOM can be employed to determine the spectral absorption characteristics of nanoparticles (Figure). Such infrared fingerprints allow for chemical identification of individual 5 nm silicon nitride particles with an absorption cross-section of 10^{-23} cm^{-2}. This corresponds to the detection of about 10.000 Si-N stretching bonds, respectively of a volume as small as $65*10^{-24}$ liters.

Our experimental results are in excellent agreement with calculated absorption spectra based on bulk silicon nitride dielectric data using extended/improved finite dipole model calculations to calculate the near-field response of small nanoparticles. This approach opens the door to nanoscale-resolved chemical imaging on the macromolecular level.

References

[1] F. Keilmann, R. Hillenbrand, Philos. T. R. Soc. Lond. A, **362** (2004), 787-805
[2] Cvitkovic et al., Phys. Rev. Lett., **97** (2006), 060801
[3] A. Cvitkovic, N. Ocelic, R. Hillenbrand, Nano Lett., **7** (2007), 3177-3181

Figures
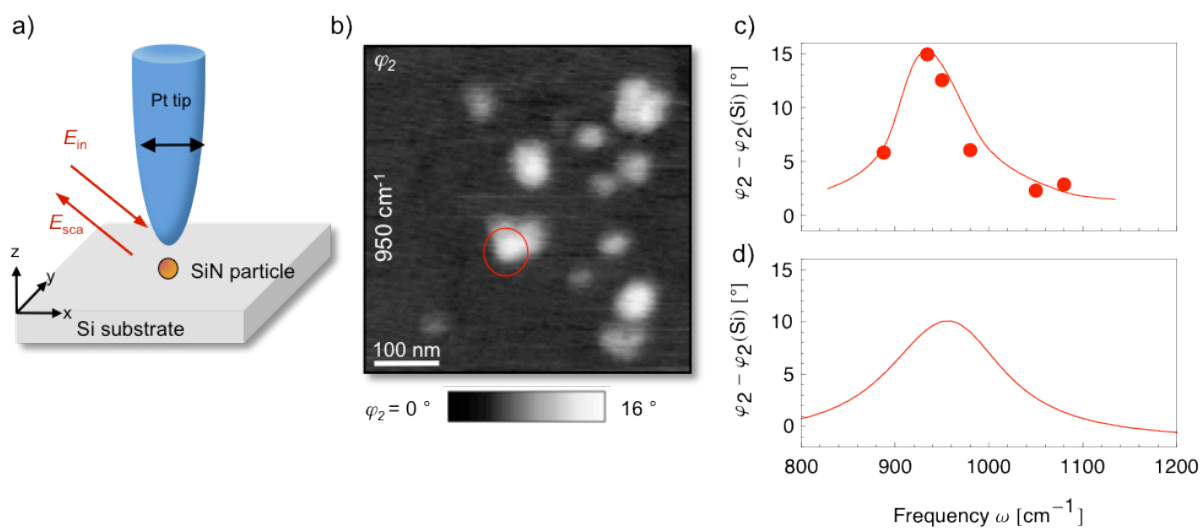
Spectral s-SNOM imaging of a 10 nm SiN nanoparticle. a) Experimental Setup. b) Experimental image showing an IR phase φ_2 image recorded at 950 cm^{-1}. c) Measured and d) calculated near-field phase φ_2 spectrum of the particle encircled in b), The solid line in c) represents a guide to the eye.

A paramagnetic to antiferromagnetic electron spin coupling transition induced by an electric field in a Polyoxometalate.

Nicolas Suaud[a], O. Svoboda[a], Nathalie Guihéry[a],
A. Gaita-Arino[b], S. Cardona-Serra[b], Juan-Modesto Clemente-Juan[b], Eugenio Coronado[b]

(a) Laboratoire de Chimie et Physique Quantiques, Université Paul Sabatier, 118 route de Narbonne, Toulouse, France
(b) Instituto de Ciencia Molecular, Universidad de Valencia, Edificios Institutos de Paterna, Catedrático José Beltrán Martínez nº 2, 46980 Paterna , Spain

suaud@irsamc.ups-tlse.fr

Polyoxometalates (**POM**) are a class of inorganic compounds that present a remarkable degree of molecular and electronic tunabilities that impact in many disciplines (catalysis, medicine, materials science). Due to their cluster-type structure, POM are specially useful as model systems for the studies of electronic and magnetic interactions. Indeed, many of these structures allow the inclusion of paramagnetic ions with various nuclearities and definite topologies and geometries. Moreover, they permit a controlled injection of electrons, giving rise to mixed-valence species in which delocalized electrons may coexist and interact with localized magnetic moments.

The possibility to handle the spin information of electrons is of the highest importance for molecular spintronic applications. This work presents a theoretical model Hamiltonian study of the influence of an external electric field on the coupling between two electrons delocalized over the $[GeV_{14}O_{40}]^{8-}$ POM. We show how the coupling, that is almost zero for a small electric field, affords a sudden rise.

References

[1] L.-H. Bi, U. Kortz *et al., J. Clust. Sc.* **17**, 143 (2006);
[2] N. Suaud, A. Gaita-Arino, J. M. Clemente-Juan, J. Marin-Sanchez, E. Coronado, *J. Am. Chem. Soc.,* **124**, 15134, (2002);
[3] N. Suaud , A.~Gaita-Arino, J. M.Clemente-Juan, E. Coronado, *Chem. Euro. J.*, **10**, 4041, (2004)
[2] N. Suaud, Y. Masaro, E. Coronado, J. M. Clemente-Juan, and N. Guihéry, *Eur. J. Inorg. Chem*. 5109 (2009)

Figures
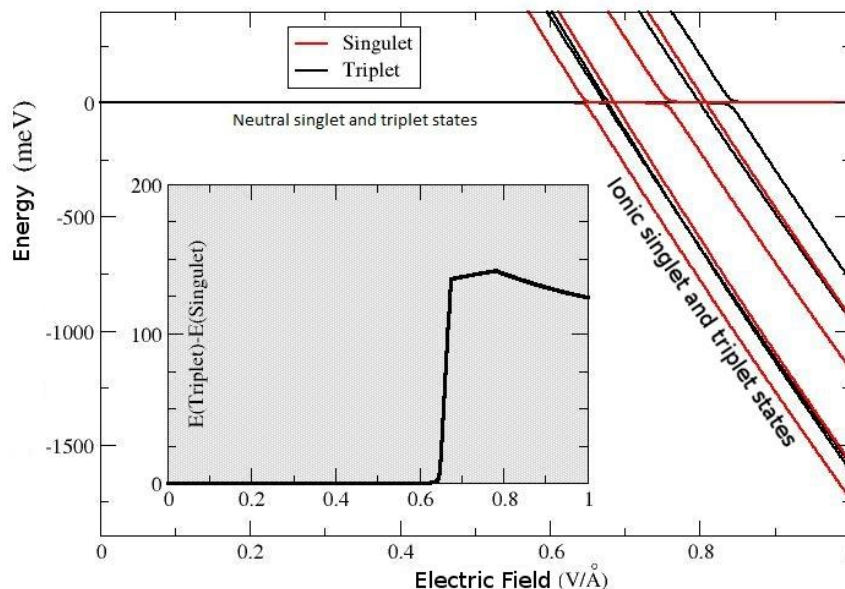
Nanostructured thermosetting systems based on block copolymers as templates for inorganic nanoparticles

Junkal Gutierrez, **Agnieszka Tercjak,** Raquel Fernandez, Maria Dolores Martin, Haritz Etxeberria, Galder Kortaberria, Iñaki Mondragon

'Materials + Technologies' Group, Department of Chemical and Environmental Engineering
University of the Basque Country, Plaza Europa 1, 20018 Donostia/San Sebastian, Spain
agnieszka.tercjaks@ehu.es

Block copolymers can self-assemble to form nanoscale structures with domain spacing that depends on molecular weight, segment size, and the strength of the interaction between the blocks, represented by the Flory-Huggins interaction parameter. In selective solvents, diblock copolymers are able to form micelles of various morphologies such as spheres, cylinders, vesicles, etc. In the bulk, microphase separation occurs, leading to various microstructures such as spheres, hexagonally packed cylinders, lamellae and discontinuous phases, among others. The ability to control both the length scale and the spatial organization of block copolymer morphologies makes these materials particularly attractive candidates for use as templates in the preparation of functional nano/mesostructured materials, which can act as templates for hybrid inorganic/organic materials.

On the other hand, block copolymers are widely used as templates for generating nanostructured epoxy or phenolic matrices with long range order in both uncured and cured states. One feasible pathway for generating self-assembled thermosetting nanostructures is the use of amphiphilic block copolymers consisting of thermoset-miscible and thermoset-immiscible blocks. As it is well known, nanostructured materials based on thermosetting matrices can find application in many different fields of nanotechnology, such as nanostructured functional surfaces, nanolithography, or building of nanostructured inorganic/organic materials.

In this study, nanostructured thermosetting systems modified with an amphiphilic block copolymer were used as templates for TiO_2 nanoparticles (both commercial and synthetized via sol-gel). In order to reach better dispersion of TiO_2 nanoparticles, in case of the commercial nanoparticles, low molecular weight 4'-(hexyl)-4-biphenyl-carbonitrile (HBC) was used as surfactant. The addition of nematic low molecular weight liquid crystals to the system allows for the achievement of thermo-responsive materials and simultaneously as dispersing agent for TiO_2 nanoparticles. On the other hand, titanium dioxide nanoparticles were employed taking into account their conductive and optical properties, which were measured using tunnelling atomic force microscopy (TUNA) at nanoscale and Keithley at macroscopic scale.

Acknowledgments

References

[1] A. Tercjak, I. Mondragon, Langmuir, 24 (2008) 11216.
[2] A. Tercjak, J. Gutierrez, I. Mondragon, Macromolecules 42 (2009) 3386.
[3] A. Tercjak, J. Gutierrez, C. Ocando, L. Peponi, I. Mondragon, Acta Materialia, 57 (2009) 4624.
[4] A. Tercjak, J. Gutierrez, C. Ocando, I. Mondragon, Langmuir, 26 (2010) 4296.
[5] J. Gutierrez, A. Tercjak, I. Mondragon, Journal of the American Chemical Society, 132 (2010) 873.
[6] J. Gutierrez, A. Tercjak, I. Mondragon, Journal of Physical Chemistry C 114 (2010) 22424.
[7] A. Tercjak, J. Gutierrez, I. Mondragon, Journal of Physical Chemistry C in press / on-line.

Gels, Xerogels and Aerogels from PbS and PbSe Quantum Dots

S. Tscharntke, A.-K. Herrmann, S. G. Hickey, A. Eychmüller

Physical Chemistry, TU Dresden, Bergstraße 66b, 01062 Dresden, Germany
s.tscharntke@chemie.tu-dresden.de

Semiconductor quantum dots attract enormous attention in the scientific world today. The synthesis of highly monodisperse nanoparticles with unique properties can provide a wide range of new materials whose potential uses range from fundamental studies to incorporation into presently existing or newly designed device architectures. The lead chalcogenides are especially interesting due to their large exciton Bohr radii leading to strong quantum confinement.

Possible applications for devices based on individual quantum dots are limited due to their small size. Most techniques are not single-particle based and do not operate in solution environments. Therefore it is imperative to be able to build 2D and 3D architectures without losing the unique characteristics inherent in these nanoscale building blocks that make nanoparticles so unique.[1]

A gel is a solid three-dimensional porous network formed through the interconnection of the primary particles. Depending on the media that fills the pores there are different terms used to describe them. For dried gels the terms aerogel and xerogel are commonly used. An aerogel is a gel that does not change its structure or volume during the drying whilst xerogels undergo shrinkage during the drying process.[2] The resulting properties depend not only on the properties of the building blocks, but are also influenced by the different steps in the gel preparation. Because of the highly porous nature of gels one can achieve very light structures which possess a very high surface area.

We have, from previous studies, gained a great deal of experience in the field of aerogel preparation using CdTe quantum dots[3] and noble metal nanoparticles[4] as building blocks and we have been able to extend these approachs successfully to the lead chalcogenides.

Combining the properties of lead sulfide and lead selenide quantum dots with the unique properties of gel structures will offer a wide market for further applications such as thermoelectric devices.

In this work we will describe the formation of lead sulfide, lead selenide and mixed lead sulfide lead selenide gel structures and their different dried equivalents. Starting from quantum dots prepared by hot injection into organic media, gels are formed from between two hours to four days depending on the chosen conditions. These three dimensional gels are supercritically dried or dried under ambient pressure to achieve aerogels and xerogels, respectively. The resulting structures are characterized with respect to their optical and electrical properties, their structure and their composition.

References

[1] S. Brock *et al.*, Comments Inorg. Chem. **27** (2006) 103.
[2] N. Hüsing *et al.*, Angew. Chem. Int. Ed. **110** (1998) 22.
[3] N. Gaponik *et al*., Adv. Mater. **40** (2008) 4257.
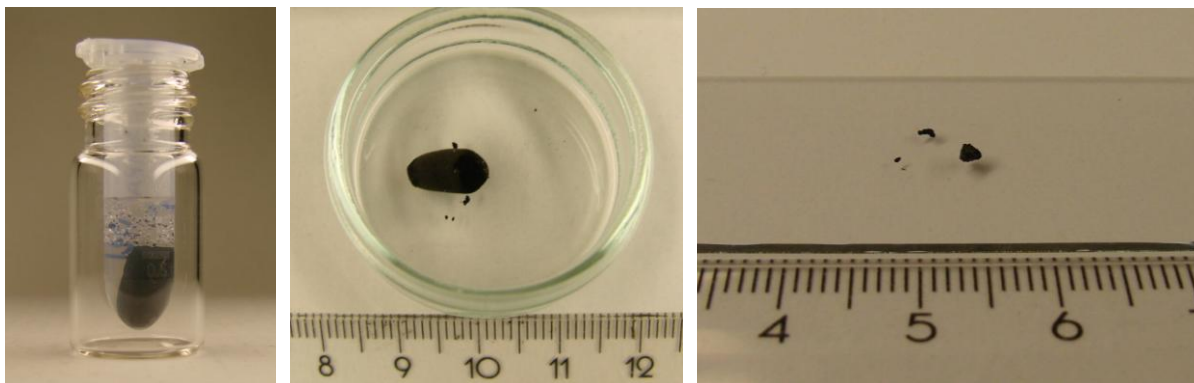[4] N. C. Bigall *et al*., Angew. Chem. Int. Ed. **48** (2009) 9731.

Figures

Figure 1: wet gel [left], gel after supercritical drying (aerogel) [middle] and gel after subcritical drying (xerogel) [right]
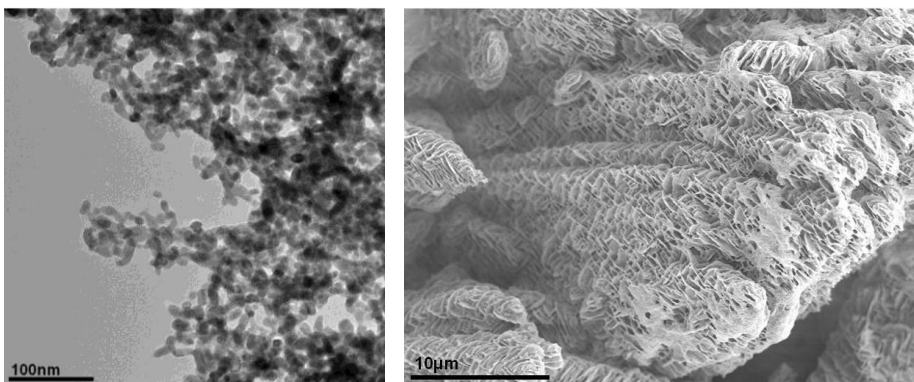

Figure 2: TEM image of a mixed PbS/PbSe aerogel [left] and SEM image of a PbS xerogel [right]

Evaluation of aprotinin-loaded microemulsion formulations for parenteral drug delivery: In vitro release studies

H. Yeşim Karasulu[1], **Neslihan Üstündağ Okur[1],** Derya İlem[2], Nevin Oruç[3], Hayal Özkılıç[4], Makbule Aşıkoğlu[2], İ. Eren Akçiçek[3], Zeynep Ay Şenyiğit[1], Funda Yılmaz[5], Ömer Özütemiz[3], Tamer Güneri[1]

[1]Department of Pharmaceutical Technology, Faculty of Pharmacy, University of Ege, Izmir, Turkey
[2]Department of Radiopharmacy, Faculty of Pharmacy, University of Ege, Izmir, Turkey
[3]Department of Gastroenterology, Faculty of Medicine, University of Ege, Izmir, Turkey
[4]Nuclear Medicine, Faculty of Medicine, Ege University, Izmir, Turkey
[5]Department of Pathology, Faculty of Medicine, University of Ege, Izmir, Turkey
neslihanustundag@yahoo.com

ABSTRACT

Microemulsions (M) are thermodynamically stable, transparent and low-viscosity colloidal dispersions consisting of microdomains of oil and/or water stabilized by an interfacial film of alternating surfactant and cosurfactant molecules [1].

Aprotinin is a monomeric globular polypeptide derived from bovine lung tissue; it has a molecular weight of 6512. It is a Kunitz protease inhibitor and has a wide action with particular against trypsin, chymotrypsin and kallikrein, making it theorically attractive in ameliorating the effects of acute pancreatitis [2].

The aim of this study was to formulate appropriate w/o and o/w microemulsion formulations for parenteral aprotinin administration to use in pancreatitis therapy.

To investigate in vitro release profile of aprotinin from newly developed microemulsion formulations, aprotinin was radiolabeled with ^{99m}Tc and comparative in vitro release studies have been performed with radiolabeled complex loaded microemulsions.

Preparation of aprotinin-loaded microemulsion formulations

The microemulsion systems (M1-2-3) were formulated with various compositions of oleic acid (OA), isopropyl myristat (IPM), Labrasol, Cremophor EL (Cr-El), ethanol, isopropyl alcohol (IPA) and 0.9 % NaCl solution. Drug-loaded microemulsions were prepared by dissolving 2 mg of aprotinin.

Preparation of ^{99m}Tc-Aprotinin

Aprotinin was dissolved in glycine phosphate alkaline buffer (GPB). While stirring, freshly prepared stannous chloride solution was added under a nitrogen atmosphere. The mixture was mixed well and filtered from a cellulose acetate filter (0.22 µm) into a vial. ^{99m}TcO$_4^-$ in saline was added to this solution and allowed to stand for 20 minutes at room temperature prior to radiochemical analysis.

Quality Control and the Stability of ^{99m}Tc-Aprotinin

The radiochemical purity of the product was analyzed by paper and Thin Layer Chromatography (TLC), using Whatman 3MM papers in acetone (100%) and Albumin-impregnated ITLC-SG strips in ammonia/ ethanol/water (1/2/5) [3]. Radiochemical purity and stability of ^{99m}Tc-Aprotinin were analyzed by TLC scanner (Bioscan AR2000) at room temperature up to 6h.

Preparation of ^{99m}Tc-Aprotinin loaded microemulsion

2 mg of aprotinin included ^{99m}Tc-Aprotinin solution was added into M1-M2 and M3 formulations.

In Vitro Release Profile of Aprotinin

^{99m}Tc-Aprotinin from microemulsions (M1-3) and solution were examined using the dialysis tube method. Dialysis tubes (Dialysis sacks, width 35 mm, diameter 21 mm, molecular weight grater than 12.000) were purchased Spectro-por and appropriate closures were purchased from Spectrum (Los Angeles, CA, USA). Inbrief, a dialysis tube containing 1 mL ^{99m}Tc-Aprotinin-microemulsion (M1-3) or solution was immersed in 50 mL of PBS (pH 7.4) as receiver. In vitro release studies were performed at 37±0.5°C and 600 rpm during the experiment. Then 100 µL of sample was withdrawn at an appropriate time intervals and an equal volume of the PBS was added. For determination of radioactivity, samples were placed in to a gamma counter (Sesa Uniscaler I/S).

RESULTS AND DISCUSSION

The optimum microemulsion formulations according to phase diagrams are shown in Table 1.

Table 1: Composition of the microemulsion formulations

	M1	M2	M3
Oil phase	OA 33.92%	OA 9.34%	IPM 10.18%
Surfactants/ co-surfactants	Cr- EL/ Ethanol 51.62%	Cr-EL / IPA 54%	Labrasol/ IPA 66.58%
Water phase	0.9% NaCl 14.46%	0.9% NaCl 36.66%	0.9% NaCl 23.25%

Radiolabeling and Quality Control and the Stability of ^{99m}*Tc-Aprotinin*

Radiolabeling efficiency of ^{99m}Tc-Aprotinin was found to be greater than 95%. The TLC studies indicated that ^{99m}Tc-Aprotinin is stable for up to 6 hrs at room temperature (
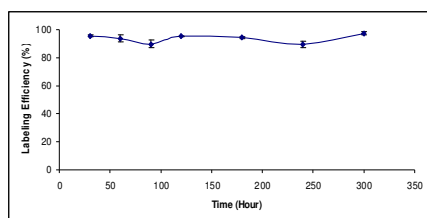
Figure **1**).

Figure 1: Stability of the ^{99m}Tc-Aprotinin at room temperature

In Vitro Release of M-Aprotinin

The in vitro release behavior of ^{99m}Tc-Aprotinin from microemulsions (M1-3) and solution is shown in Figure 2. As clearly seen in Figure 2, the release behavior of Aprotinin from M2 formulation exhibited a slower and continuous release for 6 hrs compared wih the other formulations and solution. Therefore, this suggests that release rate of Aprotinin from microemulsion could be controlled by this formulation.
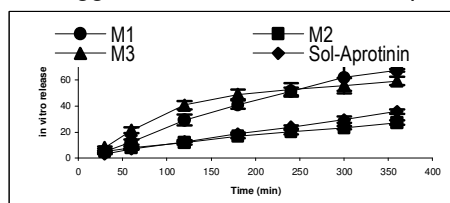
Figure 2: Release profiles of ^{99m}Tc-Aprotinin from M1-2-3 and Sol-Aprotinin (n = 3). Each value represents the mean ± S.D.

CONCLUSION

The results of in vitro release studies showed that release rate of ^{99m}Tc-Aprotinin from microemulsion could be controlled by microemulsion formulations.

REFERENCES

1- Jadhav KR, Shaikh, IM, Ambade KW, Kadam VJ. Applications of microemulsion based drug delivery system. Curr Drug Deliv 3: 267-273, 2006.

2- Smith M, Kocher HM, Hunt BJ. Aprotinin in severe acute pancreatitis. Int J Clin Pract, in press, 2009.

3- Smyth DR, Tsopelas C. 2005, An improved ^{99m}Tc-aprotinin kit formulation: quality control analysis of radiotracer stability and cold kit shelf life. Nuclear Medicine and Biology 32 (2005) 885–889.

STM and LEEM characterization of the interaction between magnesium grown on Ru(0001) and hydrogen

L. Vergara[1], B. Santos[1], T. Herranz[2], M. Monti[1], K. F. McCarty[3], J. de la Figuera[1]

[1]Instituto de Química-Física "Rocasolano", CSIC, C/ Serrano 119, 28006 Madrid, Spain
[2]Instituto de Catálisis y Petroleoquímica, CSIC, 28049 Madrid, Spain
[3]Sandia National Laboratories, 7011 East Avenue, Livermore, California 94550, USA

lvergara@iqfr.csic.es

Magnesium is a readily available non-toxic metal whose hydride (MgH_2) is being studied as a potential hydrogen storage medium, owing to its large content of 7.6% by weight of hydrogen. Magnesium is known to grow as almost perfect thin films on many substrates; in some instances, like in the case of refractory metals, with very sharp interfaces. Since a layer of $MgO/Mg(OH)_2$ grows onto the magnesium surface when it is exposed to air, changing its reactivity, the understanding of the interaction between the surface of the magnesium layer and hydrogen is of the utmost importance. Most of the few works that have been devoted to the preparation of magnesium on refractory metals study its growth on W(110) substrates [1,2]. A study about the epitaxial growth of magnesium on Ru(0001) using low-energy electron diffraction (LEED) [3] reported that magnesium keeps its own in-plane spacing when growing on such substrate, owing to the large mismatch between their respective in-plane lattice spacings (around 18%). This results in a moiré pattern on the magnesium surface, and an overlayer film without significant strain. Additionally, not much has been published about scanning tunnel microscopy (STM) characterization of epitaxial growth of magnesium up to two monolayers at room temperature.

This work is a continuation of our recent studies about the growth and hydrogenation of magnesium on Ru(0001) substrates in ultra-high vacuum [4,5]. The characterization techniques we have employed are STM and low-energy electron microscopy (LEEM), an in-situ technique that provides real-time observations at different temperatures with spatial resolution of nanometres. Magnesium was grown to a thickness of one to ten atomic layers by evaporating a rod heated by electron bombardment at a pressure in the low 10^{-10} Torr range, with a typical deposition rate of about one monolayer per minute. Up to a temperature of 430 K, the films present a layer-by-layer growth with three levels exposed at the most. The submonolayers of magnesium, detected only by STM and only in the first two atomic layers, show a moiré pattern with a periodicity of 12 Å, as can be seen in figure 1. Dark-field LEEM experiments show that films with a higher number of monolayers present stacking faults and, on stepped areas, screw dislocations are observed by STM (see figure 2), owing to the mismatch of the step heights of magnesium and ruthenium in these areas. Electron reflectivity shows quantum size effects in the unoccupied bands, indicating an abrupt interface between magnesium and ruthenium for the thicker films. Additionally, we have studied the exposure to H and H_2 of the growing films by LEEM and STM. While growth in an H_2 atmosphere produces no significant change in the magnesium films, LEEM measurements have demonstrated the nucleation of dark islands as soon as H is fed into the vacuum chamber; further exposure to H leads to their almost covering completely the field of view. Using a mass spectrometer, we have performed thermal desorption experiments in these dark islands (see figure 3), which show that hydrogen is the only gas desorbed, with a sharp peak around 470 K coinciding with the disappearance of the islands in the LEEM images. At higher temperatures, only a faint trace of them remains on the surface.

References

[1] F. Schiller, M. Heber, V.D.P. Servedio and C. Laubschat, Phys. Rev. B **70** (2004), 125106.
[2] L. Aballe, A. Barinov, A. Locatelli, T. Mentes and M. Kiskinova, Phys. Rev. B **75** (2007), 115411.
[3] H. Over, T. Hertel, H. Bludau, S. Pflanz and G. Ertl, Phys. Rev. B **48** (1993), 5572.
[4] T. Herranz, K.F. McCarty, B. Santos, M. Monti and J. de la Figuera, Chem. Mat. **22** (2010), 1291.
[5] T. Herranz, B. Santos, K. F. McCarty and J. de la Figuera, Surf. Sci., in press.

Figures

(a) (b)
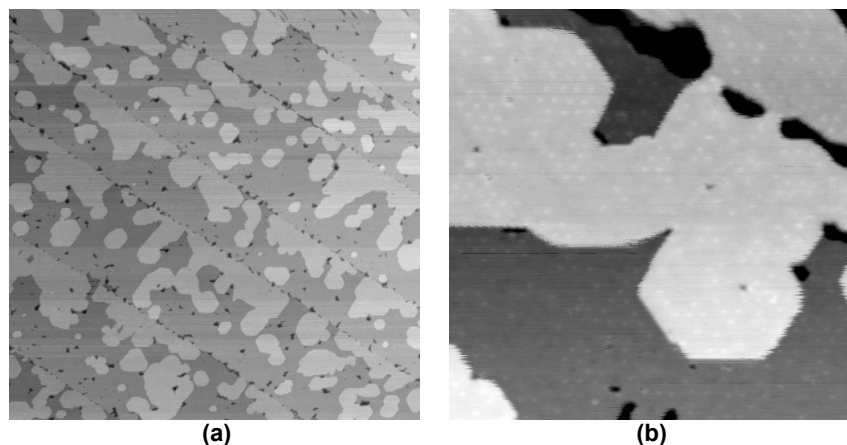
Figure 1. STM images of a magnesium film with an almost complete first monolayer and islands of the second monolayer. a) 4500-Å wide image, and b) 550-Å wide image, in which the moiré in the islands can be seen.
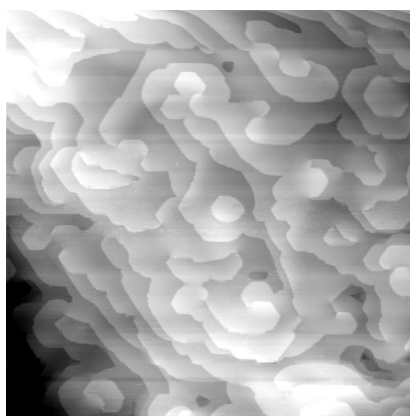
Figure 2. Screw dislocation in stepped areas seen by STM (image width and height: 3500 Å).
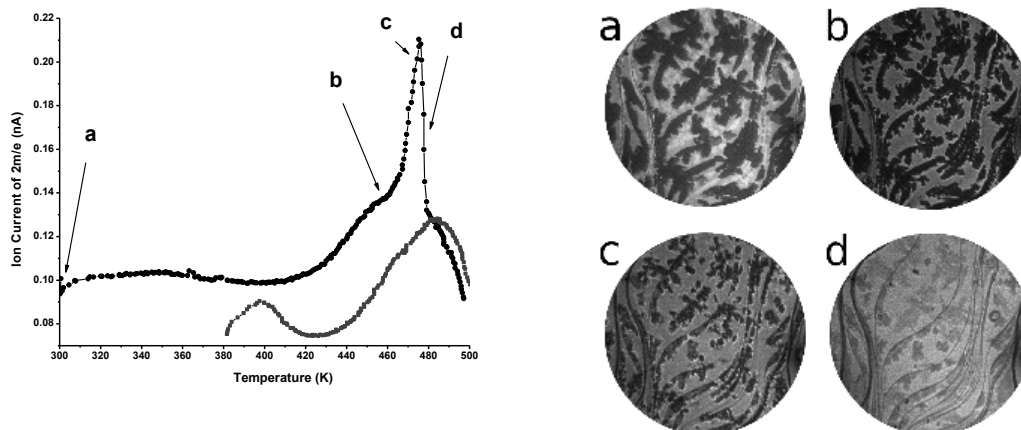
Figure 3. Thermal desorption measurements carried out in the dark islands of magnesium films with ten atomic layers grown under exposure to H_2 (lower curve) and H (upper curve). Labelled temperatures in the upper curve correspond to each of the LEEM images on the left (field of view is of 15 µm).

Macroporous foams obtained in highly concentrated Pickering emulsions stabilized solely with magnetic nanoparticles

Vílchez, A[1,*]; Rodríguez-Abreu, C[2]; Solans, C[1]; Esquena, J[1].

[1] Surface Chemistry Group, Institute for Advanced Chemistry of Catalonia (CSIC), Barcelona, Spain
[2] International Iberian Nanotechnology Laboratory (INL); Braga, Portugal

Menner, A[3]., Bismarck, A[3]

[3] Chemical Engineering Department, Imperial College of London, United Kingdom

* avvqst@cid.csic.es

Macroporous solid foams with magnetic properties may have interesting applications as adsorbents for purification and decontamination processes. High pore volume can ensure a high degree of absorption, and magnetic properties can facilitate removal from environment. Organic macroporous polymeric foams, with high pore volume and high degree of interconnectivity, can be obtained by polymerizing in the external phase of highly concentrated emulsions, stabilized with surfactants [1-4]. In the present work, the main objective was to incorporate magnetic nanoparticles on the pore walls. Therefore, an alternative method for the preparation of solid foams was used [5], based on Pickering emulsions, which are stabilized solely with nanoparticles in absence of surfactant [6-7]. Oleic-modified magnetic nanoparticles were used to prepare highly concentrated water-in-oil (W/O) Pickering emulsions, in which the monomers are located in the external continuous phase. The degree of oleic acid modification was optimized to achieve the appropriate hydrophilic-lipophilic balance of the magnetic nanoparticles, in order to maximize emulsion stability. The resulting highly concentrated Pickering emulsions showed bigger droplet size and greater stability, compared to conventional highly concentrated emulsions. Porous materials were obtained by polymerizing the monomers using an oil soluble initiator. No time-consuming purification was needed, since the emulsions did not contain any surfactant. The results showed that the polystyrene monoliths had very low density and showed big macropores with relatively closed-cell pore morphology (Fig. 1a), typical for this kind of systems. The nanoparticles remained at the pore surface (Fig. 1b), and the monolithic solid foams retained the magnetic properties resulting from the nanoparticles.

References
[1] D. Barby, Z. Haq 1982, European patent 0060138 1982.
[2]N.R. Cameron, D.C. Sherrington, *Adv. Polym. Sci.*, **126** (1996), 163.
[3] Esquena, J.; Sankar, G.S.R.; Solans, C. *Langmuir* **19**, (2003), 2983.
[4] J. Esquena, C. Solans, in J. Sjöblom (Ed.), Emulsions and Emulsion Stability, Francis & Taylor, New York 2006, 245-260.
[5] V.O Ikem, A. Menner, A. Bismarck, *Angew. Chem., Int. Ed.* **47**, (2008), 8277.
[6] S.U. Pickering, J. Chem. Soc. **91**, (1907), 2001
[7] B.P Binks, P.D.I Fletcher, *Langmuir*, **17,** (2001), 4708.

Figure 1
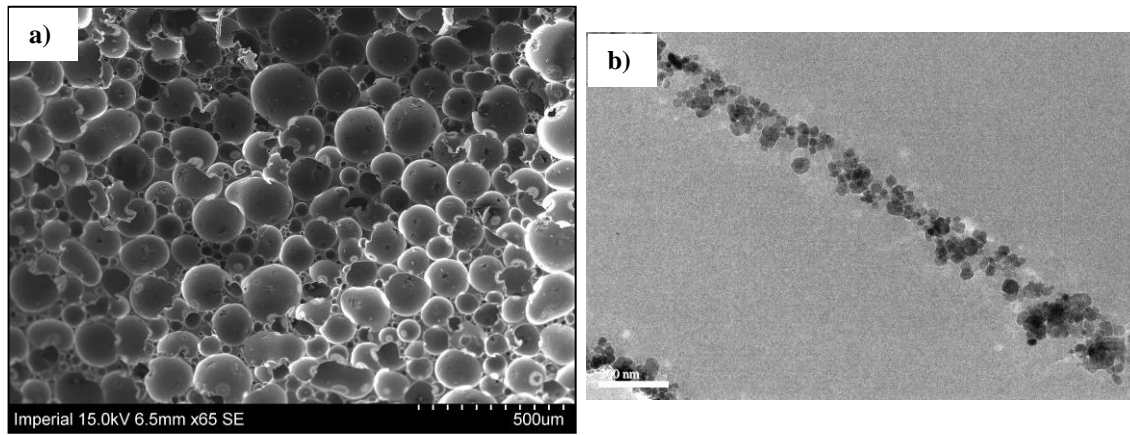
a) SEM image of a polysterene foam obtained in Pickering emulsions stabilized solely with 3wt% iron oxide nanoparticles (scale bar = 500 µm); b)TEM image of a slide (60 nm thick) showing the nanoparticles located at the polystyrene-air interface (scale bar = 200 nm).

Optimal Light Harvesting Structures in the mid Infrared

F. Villate-Guío[1], F. de León-Pérez[1,2], F.J. García-Vidal[3], and L. Martín-Moreno[1]

[1]Departamento de Física de la Materia Condensada and Instituto de Ciencia de Materiales de Aragón (ICMA), CSIC-Universidad de Zaragoza, E-50009 Zaragoza
[2]Centro Universitario de la Defensa, E-50090 Zaragoza
[3]Departamento de Física Teórica de la Materia Condensada, Universidad Autonoma de Madrid, E-28049 Madrid
fvillate@unizar.es

The ability of surface modes for squeezing visible light into metallic sub-wavelength apertures have being intensively investigated during last 10 years [1]. Efficient light harvesting (LH) structures have been proposed [2,3] and later used in the development of optical detectors, which can be integrated into standard optoelectronic devices [4]. The main goal of the present work is to translate the state of the art in LH technologies from the optical to the mid-IR regimen. As a first step into that direction, we study a typical LH structure: a sub-wavelength slit perforated in a corrugated metal film; see the inset of Fig. 1. Its IR response is computed with the coupled-mode method [1]. We show that the IR response of this 1D system can be optimized following simple design rules, based on physical intuition. Such optimal systems are next used as a seed for a conjugate gradient algorithm (CGA), which automatically scans the whole parameter space. Fig. 1 illustrates our results. It shows the spectra for a slit-grove array optimized with the CGA at a wavelength λ=4 µm. The back curve depicts the normalized-to-area transmittance (η) of a slit-groove array, where the single slit *is* surrounded by 20 grooves. An efficiency of η=60 is obtained at λ=4 µm, which means that our LH structure is 60 times more efficient than a single slit. A further enhancement of 20% is achieved for a chirped structure (blue curve of Fig. 1).

References

[1] F.J. Garcia-Vidal et al., Rev. Mod. Phys. 82, 729 (2010).

[2] F. J. García-Vidal, H. J. Lezec, et al., Phys. Rev. Lett. **90**, 213901 (2003)

[3] O. T. A. Janssen *et al*., Phys. Rev. Lett. 99, 043902 (2007).

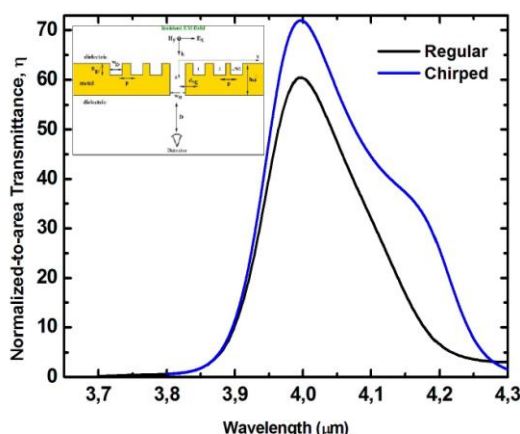[4] L. A. Dunbar *et al*., Appl. Phys. Lett. 95, 011113 (July 2009).

Figures

Figure1. Normalized to area transmittance for a slit-grooves array optimized at λ=4.0 µm. The efficiency of the regular structure described in the text is compared with a chirped slit-groove array (Slit: width=0.36 µm and depth=1.28 µm. Grooves: depth=0.5 µm, width=0.36 µm, and pitch=3.8 µm).

New aspects in the hot injection synthesis to provide large scale high quality quantum dots

C. Waurisch, L. Liebscher, E. Sperling, S. G. Hickey, A. Eychmüller

Physical Chemistry, TU Dresden, Bergstraße 66b, 01062 Dresden, Germany
c.waurisch@chemie.tu-dresden.de

Quantum dots (QDs) exhibit a range of unique optical and (opto-)electrochemical properties and thus are the subject of many research areas including chemistry, physics and material science. Amongst the applications that they may conceivably be used for are: solar cells, light emitting diodes, thermoelectric materials beside others. Such applications require high quality materials with well defined properties, and in particular for industrial implementation, large amounts. The hot injection method is a laboratory based, organo-metallic synthesis approach for the production of high quality colloidal QDs which demands up-scaling of the optimized lab scale synthesis protocols if an industrial scale is required. The synthetic route of the hot injection method involves a rapid injection of a precursor solution into a hot solution of high boiling coordinating components to affect a homogeneous nucleation event which is followed by subsequent growth at lower temperatures.[1] The precursor injection leads to monomer formation and, due to supersaturation, nuclei are formed. After lowering the reaction temperature the energy barrier for nucleation cannot further be overcome and the growth process is favored while nucleation is suppressed. Up-scaling of the precise laboratory scaled reaction conditions is a complex procedure which involves implementing changes to many parameters including those of process engineering as well as physical and chemical values.

In this contribution we present a novel way to optimize the parameters that allow the up-scaled syntheses of high quality CdSe and PbSe QDs. With a modified hot injection procedure, the seeded growth method, nuclei are introduced into the reaction and thus heterogeneous nucleation results. A special case of this approach is the *quasi* seeded growth, wherein nuclei of a different material are formed *in situ* and subsequently a cation exchange occurs whereupon the required seeds are formed and the overall process is simplified to the growth of the particles (see Figure 1).[2] Whilst in the bulk the exchange reaction is kinetically hindered, in the nanoparticular size regime it is thermodynamically favored.[3] A particular feature of the materials resulting from the up-scaled synthesis is the narrowness of the full width at half maxima of the interband transition peaks as determined by optical spectroscopy of the colloidal solutions and which is a reflection of the quality of the QDs, especially that of the particle size distribution (see Figure 2). It is envisioned that this methodology may be applied to up-scaling the synthesis of other QD materials.

References

[1] J. Park *et al.*, Angew. Chem. Int. Ed. **46** (2007) 4630.
[2] M. V. Kovalenko *et al.*, Angew. Chem. Int. Ed. **47** (2008) 3029-3033.
[3] D. H. Son *et al.*, Science **306** (2004) 1009.
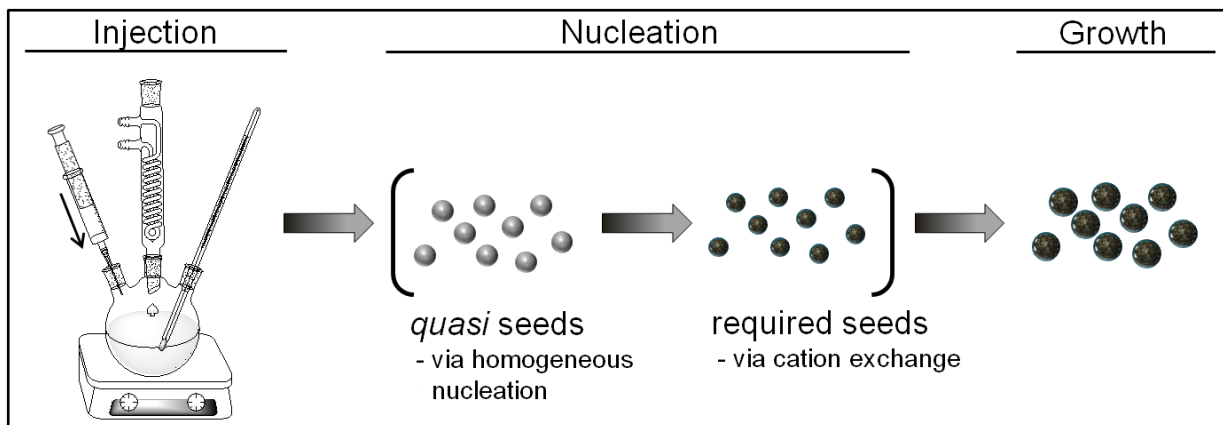
Figures

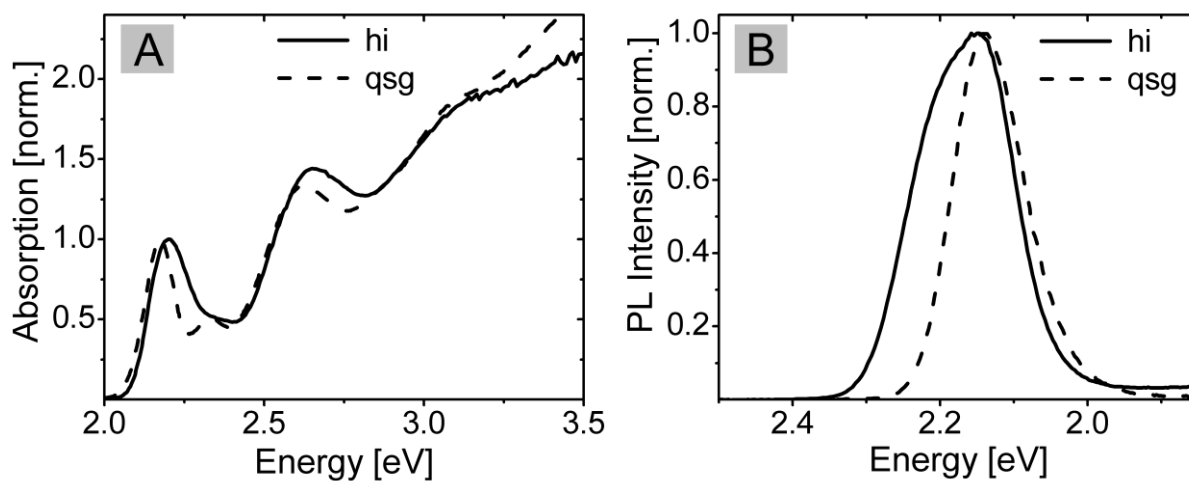*Figure 1: Mechanism of the quasi seeded growth approach.*[2]

Figure 2: Normalized absorption (A) and emission (B) spectra of the up-scaled approach to provide CdSe nanocrystals via the standard hot injection (hi) as well as the quasi seeded growth method (qsg).

Signature of clustering in Na nanocontacts

N. Zabala[1,2], A. Zugarramurdi[1,2], A.G. Borisov[3], E.V. Chulkov[2,4] and M.J. Puska[5]

[1]Department of Electricity and Electronics, FCT-ZTF, UPV-EHU, Bilbao, Spain.
[2]DIPC and CFM (CSIC-UPV/EHU), San Sebastian, Spain.
[3]CNRS, ISMO, UMR CNRS-Université Paris-Sud, 91405 Orsay CEDEX, France.
[4]Department of Materials Science, Faculty of Chemistry, UPV-EHU, San Sebastian, Spain.
[5]Department of Applied Physics, Aalto University, AALTO, Finland.

nerea.zabala@ehu.es

Nowadays, systematic studies of electronic and mechanical properties of nanocontacts are possible thanks to the mechanically controllable break junction (MCBJ) and scanning tunneling microscopy experiments [1,2]. In particular, the MCBJ is very well suited for conductance measurements, providing histograms for large sets of individual contact-breaking events as the basic input for further analysis. The electronic (atomic) shell structures of nanowires could be demonstrated with this technique [1] where the stable nanowire configurations are characterized by "magic radii" in analogy to the well-known "magic numbers" of abundance in metal clusters of different sizes [3].

Ogando et al. reported the formation of cluster-like arrangements of atoms, preceding the breakage of a stretched nanowire [4] using the ultimate jellium (UJ) model, in full agreement with previous first-principles molecular dynamics simulations [5]. The system considered in the simulations is sketched in the top of figure 1. It consists of two cylindrical UJ leads, whose potential is frozen after self-consistent calculations for an infinite wire of stable magic radius, and a central deformable part between the leads. Rearrangements upon stretching of the nanowire are only allowed in this central part. We have compared two cases in which 5 and 10 electrons are considered initially in the deformable region (this procedure is equivalent to the usual methodology followed in ab initio methods, where only a few atoms are allowed to relax. In the second case we observe the formation of a stable cluster of 8 electrons before the breakage.

Here we report on how the conductance of the elongated nanowire is affected by the formation of stable cluster-like arrangements of atoms in the break junction, by using a combined approach where the nanowire breakage is simulated with self-consistent electronic structure calculations within the density-functional theory (DFT). These self-consistent calculations provide an input for a follow-up wave packet propagation (WPP) study of the ballistic electron transport through the break junction [6,7].

We find that clustering leads to delayed and rounded conduction jumps upon the stretching of the nanowire (figure 1(a)). The results are analyzed in terms of the evolution of the transmission resonances originating from the cluster-localized electronic states [8]. The situation at hand then closely corresponds to the electron transport through molecular junctions studied in great detail in the context of molecular electronics, where the cluster would play the role of the molecular object. According to our results the resonant character of the transmission reveals itself particularly clearly in the bias voltage dependence of the differential conductance (figure 1(b)), suggesting experimental ways to evidence the presence of clusters in the break junction.

The main conclusions and results reported in this work are not determined by the specific choice of the nanowire material (Na) but rather by the very fact of the clustering at the break junction. The latter

phenomenon is of quite general nature, as it not only happens for the stretched Na nanowires but has also been reported for gold nanowires [9-11]. We hope that this work will stimulate further research on various aspects of the cluster formation during the contact breaking, such as the cluster appearance probability, stability and the effect on the conductance.

References

[1] N. Agraït, A. Levi-Yeyati, and J. van Ruitenbeek, Phys. Rep., **377** (2003) 81.

[2] G. Rubio, N. Agraït, and S. Vieira, Phys. Rev. Lett., **76** (1996) 2302.

[3] W. D. Knight, K. Clemenger, W. A. de Heer, W. A. Saunders, M. Y. Chou, and M. L. Cohen, Phys. Rev. Lett., **52** (1984) 2141.

[4] E. Ogando, T. Torsti, N. Zabala, and M. J. Puska, Phys. Rev. B, **67** (2003) 075417.

[5] R. Barnett and U. Landman, Nature (London), **387** (1997) 788.

[6] A.G. Borisov, A.K. Kazansky, J.P. Gauyacq, Phys. Rev. B, **59** (1999) 10935.

[7] E. V. Chulkov, A. G. Borisov, J. P. Gauyacq, D. Sanchez-Portal, V. M. Silkin, V. P. Zhukov, and P. M. Echenique, Chem. Rev., **106** (2006) 41601.

[8] A. Zugarramurdi, A.G. Borisov, N. Zabala, E.V. Chulkov and M.J. Puska, Phys. Rev. B, **83** (2011) 035402.

[9] P. Jelínek, R. Pérez, J. Ortega, and F. Flores, Phys. Rev. B, **77** (2008)115447.

[10] L. Hui, F. Pederiva, G. H. Wang, and B. L. Wang, J. Chem. Phys., **119** (2003) 9771.

[11] F. Tavazza, L. E. Levine, and A. M. Chaka, J. Appl. Phys., **106** (2009) 043522.

[12] A. Nakamura, M. Brandbyge, L. B. Hansen, and K. W. Jacobsen, Phys. Rev. Lett., **82** (1999) 1538.

Figures
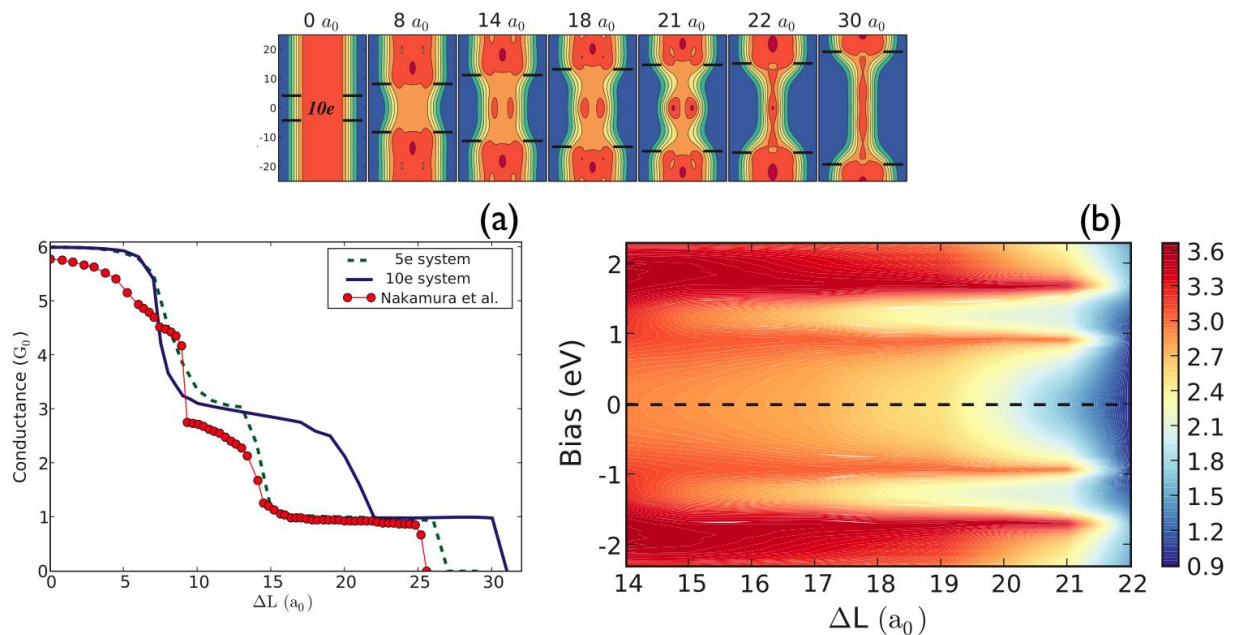
Figure 1: (Up) Snapshots of the charge density during the stretching of a Na nanowire of magic radius 10.7 a_0 and ten electrons initially in the deformable constriction for elongations ΔL= 0, 8a_0, 14a_0, 18a_0, 21a_0, 22a_0, and 30a_0. (a) Calculated conductance as a function of the nanowire elongation when 5 and 10 electrons are considered initially in the deformable part, together with ab initio data by Nakamura et al. [12]. (b) Differential conductance dI/dU map for the breakage of the same Na nanowire with ten electrons in the deformable constriction. The results are shown as a function of the applied bias voltage and nanowire elongation.

OLIGOPEROXIDE BASED SYNTHESIS OF NOVEL FUNCTIONAL POLYMERIC AND HYBRID NANOCOMPOSITES OF BIOMEDICAL APPLICATION

A. Zaichenko[1], N. Mitina[1], O. Shevchuk[1], A. Voloshinovskii[2], R. Stoika[3]

[1]Lviv Polytechnic National University, Lviv, 79013, Ukraine
[2]I. Franko National University, 6 Cyril and Methody Str., Lviv, 79005, Ukraine
[3]Institute of Cell Biology of NASU, 14/16 Drahomanov Str., Lviv, 79005, Ukraine

zaichenk@polynet.lviv.ua

Main experimental approaches based on tailored synthesis of oligoperoxide surface-active substances (SAS) and derived metal complexes (OMC) with transition or rare earth metal cations and their application for obtaining polymeric and hybrid nanoscale carriers possessing targeted functionality and biocompatibility are presented. Molecular design of novel linear, block and comb-like oligoperoxide surfactants and derived coordinating complexes of transitional and rare earth metal cations is convenient tool for the synthesis of luminescent, X-ray detectable, super paramagnetic, colored and other functional nanocomposites with controlled size distribution, and reactivity.

For the synthesis of reactive functional nanocomposites various approaches were developed and studied, namely:

1. Water and hydrocarbon dispersion polymerization including miniemulsion and emulsifier free polymerizations initiated by OMC;

2. Water dispersion co-polymerization with novel surface-active including fluorine- or galactose -, or mannose containing monomers;

3. Homogeneous nucleation of functional hybrid mineral - polymeric nanoparticles (Au, Ag, Pd, $LaPO_4...Eu^{3+}$, Fe_3O_4, Ni, Fe_2O_3 etc.) from the salt solutions in the presence of SAS or OMC including magnetic and luminescent ones;

4. Seeded polymerization initiated from the surface of functional polymeric and hybrid nanoparticles and colloids previously modified by SAS or OMC;

5. Tailored OMC based synthesis and study of comb-like and highly branched functional surface-active oligoperoxides with alternate hydrophilic and hydrophobic branches forming micelle-like nanostructures in the media of various polarities;

6. Tailored synthesis and study of surface – active functional oligoperoxides of telechelic or block structures forming micelle-like nanostructures in the media of various polarities;

7. Tailored synthesis and study of functional oligoelectrolyte based nanogels with controlled porous size and functionality capable to adsorb and release poor soluble in water drugs, form polyplexes with DNA or to be filled with gold (magnetite) nanoparticles.

The methods developed provide combining the stage of formation of polymeric, metal and metal-oxide nanoparticles with the stage of their surface irreversible modification by functional surface-active oligoperoxides capable of binding physiologically active substances. Novel functional nanoparticles are studied by chemical, colloidal-chemical, and rheological methods, X-ray diffraction technique, luminescent spectroscopy, transmission and scanning electronic microscopy. The availability of reactive ditertiary peroxide fragments appearing on the particle surface as a result of oligoperoxide sorption causes their reliable protection, hydrophilicity and ability to radical grafting functional polymer chains. Functional nanoparticles developed can be recommended for study of phagocytosis, as pathological cell markers, antimicrobial remedies and for targeted drug and DNA delivery. Some of them are untoxic and biodegradable substances and successfully studied as cell recognizing carriers for targeted anticancer drug delivery and for DNA transfection.

Nanometer-sized Au nanoparticles from mono-, bi-and tri-dentate thiolate ligands

R. Zanoni,[1] A. Boccia,[1] L. Pescatori,[2] F. Ciesa,[2] A. Arduini,[2] A. Pochini,[2] A. Secchi**,**[2] F. Rossi,[3] V. Grillo[3,4]

[1]Dipartimento di Chimica, Universita' degli Studi di Roma La Sapienza, p.le Aldo Moro 5, 00185, Roma, Italy; [2]Dipartimento di Chimica Organica e Industriale and Unita' INSTM Sez. 4 – UdR Parma, Universita' di Parma, viale Usberti 17/a, 43124 Parma, Italy; [3]IMEM-CNR, viale Usberti 37/A, 43124 Parma (Italy); [4]Centro S3, CNR-Istituto Nanoscienze, via Campi 213/A, 41125 Modena, Italy

robertino.zanoni@uniroma1.it

Ligand-stabilized nanoparticles represent an emerging class of organic–inorganic hybrid materials, constituted by a discrete aggregate of metal atoms stabilized by a shell of organic molecules that maintain their stability in solution and prevent aggregation phenomena.[1,2] A series of gold nanoparticles (AuNPs) stabilized by monodentate, bidentate, and tridentate thiolate calix[n]arene ligands was prepared by using the Brust–Schiffrin synthesis.[3] They have been characterized by NMR spectroscopy, elemental analysis, transmission electron microscopy (TEM), and X-ray Photoelectron Spectroscopy (XPS). The experimental data reveal the electronic states of different subsets of Au atoms, and show that the particular multidentate structure of calix[n]arene derivatives introduces a control element in the preparation of the nanoparticles, which allows to obtain very small (<1 nm) nanoparticles. These experimental findings are the first which identify a role of ligand denticity in the determination of the nuclearity of nanoparticles, and open the path to a ligand-assisted synthesis in the nanometer range.
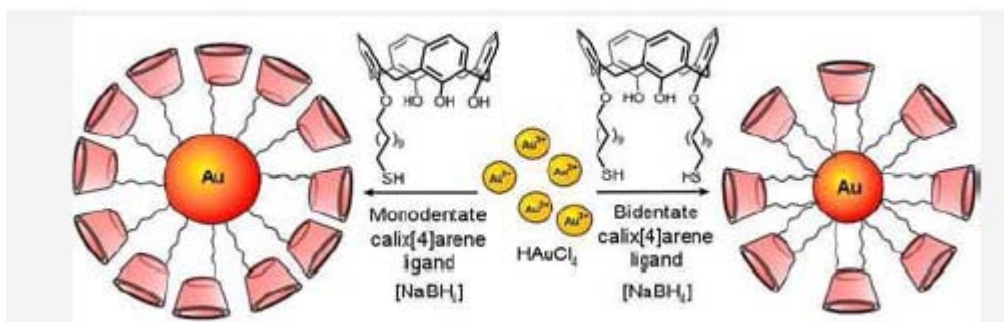
[1] J.C. Love, L.A. Estroff, J. K. Kriebel, R.G. Nuzzo, G.M. Whitesides, Chem. Rev. 2005, 105, 1103.

[2] Hybrid Materials. Synthesis Characterization, and Applications, G. Kickelbick Ed., Wiley-VCH, Weinheim, 2007.

[3] L. Pescatori, A. Boccia, F. Ciesa, F. Rossi, V. Grillo, A. Arduini, A. Pochini, R Zanoni and A. Secchi, Chem. Eur. J. 16, 11089 (2010).

Resistive switching in Hafnium oxide

R. Zazpe[1], F. Casanova[1, 2], L. E. Hueso[1, 2]

1- CIC Nanogune, Av. Tolosa 76, Donostia/San Sebastián, Spain
2- IKERBASQUE, Basque Foundation for Science, E-48011 Bilbao, Spain.

rzazpe@nanogune.eu

Metal-insulator-metal (MIM) capacitor-like structures based on transition metal oxides, have lately been considered as a promising candidate for the next generation of non-volatile memory devices. The operation of such devices is based on the resistive switching effect, which consists in the alternation two different resistance states, high resistance state (HRS) and low resistance state (LRS) by the application of electrical pulses. These resistance states are non-volatile, i.e., they are kept even when no potential is applied. In this work, we present a MIM HfO_2 based device for nonvolatile memory applications. Hafnium oxide thin film (20 nm) was deposited by atomic layer deposition at 300^oC, while both bottom (Titanium) and top electrode (Gold or Cobalt) were deposited by sputtering. To form a capacitor structure, top electrodes of different sizes were patterned (from $64x10^4$ μm^2 to $1x10^4$ μm^2). These memory cells show low working currents ($<5x10^{-5}$ A/cm^2), and a resistance ratio between HRS and LRS larger than 10^3 (Figure 1) irrespective of the top metal contact size. In addition, stable retention ($>5x10^2$ s) and stability (>400 cycles) properties (Figure 2) are found. The pristine device displays a HRS (OFF) and can be switched to a LRS (ON) by a SET process. Viceversa, the RESET process occurs by the application of a negative voltage (Figure 1). An explanation for this behavior could be the growth of conductive filaments in the hafnium oxide insulating matrix. Such conducting filaments are though to be formed by defects percolating under the application of electric field. Ohmic behavior observed in the low resistance state (LRS), agrees this filamentary conduction mechanism. The RESET process has also been found to be gradual, occurring at a relatively wide potential range. The progressive rupturing of the conducting filaments could explain this gradual RESET process which gives rise to intermediate resistive states.
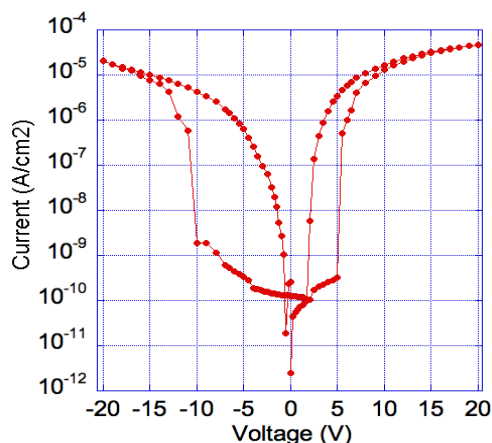
Figures

Figure 1: Current-Voltage characteristic of Ti-HfO_2-Au capacitor-like structure.
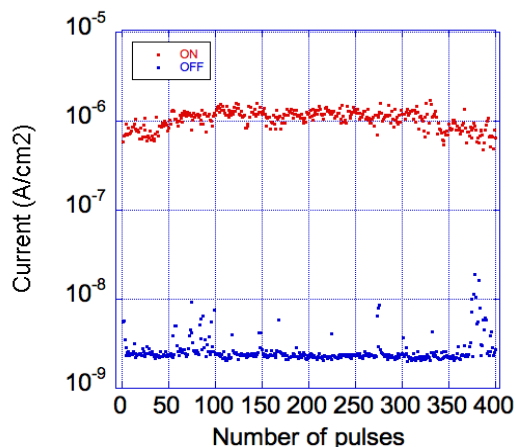

Figure 2: stability characteristics of Ti-HfO_2–Au capacitor-like structure obtained by programming ON and OFF states.

Single-Molecule Junctions Based on Nitrile-Terminated Biphenyls

Linda A. Zotti[1],
Artem Mishchenko,[2] David Vonlanthen,[3] Marius Bürkle,[4] Fabian Pauly,[4] Juan Carlos Cuevas,[1] Marcel Mayor,[3] and Thomas Wandlowski [2]

[1]Universidad Autónoma de Madrid, E-28049 Madrid, Spain
[2]University of Bern, CH-3012 Bern, Switzerland
[3]University of Basel, CH-4003 Basel, Switzerland
[4]Karlsruhe Institute of Technology, D-76131 Karlsruhe, Germany

Linda.zotti@uam.es

The electronic transport through single - molecule junctions is known to be affected by the specific molecular conformation of the central unit [1]. This has triggered the hope that molecules can be incorporated into electronic devices as switches. Recently, the conductance dependence on the torsion angle between the two phenyl rings in biphenyl based molecules has been widely investigated. For cases in which the transport is HOMO dominated, the conductance has been found to decrease with increasing torsion angle [2,3]. In this work, we analyze this dependence in a case in which the transport occurs through the molecular LUMO. This was accomplished by contacting a family of biphenyl derivatives to gold electrodes via nitrile (CN) anchoring groups. As this group is electrowithdrawing, it shifts the molecular levels downwards, affecting in turn the nature of the transport mechanism. Furthermore, studying nitriles has given us the opportunity to explore a relatively "new" binding group in this discipline. The pursuit of the best anchoring group for the formation of stable and energetically well-aligned metal-molecule contacts represents one of the most important current issues in molecular electronics [4,5]. In this perspective, understanding how the conformational induced change in the conductance depends on the specific anchoring group is one of the points which needs to be clarified.

We studied the transport through the mentioned molecules both experimentally (by scanning tunneling microscope (STM) break-junction technique) and theoretically by ab initio calculations. We found [6] that the conductance of the molecular junctions is roughly proportional to the square of the cosine of the torsion angle between the two benzene rings of the biphenyl core, which demonstrates the robustness of this structure−conductance relationship.

The calculations revealed that only atop binding geometries of the nitrile-gold contact are stable. This result is due to the coordinative nature of the covalent N-Au bond, which is established via the nitrogen lone pair. In order to evaluate whether the temperature can affect the molecular structures and in turn the conductance values, we performed molecular dynamics simulations for the isolated molecules in both vacuum and a solvent environment. They revealed that the torsion angles fluctuate around the equilibrium values. We estimated the corresponding variations in the conductance and we found that they are smaller than those due to changes in the binding geometry.

References

[1] Moresco, F.; Meyer,G.; Rieder, K. - H.; Tang, H.; Gourdon, A.; Joachim, C.; Phys. Rev. Lett. **86** (2001) 672
[2] Venkataraman, L.; Klare, J. E.; Nuckolls, C.; Hybertsen, M. S.;Steigerwald, M. L.; Nature **442** (2006) 904
[3] Mishchenko, A.; Vonlanthen, D.; Meded, V.; Burkle, M.; Li, C.; Pobelov, I. V.; Bagrets, A.; Viljas, J. K.; Pauly, F.; Evers, F.; Mayor, M.; Wandlowski, T.; Nano Lett. **10** (2010) 156
[4] Zotti, L. A.; Kirchner, T.; Cuevas, J. C.; Pauly, F.; Huhn, T.; Scheer, E.; Erbe, A.; Small **6** (2010) 1529

[5] Nichols, R.J.; Haiss, W.; Higgins, S.J.; Leary, E.; Martin, S.; Bethell, D.; Phys. Chem. Chem. Phys. **12** (2010) 2801

[6] Mishchenko, A.; Zotti, L.A.; Vonlanthen, D.; Bürkle, M.; Pauly, F.; Cuevas, J.C.; Mayor, M.; Wandlowski, T.; J.Am.Chem.Soc. **133** (2011) 184.

Figures
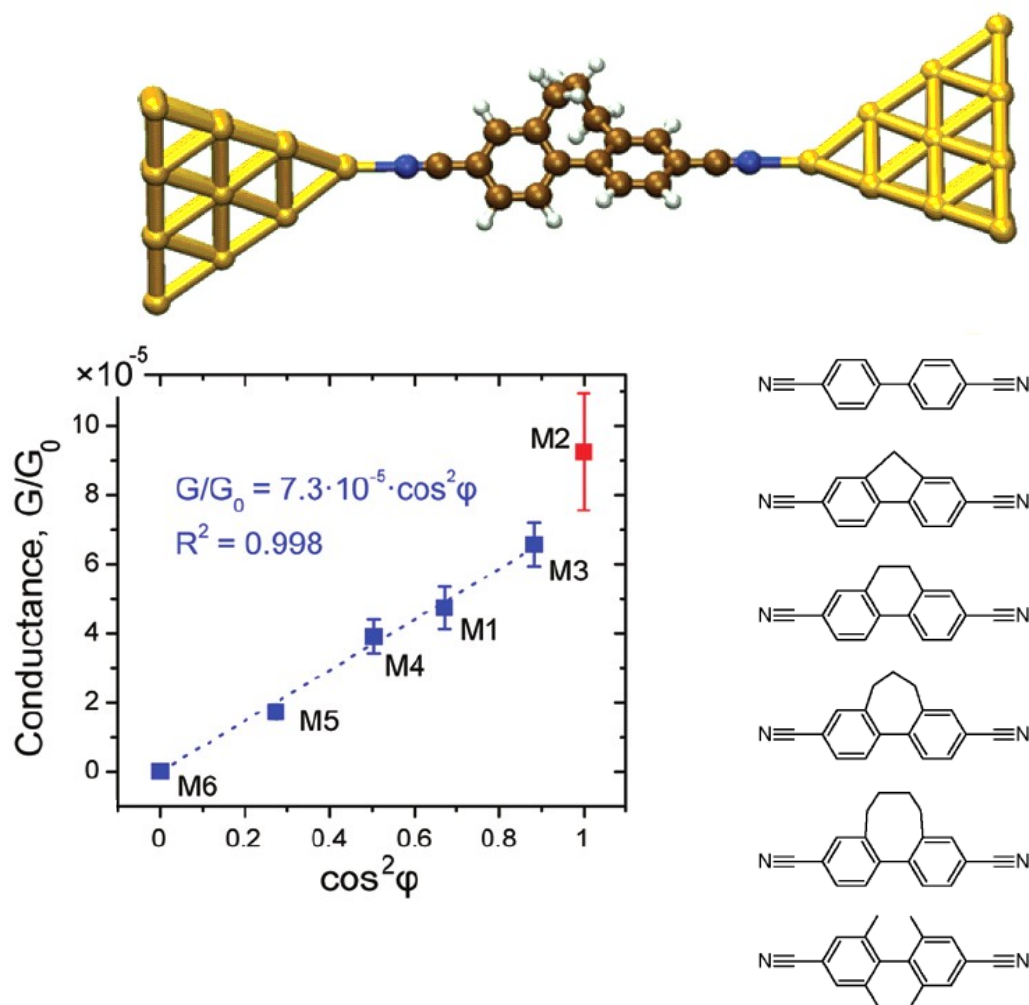
Top: Metal – molecule – metal junction for one of the studied molecules.
Lower left: Measured conductance vs cosine square of the torsion angle.
Lower right: Analyzed molecules

Influence of Boron Nitrogen pairs codoping on transport properties of Carbon nanotubes

Zoubkoff Rémi, Latil Sylvain

CEA/IRAMIS/SPCSI/LNOSC, 91191 Gif-sur-Yvette, France
remi.zoubkoff@cea.fr

In order to tune the electronic properties of carbon nanotube (CNT), a chemical doping by Boron or Nitrogen has been proposed. It appears that the Boron or Nitrogen atoms impact the transport properties and specially for injection energy corresponding to the quasi-bound states induced by the dopant [1,2]. However, these theoretical works were only considering the case of a single defect. Later different authors reported the influence of a random distribution of Boron or Nitrogen substitutive dopant [3,4]. They extracted mesoscopic informations such the mean free path and predicted rules dependence as a function of the dopant concentration or the nanotube radius.

More recentlty, Kalfoun et al [5] have investigated the effect of the BN codoping and have found that the effect of the two dopants was annealing each other when they are nearest neighbors and was cumulated when they are distant. This study was limited to a single defect thus our aim is to study the effect of the BN codoping on CNT for more realistic systems. We proposed to study the influence of BN codoping for mesoscopic system, and to investigate the effect of disorder induced by the B-N relative positions.

In order to compute the electronic properties of systems with a length scale as long as the µm, we adopt a Tight Binding formalism in a minimal basis formed by a single p orbital, that is known to give a good description of the electronic properties of CNT around the Fermi level. The influence of the N or B dopant was obtain by considering the electrostatic potential induced by a B or N on the one site element. It appears that the correction created by a BN pair is quite well described by the sum of the isolated dopant contribution. These corrections have been determined from DFT calculation performed with the SIESTA code.

We have computed the transport properties for random distribution of dopant. We consider different defects, with various distance between the B and N dopants. It appears that the mean free path behaves as an inverse of the dopant ratio, and evolves linearly with the nanotube radius. The distance between the B and N has significant effects as presented on the Figure 1. The mean free path decreases when the BN distance increases, as expected by considering results obtains for one BN pair default, the scattering potential created by the BN pair is attenuated by the proximity of the two species.

References

[1] H.J. Choi, J. Ihm, S. G. Louie, M. L. Cohen PRL, **84** (2000) 2917.
[2] C. Adessi, S. Roche, X. Blase, PRB, **73** (2006) .
[3] S. Latil,S. Roche, D.Mayou, J.C Charlier, PRL, **92** (2004) 256805.
[4] R. Avriller, S. Latil, F. Triozon, X. Blase, S. Roche, PRB, **74** (2006) 121406.
[5] H. Khalfoun, P Hermet, L. Henrad, S. Latil, PRB, **81** (2010) 193411

Figure 1
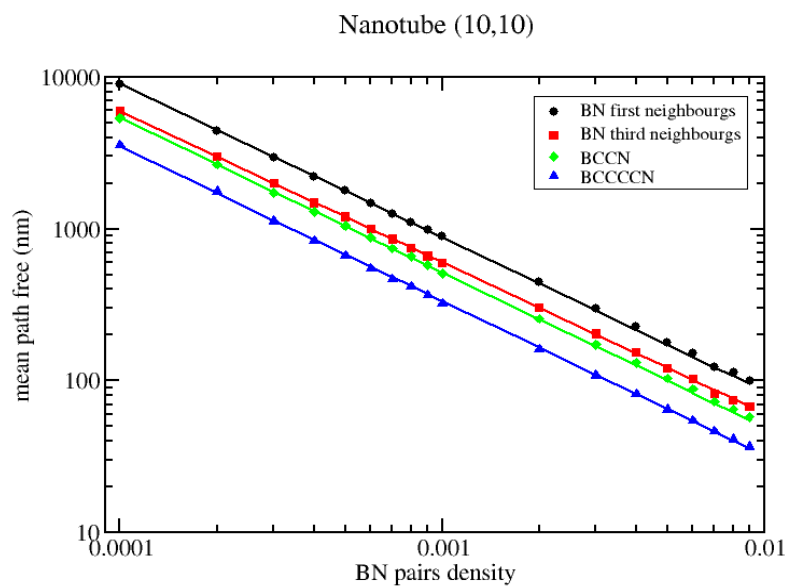
Nanotube (10,10)

Evolution of the mean free path as a function of the dopant concentration for a metallic (10,10) nanotube. The different curves are obtained for various BN pairs configuration, in a first neighbors (black), third neighbors(red), separated by two carbon atoms (green) or four atoms (blue).